VNIVERSITAT DE VALÈNCIA

INSTITUTO DE CIENCIA MOLECULAR

Programa de doctorado: Nanociencia y Nanotecnología Molecular

Mauricio López Jordà

PhD Tesis:

Materiales magnéticos híbridos formados por moléculas magnéticas biestables insertadas en redes bimetálicas de coordinación basadas en el ligando oxalato

---

Directores de la Tesis

Dr. Eugenio Coronado y Dr. Miguel Clemente León

D. Eugenio Coronado Miralles, Catedrático y **D. Miguel Clemente León**, profesor titular, del Instituto de Ciencia Molecular (ICMol) de la Universitat de València,

CERTIFICAN:

Que el trabajo que presenta D. Mauricio López Jordà en esta memoria, bajo el título: "**Materiales magnéticos híbridos formados por moléculas magnéticas biestables insertadas en redes bimetálicas de coordinación basadas en el ligando oxalato**" ha sido realizado bajo nuestra dirección en el Instituto de Ciencia Molecular de la Universitat de València.

Y para que así conste, a efectos de su presentación para optar al Grado de Doctor en Química, expedimos el presente documento.

Paterna, Mayo de 2013

Codirector	Codirector
Eugenio Coronado Miralles	Miguel Clemente León
(firma)	(firma)

A ma mare

La paciencia es un árbol de raíz amarga,
pero de frutos muy dulces.

Sinceramente, dentro de estas líneas, quisiera expresar mi agradecimiento a todas aquellas personas e instituciones que han hecho posible la realización de esta Tesis Doctoral en el Instituto de Ciencia Molecular de la Universidad de Valencia.

La primera persona que me atendió y me introdujo en el mundillo del Instituto, director del ICMol Eugenio Coronado Miralles y director de esta tesis, por su interés y confianza en mí y la oportunidad que me ha dado de poder trabajar en su grupo.

A Miguel Clemente León, director de esta investigación, por su apoyo constante durante todo el trabajo de investigación (y fuera del trabajo), por transmitirme sus conocimientos en la materia, la dedicación y paciencia que ha tenido en mi formación como químico y por su predisposición permanente para ayudarme y aclarar mis dudas. Realmente es muy difícil explicarlo en unas cuantas líneas, pero por todo ello, muchas gracias Miguel.

A todos los miembros y compañeros del grupo UIMM, que me han ayudado y colaborado en la realización de este trabajo. Esta lista es muy larga y si por error me dejase a alguien sin nombrar, desde aquí le pido disculpas:

A la gente que trabaja conmigo y que hemos compartido casi ocho horas del dia juntos, mi pecera donde tengo lo mejorcito, Sonsoles García por su buen humor, Alejandra Soriano por su continuo apoyo y cuidados. A la madre que tengo en el laboratorio Sam, que me ha ayudado en todo lo posible y ha estado siempre cuando la he necesitado. Como no, a Carlos Gómez (si no lo menciono, se pone celoso!) por su interés, sabiduría y su manera clara de transmitir sus conocimientos. Alex Abhervé (que ha venido a invadir mi espacio) realmente por ser una persona tan especial para mi; aunque lleve poco tiempo, hemos compartido buenos momentos y me ha demostrado que no es un "gamin". Por su energía y entusiasmo en todas las cosas y estar siempre disponible.

A toda la gente del grupo, que hemos compartido muchos años juntos, empezando con el Master en Nanociencia y Nanotecnología Molecular: Michele Sessolo, Julia Ponce

(JPG), Efren Navarro, Salva Cardona, Concha Bosch (mi Concha), Elena Pinilla (Pini). Luego a nuevas promociones del Master: Alex Recuenco, Toni Pertegás, Gonzalo Abellán, Hicham Brine, Jose Jaime Baldoví, Olga Malinkiewicz… Y a toda la gente que hemos compartido muchas cosas en cenas, fiestas, caminatas, findes….

Tampoco tengo suficientes palabras para decir GRACIAS a Mónica Giménez (cari!), por ser como es, su constante interés y preocupación por mi. Eres, y lo seguirás siendo, como una hermana para mi. A Guillermo Mínguez, ese sevillano, que desde el primer dia que le conocí y hasta ahora, ha estado siempre ahí, para resolverme cualquier duda. Por su simpatía y profesionalidad en el trabajo y por la "grasia andalusa".

No me gustaria olvidar a la gente que se ha ido, Filippo Bussolo y mis queridos amigos gabachos Yoann Prado (Yo-Yo o Juanito) y Florence Volatron (Flo-Flo). En estos dos últimos años han sido un gran pilar en mi vida, laboral y social. Gracias Yoann por ser tan pragmático y a ti Flo por tu sinceridad y carisma. He compartido muchas cosas con vosotros y me habeis demostrado que sois amigos de verdad.

Carlos Martí por su gran conocimiento y profesionalidad, también a Lola Gómez, Maria Monrabal por su ayuda y apoyo.

Al resto de profesores, contratados técnicos y los Ramon y Cajal, donde siempre me han ayudado cuando he tenido alguna duda.

Al grupo del profesor Andreas Hauser de la Universidad de Ginebra (Suiza) por aceptarme en su grupo para realizar mi estancia y en especial a Antoine Tissot, Enza y Elisa. Gracias por enseñarme todo lo que sé de espectroscopía y fotoexcitación en láser. Personalmente, sin vosotros mi estancia hubiera sido muy dura y más fría. Muchas gracias por vuestra hospitalidad y por esas "soirées" inolvidables.

A Chema Martínez y Gloria Agustí por las medidas magnéticas y a João C. Waerenborgh por las medidas de Mössbauer. También agradecer a Fernando Luis y Ana Repollés del

ICMA de la Universidad de Zaragoza por las medidas magnéticas a bajas temperaturas y a J.-F. Létard, Cédric Desplanches y Hongfeng Wang del ICMCB de la Universidad de Burdeos, por las medidas fotomagnéticas y tratamiento de los datos. Gracias a Paco, Marian, Manu y Estela que siempre estan informándonos de los asuntos burocráticos y problemas con las nuevas tecnologias, a Jose Usagre que nos reparte el material y productos de laboratorio.

Por otra parte, quisiera agradecer a toda mi familia, por el apoyo que me han brindado durante toda la carrera, sé que siempre han estado ahí y por los sacrificios que han tenido que hacer para poder hacer este trabajo de investigación. Con especial dedicación a mi madre por lo que ha luchado para ser algo en esta vida, mis tios y mis primos que todos ellos han creido en mí. También a todos mis amigos que me han ayudado y han estado a mi lado en los buenos y malos momentos, Vicent, Jorge Forner y Albert, Esther, Majo, Cristina, Mari, Neus, Eva, Kike.

Alex Hernández, Salva Vidal, Vicent Margarit, Sara Vidal, amigos y compañeros de piso durante algunos años, que me han acompañado durante toda esta formación desde primero de carrera, me han apoyado en todo momento, gracias por estar a mi lado.

Agradeder a Roser, Bati, Carmen, Jessica, Nadia, Miquel, Isadora, Sara, Aida, Joan, Maria, Laura, Vicent compañeros de la carrera donde todos hemos crecido y aprendido juntos, y por los buenos momentos que hemos pasado, que seguro más adelante recordaremos y reiremos.

Por último, quisiera agradecer a Guilles Ulrich, Raymond Ziessel y Antoinete Denicolla profesores que estuvieron a mi lado durante mi estancia en Strasbourg de ERASMUS, los cuales me mostraron la investigación en química y me motivaron para continuar en este mundo. Y a toda la gente erasmus que compartió esa experiencia conmigo en Strasbourg.

Índice

Capítulo 1 – Introducción

Introducción

Capítulo 1

Capítulo 1: Introducción

1. Introducción: Materiales híbridos multifuncionales

Los recientes avances tecnológicos han generado una enorme demanda en el estudio y desarrollo de nuevos materiales. La versatilidad de la química molecular actual permite el diseño y desarrollo de nuevos materiales híbridos basados en la combinación de dos o más moléculas, lo que puede dar lugar a una combinación de sus propiedades. Muchas de las nuevas aplicaciones en el campo de la ciencia de los materiales avanzados están relacionadas con los híbridos multifuncionales, ya que la combinación de propiedades de sus componentes puede dar lugar a interesantes propiedades físicas. Por otro lado, como las propiedades de un material dependen fundamentalmente de su estructura, el control de la misma nos permitirá manipular y modular sus propiedades. En la naturaleza existe un complejo orden jerárquico en la forma de construcción, desde el tamaño nanométrico hasta nivel macroscópico, donde cada componente del material tiene su función en el rendimiento del material. Esto se quiere imitar en ciencia de los materiales, de forma que la preparación de materiales, cada vez más complejos con propiedades físicas nuevas, obliga a una aproximación multidisciplinar, que implica tanto al químico sintético como al físico de materiales o al biólogo molecular.

La aproximación híbrida que hemos utilizado en esta tesis consiste en preparar nuevos materiales a través del auto-ensamblaje de varios bloques moleculares (orgánicos, inorgánicos u organometálicos), con el fin de que cada subred aporte propiedades físicas y estructurales diferentes al material multifuncional. La elección de los bloques moleculares que formarán finalmente el material deseado se realiza teniendo en cuenta las propiedades que éstos presentan cuando se ensamblan para formar un sólido. De esta forma, se busca que la combinación de estas propiedades en el material final pueda dar lugar a un comportamiento no observado con anterioridad, o incluso a una nueva propiedad como resultado de las interacciones entre los

componentes moleculares del material. Otra posibilidad muy interesante es obtener materiales inteligentes sensibles a estímulos externos, que respondan con un cambio drástico de sus propiedades a un estímulo físico o químico[1].

Siguiendo esta estrategia, se ha logrado diseñar materiales moleculares con coexistencia de propiedades (magnéticas, electrónicas, ópticas, estructurales y químicas), o acoplamiento de propiedades (magnetoópticas, fotomagnéticas, magnetoquirales, magnetoconductoras, etc.)[2]. Para el químico molecular, la síntesis de este tipo de materiales híbridos es un desafío debido a la elevada complejidad química y estructural que presentan. A su vez, estos materiales suponen para el físico una oportunidad única para estudiar la asociación inusual de propiedades físicas en un mismo sistema. Estas posibilidades ponen claramente de manifiesto el poder de los materiales híbridos para generar sistemas complejos a partir del ensamblado de bloques de construcción moleculares.

2. Materiales multifuncionales basados en redes de oxalato

2.1 Materiales multifuncionales magnéticos

Dentro del magnetismo molecular, una de las áreas más activas es la obtención y estudio de redes poliméricas. Éstas son especialmente interesantes para el diseño de nuevos materiales magnéticos híbridos. De hecho, una gran mayoría de los imanes basados en moléculas se centran en el uso de ligandos orgánicos de pequeño tamaño, que ofrecen vías electrónicas para un supercanje magnético, tales como son el oxalato ($C_2O_4^{2-}$)[3], el oxamato (pbaOH)[4], el cianuro (CN^-)[5] o la dicianamida ($[N(CN)_2]^-$)[6]. En el caso de los oxalatos, su gran versatilidad sintética ha permitido el diseño de una gran variedad de polímeros de coordinación que, además de exhibir propiedades magnéticas y electrónicas interesantes, presentan la capacidad de incorporar moleculas funcionales en sus estructuras.

2.2 Tipos de redes basadas en el ligando oxalato

Los compuestos bimetálicos basados en el ligando oxalato de fórmula $A[M^{II}M^{III}(ox)_3]$ donde M^{II} puede ser Mn, Fe, Co, Ni, Cu, Cr, Zn y M^{III} Cr, Fe, Ru y Mn, han proporcionado muchos ejemplos de imanes híbridos. Estos compuestos bimetálicos están constituidos por una red aniónica polimérica 2D[7] o 3D[8], que presenta propiedades magnéticas cooperativas (ferro- ferri- o antiferromagnetismo), y un contraión molecular. Estructuralmente están formados por subredes poliméricas cargadas negativamente separadas por cationes voluminosos del tipo $[XR_4]^+$ (X = N, P; R = Ph, nPr, nBu,…). El catión actúa como agente plantilla induciendo el auto-ensamblaje de la parte aniónica y, por consiguiente, dando lugar a polímeros de coordinación insolubles. La sustitución de estos cationes -electrónicamente "inocentes" en su mayoría- por otros con alguna propiedad física interesante, permite la introducción de nuevas propiedades al sistema. En estos compuestos el magnetismo cooperativo de la red de oxalatos puede coexistir con propiedades electrónicas proporcionadas por los cationes moleculares introducidos.

Se ha comprobado la gran versatilidad de estos sistemas para construir distintos tipos de redes con dimensionalidad controlada[9]. Así, una quiralidad alternada de los complejos metálicos octaédricos $[M(ox)_3]$ (Λ y Δ) da lugar a redes 2D formadas por anillos de seis unidades, mientras que si los octaedros presentan la misma quiralidad (Δ y Δ) o (Λ y Λ) aparecen como redes cúbicas 3D, donde el anillo que se forma tiene 10 unidades (Figura **1**). La formación de una u otra red viene condicionada por las condiciones de síntesis y sobre todo por el contraión utilizado

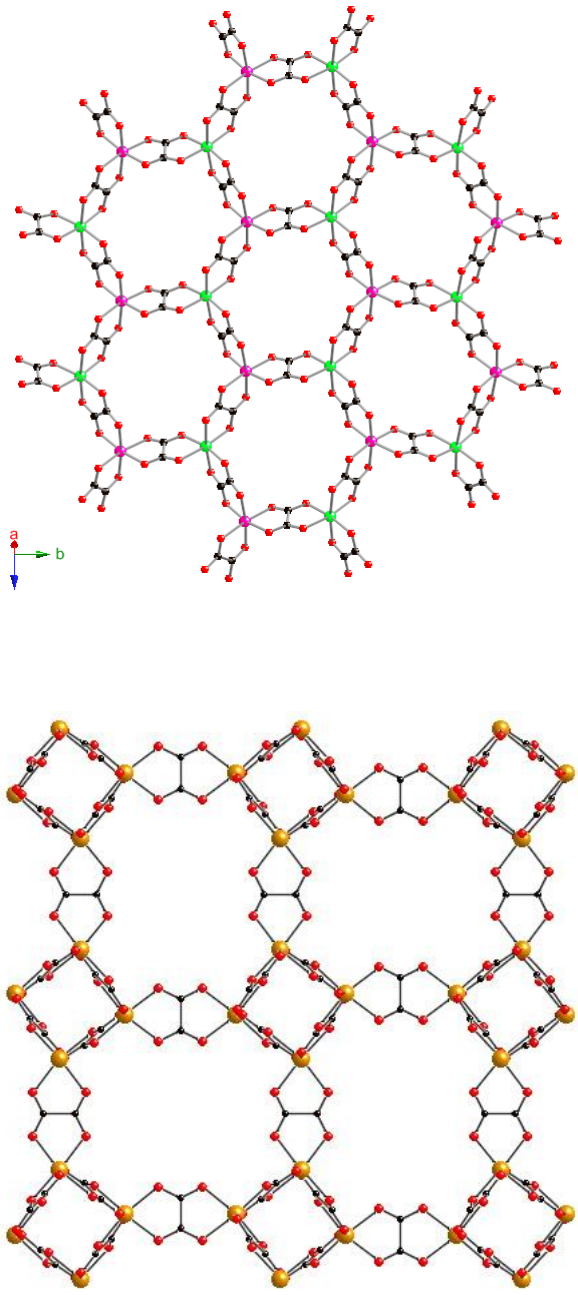

Figura 1: Estructuras bidimensional (2D, arriba) y tridimensional (3D, abajo) extendidas obtenidas a partir de los complejos octaédricos del compuesto $[M^{II}M^{III}(ox)_3]^-$.

2.2.1 Redes 2D

La redes extendidas 2D presentan la típica forma de panal de abeja formada por seis unidades $[M^{n+}(ox)_3]^{n-6}$, donde cada complejo de metal divalente se encuentra unido a tres complejos del metal trivalente y viceversa, dando una alternancia de las unidades en cada anillo hexagonal. En este tipo de sistemas los cationes se sitúan entre las capas aniónicas de oxalatos. El apilamiento de las capas de oxalato varía según el catión insertado entre ellas.

Respecto a las propiedades magnéticas, los puentes oxalato entre los centros metálicos favorecen las interacciones entre iones magnéticos iguales o diferentes y por esto han sido utilizados en la síntesis de iones magnéticos polinucleares[10]. Las redes 2D bimetálicas dan lugar a numerosos ejemplos de materiales magnéticos. En general, las interacciones M^{II}-Cr^{III} son de carácter ferromagnético, mientras que las interacciones M^{II}-Fe^{III} son antiferromagnéticas. Los compuestos de la familia $[XR_4][M^{II}Cr^{III}(ox)_3]$ (M^{II} = Mn, Fe, Co, Ni, Cu, Cr)[7a], presentan ordenamiento ferromagnético con temperaturas críticas, T_c, comprendidas entre 6 y 15 K excepto en el caso del derivado del Cr^{II} que presenta interacciones antiferromagnéticas[11]. Los compuestos $[XR_4][M^{II}Fe^{III}(ox)_3]$ presentan ordenamiento ferrimagnético cuando M^{II} = Fe o Ni, y un ferromagnetismo débil cuando (M^{II} = Mn). En este caso los espines S = 5/2 de las dos subredes se compensan dando lugar a un ordenamiento antiferromagnético[12], con ”spin canting” a 28 K. Más recientemente se ha extendido la familia de 2D a dos iones trivalentes Ru^{III} y Mn^{III}. En el caso del Ru^{III} se ha preparado la familia de compuestos de fórmula $[XR_4][M^{II}Ru^{III}(ox)_3]$ (M^{II} = Mn, Fe, Cu)[13]. En este caso se observa la presencia de interacciones ferromagnéticas para el derivado de Mn^{II} y antiferromagnéticas para los derivados de Fe^{II} y Cu^{II} con valores de T_c = 13 K. Otro ejemplo lo proporciona la familia $[NBu_4][M^{II}Mn^{III}(ox)_3]$ (M^{II} = Fe, Co, Ni). Estos iones muestran interacciones antiferromagnéticas que dan lugar a ordenamientos ferrimagnéticos en el caso de Co^{II} (T_c = 13 K) y Ni^{II} (T_c = 21 K) y a débil ferromagnetismo en el caso del Fe^{II} (T_c = 21 K)[14].

2.2.2 Redes 3D

Las primeras redes 3D, se obtuvieron al utilizar cationes plantilla de complejos metálicos similares al $[Z^{II}(bpy)_3]^{2+}$ (Z = Ru, Fe, Co, Zn, Ni; bpy = bipiridina). Se trata de una red 3D con empaquetamiento cúbico. La fórmula general para esta clase de compuestos es $[Z(bpy)_3]X[MM'(ox)_3]^{8a-d}$, $[Ru(ppy)(bpy)_2][MM'(ox)_3]$[15] y $[Ir(ppy)_2(bpy)][MM'(ox)_3]^{8e}$ (Z = Ru, Fe, Co y Ni; X = ClO_4^-, BF_4^-, PF_6^-, M, M' = Li^I, Na^I, Mn^{II}, Ni^{II}, Co^{II}, Fe^{II}, Cu^{II}, Zn^{II}, Rh^{III}, Co^{III}, Cr^{III} y Fe^{III}; bpy = 2,2'-bipiridina, ppy = fenilpiridina). A diferencia de la estructura 2D que admite una gran variedad de cationes, en las estructuras 3D los cationes deben tener el tamaño, la carga y la simetría adecuada. En estos casos, la red de oxalatos es suficientemente flexible para admitir otras cargas de los cationes, además de la +1, que se ven compensadas en el caso de cationes de carga +2, por la inclusión de pequeños aniones como BF_4^- o ClO_4^-. Esto no se ha observado en redes 2D que, por lo general, sólo admiten cationes de carga +1. En la mayoría de los casos, todos los centros metálicos de las estructuras 3D presentan la misma quiralidad en contraste con las redes 2D en las que los iones vecinos presentan quiralidad alternada. Esto ha permitido preparar compuestos 3D enantiopuros en los que cationes del tipo $[Z(bpy)_3]^{2+}$ quirales inducen el crecimiento de redes de oxalato con centros metálicos con la misma quiralidad que el catión insertado[15].

El carácter híbrido de este tipo de materiales puede generar imanes híbridos cuando las dos subredes son magnéticas. Sin embargo, la característica más interesante de esta familia es el comportamiento quiral que presenta y la posibilidad de obtener imanes quirales[15].

2.2.3 Otros tipos de redes

Por último, el ligando oxalato puede también generar redes magnéticas diferentes a las descritas con anterioridad. Esto sucede cuando parte de los oxalatos no actúa de forma bis(bidentada)[16]. Por ejemplo, mediante el uso de ligandos "tope", se han

obtenido dímeros, trímeros o tetrámeros de metales magnéticos unidos por puentes oxalato[17]. Además, el tamaño, la forma, la geometría y la carga del catión que se introduce son elementos clave para la obtención de arquitecturas de este tipo. También se han obtenido complejos basados exclusivamente en el ligando oxalato, como dímeros o trímeros, mediante el control de las condiciones de síntesis y la solubilidad de los compuestos en el medio de reacción[18].

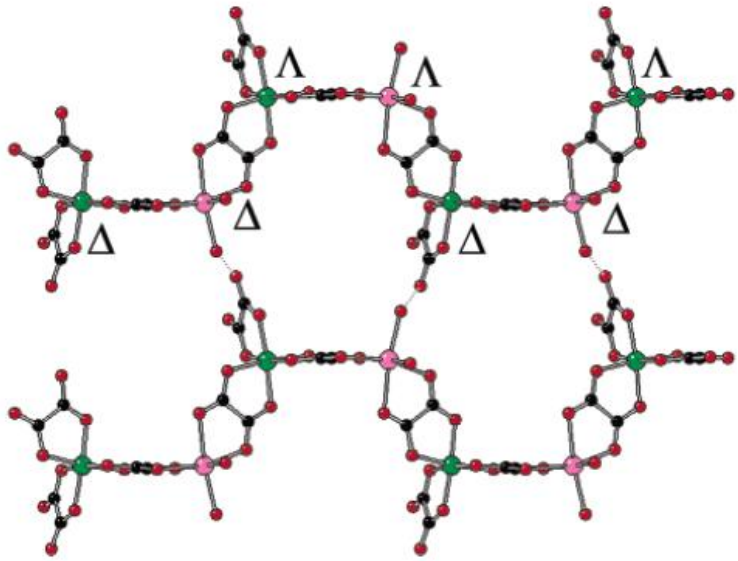

Figura 2: Cadena $[Mn(H_2O)_2Cr(ox)_3]_n^{n-}$, mostrando la quiralidad de los centros metálicos y los puentes de hidrógeno entre cadenas.

El compuesto $[K(18\text{-crown-}6)][Mn(H_2O)_2Cr(ox)_3]$[16b] es un claro ejemplo de cadena bimetálica basada en el ligando oxalato utilizando un éter corona como catión plantilla. La capa aniónica está constituida por Mn^{2+} y $(Cr(ox)_3]^{3-}$ de forma alternada dando lugar a cadenas 1D. Los Mn^{+2} están coordinados por dos oxalatos y completan la esfera de coordinación octaédrica con dos moléculas de agua. Las cadenas están formadas por los dos posibles enantiómeros presentados por pares, con una unidad de repetición

-ΔΔΛΛ-. Debido al descubrimiento de las cadenas imán o SCM (Single Chain Magnet), existe un gran interés en este tipo de compuestos con cadenas basadas en el ligando oxalato.

Este apartado ha mostrado la versatilidad intrínseca que presenta el oxalato en la construcción de diferentes estructuras cristalinas multidimensionales, que presentan propiedades magnéticas de interés. Como veremos en el siguiente apartado, el catión tiene importancia no solo estructural (como catión plantilla) sino que permite también introducir una segunda propiedad física y por lo tanto dar lugar a un material multifuncional.

2.3 Tipos de materiales multifuncionales basados en redes de oxalato

Los compuestos basados en redes extendidas de oxalato permiten preparar también compuestos multifuncionales por inserción de distintos tipos de cationes[19].

2.3.1 Conductores magnéticos

Hasta el momento, se ha obtenido un gran número de materiales híbridos que combinan propiedades conductoras con propiedades magnéticas[1a,20]. Este tipo de materiales puede brindar una oportunidad única para estudiar la interacción de estas dos propiedades. Muchos de estos materiales híbridos están formados por apilamientos segregados de moléculas orgánicas dadoras del tipo tetratiofulvaleno (TTF) y sus derivados (Figura **3**), que se encuentran parcialmente oxidadas y permiten la deslocalización electrónica, separadas por aniones magnéticos inorgánicos. El anión tris(oxalato) metalato se ha utilizado como anión inorgánico en este tipo de compuestos, tanto en forma de aniones aislados[21], oligómeros[22] o incluso, como capas extendidas[2c,23,24,25].

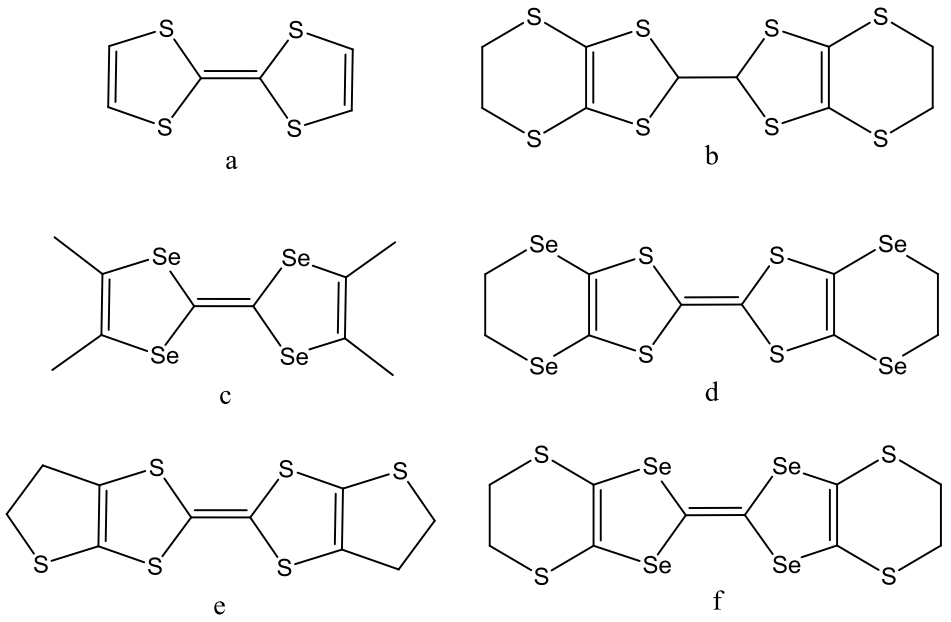

Figura 3: Dadores orgánicos de la familia del TTF. A) Tetratiofulvaleno (TTF); b) Bis(etileneditio)-TTF (BEDT-TTF o ET); c) Tetra(metil)tetraselenofulvaleno (TM-TSF); d) Bis(etilediseleno)-TTF (BEST); e) Bis(etilenetio)-TTF (BET-TTF); f) Bis(etileneditio)-TSF (BETS)

En el compuesto $[BEDT\text{-}TTF]_3[MnCr(ox)_3]^{2c}$ (BEDT = bis(etilenditio)tetrafulvaleno) se combinó por primera vez la conductividad metálica de la capa catiónica con el ordenamiento ferromagnético de la red de oxalatos. Así, este compuesto híbrido se ordena ferromagnéticamente por debajo de 5.5 K y es metálico desde temperatura ambiente hasta 0.2 K. La baja dimensionalidad es otra originalidad de este material, que unida a la débil interacción electrónica entre ambas subredes, hacen de este híbrido un compuesto muy atractivo y original desde el punto de vista de su fenomenología física. De hecho, su comportamiento magnetorresistivo presenta una gran anisotropía y peculiaridades en la conductividad provenientes del campo magnético interno generado por la componente ferromagnética. Otra de las ventajas de los materiales moleculares reside en la posibilidad de cambiar las propiedades de las moléculas componentes manteniendo una misma estructura.

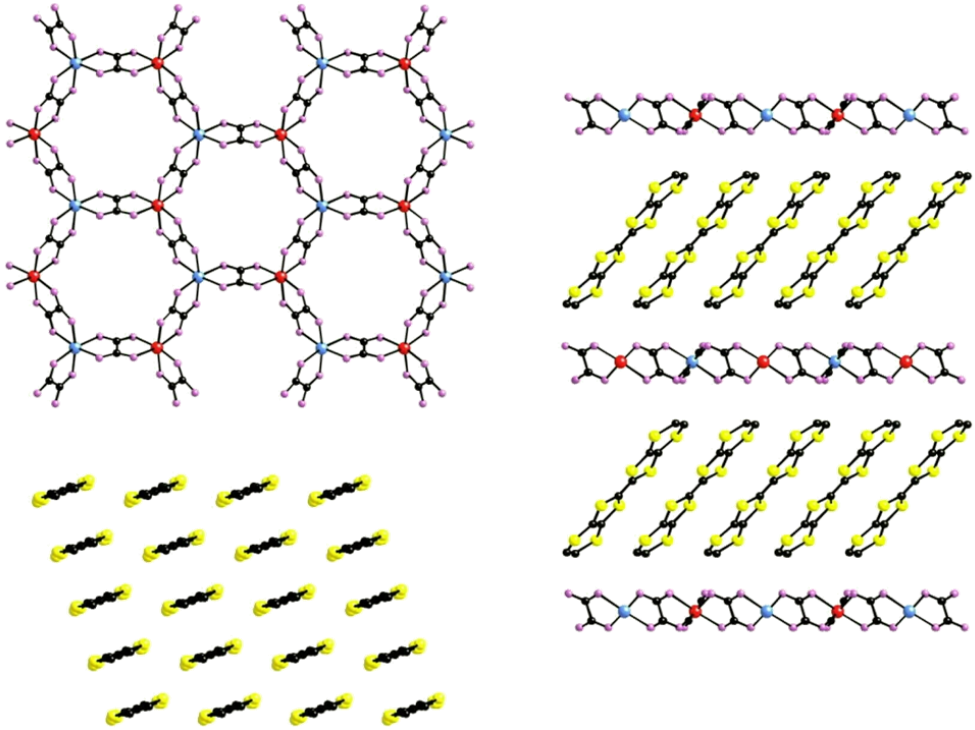

Figura 4 : Estructura del compuesto $[BEDT\text{-}TTF]_3[MnCr(ox)_3]\cdot(CH_2Cl_2)$, proyecciones de las monocapas aniónica y catiónica (izquierda) y representación de la estructura del material híbrido, mostrando la alternancia de capas orgánicas/inorgánicas (derecha).

Siguiendo este camino, se diseñaron varios compuestos de conductores moleculares magnéticos, a partir de capas aniónicas de tris(oxalato) bimetálico del compuesto anterior en los que se cambió uno de los metales de la red (Rh^{III} diamagnético en lugar del Cr^{III} paramagnético)[24], o el dador orgánico (BETS en lugar del BEDT-TTF)[25]. De esta forma, se han obtenido compuestos cristalinos multifuncionales multicapa con propiedades que varían desde aislantes a metálicos o desde paramagnéticos a ferromagnéticos, manteniendo las características estructurales globales de tal forma que las correlaciones entre las dos propiedades pueden ser apropiadamente examinadas y determinadas.

2.3.2 Multicapas magnéticas

Esta familia de compuestos se forma por la inserción de cationes paramagnéticos en redes 2D o 3D basadas en oxalato. La mayoría de estudios se ha hecho en compuestos 2D en los que las capas de oxalatos $[M^{II}M^{III}(ox)_3]^-$, ordenadas magnéticamente, se alternan con capas de cationes paramagnéticos como el decametilferricinio $[Fe^{III}Cp_2^*]^+$ [26], (Figura **5**) o radicales orgánicos catiónicos derivados de nitronil nitróxido[19]. La estructura de los compuestos con decametilferrocinio y otros cationes metalocinio está formada por un apilamiento eclipsado de las capas extendidas de oxalato separadas por capas de los cationes organometálicos. Estos materiales híbridos presentan un ordenamiento magnético similar al de otras redes 2D en función de los metales que la constituyen. Cuando se utiliza el catión paramagnético decametilferricinio, con espín S = ½ en lugar del diamagnético (S = 0), se obtiene un sistema magnético multicapa construido químicamente por capas ferromagnéticas y paramagnéticas alternadas. En el caso de los compuestos con radicales nitronil nitróxido se han utilizado distintos tipos de derivados catiónicos que se muestran en la Figura **6**. El tipo de red que se obtiene depende del método de síntesis y del catión radical. Los dos derivados de alquilpiridinio dan lugar a la formación de redes 2D amorfas en condiciones de precipitación rápida y a redes 1D y 3D en condiciones de cristalización lenta en los compuestos de fórmula $[p\text{-rad}][MnCr(ox)_3(H_2O)]\cdot 2H_2O$ y $[m\text{-rad}][MnCr(ox)_3(H_2O)_2]\cdot 2H_2O$[16a,27]. En estas redes la lenta formación de cristales favorece la coordinación de moléculas de H_2O al Mn(II) dando lugar a redes en las que parte de los oxalatos actúan como ligandos monodentados como las que se han introducido en el apartado 2.2.3. Por otro lado, el radical en el que el grupo tributilamino está unido al radical nitronil nitróxido da lugar a compuestos 2D cristalinos de fórmula $[^nBu_3NCH_2NN][MCr(ox)_3]$ (M = Mn, Ni, Zn)[19].

La diferencia principal entre el comportamiento magnético de estas dos familias de híbridos orgánicos/inorgánicos es que mientras la densidad de espín del decametilferricinio está mayoritariamente en el centro metálico situado entre los dos grupos ciclopentadieno, los radicales nitronil-nitróxido ofrecen su densidad de espín

hacia el entorno. Como consecuencia de esto, el comportamiento magnético de la primera familia corresponde a dos sub-redes magnéticas completamente independientes en la que los cationes paramagnéticos constituyen excelentes "sondas" locales para conocer el campo magnético interno generado por las capas de oxalato. Por otro lado, el comportamiento magnético de la segunda familia de compuestos es el resultado de las interacciones magnéticas entre las dos subredes, el radical orgánico y la capa inorgánica de oxalatos. Así, el estudio de estos sistemas por resonancia paramagnética electrónica (EPR) en los compuestos de decametilferricinio, ha puesto de manifiesto que las dos subredes son casi independientes ya que se observan de forma independiente las señales del decametilferricinio y de la red bimetálica de oxalatos[26c]. El único efecto del ordenamiento magnético es el desdoblamiento de Zeeman del complejo de decametilferricinio en presencia de un campo magnético interno generado por las capas de oxalato. En el caso de los compuestos 2D con radicales orgánicos, el espectro de EPR no muestra una señal intrínseca del radical orgánico distinta a la de la red, lo que indica la presencia de interacciones magnéticas débiles entre las dos subredes[19].

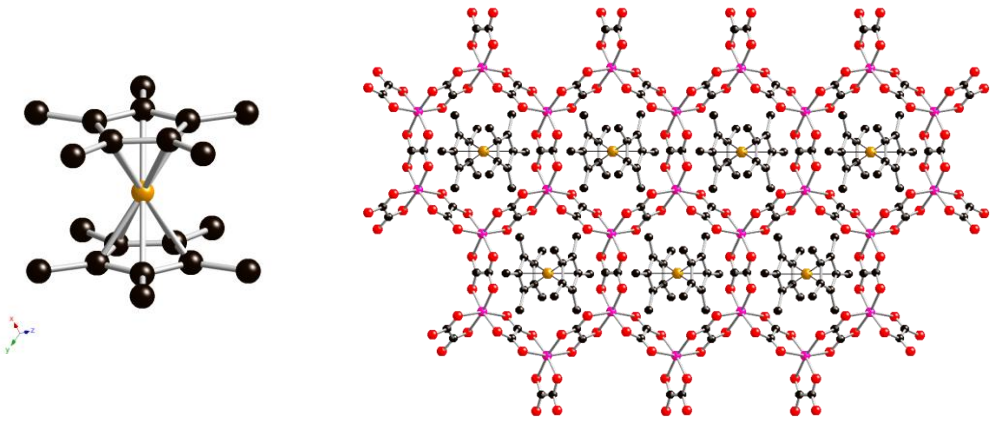

Figura 5: Estructura del catión organometálico de Fe (izquierda), estructura del compuesto $[Fe^{III}Cp_2^*][Mn^{II}Cr^{III}(ox)_3]$ (derecha).

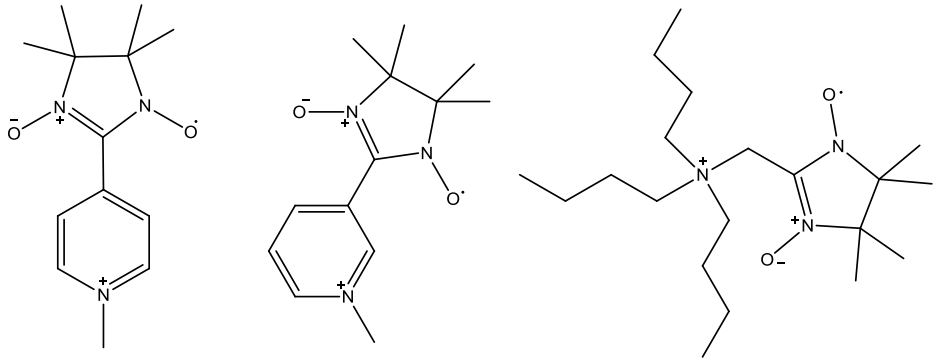

Figura 6: Diferentes radicales orgánicos insertados en redes bimetálicas de oxalato.

También existe la posibilidad de introducir cationes de transición de espín[28] entre capas de oxalato. Un esfuerzo importante se ha desarrollado en esta tesis y lo detallaremos en el apartado 2.4.3.3.

2.3.3 Fotocromismo / Óptica no lineal

Dentro de este contexto, el desarrollo de materiales basados en redes de oxalato poliméricas donde se insertan cationes que presentan propiedades fotocrómicas o de óptica no lineal (NLO, siglas en inglés), ha recibido mucha atención por sus potenciales aplicaciones en la tecnología electrónica así como en el diseño de dispositivos que puedan ser modulados mediante radiación electromagnética[29,2d]. Esto se debe al interés de obtener imanes fotosensibles, donde la molécula fotocromática orgánica provoca cambios estructurales fotoinducidos. Por otra parte, el estudio de moléculas fotocromáticas insertadas en sistemas 2D resulta muy interesante no sólo para obtener nuevos imanes magnetoópticos, sino también para obtener más información estructural y poder determinar los factores que controlan el empaquetamiento de los cromóforos dentro de las redes de oxalato y, por consiguiente, la actividad NLO[2d]. Por lo que respecta a las propiedades de óptica no lineal, el resultado más interesante lo presentan los compuestos 2D de fórmula DAMS o DAZOP[$Mn^{II}Cr^{III}$(ox)3] (Figura **7**). Estos compuestos son los que muestran una generación del segundo armónico (SHG por sus

siglas en inglés) más efectiva. Los mejores resultados de esta familia de compuestos se obtienen en los casos en los que el espaciado intercapa es menor, seguramente porque esto favorece el alineamiento de los momentos dipolares de los cromóforos, ya que cuando las distancias intercapas son mayores, aparecen huecos o defectos que favorecen la dimerización[2d]. Otra familia de compuestos con generación del segundo armónico es la de los compuestos de fórmula general $[DAMS]_4[M^{II}M^{III}{}_2(ox)_3]\cdot DAMBA\cdot 2H_2O$ (M^{III} = Rh, Fe, Co; M^{II} = Mn, Zn; DAMBA = p-dimetilaminobenzaldehido) que presentan una estructura en cadenas con oxalatos bis(bidentados) y monodentados[30]. Por último, el compuesto 2D quiral enantiopuro de fórmula $[N((S)\text{-i-Bu})MePr_2][(\Lambda)Mn\text{-}(\Delta)\text{-}Cr(ox)_3]$ (i-Bu = $CH(CH_3)C_2H_5$; Me = CH_3; Pr = C_3H_7) muestra una generación del segundo armónico importante. Además, en este compuesto aparece una señal SHG inducida por el campo magnético (MSHG)[31].

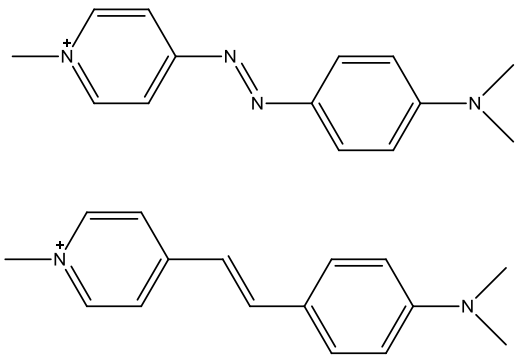

Figura 7: Cromóforos DAZOP (arriba) y DAMS (abajo).

El fotocromismo se define como una transformación fotoquímica inducida mediante la absorción de radiación electromagnética entre dos especies A y B, que se diferencian no sólo en su espectro de absorción sino también en su estructura y propiedades físicas. Un ejemplo de este tipo de compuestos es $(SP)[MnCr(ox)_3]\cdot H_2O$, donde SP^+ es un cromóforo derivado del espiropirano. Estos compuestos están formados por dos grupos heterocíclicos en planos ortogonales unidos por un átomo de carbono espiro tetraédrico común, que impide la conjugación de los dos sistemas π-electrónicos (Figura **8**). La

irradiación en la banda de absorción (365 nm) conduce, por ruptura del enlace C-O, a la formación del fotoisómero de forma abierta, y por ende, un cambio de color, debido a la deslocalización π-electrónica por conjugación.

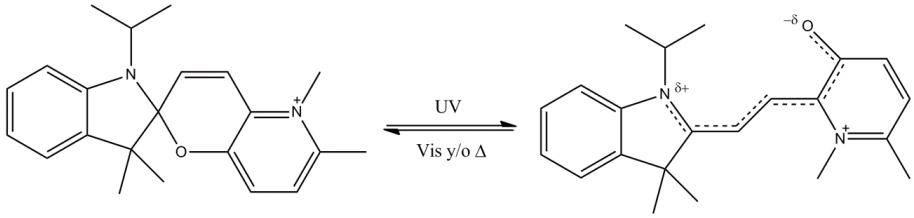

Figura 8: Equilibrio fotoinducido del catión SP.

Desafortunadamente, esta fotorreacción es irreversible en estado sólido y no interfiere en la temperatura crítica de ordenamiento magnético de la red, debido probablemente a las débiles interacciones que presenta el catión con la red. Sin embargo, el catión en forma abierta, modifica de manera significativa la curva de histéresis. Este resultado está causado posiblemente por defectos estructurales introducidos en el cristal al pasar a la forma fotoinducida[29].

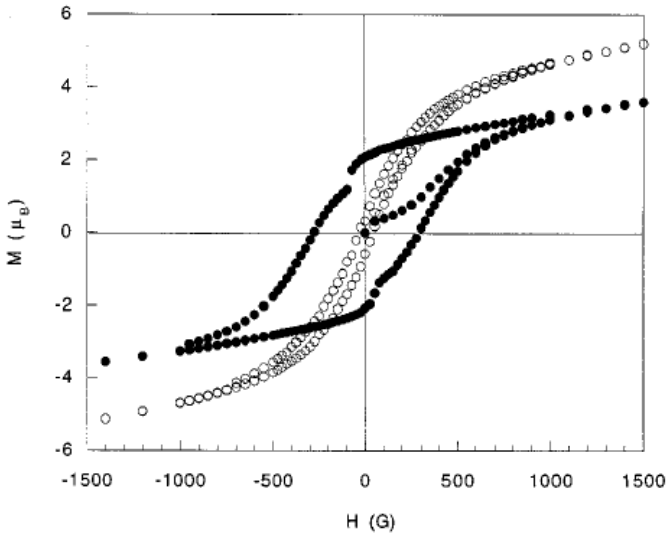

Figura 9: Curvas de histéresis antes (○) y después (●) de irradiar a 365 nm.

2.3.4 Multiferroicos

La ferroelectricidad es la capacidad de ciertos materiales para retener información en su estructura, debido a una distorsión en la red cristalina, sin necesidad de estar conectados a una fuente de energía. La información es almacenada gracias a la polarización eléctrica que poseen, que puede ser activada externamente por un voltaje, y persiste aún cuando el potencial eléctrico se retira.

Los materiales en los que coexiste esta propiedad con el ferromagnetismo se denominan materiales multiferroicos[32]. Su desarrollo ha atraído mucha atención para la preparación de nuevos dispositivos con capacidad de almacenamiento alta o dispositivos magnéticos sintonizables electrónicamente, que son de interés para la espintrónica[33].

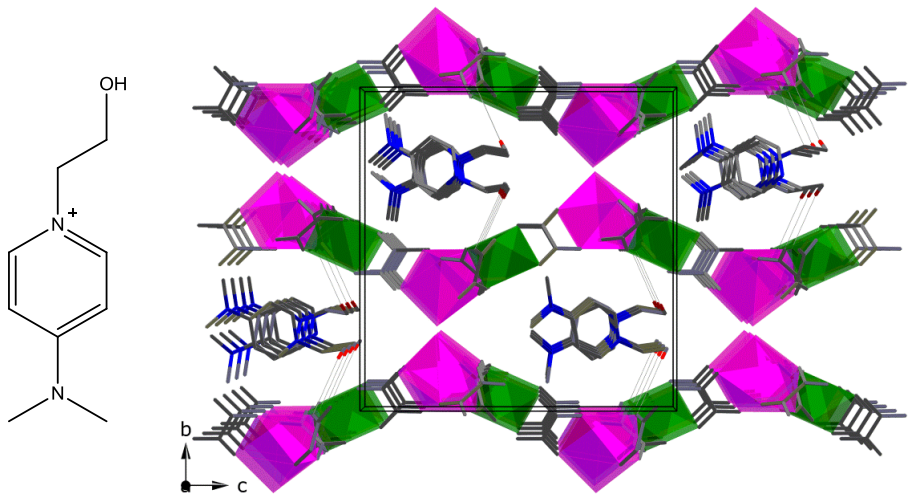

Figura 10: Empaquetamiento de los cationes entre los planos de oxalato ondulados.

Para el diseño de un multiferroico molecular se han utilizado redes bimetálicas 2D de oxalato aniónicas que proporcionan al material el orden ferromagnético a largo alcance, combinandas con cationes que aportan propiedades ferroeléctricas. Un ejemplo reciente corresponde al compuesto $C[MnCr(ox)_3(CH_3CH_2OH)]$ (C^+ = 1-(hidroxietil)-4-

(*N,N*-dimetilamino)piridina)[34] (Figura **10**). Este tipo de catión juega dos papeles importantes: 1)-favorece la formación de una red de coordinación extendida y; 2)-permite introducir un medio polar complementario, y así incrementar la posibilidad de puentes de hidrógeno, los cuales juegan un papel importante en la aparición de la ferroelectricidad.

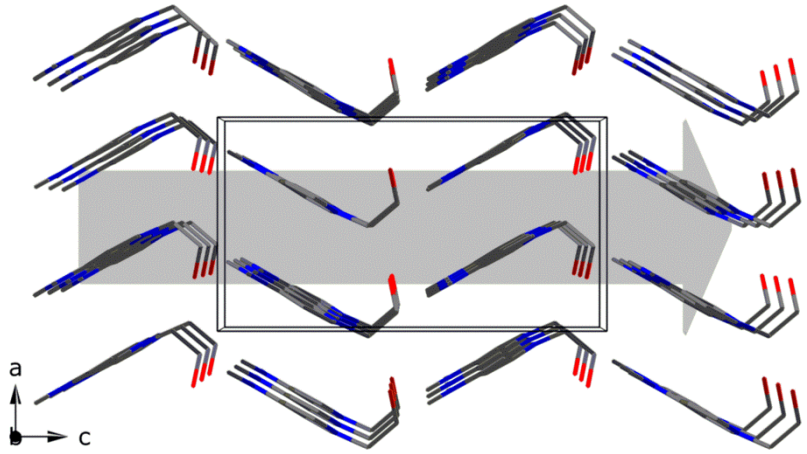

Figura 11: Organización del catión polar C^+ en el plano *ac*. La flecha gris enfatiza la dirección del orden polar.

El compuesto presenta una estructura 2D en la red de oxalatos con una coordinación heptaédrica del manganeso, debido a la presencia de una molécula de etanol. El catión y las moléculas de disolvente se sitúan entre las capas. Como se observa en la Figura **11**, la alineación polar de los cationes junto a los puentes de hidrógeno y la asimetría espacial (C_{2v}), son los principales factores para la aparición de propiedades ferroeléctricas. Así, en este compuesto se da la coexistencia del ordenamiento magnético de la red de oxalatos por debajo de 4 K, con un comportamiento ferroeléctrico en todo el intervalo de temperaturas estudiado (100-350 K). La ausencia de transición ferroeléctrica a paraeléctrica en este intervalo de temperaturas indica que la temperatura ferroeléctrica de Curie debe estar por encima de 350 K, temperatura a la cual se puede descomponer el compuesto por perdida de disolvente. Aunque la temperatura de Curie y la polarización eléctrica se observan a temperaturas muy diferentes, por lo que no se

observa un efecto magnetoeléctrico, esta aproximación demuestra que es posible obtener materiales multiferroicos con un enfoque híbrido molecular[34].

2.3.5 Conducción de protones

En la búsqueda de nuevas propiedades físicas en estos sistemas, la conducción de protones en estado sólido es hoy en día un reto, tanto para el estudio de los sistemas biológicos, como para la investigación práctica, por ejemplo en celdas de combustible[35]. Las redes metalo-orgánicas (Metal-Organic Frameworks, MOFs) pueden proporcionar poros bien diseñados para la conducción de protones. Para ello, se requiere la inserción en los poros de portadores (o transportadores) del tipo H_3O^+, NH_4^+ o H^+ pertenecientes a grupos ácidos[36].

Algunos de estos resultados se han obtenido con compuestos de oxalato porosos. Al igual que en otros materiales multifuncionales, encontramos resultados con redes 2D y 3D. El primer ejemplo es una red 3D de oxalatos bimetálica quiral de fórmula $(NH_4)_4[MnCr_2(ox)_6]\cdot 4H_2O$[37]. En esta red, dos de los tres oxalatos unidos al Cr son bis(bidentados) y están unidos a un Mn^{II}. El tercer oxalato es monodentado y presenta interacciones intermoleculares con las moléculas de disolvente. Por otra parte, el Mn^{II} está unido a través de cuatro ligandos oxalato a cuatro Cr^{III} dando la estequiometria final Mn:Cr 1:2. En los canales definidos por esta estructura 3D se sitúan las moléculas de agua y los contraiones NH_4^+. En este compuesto coexiste un ordenamiento ferromagnético a bajas temperaturas (3 K) con una conductividad protónica a temperatura ambiente debida a los cationes NH_4^+ de los canales. Los canales A, que podemos observar en la Figura **12**, presentan oxalatos terminales. Esto favorece la inserción de moléculas de agua en el centro del canal. En este compuesto, a 295 K, al aumentar la humedad, la conductividad (σ) aumenta en cinco órdenes de magnitud, de $2.4\cdot 10^{-9}$ $S\cdot cm^{-1}$ a 9% HR (Humedad Relativa) hasta $1.1\cdot 10^{-3}$ $S\cdot cm^{-1}$ a 96 % HR. Este aumento en la conductividad con el grado de humedad confirma que la conducción de protones es responsable de la elevada conductividad iónica del compuesto.

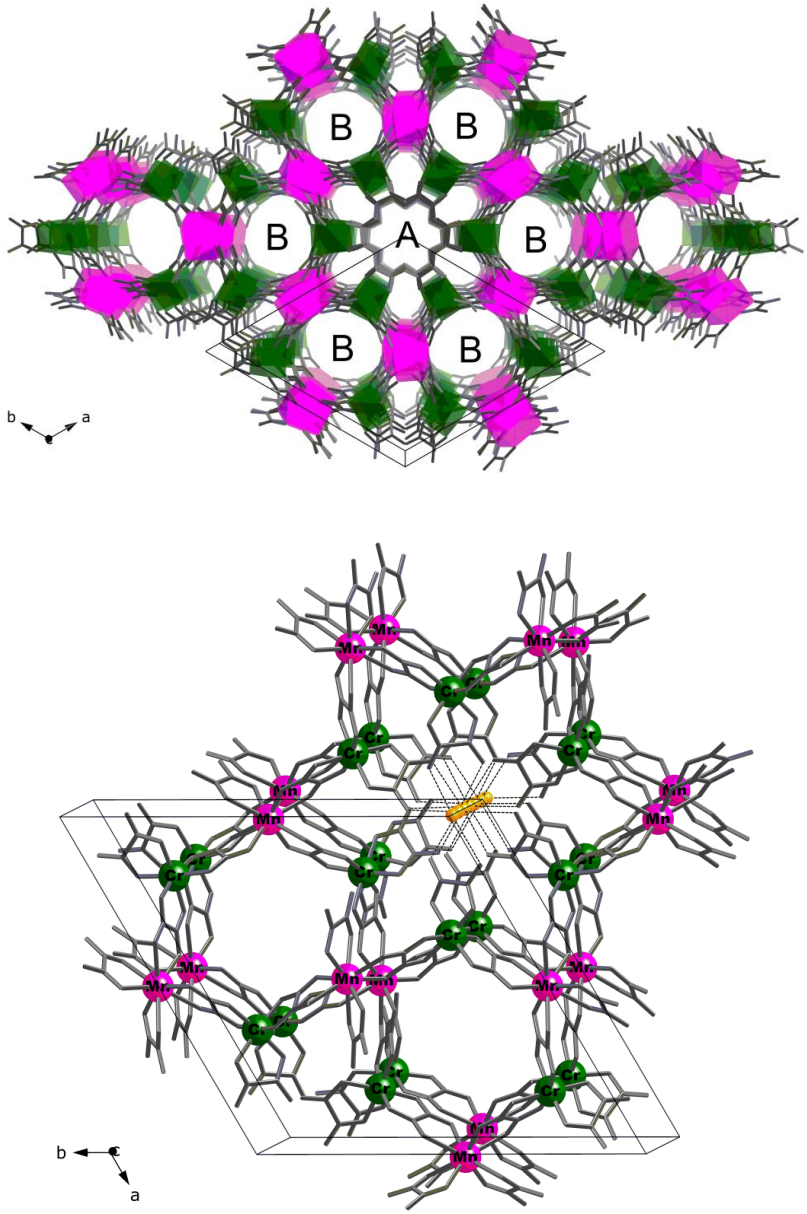

Figura 12: Estructura cristalina a lo largo del eje c de la red bimetálica de oxalato (Cr, verde; Mn, rosa). Moléculas de H_2O situadas en el canal A, de color naranja

Otro trabajo reciente, corresponde a una serie de compuestos de fórmula $[NR_3(CH_2COOH)][MCr(ox)_3]\cdot nH_2O$[38] (R = Metil, Etilo o *n*-Butil, y M = Mn o Fe). Estos

compuestos presentan una red bimetálica 2D de oxalatos, donde el catión se inserta entre las capas de oxalato (Figura **13**). Los cationes contienen un grupo ácido, el cual es responsable del transporte de protones y tres cadenas alquílicas, lo que permite modular la capacidad de transportar los protones por los huecos entre las capas de oxalato en función de su carácter hidrófilo o hidrófobo. Se ha visto que de todos ellos el que da mejores resultados es el que tiene un mayor carácter hidrófilo (cadena alquílica más corta) en el compuesto $[NMe_3(CH_2COOH)][FeCr(ox)_3]\cdot nH_2O$, ya que permite absorber más moléculas de agua, que es el requisito necesario para tener conductividad de protones con baja humedad. Este compuesto presenta una conducción de protones de 0.8×10^{-4} $S\cdot cm^{-1}$ a 65 % RH, que es la mayor entre MOFs conductores de protones con baja humedad.

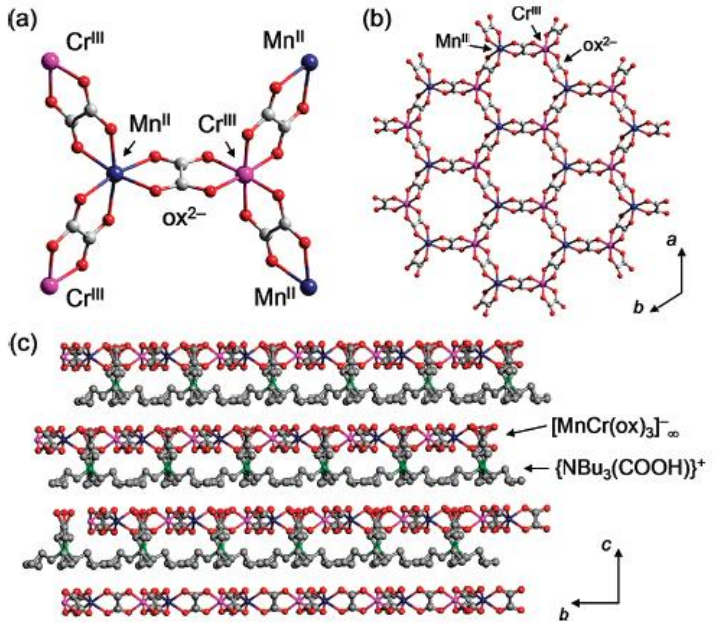

Figura 13: Estructura cristalina del compuesto $[NBu_3(CH_2COOH)][MnCr(ox)_3]\cdot nH_2O$. (a) Representación de la geometría de coordinación alrededor de Mn^{II} y Cr^{III}; (b) estructura de la capa de oxalatos; y (c) empaquetamiento de las capas.

2.4 Materiales multifuncionales basados en redes de oxalato preparadas en esta tesis. Introducción a los distintos tipos

Esta tesis se centra en materiales híbridos basados en redes bimetálicas de oxalato y en moléculas magnéticas conmutables. Además del ordenamiento magnético, se ha buscado la multifuncionalidad añadiendo una segunda propiedad en la subred catiónica. Las tres propiedades aportadas por la componente catiónica de los compuestos preparados en esta tesis son la quiralidad, memoria magnética de base molecular y la transición de espín. En este aparatado se introducen estas tres propiedades y los antecedentes de compuestos basados en redes de oxalato con estas propiedades.

2.4.1 Quiralidad

Los imanes quirales se pueden obtener en redes 3D como ya se ha mencionado anteriormente[15]. El interés en este tipo de compuestos se relaciona con la observación del dicroísmo magnetoquiral en un oxalato 2D[39].

En 1982, Wagnière y Meier[40] predijeron que la luz, al travesar un medio quiral, debería ser absorbida de diferente forma bajo la acción de un campo magnético externo. Dicho efecto que se denominó dicroísmo magnetoquiral[41] fue observado por primera vez en 1997, por Rikken y Raupach[42] en un complejo de Europio paramagnético ($[Eu((\pm)tfc)_3]$, donde tfc es (3-trifluoroacetil-±-camforato)). Puesto que este efecto es proporcional a la magnetización, se pensó que sería mucho más importante en un compuesto que presentase ordenamiento magnético. Se demostró en un oxalato 2D enantiopuro y ha despertado un gran interés en la preparación de imanes quirales[43]. Existen varias estrategias para la obtención de estos materiales quirales[2h-n,44]:

- Resolución espontanea a partir de precursores aquirales.
- El uso de ligandos quirales.
- En materiales con dos subredes, el uso de cationes o radicales con efecto plantilla.

Como ya se ha visto en aparatados anteriores, existen dos tipos de redes basadas en el ligando oxalato, las 2D y las 3D. Mientras que la red 3D es homoquiral ya que todos los metales de la red presentan la misma quiralidad incluyendo el catión insertado, en la red 2D alternan centros de quiralidad opuesta. Sin embargo, se pueden obtener un compuesto 2D quiral en redes bimetálicas en las que cada uno de los dos metales que forman la red tiene la misma quiralidad en toda la estructura, que será opuesta a la del otro metal. Esto se demostró con precursores tris(oxalato)-metalato(III), $[M^{III}(ox)_3]^{3-}$ enantiomericamente puros. Sin embargo, no fue posible obtener redes quirales 2D o 3D en forma de monocristal debido a que la velocidad de racemización de estos precursores era más rápida que la de cristalización, aunque sí que fue posible obtenerlos por precipitación rápida en forma de polvo[45]. Una estrategia alternativa que ha dado mejores resultados se basa en el uso de cationes plantilla quirales[43d]. Esta estrategia se desarrolló inicialmente en compuestos 3D como ya se ha mencionado en el apartado 2.2.2, donde los cationes metálicos quirales del tipo *tris(bipiridil)* inducen la formación de redes quirales 3D, en las que las unidades *tris(oxometalato*) presentan la misma quiralidad que los cationes[15]. El problema de estos compuestos es que presentan bandas de absorción en el visible muy intensas que enmascaran las bandas correspondientes al dicroísmo magneto-quiral y no se puede esclarecer si los compuestos presentan esa nueva propiedad[39].

Recientemente, se ha obtenido nuevos imanes quirales 2D basados en redes de oxalato, con la red de panal de abeja típica. En general, en estas estructuras los centros metálicos adyacentes presentan desorden y son indistinguibles. Sin embargo, se conocen excepciones a esta observación en las cuales la diferencia de enlace M-O característico de cada metal hace posible determinar la configuración absoluta de los dos tipos de centros metálicos octaédricos. Unos de los primeros sistemas 2D quirales fue el compuesto $[(S)\text{-}PhCH(CH_3)N(CH_3)_3][MnCr(ox)_3]$ (Figura **14**). En este caso el uso de una amina cuaternaria quiral conduce a una red 2D con sólo uno de los enantiómeros de $[Cr(ox)_3]^{-3}$, probablemente por un reconocimiento quiral[43c].

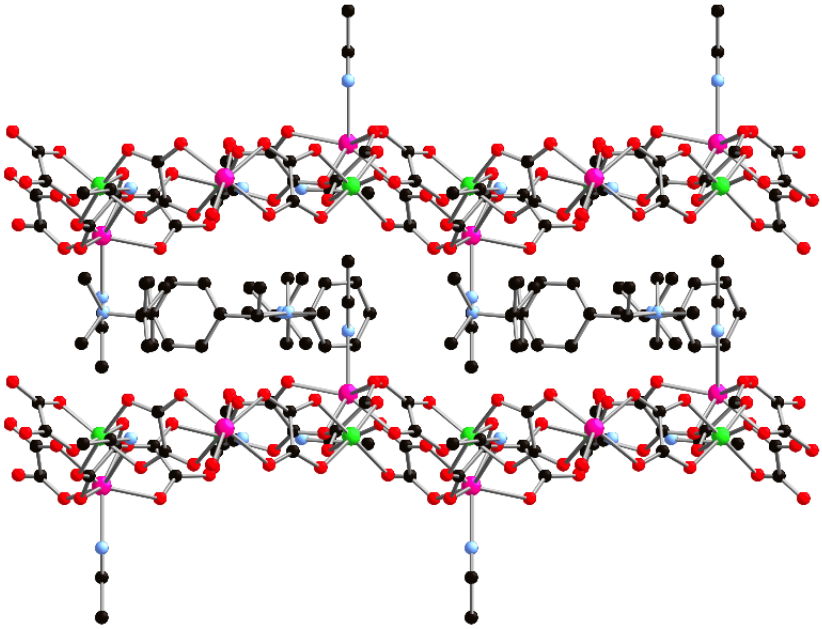

Figura 14: Estructura cristalina del compuesto [(*S*)-PhCH(CH_3)N(CH_3)$_3$][MnCr(ox)$_3$].

En 2008 se pudo observar por primera vez, el dicroísmo magneto-quiral en un imán quiral ferromagnético enantiopuro formado por una red bimetálica de oxalatos 2D con un catión quiral. Los compuestos enantiopuros tenían la fórmula [N((*S*)-i-Bu)MePr$_2$] [(Λ)Mn-(Δ)-Cr(ox)$_3$] y [N((S)-i-Bu)MePr$_2$][(Δ)Mn-(Λ)-Cr(ox)$_3$] (i-Bu = CH(CH_3)C_2H_5; Me = CH_3; Pr = C_3H_7) (Figura **15**). Este efecto aumentó en un factor de 17 al pasar de la fase paramagnética a la fase ferromagnética[39], al ser la señal de dicroísmo magneto-quiral proporcional a la magnetización (Figura **16**). Aunque este resultado es muy prometedor porque pone de manifiesto que el carácter multifuncional de un compuesto basado en redes de oxalato da lugar a la aparición de una nueva propiedad (dicroísmo magnetoquiral), es un efecto muy débil como se puede ver en la figura. Una posibilidad que se ha abordado en esta tesis para aumentar este efecto es la preparación de redes

3D enantiopuras que contengan cationes incoloros, que era la principal limitación para la medida de esta propiedad en redes 3D. En estas redes se espera un mayor efecto que en las 2D, al tener sólo un tipo de enantiómero de los dos metales. Esta posibilidad se ha abordado en los capítulos 6 y 8.

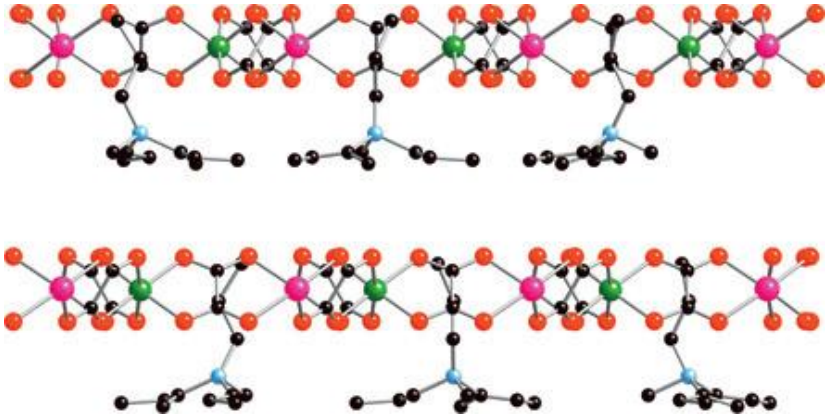

Figura 15: Estructura cristalina del compuesto [N((*S*)-i-Bu)MePr$_2$][(Λ)Mn-(Δ)-Cr(ox)$_3$].

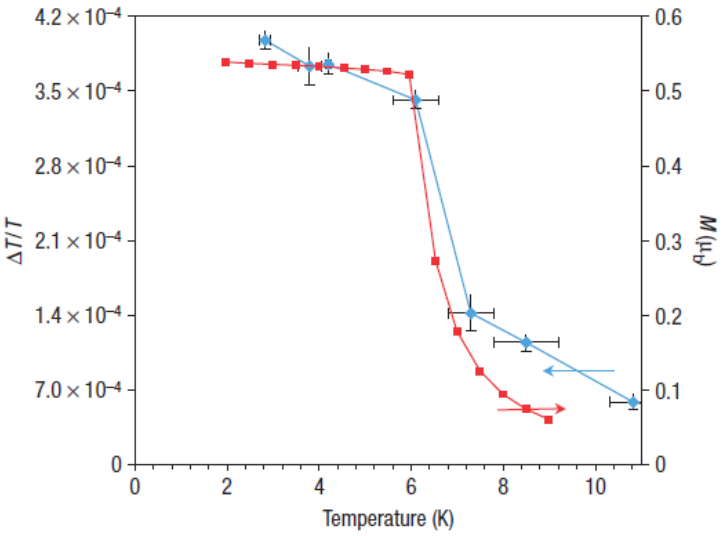

Figura 16: Dependencia del dicroísmo magnetoquiral con la temperatura medido a 615 nm del compuesto [N((*S*)-i-Bu)MePr$_2$][(Λ)Mn-(Δ)-Cr(ox)$_3$].

2.4.2 Memorias magnéticas de base molecular

La continua miniaturización de los sistemas de almacenamiento de información magnéticos así como el rápido desarrollo de ordenadores de alta velocidad han implicado un creciente interés en la obtención y estudio de materiales con memoria magnética a escala nanométrica. Hasta hace unos años, estos materiales se obtenían por fragmentación de unidades (aproximación descendente), es decir, mediante una reducción en el tamaño del material macroscópico hasta alcanzar las dimensiones deseadas. Una alternativa desarrollada en los últimos años es un método químico en el que se construyen compuestos polinucleares por métodos sintéticos (aproximación ascendente). Desde el descubrimiento a principios de los 90, de que algunos complejos polimetálicos discretos pueden presentar memoria magnética -los llamados imanes unimoleculares "*Single Molecule Magnets o SMM"* (por sus siglas en inglés)- se ha sintetizado un gran número de moléculas de alto espín que presentan memoria magnética[46].

A bajas temperaturas, estos sistemas exhiben una lenta relajación de su magnetización inducida debido a la combinación de dos propiedades intrínsecas: un estado fundamental de espín elevado y una gran anisotropía magnética uniaxial. La combinación de estas dos propiedades puede crear una barrera energética entre los estados con m_S positivo y m_S negativo, de manera que el sistema presenta un bloqueo superparamagnético a bajas temperaturas. Esta característica hace que los SMM sean unos candidatos posibles para el almacenamiento de la información a nivel molecular.

El complejo $[Mn_{12}O_{12}(O_2CCH_3)_{16}(H_2O)_4]\cdot 4H_2O\cdot 2CH_3CO_2H$ y sus derivados (Mn_{12}) fueron los primeros compuestos donde se observó este efecto[47]. Esta molécula presenta un elevado estado fundamental de espín S = 10. Además posee una marcada anisotropía magnética uniaxial (D < 0), dando lugar a una de las barreras energéticas (U) más altas conocidas (66 K) y, por consiguiente, a fenómenos de relajación lenta de magnetización por debajo de 3.5 K. (Figura **17**)

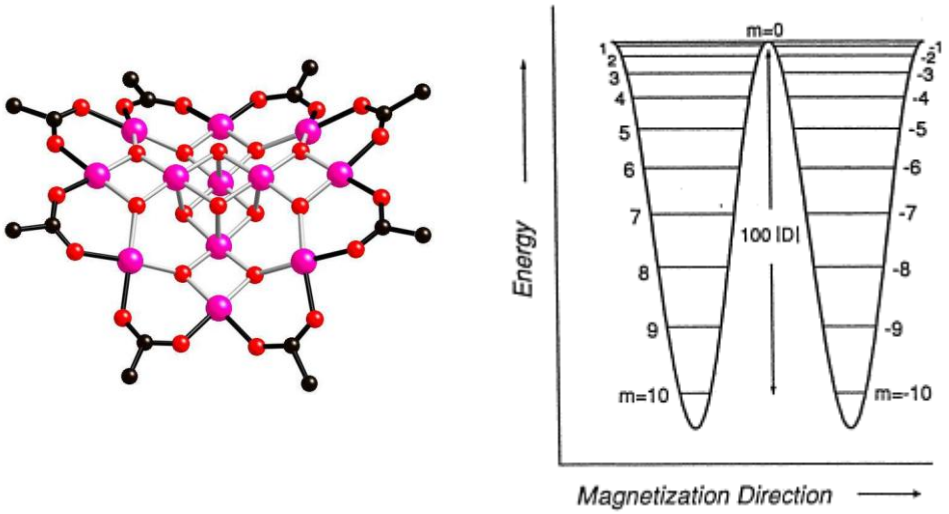

Figura 17: Estructura de la molécula de Mn_{12}, Mn (rosa), O (rojo), C (negro); pozos de potencial energético.

Las propiedades magnéticas de estas moléculas abren un abanico de perspectivas para su aplicación en dispositivos de almacenamiento de información. En los últimos años se han realizado numerosos estudios de compuestos de distinta nuclearidad con un comportamiento SMM. En un primer momento la estrategia más común se basó en intentar aumentar la nuclearidad para tener un espín mayor que diese lugar a mayores temperaturas de bloqueo. Sin embargo, los resultados obtenidos no mejoraban mucho los de los primeros SMMs de Mn_{12}. Uno de los compuestos sobre los que se ha realizado más estudios son los clusters de ocho hierros de fórmula $[Fe_8O_2(OH_{12})(tacn)_6]Br_8$ (tacn = 1,4,7-triazaciclononano) (Fe_8). Este cluster presenta un estado fundamental con un S = 10, que se puede justificar poniendo seis espines S = 5/2 acoplados ferromagneticamente y 2 antiferromagneticamente (Figura **18**)[48]. En los últimos años ha aparecido una estrategia diferente que consiste en aumentar la anisotropía magnética preparando complejos con un solo centro metálico (generalmente un lantánido). Estos compuestos se conocen como moléculas imán mononucleares (single ion magnets)[49,50].

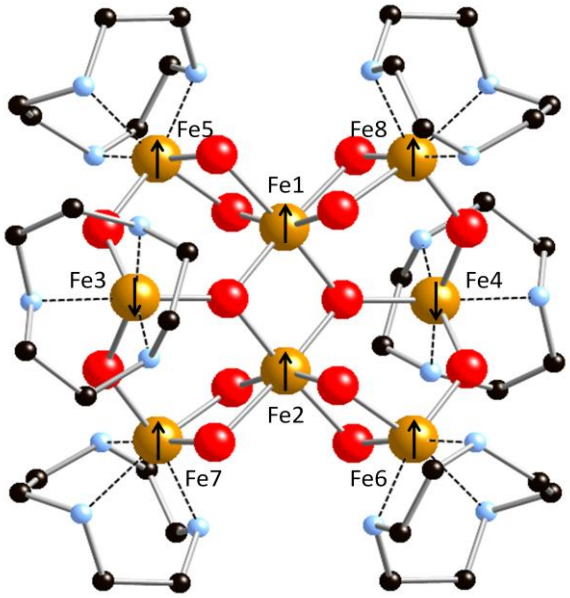

Figura 18: Estructura esquemática del cluster Fe_8 con la orientación preferida de los espines individuales.

En esta tesis se ha utilizado complejos dinucleares de Mn^{III} del tipo salen (bases de Schiff tetradentadas, salen = N,N'-etilen-bis(salicilideneiminato)), que presentan en algunos casos un comportamiento SMM, para el diseño de redes magnéticas basadas en el ligando oxalato. Esta elección ha estado motivada por el carácter catiónico y la estabilidad. El comportamiento SMM de estos compuestos se debe a que el eje de la distorsión Jahn-Teller del complejo dinuclear en la esfera de coordinación del complejo coincide con el de fácil anisotropía magnética. Además, las unidades diméricas presentan interacciones intramoleculares ferromagnéticas entre los Mn^{III}, generando un estado fundamental de espín $S_T = 4$ que da lugar a propiedades de SMM[51]. La primera investigación que mostró un comportamiento de SMM de una especie dinuclear se publicó en 2004 en el compuesto $[Mn_2(saltmen)_2\text{-}(ReO_4)_2]$ (saltmen = 1,1,2,2-tetrametileno)bis(salicilideneiminato). Propiedades magnéticas similares se han observado en otros complejos dinucleares como $[Mn_2(saltmen)_2(X)_2]$ donde X^- =

CH_3COO^-, N_3^-, $[Mn_2(salen)_2(NCO)_2]$ y $[Mn_2(3,5\text{-Br-salen})_2(3,5\text{-Br-salicilaldehido})_2]$ (3,5-Br-salen = N, N'-etilene-bis(3,5-dibromosalicilideneiminato)). Estas unidades diméricas se han unido a través de complejos paramagnéticos para dar lugar a sistemas 1D y 2D que en muchos casos presentan ordenamientos ferromagnéticos o comportamientos del tipo SCM u otro tipo de comportamientos intermedios. Por ejemplo, el compuesto $[Mn_2(salpn)_2(H_2O)_2](ClO_4)_2$ (salpn = N,N'-propano-bis-(salicilideneiminato)) presenta un comportamiento intermedio entre SMM y SCM, debido a las interacciones magnéticas a través de los puentes de hidrógeno entre las unidades dinucleares[52]. En estos sistemas se ha visto que un punto importante para el diseño de este tipo de imanes unimoleculares es reducir las interacciones intermoleculares entre los dímeros. Se ha demostrado que el uso de contraiones voluminosos diamagnéticos como los polioxometalatos es una estrategia eficiente para separar las entidades magnéticas y tener un comportamiento de imán unimolecular[53].

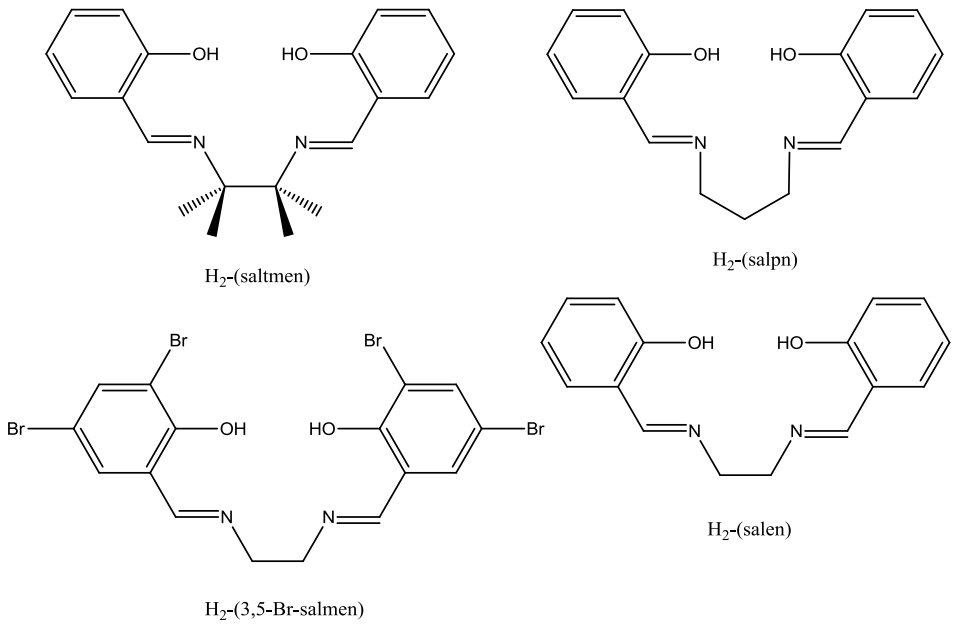

Figura 19: Estructura esquemática de los ligandos para obtener las especies diméricas.

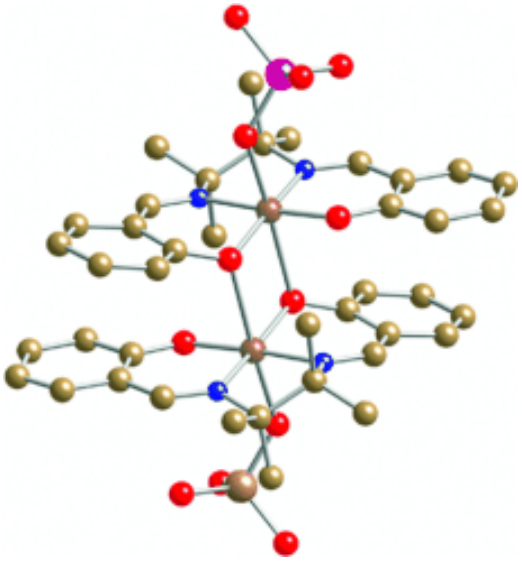

Figura 20: Estructura molecular del dímero compuesto $[Mn_2(saltmen)_2\text{-}(ReO_4)_2]$.

2.4.3 Multicapas magnéticas con complejos de transición de espín

2.4.3.1 Introducción al fenómeno

El fenómeno de la transición de espín se enmarca en el campo de la magnetoquímica y está enlazado fuertemente con el desarrollo de la química de coordinación. Los centros metálicos en los que tiene lugar este fenómeno presentan configuraciones electrónicas lábiles intercambiables entre los estados de alto espín (HS) y bajo espín (LS), dando lugar a cambios característicos en el magnetismo, el color y la estructura, que pueden ser inducidos por variaciones de temperatura, presión o por irradiación de luz. Por tanto, es un ejemplo claro de biestabilidad molecular en el que una molécula puede presentar dos estados que se pueden interconvertir mediante un estímulo externo, tal y como sucede en un interruptor binario[54]. La idea de que una molécula o conjunto de moléculas pueda comportarse como un dispositivo electrónico ha estimulado el desarrollo de este campo.

En simetría octaédrica, según la teoría del campo de ligandos, los complejos de metales de transición con configuraciones electrónicas $[Ar]3d^4$-$3d^7$ pueden presentar dos estados electrónicos fundamentales distintos, según el desdoblamiento de los orbitales *d* en los subconjuntos e_g y t_{2g}. Cuando la separación energética entre estos subconjuntos (fuerza del campo de ligandos), Δ, es mayor que la energía de repulsión interelectrónica, P, los electrones tienden a ocupar los orbitales de más baja energía, t_{2g}, y el complejo metálico adopta el estado de bajo espín. Si Δ es menor que P, los electrones *d* cumplen la regla de máxima multiplicidad de Hund y el complejo adopta el estado de alto espín. La mayoría de los complejos de Cr(II), Mn(II), Mn(III), Fe(II), Fe(III), Co(II) y Co(III) pueden presentar estas dos configuraciones electrónicas[55], si bien la familia de compuestos de Fe(II) que presentan transición de espín es la más importante y la más numerosa.

Aunque el origen del fenómeno de transición de espín es puramente molecular, la manifestación macroscópica en el sólido es el resultado de la interacción cooperativa entre las moléculas que constituyen el material. La naturaleza cooperativa de la transición de espín ha estimulado mucho interés dado que las transiciones de fase de primer orden que se producen acompañadas de histéresis térmica confieren a estos materiales un cierto grado de memoria, que podría ser potencialmente aprovechada en futuras aplicaciones. En la Figura **22** se observa el cambio de la fracción de alto espín (γ_{HS}) con la temperatura gradual típico de sistemas poco cooperativos y el abrupto con histéresis típico de sistemas muy cooperativos.

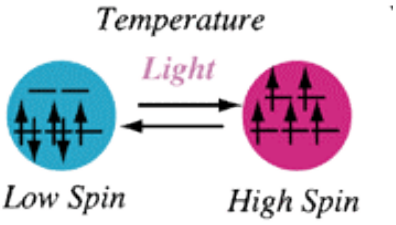

Figura 21: Biestabilidad de complejos de Fe^{III}.

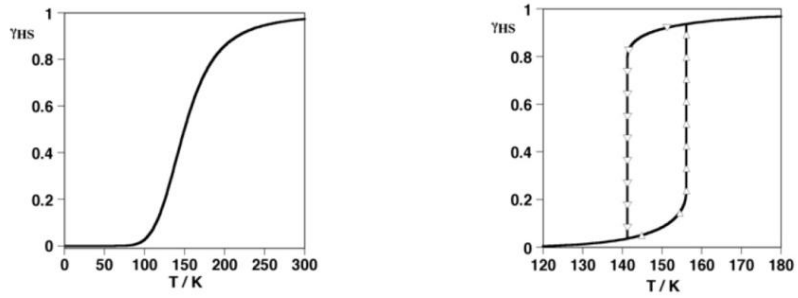

Figura 22: Tipos principales de curvas de transición de espín representadas en la forma de γ_{HS} frente a T: gradual (izquierda) y abrupta y con histéresis (derecha).

2.4.3.2 Efecto LIESST (Light Induced Excited Spin State Trapping)

Un problema importante a la hora de insertar compuestos de transición de espín en redes de oxalatos para que coexistan en un mismo compuesto el ordenamiento magnético y la transición de espín, es que estas dos propiedades aparecen en un intervalo de temperaturas muy distinto. En el caso de los oxalatos las temperaturas de ordenamiento son inferiores a 10 K, mientras que la transición de espín tiene lugar a temperaturas más altas en la mayoría de complejos de Fe^{II} y Fe^{III}. Una forma de solventar este problema consiste en hacer uso del efecto LIESST que es el cambio de espín fotoinducido que en estado sólido, tiene lugar a bajas temperaturas (similares a las del ordenamiento magnético de la redes de oxalato).

La luz es un medio muy eficaz para "comunicarse" con un sistema molecular cuando se trata de encontrar posibles aplicaciones tecnológicas. La fotoinducción de la transición de espín fue observada por primera vez por Mc Garvey y Lawthers en disolución a temperaturas relativamente altas[56], sin embargo, el tiempo de vida media de los estados inducidos era muy corto. Hace unos treinta años Buhks y col[57]. sugirieron que el cruzamiento intersistema dinámico de los compuestos de transición de espín tras irradiación se debería tratar como un proceso no-adiabático dentro de la teoría de relajación multifonónica no radiativa. Este fenómeno fue conocido posteriormente como efecto LIESST (Light-Induced Excited Spin State Trapping)[58] (Figura **23**). Estos

autores predijeron que la relajación del estado metaestable HS→LS obtenida tras irradiar la muestra se trataba de un proceso activado térmicamente a altas temperaturas, pero un proceso vía túnel a bajas temperaturas. Este fenómeno fue observado originalmente para los complejos de Fe^{II} a bajas temperaturas (normalmente por debajo de 50 K).[59]

A temperaturas suficientemente bajas el estado de bajo espín está totalmente poblado y al irradiar el compuesto se pueblan los estados excitados superiores. El tiempo de vida media de estos estados es de unos pocos nanosegundos, por lo que el sistema se relaja rápidamente. Dicha relajación debería tener lugar normalmente al estado inicial ($^1A_1$ para Fe^{II}) pero, no obstante, existe una pequeña probabilidad de relajación a través de los estados de espín intermedio por mecanismos de cruce entre sistemas ("intersystem crossing", ISC) permitidos por acoplamientos espín-orbita de segundo orden. La relajación desde los estados de espín intermedio puede ocurrir de nuevo por medio de dos procesos ISC, uno implica la relajación al estado fundamental y otro al metaestable $^5T_2$ (para Fe^{II}) donde las moléculas del compuesto permanecen atrapadas, siempre que la energía térmica (K_BT) sea suficientemente menor que E^a_{HL} (Figura **23**). A bajas temperaturas el estado metaestable $^5T_2$ tiene un tiempo de vida media detectable, dado que la relajación $^5T_2 \rightarrow {}^1A_1$ está prohibida.

Desde que Gütlich y col. observaron esta transición fotoinducida LS $\rightarrow$ HS en un complejo de transición de espín de Fe^{II} en 1984[60], se han realizado muchos trabajos sobre este tema, ya que el descubrimiento del efecto LIESST sugirió que este tipo de compuestos se podría utilizar como interruptores ópticos. Este efecto es mucho más común en los complejos de Fe^{II} que en los complejos de Fe^{III}. Esto se explica con el modelo SCC (Single Coordinate Configuration) propuesto por el profesor Andreas Hauser. En general, este modelo considera principalmente la coordenada de reacción (Q, o modo de estiramiento) expresada como la diferencia en la longitud del enlace metal-ligando entre ambos estados ($\Delta r_{HL} = r_{HS} - r_{LS}$), es decir, como el desplazamiento horizontal de los dos pozos de potencial de alto espín y bajo espín.

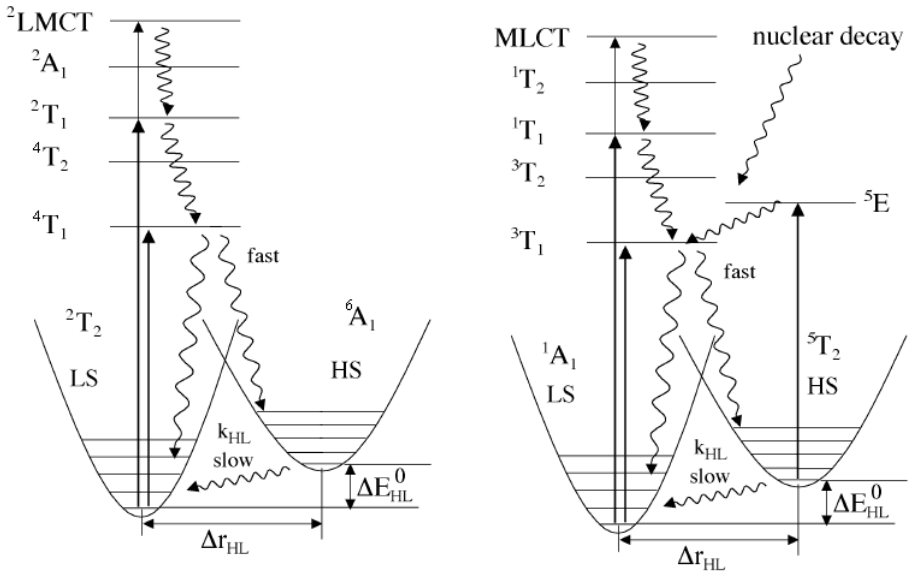

Figura 23: Diagrama de Jablonski para un sistema d^5 como el de los complejos de Fe^{III} (izquierda) y para un sistema d^6 como los complejos de Fe^{II} (derecha).

En la Figura **24** se muestran los pozos de potencial de los estados HS y LS de complejos de Fe^{II} y Fe^{III} con transición de espín. La distancia metal-ligando se ve más afectada en la transición de espín de los complejos de Fe^{II}, alrededor de 0.2 Å, que en los complejos de Fe^{III}, ~ 0.13 Å. A bajas temperaturas observamos la relajación por el efecto túnel entre el estado vibracional más bajo del estado fotoexcitado al estado de bajo espín[61]. Los complejos de Fe^{II} presentan un desplazamiento relativamente grande entre estos dos estados, por lo que el estado metaestable fotoexcitado debería adquirir bastante energía térmica para poder superar la barrera energética que hay entre los dos pozos, observando tiempos de vida media del estado fotoexcitado del orden de 10^2-10^6 s a bajas temperaturas[62]. En cambio, en los complejos de Fe^{III} el solapamiento de los pozos es mayor y esto da como resultado que observar el efecto LIESST en los complejos de Fe^{III} sea muy raro, incluso a bajas temperaturas, porque la barrera energética entre los pozos es inferior, presentando valores de tiempo de vida media 5 o 6 órdenes de magnitud inferiores a los observados en los complejos de Fe^{II}.

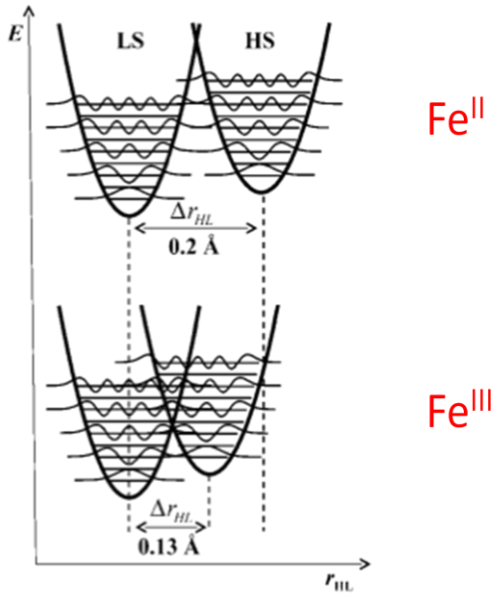

Figura 24: Pozos de potencial de complejos de Fe^{II} y Fe^{III}.

Sin embargo, existen algunos ejemplos de complejos de Fe^{III}, sintetizados por el grupo del profesor O. Sato, que presentan efecto LIESST[61,63] como $[Fe^{III}(pap)_2]^+$ y $[Fe^{III}(qsal)_2]^+$ (Figura **25** y **26**). Se piensa que en estos sistemas, el modelo SCC no es adecuado, porque en estos compuestos aparece una distorsión geométrica muy importante en el entorno octaédrico del metal al cambiar de estado LS → HS.

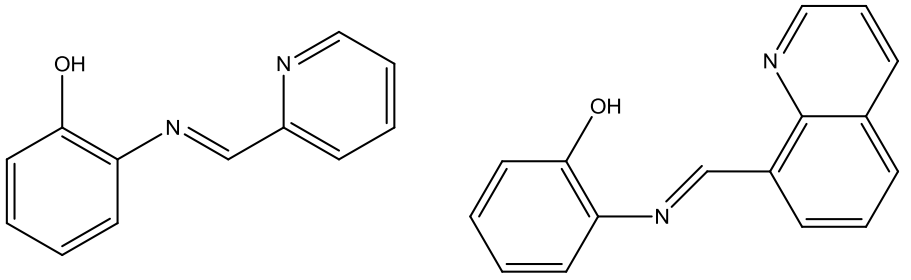

Figura 25: Estructura de los ligandos Hpap y Hqsal.

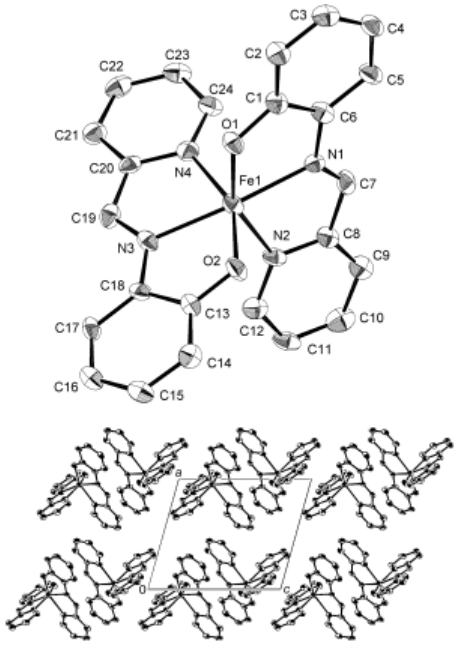

Figura 26: Estructura del complejo $[Fe(pap)_2]^{2+}$ (arriba) y empaquetamiento de los complejos en el cristal. (abajo)

De acuerdo con el profesor O. Sato, para estudiar y comprender mejor este comportamiento en los complejos de Fe^{III}, además de considerar el modo de estiramiento habría que considerar el modo de torsión, es decir, la distorsión que sufre el complejo al cambiar bruscamente del estado de bajo espín al estado metaestable de alto espín. (Figura **27**). Esto haría que la diferencia entre los pozos de potencial del estado fotoinducido de alto espín y el de bajo espín fuera mayor de la calculada por el modelo SCC, y explicaría el largo tiempo de vida media de este estado en estos sistemas y la observación del efecto LIESST. Otra de las razones que aportan los autores para que se observe este efecto son las fuertes interacciones intermoleculares que existen entre los complejos de Fe^{III} y que juegan un papel importante.

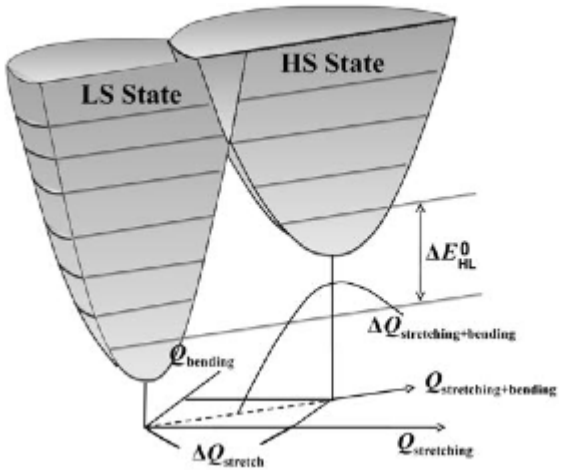

Figura 27: Pozos de potencial de un complejo de Fe^{III} considerando las dos contribuciones modo de estiramiento y modo de torsión ("the stretching mode" y "the bending mode").

2.4.3.3 Materiales híbridos basados en complejos de transición de espín insertados en redes de oxalato

Los complejos de transición de espín son especialmente adecuados para preparar materiales magnéticos multifuncionales[64] ya que representan uno de los mejores ejemplos de biestabilidad molecular. La inserción de complejos de transición de espín entre las redes de oxalato, que son aniónicas, permitiría modificar el ordenamiento magnético de la red de oxalatos induciendo el cambio del espín del catión insertado mediante luz o presión.

Decurtins y col. Publicaron el primer ejemplo de inserción de este tipo de cationes dentro de redes de oxalato. Se basaba en la introducción de un complejo de transición de espín de Co^{II} dentro de una red 3D de oxalatos de fórmula $[Co^{II}(bpy)_3][LiCr(ox)_3]$[65]. Este compuesto no presenta coexistencia de la transición de espín y ordenamiento magnético, ya que la red de oxalatos es paramagnética. Unos años más tarde, nuestro grupo consiguió introducir un complejo de transición de espín de Fe^{II}, $[Fe^{II}(bpp)_2]^{2+}$

(Figura **28**), dentro de una red de oxalatos 3D ferromagnética aquiral[66]. Sin embargo, no se pudo observar el cambio de espín, ya que la mayoría de los complejos de hierro permanecían en bajo espín en todo el rango de temperaturas. La coexistencia de transición de espín y el ordenamiento magnético en una red de oxalatos se encontró por primera vez en el compuesto de fórmula $[Fe^{III}(sal_2\text{-trien})]_2[Mn_2{}^{II}(ox)_3]\cdot 4H_2O\cdot C_3H_7NO$. La estructura de este compuesto está formada por una capa 2D homometálica formada por iones Mn^{II} unidos por ligandos oxalato[64]. Entre estas capas aniónicas se sitúa una doble capa de cationes $[Fe^{III}(sal_2\text{-trien})]^+$ y moléculas de disolvente (Figura **29**). Este compuesto presenta débil ferromagnetismo a T_c = 8.1 K y un cambio de espín gradual del complejo $[Fe^{III}(sal_2\text{-trien})]^+$ insertado con la temperatura.

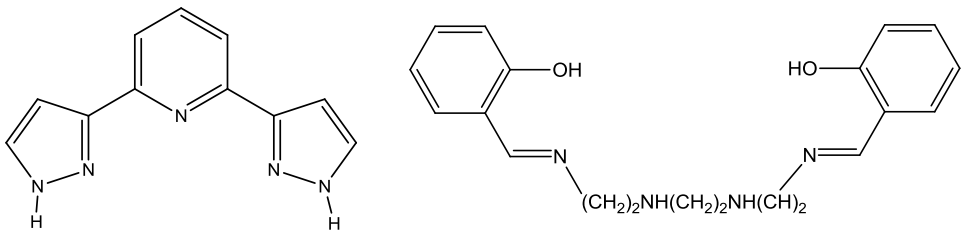

Figura 28: Estructura molecular del ligando bpp (izquierda) y del sal_2trien (derecha).

En esta tesis se ha seguido con esta estrategia de inserción del $[Fe^{III}(sal_2trien)]^+$ y sus derivados dentro de redes heterometálicas de oxalatos (capítulos 2-7). Esto presenta varias ventajas respecto a los compuestos mencionados anteriormente. Por una parte, el uso de redes heterometálicas, que presentan comportamientos ferro o ferrimagnéticos en lugar del débil ferromagnetismo del último compuesto, puede facilitar la observación de interacciones magnéticas con el catión $[Fe^{III}(sal_2\text{-trien})]^+$ insertado. Por otro lado, si el uso de otros derivados de $[Fe^{III}(sal_2\text{-trien})]^+$ consiguiese dar lugar a redes 3D, se podría aumentar el efecto de la transición de espín del catión insertado en el ordenamiento magnético de las redes de oxalatos, ya que el magnetismo de las redes 3D es mucho más sensible a los cambios en distancias y ángulos del catión insertado que las redes 2D[8e]. Para que este cambio de espín coincida con la temperatura

de ordenamiento magnético, se ha buscado el efecto LIESST del compuesto insertado. Aunque esto es en principio bastante improbable para un compuesto de Fe^{III} como el $[Fe^{III}(sal_2\text{-trien})]^+$, los antecedentes descritos en el apartado anterior de complejos de Fe^{III} que presentan efecto LIESST nos animaron en la búsqueda de esta propiedad en complejos de transición de espín de Fe^{III} insertados en redes de oxalato.

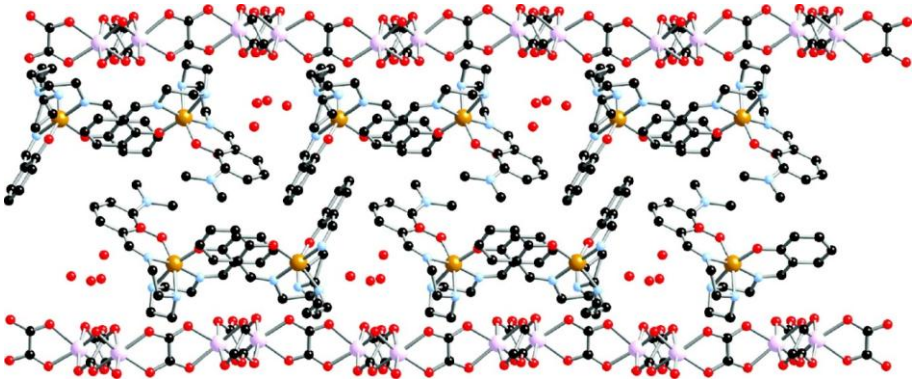

Figura 29: Estructura del compuesto $[Fe^{III}(sal_2\text{-trien})]_2[Mn_2{}^{II}(ox)_3]\cdot 4H_2O\cdot C_3H_7NO$.

3. Resumen

En el Capítulo 2 se presenta la obtención y caracterización de los dos primeros materiales multifuncionales $[Fe^{III}(sal_2\text{-trien})][Mn^{II}Cr^{III}(ox)_3]\cdot CH_2Cl_2$ y $[Fe^{III}(sal_2\text{-trien})][Mn^{II}Cr^{III}(ox)_3]\cdot 0.75CH_3OH\cdot 0.5H_2O$. La utilización del complejo $[Fe^{III}(sal_2\text{-trien})]^+$ ha dado lugar, dependiendo de las condiciones de síntesis, a dos estructuras diferentes. En el compuesto $[Fe^{III}(sal_2\text{-trien})][Mn^{II}Cr^{III}(ox)_3]\cdot CH_2Cl_2$, que presenta una red de oxalatos bidimensional, coexiste una transición de espín completa con el ordenamiento ferromagnético de la red bimetálica de oxalatos alrededor de 5 K. El segundo compuesto, $[Fe^{III}(sal_2\text{-trien})][Mn^{II}Cr^{III}(ox)_3]\cdot 0.75CH_3OH\cdot 0.5H_2O$, con una red tridimensional aquiral, presenta una transición de espín parcial además del ordenamiento magnético. La formación de dos redes de oxalatos diferentes con el mismo catión plantilla es un hecho inusual en la química de este tipo de compuestos que atribuimos a la flexibilidad que presenta el ligando orgánico del complejo $[Fe^{III}(sal_2\text{-trien})]^+$ en presencia de distintos disolventes. En el Capítulo 3 se realiza el estudio de las propiedades fotomagnéticas del compuesto $[Fe^{III}(sal_2\text{-trien})][Mn^{II}Cr^{III}(ox)_3]\cdot CH_2Cl_2$, el cual presenta efecto LIESST por debajo de 42 K. Dicho efecto es muy poco frecuente en complejos de Fe^{III}. En el Capítulo 4, se han preparado análogos del compuesto $[Fe^{III}(sal_2\text{-trien})][Mn^{II}Cr^{III}(ox)_3]\cdot CH_2Cl_2$ en otros disolventes halogenados ($CHCl_3$, CH_2Br_2 y $CHBr_3$). Los compuestos obtenidos de fórmula $[Fe^{III}(sal_2\text{-trien})][Mn^{II}Cr^{III}(ox)_3]\cdot CH_2Br_2$, $[Fe^{III}(sal_2\text{-trien})][Mn^{II}Cr^{III}(ox)_3]\cdot CHBr_3$, $[Fe^{III}(sal_2\text{-trien})][Mn^{II}Cr^{III}(ox)_3]\cdot CHCl_3$, mantienen la misma estructura 2D. El cambio de CH_2Cl_2 por disolventes más voluminosos permite modular la $T_{1/2}$, que se desplaza a temperaturas menores, y la T_{LIESST}, que se desplaza a valores mayores. En este capítulo se ha diluido el complejo de Fe^{III} con otros complejos similares de Ga^{III} diamagnéticos. Esto ha permitido estudiar la evolución de la transición de espín del complejo de Fe^{III} aislado por métodos espectroscópicos en el compuesto $[Ga_{0.99}Fe_{0.01}(sal_2\text{-trien})][Mn^{II}Cr^{III}(ox)_3]\cdot CH_2Cl_2$ que, al igual que el compuesto puro, presenta una transición de espín con la temperatura y efecto LIESST. Por último, en este capítulo se realiza un análisis estructural de estos compuestos y otros de Fe^{III}, descritos en la bibliografía que presentan efecto LIESST.

En los Capítulos 5, 6 y 7 se ha continuado la búsqueda de híbridos magnéticos basados en redes bimetálicas de oxalato con derivados del complejo $[Fe^{III}(sal_2\text{-trien})]^+$. En el Capítulo 5 se presenta los compuestos $[Fe^{III}(5\text{-}NO_2\text{-}sal_2trien)][Mn^{II}Cr^{III}(ox)_3]\cdot MeNO_2\cdot 0.5H_2O$ y $[Fe^{III}(5\text{-}CH_3O\text{-}sal_2trien)][Mn^{II}Cr^{III}(ox)_3]$ con una estructura 2D y 3D aquiral respectivamente. Los dos compuestos presentan un ordenamiento magnético alrededor de 5 K y no presentan transición de espín. En el Capítulo 6 se describe la síntesis, estructura y propiedades magnéticas de los compuestos $[Fe^{III}(5\text{-}Cl\text{-}sal_2trien)][Mn^{II}Cr^{III}(ox)_3]\cdot 0.5MeNO_2$, $[Fe^{III}(5\text{-}Br\text{-}sal_2trien)][Mn^{II}Cr^{III}(ox)_3]$ y $[In^{III}(5\text{-}Cl\text{-}sal_2trien)][Mn^{II}Cr^{III}(ox)_3]$. Estos compuestos muestran una nueva estructura 3D quiral, con lo que se aporta una tercera propiedad al material multifuncional, que es la quiralidad de la red, además del ordenamiento magnético y la transición de espín parcial en los dos compuestos de Fe^{III}. Por último, el $[Fe^{III}(sal_2\text{-trien})]^+$ con substituyentes en las posiciones 3 o 4, se ha obtenido los compuestos $[Fe^{III}(4\text{-}Br\text{-}sal_2trien)][Mn^{II}Cr^{III}(ox)_3]_{0.67}\cdot Cl_{0.33}\cdot MeOH$, $[Fe^{III}(3\text{-}Cl\text{-}sal_2trien)][Mn^{II}Cr^{III}(ox)_3]\cdot(CH_3OH)_2\cdot(CH_3CN)_2$, $[Fe^{III}(3\text{-}Br\text{-}sal_2trien)][Mn^{II}Cr^{III}(ox)_3]\cdot(CH_3CN)_2$, y $[Fe^{III}(3\text{-}MeO\text{-}sal_2trien)][Mn^{II}Cr^{III}(ox)_3]\cdot(CH_3OH)\cdot(H_2O)_{1.5}\cdot(CH_2Cl_2)_{0.5}$, que presentan una estructura 2D. Todos ellos muestran un ordenamiento magnético alrededor de 5 K que coexiste con una transición de espín completa entre 300 y 400 K para $[Fe^{III}(4\text{-}Br\text{-}sal_2trien)][Mn^{II}Cr^{III}(ox)_3]_{0.67}\cdot Cl_{0.33}\cdot MeOH$ y transiciones de espín parciales para $[Fe^{III}(3\text{-}Cl\text{-}sal_2trien)][Mn^{II}Cr^{III}(ox)_3]\cdot(CH_3OH)_2\cdot(CH_3CN)_2$ y $[Fe^{III}(3\text{-}Br\text{-}sal_2trien)][Mn^{II}Cr^{III}(ox)_3]\cdot(CH_3CN)_2$. El compuesto $[Fe^{III}(3\text{-}MeO\text{-}sal_2trien)][Mn^{II}Cr^{III}(ox)_3]\cdot(CH_3OH)\cdot(H_2O)_{1.5}\cdot(CH_2Cl_2)_{0.5}$ permanece en estado de alto espín.

En los Capítulos 8 y 9, se ha estudiado la inserción de complejos de Mn^{III} de $[Mn^{III}(salen)]^+$ y derivados en redes bimetálicas de oxalato, obteniendo una gran variedad de estructuras. En el Capítulo 8 se muestra que cuando se utilizan derivados de $[Mn^{III}(salen)]^+$ se estabilizan los monómeros de Mn^{III} unidos a la base de Schiff tetradentada con dos moléculas de disolvente. Algunos de estos compuestos como $[Mn((R)\text{-salmen})(CH_3OH)_2][MnCr(ox)_3](CH_2Cl_2)_{0.375}\cdot(CH_3OH)_{0.125}\cdot(H_2O)_{0.375}$ y $[Mn((S)\text{-salmen})(CH_3OH)_2][MnCr(ox)_3](CH_2Cl_2)_{0.375}\cdot(CH_3OH)_{0.375}\cdot(H_2O)_{0.125}$ presentan estructuras 3D aquirales totalmente distintas a las obtenidas con anterioridad. El resultado más

prometedor lo constituyen los compuestos [Mn((*R*)-salmen)(CH_3OH)(CH_3CN)] [$MnCr(ox)_3$]·(CH_3OH)$_{0.5}$·(CH_3CN)$_{1.25}$ y [Mn((*S*)-salmen)(CH_3OH)(CH_3CN)][$MnCr(ox)_3$] ·(CH_3OH)$_{0.5}$·(CH_3CN)$_{1.25}$, con una estructura 2D quiral, que se pueden obtener de forma enantioméricamente pura. En contraste con sus derivados, el complejo $[Mn^{III}(salen)]^+$ mantiene la estructura dimérica del precursor y da lugar al compuesto de fórmula $[Mn^{III}(salen)(H2O)]_2[Mn^{II}Cr^{III}(ox)_3]_2\cdot(CH_3OH)_3\cdot(H_2O)$ y al análogo con una red paramagnética de fórmula $[Mn^{III}(salen)(H_2O)]_2[Zn^{II}Cr^{III}(ox)_3]_2\cdot(MeOH)_3\cdot(H_2O)$ formados por dímeros $[Mn^{III}(salen)(H_2O)]_2^{2+}$ insertados en una red 3D aquiral muy parecida a la obtenida con $[Fe^{III}(sal_2\text{-trien})]^+$ estudiados en el Capítulo 2. La conservación de la estructura del dímero de Mn^{III} del precursor permite observar un comportamiento de imán molecular en el compuesto paramagnético de Zn^{II}, aunque solo a muy bajas temperaturas (por debajo de 0.5 K). La caracterización magnética del compuesto ferromagnético $[Mn^{III}(salen)(H2O)]_2[Mn^{II}Cr^{III}(ox)_3]_2\cdot(CH_3OH)_3\cdot(H_2O)$ es consistente con la coexistencia de un ordenamiento magnético alrededor de 5 K y un comportamiento de imán unimolecular con importantes cambios en las dos propiedades debidos a la interacción entre la red bimetálica de oxalatos y las moléculas imán.

3. Summary

The preparation and characterisation of $[Fe^{III}(sal_2\text{-trien})][Mn^{II}Cr^{III}(ox)_3]\cdot CH_2Cl_2$ and $[Fe^{III}(sal_2\text{-trien})][Mn^{II}Cr^{III}(ox)_3]\cdot 0.75CH_3OH\cdot 0.5H_2O$ is presented in Chapter 2. The use of $[Fe^{III}(sal_2\text{-trien})]^+$ leads, depending on the synthetic conditions, to two different structures. Compound $[Fe^{III}(sal_2\text{-trien})][Mn^{II}Cr^{III}(ox)_3]\cdot CH_2Cl_2$ presents a 2D network and shows coexistence of a complete spin-crossover and a ferromagnetic ordering from the bimetallic oxalate network around 5 K. The second compound, $[Fe^{III}(sal_2\text{-trien})]$ $[Mn^{II}Cr^{III}(ox)_3]\cdot 0.75CH_3OH\cdot 0.5H_2O$, with a 3D achiral network, exhibits a partial spin-crossover besides the ferromagnetic ordering. The formation of two different oxalate networks with the same templating cation is a very unusual fact for this type of compounds that we attribute to the flexibility of the organic ligands of $[Fe^{III}(sal_2\text{-trien})]^+$ complex in the presence of different solvents. The photomagnetic properties of $[Fe^{III}(sal_2\text{-trien})]$ $[Mn^{II}Cr^{III}(ox)_3]\cdot CH_2Cl_2$ are studied in Chapter 3. This compound shows LIESST effect below 42 K. This is a very unusual result as this effect is rarely observed in Fe^{III} complexes. In Chapter 4, the preparation of several analogs of $[Fe^{III}(sal_2\text{-trien})]$ $[Mn^{II}Cr^{III}(ox)_3]\cdot CH_2Cl_2$ in other halogenated solvents ($CHCl_3$, CH_2Br_2 y $CHBr_3$) is described. The same 2D structure is maintained in the compounds of formula $[Fe^{III}(sal_2\text{-trien})]$ $[Mn^{II}Cr^{III}(ox)_3]\cdot CH_2Br_2$, $[Fe^{III}(sal_2\text{-trien})][Mn^{II}Cr^{III}(ox)_3]\cdot CHBr_3$ and $[Fe^{III}(sal_2\text{-trien})]$ $[Mn^{II}Cr^{III}(ox)_3]\cdot CHCl_3$. The change of CH_2Cl_2 by bulkier solvents allows tuning $T_{1/2}$, which is shifted toward lower temperatures, and T_{LIESST}, which is shifted towards higher values. The Fe^{III} complexes of these compounds have been diluted with similar diamagnetic Ga^{III} complexes. This has allowed to study the spin-crossover of the isolated Fe^{III} complexes by spectroscopic methods in $[Ga_{0.99}Fe_{0.01}(sal_2\text{-trien})][Mn^{II}Cr^{III}(ox)_3]\cdot CH_2Cl_2$. This compound shows a thermal spin-crossover and LIESST effect as the Fe^{III} pure compound. Finally, a structural analysis of these compounds and other Fe^{III} ones described in the literature showing LIESST effect has been performed.

In Chapter 5, 6 and 7 the search of other oxalate-based magnetic hybrids with derivatives of $[Fe^{III}(sal_2\text{-trien})]^+$ complex has been continued. $[Fe^{III}(5\text{-}NO_2\text{-}sal_2trien)]$

$[Mn^{II}Cr^{III}(ox)_3]\cdot MeNO_2\cdot 0.5H_2O$ and $[Fe^{III}(5\text{-}CH_3O\text{-}sal_2trien)][Mn^{II}Cr^{III}(ox)_3]$ with 2D and 3D achiral structures, respectively, are presented in Chapter 5. The two compounds show a magnetic ordering around 5 K but they do not present spin-crossover. The syntheses, structure and magnetic properties of $[Fe^{III}(5\text{-}Cl\text{-}sal_2trien)][Mn^{II}Cr^{III}(ox)_3]\cdot 0.5MeNO_2$, $[Fe^{III}(5\text{-}Br\text{-}sal_2trien)][Mn^{II}Cr^{III}(ox)_3]$ and $[In^{III}(5\text{-}Cl\text{-}sal_2trien)][Mn^{II}Cr^{III}(ox)_3]$ are shown in Chapter 6. They present a new chiral 3D structure that affords a new property to the multifunctional system, chirality, besides magnetic ordering and spin-crossover in the Fe^{III} compounds. Finally, derivatives of $[Fe^{III}(sal_2\text{-}trien)]^+$ with substituent in 3 or 4 positions lead to the compounds of formula $[Fe^{III}(4\text{-}Br\text{-}sal_2trien)][Mn^{II}Cr^{III}(ox)_3]_{0.67}\cdot Cl_{0.33}\cdot MeOH$, $[Fe^{III}(3\text{-}Cl\text{-}sal_2trien)][Mn^{II}Cr^{III}(ox)_3]\cdot(CH_3OH)_2\cdot(CH_3CN)_2$, $[Fe^{III}(3\text{-}Br\text{-}sal_2trien)][Mn^{II}Cr^{III}(ox)_3]\cdot(CH_3CN)_2$, and $[Fe^{III}(3\text{-}MeO\text{-}sal_2trien)][Mn^{II}Cr^{III}(ox)_3]\cdot(CH_3OH)\cdot(H_2O)_{1.5}\cdot(CH_2Cl_2)_{0.5}$ with 2D structures. The magnetic ordering around 5 K of all of them coexists with a complete spin-crossover from 300 to 400 K for $[Fe^{III}(4\text{-}Br\text{-}sal_2trien)][Mn^{II}Cr^{III}(ox)_3]_{0.67}\cdot Cl_{0.33}\cdot MeOH$ and partial spin-crossover for $[Fe^{III}(3\text{-}Cl\text{-}sal_2trien)][Mn^{II}Cr^{III}(ox)_3]\cdot(CH_3OH)_2\cdot(CH_3CN)_2$ and $[Fe^{III}(3\text{-}Br\text{-}sal_2trien)][Mn^{II}Cr^{III}(ox)_3]\cdot(CH_3CN)_2$. Fe^{III} complexes of $[Fe^{III}(3\text{-}MeO\text{-}sal_2trien)][Mn^{II}Cr^{III}(ox)_3]\cdot(CH_3OH)\cdot(H_2O)_{1.5}\cdot(CH_2Cl_2)_{0.5}$ are in the High-Spin state in all the range of temperature studied.

The insertion of $[Mn^{III}(salen)]^+$ complexes and derivatives into oxalate-based bimetallic networks has been studied in Chapters 8 and 9. These complexes give rise to a great variety of structures. The insertion of derivatives of $[Mn^{III}(salen)]^+$ leads to the stabilization of Mn^{III} monomers coordinated to the tetradentate Schiff base and two solvent molecules as shown in Chapter 8. Some of these compounds of formula $[Mn((R)\text{-}salmen)(CH_3OH)_2][MnCr(ox)_3](CH_2Cl_2)_{0.375}\cdot(CH_3OH)_{0.125}\cdot(H_2O)_{0.375}$ and $[Mn((S)\text{-}salmen)(CH_3OH)_2][MnCr(ox)_3](CH_2Cl_2)_{0.375}\cdot(CH_3OH)_{0.375}\cdot(H_2O)_{0.125}$ present 3D achiral structures totally different to those obtained before. The compounds $[Mn((R)\text{-}salmen)(CH_3OH)(CH_3CN)][MnCr(ox)_3]\cdot(CH_3OH)_{0.5}\cdot(CH_3CN)_{1.25}$ and $[Mn((S)\text{-}salmen)(CH_3OH)(CH_3CN)][MnCr(ox)_3]\cdot(CH_3OH)_{0.5}\cdot(CH_3CN)_{1.25}$ with a chiral 2D structure constitute the most promising result, as the they can be obtained enantiomerically pure. In contrast to its derivatives, $[Mn^{III}(salen)]^+$ inserted into bimetallic networks maintains its

dimeric structure in the compound $[Mn^{III}(salen)(H_2O)]_2[Mn^{II}Cr^{III}(ox)_3]_2\cdot(MeOH)_3\cdot(H_2O)$ and the paramagnetic analog of formula $[Mn^{III}(salen)(H_2O)]_2[Zn^{II}Cr^{III}(ox)_3]_2\cdot(MeOH)_3\cdot(H_2O)$. They are formed by $[Mn^{III}(salen)(H_2O)]_2^{2+}$ dimers inserted into an achiral 3D network very similar to that obtained with $[Fe^{III}(sal_2\text{-trien})]^+$, in Chapter 2. The preservation of the dimeric structure of Mn^{III} precursor, allows a single molecule magnet (SMM) behavior in the Zn^{II} paramagnetic compound although at very low temperatures (below 0.5 K). Magnetic characterization of the ferromagnetic $[Mn^{III}(salen)(H_2O)]_2[Mn^{II}Cr^{III}(ox)_3]_2\cdot(MeOH)_3\cdot(H_2O)$ compound is consistent with coexistence of magnetic ordering and a SMM behavior with important changes in the two properties due to the interaction between the bimetallic oxalate network and the SMMs.

4. Bibliografía

[1] (a) E. Coronado, P. Day, *Chem. Rev.*, 2004, **104**, 5419; (b) E. Coronado, J. R. Galán-Mascarós, *J. Mater. Chem.*, 2005, **15**, 66; (c) E. Coronado, M. Giménez-Marqués, G. Mínguez-Espallargas, L. Brammer, *Nature Communication*, 2012, **3**, 828;(d) E. Coronado, G. Minguez-Espallargas, *Chem. Soc. Rev.*, 2013, **42**, 1525.

[2] (a) O. Sato, T. Iyoda, A. Fujishima, K. Hashimoto, *Science*, 1996, **272**, 704; (b) P. J. Hagrman, D. Hagrman, J. Zubieta, *Angew. Chem. Int*., *Ed. Engl.*, 1999, **38**, 2638; (c) E. Coronado, J. R. Galán-Mascarós, C. J. Gómez-García, V. Laukhin, *Na*ture, 2000, **408**, 447; (d) S. Bénard, P. Yu, J. P. Audiére, V. Riviére, R. Clèment, J. Ghilhelm, L. Tchertanov, K. Nakatani, *J. Am. Chem. Soc.*, 2000, **122**, 9444; (e) A. Bleuzen, C. Lomonech, V. Escax, F. Villain, F. Varret, C. Cartier, M. Verdaguer, *J. Am. Chem. Soc.*, 2000, **122**, 6648; (f) B. Moulton, M. J. Zaworotko, *Chem. Rev.*, 2001, **101**, 1629; (g) S. R. Batten, *Current Opinion in Solid State and Materials Science*, 2001, **5**, 107; (h) M. Minguet, D. Luneau, E. Lhotel, V. Villar, C. Paulsen, D. B. Amabilino, J. Veciana, *Angew. Chem., Int. Ed.*, 2002, **41**, 586; (i) E. Coronado, C. J. Gómez-García, A. Nuez, F. M. Romero, E. Rusanov, H. Stoeckli-Evans, *Inorg. Chem.*, 2002, **41**, 4615; (j) N. Guillou, C. Livage, M. Drillon, G. Ferey, *Angew. Chem., Int. Ed.*, 2003, **42**, 5314; (k) K. Inoue, K. Kikuchi, M. Ohba, H. Okawa, *Angew. Chem., Int. Ed*., 2003, **42**, 4810; (l) S. Kitagawa, R. Kitaure, S.-I. Noro*, Angew. Chem.*, *Int. Ed.*, 2004, **43**, 2334; (m) E. Q. Gao, Y. F. Yue, S. Q. Bai, Z. He, C. H. Yan, *J. Am. Chem. Soc.*, 2004, **126**, 1419; (n) E. Coronado, C. J. Gómez-García, A. Nuez, F. M. Romero, J. C. Waerenborgh, *Chem. Mater.*, 2006, **18**, 2670; (o) G. Rogez, N. Viart, M. Drillon, *Angew. Chem., Int. Ed*., 2010, **49**, 1921.

[3] M. Pilkingston, S. Decurtins, *Magnetism: Molecular to Materials II: Models and Experiments*, ed. J. S. Miller and M. Drillon, Wiley, 2003, p. 339.

[4] O. Kahn, Y. Pei, M. Verdaguer, J. P. Renard, J. Sletten, *J. Am. Chem. Soc.*, 1998, **110**, 782.

[5] M. Shatruk, C. Avendano, K. R. Dunbar, *Prog. Inorg. Chem.*, 2009, **56**, 155.

[6] (a) M. Kurmoo, C. J. Kepert, *New J. Chem.*, 1998, **22**, 1515; (b) S. R. Batten, K. S. Murray, *Coord. Chem. Rev.*, 2003, **246**, 103.

[7] (a) H. Tamaki, Z. J. Zhong, N. Matsumoto, S. Kida, M. Koikawa, N. Achiwa, Y. Hashimoto, H. Okawa, *J. Am. Chem. Soc.*, 1992, **114**, 6974; (b) H. Tamaki, M. Mitsumi, N. Nakamura, N. Matsumoto, S. Kida, H. Okawa, S. Ijima, *Chem. Lett.*, 1992, 1975; (c) C. Mathonière, J. Nutall, S. G. Carling, P. Day, *Inorg. Chem.*, 1996, **35**, 1201; (d) R. Pellaux, H. W. Schmalle, R. Huber, P. Fisher, T. Hauss, B. Ouladdiaf, S. Decurtins, *Inorg. Chem.*, 1997, **36**, 2301; (e) E. Coronado, J. R. Galán-Mascarós, C. J. Gómez-García, J. M. Martínez-Agudo, E. Martínez-Ferrero, J. C. Waerenborgh, M. Almeida, *J. Solid State*

Chem., 2001, **159**, 391; (f) K. S. Min, A. L. Rhinegold, J. S. Miller, *Inorg. Chem.*, 2005, **44**, 8433.

[8] (a) S. Decurtins, H. W. Schmalle, P. Schneuwly, H. R. Oswald, *Inorg. Chem.*, 1993, **32**, 1888; (b) S. Decurtins, H. W. Schmalle, P. Schneuwly, J. Ensling, P. Gülich, *J. Am. Chem. Soc.*, 1994, **116**, 9512; (c) M. Hernández-Molina, F. Lloret, C. Pérez-Ruiz, M. Julve, *Inorg. Chem.*, 1998, **37**, 4141; (d) E. Coronado, J. R. Galán-Mascarós, C. J. Gómez-García, J. M. Martínez-Agudo, *Inorg. Chem.*, 2001, **40**, 113; (e) M. Clemente-León, E. Coronado, C. J. Gómez-García, A. Soriano-Portillo, *Inorg. Chem.*, 2006, **45**, 5653.

[9] S. Decurtins, R. Pellaux, A. Hauser; M.E. Arxvon, M.E.; *Magnetism: A Supramolecular Function*. Ed. O.*Khan, Kluwer Academic*. Press. NATO-ASI Series, Vol. C484, Nº1, 487, 1996, C484.

[10] O. Kahn; *Struct. Bonding,* 1987, **68**, 89.

[11] C.J. Nuttall, C. Bellito, P. Day; *J. Chem. Soc., Chem. Commun*., 1995, 1513.

[12] (a) H. Okawa, N. Matsumoto, H. Tamaki, H. Okawa; *M: Cryst. Liq. Cryst.*, 1993, **233**, 257; (b) C. Mathonière, S.G. Carling, D. Yuscheng, P. Day; *J. Chem. Soc., Chem. Commun.*, 1994, 1551.

[13] J. Larionova, B. Monbelli, J. Sanchiz, O. Kahn, *Inorg. Chem.*, 1998, **37**, 679.

[14] E. Coronado, J.R. Galán-Mascarós, C. Gastaldo-Martí; *J. Mater. Chem*., 2006, **10**, 1039.

[15] (a) R. Andrés, M. Gruselle, B. Malézieux, M. Verdaguer, J. Vaissermann, *Inorg. Chem.*, 1999, **38**, 4637; (b) R. Andrés, M. Brissard, M. Gruselle, C. Train, J. Vaissermann, B. Malézieux, J. P. Jamet, M. Verdaguer, *Inorg. Chem.*, 2001, **40**, 4633 ; (c) F. Pointillart, C. Train, M. Gruselle, F. Villain, H. W. Schmalle, D. Talbot, P. Gredin, S. Decurtins, M. Verdaguer, *Chem. Mater.*, 2004, **16**, 832.

[16] (a) G. Ballester, E. Coronado, C. Giménez-Saiz, F. M. Romero, *Angew. Chem.*, *Int. Ed.*, 2001, **40**, 792; (b) E. Coronado, J. R. Galán-Mascarós, C. J. Gómez-García, C. Martí-Gastaldo, *Inorg. Chem.*, 2005, **44**, 6197; (c) E. Coronado, J. R. Galán-Mascarós, C. Martí-Gastaldo, *Inorg. Chem.*, 2006, **45**, 1882; (d) E. Coronado, J. R. Galán-Mascarós, C. Martí-Gastaldo, A. Murcia-Martínez, *Dalton Trans.*, 2006, 3294; (e) H. Z. Kou, O. Sato, *Inorg. Chem.*, 2007, **46**, 9513; (f) E. Cariati, R. Macchi, D. Roberto, R. Ugo, S. Galli, N. Casati, P. Macchi, A. Sironi, L. Bogani, A. Caneschi, D. Gatteschi, *J. Am. Chem. Soc.*, 2007, **129**, 9410; (g) H. Z. Kou, J. Tao, O. Sato, *Dalton Trans.*, 2008, 3652.

[17] (a) F. D. Rochon, R. Melanson, M. Andruh, *Inorg. Chem.*, 1996, **35**, 6086; (b) M. Andruh, R. Melanson, C. V. Stager, F. D. Rochon, *Inorg. Chim. Acta*, 1996, 309. (c) N.

Stanica, C. V. Stager, M. Cimpoesu, M. Andruh, *Polyhedron*, 1998, **17**, 1787; (d) G. Marinescu, M. Andruh, R. Lescouëzec, M. C. Muñoz, J. Cano, F. Lloret, M. Julve, *New J. Chem.*, 2000, **24**, 527; (e) S. Triki, F. Berezovsky, J. S. Pala, E. Coronado, C. J. Gómez-García, J. M. Clemente, A. Riou, P. Molinie, *Inorg. Chem.*, 2000, **39**, 3771; (f) E. Coronado, M.C. Giménez, C. J. Gómez-García, F. M. Romero, *Polyhedron*, 2003, **22**, 3115

[18] (a) E. Coronado, J. R. Galán-Mascarós, C. J. Gómez-García, *Dalton Trans.*, 2000, 205; (b) S. Rashid, S. S. Turner, P. Day, M. E. Light, M. B. Hursthouse, *Inorg. Chem.,* 2000, **39**, 2426; (c) E. Coronado, J. R. Galán-Mascarós, C. Giménez-Saiz, C. J. Gómez-García, C. Ruiz-Pérez, S. Triki, *Adv. Mater.*, 1996, **8**, 737; (d) E. Coronado, C. Giménez-Saiz, J. R. Galán-Mascarós, C. J. Gómez-García, C. Ruiz-Pérez, *Eur. J. Inorg. Chem.*, 2003, 2290.

[19] M. Clemente-León, E. Coronado, C. Martí-Gastaldo, F. M. Romero, *Chem. Soc. Rev.*, 2011, **40**, 473.

[20] (a) T. Enoki, A. Miyazaki, *Chem. Rev.*, 2004*,* **104**, 5449; (b) H. Kobayashi, H. Cui, A. Kobayashi, *Chem. Rev.*, 2004*,* **104**, 5265; (c) E. Coronado, C. Martí-Gastaldo, E. Navarro-Moratalla, A. Ribera, S. J. Blundell, P. J. Baker, *Nature Chem.*, 2010*,* **2**, 1031.

[21] E. Coronado, S. Curreli, C. Giménez-Saiz, C. J. Gómez-García, *Inorg. Chem.*, 2012, **51**, 1111.

[22] E. Coronado, J. R. Galán-Mascarós, C. J. Gómez-García, *J. Chem., Dalton Trans.*, 2000, 205.

[23] (a) E. Coronado, J. R. Galán-Mascarós, C. Giménez-Saiz, C. J. Gómez-García, J. M. Martínez-Agudo, E. Martínez-Ferrero, *Polyhedron*, 2003, **22**, 2381.

[24] E. Coronado, J. R. Galán-Mascarós, C. J. Gómez-García, E. Martínez-Ferrero, S. Van Smaalen, *Inorg. Chem.*, 2004, **43**, 4808.

[25] A. Alberola, E. Coronado, J. R. Galán-Mascarós, C. Giménez-Saiz, C. J. Gómez-García, *J. Am. Chem. Soc.*, 2003, **125**, 10774.

[26] (a) M. Clemente-León, J. R. Galán-Mascarós, C. J. Gómez-García, *Chem. Commun.*, 1997, 1727; (b) E. Coronado, J. R. Galán-Mascarós, C. J. Gómez-García, J. M. Martínez-Agudo, *Adv. Mater.*, 1999, **11**, 558; (c) E. Coronado, J. R. Galán-Mascarós, C. J. Gómez-García, J. Ensling, P. Gutlich, *Chem. Eur. J.*, 2000, **6**, 552.

[27] A. Alberola, E. Coronado, C. Giménez-Saiz, C. J. Gómez-García, F. M. Romero, A. Tarazón, *Eur. J. Inorg. Chem.*, 2005, 389.

[28] M. Clemente-León, E. Coronado, M. C. Giménez-López, A. Soriano-Portillo, J. C. Waerenborgh, F. S. Delgado, C. Ruiz-Pérez, *Inorg. Chem.*, 2008, **47**, 9111.

[29] (a) S. Bénard, E. Rivière, P. Yu, K. Nakatami, J. F. Delouis, *Chem. Mater.*, 2001, **13**, 159; (b) S. M. Aldoshin, N. A. Sanina, V. I. Minkin, N. A. Voloshin, V. N. Ikorskii, V. I. Ovcharenko, V. A. Smirnov, N. K. Nagaeva, *J. Mol. Struct.*, 2007, **826**, 69.

[30] E. Cariati, R. Macchi, D. Roberto, R. Ugo, S. Galli, N. Casati, P. Macchi, A. Sironi, L. Bogani, A. Caneschi, D. Gatteschi, *J. Am. Chem. Soc.*, 2007, **129**, 9410.

[31] C. Train, T. Nuida, R. Gheorghe, M. Gruselle, S. Ohkoshi, *J. Am. Chem. Soc.,* 2009, **131**, 16838.

[32] (a) W. Eerenstein, N. D. Mathur, J. F. Scott, *Nature*, 2006, **442**, 759; (b) H. Zheng, J. Wang, S. E. Lofland, Z. Ma, L. Mohaddes-Ardabili, T. Zhao, L. Salamanca-Riba, S. R. Shinde, S. B. Ogale, F. Bai, D. Viehland, Y. Jia, D. G. Schlom, M. Wuttig, A. Roytburd, R. Ramesh, *Science*, 2004, **303**, 661.

[33] (a) S. W. Cheong, M. Mostovoyo, *Nat. Mater.*, 2007, **6**, 13; (b) D. Khomskii, *Physics*, 2009, **2**, 20.

[34] E. Pardo, C. Train, H. Liu, L.-M. Chamoreau, B. Dkhil, K. Boubekeur, F. Lloret, K. Nakatani, H. Tokoro, S.-i. Ohkoshi, M. Verdaguer, *Angew. Chem.*, *Int. Ed*., 2012, **51**, 8356.

[35] (a) M. Sadakiyo, T. Yamada, H. Kitagawa, *J. Am. Chem. Soc.*, 2009, **131**, 9906; (b) T. Yamada, M. Sadakiyo, H. Kitagawa, *J. Am. Chem. Soc.*, 2009, **131**, 3144; (c) T. Yamada, H. Kitagawa, *J. Am. Chem. Soc.*, 2009, **131**, 6312.

[36] (a) H. Kitagawa, Y. Nagao, M. Fujishima, R. Ikeda, S. Kanda, *Inorg. Chem. Commun*., 2003, **6**, 346; (b) Y. Nagao, T. Kubo, K. Nakasuji, R. Ikeda, T. Kojima, H. Kitagawa, *Synth. Met*., 2005, **154**, 89; (c) M. Fujishima, M. Enyo, S. Kanda, R. Ikeda, H. Kitagawa, *Chem. Lett.*, 2006, **35**, 546; (d) S. Bureekaew, S. Horike, M. Higuchi, M. Mizuno, T. Kawamura, D. Tanaka, N. Yanai, S. Kitagawa, *Nat. Mater*., 2009, **8**, 831; (e) J. A. Hurd, R. Vaidhyanathan, V. Thangadurai, C. I. Ratcliffe, I. L. Moudrakovski, G. K. H. Shimizu, *Nat. Chem.*, 2009, **1**, 705 (f) H. Okawa, A. Shigematsu, M. Sadakiyo, T. Miyagawa, K. Yoneda, M. Ohba, H. Kitagawa, *J. Am. Chem. Soc.*, 2009, **131**, 13516.

[37] E. Pardo, C. Train, G. Gontard, K. Boubekeur, O. Fabelo, H. Liu, B. Dkhil, F. Lloret, K. Nakagawa, H. Tokoro, S.-I. Ohkoshi, M. Verdaguer, *J. Am. Chem. Soc.*, 2011, **133**, 15328.

[38] M. Sadakiyo, H.Okawa, A. Shigematsu, M. Obha, T. Yamada, H. Kitagawa, *J. Am. Chem. Soc.*, 2012, **134**, 5472.

[39] C. Train, R. Gheorghei, V. Krstic, L. M. Chamoreau, N. S. Ovanesyan, G. L. J. A. Rikken; M. Gruselle, M. Verdaguer, *Nature Mater.*, 2008, **7**, 729.

[40] G. H. Wagnière, A. Meier, *Chem Phys Lett*., 1982, **93**, 78.

[41] D. L. Barron, J. Vrbancich, *J. Mol. Phys.*, 1984, **51**, 715.

[42] (a) G. L. J. A. Rikken, E. Raupach, *Nature*, 1997, **390**, 493; (b) G. L. J. A. Rikken, E. Raupach, *Phys. Rev.*, 1998, **390**, 493.

[43] (a) A. Caneschi, D. Gatteschi, P. Rey, R. Sessoli, *Inorg. Chem.*, 1991, **30**, 3936; (b) E. Coronado, J. R. Galán-Mascarós, C. J. Gómez-García, A. Murcia-Martínez, E. Canadell, *Inorg. Chem.*, 2004, **43**, 8072; (c) M. Clemente-León, E. Coronado, J. C. Dias, A. Soriano-Portillo, R. D. Willett, *Inorg. Chem.*, 2008, **47**, 6458; (d) C. Train, M. Gruselle, M. Verdaguer, *Chem. Soc. Rev.*, 2011, **40**, 3297.

[44] (a) E. Coronado, J. R. Galán-Mascarós, C. J. Gómez-García, A. Murcia-Martínez, *Chem. Eur. J.*, 2006, **12**, 3484; (b) W. Kaneko, S. Kitagawa, M. Ohba, *J. Am. Chem. Soc.*, 2007, **129**, 248; (c) J. Millon, M. C. Daniel, A. Kaiba, P. Guionneau, S. Brandes, J. P. Sutter, *J. Am. Chem. Soc.*, 2007, **129**, 13872.

[45] M. Grusselle, C. Train, K. Boubekour, P. Gredin, N. Ovanesyan, *Coord. Chem. Rev.*, 2006, **250**, 2491.

[46] (a) P. D. W. Boyd, Q. Li, J. B. Vincent, K. Folting, H.-R. Chang, W. E. Streib, J. C. Huffman, G. Christou, D. N. Hendrickson, *J. Am. Chem. Soc.*, 1988, **110**, 8537; (b) R. Sessoli, H.-L. Tsai, A. R. Schake, S. Wang, J. B. Vincent, K. Folting, D. Gatteschi, G. Christou, D. N. Hendrickson, *J. Am. Chem. Soc.*, 1993, **115**, 1804; (c) M. N. Leuenberg, D. Loss, *Nature*, 2001, **410**, 789; (d) J. Lehmann, A. Gaita-Ariño, E. Coronado, D. Loss, *Nat. Nanotechnol.*, 2007, **2**, 312.

[47] (a) R. Sessoli, D. Gatteschi, , A. Caneschi, M.A. Novak, *Nature,* 1993, **365**, 141; (b) D. Gatteschi, A. Caneschi, L. Pardi, R. Sessoli, *Science,* 1994, **265**, 1054; (c) H. J. Eppley, H.-L. Tsai, N. de Vries, K. Folting, G. Christou, D. N. Hendrickson*, J. Am. Chem. Soc*., 1995, **117**, 301; (d) J. Friedman, M.P. Sarachik, J. Tejada, R. Ziolo, *Phys. Rev. Lett.,* 1996, **76**, 3830-3833; (e) L. Thomas, F. Lionti, R. Ballou, D. Gatteschi, R. Sessoli, B. Barbara, *Nature,* 1996, **383**, 145-147.

[48] (a) C. Delfs, D. Gatteschi, L. Pardi, R. Sessoli, K. Wieghardt, D. Hanke, *Inorg. Chem.*, 1993, **32**, 3099; (b) A. L. Barra, P. Debrunner, D. Gatteschi, C. E. Schukz, R. Sessoli, *Europhys. Lett.*, 1996, **35**, 133; (c) W. Wernsdorfer, A. Caneschi, R. Sessoli, D. Gatteschi, A. Cornia, V. Villar, C. Paulsen, *Phys. Rev. Lett.*, 2000, **84**, 2965; (d) W. Wernsdorfer, A.

Caneschi, R. Sessoli, D. Gatteschi, A. Cornia, *Europhys. Lett.*, 2000, **50**, 552; (e) D. Gatteschi, R. Sessoli, *Angew. Chem., Int. Ed.*, 2003, **42**, 268.

[49] (a) N. Ishikawa, M. Sugita, T. Ishikawa, S. Koshihara, Y. Kaizu, *J. Am. Chem. Soc.*, 2003, **125**, 8694; (b) M. A. AlDamen, J. M. Clemente-Juan, E. Coronado, C. Martí-Gastaldo, A. Gaita-Ariño, *J. Am. Chem. Soc.*, 2008, **130**, 8874 ; (c) M. A. AlDamen, S. Cardona-Serra, J. M. Clemente-Juan, E. Coronado, A. Gaita-Ariño, C. Martí-Gastaldo, F. Luis, O. Montero, *Inorg. Chem.*, 2009, **48**, 3467; (d) J. D. Rinehart, K. R. Meihaus, J. R. Long, *J. Am. Chem. Soc.*, 2010, **132**, 7572; (e) S. Jiang, B. Wang, G. Su, Z. Wang, S. Gao, *Angew. Chem., Int. Ed.*, 2010, **49**, 7448; (f) L. Sorace, C. Benelli, D. Gatteschi, *Chem. Soc. Rev.*, 2011, **40**, 3092; (g) S. Jiang, B. Wang, H. Sun, Z. Wang, S. Gao, *J. Am. Chem. Soc.*, 2011, **133**, 4730; (h) M. A. Antunes, L. C. J. Pereira, I. C. Santos, M. Mazzanti, J. Marçalo, M. Almeida, *Inorg. Chem.*, 2011, **50**, 9915; (i) N. Magnani, C. Apostolidis, A. Morgenstern, E. Colineau, J. C. Griveau, H. Bolvin, O. Walter, R. Caciuffo, *Angew. Chem., Int. Ed.*, 2011, **50**, 1696.

[50] (a) L. Maria, M. P. Campello, A. Domingos, I. Santos and R. J. Andersen, *Chem. Soc., Dalton Trans.*, 1999, **43**, 2015; (b) R. Schenker, M. N. Leuenberger, G. Chaboussant, H.-U. Güdel, D. Loss, *Chem. Phys. Lett.*, 2002, **358**, 413; (c) S. Karasawa, G. Zhou, H. Morikawa, N. Koga, *J. Am. Chem. Soc.*, 2003, **125**, 13676; (d) J. D. Rinehart, J. R. Long, *J. Am. Chem. Soc.*, 2009, **131**, 12558; (e) N. Magnani, E. Colineau, R. Eloirdi, J.-C. Griveau, R. Caciuffo, S. M. Cornet, I. May, C. A. Sharrad, D. Collison, R. E. P. Winpenny, *Phys. Rev. Lett.*, 2010, **104**, 197202; (f) D. P. Mills, F. Moro, J. McMaster, J. van Slageren, W. Lewis, A. J. Blake, S. T. Liddle, *Nat. Chem.*, 2011, **3**, 454; (g) S. Mossin, B. L. Tran, D. Adhikari, M. Pink, F. W. Heinemann, J. Sutter, R. K. Szilagyu, K. Meyer, D. J. Mindiola, *J. Am. Chem. Soc.*, 2012, **134**, 13651; (h) S. Cardona-Serra, J. M. Clemente-Juan, E. Coronado, A. Gaita-Ariño, A. Camón, M. Evangelisti, F. Luis, M. J. Martínez-Pérez, J. Sesé, *J. Am. Chem. Soc.*, 2012, **134**, 14982.

[51] (a) H. Miyasaka, R. Clérac, W. Wernsdorfer, L. Lecren, C Bonhomme, K.-I. Sugiura, M. Yamasita, *Angew. Chem., Int. Ed.,* 2004, **43**, 2801; (b) Z. Lu, M. Yuan, F. Pan, S. Gao, D. Zhang, D. Zhu, *Inorg. Chem.*, 2006, **45**, 3538; (c) I.-R. Jeon, R. Clérac, *Dalton Trans.*, 2012, **41**, 9569.

[52] (a) H. Miyasaka, M. Yamashita, *Dalton Trans.*, 2007, **4**, 399; (b) L. Lecren, W. Wernsdorfer, Y.-G. Li, A. Vindigni, H. Miyasaka, R. Clérac, *J. Am. Chem. Soc.*, 2007, **129**, 5045.

[53] (a) Wu, Q.; Li, Y.-G.; Wang, Y.-H.; Clérac, R.; Lu, Y.; Wang, E.-B.*Chem. Commun.*, 2009, 5743; (b) Y. Sadawa, W. Kosaka, Y. Hayashi, H. Miyasaka, *Inorg. Chem.*, 2012, **51**, 4824.

[54] (a) O. Kahn, *Molecular Magnetism*, VCH, New York, 1993; (b) W. A. Little, *Phys. Rev.*, 1964, **A 134**, 1416; (c) F. L. Cater, *Ed., Molecular Electronic Devices I & II*, M. Dekker, New York, 1982 & 1987; (d) J. S. Miller, *Adv. Mater.*, 1990, **2**, 378; (e) D. Goldhaber-

Gordon, M. S. Montemerlo, J. C. Love, G. J. Opiteck, J. C. Ellenbogen, *Proceeding of the IEEE*, 1997, **85**, 521; (f) R. C. Haddon, A. A. Lamola, *Proc. Natl. Acad. Sci. USA*, 1985, **82**, 1874.

[55] (a) P. Gütlich, A. H., *Coord. Chem. Rev.*, 1990, **97**, 1; (b) A. B. Gaspar, M. C. M., V. Niel, J. A. Real, *Inorg. Chem.*, 2001, **40**, 9; (c) H. A. Goodwin, *Topics in Current Chemistry*, 2004, **234**, 786; (d) P. J. van Koningsbruggen, Y. M., H. Oshio, *Topics in Current Chemistry*, 2004, **233**, 259; (e) I. Krivokapic, M. L. Daku, a. Vargas, C. Enachescu, C. Ambrus, P. Treganna-Piggott, N. Amstutz, E. Krausz, A. Hauser, *Coord. Chem. Rev.*, 2007, **251**, 364; (f) M. Nihei, T.S., Y. Maeda, H. Oshio, *Coord. Chem. Rev.*, 2007, **251**, 2606; (g) M. A. Halcrow, *Polyhedron*, 2007, **26**, 3523; (h) M. A. Halcrow, *Coord. Chem. Rev.*, 2009, **253**, 2493.

[56] J. J. McGravey, I. Lawthers, *J. Chem. Soc., Chem. Commun.*, 1982, 906.

[57] E. Buhks, G. Navon, M. Bixon, J. Jortner, *J. Am. Chem. Soc.*, 1980, **102**, 3966.

[58] P. Gütlich, A. Hauser, H. Spiering, *Angew. Chem.Int.*, *Ed. Engl.*, 1994, **33**, 2024.

[59] (a) A. Hauser, *Chem. Phys. Lett.*, 1986, **124**, 543; b) A. Hauser, P. Gütlich, H. Spiering, *Inorg. Chem.*, 1986, **25**, 4245.

[60] (a) S. Decurtins, P. Gütlich, C.P. Köhler, H. Spiering, A. Hauser, *Chem. Phys. Lett.*, 1984, **105**, 1; (b) S. Decurtins, P. Gütlich, K. M. Hasselbach, A. Hauser, H. Spiering, *Inorg. Chem.*, 1985, **24**, 2174.

[61] S. Hayami, K. Hiki, T. Kawahara, Y. Maeda, D. Urakami, K. Inoue, M. Ohama, S. Kawata, O. Sato, *Chem. Eur. J.*, 2009, **15**, 3497.

[62] A. Hauser, A. Vef, P. Adler, *J. Chem. Phys.*, 1991, **95**, 8710.

[63] (a) S. Hayami, Z. Gu, M. Shiro, T. Einaga, A. Fujishima, O. Sato, *J. Am. Chem. Soc.*, 2000, **122**, 7126; (b) G. Juhász, S. Hayami, O. Sato, Y. Maeda, *Chem. Phys. Lett.*, 2002, **364**, 164; (c) O. Sato, *Acc. Chem. Res.*, 2003, **36**, 692 ; d) S. Hayami, T. Kawahara, Y. Maeda, K. Inoue, O. Sato, *J. Radioanal. Nucl. Chem.*, 2005, **266**, 521; e) T. Shimizu, Y. Komatsu, H. Kamihata, Y. H. Lee, A. Fuyuhiro, S. Iijima, S. Hayami, *J. Incl. Phenom. Macrocycl. Chem.*, 2011, **71**, 363.

[64] M. Clemente-León, E. Coronado, M. C. Giménez-López, A. Soriano-Portillo, J. C. Waerenborgh, F. S. Delgado, C. Ruiz-Pérez, *Inorg. Chem.*, 2008, **47**, 9111.

[65] R. Sieber, S. Decurtins, H. Stoeckli-Evans, C. Wilson, D. Yufit, J. A. K. Howard, S. C. Capelli, A. Hauser, *Chem. Eur. J.*, 2000, **6**, 361.

[66] E. Coronado, J. R. Galán-Mascarós, M. C. Giménez-López, M. Almeida, J. C. Waerenborgh, *Polyhedron*, 2007, **26**, 1838.

Multifunctional magnetic materials obtained by insertion of a spin-crossover Fe^{III} complex into bimetallic oxalate-based

CHEMISTRY
A EUROPEAN JOURNAL

Capítulo 2

Capítulo 2: Multifunctional magnetic materials obtained by insertion of a spin-crossover Fe^{III} complex into bimetallic oxalate-based ferromagnets

Abstract: The syntheses, structures and magnetic properties of the compounds of formula $[Fe^{III}(sal_2\text{-trien})][Mn^{II}Cr^{III}(ox)_3]\cdot(CH_2Cl_2)$ (**1**), $[Fe^{III}(sal_2\text{-trien})][Mn^{II}Cr^{III}(ox)_3]\cdot(CH_3OH)$ (**2**), $[In^{III}(sal_2\text{-trien})][Mn^{II}Cr^{III}(ox)_3]\cdot0.25(H_2O)\cdot0.25(CH_3OH)\cdot0.25(CH_3CN)$ (**3**) and $[In^{III}(sal_2\text{-trien})][Mn^{II}Cr^{III}(ox)_3]\cdot(CH_3NO_2)\cdot0.5(H_2O)$ (**4**) are reported. The structure of **1** presents a 2D honeycomb anionic layer formed by Mn^{II} and Cr^{III} ions linked through oxalate ligands and a cationic layer of $[Fe(sal_2\text{-trien})]^+$ complexes intercalated between the 2D oxalate network. The structures of **2**, **3** and **4** present a 3D achiral anionic network formed by Mn^{II} and Cr^{III} ions linked through oxalate ligands with $[Fe(sal_2\text{-trien})]^+$ or $[In(sal_2\text{-trien})]^+$ complexes and solvent molecules intercalated within the 3D oxalate network. The magnetic properties and Mössbauer spectroscopy of **1** and **2** indicate that these compounds undergo a long-range ferromagnetic ordering at ca. 5 K and a spin crossover of the intercalated $[Fe(sal_2\text{-trien})]^+$ complexes above 130 K, which is complete in the case of **1**. The magnetic properties of the compounds **3** and **4** confirm the ferromagnetic ordering of the bimetallic oxalate network.

Introduction

One of the most exciting developments in molecular magnetism is the preparation of multifunctional compounds. The versatility of molecular chemistry makes possible the design of new molecule-based materials that combine two (or more) physical properties of interest. Thus, a wise choice of the constituent molecules could allow the appearance in the same compound of an unusual combination of physical properties, or even a mutual interplay –synergy– of the properties involved. A suitable approach to obtain such materials is the so-called hybrid approach in which two-network solids are constructed via self-assembling of two different molecular fragments (organic, inorganic or organometallic), with each network furnishing the solid with distinct properties.[1]

Bimetallic oxalate-bridged complexes of formula $A[M^{II}M^{III}(ox)_3]$ (M^{III} = Cr, Fe, Ru, V, Mn; M^{II} = Mn, Fe, Co, Ni, Cu, Zn; A = Cation) have provided many examples of hybrid magnets. These bimetallic salts are most often composed by polymeric 2D anionic networks, which furnish the cooperative magnetic properties (ferro- ferri- or canted antiferromagnetism),[2] and a bulky charge-compensating molecular cation, which templates the network formation. In these compounds, the cooperative magnetism of the oxalate network can coexist with the electronic property provided by the cationic molecular lattice. Some illustrative examples of this concept are provided by the use of paramagnetic decamethylferrocenium[3] or organic radical cations,[4] photochromic molecules,[5] NLO-active molecules,[6] organic π-electron donors,[7] and chiral cations[8] which lead to the formation of magnetic multilayers, photochromic magnets, ferromagnetic molecular metals or chiral magnets. More recently, the magnetochiral dichroic effect has been observed for the first time on a chiral magnet in enantiopure 2D oxalate-based magnets prepared by Train et al.[9] Other magnetic networks, different from the 2D honeycomb-like network, can also be obtained depending on the nature of the templating cation (size, shape and charge) with dimensionalities ranging from 0D to 3D.[10] The most extensive one is represented by the family of 3D chiral structures in which the chirality of a templating cation of the type $[Z^{II}(bpy)_3]^{2+}$ (Z^{II} = Fe, Co, Ni, Ru; bpy = 2,2'-bipyridine) induces the building blocks to adopt an homochiral configuration,[11] which provides an opportunity to obtain chiral magnets.[11e,12] In addition, the hybrid character of these series also leads to examples in which the two sublattices are magnetic.[11d]

In this context, spin-crossover cations are particularly suitable to prepare multifunctional magnetic materials since they represent one of the best examples of molecular bistability. This may open a way to design switching magnets in which the magnetic ordering of the oxalate network could be tuned, thus taking advantage of the possibility of inducing the spin-crossover phenomenon by applying an external stimuli such as light or pressure. However, this challenging goal requires first the preparation of hybrid materials formed by a magnetic network and a spin-crossover complex.

The first example of the insertion of spin-crossover cations into oxalate networks was reported by Decurtins et al. in a compound of formula $[Co(bpy)_3][LiCr(ox)_3]$.[13] In that case, the insertion of a Co^{II} complex into a 3D oxalate-based network resulted in the observation of spin crossover in the Co^{II} sublattice. However, the compound did not show coexistence of spin crossover and magnetic ordering since the oxalate network was paramagnetic. More recently, our group reported the insertion of the Fe^{II} spin-crossover complex, $[Fe(bpp)_2]^{2+}$ [bpp = 2,6(bis(pyrazol-3-yl)pyridine)], into a ferromagnetic achiral 3D oxalate-based network, $[Fe(bpp)_2][MnCr(ox)_3]\cdot(bpp)\cdot(CH_3OH)$,[14] although spin crossover was not observed as most of Fe^{II} complexes remained in the low spin (LS) state throughout the entire temperature range. The coexistence of a spin crossover and magnetic ordering has successfully been obtained very recently by insertion of Fe^{III} complexes in homometallic oxalate layers.[15] As a result, the compound $[Fe^{III}(sal_2\text{-trien})]_2[Mn^{II}_2(ox)_3]\cdot 4(H_2O)\cdot(C_3H_7NO)$ (sal_2-trien = hexadentate ligand, see Scheme 1) formed by homometallic Mn^{II} oxalate layers and $[Fe(sal_2\text{-trien})]^+$ cations behaves as a weak ferromagnet below T_c = 8.1 K, exhibiting at the same time a gradual spin crossover of half of the intercalated $[Fe(sal_2\text{-trien})]^+$ complexes from 300 to 80 K. In this compound, however, the two properties seems to be independent since the change in the spin state of the inserted $[Fe(sal_2\text{-trien})]^+$ cations after desolvation does not produce important changes in the magnetic ordering of the homometallic oxalate network.

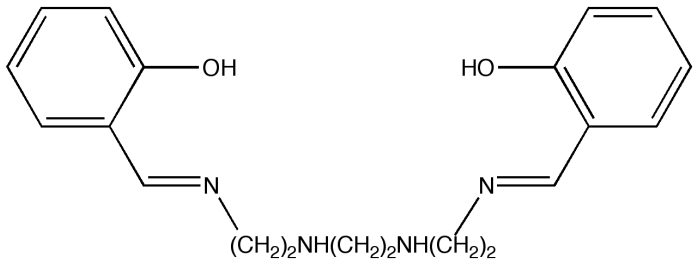

Scheme 1. H_2sal_2-trien

In view of this first result, we have explored the insertion of $[Fe(sal_2\text{-trien})]^+$ complex into bimetallic oxalate anionic networks. This approach has several advantages with respect to the previous one. On one hand, the use of bimetallic oxalate networks can give rise to ferro- or ferrimagnetism instead of weak ferromagnetism due to a spin canting in the antiferromagnetic state. On the other hand, the possibility of inserting the spin crossover complex into a 3D lattice could improve the effect of the spin crossover on the magnetic ordering of the oxalate network since the 3D oxalate networks are much more sensitive to small structural and size changes of the inserted cation than the 2D oxalate networks.[11f]

In this work we report the preparation and structural and magnetic characterization of the compounds $[Fe^{III}(sal_2\text{-trien})][Mn^{II}Cr^{III}(ox)_3]\cdot(CH_2Cl_2)$ (**1**), that presents a 2D oxalate-based anionic network, and $[Fe^{III}(sal_2\text{-trien})][Mn^{II}Cr^{III}(ox)_3]\cdot(CH_3OH)$ (**2**), $[In^{III}(sal_2\text{-trien})][Mn^{II}Cr^{III}(ox)_3]\cdot 0.25(H_2O)\cdot 0.25(CH_3OH)\cdot 0.25(CH_3CN)$ (**3**) and $[In^{III}(sal_2\text{-trien})][Mn^{II}Cr^{III}(ox)_3]\cdot(CH_3NO_2)\cdot 0.5(H_2O)$ (**4**) that present an achiral 3D oxalate-based anionic network. The compounds containing the diamagnetic $[In(sal_2\text{-trien})]^+$ complex have been studied as reference compounds.

Results and Discussion

Synthesis: The method used to prepare this family of compounds is analogous to that used to prepare the chiral oxalate 2D compound of formula $[(S)\text{-}[PhCH(CH_3)N(CH_3)_3]][Mn(CH_3CN)_{2/3}Cr(ox)_3]\cdot(CH_3CN)\cdot(solvate)$.[8] It is based in the use of $Ag_3[Cr(ox)_3]$ to avoid the presence of alkali ions in the structure. It consists on the slow diffusion of a methanol solution containing the precursors of the oxalate network, Mn^{2+} and $[Cr(ox)_3]^{3-}$ ions, in methanol, into a solution of $[M(sal_2\text{-trien})]^+$ (M^{III} = Fe or In) in different solvents. The use of different solvents to dissolve the $[M(sal_2\text{-trien})]^+$ complex gives rise to different structures. Thus, **1** is obtained by using CH_2Cl_2, while **2** and **3** by using CH_3CN and **4** by using CH_3NO_2. The composition of these crystals, checked by microanalysis, shows in all cases a M/Mn/Cr ratio of 1:1:1. Furthermore, crystals of **1** show the presence of Cl from CH_2Cl_2 in a ratio 2:1 with respect to Mn, Cr and Fe. It has

not been possible to obtain the crystal structure of the 2D oxalate network with the $[In(sal_2\text{-trien})]^+$ cation dissolved in dichloromethane. Due to this, we have tried with other solvents such as CH_3NO_2, but this has resulted in a new compound, **4**, that presents a 3D oxalate network slightly different to that of **2** and **3**. The crystal structures of the four compounds have been solved by single-crystal X-ray diffraction. Unit cells of several crystals obtained in the same diffusion tube have been measured by single-crystal X-ray diffraction giving similar results in all cases. This excludes the possibility of crystallisation of the different structures by using the same solvent mixture. Attempts to obtain analogous compounds with other paramagnetic M^{2+} ions (M = Ni, Fe, Co and Cu) or with other M^{III} ions (M^{III} = Fe) in the place of Cr^{III} have been unsuccessful.

Structure of $[Fe^{III}(sal_2\text{-trien})][Mn^{II}Cr^{III}(ox)_3]\cdot CH_2Cl_2$ (1): The structure of this compound is formed by anionic sheets in the *bc* plane of formula $[MnCr(ox)_3]^-$ with interlamellar $[Fe(sal_2\text{-trien})]^+$ cations and dichloromethane solvent molecules (Figure 1). The anionic layer is formed by an extended network with Mn^{II} and Cr^{III} ions linked through oxalate bridges. It presents the well-known 2D honeycomb structure. It is formed by oxalate ligands connecting Mn^{II} with Cr^{III} ions in such a way that each Mn^{II} is surrounded by three neighbouring Cr^{III} and vice versa (Figure 2). The neighbouring metal centers of these layers present alternated chirality as usual for this type of networks. There are two metals crystallographically independent with M–O distances lying between 2.061(3) and 2.107(3) Å. These distances are intermediate between the ones expected for Cr^{III}–O and Mn^{II}–O. Therefore, it is not possible to distinguish between the two metals in this structure. Mean metal-metal distances between adjacent centers are in the range 5.3941(13)-5.4432(13) Å. These distances are similar to those found in other 2D oxalate networks reported in the literature[2,3] and shorter than those found in 3D systems.[11,13] The distances between metals of different layers are 11.6440(2) Å which are higher than those found in other oxalate-based 2D compounds with decamethylferrocenium or alkylammonium cations (9.2-9.7 Å)[2,3] but lower than those of the $[Fe^{III}(sal_2\text{-trien})]_2[Mn^{II}_2(ox)_3]\cdot 4H_2O\cdot C_3H_7NO$ compound (17.489(7) Å) in which a double layer of

cations is necessary to compensate the higher charge of the $[Mn^{II}_2(ox)_3]^{2-}$ anionic layer with respect to the $[M^{II}M^{III}(ox)_3]^-$ anionic layer.[15]

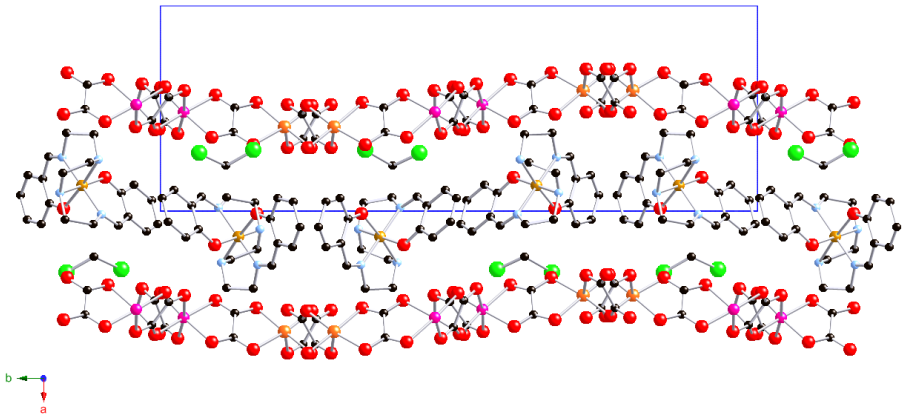

Figure 1. Projection on the *ab* plane of the structure of **1** (neighbouring atoms corresponding to disordered Mn/Cr have been assigned for Mn and Cr separately for clarity). Hydrogen atoms have been omitted for clarity.

These anionic layers are stacked one over the other in a *AA*···fashion. The Mn^{II} and Cr^{III} ions and oxalate ligands do not form a perfect 2D layer, as there is a certain amount of undulation of the inorganic layer (see Figure 1). The presence of ethylene groups from $[Fe(sal_2\text{-trien})]^+$ that extend alternatively above and below the layer of inserted $[Fe(sal_2\text{-trien})]^+$ complexes could be the responsible of this effect. Finally, the minimum distance between the metallic ions from the oxalate network and the Fe atoms is 6.3795(9) Å.

The space between the oxalate layers is occupied by one crystallographically independent $[Fe(sal_2\text{-trien})]^+$ complex and one dichloromethane molecule (Figures 1 and 2). The $[Fe(sal_2\text{-trien})]^+$ cations lie with their longer axis parallel to the oxalate layers. They form double chains running along the *c* axis (Figure 1 and Figure 1SS of the Supporting information) in which $[Fe(sal_2\text{-trien})]^+$ complexes are connected through C–H···π and N–H···π interactions.[16] Only one of the two phenoxy rings of sal_2-trien, which is placed in the internal part of the double chain, is involved in these C–H···π and

N–H···π interactions with two adjacent $[Fe(sal_2\text{-trien})]^+$ complexes that belong to the same chain. These are edge-to-face interactions with a shortest distance of 3.592(7) Å between C4 and C1 of neighbouring rings and 3.356(6) Å between C4 and N3 of neighbouring rings (Figure 1SS of the Supporting Information).

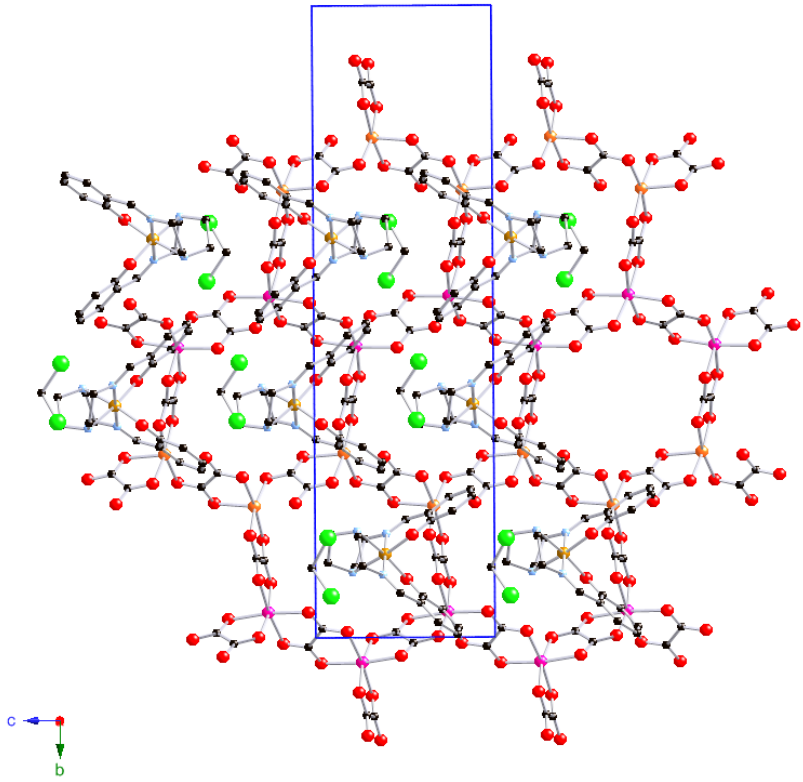

Figure 2. Projection on the bc plane of the structure of **1** (neighbouring atoms corresponding to disordered Mn/Cr have been assigned for Mn and Cr separately for clarity). Hydrogen atoms have been omitted for clarity.

Furthermore, the phenoxy rings from $[Fe(sal_2\text{-trien})]^+$ complexes that belong to different double chains that are not involved in these interactions present short contacts with O atoms from the oxalate network ($d_{C16–O14}$ = 3.384(6) Å). Finally, there are short contacts between C atoms from ethylene groups of sal_2-trien and the oxalate ligands ($d_{C10–O13}$ = 3.152(6) Å). The average Fe–N and Fe–O bond distances in $[Fe(sal_2\text{-}$

trien)]$^{+}$ complexes are 1.989(4) and 1.866(3) Å respectively. These values are in the range of those obtained for other low-spin [Fe(sal$_2$-trien)]$^{+}$ compounds[17] and are in full agreement with the magnetic measurements and Mössbauer spectroscopy (see below), which indicate that all Fe are LS at 180 K (temperature at which the crystal structure has been determined). On the other hand, the dichloromethane molecules occupy the holes situated in between the [Fe(sal$_2$-trien)]$^{+}$ cations and the oxalate network. They are placed alternatively above and below the layer formed by [Fe(sal$_2$-trien)]$^{+}$ cations. They present short contacts with oxalate ligands ($d_{Cl1–O10}$ = 3.258(3) and $d_{Cl2–O12}$ = 2.979(3) Å).

Structure of [Fe^{III}(sal$_2$-trien)][Mn^{II}Cr^{III}(ox)$_3$]·(CH$_3$OH) (2): The structure of **2** is formed by an anionic 3D polymeric oxalate-bridged bimetallic network with [Fe(sal$_2$-trien)]$^{+}$ cations and solvent molecules occupying the cavities (Figure 3).

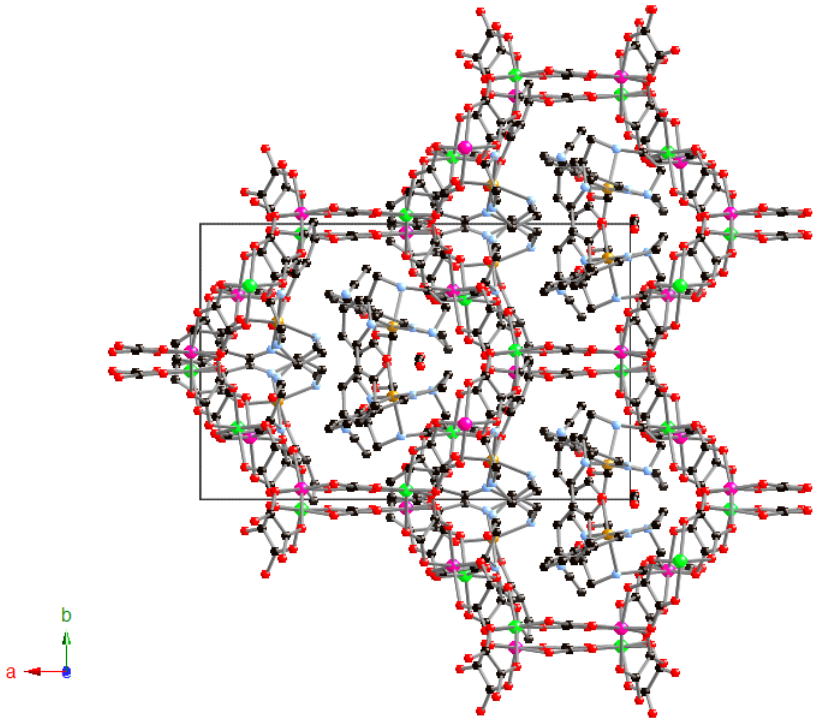

Figure 3. Projection on the *ab* plane of the structure of **2** (neighbouring atoms corresponding to disordered Mn/Cr have been assigned for Mn and Cr separately for clarity). Hydrogen atoms have been omitted for clarity.

This anionic polymeric structure is formed by bis-chelating oxalate ligands that connect Mn^{II} and Cr^{III} ions in such a way that each Mn^{II} is surrounded by three Cr^{III} and vice versa, thus building ten-membered rings in a (10,3) topology. In contrast to typical chiral structures exhibited by the oxalate-based 3D network, compound **2** possesses metal centers of both chiralities. In fact, **2** crystallizes in the acentric *Cc* space group. A similar achiral 3D oxalate network has been found in the compound of formula $[Fe(bpp)_2][MnCr(ox)_3]_2 \cdot bpp \cdot CH_3OH$ that crystallizes in the centrosymmetric $P2_1/n$ space group.[14] The (10,3) decagon rings perpendicular to the *c* axis are formed by metal centers with the same chirality (see Figure 3). Two of these neighbouring metal rings, which are linked trough two oxalate ligands, present opposite chirality (see Figure 4). Projection of the oxalate network on the *ac* plane is almost identical to that of the chiral 3D oxalate network in the *ab*, *bc* or *ac* planes (see Figure 5). However, projection on the *bc* or *ab* planes (see Figure 3 and 4) are different as a result of the different chirality of the neighbouring (10,3) decagon rings. Thus, in the *ab* projection an eclipsed disposition of the neighbouring oxalate rings is observed as a result of the heterochiral oxalate junctions among them (see Figure 3). This anionic network contains four metals crystallographically independent with M–O bond lengths lying between 2.004(14) and 2.141(13) Å. Again, these bond lengths are intermediate between the ones expected for Cr^{III}–O and Mn^{II}–O and hence it is not possible to distinguish between the two metals in this structure. Metal-metal distances between adjacent centers are in the range 5.396(3)-5.408(3) Å. These metal-metal distances are significantly shorter than those exhibited by the 3D chiral structures. For instance, Mn–Cr distance in $[Ir(ppy)_2(bpy)][MnCr(ox)_3] \cdot 0.5H_2O$ is 5.503 Å.[11f] These metal-metal distances are shorter than those found for compound **1** although it is important to note that the crystal structure of compound **2** was determined at lower temperature (120 versus 180 K). In addition, the minimum distance between the metallic ions from the oxalate network and the Fe atoms is also shorter than in compound **1**. Thus, a value of 5.905(4) Å is obtained between Mn4/Cr4 and Fe1.

$[Fe(sal_2\text{-trien})]^+$ complexes and solvent molecules are intercalated in the holes described by this 3D oxalate network. There are two crystallographically independent $[Fe(sal_2\text{-trien})]^+$ complexes ([Fe1] and [Fe2]), and disordered methanol. The phenoxy rings from two neighbouring crystallographically independent $[Fe(sal_2\text{-trien})]^+$ complexes present edge-to-face interactions with a shortest distance of 3.46(12) Å between C19 and C26 of neighbouring rings. Furthermore, [Fe1] complex presents hydrogen-bonds through the NH groups with one disordered methanol molecule and one oxalate ligand ($d_{N3–O3M}$ = 3.11(2) and $d_{N2–O24}$ = 3.100(18) Å) and short contacts with oxalate ligands ($d_{C14–O19}$ = 3.21(2) and $d_{C19–O22}$ = 3.137(16) Å), whereas [Fe2] complex forms hydrogen-bonds with two disordered methanol molecules ($d_{N6–O2M}$ = 3.15(3) and $d_{O4–O3M}$ = 2.94(3) Å) and presents short contacts with oxalate ligands from the oxalate network ($d_{C29–O12}$ = 3.05(3) Å). The average Fe–N and Fe–O bond distances are 2.042(17) and 1.891(13) Å in [Fe1] complexes and 2.15(2) and 1.877(15) Å in [Fe2] complexes. These values are higher than those found in **1** and close to those obtained for other high-spin (HS) $[Fe(sal_2\text{-trien})]^+$ compounds. We have to take into account that magnetic measurements and Mössbauer spectroscopy (see below) indicates that around 28 % of Fe is LS at 120 K (temperature at which the crystal structure has been determined).

Interestingly, the use of the same templating cation in different solvents has afforded different structures. This finding is very unusual for this type of oxalate compounds. The few examples in the literature in which that occurs involve either a change in the coordination mode of the oxalate ligand, or the presence of solvent molecules that complete the coordination of the metals from the oxalate network.[10k,10l,18] In our case, the two different structures -a 2D and an achiral 3D oxalate network- present bis-chelating oxalate ligands connecting M^{II} and M^{III} ions. To our knowledge, this is a novel feature in this type of compounds. A possible explanation may be related to the flexibility of $[Fe(sal_2\text{-trien})]^+$ cation. This complex presents two phenoxy arms projecting from the same face of the molecule.[17] The relative orientation of these arms differs notably in different compounds. Therefore, a different configuration of the phenoxy rings may have a different templating effect on the oxalate network, thus

giving rise to different structures. Indeed, the configuration of $[Fe(sal_2\text{-trien})]^+$ cations in the structures of **1** and **2** confirms this point. The dihedral angles (α) between the least-squares planes of the two phenoxy rings have very different values in the 2D or 3D structures presented in this paper. Thus, α = 71.65(13)° is present in **1**, whereas α = 120.13(67)° ([Fe1] complex) and α = 103.02(75)° ([Fe2] complex) are present in **2**. Whereas in the 2D compound the two phenoxy rings are clearly below 90°, the ideal value for an octahedral complex, the opposite behavior is observed in the 3D compound for the two crystallographically independent $[Fe(sal_2\text{-trien})]^+$ cations, which present α higher than 90°. Such a difference may be induced by the different solvent mixture used to dissolve the $[Fe(sal_2\text{-trien})]^+$ cations in the two compounds.

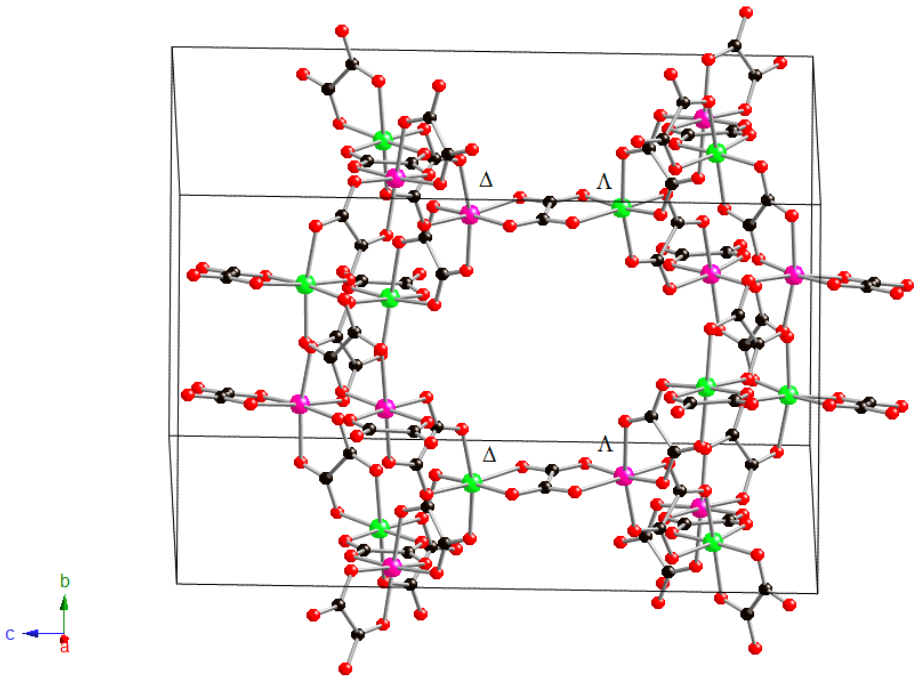

Figure 4. Two neighbouring ten-membered rings of the oxalate network of **2** of opposite chirality connected through two oxalate ligands along the *c* direction (neighbouring atoms corresponding to disordered Mn/Cr have been assigned for Mn and Cr separately for clarity). Hydrogen atoms have been omitted for clarity.

It is also possible to relate this configuration with the magnetic behavior of the $[Fe(sal_2\text{-trien})]^+$ complexes in the two compounds. Pritchard et al. have shown that there is a correlation between the disposition of the two phenoxy groups and the spin state of $[Fe(sal_2\text{-trien})]^+$ salts.[17] All $[Fe(sal_2\text{-trien})]^+$ compounds with LS state adopt a configuration with an α angle of 61.8-73.6°, whereas those presenting a HS state are much more structurally variable. They conclude that compounds presenting a low α angle, which is the preferred configuration for the LS state, can undergo a spin-crossover. On the contrary, those presenting high α angles remain in the HS state, as the structural changes needed to adopt a LS state prevent the spin-crossover from occurring. This is confirmed for the two compounds presented in this paper. Thus, in compound **1**, which shows a clear spin-crossover (see below), α = 71.65(13)°, while in compound **2**, which remains mostly in the HS state in all the range of temperatures, α values of 120.13(67)° and 103.02(75) ° are observed.

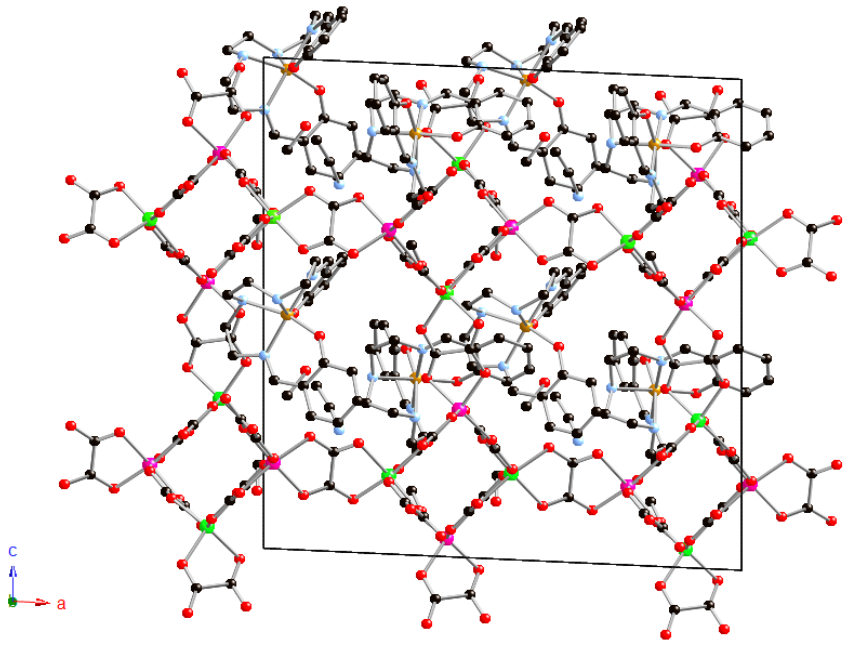

Figure 5. Projection on the *ac* plane of the structure of **2** (neighbouring atoms corresponding to disordered Mn/Cr have been assigned for Mn and Cr separately for clarity). Hydrogen atoms have been omitted for clarity.

Structure of $[In^{III}(sal_2\text{-trien})][Mn^{II}Cr^{III}(ox)_3]\cdot 0.25(H_2O)\cdot 0.25(CH_3OH)\cdot 0.25(CH_3CN)$ (3): The structure of **3** resembles that of **2** with $[In(sal_2\text{-trien})]^+$ cations in the place of $[Fe(sal_2\text{-trien})]^+$ (see Figures 2SS, 3SS and 4SS of the Supporting Information). The bimetallic oxalate 3D network is similar to that of **2**. It is formed by four metals that are crystallographically independent with M–O bond lengths that lie between 2.050(6) and 2.103(6) Å. Again, it is not possible to distinguish between Mn or Cr in this structure. Metal-metal distances between adjacent centers are in the range 5.3545(14)-5.4157(14) Å. The cavities of the oxalate network are occupied by two crystallographically independent $[In(sal_2\text{-trien})]^+$ complexes ([In1] and [In2]), and disordered water, methanol and acetonitrile molecules. The disposition of the solvent molecules and $[In(sal_2\text{-trien})]^+$ differs with respect to that of **2**. In this case, the complex [In1] forms hydrogen-bonds with one methanol molecule (d_{N7-O1M} = 3.084(16) Å) and one water molecule ($d_{O50-O1W}$ = 3.038(13) Å), and has at the same time a short contact with an oxalate ligand (d_{N7-O2} = 3.269(13) Å) as well as C–H···π and N–H···π interactions with the neighbouring [In2]. Apart from this short interaction between the two crystallographically independent complexes, [In2] presents one hydrogen-bond with one water molecule (d_{N2-O1W} = 3.033(10) Å) and two short interactions with an oxalate ligand (d_{N3-O11} = 3.199(7) and d_{N3-O12} = 3.122(7) Å). Dihedral angles between the phenoxy rings of [In1] and [In2] are respectively 120.22(52)° and 102.96(60)°, similar to those found for $[Fe(sal_2\text{-trien})]^+$ complexes in compound **2**.

Structure of $[In^{III}(sal_2\text{-trien})][Mn^{II}Cr^{III}(ox)_3]\cdot(CH_3NO_2)\cdot 0.5(H_2O)$ (4): Compound **4** crystallizes in the acentric orthorhombic space group *Pna2₁*, which contains metal centers of both chiralities. It is formed by an anionic 3D polymeric oxalate-bridged bimetallic network similar to that of **2** and **3**. The cavities of this 3D network are occupied by the $[In(sal_2\text{-trien})]^+$ cations and nitromethane and water solvent molecules (Figure 6). In contrast to **2** and **3**, it is possible to distinguish between Mn and Cr ions of this oxalate network. Thus, there are two crystallographically independent Mn ions (Mn1 and Mn2) with Mn–O bond lengths lie between 2.151(6) and 2.196(6) Å and two

crystallographically independent Cr ions (Cr1 and Cr2) with Cr–O bond lengths lie between 1.957(6) and 1.988(6) Å. These are typical Cr^{III}–O and Mn^{II}–O distances similar to those found in other oxalate networks. Metal-metal distances between adjacent centers are in the range 5.3795(17)-5.4342(18) Å. These metal-metal distances are slightly shorter than those exhibited by **3** measured at the same temperature. This shortening may have some consequences in the magnetic properties (see below).

The (10,3) decagon rings formed by metal centers with the same chirality are in this case perpendicular to the *a* axis (Figure 6). Two of these neighbouring metal rings, which are linked trough two oxalate ligands, present opposite chirality as in the structure of **2** and **3** (see figure 5SS of the Supporting Information). Projection of the oxalate network on the *ab* plane is almost identical to that of the chiral 3D oxalate network in the *ab*, *bc* or *ac* planes (see Figure 6SS), whereas projections on the *bc* or *ac* planes (see Figure 6 and 5SS of the Supporting Information) are different as a result of the different chirality of the neighbouring (10,3) decagon rings, as observed for **2** and **3**. In this case, the eclipsed disposition of the neighbouring rings is observed in the *bc* projection view (see Figure 6). In contrast to compounds **2** and **3**, which crystallize in a monoclinic space group, the eclipsed disposition of the rings is almost complete, as a result of the higher symmetry of the space group of compound **4**.

The disposition of $[In(sal_2\text{-trien})]^+$ complexes and solvent molecules intercalated in the holes of this 3D oxalate network differs from that of **2** and **3**. There are two crystallographically independent $[In(sal_2\text{-trien})]^+$ complexes ([In1] and [In2]), one nitromethane molecule and disordered nitromethane and water molecules. [In1] presents short contacts with the oxalate ligands through one of the two phenoxy rings ($d_{C14–O16}$ = 2.924(11) and $d_{C15–O16}$ = 3.168(11) Å). [In1] presents short contacts with two neighbouring [In2] complexes. There are two types of short contacts. The first one is between the phenoxy ring of [In1] and one of the ethylene groups of [In2] ($d_{C19–C31}$ = 3.280(18) and $d_{C19–N7}$ = 3.237(15) Å). The second one is between one NH from [In1] and atoms from the phenoxy ring of [In2] ($d_{N3–C39}$ = 3.218(11) and $d_{N3–C40}$ = 3.294(11) Å).

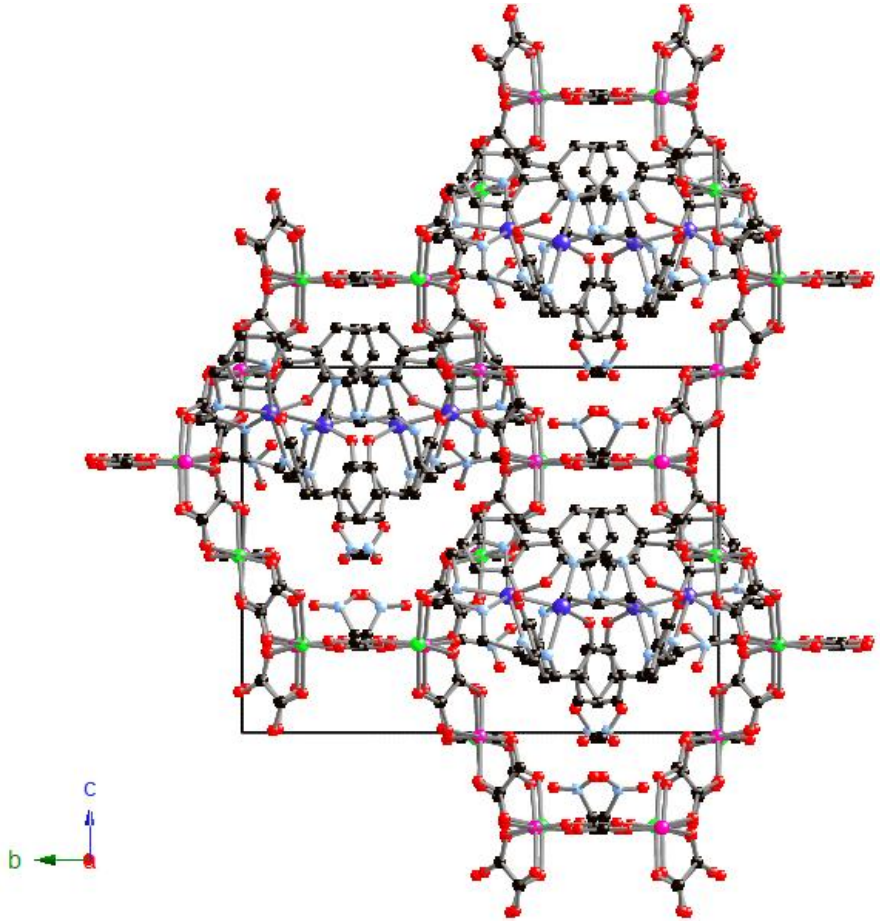

Figure 6. Projection on the *bc* plane of the structure of **4**. Hydrogen atoms have been omitted for clarity.

These are edge-to-face interactions. [In2] also presents short contacts with the oxalate ligands through one of the two phenoxy rings ($d_{C39–C55}$ = 3.310(12) and $d_{C39–O28}$ = 3.154(11) Å). Furthermore, the imine C linked to this phenoxy ring (C34) presents a short contact with another oxalate ligand ($d_{C34–O17}$ = 2.901(12) Å). [In2] is also connected to two neighbouring [In1] complexes through the short contacts mentioned above. The absence of methanol molecules in this structure could induce shorter contacts between neighbouring $[M(sal_2\text{-trien})]^+$ complexes than those observed in **2** or **3** compounds. We

have to take into account that methanol molecules of **2** and **3** are linked to sal_2-trien ligands through hydrogen-bonds. Dihedral angles between the phenoxy rings of [In1] and [In2] are respectively 114.84(46)° and 96.59(38)°.

Magnetic properties of 1: The thermal dependence of the product of the molar magnetic susceptibility with the temperature (χT) of **1** is shown in Figure 7. χT shows a constant value of 10.0 emu·K·mol^{-1} from 400 to 350 K. This value is approximately equal to the sum of the expected contributions for the isolated paramagnetic ions with the Fe^{III} spin-crossover complex in a HS state. χT decreases gradually from 350 to 165 K as temperature decreases with a more abrupt decrease below 300 K. The χT value at 165 K is 7.2 emu·K·mol^{-1}. This value of χT is consistent with the Mössbauer data that suggest that Fe^{III} is 94 % LS at this temperature. Therefore, in this range of temperatures a full HS→LS spin conversion of the Fe^{III} complex takes place. At lower temperatures there is an increase of χT which is very sharp below 50 K. This indicates the presence of ferromagnetic interactions between neighbouring Mn^{II}–Cr^{III} magnetic ions and suggests the onset of long-range ferromagnetic ordering, as observed for other M^{II}–Cr^{III} 2D oxalate networks.[2a,3] To confirm the presence of long-range magnetic ordering and to determine precisely the critical temperatures, alternating current (AC) susceptibility measurements were carried out. A maximum in the in-phase signal (χ') near T_c and an out-of-phase signal (χ'') that starts to appear at temperatures just below T_c is observed (Figure 8). From this data, the T_c of **1** is 5.4 K, similar to those reported for other Mn^{II}-Cr^{III} 2D Mn^{II}–Cr^{III} 2D oxalate compounds.[2a,3] These signals are frequency independent as expected for a ferromagnet (Figure 8). In the ordered phase an additional peak in χ'' at temperatures below 3 K is also detected. The presence of such a frequency-dependent peak has already been observed in other 2D M^{II}–Cr^{III} 2D oxalate compounds.[3] It can be related to the formation of magnetic domains and domain-wall movement.[19]

To confirm the ferromagnetic ordering of the spins, isothermal magnetization at 2 K has been performed (Figure 9). It presents a sharp increase at low fields which is much faster than that expected for non-interacting Cr^{III} and Mn^{II} centers; this increase is more

gradual at higher fields and no saturation is reached up to 5 T. The magnetization (*M*) value at 5 T is 8.5 μ_B (μ_B = Bohr magneton), which is slightly lower than the expected value for a parallel alignment of the spins in the bimetallic lattice (9 μ_B). It can be due to a spin canting of the ferromagnetic phase, as for other M^{II}–Cr^{III} 2D oxalate compounds.[3] The hysteresis loops at 2 K shows that this compound is a soft ferromagnet with a coercive field of 2 mT.

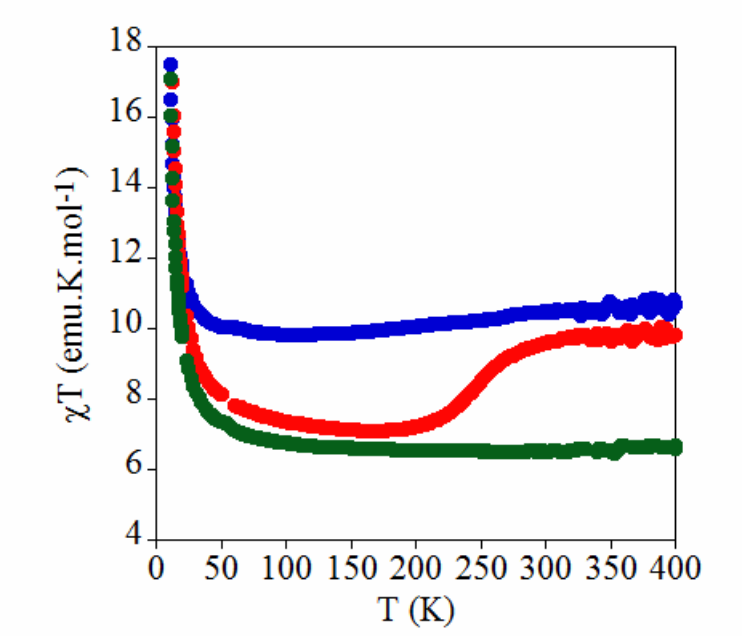

Figure 7. Temperature dependence of the product of the molar magnetic susceptibility with temperature (χT) at 0.1 T for compounds **1** (red), **2** (blue) and **3** (green)

The magnetic behavior of this compound after heating at 400 K under vacuum for 1 hour has been studied because removal of solvent molecules may cause drastic changes in the spin crossover behavior of this cation, as shown in other $[Fe(sal_2\text{-trien})]^+$ salts.[15,20] However, in contrast to similar compounds,[15] desolvation could not achieved as microanalysis continued to show the presence of Cl in a 2:1 ratio with respect to Mn, Cr and Fe.

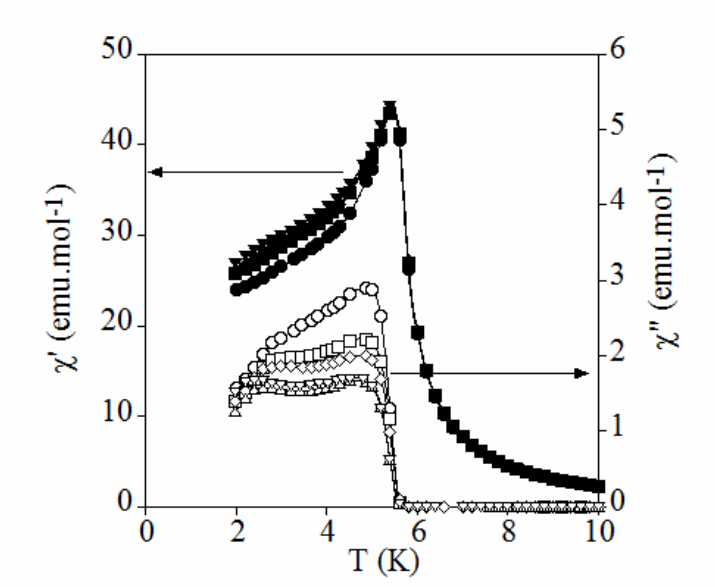

Figure 8. Temperature dependence of the in-phase AC susceptibility (χ') (filled symbols) and the out-of-phase AC susceptibility (χ'') (empty symbols) for **1**.

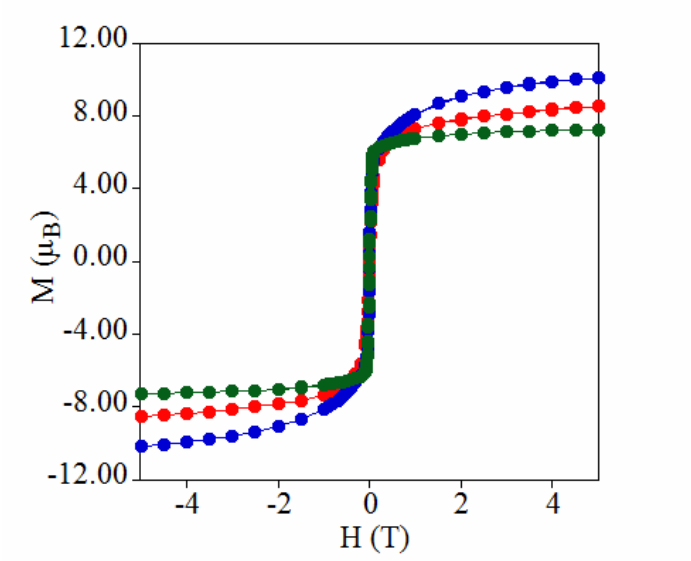

Figure 9. Field dependence of the magnetization (M) for **1** (filled circles) **2** (empty circles) and **3** (empty squares).

Magnetic properties of 2 and 3: The thermal dependence of χT for **2** shows a value of 10.7 emu·K·mol^{-1} at 400 K (Figure 7). This value is close to the sum of the expected contributions for the isolated paramagnetic ions with 100 % of Fe^{III} in a HS state. Furthermore, this value is 4.2 emu·K·mol^{-1} higher than that obtained for the reference compound (**3**) with diamagnetic $[In(sal_2\text{-trien})]^+$ in the place of $[Fe(sal_2\text{-trien})]^+$. This confirms that $[Fe(sal_2\text{-trien})]^+$ is 100 % HS at this temperature. χT presents a smooth decrease from 300 (10.5 emu·K·mol^{-1}) to 115 K (9.8 emu·K·mol^{-1}) as temperature decreases. The χT value of **2** at 300 K and the difference with that of **3** (4.0 emu·K·mol^{-1}) are consistent with the Mössbauer data that suggest that Fe^{III} is 93 % HS at this temperature. On the other hand, difference of χT values of **2** and **3** at 115 K is 3.1 emu·K·mol^{-1} which is again consistent with the Mössbauer data that suggest that the fraction of LS Fe^{III} remains constant and close to 30 % below 130 K. Therefore, the HS$\rightarrow$LS spin conversion of 30 % of the Fe^{III} complexes takes place between 300 and 130 K. This contrasts with the magnetic behavior of **1** that presents a complete spin conversion. At temperatures below 115 K there is an increase of χT, which is very sharp below 50 K. This indicates the presence of ferromagnetic interactions between neighbouring Mn^{II}–Cr^{III} magnetic ions and the onset of long-range ferromagnetic ordering as usual for this type of compounds. The χ^{-1} versus T curve of **3** is linear in the 50-300 K temperature range. This allows one to fit it to a Curie-Weiss law ($\chi^{-1}=(T-\theta)/C$, in which C is the Curie constant) and thus to a Weiss constant, θ (K), of 3.7 K, which is slightly lower than that obtained for a chiral 3D Mn^{II}-Cr^{III} oxalate network in the $[Ir(ppy)_2(bpy)][M^{II}Cr^{III}(ox)_3]\cdot 0.5H_2O$ compound (6.1 K).[11f] The long-range ferromagnetic ordering of the two compounds is confirmed by AC susceptibility measurements (see Figure 10) that show frequency-independent χ' and χ'' peaks. From this data the T_c of the **2** and **3** compounds is in both cases 5.2 K.

Isothermal magnetization at 2 K of the two compounds presents a sharp increase at low fields (below 0.1 T), and a hysteresis loop with a coercive field of approximately 3 mT, which is usual for this type of compounds (Figure 9). In **3** only the bimetallic oxalate sublattice is magnetic, so the magnetization tends to saturate and only a slight

linear increase of *M* versus magnetic field (*H*) is observed at fields above 0.1 T as a consequence of spin canting in the ferromagnetic phase. In contrast, in **2** the presence of a fraction of paramagnetic Fe^{III} produces a pronounced curvature in the *M* versus *H* curve with *M* increasing from 7.5 to 10 μ_B when *H* increases from 0.1 to 5 T. In these two compounds the difference between the *M* values at 5 T (ca. 3 μ_B) is consistent with the presence of a 70 % of Fe^{III} in the HS state in **2**.

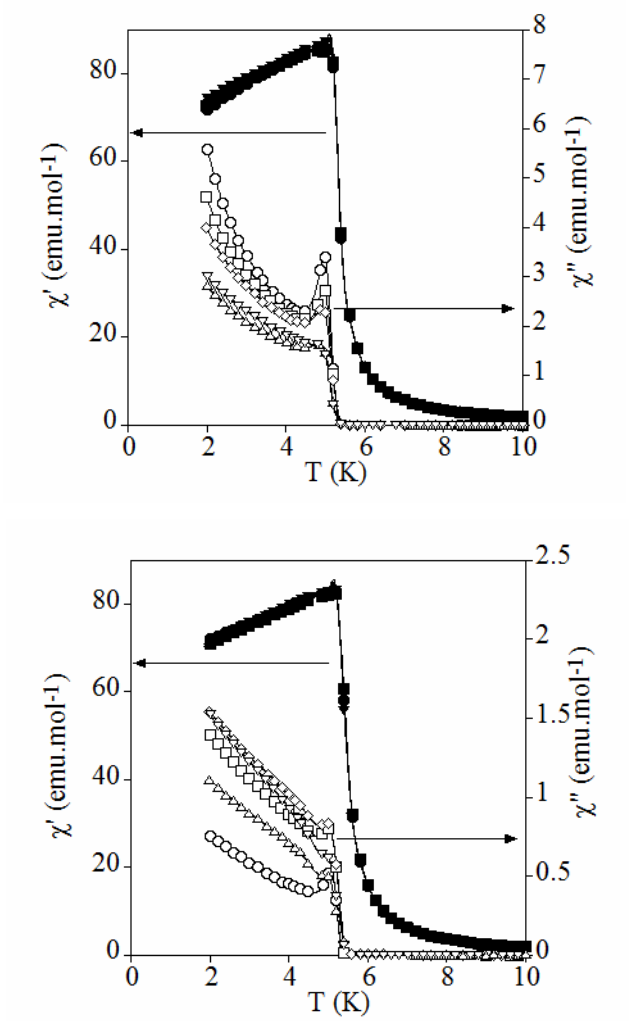

Figure 10. Temperature dependence of the in-phase AC susceptibility (χ') (filled symbols) and the out-of-phase AC susceptibility (χ'') (empty symbols) for **2** (up) and **3** (down).

The magnetic behavior of **2** and **3** after desolvation has also been studied. In both cases, there are small differences with respect to the solvated sample. χT of the desolvated sample presents a more gradual decrease upon lowering the temperature, with values slightly higher than those of the initial sample from 300 to 100 K (see Figure 7SS of the Supporting Information). Thus, χT of the desolvated sample at 115 K is 0.3 emu·K·mol^{-1} higher than that of the solvated one. We could relate these differences to changes in the spin-state of Fe^{III}. However, this is a very small effect that could be related also to structural changes in the oxalate network (changes in distances and angles between the metallic centers). Thus, a slight increase of χT is also observed for the In^{III} analogous, **3**, which does not contain a spin-crossover cation. Some differences appear also in AC susceptibility measurements of **2** and **3** with respect to the initial sample. Thus, both the χ' and χ'' peaks are shifted towards lower (T_c of 5.0 versus 5.2 K) temperatures and their intensity decreases with respect to the initial compound (see Figure 8SS of the Supporting Information). Again these changes may be related to the oxalate network as they occur in both compounds.

Magnetic properties of 4: χT of **4** presents a value of 6.5 emu·K·mol^{-1} at 300 K and an increase on lowering the temperature with a sharp increase below 50 K (Figure 9SS). This confirms the ferromagnetic interaction between Mn^{II} and Cr^{III} ions of the oxalate network and the ferromagnetic behavior already observed in **2** and **3**. AC susceptibility measurements show a frequency-independent peak that starts to appear at 5.0 K and defines T_c (Figure 10SS of the Supporting Information). The isothermal magnetization at 2 K shows a very sharp increase at low fields and does not saturate completely at 5 T (see Figure 11SS of the Supporting Information). A M value of 7.8 μ_B is obtained at 5 T as expected for a Mn^{II}-Cr^{III} ferromagnet. A hysteresis loop of the magnetization with a coercive field of 3 mT is observed at 2 K. All these features indicate that the ferromagnetic behavior of this 3D oxalate network is analogous to that of **3**. The slight decrease of T_c with respect to that of **2** and **3** may be explained by the slightly longer

mean Mn^{II}–Cr^{III} distances shown by **4** (5.408 Å for **4** compared to 5.399 Å for **3**) and by slight differences in the bonding angles.

In any case, the T_c values obtained in the reported Mn^{II}–Cr^{III} 3D oxalate compounds are all very close (5.2 K in **2** and **3**; 5.0 K in **4**) and similar to that shown by the chiral compound $[Ir(ppy)_2(bpy)][Mn^{II}Cr^{III}(ox)_3]\cdot 0.5H_2O$ (T_c = 5.1 K[11f]). Still, in the compound $[Fe(bpp)_2][MnCr(ox)_3]\cdot bpp\cdot CH_3OH$, which presents an achiral 3D oxalate network but longer Mn^{II}-Cr^{III} distances (5.503 Å), a significantly lower T_c value has been observed (T_c = 3.0 K).[14] It seems therefore that a correlation purely based on the Mn^{II}–Cr^{III} distances (longer for most of the chiral compounds) is not correct in this case, and other factors should also be involved. In this context we have demonstrated in a recent study that the decrease in T_c observed in the 3D series of bimetallic oxalates with respect to the 2D ones can be explained by the noncollinear alignment of the chiral axis in the 3D compounds, as they produce differences in the relative orientation of the magnetic orbitals.[21] Hence, in an achiral 3D lattice, the T_c values should be intermediate between those shown by the 2D and the chiral 3D lattices if the distances between metals ions and other structural factors are kept similar. That is so because an achiral 3D lattice contains both homochiral (similar to those found in chiral 3D structures) and heterochiral (similar to those found in 2D structures) pairs of neighbouring magnetic ions. Preliminary results in a chiral 3D analogue of **2** exhibiting a lower T_c value (4.8 K, compared to 5.2 K in **2**) confirm this point.[22]

Mössbauer spectroscopy of 1: The Mössbauer spectrum of **1** obtained at 4 K shows only two well-defined peaks and may be fitted with a quadrupole doublet with isomer shift (IS) and quadrupole splitting (QS) typical of LS Fe^{III} (see Figure 11).[20a,23] Up to 160 K there is no change in the shape of the Mössbauer spectra. At 165 K, a very small absorption is observed between both peaks of the LS Fe^{III} doublet. This absorption increases as the temperature increases and may be fitted with two broad peaks with IS and QS typical for HS Fe^{III}.[20a,23] The coexistence of LS and HS Fe^{III} above 165K, as well as the increase in

the relative areas (*I*) of the HS Fe^{III} with increasing temperature, agree with magnetization data.

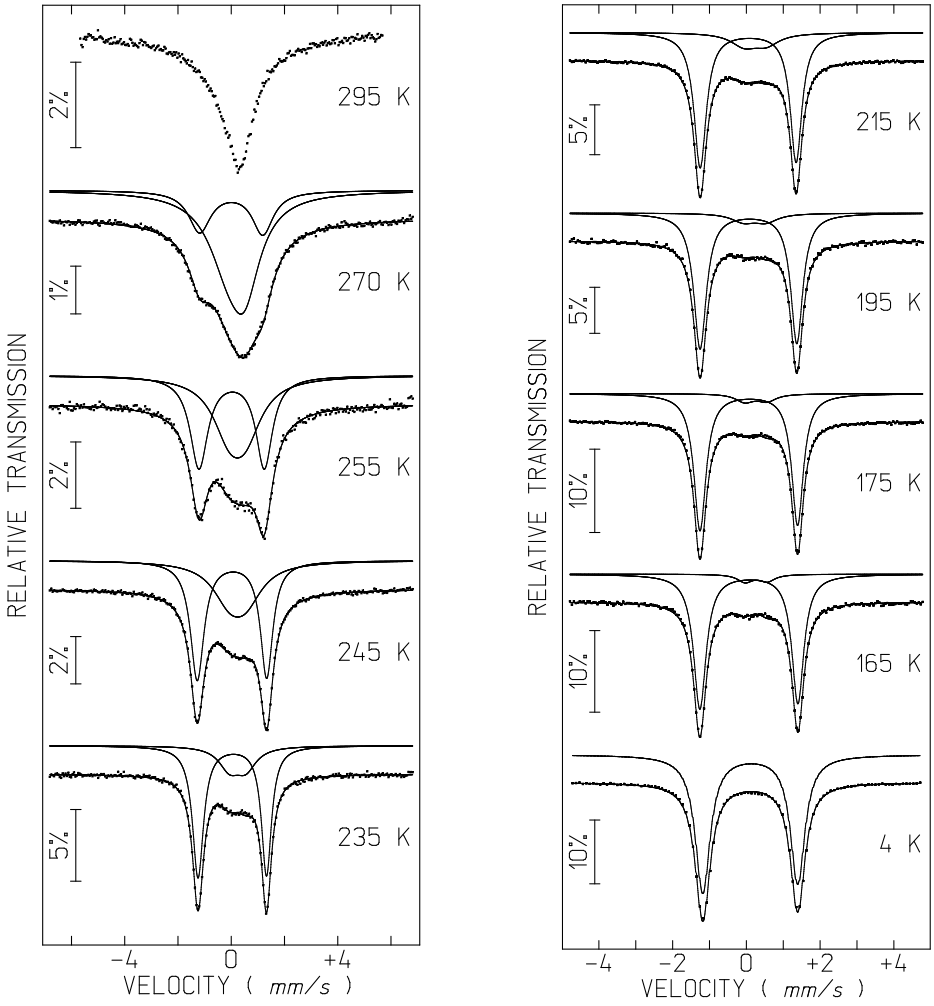

Figure 11. Mössbauer spectra of **1** taken at different temperatures. The lines over the experimental points are the sum of two doublets corresponding to HS and LS Fe^{III}. The estimated parameters for these doublets are collected in Table 1SS.

The HS Fe^{III} absorption peaks significantly broaden with increasing temperature and above 235K the same is observed for LS Fe^{III} peaks. At 255K the LS Fe^{III} peaks, although quite broad, are still resolved, but at 270K and above this is no longer the case. Such behavior of the spectra may be understood if a dynamic $^2T \leftrightarrow {}^6A$ spin interconversion occurs and the spin state lifetimes are comparable to the Mössbauer time scale, 10^{-7} s^{-1}.[23c] Up to 255 K, since the HS and LS signals are distinct we may infer that the spin-state interconversion rate is still slow relative to the Mossbauer timescale. At 270 K signals for the HS and LS species strongly overlap, and at 295 K it is not possible to distinguish them, although magnetic susceptibility data indicate that an appreciable LS population is still present at this temperature.

The estimated HS Fe^{III} fractions from Mössbauer and magnetization data are in good agreement up to 270 K. Between 165 and 255 K the LS fraction deduced from magnetic susceptibility is slightly lower than the corresponding relative areas (*I*) estimated from the Mössbauer spectra (see Table 1SS). There are many effects that may contribute to differences between the values estimated from both techniques. In general, due to the shorter and stronger Fe-ligand chemical bonds in the LS Fe^{III} molecules, the recoilless fraction of these Fe^{III} species is higher than that of the HS Fe^{III}, particularly above 80 K. Consequently the estimated *I* for LS Fe^{III} may be higher than the actual fraction. Broad peaks in the spectra of compound **1** also lead to higher uncertainties in the estimated *I*. Moreover, the fraction of HS Fe^{III} deduced from magnetic susceptibility data may be overestimated, particularly at lower temperatures, due to the ferromagnetic coupling between Mn^{II} and Cr^{III} neighbours. It should also be noticed that the ferromagnetic ordering that occurs in the oxalate layer, detected by magnetization data, has no effect in the Mössbauer spectra. The LS Fe^{III} remains paramagnetic below T_c.

Mössbauer spectroscopy of 2: In the Mössbauer spectra of **2**, two contributions are observed in the temperature range 2.2 - 297 K (see Figure 12). One is a quadrupole doublet with estimated parameters typical of LS Fe^{III}. The other one consists of an unresolved absorption centred at IS ≈ 0.34 (297K) - 0.45 mm/s (4K). This contribution

gradually broadens as the temperature decreases. At 10 K, the maxima of four peaks belonging to a sextet appears on the absorption band. This sextet is clearly observed at 4 K with an estimated magnetic hyperfine field B_{hf} ≈ 51 T, the corresponding peaks sharpening down to 2.2 K (B_{hf} ≈ 52 T). The estimated IS and B_{hf} for this contribution are typical of HS Fe^{III}.

Broadening of the HS Fe^{III} peaks was also observed in $[Fe(acac)_2trien]BPh_4$ and $[Fe(acac)_2trien]PF_6$[23a] (acac = acetylacetonate), and has been attributed to dynamic effects in the time scale 10^{-6} - 10^{-8} s, the order of magnitude of the lifetime of the Mössbauer excited nuclear state.[23] These effects may be either related to the lifetimes of the electronic S = 1/2 and S = 5/2 states in the temperature range in which both states coexist, or to fluctuations of the directions of the Fe magnetic moments, μ_{Fe}, with a frequency along the order of 10^7 s^{-1}. When the spin-state interconversion between the HS and LS states is comparable or faster than the reciprocal of the Mössbauer time window, the corresponding doublets are expected to fuse into a single one with increasing temperature[23c] as observed for compound **1**. Since both LS and HS Fe^{III} contributions are separately observed in the spectra of compound **2**, the fluctuations between spin states (frequencies < 10^7 s^{-1}) are slow compared to the Mossbauer timescale at all measured temperatures. Therefore the HS Fe^{III} absorption broadening is only related to slow fluctuations of the magnetic hyperfine interaction caused by the slow relaxation of μ_{Fe} directions.

A sextet is observed when the frequency of fluctuation of the μ_{Fe} directions is lower than 10^7 s^{-1}.[24] This is the case when μ_{Fe} are magnetically ordered. However, such low frequencies may also be observed in the case of paramagnetic Fe atoms with slow μ_{Fe} relaxation. For compound **2** one should be cautious since no sudden freezing of the μ_{Fe} in the $[Fe(sal_2\text{-trien})]^+$ occurs at the magnetic ordering temperature of the $[MnCr(ox)_3]^-$ layers. Instead, a slow paramagnetic relaxation frequency of 10^7 - 10^9 s^{-1} is already observed at 170 K and it slows down gradually as the temperature decreases.

Furthermore, no effect of the ferromagnetic ordering is observed in the LS Fe^{III} contribution as in the case of compound **1**.

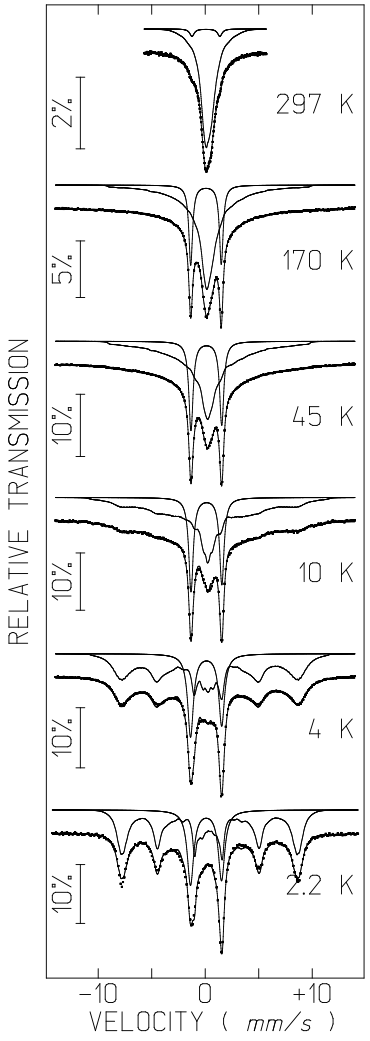

Figure 12. Mössbauer spectra of **2** taken at different temperatures. The lines over the experimental points are the sum of a doublet and a distribution of B_{hf} corresponding to LS and HS Fe^{III}. The estimated parameters for these doublets are collected in Table 2SS.

The LS Fe^{III} contributions to the spectra are well defined quadrupole doublets within the 297 - 2.2 K temperature range. This means that, as usual, slow relaxation of μ_{Fe} is only observed for HS Fe^{III} and not for LS Fe^{III}. In fact HS Fe^{III}, in the electronic ^6S state, is characterized by vanishing orbital momentum. The only relaxation mechanism available in this case is spin-spin (i.e., energy transfer may only occur between interacting spins). A sizeable orbital moment is, however, expected for LS Fe^{III}, and the corresponding spins may interact by means of spin-orbit and orbital-phonon coupling with the phonons, the so called spin-lattice relaxation mechanism. This mechanism explains why μ_{Fe} relaxation is fast for LS Fe^{III}. By simulating the broad absorption of HS Fe^{III} with a distribution of B_{hf}, the estimated relative areas (table 2SS in the Supporting Information) suggest that the fraction of HS Fe^{III} drops from ≈ 93% at 297 K to ≈ 72% at 130K. Below this temperature it remains approximately constant (≈ 70%) down to 2.2K. At 4 and 2.2 K the distribution of B_{hf} narrows significantly and, as mentioned above, is centred at B_{hf} ≈ 51 and 52 T, respectively.

Conclusion

We have reported in this paper the first examples of molecular materials with coexistence of ferromagnetism and spin crossover. The materials are salts formed by insertion of a spin-crossover Fe^{III} cation complex into anionic coordination polymers based on bimetallic oxalate complexes. From the chemical point of view, we have shown that the use of different mixed solvents and the same templating cation, which can adopt a variable configuration in the crystalline lattice, is a suitable strategy to obtain different oxalate networks. Thus, by changing the experimental conditions, two different oxalate networks, a 2D structure in compound **1** and an unusual achiral 3D structure in compounds **2**, **3** and **4**, have been obtained with the same templating cation, $[Fe(sal_2\text{-trien})]^+$.

From the point of view of the physical properties, we have found that the magnetic properties and the Mössbauer spectroscopy of **1** indicate the coexistence of an almost complete spin crossover of 100 % of Fe^{III} ions from 300 to 160 K, and a ferromagnetic

ordering below 5.4 K in the layered magnet. In turn, **2** shows a gradual spin-crossover of 30 % of the Fe^{III} from 300 to 130 K, together with a ferromagnetic ordering in the 3D lattice below 5.2 K. The preparation of the reference compounds **3** and **4** has allowed us to study the magnetic properties of the 3D lattice alone. They have shown that, in this case, the spin-crossover phenomenon does not influence the magnetic ordering. On the other hand, the magnetic properties of **2**, **3** and **4** indicate that the ordering temperature of this achiral 3D network, T_c, is slightly higher than those observed in the chiral 3D analogues.

A very promising possibility provided by this hybrid strategy is to tune the magnetic ordering of the $Mn^{II}Cr^{III}$ oxalate network, thereby inducing the spin crossover of the intercalated spin-crossover cations by applying light or pressure. Compound **1** seems a better candidate for this purpose as it undergoes a complete spin-crossover; however, it is unexpected that the changes in structure of the intercalated compound could modify the T_c of the 2D oxalate network, as 2D oxalate networks with different interlayer separations present similar T_c values. In fact, the spin-crossover transition can be seen as an internal anisotropic pressure that may induce small structural changes in the ferromagnetic sublattice. In this sense, compound **2**, which is formed by a 3D magnetic network, is expected to be much more sensitive to the influence of this internal pressure. Unfortunately, in this case the HS state is highly favoured; therefore, the occurrence of a spin-crossover and its influence on the ferromagnetic sublattice is very limited.

We can conclude that hybrid magnets with coexistence of magnetic ordering and spin crossover can be designed using this molecular approach. Although the preparation of hybrid switchable magnets has not yet been reached, the synthetic strategy presented in this paper opens the way to the preparation of these new type of magnets. Apart from this final goal, the versatility of this method to combine two molecular sub-networks in the same compound, could give rise to new physical properties that stem from this unusual combination. This has been achieved in one of the compounds

presented in this paper. Thus, in the ordered ferromagnetic state (below 5 K) Mössbauer spectrum of compound **2** has shown the appearance of a sextet associated to HS Fe^{III}. However, this new phenomenon in $[Fe(sal_2\text{-trien})]^+$ compounds, the slow relaxation of the magnetic moment of HS Fe^{III}, is also observed at temperatures much higher than the magnetic ordering of the oxalate network. There is therefore no clear evidence of a relation between both phenomena.

Experimental Section

Synthesis: The complexes $[Fe(sal_2\text{-trien})]PF_6$ and $[In(sal_2\text{-trien})]PF_6$ were prepared according to literature methods.[23a] $Ag_3[Cr(ox)_3]$ was prepared by metathesis from the corresponding potassium salt.[25] All other materials and solvents were commercially available and used without further purification.

$[Fe^{III}(sal_2\text{-trien})][Mn^{II}Cr^{III}(ox)_3]\cdot(CH_2Cl_2)$ (1): Crystals of this compound were obtained by slow diffusion of two solutions. The first solution was prepared by adding $MnCl_2\cdot 4H_2O$ (0.053 g, 0.268 mmol) to a suspension of $Ag_3Cr(Ox)_3$ (0.114 g, 0.179 mmol) in 8 mL of methanol. The AgCl precipitate was filtered. The second solution was obtained by dissolving $[Fe(sal_2\text{-trien})]PF_6$ (0.100 g, 0.179 mmol) in 8 mL of dichloromethane. After two weeks, brown crystals were obtained.

$[Fe^{III}(sal_2\text{-trien})][Mn^{II}Cr^{III}(ox)_3]\cdot(CH_3OH)$ (2): Crystals of this compound were obtained by slow diffusion of two solutions. The first solution was prepared by adding $MnCl_2\cdot 4H_2O$ (0.053 g, 0.268 mmol) to a suspension of $Ag_3Cr(ox)_3$ (0.114 g, 0.179 mmol) in 7 mL of methanol. The AgCl precipitate was filtered. The second solution was obtained by dissolving $[Fe(sal_2\text{-trien})]PF_6$ (0.100 g, 0.179 mmol) in 7 mL of acetonitrile. After two weeks, brown crystals were obtained.

$[In^{III}(sal_2\text{-trien})][Mn^{II}Cr^{III}(ox)_3]\cdot 0.25(H_2O)\cdot 0.25(CH_3OH)\cdot 0.25(CH_3CN)$ (3): Crystals of this compound were obtained by slow diffusion of two solutions. The first solution was prepared by adding $MnCl_2\cdot 4H_2O$ (0.053 g, 0.268 mmol) to a suspension of $Ag_3Cr(Ox)_3$

(0.114 g, 0.179 mmol) in 8 mL of methanol. The AgCl precipitate was filtered. The second solution was obtained by dissolving [In(sal_2-trien)]PF_6 (0.110 g, 0.179 mmol) in 8 mL of acetonitrile. After three weeks, violet crystals were obtained.

[In^{III}(sal_2-trien)][$Mn^{II}Cr^{III}(ox)_3$]·0.5(CH_3NO_2) · 0.5(H_2O) (4): Crystals of this compound were obtained by slow difussion of two solutions. The first solution was prepared by adding $MnCl_2·4H_2O$ (0.072 g, 0.364 mmol) to a suspension of $Ag_3Cr(Ox)_3$ (0.155 g, 0.242 mmol) in 12 mL of methanol. The AgCl precipitate was filtered. The second solution was prepared by dissolving [In(sal_2-trien)]PF_6 (0.150 g, 0.242 mmol) in 12mL of nitromethane. After three weeks violet, crystals were obtained.

Structural characterisation: Single crystal X-ray data were collected at 180 K for compound **1**, 120 K for compound **2** and 150 K for compounds **3** and **4** by using a Nonius KappaCCD diffractometer equipped with a graphite-monochromated $Mo_{K\alpha}$ radiation (λ = 0.71073 Å). The Denzo and Scalepack programs were used for cell refinements and data reduction of the four compounds.[26] Crystal structures were solved by direct methods using the SIR97 program,[27] and refined against all F^2 values using the SHELXL-97 program.[28] Non-hydrogen atoms were refined anisotropically (except as noted), and hydrogen atoms were placed in calculated positions refined using idealized geometries (riding model) and assigned fixed isotropic displacement parameters. In **3**, one of the two crystallographically independent sal_2-trien ligands was modeled in two orientations in a 59.7(10): 40.3(10) ratio. Carbon, nitrogen and oxygen atoms of some of the sal_2-trien ligands could only be modeled isotropically for compounds **2** and **3**, possibly due to the flexibility of the ligand. The use of restraints and/or constraints in the refinement of the structures is documented in the corresponding CIFs. Data collection and refinement statistics are collected in Table 1. CCDC-749068 (**1**), -749069 (**2**), -749070 (**3**) and -749071 (**4**) contain the supplementary crystallographic data for this paper. These data can be obtained free of charge from The Cambridge Crystallographic Data Centre via www.ccdc.cam.ac.uk/data_request/cif.

Table 1. Crystallographic data for compounds **1**, **2**, **3** and **4**.

Compound	**1**	**2**	**3**	**4**
Empirical formula	$C_{27}H_{26}Cl_2CrFe$ MnN_4O_{14}	$C_{54}H_{56}Cr_2Fe_2$ $Mn_2N_8O_{30}$	$C_{53.5}H_{52.5}Cr_2In_2$ $Mn_2N_{8.5}O_{29}$	$C_{54}H_{48}Cr_2In_2$ $Mn_2N_{10}O_{33}$
Formula weight	864.2065	1622.6329	1722.0495	1808.5270
Crystal color	Brown	Brown	Violet	Violet
Temperature (K)	180	120	150	150
Wavelength (*Å*)	0.71073	0.71073	0.71073	0.71073
Crystal system, Z	Monoclinic, 4	Monoclinic, 4	Monoclinic, 4	Orthorombic, 4
Space group	$P2_1/c$	Cc	Cc	$Pna2_1$
a (Å)	11.6440(2)	21.9180(9)	21.5690(7)	20.4650(3)
b (Å)	31.7710(5)	14.0330(9)	14.1590(7)	21.2430(5)
c (Å)	9.5340(3)	22.4670(15)	22.7360(9)	16.2740(5)
β °	110.2370(11)	92.639(4)	91.116(2)	90
V (Å^3)	3309.30(13)	6903.0(7)	6942.2(5)	7074.9(3)
ρcalc (Mg/m^3)	1.735	1.561	1.659	1.698
μ($Mo_{K\alpha}$) (mm^{-1})	1.367	1.157	1.405	1.378
θ range (°)	1.28 to 27.48	1.72 to 21.77	1.72 to 27.45	1.38 to 27.49
Reflns collected	13485	8013	12959	15664
Independent reflns, (R_{int})	7451 (0.0471)	8006 (0.0273)	12955 (0.0617)	15664 (0.1364)
L. S. parameters/ restraints	475/0	671/2	790/36	790/1
$R1(F)$,[a] $I>2\sigma(I)$]	0.0557	0.0798	0.0710	0.0621
$wR2(F^2)$,[b] all data	0.1519	0.1435	0.1440	0.1120
$S(F^2)$,[c] all data	1.116	1.017	0.970	1.033

[a] $R1(F) = \Sigma(||F_O| - |F_C||)/\Sigma|F_O|$; [b] $wR2(F^2) = [\Sigma w(F_O^2 - F_C^2)^2/\Sigma wF_O^4]^{1/2}$; [c] $S(F^2) = [\Sigma w(F_O^2 - F_C^2)^2/(n - p)]^{1/2}$

Physical measurements. Magnetic susceptibility measurements were performed on polycrystalline samples by using a magnetometer (Quantum Design MPMS-XL-5) equipped with a SQUID sensor. Variable-temperature measurements were carried out in the temperature range 2-400 K. The AC measurements were performed in the temperature range 2-10 K at different frequencies with an oscillating magnetic field of 0.395 mT. The magnetisation and hysteresis studies were performed between 5 and –5 T and by cooling the samples at zero field. The Fe/Mn/Cr/Cl and In/Mn/Cr ratios were measured on a Philips ESEM X230 scanning electron microscope equipped with an EDAX DX-4 microsonde. Mössbauer spectra were collected in transmission mode using a conventional constant-acceleration spectrometer and a 25 mCi ^{57}Co source in a Rh matrix. The velocity scale was calibrated using α-Fe foil. The absorber was obtained by pressing powdered single crystals of **1** or **2** into a perspex holder. Low-temperature spectra were collected using a bath cryostat with the sample immersed in liquid He for measurements at 4.1 and 2.2 K, or by using flowing He gas to cool the sample above 4.1 K (temperature stability of 0.2 K). The spectra were fitted to Lorentzian lines using a non-linear least-squares method.[29] Isomer shifts (Tables 1SS and 2SS in the Supporting Information) are given relative to metallic α-Fe at room temperature.

Acknowledgements

Financial support from the European Union (MolSpinQIP and SPINMOL ERC Advanced Grrant), the Spanish Ministerio de Ciencia e Innovación (Project Consolider-Ingenio in Molecular Nanoscience, CSD2007-00010, and projects CTQ2005-09385-C03 and MAT2007-61584), and the Generalitat Valenciana (Prometeo Program) are gratefully acknowledged. The authors also thank J. M. Martínez-Agudo of the University of Valencia for assistance with the preparation and magnetic characterization of the samples.

References

[1] (a) E. Coronado, P. Day, *Chem. Rev.*, 2004, **104**, 5419; (b) E. Coronado, J. R. Galán-Mascarós, *J. Mater. Chem.*, 2005, **15**, 66.

[2] (a) H. Tamaki, Z. J. Zhong, N. Matsumoto, S. Kida, M. Koikawa, N. Achiwa, Y. Hashimoto, H. Okawa, *J. Am. Chem. Soc.*, 1992, **114**, 6974; (b) H. Tamaki, M. Mitsumi, N. Nakamura, N. Matsumoto, S. Kida, H. Okawa, S. Ijima, *Chem. Lett.*, 1992, 1975; (c) C. Mathonière, S. G. Carling, D. Yuscheng, P. Day, *J. Chem. Soc., Chem. Commun.*, 1994, 1551; (d) C. Mathonière, J. Nutall, S. G. Carling, P. Day, *Inorg. Chem.*, 1996, **35**, 1201; (e) R. Pellaux, H. W. Schmalle, R. Huber, P. Fisher, T. Hauss, B. Ouladdiaf, S. Decurtins, *Inorg. Chem.*, 1997, **36**, 2301; (f) E. Coronado, J. R. Galán-Mascarós, C. J. Gómez-García, J. M. Martínez-Agudo, E. Martínez-Ferrero, J. C. Waerenborgh, M. Almeida, *J. Solid State Chem.*, 2001, **159**, 391; (g) K. S. Min, A. L. Rhinegold, J. S. Miller, *Inorg. Chem.*, 2005, **44**, 8433; (h) E. Coronado, J. R. Galán-Mascarós, C. Martí-Gastaldo, *J. Mater. Chem.*, 200**6**, **16**, 2685.

[3] (a) M. Clemente-León, J. R. Galán-Mascarós, C. J. Gómez-García, *Chem. Commun.*, 1997, 1727; (b) E. Coronado, J. R. Galán-Mascarós, C. J. Gómez-García, J. M. Martínez-Agudo, *Adv. Mater.*, 1999, **11**, 558; (c) E. Coronado, J. R. Galán-Mascarós, C. J. Gómez-García, J. Ensling, P. Gutlich, *Chem. Eur. J.*, 2000, **6**, 552.

[4] E. Coronado, C. Giménez-Saiz, C. J. Gómez-Garcia, F. M. Romero, A. Tarazón, *J. Mater. Chem.* 2008, **18**, 929.

[5] (a) S. Bénard, P. Yu, J. P. Audière, E. Rivière, R. Clèment, J. Ghilhem, L. Tchertanov, K. Nakatami, *J. Am. Chem. Soc.*, 2000, **122**, 9444; (b) S. M. Aldoshin, N. A. Sanina, V. I. Minkin, N. A. Voloshin, V. N. Ikorskii, V. I. Ovcharenko, V. A. Smirnov, N. K. Nagaeva, *J. Mol. Struct.*, 200**7**, **826**, 6.

[6] S. Bénard, E. Rivière, P. Yu, K. Nakatami, J. F. Delouis, *Chem. Mater.*, 2001, **13**, 159.

[7] (a) E. Coronado, J. R. Galán-Mascarós, C. J. Gómez-García V. Laukhin, *Nature*, 2000, **408**, 447; (b) A. Alberola, E. Coronado, J. R. Galán-Mascarós, C. Giménez-Saiz, C. J. Gómez-García, *J. Am. Chem. Soc.*, 2003, **125**, 10774; (c) E. Coronado, J. R. Galán-Mascarós, C. J. Gómez-García, E. Martínez-Ferrero, S. Van Smaalen, *Inorg. Chem.*, 200**4**, **43**, 4808.

[8] M. Clemente-León, E. Coronado, J. C. Dias, A. Soriano-Portillo, R. D. Willett, *Inorg. Chem.*, 2008, **47**, 6458.

[9] C. Train, R. Gheorghei, V. Krstic, L. M. Chamoreau, N. S. Ovanesyan, G. L. J. A. Rikken, M. Gruselle, M. Verdaguer, *Nature Mater.*, 2008, **17**, 729.

[10] (a) F. D. Rochon, R. Melanson, M. Andruh, *Inorg. Chem.*, 1996, **35**, 6086; (b) M. Andruh, R. Melanson, C. V. Stager, F. D. Rochon, *Inorg. Chim. Acta*, **1996**, 309; (c) N. Stanica, C. V. Stager, M. Cimpoesu, M. Andruh, *Polyhedron*, 1998, **17**, 1787; (d) G. Marinescu, M. Andruh, R. Lescouëzec, M. C. Muñoz, J. Cano, F. Lloret, M. Julve, *New J. Chem.*, 2000, **24**, 527; (e) S. Triki, F. Berezovsky, J. S. Pala, E. Coronado, C. J. Gómez-García, J. M. Clemente, A. Riou, P. Molinie, *Inorg. Chem.*, 2000, **39**, 3771; (f) G. Ballester, E. Coronado, C. Giménez-Saiz, F. M. Romero, *Angew. Chem., Int. Ed.*, 2001, **40**, 792; (g) E. Coronado, C. Giménez-Saiz, J. R. Galán-Mascarós, C. J. Gómez-García, C. Ruiz-Pérez, *Eur. J. Inorg. Chem.*, 2003, 2290; (h) E. Coronado, J. R. Galán-Mascarós, C. J. Gómez-García, C. Martí-Gastaldo, *Inorg. Chem.*, 2005, **44**, 6179; (i) E. Coronado, J. R. Galán-Mascarós, C. Martí-Gastaldo, *Inorg. Chem.*, 2006, **45**, 1882; (j) E. Coronado, J. R. Galán-Mascarós, C. Martí-Gastaldo, A. Murcia-Martínez, *Dalton Trans.*, 2006, 3294; (k) H. Z. Kou, O. Sato, *Inorg. Chem.*, 2007, **46**, 9513; (l) E. Cariati, R. Macchi, D. Roberto, R. Ugo, S. Galli, N. Casati, P. Macchi, A. Sironi, L. Bogani, A. Caneschi, D. Gatteschi, *J. Am. Chem. Soc.*, 2007, **129**, 9410; (m) H. Z. Kou, J. Tao, O. Sato, *Dalton Trans.*, 2008, 3652.

[11] (a) S. Decurtins, H. W. Schmalle, P. Schneuwly, H. R. Oswald, *Inorg. Chem.*, 1993, **32**, 1888; (b) S. Decurtins, H. W. Schmalle, P. Schneuwly, J. Ensling, P. Gütlich, *J. Am. Chem. Soc.*, 1994, **116**, 9521; (c) M. Hernández-Molina, F. Lloret, C. Ruiz-Pérez, M. Julve, M. *Inorg. Chem.,* 1998, **37**, 4141; (d) E. Coronado, J. R. Galán-Mascarós, C. J. Gómez-García, J. M. Martínez-Agudo, *Inorg. Chem.*, 2001, **40**, 113; (e) F. Pointillart, C. Train, M. Gruselle, F. Villain, H. W. Schmalle, D. Talbot, P. Gredin, S. Decurtins, M. Verdaguer, *Chem. Mater.*, 2004, **16**, 832; (f) M. Clemente-León, E. Coronado, C. J. Gómez-García, A. Soriano-Portillo, A. *Inorg. Chem.*, 2006, **45**, 5653.

[12] (a) R. Andrés, M. Gruselle, B. Malézieux, M. Verdaguer, J. Vaissermann, *Inorg. Chem.*, 1999, **38**, 4637; (b) R. Andrés, M. Brissard, M. Gruselle, C. Train, J. Vaissermann, B. Malézieux, J. P. Jamet, M. Verdaguer, *Inorg. Chem.*, 2001, **40**, 4633.

[13] R. Sieber, S. Decurtins, H. Stoeckli-Evans, C. Wilson, D. Yufit, J. A. K. Howard, S. C. Capelli, A. Hauser, *Chem. Eur. J.*, 2000, **6**, 361.

[14] E. Coronado, J. R. Galán-Mascarós, M. C. Giménez-López, M. Almeida, J. C. Waerenborgh, *Polyhedron*, 2007, **26**, 1838.

[15] M. Clemente-León, E. Coronado, M. C. Giménez-López, A. Soriano-Portillo, J. C. Waerenborgh, F. S. Delgado, C. Ruiz-Pérez, *Inorg. Chem.*, 2008, **47**, 9111.

[16] C. Janiak, *J. Chem. Soc., Dalton Trans.*, 2000, 3885.

[17] R. Pritchard, S. A. Barrett, C. A. Kilner, M. A. Halcrow, *Dalton Trans.*, 2008, 3159.

[18] A. Alberola, E. Coronado, C. Giménez-Saiz, C. J. Gómez-García, F. M. Romero, A. Tarazón, *Eur. J. Inorg. Chem.*, 2005, 389.

[19] N. A. Chernova, Y. Song, P. Y. Zavalij, M. S. Wittingham, Phys. Rev. B, 2004, **70**, 144405.

[20] (a) S. Floquet, S. Salunke, M. L. Boillot, R. Clément, F. Varret, K. Boukheddaden, E. Rivière, *Chem. Mater.*, 2002, **14***,* 4164-4171; (b) S. Floquet, M. C. Muñoz, E. Rivière, R. Clément, J. P. Audière, M. L. Boillot, *New J. Chem.*, 2004, **28**, 535.

[21] R. S. Fishman, M. Clemente-León, E. Coronado, *Inorg. Chem.*, 2009, **48**, 3039.

[22] Unpublished results.

[23] (a) E. Sinn, G. Sim, E. V. Dose, M. F. Tweedle, L. J. Wilson *J. Am. Chem. Soc*., 1978, **100**, 3375; (b) Y. Maeda, N. Tsutsumi Y. Takashima, *Inorg. Chem.*, 1984, **32**, 2440; (c) M. Nihei, T. Shiga, Y. Maeda, H. Oshio, *Coord. Chem. Rev.*, 2007, **251**, 2606.

[24] N. N. Greenwood, T. C. Gibb, *Mossbauer Spectroscopy*, Chapman and Hall, Ltd. Publishers, London, 1971, pp. 72.

[25] J. C. Baylar, E. M. Jones, *Inorganic Synthesis, Vol 5,* (Ed. H. S. Booth), McGraw-Hill, New York, 1939, p. 35.

[26] Z. Otwinowski, W. Minor, *Methods in Enzymology*, *Vol 276,* (Ed. C. W. Carter Jr., R. M. Sweet), Academic Press, 1997, p. 307.

[27] A. Altomare, M. C. Burla, M. Camalli, G. L. Cascarano, C. Giacovazzo, A. Guagliardi, A. G. G. Moliterni, G. Polidori, R. Spagna, *J. Appl. Cryst*., 1999, **32**, 115.

[28] SHELXL-97: G. M. Sheldrick, University of Göttingen, Germany, 1997.

[29] J. C. Waerenborgh, M. O. Figueiredo, J. M. P. Cabral, L. C. Pereira, *J. Solid State Chem.*, 1994**, 111**, 300.

A hybrid magnet with coexistence of ferromagnetism and photoinduced Fe(III) spin-crossover

Chemical Science

Capítulo 3

Capítulo 3: A hybrid magnet with coexistence of ferromagnetism and photoinduced Fe(III) spin-crossover

The insertion of a $[Fe(sal_2\text{-trien})]^+$ complex cation into a 2D oxalate network results in a hybrid magnet with coexistence of magnetic ordering and photoinduced spin-crossover (LIESST effect) in compound $[Fe^{III}(sal_2\text{-trien})][Mn^{II}Cr^{III}(ox)_3]\cdot(CH_2Cl_2)$ (**1**). A complete photomagnetic characterization together with a detailed structural analysis of the low-spin (LS) and high-spin (HS) structures of **1** is presented in order to understand such unusual behavior. This very rare and unexpected property in a Fe^{III} spin-crossover complex, has been attributed to the strong distortion exhibited by the metastable HS state. Furthermore, **1** has shown that, in contrast to what has been previously proposed, a cooperative spin-crossover is not a necessary condition to observe LIESST effect in Fe^{III} compounds. The photo-induced spin conversion of the inserted Fe^{III} complex has shown to have a negligible influence on the cooperative magnetic behavior of the 2D oxalate network.

Introduction

Multifunctionality is one of the most appealing topics in chemical science. A rational approach to design multifunctional materials consists of building up two-network hybrid solids formed by two molecular fragments where each network furnishes distinct physical properties. If the two networks are quasi-independent, a coexistence of the two physical properties is anticipated.[1] If the two molecular networks are coupled, an interplay between their properties may be observed.[1b] Finally, if one of these two networks is physically (or chemically) responsive (i.e., if it changes its properties under the application of an external stimulus, like for example light, pressure or temperature), a switchable multifunctional material can be obtained in which the responsive network can influence the properties of the other network.[2]

Bimetallic oxalate-bridged complexes of formula $A[M^{II}M^{III}(ox)_3]$ (M^{III} = Cr, Fe, Ru, V, Mn; M^{II} = Mn, Fe, Co, Ni, Cu, Zn; A = Cation; ox = oxalate) have provided remarkable examples of these types of materials.[3] They are composed by polymeric 2D[4] or 3D[5] anionic networks, which furnish the cooperative magnetic properties (ferro- ferri- or canted antiferromagnetism), and a bulky charge-compensating molecular cation, which templates the network formation and adds a second physical property to the solid. The insertion of different cations into oxalate networks has led to compounds combining the long-range magnetic ordering from the oxalate network with paramagnetism,[6] photochromism,[7] electric conductivity,[8] proton conduction,[9] chirality[10] or very recently chirality and conductivity in the same compound.[11]

The interplay between the properties of the two molecular networks has been observed, for example, in enantiopure 2D oxalate-based magnets prepared by Train *et al.* that exhibit magneto-chiral dichroic effect and magnetisation-induced second harmonic generation.[12]

The design of switchable magnets has been less explored. A promising approach to reach this goal consists of combining the bimetallic oxalate network with spin-crossover complexes. These kinds of molecular complexes change their spin state from low-spin (LS) to high-spin (HS) configurations when submitted to an external stimulus such as temperature, light-irradiation or pressure. As this magnetic switching is accompanied by changes in the molecular size, the spin-crossover process should act as an internal pressure in the hybrid material and therefore, it might affect the long-range magnetic ordering in the extended magnetic network.

Although several compounds combining spin-crossover cations and bimetallic oxalate anion networks have been reported,[13,14] the only one showing coexistence of spin-crossover and ferromagnetism is $[Fe^{III}(sal_2\text{-trien})][Mn^{II}Cr^{III}(ox)_3]\cdot(CH_2Cl_2)$ (**1**) reported very recently by our group.[14] This compound is formed by $[Fe(sal_2\text{-trien})]^+$

cations inserted between $Mn^{II}Cr^{III}$ bimetallic oxalate layers. It presents a gradual spin crossover transition from 350 to 160 K, and a ferromagnetic ordering at 5.6 K. Furthermore, by changing the synthetic conditions a second compound of formula $[Fe^{III}(sal_2\text{-trien})][Mn^{II}Cr^{III}(ox)_3]\cdot(CH_3OH)$ (**2**) has also been obtained. This compound shows an unusual non-chiral 3D network with inserted $[Fe(sal_2\text{-trien})]^+$ cations, exhibiting a gradual spin-crossover of 30 % of the Fe(III) from 300 to 130 K, together with a ferromagnetic ordering at 5.2 K. Unfortunately, in these compounds no interplay between these two properties -spin-crossover and ferromagnetism- has been detected. This is probably due to the large difference in temperature at which the two phenomena occur. Thus, while the spin-crossover occurs at high temperatures (in the range 130-350 K), the ferromagnetic ordering occurs below 5.2-5.6 K.

A way to overcome this limitation is to take advantage of the photo-induced spin-crossover effect, also known as LIESST effect (Light-Induced Excited Spin-State Trapping).[15] This phenomenon was originally established for Fe^{II} complexes at low-temperatures (typically below 50 K).[16] In principle, the relaxation *via* a tunneling process from the HS to the LS state is much faster in Fe^{III} compounds because the changes in the metal-ligand bond lengths between the two states are significantly smaller. However, there are two examples of Fe^{III} complexes showing the LIESST effect reported by Sato *et al*.[17,18] The explanation given by these authors for such unexpected behavior is related to the large structural distortion between the LS and HS states, with the intermolecular interactions playing an important role in the relaxation behavior.[18]

In this work we will explore the possibility of using light irradiation to induce spin-crossover in these hybrid materials. We will show that the confinement of $[Fe(sal_2\text{-trien})]^+$ cations provided by the 2D bimetallic oxalate layers in **1** can also induce LIESST effect in Fe^{III} complexes. A complete photomagnetic characterization together with a detailed structural analysis of the LS and HS structures of **1** is

presented in order to understand such unusual behavior. Finally, the possibility of using this family of compounds as switching magnets will be explored.

Results

Crystal structure of 1

The syntheses, crystal structures, Mössbauer spectroscopy and magnetic properties of **1** and **2** were reported previously.[14] In this work, four crystal structures of **1** at 92, 120, 250 and 300 K were solved to study the structural changes between the LS and HS structures.[19] Furthermore, we used for comparison the structural data at 180 K from the previous work[14] and measured the unit cell of one crystal between 92 and 290 K.

The structure of **1** is formed by anionic $[MnCr(ox)_3]^-$ sheets in the *bc* plane alternating with inter-lamellar $[Fe(sal_2\text{-trien})]^+$ cations and dichloromethane solvent molecules (see Fig. 1 and Fig. 2).

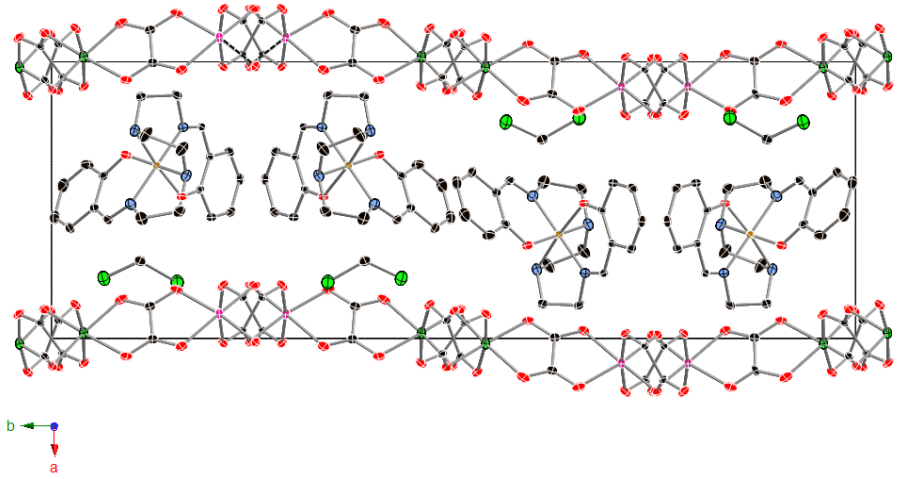

Fig. 1. Projection of the structure of **1** in the *ab* plane at 120 K. Fe (yellow), Cl (green), C (black), N (blue), O (red), Mn (pink), Cr (green). Hydrogen atoms have been omitted for clarity.

To evaluate the structural distortion between the LS and HS octahedral coordination geometries of $[Fe(sal_2\text{-trien})]^+$ in **1**, we have focused in the differences observed in the crystal structures measured at 120 and 300 K for the same crystal because they correspond roughly to the LS and HS structures.

The first difference is a shortening on metal-ligand bond lengths as expected for a spin-crossover. Thus, the average Fe–N and Fe–O bond distances in the structure solved at 300 K are respectively 2.124(4) and 1.890(4) Å, while those solved at 92 K are 1.975(2) and 1.866(2) Å. This results in average bond length differences $\Delta r_{HL,Fe\text{-}N}$ = 0.149 Å and $\Delta r_{HL,Fe\text{-}O}$ = 0.024 Å.

The second difference concerns the distortion of the octahedral coordination site, which is significantly larger for the HS state. Thus, at 300 K two of the three diagonals from the octahedron, defined by the bonds N(amine)-Fe-O(Phenoxo) (N(amine) = N2,N3), differ strongly from 180° (158.08(19) and 161.23(15)°), while the remaining one, defined by the bond N(imine)-Fe-N(imine), is 176.78(15)° (N(imine) = N1,N4). On the contrary, the coordination octahedron is much more regular at 120 K. The three diagonals are much closer to 180° with N(amine)-Fe-O(Phenoxo) angles of 173.18(10) and 173.82(9)° and N(imine)-Fe-N(imine) angle of 179.63(11)°. Different parameters have been used by several authors to quantify the distortions of $[Fe(sal_2\text{-trien})]^+$ salts, such as Σ and Θ (see Table 1).[20,21,22] As expected, angular and trigonal distortions, which are evaluated respectively by Σ and Θ, are much more important when the Fe^{III} complex is in the HS state (300 K). On the other hand, Σ and Θ parameters of the LS structures (92, 120 and 180 K) present very similar values while the structure with intermediate spin state (250 K) present intermediate values between the LS and HS structures as expected (see Table 1).

The third difference concerns the structural disorder shown by one of the ethylene groups at 300 K, which can be solved by considering two possible configurations with occupancies of 58 and 42 %. This disorder is not observed in the

structures close to the LS state at 180, 120 and 92 K but it is maintained in the structure with ~50 % of Fe^{III} in the HS state (250 K) with occupancies of 56 and 44 %. Dichloromethane molecules that occupy the holes left by the $[Fe(sal_2\text{-trien})]^+$ cations and the oxalate network, present a similar disorder at 250 and 300 K, which disappears at 92, 120 and 180 K.

Table 1. Structural parameters of **1** and **2**

	Spin state	Mean Fe-N (Å)	Mean Fe-O (Å)	Σ (º) [a]	Θ (º)[b]
1 (300 K)	~ 80 %HS	2.124(4)	1.890(4)	88	244
1 (250 K)	~ 50 %HS	2.076(4)	1.871(3)	72	217
1 (180 K)	~ 90 %LS	1.989(4)	1.866(3)	52	89
1 (120 K)	LS	1.975(2)	1.866(2)	49	87
1 (92 K)	LS	1.978(3)	1.864(2)	50	86
2 (120 K)	~ 72 %HS				
[Fe1]		2.039(15)	1.886(12)	71	190
[Fe2]		2.14(2)	1.859(14)	89	235

[a] $\Sigma = \sum_{i=1}^{12} |90 - \alpha i|$ where α_i are the12 cis-N/O-Fe-N/O angles around the iron atom. [b] $\Theta = \sum_{j=1}^{24} |60 - \theta j|$ where θj are the 24 unique N/O-Fe-N/O angles measured on the projection of two triangular faces of the octahedron along their common pseudo-threefold axis.

The crystal packing of $[Fe(sal_2\text{-trien})]^+$ complexes between the low and high temperature structures also presents some changes, which are reflected in the lattice parameters. Changes in the unit cell of **1** indicate a shortening of *a* and *b* axis from 300 to 92 K whereas the *c* axis remains almost constant with a small increase at decreasing temperature (see Fig. S1). Furthermore, the β angle decreases gradually from 300 to 92 K. All these changes are more important in the spin-crossover region from 300 to 175 K indicating that they are associated to the change of spin state of $[Fe(sal_2\text{-trien})]^+$. To understand these changes, let us first describe

the intermolecular contacts between the Fe^{III} complexes. In the present case, this packing is restricted in the *bc* plane as the Fe^{III} complexes are confined between two anionic bimetallic oxalate layers. They lie with their longer axis parallel to the oxalate layers, and they are connected through edge-to-face C–H···π and N–H···π interactions[23] (see Figs. S2 and S3) forming double chains running along the *c* axis. From the two phenoxy rings of sal_2-trien, only the one placed in the internal part of the double chain is involved in these C–H···π and N–H···π interactions with four adjacent Fe^{III} complexes belonging to the same double chain. Furthermore, the phenoxy ring belonging to different double chains present π–π stacking interactions. Finally, there are numerous short contacts with the oxalate ligands of the two neighboring layers (see Figs S4 and S5).

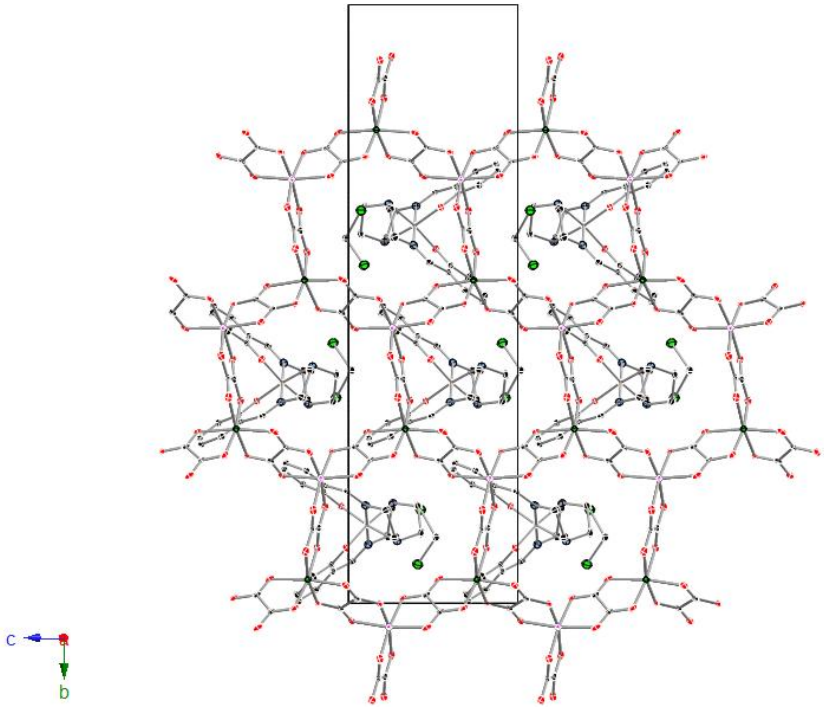

Fig. 2. Projection of the structure of **1** in the *bc* plane at 120 K. Fe (yellow), Cl (green), C (black), N (blue), O (red), Mn (pink), Cr (green). Hydrogen atoms have been omitted for clarity.

As the *a* parameter gives the separation between the oxalate layers (from 12.096(5) Å at 300 K to 11.5561(3) Å at 120 K), the shortening of *a* axis arises from the change in the spin state of the Fe^{III} complex. The most important consequence of this shortening is that at 120 K there are shorter contacts between O atoms from oxalate layers and CH groups from $[Fe(sal_2\text{-trien})]^+$ (see SI). On the other hand, the most important effect of the shortening of *b* axis (from 32.135(5) Å at 300 K to 31.6369(7) Å at 120 K) is the presence of shorter contacts at 120 K between Fe^{III} complexes belonging to the same double chains through N–H···π edge-to-face interactions and between Fe^{III} complexes belonging to different double chains through π–π stacking interactions. On the contrary, offset π–π stacking interactions appear in the structure at 300 K between C atoms of phenoxy rings belonging to different double chains (in green in Figure S2) with weaker contacts in the structure solved at 120 K (see SI.).

Change in the Magnetic properties of 1 upon irradiation.

In Fig. 3, we plot the magnetic behavior of **1** before and after light irradiation. Before irradiation χT shows a constant value of 10.0 emu·K·mol^{-1} in the high temperature range (from 400 to 350 K), which is approximately equal to the sum of the expected contributions for the isolated paramagnetic ions with ~ 80 % of Fe^{III} spin-crossover complex in a HS state. From 350 to 165 K χT decreases gradually to reach a minimum χT value at 165 K of 7.2 emu·K·mol^{-1}. This value is consistent with the Mössbauer data that indicates that Fe^{III} is 94 % LS at this temperature.[14] Therefore, in this range of temperatures a HS→LS spin conversion of the Fe^{III} complex takes place. Below 165 K, χT increases due to the Mn^{II}–Cr^{III} ferromagnetic interactions within the bimetallic oxalate layers. This increase is very sharp at lower temperatures suggesting the onset of long-range ferromagnetic ordering at 5.6 K, as confirmed by AC susceptibility and field cooled (FC) and zero-field cooled (ZFC) magnetization measurements (Figs. S6 and S7).[14]

During irradiation at 647 nm wavelength (power 8 mW cm^{-2}), at 10 K inside a SQUID cavity, an increase in χT was observed at low temperatures. Thus, after about 1.5 h the light irradiation has been switched off. The temperature has been then increased at 0.3 K min^{-1} and the magnetic susceptibility recorded. Below 50 K, the χT value after irradiation is clearly higher than the one before irradiation, while above 50 K, the two curves are superimposed (Fig. 3).

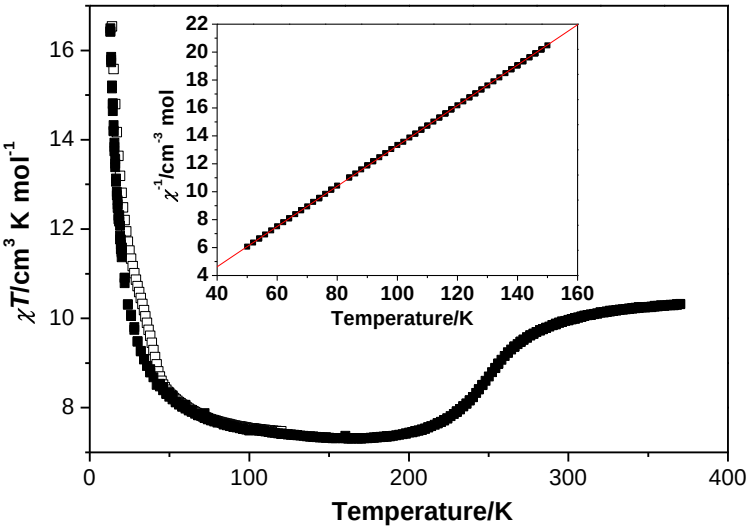

Fig. 3. Magnetic and Photo-Magnetic behavior for compound **1**. ■ Magnetic behavior measured in dark. □ Photo-magnetic behavior measured after irradiation by 647 nm wavelength laser. Inserted graph: Curie-Weiss law between 50 K and 150 K.

This result suggests that a photomagnetic effect has occurred, which can be attributed to the spin photoconversion of the $[Fe(sal_2\text{-trien})]^+$ from its LS ground state at low temperature to its HS metastable state. In order to estimate the fraction of photoconverted Fe^{III}, the magnetism of the $Mn^{II}Cr^{III}$ bimetallic layers needs to be substrated as it presents a strong underlying magnetism. To estimate the magnetism of the bimetallic layers we have taken advantage of the fact that

below the thermal spin transition (*i.e.* below 150 K) and well above the Curie temperature (*i.e.* above 50 K), the magnetic response can be satisfactorily simulated by a Curie-Weiss law (see inset in Fig. 3). Below 50 K, this simple Curie-Weiss law is unable to reproduce properly the χT values due to the vicinity of the ferromagnetic ordering. In this region, we have used the molecular field model proposed by Néel that explicitly takes into account the fact that there are two distinct sub-networks in the $Mn^{II}Cr^{III}$ layers.[24] Differences between experimental χT values and those obtained with this model are lower than 0.04 $cm^3 \cdot K \cdot mol^{-1}$ in between 25 K and 175 K. Details of this fitting are given as supporting information. In Fig. 4, we plot the temperature dependence of the fraction of HS Fe^{III} (γ_{HS}) before and after irradiation after substracting the contribution from the $Mn^{II}Cr^{III}$ oxalate network.

γ_{HS} is almost zero below 170 K in the measurements performed in the dark. Increasing the temperature above 170 K leads to a gradual increase of γ_{HS} with a maximum value of 0.86 at 370 K in agreement with Mössbauer measurements.[14] γ_{HS} from the curve obtained after irradiation reaches a maximum value of 0.37 at 25 K. When the temperature increases, a decrease in γ_{HS} is observed, and γ_{HS} reaches 0 at about 75 K. At higher temperatures γ_{HS} curve is superimposed with that recorded in the dark. The T(LIESST), estimated from the minimum of the derivative of γ_{HS} by the temperature (inset in Fig. 4), is determined to be 41 K.[25] This represents somewhat the limit of the long-lived photo-induced lifetime of the HS state. In order to get some insight into the decay of the photoinduced HS state, some kinetics have been recorded at 10 K and every 2 K between 36 and 44 K (figure 5).

At 10 K, almost no decay of the photo-induced HS state was noticed. More precisely, the decrease of the HS fraction was less than 2 % after 7 h. Fig. 5 shows the relaxation kinetics recorded between 36 and 44 K. The maximum of HS fraction at initial time, for a given kinetic is different: the higher the temperature, the lower the photoexcitation. This suggests that the kinetic process is thermally activated.

Interestingly, these relaxation curves show strong deviation from a single exponential, with a marked stretched exponential behavior, and with a fast component at earlier times and a long decay process at infinite time. For reproducing this type of curves, Hauser et al.[26] used a distribution of relaxation rates at a given temperature with a Gaussian distribution of the activation energy. Following this procedure, the relaxation curves of compound **1** can be satisfactorily fitted as illustrated by the solid lines in Fig. 5. The apparent activation energy, E_a (= 200 cm^{-1}), and the apparent preexponential factor, k_∞ (= 0.49 s^{-1}) of the activated region are calculated from the straight line of the $\ln k_{HL}(T)$ *vs*. $1/T$ plot. The standard deviation of the activation energy is 52 ± 6 cm^{-1}.

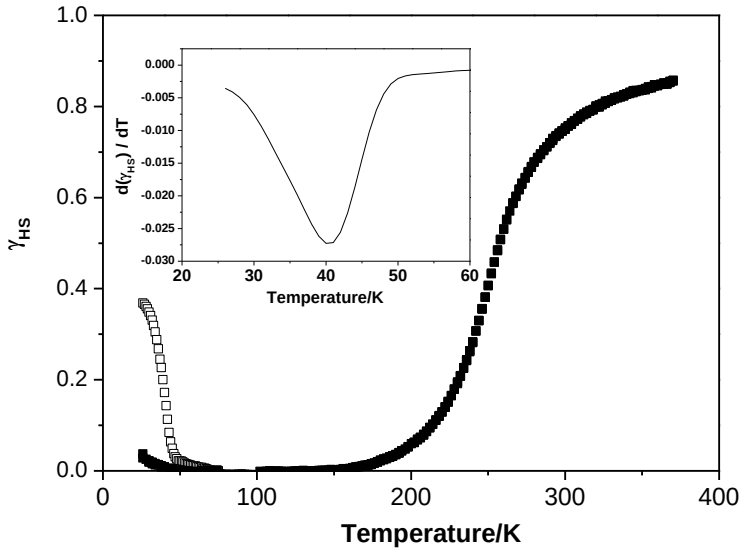

Fig. 4 Fraction of HS Fe^{III} (γ_{HS}) before (■) and after (□) irradiation). Inserted graph: χT derivative for photo-magnetism

Effect of photoexcitation on the magnetic ordering

FC and ZFC magnetization (Fig. S6) and AC susceptibility measurements (Fig. S7) have been recorded between 2 and 10 K, before and after photoirradiation of 1.5 h

at 10 K to test if the photoconversion of the Fe^{III} complex affects the Curie temperature (T_c) of the compound. We have to take into account that at 10 K the lifetime of the photoinduced HS state is very long, and consequently the HS fraction remains almost constant during the experiment. ZFC and FC magnetization measurements start to bifurcate at 5.6 K, both before and after irradiation. Similarly, AC susceptibility measurements show the appearance of an out-of-phase signal (χ'') below T_c = 5.6 K that remains almost constant upon irradiation, showing a shift to higher values by 0.1 K after photoirradiation.

Crystal structure and photomagnetism of 2

The structure of **2** was solved at 120 K.[14] It is formed by an anionic 3D polymeric oxalate-bridged bimetallic network with $[Fe(sal_2\text{-trien})]^+$ cations and methanol solvent molecules occupying the cavities.

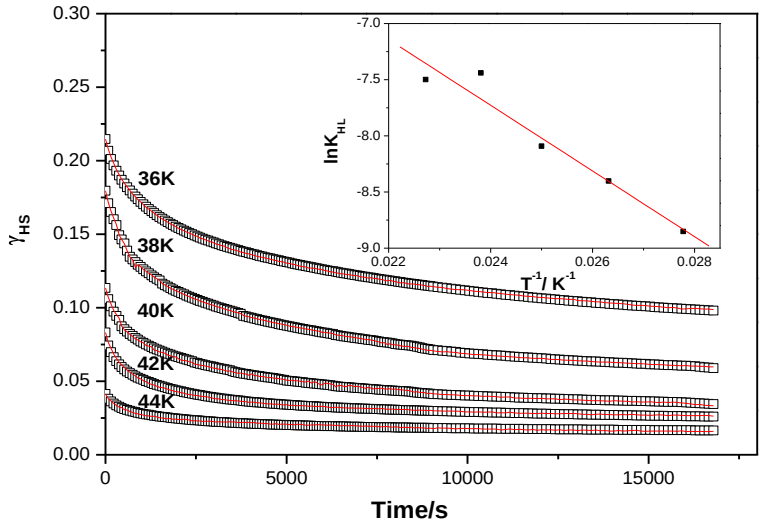

Fig. 5. Relaxation kinetics and simulation of the HS fraction *vs.* time at different temperatures. Inserted graph: $\ln k_{HL}(T)$ *vs.* $1/T$ dependence. k_{HL} corresponds to the rate constant for the HS→LS relaxation. The fitting procedure has been performed by adding a small residual HS at long time.

Magnetic measurements and Mössbauer spectroscopy[14] indicate that 100 % of Fe^{III} complexes are in the HS at room temperature and the HS $\rightarrow$ LS spin conversion of 30 % of the Fe^{III} complexes from 300 and 130 K. There are two crystallographically independent $[Fe(sal_2\text{-trien})]^+$ complexes ([Fe1] and [Fe2]). The average Fe–N and Fe–O bond distances are close to those obtained for other high-spin (HS) $[Fe(sal_2\text{-trien})]^+$ compounds (see Table 1). At lower temperatures the HS fraction remains constant and there is a ferromagnetic ordering with a T_c of 5.2 K, as usual for this type of compounds. In contrast to **1**, this compound does not present LIESST effect.

Discussion

The lifetime of the HS photoexcited state has been rationalized by Hauser,[27] on the basis of a non-adiabatic mutiphonon relaxation model. In the framework of this theory, the Metal-Ligand distance is taken as the reaction coordinate, related to only one vibrational mode, namely the completely symmetrical one. This is the so-called SCC (Single Configurational Coordinate) approach. Based on this theory, it is possible to estimate theoretically the rate constant for the HS $\rightarrow$ LS relaxation (k_{HL}) at different temperatures for the different ions that could exhibit LIESST effect such as Fe^{II}, Fe^{III} or Co^{II}.[28] The main difference between these three ions is the bond length difference between the LS and the HS states, being typically 0.2 Å for Fe^{II}, 0.13-0.16 Å for Fe^{III} and 0.09-0.12 Å for Co^{II}. This change in bond length difference is expected to directly affect the decay of the photo-induced state, being much faster for Co^{II} than for Fe^{II} and Fe^{III}. Particularly, according to SCC theory, the low-temperature (tunneling regime) lifetime of the HS state for Fe^{III} spin-crossover compounds is expected to be of the order of milliseconds, whereas it can go from seconds to months for Fe^{II} spin-crossover compounds. According to such a short lifetime, it should be impossible to observe the decay of the photoinduced state for Fe^{III} by using standard SQUID techniques. However, as mentioned above, the LIESST effect has been observed by Sato in two Fe^{III} complexes, $[Fe(pap)_2]^+$ and $[Fe(qsal)_2]^+$.[18] This author attributed such an extraordinary result to the strong

distortion of the Fe^{III} site from its octahedral geometry, which can be enhanced by the presence of strong intermolecular interactions, such as π-π stacking. Thus, when passing from the ideal octahedral site $[Fe^{II}N_6]$ to a distorted $[Fe^{III}N_4O_2]$ geometry, in addition to the completely symmetrical vibrational mode, other vibrational modes such as the bending mode should also be taken into account.[18,29] This results in a displacement between the potential walls of the HS and LS states, which is larger than that expected considering only the changes in metal-ligand distances, and could explain the long lifetime of the photogenerated HS state.

To evaluate the distortion of $[Fe(sal_2\text{-trien})]^+$ in **1**, we have focused our attention in the differences between the 120 and 300 K structures of the compound as they are close to the LS and HS structures. The structure at 120 K corresponds to the LS structure since magnetic and Mössbauer data indicate that 100 % of the Fe^{III} are in the LS state at this temperature. On the other hand, the structure at 300 K is close to the HS structure as magnetic data indicate that around 80 % of Fe^{III} are in the HS state at this temperature.[14]

The first difference between the two structures is a shortening in the Fe-N and Fe-O bond lenghts as expected for a spin-crossover. Thus, the average bond length differences are $\Delta r_{HL,Fe\text{-}N}$ = 0.149 Å and $\Delta r_{HL,Fe\text{-}O}$ = 0.024 Å. If we take into account that at 300 K about 20 % of Fe^{III} remains in the LS state, we could expect $\Delta r_{HL,Fe\text{-}N}$ = 0.186 Å and $\Delta r_{HL,Fe\text{-}O}$ = 0.03 Å values between the LS and HS states of this compound. These values are very close to those exhibited by the two Fe^{III} compounds known to date presenting LIESST effect (in $[Fe(pap)_2]X$, $\Delta r_{HL,Fe\text{-}N}$ = 0.19 Å and $\Delta r_{HL,Fe\text{-}O}$ = 0.05 Å, and in $[Fe(qsal)_2]Y$, $\Delta r_{HL,Fe\text{-}N}$ = 0.18 Å and $\Delta r_{HL,Fe\text{-}O}$ = 0.02 Å).[18] Notice that these values are also similar to those reported for $[Fe(sal_2\text{-trien})][Ni(dmit)_2]$ ($\Delta r_{HL,Fe\text{-}N}$ = 0.188 Å and $\Delta r_{HL,Fe\text{-}O}$ = 0.036 Å)[30] which is the only other $[Fe(sal_2\text{-trien})]^+$ salt reported so far for which both the LS and HS structural data are available.[31] This salt is the first example of $[Fe(sal_2\text{-trien})]^+$ salt presenting a strong cooperative transition and wide hysteresis but no LIESST effect has been reported for this compound.

Furthermore, the synthesis of this compound presents serious problems of reproducibility that could limit further studies.[32]

A second set of parameters accounting for angular and trigonal distortions from the ideal octahedron is provided by Σ and Θ parameters. However, Σ and Θ values of the 300 and 120 K structrures lie in the range of those found for other HS and LS $[Fe(sal_2\text{-trien})]^+$ compounds.[31] Therefore, it is difficult to get some conclusions from these parameters.

The third difference concerns the changes in selected bond angles (*cis* and *trans* N/O-Fe-N/O bond angles) between the LS and HS structures ($\Delta\measuredangle_{HL}$). In **1**, a value of $\Delta\measuredangle_{HL}$ = 93.64° is obtained. This value is intermediate between that of $[Fe(pap)_2]^+$ ($\Delta\measuredangle_{HL}$ =136.06°), for which LIESST effect is observed, and that of $[Fe(acpa)_2]^+$ ($\Delta\measuredangle_{HL}$ = 74.32°), which does not present LIESST effect, but a larger value could be expected taking into account that there are still around 20 % of Fe^{III} in the LS state in the structure solved at 300 K. Therefore, we can conclude that, in analogy with $[Fe(pap)_2]^+$, the strong distortion from the ideal octahedral geometry in **1** is at the origin of the LIESST effect.

In turn, a sharp structural difference between **1** and $[Fe(pap)_2]^+$ concerns the nature and dimensionality of the intermolecular interactions. Thus, while in $[Fe(pap)_2]^+$ the π–π 2D stacking between pyridine and phenyl rings seems to enhance the structural distortion of the LIESST complex, in **1**, π–π interactions between pairs of $[Fe(sal_2\text{-trien})]^+$ complexes belonging to different chains coexist with edge-to-face CH···π and NH···π interactions. As a consequence, **1** shows a gradual spin-crossover with no hysteresis, while $[Fe(pap)_2]^+$ presents a cooperative spin-crossover with hysteresis. Furthermore, the decay of the photo-induced HS state of the two compounds follows a different relaxation kinetics. Whereas the time dependence of the HS fraction after photoexcitation of $[Fe(pap)_2]^+$ can be fitted to a sigmoidal-type curve as a result of self-acceleration of the HS → LS

relaxation due to cooperative effects, the one from **1** can be fitted to a multiexponential curve with a fast component at earlier times and a long decay process at infinite times. The broad distribution of activation energies is the cause of this type of relaxation kinetics. These curves are typical of non-cooperative systems that rarely present a single-exponential behavior. It appears in poorly crystalline solids and in some cases it has been related to the presence of disorder in the structure in compounds presenting a cooperative spin-crossover.[33] Hence, it could have some relation with the disorder observed in the structure of **1** even it is only observed at high temperature. In any case, we can conclude that both the magnetic behavior and the decay of the photo-induced HS state in **1**, indicate that in contrast to the previous examples, cooperativity it is not a necessary condition to have LIESST effect in Fe^{III} compounds.

A second structural difference of **1** with respect to the other Fe^{III} compounds exhibiting LIESST effect is the presence of an anionic extended network (the bimetallic oxalate network) instead of a discrete small counterion. This rigid network could play a similar role in the stabilisation of the metastable HS state of **1** to that played by the strong π–π intermolecular interactions in $[Fe(pap)_2]^+$. In favour of this hypothesis are the numerous short contacts between the $[Fe(sal_2\text{-trien})]^+$ cations with the oxalate ligands, which are different in the low and high-temperature structures (see SI). Maybe the interactions with the oxalate network enhance the distortion of the LIESST complex but, at the same time, they prevent a cooperative spin-crossover since they restrict the structural dimensionality to 2. Photomagnetic measurements on salts of $[Fe(sal_2\text{-trien})]^+$ and derivatives in different anionic environments are needed to clarify this point. This work is in progress in our group.[13d]

The question remains why no LIESST has been observed on the remaining 30 % HS fraction at 10 K for compound **2**. Further work is necessary to answer to such question. For now, it remains unclear if the absence of LIESST is linked to: (a) a

distortion effect and/ or (b) the difference of rigidity between 2D and 3D networks and/or (c) the small amount of Fe^{III} that can be converted. As far as the distortion (a) is concerned, it would be helpful to compare the geometries of the $[Fe(sal_2\text{-trien})]^+$ complexes in the HS and the LS state. Unfortunately, this is not possible as the HS fraction remains of 70 % at temperature as low as 10 K. The influence of the rigidity of the network (b) can be seen in the fact that the contraction of the interlayer distance that follows the spin-crossover in **1** cannot be present in **2** that present a more isotropic 3D network. Finally, the low amount of low spin fraction at low temperature (c) makes it difficult to observe the possible small increase of magnetic response under light, as it will be difficult to distinguish this increase from the important magnetic signal of the oxalate network. New compounds are to be synthesized, 2D and 3D, in order to have more data to draw conclusions.

Conclusions

In this work we have shown that the insertion of a $[Fe(sal_2\text{-trien})]^+$ complex cation into a 2D oxalate network results in a hybrid magnet with coexistence of magnetic ordering and photoinduced spin-crossover in compound **1**. The use of a molecular approach has led to the coexistence of two properties -ferromagnetism and photo-induced spin crossover- that normally do not appear together in the same compound. This could open the way to prepare switching magnets. Still, in the present case the photo-induced spin conversion of the inserted Fe^{III} complex has shown to have a negligible influence on the cooperative magnetic behavior of the 2D oxalate network. This is not an unexpected result, as 2D oxalate networks with very different interlayer separations present similar T_c values. In this sense, hybrid compounds formed by insertion of these spin-crossover cations into a 3D oxalate network are expected to be more suitable, as this magnetic network has shown to be much more sensitive to the influence of an internal pressure. Unfortunately, the compound **2** obtained by insertion of a $[Fe(sal_2\text{-trien})]^+$ cation into a 3D oxalate network does not present LIESST effect.

Another remarkable result has been the observation of LIESST effect in **1**. This very rare and unexpected property in a Fe^{III} spin-crossover complex, has been attributed to the strong distortion exhibited by the metastable HS state. However, **1** has shown that, in contrast to what has been previously proposed, a cooperative spin-crossover is not a necessary condition to observe LIESST effect in Fe^{III} compounds. The presence of an extended anion network able to establish strong intermolecular interactions with the spin-crossover cation could also enhance this distortion. If this was true, the confinment of spin-crossover cations into extended networks could be a suitable strategy to induce LIESST effect on other Fe^{III} cations, or to improve LIESST properties in Fe^{II} complexes.

Finally, the discovery that $[Fe(sal_2\text{-trien})]^+$ complexes can present LIESST effect opens the way to the use of this compound in the preparation of new multifunctional switchable compounds with other properties different from the magnetic ones. An interesting possibility could be the switching of the conductivity in $[Fe(sal_2\text{-trien})]^+$ salts of $[Ni(dmit)_2]$ anions already reported in the literature.[34]

Acknowledgments

Financial support from the EU (SPINMOL ERC Advanced Grant to EC), the Spanish Ministerio de Ciencia e Innovación (Project Consolider-Ingenio in Molecular Nanoscience and projects MAT2007-61584 and CTQ-2008-06720) and the Generalitat Valenciana (Prometeo Program) are gratefully acknowledged.

Notes and references

[1] (a) E. Coronado and P. Day, *Chem. Rev.,* 2004, **104**, 5419; (b) E. Coronado, C. Martí-Gastaldo, E. Navarro-Moratalla, A. Ribera, S. J. Blundell and P. J. Baker, *Nat. Chem.,* 2010, **2**, 1031.

[2] (a) E. Coronado, M. C. Giménez-López, G. Levchenko, F. M. Romero, V. García-Baonza, A. Milner and M. Paz-Pasternak, *J. Am. Chem. Soc.,* 2005, **127**, 4580; (b) E. Coronado, M. C. Giménez-López, T. Korzeniak, G. Levchenko, F. M. Romero, A. Segura, V. García-Baonza, J. C. Cezar, F. M. F. De Groot, A. Milner and M. Paz-Pasternak, *J. Am. Chem. Soc.,* 2008, **130**, 15519.

[3] M. Clemente-León, E. Coronado, C.Martí-Gastaldo and F. M. Romero, *Chem. Soc. Rev.,* 2011, **40**, 473.

[4] (a) H. Tamaki, Z. J. Zhong, N. Matsumoto, S. Kida, M. Koikawa, N. Achiwa, Y. Hashimoto and H. Okawa, *J. Am. Chem. Soc.,* 1992, **114**, 6974; (b) H. Tamaki, M. Mitsumi, N. Nakamura, N. Matsumoto, S. Kida, H. Okawa and S. Ijima, *Chem. Lett.,* 1992, 1975; (c) C. Mathonière, S. G. Carling, D. Yuscheng and P. Day, *J. Chem. Soc., Chem. Commun.,* 1994, 1551; (d) C. Mathonière, J. Nutall, S. G. Carling and P. Day, *Inorg. Chem.,* 1996, **35**, 1201; (e) R. Pellaux, H. W. Schmalle, R. Huber, P. Fisher, T. Hauss, B. Ouladdiaf and S. Decurtins, *Inorg. Chem.,* 1997, **36**, 2301; (f) E. Coronado, J. R. Galán-Mascarós, C. J. Gómez-García, J. M. Martínez-Agudo, E. Martínez-Ferrero, J. C. Waerenborgh and M. Almeida, *J. Solid State Chem.,* 2001, **159**, 391; (g) K. S. Min, A. L. Rhinegold and J. S. Miller, *Inorg., Chem.,* 2005, **44**, 8433; (h) E. Coronado, J. R. Galán-Mascarós and C. Martí-Gastaldo*, J. Mater. Chem.,* 2006, **16**, 2685.

[5] (a) S. Decurtins, H. W. Schmalle, P. Schneuwly and H. R. Oswald, *Inorg. Chem.,* 1993, **32**, 1888; (b) S. Decurtins, H. W. Schmalle, P. Schneuwly, J. Ensling and P. Gütlich, *J. Am. Chem. Soc.,* 1994, **116**, 9521; (c) M. Hernández-Molina, F. Lloret, C. Ruiz-Pérez and M. Julve, *Inorg. Chem.,* 1998, **37**, 4141; (d) E. Coronado, J. R. Galán-Mascarós, C. J. Gómez-García and J. M. Martínez-Agudo, *Inorg. Chem.,* 2001, **40**, 113; (e) F. Pointillart, C. Train, M. Gruselle, F. Villain, H. W. Schmalle, D. Talbot, P. Gredin, S. Decurtins and M. Verdaguer, *Chem. Mater.,* 2004, **16**, 832; (f) M. Clemente-León, E. Coronado, C. J. Gómez-García and A. Soriano-Portillo, *Inorg. Chem.,* 2006, **45**, 5653.

[6] (a) M. Clemente-León, J. R. Galán-Mascarós and C. J. Gómez-García, *Chem. Commun.,* 1997, 1727; (b) E. Coronado, J. R. Galán-Mascarós, C. J. Gómez-García and J. M. Martínez-Agudo, *Adv. Mater.,* 1999, **11**, 558; (c) E. Coronado, J. R. Galán-Mascarós, C. J. Gómez-García, J. Ensling and P. Gutlich, *Chem. Eur. J.,* 2000, **6**, 552.

[7] (a) S. Bénard, P. Yu, J. P. Audière, E. Rivière, R. Clèment, J. Ghilhem, L. Tchertanov and K. Nakatami, *J. Am. Chem. Soc.,* 2000, **122**, 9444; (b) S. M. Aldoshin, N. A. Sanina, V. I.

Minkin, N. A. Voloshin, V. N. Ikorskii, V. I. Ovcharenko, V. A. Smirnov and N. K. Nagaeva, *J. Mol. Struct.,* 2007, **826**, 6.

[8] (a) E. Coronado, J. R. Galán-Mascarós, C. J. Gómez-García and V. Laukhin, *Nature*, 2000, **408**, 447; (b) A. Alberola, E. Coronado, J. R. Galán-Mascarós, C. Giménez-Saiz and C. J. Gómez-García, *J. Am. Chem. Soc.,* 2003, **125**, 10774; (c) E. Coronado, J. R. Galán-Mascarós, C. J. Gómez-García, E. Martínez-Ferrero and S. Van Smaalen, *Inorg. Chem.*, 2004, **43**, 4808.

[9] H. Okawa, A. Shigematsu, M. Sadakiyo, T. Miyagawa, K. Yoneda, M. Ohba and H. Kitagawa, *J. Am. Chem. Soc.*, 2009, **131**, 13516.

[10] (a) R. Andrés, M. Gruselle, B. Malézieux, M. Verdaguer and J. Vaissermann, *Inorg. Chem*., 1999, **38**, 4637; (b) R. Andrés, M. Brissard, M. Gruselle, C. Train, J. Vaissermann, B. Malézieux, J. P. Jamet and M. Verdaguer, *Inorg. Chem.*, 2001, **40**, 4633; (c) M. Clemente-León, E. Coronado, J. C. Dias, A. Soriano-Portillo and R. D. Willett, *Inorg. Chem.,* 2008, **47**, 6458.

[11] J. R. Galán-Mascarós, E. Coronado, P. A. Goddard, J. Singleton, A. I. Coldea, J. D. Wallis, S. J. Coles and A. Alberola, *J. Am. Chem. Soc.,* 2010, **132**, 9271.

[12] (a) C. Train, R. Gheorghe, V. Krstic, L. M. Chamoreau, N. S. Ovanesyan, G. L. J. A. Rikken, M. Gruselle and M. Verdaguer, *Nat. Mater.*, 2008, **17**, 729; (b) C. Train, T. Nuida, R. Gheorghe, M. Gruselle and S. Ohkoshi, *J. Am. Chem. Soc.,* 2009, **131**, 16838.

[13] (a) R. Sieber, S. Decurtins, H. Stoeckli-Evans, C. Wilson, D. Yufit, J. A. K. Howard, S. C. Capelli and A. Hauser, *Chem. Eur. J.,* 2000, **6**, 361; (b) E. Coronado, J. R. Galán-Mascarós, M. C. Giménez-López, M. Almeida and J. C. Waerenborgh, *Polyhedron,* 2007, **26**, 1838; (c) M. Clemente-León, E. Coronado, M. C. Giménez-López, A. Soriano-Portillo, J. C. Waerenborgh, F. S. Delgado and C. Ruiz-Pérez, *Inorg. Chem.,* 2008, **47**, 9111; (d) M. Clemente-León, E. Coronado and M. López-Jordà, *Dalton Trans.,* 2010, **39**, 4903.

[14] M. Clemente-León, E. Coronado, M. López-Jordà, G. Mínguez Espallargas, A. Soriano-Portillo and J. C. Waerenborgh, *Chem. Eur. J.,* 2010, **16**, 2207.

[15] S. Decurtins, P. Gütlich, K. M. Hasselbach, A. Hauser and H. Spiering, *Inorg. Chem.,* 1985, **24**, 2174.

[16] C. Enachescu, A. Hauser, J.-J. Girerd and M.-L. Boillot, *Chem. Phys. Chem.,* 2006, **7**, 1127.

[17] (a) S. Hayami, Z.-Z. Gu, M. Shiro, Y. Einaga, A. Fujishima and O. Sato, *J. Am. Chem. Soc.,* 2000, **122**, 7126; (b) G. Juhász, S. Hayami, O. Sato and Y. Maeda, *Chem. Phys. Lett.,* 2002, **364**, 164.

[18] S. Hayami, K. Hiki, T. Kawahara, Y. Maeda, D. Urakami, K. Inoue, M. Ohama, S. Kawata and O. Sato, *Chem. Eur. J.,* 2009, **15**, 3497.

[19] Crystal data for **1** at 300 K: $C_{27}H_{26}Cl_2CrFeMnN_4O_{14}$, M = 864.21, monoclinic, space group $P2_1/c$ (no. 14), a = 12.096(5) Å, b = 32.135(5) Å, c = 9.467(5) Å, β = 111.981(5)°, V = 3412(2) Å^3, Z = 4, μ = 1.325 mm^{-1}, F(000) = 1748, T = 300(2) K, 44282 reflections measured, 11352 unique (R_{int} = 0.0589), R1 = 0.0635, wR2 = 0.1689 for I > 2σ(I). CCDC 807173. Crystal data for **1** at 250 K: $C_{27}H_{26}Cl_2CrFeMnN_4O_{14}$, M = 864.21, monoclinic, space group $P2_1/c$ (no. 14), a = 11.9215(15)Å, b = 31.910(3)Å, c = 9.4841(11)Å, β = 111.535(13)°, V = 3356.1(6)Å3, Z = 4, μ = 1.348 mm-1, F(000) = 1748, T = 250(2) K, 43973 reflections measured, 11354 unique (R_{int} =0.0590), R1 = 0.0530, wR2 = 0.1240 for I > 2σ(I). CCDC 813345. Crystal data for **1** at 120 K: $C_{27}H_{26}Cl_2CrFeMnN_4O_{14}$, M = 864.21, monoclinic, space group $P2_1/c$ (no. 14), a = 11.5561(3) Å, b = 31.6369(7) Å, c = 9.5457(3) Å, β = 109.984(3)°, V = 3279.77(15) Å^3, Z = 4, μ = 1.379 mm^{-1}, F(000) = 1748, T = 120(2) K, 26791 reflections measured, 10705 unique (R_{int} = 0.0302), R1 = 0.0477, wR2 = 0.0951 for I > 2σ(I). CCDC 807172. Crystal data for **1** at 92 K: $C_{27}H_{26}Cl_2CrFeMnN_4O_{14}$, M = 864.21, monoclinic, space group $P2_1$/c (no. 14), a = 11.5602(4) Å, b = 31.6268(12) Å, c = 9.5237(4) Å, β = 110.199(4)°, V = 3267.8(2) Å^3, Z = 4, μ = 1.379 mm^{-1}, F(000) = 1748, T = 92(2) K, 29715 reflections measured, 10846 unique (R_{int} = 0.0557), R1 = 0.0546, wR2 = 0.1230 for I > 2σ(I). CCDC 807172. Crystal data of **1** at 180 K have been taken from reference 14.

[20] P. Guionneau, M. Marchivie, G. Bravic and J.-F. Létard, D. Chasseau, *Top. Curr. Chem.,* **2004**, *234*, 97.

[21] J. K. McCusker, A. L. Rheingold and D. N. Hendrickson, *Inorg. Chem.,* **1996**, *35*, 2100.

[22] M. Marchivie, P. Guionneau, J.-F. Létard and D. Chasseau, *Acta Crystallogr., Sect. B: Struct. Sci.,* 2005*,* **61**, 25.

[23] C. Janiak, J. Chem. Soc. Dalton Trans., 2000, 3885.

[24] L. Néel, *Ann. Phys.,* 1948, **3**, 137.

[25] J.-F. Létard, *J. Mater. Chem.,* 2006, **16**, 2550.

[26] A. Hauser, J. Adler and P. Gütlich, *Chem. Phys. Lett.,* 1988, **152**, 468.

[27] A. Hauser, *J. Chem. Phys.,* 1991*,* **94**, 2741.

[28] A. Hauser *Top. Curr. Chem.,* 2004, **234**, 155

[29] S. Schenker, A. Hauser and R. M. Dyson, *Inorg. Chem.,* 1996, **35**, 4676.

[30] S. Dorbes, L. Valade, J. A. Real and C. Faulmann, *Chem. Commun.,* 2005, 69.

[31] R. Pritchard, S. A. Barrett, C. A. Kilner and M. A. Halcrow, *Dalton Trans.,* 2008, 3159.

[32] C. Faulmann, P. A. Szilágyi, K. Jacob, J. Chahine, L. Valade, *New J. Chem.,* 2009, **33**, 1268.

[33] V. Mishra, R. Mukherjee, J. Linares, C. Balde, C. Desplanches, J.-F. Létard, E. Collet, L. Toupet, M. Castro, F. Varret, *Inorg. Chem.,* 2008, **47**, 7577.

[34] C. Faulmann, S. Dorbes, J. A. Real and L. Valade, *J. Low. Temp. Phys.,* 2006, **142**, 261.

Stimuli responsive hybrid magnets: Tuning the photoinduced spin-crossover in Fe(III) complexes inserted into layered magnets

JACS
JOURNAL OF THE AMERICAN CHEMICAL SOCIETY

Capítulo 4

Capítulo 4: Stimuli responsive hybrid magnets: Tuning the photoinduced spin-crossover in Fe(III) complexes inserted into layered magnets

Abstract

The insertion of a $[Fe(sal_2\text{-trien})]^+$ complex cation into a 2D oxalate network in the presence of different solvents results in a family of hybrids magnets with coexistence of magnetic ordering and photoinduced spin-crossover (LIESST effect) in compounds, $[Fe^{III}(sal_2\text{-trien})][Mn^{II}Cr^{III}(ox)_3]\cdot CHCl_3$ (**1·CHCl$_3$**), $[Fe^{III}(sal_2\text{-trien})][Mn^{II}Cr^{III}(ox)_3]\cdot CHBr_3$ (**1·CHBr$_3$**) and $[Fe^{III}(sal_2\text{-trien})][Mn^{II}Cr^{III}(ox)_3]\cdot CH_2Br_2$ (**1·CH$_2$Br$_2$**). The three compounds crystallize in a 2D honeycomb anionic layer formed by Mn^{II} and Cr^{III} ions linked through oxalate ligands and a layer of $[Fe(sal_2\text{-trien})]^+$ complexes and solvent molecules ($CHCl_3$, $CHBr_3$, or CH_2Br_2) intercalated between the 2D oxalate network. The magnetic properties and Mössbauer spectroscopy indicate that they undergo a long-range ferromagnetic ordering at 5.6 K and a spin crossover of the intercalated $[Fe(sal_2\text{-trien})]^+$ complexes at different $T_{1/2}$. The three compounds present a LIESST effect with a relaxation temperature T_{LIESST} inversely proportional to $T_{1/2}$. The isostructural paramagnetic compound, $[Fe^{III}(sal_2\text{-trien})][Zn^{II}Cr^{III}(ox)_3]\cdot CH_2Cl_2$ (**2·CH$_2$Cl$_2$**) was also prepared. This compound presents a partial spin crossover of the inserted Fe^{III} complex as well as a LIESST effect. Finally, spectroscopic characterization of the Fe^{III} doped compound $[Ga_{0.99}Fe_{0.01}(sal_2trien)][Mn^{II}Cr^{III}(ox)_3]\cdot CH_2Cl_2$ (**3·CH$_2$Cl$_2$**) shows a gradual and complete thermal spin crossover and a LIESST effect on the isolated Fe^{III} complexes. This result confirms that cooperativity is not necessary condition to observe the LIESST effect in an Fe^{III} compound.

Introduction

Multifuncionality is one of the most appealing topics in chemical science. A rational approach to design multifunctional materials consists of creating hybrid solids constituted of two networks formed by two molecular fragments, where each network furnishes distinct physical properties.[1] A coexistence of the two physical properties is anticipated if the two networks are quasi-independent. Materials for which physical properties can be tuned by applying an external stimulus are attracting considerable interest in view of their potential applications as chemical switches, memories or molecular sensors.[2] Most of the responsive magnetic materials obtained so far are one-network materials in which the magnetic order is tuned by light or pressure.[3] Two-network materials formed by a magnetic lattice and a switchable molecular component are promising candidates for the preparation of multifunctional responsive materials.

A potential source for this type of materials is the bimetallic oxalate-bridged complexes that have provided remarkable examples of multifunctional magnetic materials.[4] An interesting example prepared by our group is the compound $[Fe^{III}(sal_2\text{-trien})][Mn^{II}Cr^{III}(ox)_3]\cdot CH_2Cl_2$ (**1·CH_2Cl_2**, H_2sal_2-trien = N,N'-disalicylidenetriethylene-tetramine, ox = oxalate).[5] This compound shows an unusual combination of properties in the same compound; a spin crossover (SCO) transition of the inserted complex cation and a ferromagnetic ordering of the oxalate network. Unfortunately, no interplay between these two properties has been detected due to the large difference in temperature at which the two phenomena occur. Thus, while the spin crossover occurs at comparatively high temperatures, that is, in the range of 130-350 K, the ferromagnetic ordering occurs below 5.2-5.6 K. A way to overcome this limitation is to take advantage of the photo-induced spin crossover effect, also known as LIESST effect (Light-Induced Excited Spin-State Trapping) originally establisched for Fe^{II} complexes at temperatures typically below 50 K.[6] Light irradiation at low temperature, induces a LIESST effect for **1·CH_2Cl_2** with a T(LIESST) = 41 K, which defines the limiting temperature above which the photo-inscribed information is erased.[7] The photo-induced spin

conversion of the inserted Fe^{III} complex, however, has a negligible influence on the magnetic behavior or the 2D oxalate network. This is not unexpected, as 2D oxalate networks with very different interlayer separation present a similar behavior.

Although the preparation of a switchable magnet has not been achieved, the LIESST effect of this compound constitutes a remarkable finding, as this phenomenon is rarely observed in Fe^{III} complexes. SCO Fe^{II} compounds present an average bond length change of about 0.20 Å between the LS and HS state, whereas that of Fe^{III} SCO complexes is about 0.13 Å. Obviously, the structural reorganization influences the kinetics of the spin-state interconversion. It is presumed that the lifetime of the photoinduced excited HS state for Fe^{III} complexes is shorter than that for Fe^{II} complexes, as the smaller energy barrier between the HS and LS state in Fe^{III} complexes cannot prevent the relaxation of the metastable HS state back to the LS ground state effectively. Only a few examples of Fe^{III} complexes showing the LIESST effect have been reported by Sato, Hayami et al. namely $[Fe^{III}(pap)_2]^+$, $[Fe^{III}(qsal)_2]^+$, and $[Fe^{III}(qnal)_2]^+$ (Hpap = 2-(2-pyridilmethylamino) phenol, Hqsal = 2-[(8-quinolinyilimino)methyl]phenol and Hqnal = 1-[(8-quinolinylamino)methyl]-2-naphthalenol).[8,9,10] The LIESST effect of these compounds is attributed to the strong distortion of the Fe^{III} sites from their octahedral geometry, which is enhanced by the presence of strong intermolecular interactions, such as π–π stacking.[9] In contrast to the above Fe^{III} complexes in the form of salts of small anions such as BF_4^- or ClO_4^-, **1·CH_2Cl_2** presents an extended 2D anionic network formed by Mn^{II} and Cr^{III} ions linked through oxalate ligands. $[Fe^{III}(sal_2\text{-trien})]^+$ cations and CH_2Cl_2 solvent molecules are intercalated between these oxalate layers.[5] Besides **1·CH_2Cl_2**, other compounds formed by insertion of $[Fe^{III}(sal_2\text{-trien})]^+$ or $[Fe^{III}(X\text{-}sal_2\text{-trien})]^+$ (X = 5-Cl, 5-Br, 5-NO_2, 5-CH_3O, 4-Br, 3-Br, 3-Cl, 3-CH_3O) into 2D or 3D bimetallic oxalate networks have been prepared by us,[5,11] but the LIESST effect has so far only been observed in **1·CH_2Cl_2**.[7]

In this work, a family of compounds with a similar structure to that of **1·CH_2Cl_2** has been prepared by replacing CH_2Cl_2 with other halogenated solvents. Furthermore, a fraction of the Fe^{III} spin crossover complexes of **1·CH_2Cl_2** have been replaced with the

diamagnetic dopant, $[Ga^{III}(sal_2\text{-trien})]^+$ complex, to prepare compounds of formula $[Ga^{III}_{1-x}Fe^{III}_x(sal_2\text{-trien})][Mn^{II}Cr^{III}(ox)_3]\cdot(CH_2Cl_2)$. The aim of this work is to obtain new Fe^{III} compounds presenting a LIESST effect that could provide more data to understand this rare property. On the other hand, substitution of the solvent molecule may allow tuning the temperatures of the thermal and photoinduced spin-crossover of the inserted Fe^{III} cations. We have to take into account that replacement of the solvent molecules induces changes in the internal chemical pressure on the inserted Fe^{III} SCO complex and the intermolecular interaction with the oxalate network, that are key factors for the SCO properties. Finally, dilution of the $[Fe^{III}(sal_2\text{-trien})]^+$ complex with an inert $[Ga^{III}(sal_2\text{-trien})]^+$ complex reduces cooperativity and may help to clarify the role of intermolecular interactions between SCO complexes in this type of compounds. An additional advantage of dilution is that it permits to perform spectroscopic characterization on single crystals, which is not possible for pure Fe^{III} compounds due to the strong absorption of $[Fe^{III}(sal_2\text{-trien})]^+$ complexes.

Experimental section

Syntesis: $[Fe(sal_2\text{-trien})]PF_6$ and $[Ga(sal_2\text{-trien})]PF_6$ were prepared according to literature methods.[12] $Ag_3Cr(ox)_3$ was prepared by metathesis from the corresponding potassium salt.[13] All other materials and solvents were commercially available and used without further purification. Single crystals of the five compounds $[Fe^{III}(sal_2\text{-trien})][Mn^{II}Cr^{III}(ox)_3]\cdot CHCl_3$ (**1·CHCl$_3$**), $[Fe^{III}(sal_2\text{-trien})][Mn^{II}Cr^{III}(ox)_3]\cdot CHBr_3$ (**1·CHBr$_3$**), $[Fe^{III}(sal_2\text{-trien})][Mn^{II}Cr^{III}(ox)_3]\cdot CH_2Br_2$ (**1·CH$_2$Br$_2$**), $[Fe^{III}(sal_2\text{-trien})][Zn^{II}Cr^{III}(ox)_3]\cdot CH_2Cl_2$ (**2·CH$_2$Cl$_2$**) and $[Ga^{III}_{1-x}Fe^{III}_x(sal_2\text{-trien})][Mn^{II}Cr^{III}(ox)_3]\cdot CH_2Cl_2$ (**3·CH$_2$Cl$_2$**, x = 0.01) were obtainded by slow diffusion of two solutions. The first solution was prepared by adding $MnCl_2\cdot 4H_2O$ (0.040 g, 0.202 mmol for **1·CHBr$_3$**, **1·CHCl$_3$** and **1·CH$_2$Br$_2$**) or $ZnCl_2$ (0.075 g, 0.536 mmol for **2·CH$_2$Cl$_2$**) to a suspension of $Ag_3Cr(ox)_3$ (0.086 g, 0.134 mmol) in 9 mL of methanol. The AgCl precipitate was filtered. The second solution was obtained by dissolving $[Fe(sal_2\text{-trien})]PF_6$ (0.075 g, 0.134 mmol) in 9 mL of chloroform (**1·CHCl$_3$**), bromoform (**1·CHBr$_3$**), dibromomethane (**1·CH$_2$Br$_2$**) and dichloromethane (**2·CH$_2$Cl$_2$**), or a mixture of

0.1 and 9.9 mL of 15 mM solutions of [Fe(sal_2-trien)]PF_6 and [Ga(sal_2-trien)]PF_6, respectively, in dichloromethane (**3·CH_2Cl_2**). After two weeks brown or violet (**3·CH_2Cl_2**) crystals were obtained.

Stuctural characterization: Single crystals of all five compounds were mounted on glass fibres using a viscous hydrocarbon oil to coat the crystal and then transferred directly to the cold nitrogen stream for data collection. X-ray data were collected at 100 and 300 K for **1·$CHCl_3$**, **1·$CHBr_3$** and **1·CH_2Br_2**, at 120 K for **2·CH_2Cl_2** and at 300 K for **3·CH_2Cl_2** on a diffractometer equipped with a graphite-monochromated Enhance (Mo) X-ray Source (λ = 0.71073Å). The program CrysAlisPro, Oxford Diffraction Ltd., was used for unit cell determinations and data reduction. Empirical absorption correction was performed using spherical harmonics, implemented in the SCALE3 ABSPACK scaling algorithm. Crystal structures were solved by direct methods with the SIR97 program,[14] and refined against all F^2 values with the SHELXL-97 program[15], using the WinGX graphical user interface.[16] Non-hydrogen atoms were refined anisotropically (except as noted), and hydrogen atoms were placed in calculated positions refined using idealized geometries (riding model) and assigned fixed isotropic displacement parameters. In compound **1·$CHCl_3$**, the small size of the crystals gave rise to a very weak scattering. Due to this, the number of reflections was not enough to carry out anisotropic refinement of all the atoms. Thus, carbon atoms at 100 K and carbon, nitrogen and oxygen atoms at 300 K could only be modeled isotropically. Furthermore, this caused a too low observed/unique reflections ratio in the structure solved at 300 K. This problem disappeared in the structure of the same crystal solved at 100 K. Data collection and refinements statistics are collected in Table 1. CCDC-929201 to 929208 contain the supplementary crystallographic data for this paper. These data can be obtained free of charge from The Cambridge Crystallographic Data Centre via www.ccdc.ac.uk./data_request/cif.

Table 1a. Crystallographic data for compounds **1·$CHCl_3$**, **1·$CHBr_3$** and **1·CH_2Br_2** at 100 K and **2·CH_2Cl_2** at 120 K.

Compound	**1·$CHCl_3$**	**1·$CHBr_3$**	**1·CH_2Br_2**	**2· CH_2Cl_2**
Empirical formula	$C_{27}H_{25}Cl_3CrFeMnN_4O_{14}$	$C_{27}H_{25}Br_3CrFeMnN_4O_{14}$	$C_{27}H_{26}Br_2CrFeMnN_4O_{14}$	$C_{27}H_{26}Cl_2CrFeZnN_4O_{14}$
Formula weight	898.65	1032.03	953.13	874.64
Crystal color	Brown	Brown	Brown	Brown
Temperature (K)	100	100	100	120
Wavelength (*Å*)	0.71073	0.71073	0.71073	0.71073
Crystal system, Z	Monoclinic, 4	Monoclinic, 4	Monoclinic, 4	Monoclinic, 4
Space group	$P2_1/c$	$P2_1/c$	$P2_1/c$	$P2_1/c$
a (Å)	11.7374(14)	11.9224(5)	11.7115(4)	11.6634(6)
b (Å)	31.6700(30)	31.8487(8)	31.9453(7)	31.4028(11)
c (Å)	9.5800(9)	9.6032(3)	9.5068(3)	9.3270(4)
β (°)	111.136(12)	110.582(4)	109.821(4)	109.747(5)
V ($Å^3$)	3321.5(6)	3413.7(2)	3346.04(17)	3215.2(2)
ρcalc (Mg/m^3)	1.797	2.008	1.892	1.807
μ($Mo_{K\alpha}$) (mm^{-1})	1.443	4.681	3.580	1.760
θ range (°)	2.98 to 28.30	2.97 to 30.56	2.97 to 30.49	2.26 to 32.51
Reflns collected	8291	10433	10248	10735
Independent reflns, *n*, (R_{int})	2839 (0.1888)	7423 (0.1048)	8128 (0.0696)	3454 (0.1214)
L. S. parameters/ restraints	325/0	460/0	451/0	421/0
$R1(F)$,[a] $I>2\sigma(I)$]	0.0481	0.0608	0.0545	0.0493
$wR2(F^2)$,[b] all data	0.0813	0.1425	0.1098	0.0867
$S(F^2)$,[c] all data	0.638	1.061	1.176	0.665

[a] $R1(F) = S(|F_O| - |F_C|)/S|F_O|$; [b] $wR2(F^2) = [Sw(F_O^2 - F_C^2)^2/SwF_O^4]^{½}$; [c] $S(F^2) = [Sw(F_O^2 - F_C^2)^2/(n - p)]^{½}$

Table 1b. Crystallographic data for compounds **1·CHCl$_3$**, **1·CHBr$_3$** and **1·CH$_2$Br$_2$** and **3·CH$_2$Cl$_2$** at 300 K.

Compound	**1·CHCl$_3$**	**1·CHBr$_3$**	**1·CH$_2$Br$_2$**	**3·CH$_2$Cl$_2$**
Empirical formula	$C_{27}H_{25}Cl_3CrFeMnN_4O_{14}$	$C_{27}H_{25}Br_3CrFeMnN_4O_{14}$	$C_{27}H_{26}Br_2CrFeMnN_4O_{14}$	$C_{27}H_{26}Cl_2CrGaMnN_4O_{14}$
Formula weight	898.65	1032.03	953.13	878.08
Crystal color	Brown	Brown	Brown	Brown
Temperature (K)	300	300	300	300
Wavelength (*Å*)	0.71073	0.71073	0.71073	0.71073
Crystal system, Z	Monoclinic, 4	Monoclinic, 4	Monoclinic, 4	Monoclinic, 4
Space group	$P2_1/c$	$P2_1/c$	$P2_1/c$	$P2_1/c$
a (Å)	12.1519(17)	12.2769(4)	12.1735(6)	12.0528(9)
b (Å)	31.939(4)	32.0813(8)	32.3048(9)	32.1554(15)
c (Å)	9.4867(12)	9.5335(3)	9.4392(4)	9.4707(6)
β (°)	111.480(15)	110.849(4)	111.274(5)	112.297(8)
V (Å^3)	3426.2(8)	3508.99(18)	3459.1(2)	3396.0(4)
ρcalc (Mg/m^3)	1.742	1.954	1.830	1.717
μ($Mo_{K\alpha}$) (mm^{-1})	1.399	4.5554	3.463	8.594
θ range (°)	2.99 to 28.27	2.97 to 30.48	2.98 to 30.47	2.75 to 75.29
Reflns collected	8222	10725	10590	6650
Independent reflns, *n*, (R_{int})	1757 (0.2370)	5973 (0.1012)	4921 (0.1229)	4235 (0.0541)
L. S. parameters/ restraints	252/0	497/0	461/0	489/0
$R1(F)$,[a] $I>2\sigma(I)$]	0.0510	0.0649	0.0794	0.0709
$wR2(F^2)$,[b] all data	0.1078	0.1701	0.2291	0.2248
$S(F^2)$,[c] all data	0.577	1.030	1.025	1.074

[a] $R1(F) = S(|F_O| - |F_C|)/S|F_O|$; [b] $wR2(F^2) = [Sw(F_O^2 - F_C^2)^2/SwF_O^4]^{1/2}$; [c] $S(F^2) = [Sw(F_O^2 - F_C^2)^2/(n - p)]^{1/2}$

Physical measurements: Magnetic susceptibility measurements were performed on polycrystalline samples using a magnetometer (Quantum Design MPMS-XL-5) equipped with a SQUID sensor. Variable-temperature measurements were carried out in the temperature range 2 - 400 K. The AC measurements were performed in the temperature range 2 - 10 K at different frequencies with an oscillating magnetic field of 0.395 mT. The magnetization and hysteresis studies were perfomed between 5 and -5 T, cooling the sample at zero field. The Ga:Fe:M:Cr:X (M = Mn or Zn, and X = Br or Cl) ratios were measured on a Philips ESEM X230 scanning electron microscope equipped with an EDAX DX-4 microprobe.

Mössbauer spectra were collected in transmission mode using a conventional constant-acceleration spectrometer and a 25 mCi ^{57}Co source in a Rh matrix. The velocity scale was calibrated using an α-Fe foil. The absorber was obtained by gently packing single crystals of **1·CHCl$_3$**, **1·CHBr$_3$** and **1·CH$_2$Br$_2$** into a prespex holder. Low-temperature spectra were collected using a bath cryostat with the sample immersed in liquid He for measurements at 4.2 K, or by using flowing He gas to cool the sample above 4.2 K (temperature stability of 0.5 K). The spectra were fitted to Lorentzian lines using a non-linear least-squares method.[17] Isomer shifts are given relative to metallic α-Fe at room temperature.

Variable temperature optical single crystal absorption spectra of **3·CH$_2$Cl$_2$** were recorded with a commercial double beam spectrometer (Varian, Cary 5000). To this end a small crystal was mounted with silver paste so as to cover an aperture on a copper sample holder, which in turn was mounted on the cold finger of an optical close cycle cryostat (Janis, sumitomo SHI-4.5) capable of achieving a base temperature of 4 K.

Results

Synthesis: The method used to prepare the family of five compounds of the present work was described in the experimental section and is analogous to that used to prepare **1·CH$_2$Cl$_2$**.[5] In previous work, two different types of structures were obtained

depending on the solvent used to dissolve $[Fe^{III}(sal_2\text{-trien})]PF_6$.[5] A 2D bimetallic oxalate network is obtained with CH_2Cl_2 in **1·CH_2Cl_2**, while a 3D bimetallic oxalate network is obtained with CH_3CN or CH_3NO_2. In this work, we have discovered that the halogenated solvents, $CHCl_3$, $CHBr_3$ and CH_2Br_2, give rise to 2D structures similar to that of **1·CH_2Cl_2**. This confirms that the formation of 2D or 3D networks is controlled by the size and configuration of the templating cation, which change in the different solvents. An interesting example of how subtle changes lead to 2D or 3D structures is the use of other $[M^{III}(sal_2\text{-trien})]^+$ complexes in the same solvent (CH_2Cl_2). Thus, the largest cation, $[In^{III}(sal_2\text{-trien})]^+$, gives rise to a 3D structure[18] while the smallest one, $[Ga^{III}(sal_2\text{-trien})]^+$,[19] leads to a 2D one. Therefore, the halogenated solvents, CH_2Cl_2, CH_2Br_2, $CHCl_3$ and $CHBr_3$ lead to 2D structures with $[Fe^{III}(sal_2\text{-trien})]^+$ because they induce a configuration of the cation suitable for the growth of the 2D network, which is also stabilized by the insertion of the solvent molecules. When a similar cation of larger size such as $[In^{III}(sal_2\text{-trien})]^+$ is used, the 3D network is favoured and the solvent molecules do not enter the structure. This allows preparing 2D compounds containing two different cations of similar size and to dilute the SCO Fe^{III} complexes with diamagnetic Ga^{III} complexes. In the compounds of formula $[Ga^{III}_{1-x}Fe^{III}_x(sal_2\text{-trien})][Mn^{II}Cr^{III}(ox)_3]\cdot CH_2Cl_2$, most of the $[Fe^{III}(sal_2\text{-trien})]^+$ complexes of **1·CH_2Cl_2** are replaced by the diamagnetic $[Ga^{III}(sal_2\text{-trien})]^+$ complexes. They are prepared by mixing the $[Ga^{III}(sal_2\text{-trien})]PF_6$ and $[Fe^{III}(sal_2\text{-trien})]PF_6$ precursors in the desired ratio.

The composition of the compounds was checked by microanalysis, which shows the presence of the solvent molecules in the structures. Thus, a 1:1:1:3 Fe:M (Mn or Zn):Cr:X (Cl or Br) ratio is found for **1·$CHCl_3$** and **1·$CHBr_3$**, while a 1:1:1:2 one is found for **1·CH_2Br_2** and **2·CH_2Cl_2**. The Ga:Fe ratio for $[Ga^{III}_{1-x}Fe^{III}_x(sal_2\text{-trien})]$ $[Mn^{II}Cr^{III}(ox)_3]\cdot CH_2Cl_2$ was found to be close to the ratio of the solutions used in the synthesis. For the lightly doped compound $[Ga^{III}_{1-x}Fe^{III}_x(sal_2\text{-trien})][Mn^{II}Cr^{III}(ox)_3]\cdot CH_2Cl_2$, (x = 0.01, **3·$CH_2Cl_2$**) used for optical spectroscopic characterization, the iron content was found to be less than 1 % and could not determined accurately. Still, the presence of Fe in the single crystals of

3·CH_2Cl_2 is verified by the presence of the characteristic LMCT bands in the absorption spectrum (see below).

Structure: The single crystal X-ray diffraction study of **1·$CHCl_3$**, **1·$CHBr_3$**, **1·CH_2Br_2**, **2·CH_2Cl_2** and **3·CH_2Cl_2** shows that they present a very similar structures to that of **1·CH_2Cl_2**. Indeed, their unit cell parameters are very close to the one of **1·CH_2Cl_2** (see Table 1). The structures of **1·$CHCl_3$**, **1·$CHCBr_3$** and **1·CH_2Br_2** were solved at 100 and 300 K as at these temperatures the Fe^{III} complexes are close to 100 % in the LS or the HS state, respectively. On the other hand, the structure of **2·CH_2Cl_2** could only be solved at 120 K due to lower quality of the crystals and the only a partial spin crossover exhibited by this compound (see below).

As in the case of **1·CH_2Cl_2**, the four compounds are formed by anionic $[M^{II}Cr^{III}(ox)_3]^-$ (M = Mn or Zn) sheets in the *bc* plane alternating with inter-lamellar $[Fe^{III}(Sal_2\text{-trien})]^+$ cationic complexes and solvent molecules (see Figure 1). The anionic layers present a 2D honeycomb structure with two crystallographically independent metals linked through oxalate ligands. The intermediate metal-oxygen distances with respect to the ones expected for Cr^{III}-O and Mn^{II}-O (Zn^{II}-O for **2·CH_2Cl_2**), do not allow distinguishing between the two metals in these structures. The cationic layer contains one crystallographically independent $[Fe^{III}(sal_2\text{-trien})]^+$ (or $[Ga^{III}(sal_2\text{-trien})]^+$ in **3·CH_2Cl_2**) complex and one solvent molecule (CH_2Cl_2, $CHCl_3$, $CHCBr_3$ or CH_2Br_2).

We will now focus on the difference between the crystal structures measured at 100 and 300 K as they may help to understand the structural changes associated with the spin crossover. Furthermore, they will be compared with those observed in **1·CH_2Cl_2**. We will look first at the usual changes in the coordination geometry of the Fe^{III} complex between the LS and HS states (Fe-N or Fe-O bond lengths and distorsions from the octahedral geometry) and then at the differences in crystal packing.

The first effect of lowering the temperature is a shortening on a metal-ligand bond lengths (see Table 2), which is similar to that found for **1·CH_2Cl_2** (average bond length

differences of $\Delta r_{HL,Fe\text{-}N}$ = 0.149 Å and $\Delta r_{HL,Fe\text{-}O}$ = 0.024 Å[7]). The small variation in these values between the different compounds may be attributed to a different fraction of Fe^{III} complexes undergoing spin crossover from 300 to 100 K.

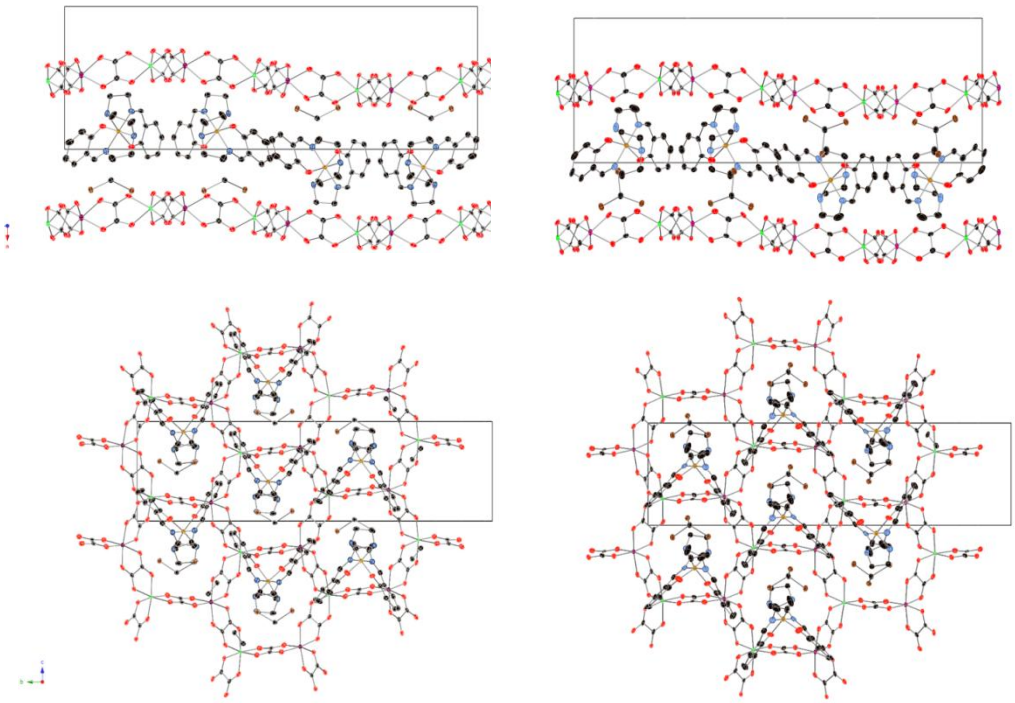

Figure 1. Projection on the *ab* (top) and *bc* (bottom) planes of the structures of **1·CH_2Br_2** (left) and **1·$CHBr_3$** (right) at 100 K; Mn (pink), Cr (green), Fe (yellow), C (black), N (blue), O (red), Br (brown); neighboring atoms corresponding to disordered Mn/Cr have been assigned as Mn and Cr separately for clarity; hydrogen atoms have been omitted for clarity.

The second difference concerns the distortion of the octahedral coordination site, which is larger for the HS state as observed in **1·CH_2Cl_2**.[7] Thus, at 300 K the angles of two of the three diagonals from the octahedron, defined by the bonds N(amine)-Fe-O(Phenoxo), N(amine) = N2,N3, differ strongly from 180°, while the remaining one, defined by the bond N(imine)-Fe-N(imine), N(imine) = N1,N4, is closer to 180°. The coordination octahedron is much more regular at 100 K with angles of all three diagonals closer to 180° (see Table 2).

The third difference between the LS and HS structures is related to the disorder of the ethylene groups of $[Fe(sal_2\text{-trien})]^+$ and solvent molecules. At 300 K, two of the three ethylene groups of $[Fe(sal_2\text{-trien})]^+$ in **1·CHBr$_3$** and **1·CHCl$_3$** and the three of them in **1·CH$_2$Br$_2$** present a disorder, which has been solved by considering two possible configurations with occupancies of 62 and 38 % for **1·CHBr$_3$**, 69 and 31 % for **1·CHCl$_3$** and 63 and 37 % for **1·CH$_2$Br$_2$**. This disorder is not observed in the structures of these compounds solved at 100 K. This disorder could be related to the presence of HS Fe^{III} complexes as it disappears at low temperatures with where Fe is in the LS state. On the other hand, in **1·CH$_2$Br$_2$** one over the two Br atoms of the CH_2Br_2 solvent presents a disorder at 300 K that could be solved assuming two possible configurations with occupancies of 85 and 15 %. This disorder disappears at 100 K. **1·CH$_2$Cl$_2$** presents a similar disorder of the ethylene groups and in the Cl atoms of CH_2Cl_2 molecules at 250 and 300 K, which disappears below 180 K.[7] This disorder is not present for $CHBr_3$ or $CHCl_3$ solvent molecules in **1·CHCl$_3$** and **1·CHBr$_3$**.

Finally, the crystal packing of $[Fe^{III}(sal_2\text{-trien})]^+$ complexes in the four neat compounds also presents important differences between low and high temperature structures. As in the case of **1·CH$_2$Cl$_2$**, the *a* parameter, that gives the interlayer separation, decreases with the temperature (see table 1). Therefore, the spin crossover from HS to LS states leads to a decrease of the interlayer separation. This shortening results in contacts between O atoms from oxalate layers and CH or CH_2 groups from $[Fe^{III}(sal_2\text{-trien})]^+$, which are shorter at 100 K than at 300 K. Therefore, stronger interactions with the oxalate network are expected when the Fe^{III} complexes are in the LS state (see Tables S1-S6 of the supporting information). On the other hand, interlayer distances of **1·CH$_2$Cl$_2$** are shorter than those of **1·CHCl$_3$**, **1·CHBr$_3$** and **1·CH$_2$Br$_2$** (11.5602(4) Å at 92 K and 12.096(5) Å at 300 K for **1.CH$_2$Cl$_2$**)[7] at the same temperatures. Two factors could explain these differences: the changes of CH_2Cl_2 by the more voluminous $CHCl_3$, $CHBr_3$ or CH_2Br_2 solvents, and a different fraction of $[Fe^{III}(sal_2\text{-trien})]^+$ in the HS state. Thus, at low temperatures, when 100% of Fe^{III} are in the LS state, a comparison of the *a* parameter for **1·CHCl$_3$** and **1·CH$_2$Br$_2$** at 100 K with that of **1·CH$_2$Cl$_2$**

at 92 K demonstrates that the interlayer distance increases with the volume of the solvent. In the case of **1·CHBr$_3$**, the ~ 25 % of Fe^{III} are in the HS state at this temperature (see Mössbauer data below). This may be an additional factor contributing to the increase of interlayer separation. This indicates that the internal pressure on the inserted [Fe^{III}(sal$_2$-trien)]$^+$ complexes decreases as the size of the solvent increases. This could explain the stabilization of the HS state in the presence of the bulkier solvents. Magnetic measurements and Mössbauer spectra are consistent with this feature (see below).

Table 2. Structural parameters of **1·CHCl$_3$**, **1·CHBr$_3$**, **1·CH$_2$Br$_2$** and **2·CH$_2$Cl$_2$**

	Spin state	Mean Fe-N (Å)	Mean Fe-O (Å)	N(amine)-Fe-O(Phenoxo) (°)	N(imine)-Fe-N(imine) (°)
1·CHCl$_3$ (300 K)	100 % HS	2.142(5)	1.905(5)	156.9(2) and 157.9(2)	177.2(2)
1·CHCl$_3$ (100 K)	~5 % HS	1.985(4)	1.865(3)	171.86(15) and 170.75(15)	178.72(16)
1·CHBr$_3$ (300 K)	100 % HS	2.148(5)	1.897(4)	156.2(2) and 156.73(2)	176.7(2)
1·CHBr$_3$ (100 K)	~25 % HS	2.013(5)	1.875(4)	168.5(2) and 167.45(19)	177.90(19)
1·CH$_2$Br$_2$ (300 K)	100 % HS	2.135(6)	1.885(6)	158.1(3) and 160.1(2)	176.3(3)
1·CH$_2$Br$_2$ (100 K)	100 % LS	1.982(3)	1.865(3)	173.49(14) and 173.17(13)	179.14(15)
2·CH$_2$Cl$_2$ (120 K)	100 % LS	1.969(4)	1.857(3)	172.99(14) and 173.47(14)	178.91(16)

Magnetic properties: The thermal dependence of the product of the molar magnetic susceptibility times the temperature (χ_MT) of the three compounds is shown in Figure 2. The values for χ_MT are 10.9, 10.1 and 9.9 cm^3·K·mol^{-1} at 300K for **1·CHCl$_3$**, **1·CHBr$_3$** and **1·CH$_2$Br$_2$**, respectively. These values are close to the sum of the expected contributions for the isolated paramagnetic ions with most of the Fe^{III} spin-crossover complexes in the HS state. The lower χ_MT values of **1·CHBr$_3$** and **1·CH$_2$Br$_2$** with respect of that of **1·CHCl$_3$** indicate that in these two compounds there is still a small Fe^{III} LS fraction at 300 K. This is consistent with Mössbauer data at 250 K (see below and Table 3). χ_MT decrease gradually in the three compounds from 300 K to reach minimum values at 140 K for **1.CH$_2$Br$_2$**, 95 K for **1.CHCl$_3$** and 80 K for **1.CHBr$_3$**. Mössbauer data (see below) indicate

that almost 100 % of Fe^{III} are in the LS state below 80 K for **1·CH_2Br_2** and **1·$CHCl_3$**. In the case of **1·$CHBr_3$** at 77 K, there is still a significant fraction of Fe^{III} in the HS state (~ 18 %), that disappears at 4 K. Therefore, the three compounds undergo an almost complete spin crossover with different $T_{1/2}$ values ($T_{1/2}$ = temperature of 50 % HS $\rightarrow$ LS spin conversion). These values, calculated from Mössbauer data are 230 K for **1·CH_2Br_2**, 180 K for **1·$CHCl_3$** and 140 K for **1·$CHBr_3$**. This confirms that the presence of bulkier solvent molecules shifts the $T_{1/2}$ towards lower values due to the lowering of the chemical pressure on the inserted $[Fe^{III}(sal_2\text{-trien})]^+$ complexes. At lower temperatures, $\chi_M T$ increases due to the ferromagnetic interactions between nieghbouring Mn^{II}-Cr^{III} magnetic ions as observed for **1·CH_2Cl_2** and other M^{II}-Cr^{III} 2D oxalate networks. AC susceptibility measurements confirm the presence of long-range magnetic ordering and permit to determinate precisely the critical temperatures (T_c). A maximum in the in-phase signal (χ_M') near T_c and an out-phase signal (χ_M'') that starts to appear at temperatures just below T_c is observed in the three compounds (Figure 3). From this data the T_c of the three compounds is 5.6 K, which is similar to that of **1·CH_2Cl_2** and other Mn^{II}-Cr^{III} 2D oxalate compounds.[5,11a-c] These signals are frequency independent as expected for a ferromagnet.

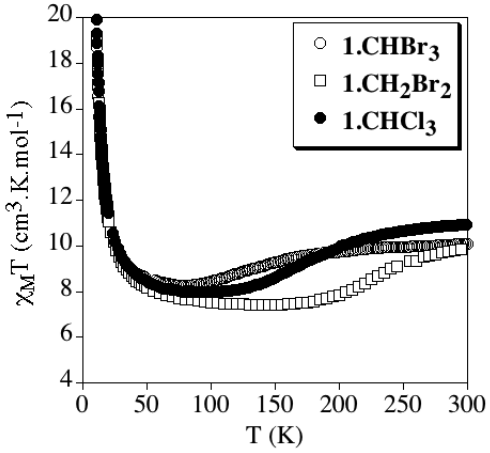

Figure 2. Temperature dependence of the product of the molar magnetic susceptibility with temperature ($\chi_M T$) at 0.1 T for compounds **1·$CHCl_3$** (filled circles), **1·$CHBr_3$** (empty circles) and **1·CH_2Br_2** (empty squares).

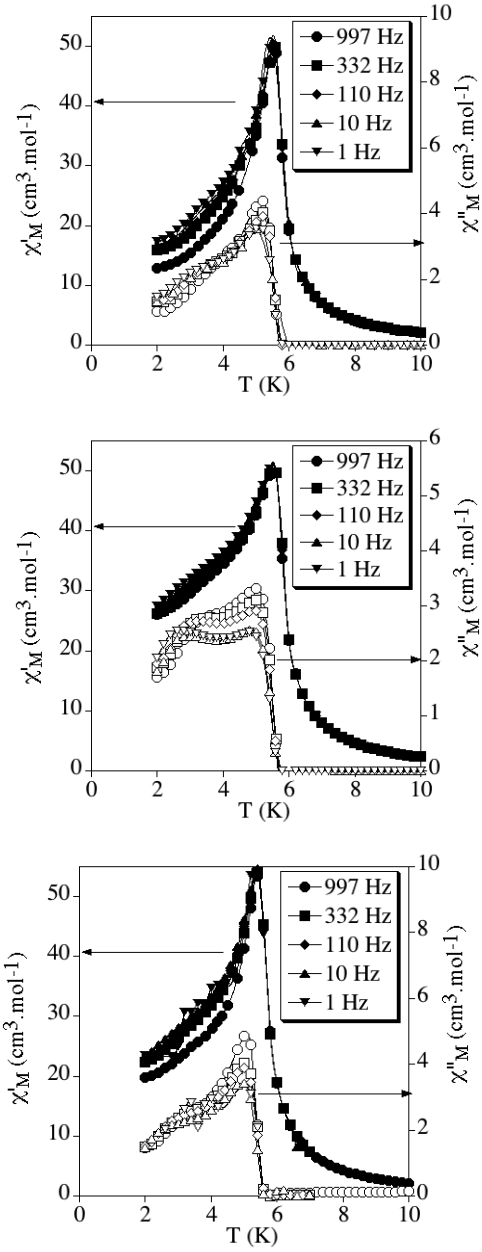

Figure 3. Temperature dependence of the in-phase AC susceptibility (χ') (filled symbols) and the out-of-phase AC susceptibility (χ'') (empty symbols) for **1·CHBr$_3$** (top), **1·CHCl$_3$** (middle) and **1·CH$_2$Br$_2$** (bottom).

Isothermal magnetization at 2 K of the three compounds shows the expected behavior for a ferromagnet (Figure S1 in SI). The magnetization (*M*) value at 5 T of the three compounds is 8.7 μ_B, which is close to the expected value of 9 μ_B for a parallel alignment of the spins in the bimetallic lattice with Fe^{III} in the LS state, thus confirming the complete HS $\rightarrow$ LS spin conversion at this temperature for the three compounds. The hysteresis loops at 2 K shows that these compounds are soft ferromagnets with coercitive fields of 3 mT for **1·CHBr$_3$** and 1mT for **1·CH$_2$Br$_2$** and **1·CHCl$_3$**.

The temperature dependence of $\chi_M T$ of **2·CH$_2$Cl$_2$** is shown in Figure S2 in SI. $\chi_M T$ shows a value of 4.5 $cm^3 \cdot K \cdot mol^{-1}$ at 300K. This value is approximately equal to the sum of the expected contributions for the isolated paramagnetic ions (Cr^{III} and Fe^{III}) with ca. 50 % of the Fe^{III} spin-crossover complexes in a HS state. $\chi_M T$ decrease gradually from 300 to 150 K. Below this temperature, the decreas is less abrupt and reaches a plateau below 100 K with $\chi_M T$ values of 2.3 $cm^3 \cdot K \cdot mol^{-1}$ close to the expected value for isolated Cr^{III} ions and 100% of the Fe^{III} complexes in a LS state. Finally, below 10 K, there is a decrease of a $\chi_M T$ that can be due to spin-orbit coupling and zero-field splitting effects. These results demonstrates that inside the bimetallic oxalate framework the two metals are ordered in such a way that each Cr^{III} center is surrounded by three non-magnetic Zn centers and that a 50 % HS $\rightarrow$ LS spin conversion takes place from 300 to 100 K.

Photomagnetic properties: **1·CHBr$_3$**, **1·CHCl$_3$**, **1·CH$_2$Br$_2$** and **2·CH$_2$Cl$_2$** were introduced into SQUID at 10 K and irradiated with red light (λ = 647 nm). An increase of the magnetic signal was observed. After about 1 hour, the irradiation was switched off. The temperature was then increased at a rate of 0.3 $K \cdot min^{-1}$ and the magnetic susceptibility recorded. For the three compounds, $\chi_M T$ recorded at low temperature after irradiation is higher than the value recorded in the dark. Upon increasing the temperature, the difference vanishes and becomes zero above at temperature between 60 and 80 K, depending on the compound. In order to see clearly the magnetic differences after and before irradiation, $\chi_M T$ after irradiation has been subtracted to the one recorded before

irradiation using an interpolation procedure. Interpolated differences are presented in Figure 4. At 20 K, the difference in $\chi_M T$ values are 1.5, 0.8, 1.0 and 0.45 $cm^3 \cdot K \cdot mol^{-1}$ respectively for **1·CHCl$_3$**, **1·CH$_2$Br$_2$**, **1·CHBr$_3$** and **2·CH$_2$Cl$_2$**. Taking the mean values of 4.375 $cm^3 \cdot K \cdot mol^{-1}$ for Fe^{III} HS and 0.6 $cm^3 \cdot K \cdot mol^{-1}$ for Fe^{III} LS, the fraction of Fe^{III} photoconverted after irradiation is calculated to be 40, 21, 26 and 13 % for **1·CHCl$_3$**, **1·CH$_2$Br$_2$**, **1·CHBr$_3$** and **2·CH$_2$Cl$_2$**, respectively. As already described, the difference in $\chi_M T$ decreases when the temperature increases, being zero when the temperature is higher than 80 K. For the four compounds, T(LIESST) temperatures, defined as the minimum of the derivate of this $\chi_M T$ difference with regard to temperature, are respectively 58, 45, 62 and 45 K.

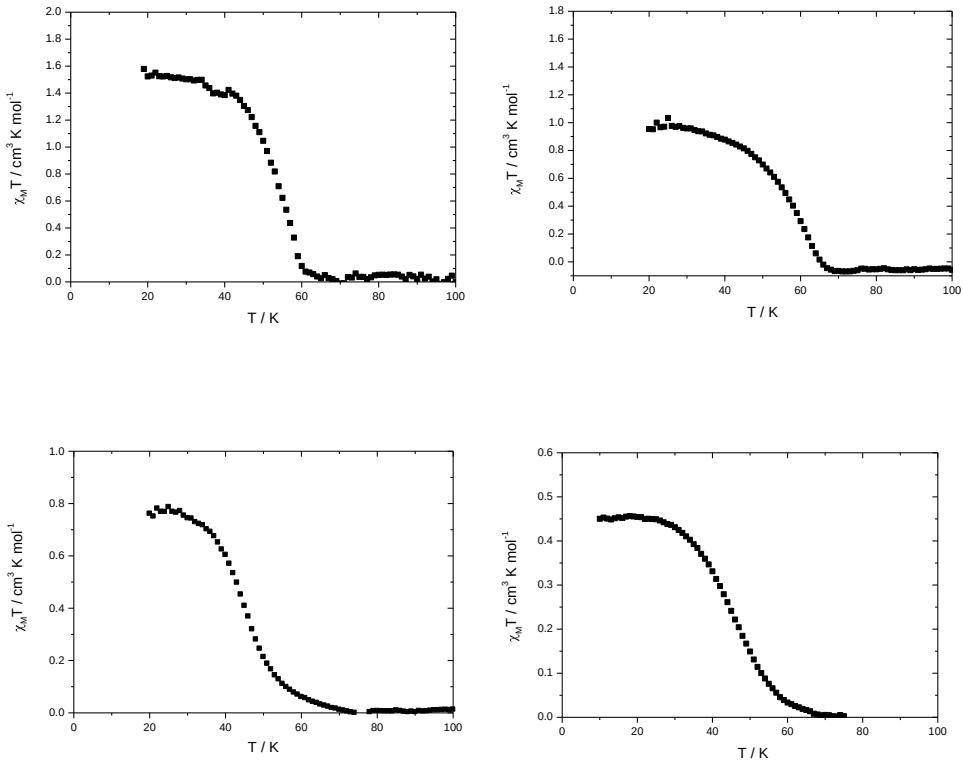

Figure 4. Difference between magnetic signal after and before photoconversion for compounds **1·CHCl$_3$**, (top left) **1·CH$_2$Br$_2$**, (top right) **1·CHBr$_3$**, (bottom left) and **2·CH$_2$Cl$_2$** (bottom right).

In order to get some insight into the decay of the photoinduced HS state, HS $\rightarrow$ LS relaxation curves were recorded for **1·CHCl$_3$**, **1·CH$_2$Br$_2$** and **1·CHBr$_3$**. These are presented in Figure S3 in SI. For the three compounds, the relaxation curves show strong deviations from single exponential in the shape of stretched exponentials. The best fit (solid lines in Figure S3 in SI) was obtained with a distribution of relaxation rate constants at a given temperature from a Gaussian distribution of activation energies as already observed in **1·CH$_2$Cl$_2$**.[7] The apparent activation energy, E_a, apparent pre-exponential factor, k_∞, and standard deviation of the mean activation energy, σ, are reported in table S7 in SI for the three compounds. These curves are typical of non-cooperative systems, which rarely show a single-exponential behavior, because of inhomogeneous distribution due to poory crystalline solids and the presence of disorder.[20] Hence, in the present case the deviations could be related to the disorder observed in the ethylene groups of $[Fe^{III}(sal_2\text{-trien})]^+$ in **1·CHCl$_3$**, **1·CH$_2$Br$_2$** and **1·CHBr$_3$**, indicating different possible configurations of the cation in the HS state.

Mössbauer spectroscopy: Mössbauer spectra of **1·CHBr$_3$**, **1·CHCl$_3$** and **1·CH$_2$Br$_2$** shown in Figures 5, 6 and 7 are similar to those published for **1·CH$_2$Cl$_2$**, the achiral 3D compound $[Fe^{III}(sal_2trien)][Mn^{II}Cr^{III}(ox)_3]\cdot CH_3OH$, or other compounds formed by the insertion of $[Fe^{III}(5X\text{-}sal_2\text{-trien})]^+$ (X = Cl, Br) into chiral 3D oxalate networks.[5,11b] In the present compounds, only a quadrupole doublet with estimated parameters typical of LS Fe^{III} is observed at 4K (Table 3). Above 77 K for **1·CHCl$_3$** and **1·CHBr$_3$** and 160 K for **1·CH$_2$Br$_2$**, an unresolved absorption, centered at IS $\sim$ 0.30 - 0.36 mm/s at 295K, is observed. This broad absorption is assigned to HS Fe^{III}. As discussed in detail in previous papers[5,11b] broadening of the HS Fe^{III} contribution below 180 K may hardly be attributed to a slow spin state interconversion, since the LS Fe^{III} doublet peaks remain sharp with relatively thin line widths. In the 4-180 K temperature range broadening of the HS Fe^{III} seems to be rather due to slow relaxation of the HS Fe^{III} magnetic moments directions with a frequency (10^7 - 10^9 s^{-1}) whose reciprocal is of the same order of magnitude of the Mössbauer effect observation time. Below the temperatures referred to above, all the Fe centers are present as LS Fe^{III} and therefore no sextets are observed at 4 K in contrast

to $[Fe(5\text{-}Cl\text{-}sal_2trien)][MnCr(ox)_3]\cdot 0.5CH_3NO_2$, $[Fe(5\text{-}Br\text{-}sal_2trien)][MnCr(ox)_3]$ and $[Fe(sal_2trien)][MnCr(ox)_3]\cdot CH_3OH$ where a significant fraction of Fe^{III} was still in the HS state at temperatures ≤ 4 K.[5,11b]

Table 3. Estimated parameters from the Mössbauer spectra of **1·$CHCl_3$**, **1·$CHBr_3$** and **1·CH_2Br_2**.

Compound	T		IS	QS	I
1·$CHCl_3$	250 K	Fe L. S.	0.12	2.35	10 %
		Fe H. S.	0.30	0.18	90 %
	230 K	Fe L. S.	0.14	2.43	17 %
		Fe H. S.	0.29	0.21	83 %
	220 K	Fe L. S.	0.15	2.43	26 %
		Fe H. S.	0.29	0.20	74 %
	175 K	Fe L. S.	0.19	2.50	54 %
		Fe H. S.	0.30	0.20	46 %
	150 K	Fe L. S.	0.20	2.54	77 %
		Fe H. S.	0.28	0.20	22 %
	100 K	Fe L. S.	0.21	2.52	93 %
		Fe H. S.	0.33	0.40	7 %
	80 K	Fe L. S.	0.21	2.54	93 %
		Fe H. S.	0.27	0.34	7 %
	4K	Fe L. S.	0.21	2.45	100 %
1·$CHBr_3$	250 K	Fe L. S.	0.14	2.35	15 %
		Fe H. S.	0.36	0.34	85 %
	230 K	Fe L. S.	0.15	2.40	22 %
		Fe H. S.	0.36	0.40	78 %
	210 K	Fe L. S.	0.16	2.50	27 %
		Fe H. S.	0.36	0.41	73 %
	190 K	Fe L. S.	0.17	2.56	28 %
		Fe H. S.	0.37	0.40	72 %
	170 K	Fe L. S.	0.18	2.59	34 %
		Fe H. S.	0.36	0.35	66 %
	130 K	Fe L. S.	0.20	2.57	57 %
		Fe H. S.	0.36	0.31	43 %
	100 K	Fe L. S.	0.20	2.56	72 %
		Fe H. S.	0.36	0.35	28 %
	77 K	Fe L. S.	0.21	2.59	82 %
		Fe H. S.	0.37	0.44	18 %
	4K	Fe L. S.	0.22	2.61	100 %

IS isomer shift relative to metallic Fe at 295 K; QS quadrupole splitting; I relative area; Estimated errors are < 0.03 mm/s for IS and QS and < 2 % for I

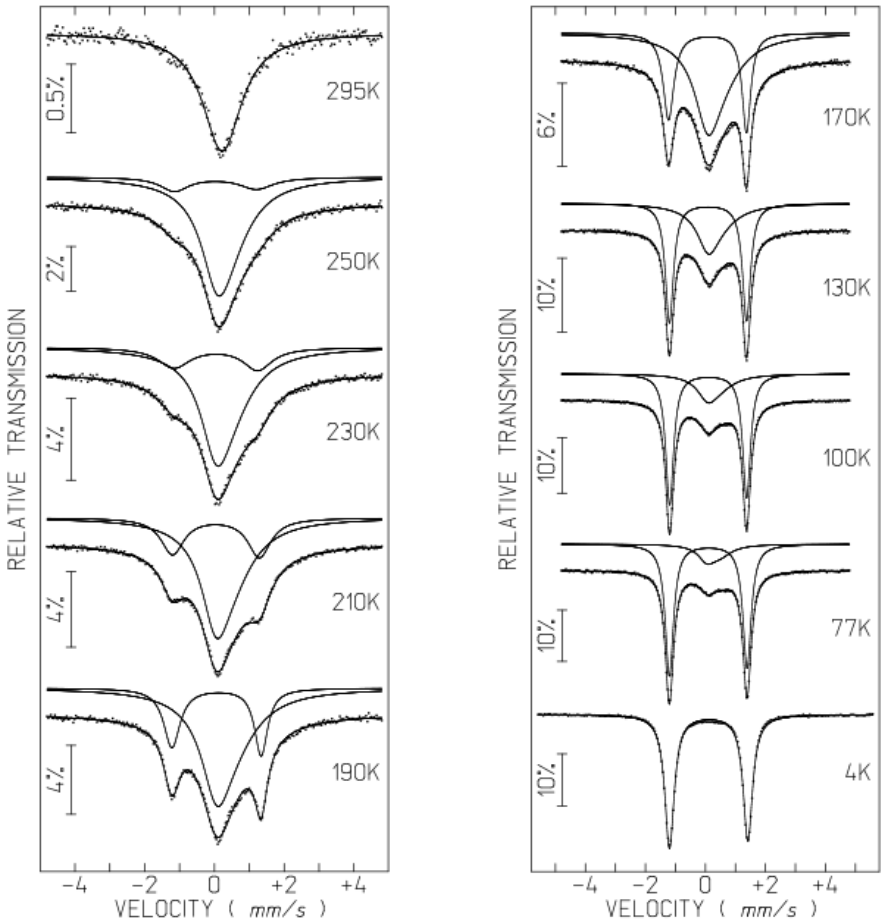

Figure 5. Mössbauer spectra of **1·CHBr$_3$** taken at different temperaturas. The lines over the experimental points are the sum of two doublets corresponding to HS and LS Fe^{III}. The estimated parameters for these doublets are collected in Table 3.

The temperature dependence of the estimated relative areas of the HS and LS Fe^{III} subspectra of the three compounds are plotted in Figure S4 of the supporting information. They follow the same trend as the temperature dependence of $\chi_M T$ and permit to calculate the transition temperature $T_{1/2}$.

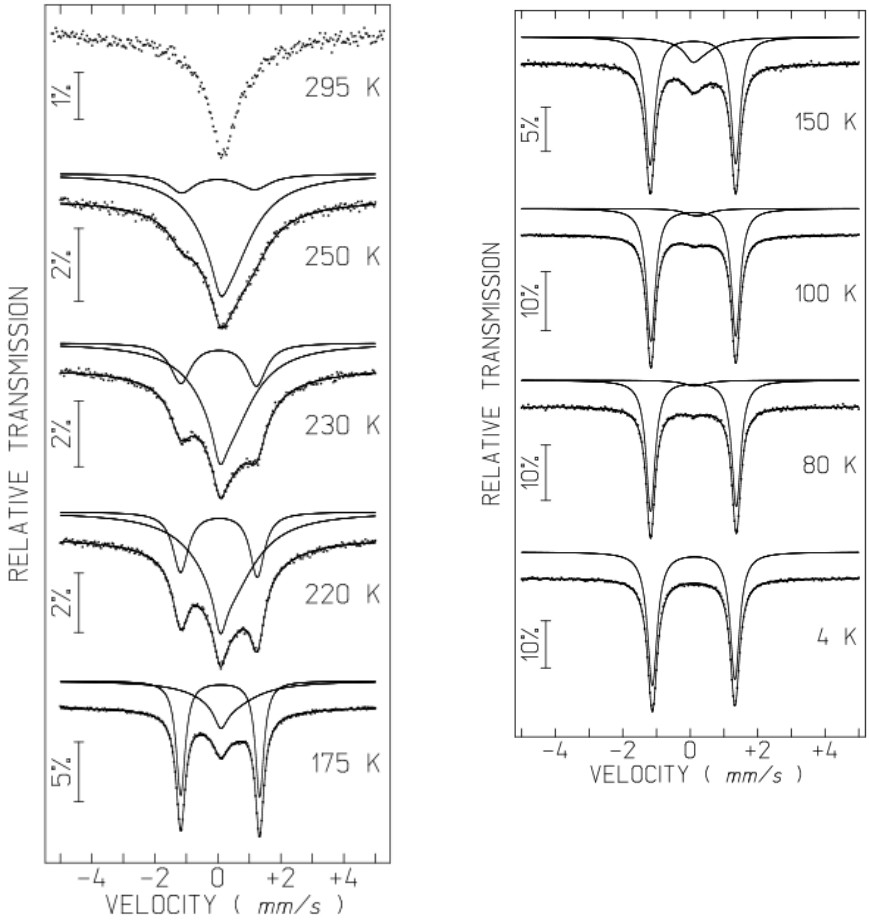

Figure 6. Mössbauer spectra of **1·CHCl$_3$** taken at different temperaturas. The lines over the experimental points are the sum of two doublets corresponding to HS and LS Fe^{III}. The estimated parameters for these doublets are collected in Table 3.

Compound	T		IS	QS	I
1·CH$_2$Br$_2$	245 K	Fe L. S.	0.15	2.53	28 %
		Fe H. S.	0.32	-	72 %
	199 K	Fe L. S.	0.16	2.52	78 %
		Fe H. S.	034	0.46	22 %
	180 K	Fe L. S.	0.18	2.57	85 %
		Fe H. S.	0.34	0.49	15 %

	160 K	Fe L. S.	0.19	2.60	90 %
		Fe H. S.	0.35	0.49	10 %
	77 K	Fe L. S	0.20	2.56	100 %
	63 K	Fe L. S.	0.21	2.60	100 %
	4 K	Fe L. S	0.21	2.61	100%

IS isomer shift relative to metallic Fe at 295 K; QS quadrupole splitting; I relative area; Estimated errors are < 0.03 mm/s for IS and QS and < 2 % for I

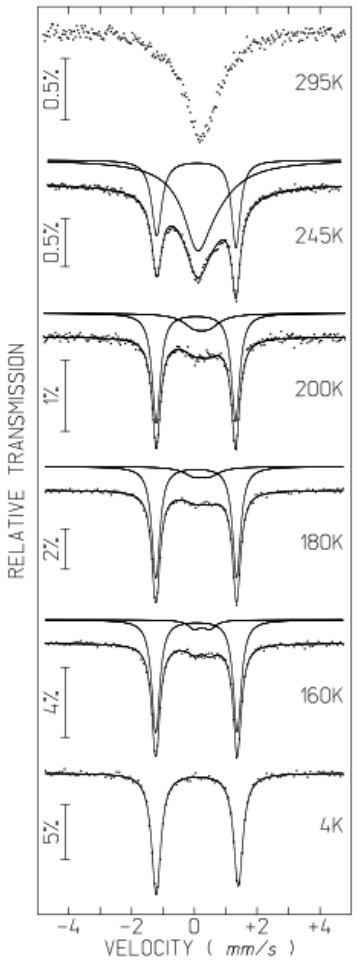

Figure 7. Mössbauer spectra of **1·CH_2Br_2** taken at different temperaturas. The lines over the experimental points are the sum of two doublets corresponding to HS and LS Fe^{III}. The estimated parameters for these doublets are collected in Table 3.

Spectroscopic measurements on the diluted system. The spin-crossover behavior of this family of Fe^{III} complexes has been studied by optical spectroscopy on single crystals. It is not possible to perform this type of measurements with the pure Fe compounds because the ligand-metal charge transfer (LMCT) absorption bands of the Fe complexes are very intense in the visible region and saturate the signal. To avoid this problem, doped $[Ga^{III}_{x}Fe^{III}_{1-x}(sal_2\text{-trien})][Mn^{II}Cr^{III}(ox)_3]\cdot CH_2Cl_2$ crystals were prepared. They show much less intense absorption bands, as Ga^{III} complexes do not absorb in the visible region of the spectrum. For good quality spectra, it was necessary to reduce the Fe content to 1 mole% (**3·CH_2Cl_2**).

Absorption spectra at different temperatures on single crystal of **3·CH_2Cl_2** were recorded in order to follow the thermal spin crossover of the compound (Figure 8a). At room temperature, the characteristic LMCT band of the HS Fe^{III} complex is observed as a shoulder around 500 nm of an intense band at 570 nm assigned to the spin allowed $^4A_2 \rightarrow {}^4T_2$ *d-d* transition of $[Cr(ox)_3]^{3-}$ of the bimetallic oxalate network. The latter practically does not change with the temperature. Upon cooling, a band around 650 nm, due to an LMCT absorption of the LS complex, gradually appears and increases in intensity. At the same time, the intensity of the above-mentioned HS band decreases gradually. The temperature dependence of the HS fraction was monitored by analyzing the evolution of the absorbance of the LMCT absorption bands. For a quantitative evaluation of the resultant thermal spin transition, the evolution of the optical density at 665 nm as a function of temperature has been normalized with the data from the magnetic measurements performed on **1·CH_2Cl_2**.[5] Comparison of this result with magnetic data of the pure Fe compound **1·CH_2Cl_2** is shown in Figure 8b. For both compounds a gradual variation of the HS fraction is observed, with an estimated HS fraction at room temperature of 80 %. For the doped system **3·CH_2Cl_2**, $T_{1/2}$ is shifted to lower temperatures ($T_{1/2}$ = 225 K) compared to **1·CH_2Cl_2** ($T_{1/2}$ = 245 K).[7] Furthermore, the transition is more gradual in **3·CH_2Cl_2** than in the pure Fe compound **1·CH_2Cl_2**. This observation can be explained by the lack of cooperative interactions in lightly doped crystals.

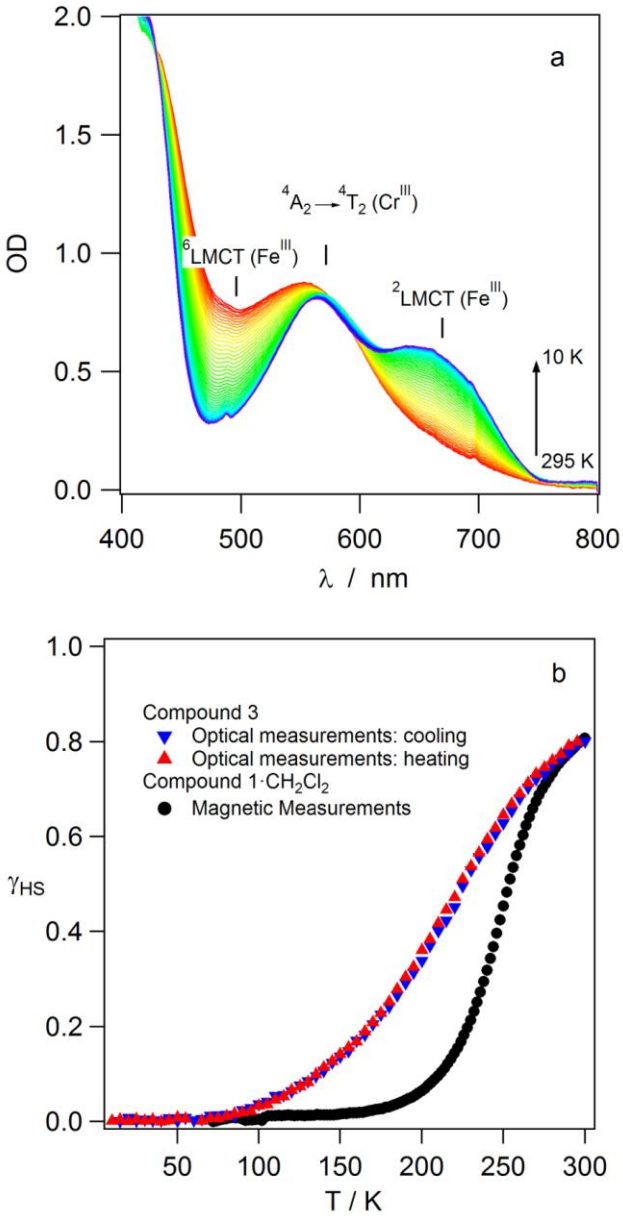

Figure 8. (a) Variable temperature single crystal absorption spectra of **3·CH_2Cl_2**. (b) Thermal spin crossover for **3·CH_2Cl_2** extracted from spectroscopic measurements (red and blue triangles) and of **1·CH_2Cl_2** from magnetic measurements from reference 5 (black circles).

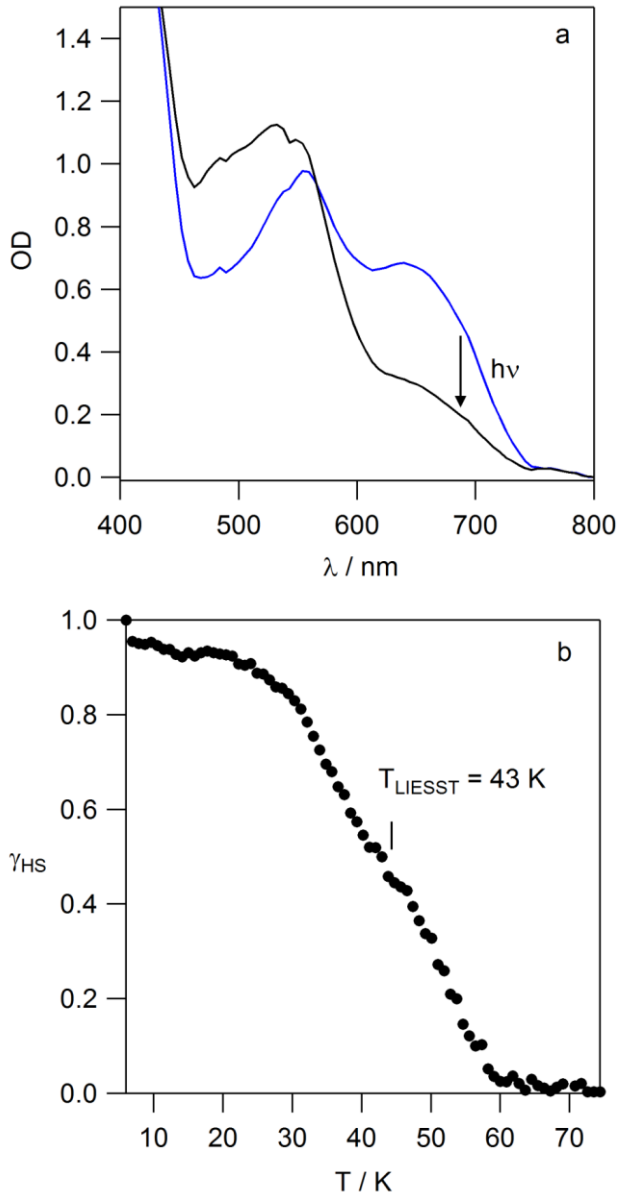

Figure 9. (a) Absorption spectra before and after irradiation at 4 K with light from 690 nm Laser of **3·CH_2Cl_2**. (b) Evolution of the photo-excited HS fraction during a heating cycle at 0.3 K/min after irradiation at 4 K on a crystal of **3·CH_2Cl_2**.

For LIESST experiments the sample was irradiated at 5 K with a continuous diode pumped solid-state laser at 690 nm. Irradiation at this wavelength, which is within the LMCT absorption of the LS species, resulted in a light-induced population of the metastable HS state at the expense of the LS state. Irradiation for only 2 minutes at 1 mW/mm^2 in fact resulted in an almost quantitative transformation from the LS state to the photo-excited HS state (Figure 9a), since the absorption spectra of **3·CH$_2$Cl$_2$** in the photo-excited state at low temperature is almost identical to the one obtained at room temperature. Absorption spectra after photo-excitation were subsequently recorded between 5 and 70 K with a heating rate of 0.3 K/min. The HS fraction at every temperature was calculated from the evolution of the absorbance at 665 nm, taking the spectra at 5 K as the LS reference and the one obtained just after irradiation at this temperature as the HS reference. The HS fraction remains close to 100 % from 5 to 30 K. At higher temperatures it decreases to reach a value close to zero at around 60 K (Figure 9b). This gives a T(LIESST) of 43 K, which is similar to the result obtained in the magnetic measurements for the pure Fe compound **1·CH$_2$Cl$_2$**.[7] In contrast to the magnetic measurements on the pure Fe crystals, for which a light induced HS fraction of only 0.4 could be achieved,[7] in the very dilute system it proved possible to achieve a quantitative population of the HS state. This is due to the comparatively weak optical density of the dilute crystals, which results in a good penetration and propagation of the light through the crystal, whereas the strong absorption of the pure Fe crystals only results in the photo-excitation of the complexes close to the surface and not in the bulk.

Discussion

T(LIESST). In the quest for high T(LIESST) values, chemists have searched for parameters allowing to rationalize and predict the T(LIESST) value, in order to reach the highest T(LIESST) possible. Létard et al. have proposed a relationship between T(LIESST) and $T_{1/2}$ for Fe(II) complexes.[21] They proposed that these two experimental parameters are related by a linear relationship, T(LIESST) = T_0 - 0.3 $T_{1/2}$. T_0 has been proposed to be equal to 100, 120, 150, 180 and 200 for monodentate, bidentate, tridentate,

macrocyclic ligands and Prussian Blue analogous, respectively. Sato et al. have looked for an analogous relationship for the Fe^{III} complexes presenting a LIESST effect. Thus, they reported a linear relationship $T(LIESST) = T_0 - 0.4 \cdot T_{1/2}$, with $T_0 = 185$ K for the six compounds derived from $[Fe(pap)]^+$ complex.[8c] In a second article, two more examples of Fe^{III} complexes presenting a LIESST effect containing the complex $[Fe(qsal)_2]^+$, were added.[9] These two compounds were shown to have substantially lower T(LIESST) values than expected from the above relation.

The T(LIESST) / $T_{1/2}$ values for the SCO compounds based on $[Fe^{III}(sal_2\text{-trien})]^+$ inserted into bimetallic oxalate networks as well as the other compounds reported by Sato et al.[8,9] are given in Table 4 and Figure 10.

All the $[Fe(pap)_2]^+$ complexes (points 1 to 6) lie quite close to the line with $T_0 = 150$ K, the one obtained for tridentate ligands in Fe^{II} complexes using the relation of Létard et al.[20]. Since the pap^- ligand is tridentate in nature, it can be supposed that the Fe^{III} complexes exhibiting LIESST effect follow the same law as Fe^{II} complexes. The two $[Fe(qsal)_2]^+$ compounds (points 7 and 8) lie sensibly bellow this line, although the $qsal^-$ ligand is also tridentate. Sato et al. indicated that this could be due to the incomplete LIESST effect of this complex.[9] The four $[Fe^{III}(sal_2\text{-trien})][Mn^{II}Cr^{III}(ox)_3]\cdot S$ (S = CH_2Cl_2, $CHCl_3$, CH_2Br_2, $CHBr_3$) compounds (points 9 - 12) lie notably lower than the previous Fe^{III} compounds. This behavior is significantly different to that of the pap^- ligand. Indeed, the $sal_2\text{-trien}^{2-}$ ligand is a hexadentate ligand. Thus, a priori, we would have expected the T(LIESST) / $T_{1/2}$ points to be situated on an upper line ($T_0 = 180$ K for example). A possible explanation may be related to the flexibility of the ligand. Tridentate pap^- and $qsal^-$ ligands are both entirely conjugated incontrast of the $sal_2\text{-trien}^{2-}$ ligand, which possesses three flexible ethylene bridges $-CH_2CH_2-$. A high flexibility has been recognized as a factor decreasing T(LIESST).[21]

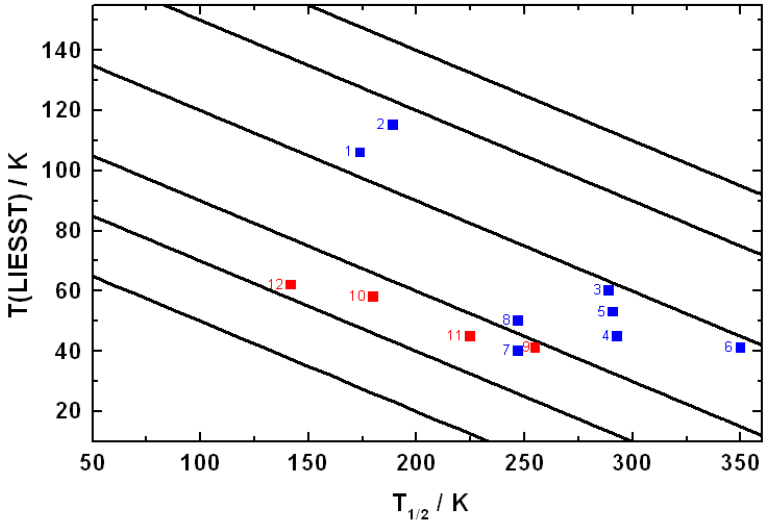

Figure 10. T(LIESST)/$T_{1/2}$ of different Fe^{III} compounds. Blue points are for $[Fe(pap)]^+$ and $[Fe(qsal)^2]^+$, whereas red points are for $[Fe^{III}(sal_2\text{-trien})][Mn^{II}Cr^{III}(ox)_3]\cdot S$ (S = CH_2Cl_2, $CHCl_3$, CH_2Br_2, $CHBr_3$). Parallel lines are for T(LIESST) = $T_0 - 0.3\cdot T_{1/2}$, with T_0 = 80, 100, 120, 150, 180 and 200 K.

Table 4. $T_{1/2}$ and T(LIESST) for different reported Fe(III) complexes

Nb	$T_{1/2}$ / K	T(LIESST) / K	Compound
1	174	106	$[Fe(pap)_2]ClO_4\cdot H_2O$
2	189	115	$[Fe(pap)_2]BF_4\cdot H_2O$
3	289	60	$[Fe(pap)_2]PF_6\cdot CH_3OH$
4	293	45	$[Fe(CH_3\text{-pap})_2]ClO_4\cdot H_2O$
5	291	53	$[Fe_{0.5}Al_{0.5}(pap)_2]ClO_4\cdot CH_3OH$
6	350	41	$[Fe_{0.25}Al_{0.75}(pap)_2]ClO_4\cdot CH_3OH$
7	247	40	$[Fe(qsal)_2]NCS$ *
8	247	50	$[Fe(qsal)_2]NCSe$ *
9	255	41	**$1\cdot CH_2Cl_2$**
10	180	58	**$1\cdot CHCl_3$**
11	225	45	**$1\cdot CH_2Br_2$**
12	142	62	**$1\cdot CHBr_3$**
13	220	45	**$2\cdot CH_2Cl_2$****
14	225	43	**$3\cdot CH_2Cl_2$**

* These two compounds present only a low light-induced HS fraction; ** partial transition only

Sato et al. have related the low T(LIESST) of $[Fe(qsal)_2]NCS$ and $[Fe(qsal)_2]NCSe$ to the low photo-conversion. Approximately 17 % and 8 % of LS species were transformed into photo-induced HS species at 5 K for $[Fe(qsal)_2]NCS$ and $[Fe(qsal)_2]NCSe$ respectively. It seems however, that in $[Fe^{III}(sal_2\text{-trien})][Mn^{II}Cr^{III}(ox)_3]\cdot S$ compounds, the situation is more complex. For example, **$1\cdot CHCl_3$** presents a T(LIESST) of 58 K with a photoconversion of about 40 % whereas **$1\cdot CHBr_3$** presents a slightly higher T(LIESST) of 62 K with a photoconversion of about 26 %. In the dilute system **$3\cdot CH_2Cl_2$**, the photoconversion is 100 % and T (LIESST) is 43 K.

Origin of the LIESST effect in Fe^{III} complexes The lifetime of the HS photoexcited state has been rationalized on the basis of a non-adiabatic mutiphonon relaxation model.[22] Within the framework of this theory, the Single Configurational Coordinate (SCC) approach considers the Metal-Ligand distance as the reaction coordinate, related to only one vibrational mode, the completely symmetrical one. According to SCC theory, the low-temperature (tunneling regime) lifetime of the HS state for Fe^{III} spin crossover compounds is expected to be of the order of milliseconds, whereas it can go from seconds to months for Fe^{II} spin crossover compounds. With this short lifetime, it should be impossible to observe the decay of the photoinduced state for Fe^{III} by using standard SQUID techniques. However, as mentioned above, the LIESST effect has been observed by Sato et al. in several Fe^{III} complexes.[8-10] These authors attributed their observations to the strong distortion of the Fe^{III} site from its octahedral geometry, enhanced by the presence of strong intermolecular interactions such as π-π stacking. Thus, when passing from the ideal octahedral site $[Fe^{II}N_6]$ site to a distorted $[Fe^{III}N_4O_2]$ geometry, in addition to the completely symmetrical vibrational mode, other vibrational modes such as the bending modes should also be taken into account.[9,23] This results in a displacement between the potential walls of the HS and LS states, which is larger than that expected considering only the changes in metal-ligand distances, and could explain the long lifetime of the photogenerated HS state.

To evaluate the structural changes of $[Fe(sal_2\text{-trien})]^+$ in **1·CH_2Cl_2**, **1·CH_2Br_2**, **1·$CHCl_3$** and **1·$CHBr_3$**, we have focused our attention on the differences between the 100 and 300 K structures as they are close to the LS and HS structures. A limitation of this comparison is that we assume that the photoinduced and high temperature HS states to present similar structures. X-ray structure determination of crystals of **1·CH_2Cl_2** after light irradiation at 10 K is in progress to verify this.

As the shortening in the Fe-N and Fe-O bond lenghts between the HS and LS structures in these compounds are similar to those of other Fe^{III} complexes, other structural factor such as the distortion of the octahedral geometry may be at the origin of the LIESST effect in these compunds. To evaluate and compare this distortion with that of other Fe^{III} complexes, we have used the program SHAPE that can be obtained from its authors upon request.[24] This program calculates continuous shape measures of a set of points (e.g. atomic positions) relative to the vertices of ideal polyhedra and has already been used to find structure-property correlations in SCO complexes.[25] It also calculates the path deviation function for the minimal distortion interconversion path between the two ideal polyhedra (octahedron and a trigonal prism in our case). In the case, SHAPE calculations show that at all temperatures, the coordination geometry around Fe falls along the minimal distortion path between a perfect octahedron and a perfect trigonal prism with a deviation of less than 10 %. We have then calculated the generalized coordinate between the two ideal polyhedra that gives the trigonal prismacity of a given coordination sphere with respect to a pure octahedron. Thus, complexes with a perfect octahedral geometry or a perfect trigonal prismatic one would have generalized coordinate values of 0 % and 100 %, respectively. Figure 11 shows that the changes of the generalized coordinate of the Fe^{III} complexes of **1·CH_2Cl_2** with the temperature follow the same trend as the increase of HS fraction extracted from magnetic and Mössbauer measurements.[5] The distortion of the octahedral geometry of these complexes from the LS to the HS state follows then a Bailar twist with a higher distortion for the HS state. The trigonal prismacity of the Fe^{III} complexes of **1·$CHCl_3$**, **1·$CHBr_3$** and **1·CH_2Br_2** in the LS and HS state are similar to those of **1·CH_2Cl_2** at the same

temperatures with small differences that can be related to small differences in the LS/HS ratio (see Figure 11). Therefore, the HS Fe^{III} complexes in **1·CH_2Cl_2**, **1·$CHCl_3$**, **1·$CHBr_3$** and **1·CH_2Br_2** present a Bailar distortion with respect to the LS complexes.

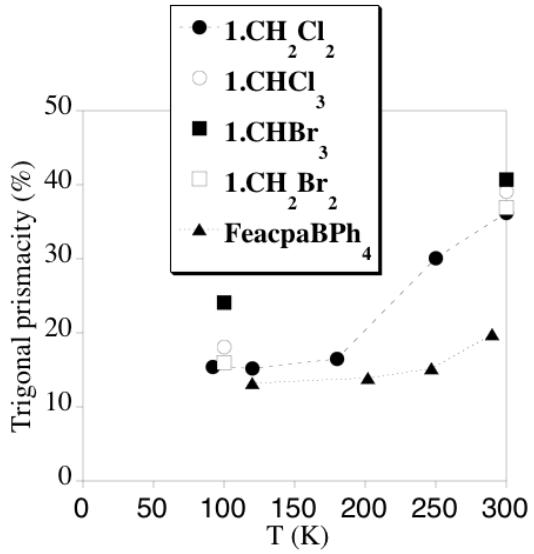

Figure 11. Trigonal prismicity of **1·$CHBr_3$**, **1·$CHCl_3$**, **1·CH_2Br_2**, **1·CH_2Cl_2** and [Fe(acpa)]BPh_4 at different temperatures calculated with SHAPE program.

To see whether the LIESST effect could be related to this distortion, the trigonal distortion of other $[Fe(sal_2\text{-trien})]^+$ salts in which LIESST is not detected, such as the reference compound, $[Fe(sal_2\text{-trien})]ClO_4$ and the compound $[Fe^{III}(sal_2\text{-trien})][Mn^{II}Cr^{III}(ox)_3]\cdot(CH_3OH)$ were calculated.[5,7,26] The result show that they present a similar trigonal distortion as those of $[Fe(sal_2\text{-trien})]^+$ salts presenting a LIESST effect.[27] Then, the same method was used to evaluate the distortion of other Fe^{III} complexes not presenting a LIESST effect such as $[Fe(acpa)_2]^+$. This complex presents a Bailar twist in $[Fe(acpa)_2]BPh_4$ that follows the same trend as the magnetic measurements (see Figure 11), but the relative changes are much smaller than those found for the $[Fe^{III}(sal_2\text{-trien})]^+$. Finally, the distortion of the octahedral geometry of $[Fe^{III}(pap)_2]^+$, the Fe^{III} complex exhibiting the clearest LIESST effect, has been evaluated. In this case, the

coordination geometry is far from the pure octahedral one even for the LS state. In contrast to $[Fe(sal_2\text{-trien})]^+$ complexes, the changes of the coordination sphere from LS to HS do not follow a Bailar distortion. This may be related to the tridentate character of the pap^- ligands that favours a different type of distortion path (D_{2d}) rather than the trigonal twist.[25a]

We conclude that the Fe^{III} complexes exhibiting a LIESST effect present a large distortion of the octahedral geometry in their HS state. However, in $[Fe^{III}(sal_2\text{-trien})]^+$ salts, other factors may contribute to this rare property as several salts of this cation with a similar distortion of the octahedral geometry do not present a LIESST effect such as ClO_4^- and 3D $[Mn^{II}Cr^{III}(ox)_3]^-$ salts. In the case of $[Fe^{III}(pap)_2]^+$ salts, which present a different distortion of the octahedral geometry between the LS and HS states, it has been proposed that cooperative interactions due to strong π-π stacking intermolecular interactions may be at the origin of the LIESST effect. This factor cannot be used to explain the LIESST effect of $[Fe^{III}(sal_2\text{-trien})]^+$ compounds as they do not present the abrupt spin-crossover transitions characteristic of cooperative systems. Furthermore, spectroscopic measurements on single crystals of the doped compound **3·CH_2Cl_2**, which is isostructural to **1·CH_2Cl_2**, confirm that the LIESST effect in this type of compounds is not related to cooperativity. An important structural difference between the compounds reported in this paper and the other Fe^{III} compounds exhibiting LIESST effect is the presence of the bimetallic anionic extended oxalate network, instead of discrete small counterions. This rigid network could play an important role in the stabilization of the metastable HS state. In favor of this hypothesis are the numerous short contacts between the $[Fe(sal_2\text{-trien})]^+$ cations and the oxalate ligands, which are different in the low and high temperature structures. These interactions may stabilize the photo-generated LIESST complex and prevent fast relaxation to the LS ground state. In other words, the increase of volume of the $[Fe^{III}(sal_2\text{-trien})]^+$ complexes after the photoinduced spin-crossover may result in new interactions with the bimetallic oxalate layers, which prevent fast relaxation to the LS ground state. A structure determination

of the metastable LIESST state is in progress to confirm this hipothesis, but this is not a tivial task.

Possible explanations for the absence of LIESST in other $[Fe(sal_2\text{-trien})]^+$ complexes inserted in 2D and 3D extended oxalate-base networks are:[7,11c] (a) a too high $T_{1/2}$ leading to a too fast HS-LS relaxation to be detected on the time scale of SQUID measurements; (b) the small amount of Fe^{III} that can undergo spin crossover, and (c) a different organization of the $[Fe(sal_2\text{-trien})]^+$ complexes in which only weak contacts with the oxalate network are stablished. Synthesis of more Fe^{III} complexes showing LIESST together with further characterization are needed to understand this unusual property.

Conclusion

We have demonstrated that the substitution of CH_2Cl_2 for other halogenated solvents in the synthesis of the 2D oxalate-based ferromagnet of formula $[Fe^{III}(sal_2\text{-trien})][Mn^{II}Cr^{III}(ox)_3]\cdot CH_2Cl_2$ permits the preparation of a family of compounds with an analogous structure that maintain the interesting physical properties of this compound, i. e., a coexistence of magnetic ordering and the LIESST effect. The subtle structural changes provide a model system for studying in detail the LIESST effect in Fe^{III} complexes. In fact, the change of solvent modifies the chemical pressure exerted on the inserted cation leading to different temperatures of the thermal and photoinduced spin crossover for each compound. Thus, the bulkiest $CHBr_3$ solvent increases the interlayer separation between layers in the structure of **1·CHBr$_3$** and favours the HS state, while the opposite is observed for the solvent of smallest volume, that is, CH_2Cl_2. As a consequence, **1·CHBr$_3$** and **1·CH$_2$Cl$_2$** presents respectively the lowest and highest $T_{1/2}$ and the highest and lowest T_{LIESST} of this family of compounds. Therefore, substitution of CH_2Cl_2 in **1·CH$_2$Cl$_2$** by the bulkier $CHBr_3$, CH_2Br_2 and $CHCl_3$ solvent molecules has proven to be a successful strategy to obtain Fe^{III} complexes exhibiting a LIESST effect at higher temperatures.

The versatility of this system has also allowed us to show that the replacement of Fe^{III} complexes by the diamagnetic Ga^{III} is a successful strategy to perform a spectroscopic characterization on single crystals. Thus, we have demonstrate that $[Ga_{1-x}Fe_x(sal_2trien)][Mn^{II}Cr^{III}(ox)_3]\cdot CH_2Cl_2$, x = 0.01 (**3·$CH_2Cl_2$**) also presents a complete thermal spin crossover and a quantitative LIESST effect. These measurements on diluted samples confirm that, in contrast to the results obtained by Sato et al., cooperativity is not a necessary condition to observe the LIESST effect in Fe^{III} complexes, as cooperativity is excluded in these doped systems due to the long distance between the Fe^{III} centers.

Structural analysis of these compounds and other Fe^{III} complexes indicates that several factors may explain the LIESST effect of Fe^{III} complexes. In the case of $[Fe^{III}(pap)_2]^+$ complexes, the presence of a rigid tridentate ligand that induces a distorted octahedral geometry together with strong π-π interactions between the Fe^{III} complexes could be at the origin of this effect, while in the $[Fe^{III}(sal_2\text{-trien})]^+$ complexes reported here, which contain a more flexible ligand, it could be related to the interactions with a bimetallic oxalate extended network. Further experiments are needed to confirm this point.

Associated Content

Supporting Information. Magnetization curves of **1·CH_2Br_2**, **1·$CHCl_3$**, and **1·$CHBr_3$**, the temperature dependence of $\chi_M T$ for **2·CH_2Cl_2**, relaxation kinetics and simulation of the $\chi_M T$ product vs. time at different temperatures of **1·CH_2Br_2**, **1·$CHCl_3$**, and **1·$CHBr_3$**, temperature dependence of the estimated relative areas of HS Fe^{III} from the Mössbauer spectra for compounds **1·CH_2Br_2**, **1·$CHCl_3$**, and **1·$CHBr_3$** and tables with the intermolecular contacts and the parameters from the relaxation kinetics curves of **1·CH_2Br_2**, **1·$CHCl_3$**, and **1·$CHBr_3$**. This material is available free of charge via the Internet at http://pubs.acs.org.

Acknowledgment

Finantial support from the European Union (MolSpinQIP and SPINMOL ERC Advanced Grant), the Spanish Ministerio de Economía y Competitividad (Projects Consolider-Ingenio in Molecular Nanoscience CSD2007-00010, MAT2011-22785 and CTQ2011-26507), and the Generalitat Valenciana (Prometeo Program) are gratefully acknowledgment. The authors also thank J. M. Martínez-Agudo, Dr. Gloria Agustí-López, University of Valencia, for magnetic characterization of the sample, Prof. S. Hayami and Prof. O. Sato by kindly providing the structural data of $[Fe^{III}(pap)_2]PF_6 \cdot CH_3OH$ compound and Prof. S. Álvarez by kindly providing the SHAPE program and for helpful discussions. AT acknowledgment a Marie-Curie Fellowship of the European Union, C. Besnard is acknowledged for the structure determination of the compound **3·CH_2Cl_2**.

References

[1] (a) E. Coronado, P. Day, *Chem. Rev.*, 2004, **104**, 5419; (b) E. Coronado, C. Martí-Gastaldo, E. Navarro-Moratalla, A. Ribera, S. J. Blundell, P. J. Baker, *Nat. Chem.*, 2010, **2**, 1031; (c) E. Coronado, C. Martí-Gastaldo, E. Navarro-Moratalla, E. Burzuri, E. Camon, F. Luis, *Adv. Mater.*, 2011, **23**, 5021.

[2] E. Coronado, G. Mínguez-Espallargas, *Chem. Soc. Rev.*, 2013, **42**,1525.

[3] (a) O. Sato, T. Iyoda, A. Fujishima, K. Hashimoto, *Science*, 1996, **272**, 704; (b) E. Coronado, M. C. Giménez-López, G. Levchenko, F. M. Romero, V. García-Baonza, A. Milner, M. Paz-Pasernak, *J. Am. Chem. Soc.*, 2005, **127**, 4580; (c) E. Coronado, M. C. Giménez-López, T. Korzeniak, G. Levchenko, F. M. Romero, A. Segura, V. García-Baonza, J. C. Cezar, F. M. F. De Groot, A. Milner, M. Paz-Pasernak, *J. Am. Chem. Soc.*, 2008, **130**, 15519; (d) S.-L. Ohkoshi, K. Imoto, S. Takano, H. Tokoro, *Natur. Chem.*, 2011, **3**, 564.

[4] (a) S. Bérnard, P. Yu, J. P. Audière, E. Rivière, R. Clèment, J. Ghulhem, L. Tchertanov, K. Nakatami, *J. Am. Chem. Soc.*, 2000, **122**, 9444: (b) E. Coronado, J. R. Galán-Mascarós, C. J. Gómez-García, V. Laukhin, *Nature*, 2000, **408**, 407; (c) C. Train, R. Gheorghe, V. Krstic, L. M. Chamoreau, N. S. Ovanesyan, G. L. J. A. Rikken, M. Gruselle, M. Verdaguer, *Nat. Mater.*, 2008, **7**, 729; (d) H. Okawa, A. Shigematsu, M. Sadakiyo, T. Miyagawa, K. Yoneda, M. Ohba, H. Kitagawa, *J. Am. Chem. Soc.*, 2009, **131**, 13516; (e) C. Train, T. Nuida, R. Gheorghe, M. Gruselle, S. Ohkoshi, *J. Am. Chem. Soc.*, 2009, **131**, 16383; (f) M. Clemente-León, E. Coronado, C. Martí-Gastaldo, F. M. Romero, *Chem. Soc. Rev.*, 2011, **40**, 473; (g) E. Pardo, C. Train, H. Liu, L.-M- Chamoreau, B. Dkhil, K. Boubekeur, F. Lloret,

K. Nakatani, H. Tokoro, S.-I. Ohkoshi, M. Verdaguer, *Angew. Chem., Int. Ed*., 2012, **51**, 8356; (h) M. Sadayiko, H. Okawa, A. Shigematsu, M. Ohba, T. Yamada, H. Kitagawa, *J. Am. Chem. Soc.*, 2012, **134**, 5472; (i) H. Okawa, M. Sadayiko, T. Yamada, M. Maesato, M. Ohba, H. Kitagawa, *J. Am. Chem. Soc.*, 2013, **135**, 2256.

[5] M. Clemente-León, E. Coronado, M. López-Jordà, G. Mínguez-Espallargas, A. Soriano-Portillo, J. C. Waerenborgh, *Chem Eur. J.*, 2010, **16**, 2207.

[6] (a) S. Decurtins, P. Gütlich, C. P. Köhler, H. Spiering, A. Hauser, *Chem. Phys. Lett.*, 1984, **105**, 1; (b) A. Hauser, T*op. Curr. Chem.*, 2004, **234**, 155.

[7] M. Clemente-León, E. Coronado, M. López-Jordà, C. Desplanches, S. Asthana, H. Wang, J.-F. Létard, *Chem. Sci.*, 2011, **2**, 1121.

[8] (a) S. Hayami, Z.-Z. Gu, M. Shiro, Y. Einaga, A. Fujishima, O. Sato, *J. Am. Chem. Soc.*, 2000, **122**, 7126; (b) G. Juhász, S. Hayami, O. Sato, Y. Maeda, *Chem. Phys. Lett.*, 2002, **364**, 164 ; (c) S. Hayami, T. Kawahara, Y. Maeda, K. Inoue, O. Sato, *J. Radioanal. Nucl. Chem.*, 2005, **266**, 521.

[9] S. Hayami, K. Hiki, T. Kawahara, Y. Maeda, D. Urakami, K. Inoue, M. Ohama, S. Kawata, O. Sato, *Chem. Eur. J.*, 2009, **15**, 3497.

[10] T. Shimizu, Y. Komatsu, H. Kamihata, Y. H. Lee, A. Fuyuhiro, S. Iijima, S. Hayami, *J. Incl. Phenom. Macrocycl. Chem.*, 2011, **71**, 363.

[11] (a) M. Clemente-León, E. Coronado, M. López-Jordà, *Dalton Trans.*, 2010, **39**, 4903; (b) M. Clemente-León, E. Coronado, M. López-Jordà, J. C. Waerenborgh, *Inorg. Chem.*, 2011, **50**, 9122; (c) M. Clemente-León, E. Coronado, M. López-Jordà, *Eur. J. Inorg. Chem.*, 2013, 753.

[12] M. F. Tweedle, L. J. Wilson, *J. Am. Chem. Soc.*, 1976, **98**, 4824.

[13] J. C. Baylar, E. M. Jones, *Inorganic Synthesis*; H. S. Booth, Ed. McGraw-Hill, New York, 1939, Vol. 1, p 35.

[14] A. Altomare, M. C. Burla, M. Camalli, G. L. Cascarano, C. Giacovazzo, A. Guagliardi, A. G. G. Moliterni, G. Polidori, R. Spagna*, J. Appl. Cryst*., 1992, **32**, 115.

[15] SHELXL-97: G. M. Sheldrick, University of Göttingen, Germany, 1997.

[16] L. J. Farrugia, *J. Appl. Cryst*., 1997, **32**, 837.

[17] J. V. Rodrigues, I. C. Santos, V. Gama, R. T. Henriques, J. C. Waerenborgh, M. T. Duarte, M. Almeida, *J. Chem. Soc. Dalton Trans.*, 1994, 2655.

[18] Unit cell of compound $[In^{III}(sal_2\text{-trien})][Mn^{II}Cr^{III}ox)_3]$ obtained in CH_2Cl_2 measured with single crystal X-ray data diffraction (a = 15.841 (12) Å, b = 20.639 (16) Å, c = 21.285 (18) Å, β = 90°, V = 6947 (10) $Å^3$) is similar to that of other 3D compounds obtained in CH_3CN or CH_3NO_2 such as compound **4** from reference 5.

[19] Unit cell of compound $[Ga^{III}(sal_2\text{-trien})][Mn^{II}Cr^{III}ox)_3]\cdot CH_2Cl_2$ measured with single crystal X-ray data diffraction (a = 11.851 (8) Å, b = 31.972 (18) Å, c = 9.486 (7) Å, β = 111.62 (6)°, V = 3342 (4) $Å^3$) is similar to that of the 2D compounds obtained in CH_2Cl_2 with $[Fe^{III}(sal_2\text{-trien})]$ (**1·CH_2Cl_2**).

[20] V. Mishra, R. Mukherjee, J. Linares, C. Baldé, C. Desplanches, J.-F. Létard, E. Collet, L. Toupet, M. Castro, F. Varret, *Inog. Chem.*, 2008, **47**, 7577.

[21] (a) J.-F. Létard, P. Guionneau, O. Nguyen, J. Sanchez Costa, S. Marcen, G. Chastanet, M. Marchivie, L. Goux-Capes, *Chem. Eur. J.* 2005, **11**, 4582 ; (b) J.-F. Létard, *J. Mater. Chem.* 2006, **16**, 2550.

[22] A. Hauser, *J. Chem. Phys.* **1991***, 94*, 2741.

[23] S. Schenker, A. Hauser, R. M. Dyson, *Inorg. Chem.* 1996, **35**, 4676.

[24] M. Llunell, D. Casanova, J. Cirera, J. M. Bofill, P. Alemany, S. Alvarez, M. Pinski, D. Avnir, SHAPE (2.0); Barcelona 2010

[25] (a) S. Alvárez, *J. Am. Chem. Soc.* 2003, **125**, 6795; (b) G. S. Matouzenko, S. A. Borshch, E. Jeanneau, M. B. Bushuev, *Chem. Eur. J.* 2009, **15**, 1252.

[26] R. Pritchard, S. A. Barrett, C. A. Kilner, M. A. Halcrow, *Dalton Trans.*, 2008, 3159.

[27] Trigonal prismacity of the two crystallographically independent iron atoms of $[Fe^{III}(sal_2\text{-trien})]$ $[Mn^{II}Cr^{III}ox)_3]\cdot CH_3OH$ is 29.1 and 34.9 % at 120 K, temperature at which 70 % of FeIII is in the HS state. Trigonal prismacity or the four crystallographically independent iron atoms of $[Fe^{III}(sal_2\text{-trien})]ClO_4$ is 37.4 and 41.8 % for the HS Fe^{III} and 14.1 and 19.2 % fo the LS Fe^{III} at 105 K. At this temperature half of the Fe^{III} is in the HS state (see reference 26).

2D and 3D bimetallic oxalate-based ferromagnets prepared by insertion of different Fe^{III} spin crossover complexes

Dalton Transactions

Capítulo 5

Capítulo 5: 2D and 3D bimetallic oxalate-based ferromagnets prepared by Insertion of a Fe^{III} Spin-Crossover Complexes

The syntheses, structures and magnetic properties of the compounds of formula $[Fe^{III}(5\text{-}NO_2sal_2\text{-}trien)][Mn^{II}Cr^{III}(ox)_3]\cdot(CH_3NO_2)\cdot 0.5(H_2O)$ **(1)** and $[Fe^{III}(5\text{-}CH_3Osal_2\text{-}trien)][Mn^{II}Cr^{III}(ox)_3]$ **(2)** are reported. The structure of **1**, that crystallizes in the $P2_1$ chiral space group, presents a 2D honeycomb anionic layer formed by Mn^{II} and Cr^{III} ions linked through oxalate ligands and a cationic layer of $[Fe^{III}(5\text{-}NO_2sal_2\text{-}trien)]^+$ complexes intercalated between the 2D oxalate network. The structure of **2**, that crystallizes in the $Pna2_1$ acentric space group, presents a 3D achiral anionic network formed by Mn^{II} and Cr^{III} ions linked through oxalate ligands with $[Fe(5\text{-}CH_3Osal_2\text{-}trien)]^+$ complexes intercalated within the 3D oxalate network. The magnetic properties of **1** and **2** indicate that both compounds undergo a long-range ferromagnetic ordering at ca. 5 K. On the other hand, the inserted Fe^{III} cations remain mainly in the low-spin (LS) state in the case of **1** and in the high-spin (HS) state in the case of **2**.

Introduction

For more than 30 years molecular magnetism has been a source of novel materials. The flexibility offered by the molecular approach has afforded the development of materials with novel and unprecedented properties. In this direction the multifunctional materials that combine two (or more) physical properties of interest are one of the most promising areas.[1] A wise choice of the constituent molecules could allow the appearance in the same compound of an unusual combination of physical properties, or even a mutual interplay or synergy of the properties involved. A suitable approach to obtain such materials is the so-called hybrid approach in which two network solids are constructed *via* self-assembling of two different molecular fragments (organic, inorganic or organometallic), with each network furnishing distinct properties to the solid.

Bimetallic oxalate-bridged complexes of formula $A[M^{II}M^{III}(ox)_3]$ (M^{III} = Cr, Fe, Ru, V, Mn; M^{II} = Mn, Fe, Co, Ni, Cu, Zn; A = Cation; ox = oxalate) have provided many examples of hybrid magnets. These bimetallic salts are most often composed by polymeric 2D anionic networks, which furnish the cooperative magnetic properties (ferro-, ferri- or canted antiferromagnetism),[2] and a bulky charge-compensating molecular cation, which templates the network formation. In these compounds the cooperative magnetism of the oxalate network can co-exist with the electronic property provided by the cationic molecular lattice. Thus, paramagnetic decamethylferrocenium[3] or organic radical cations,[4] photochromic molecules,[5] NLO-active molecules,[6] organic π-electron donors,[7] and chiral molecules[8,9] have led to the formation of magnetic multilayers, photochromic magnets, ferromagnetic molecular metals or chiral magnets. New properties for this type of compounds such as the magnetisation-induced second harmonic generation,[10] observed in an enantiopure 2D oxalate-based magnet, and proton conduction, observed in a 2D oxalate-based magnet containing a hydrophilic ammonium cation,[11] have been reported very recently. Other magnetic networks, different from the 2D honeycomb-like network, can also be obtained depending on the nature of the templating cation (size, shape and charge) with dimensionalities ranging from 0D to 3D.[12] The most extensive one is represented by the family of 3D chiral structures in which the chirality of a templating cation of the type $[Z^{II}(bpy)_3]^{2+}$ (Z^{II} = Fe, Co, Ni, Ru; bpy = 2,2'-bipyridine) induces the building blocks to adopt an homochiral configuration,[13] which provides an opportunity to obtain chiral magnets.[13e,14] In addition, the hybrid character of these series also leads to examples in which the two sublattices are magnetic.[13d]

Spin crossover cations are particularly suitable to prepare multifunctional magnetic materials since they represent one of the best examples of molecular bistability. This may open a way to design switching magnets in which the magnetic ordering of the oxalate network could be tuned by inducing the spin crossover phenomenon applying external stimuli such as light or pressure.

The first example of the insertion of spin crossover cations into oxalate networks was reported by Decurtins et al. in a compound of formula $[Co(bpy)_3][LiCr(ox)_3]$.[15] This compound did not show coexistence of spin crossover and magnetic ordering since the oxalate network was paramagnetic. More recently, our group reported the insertion of the Fe^{II} spin-crossover complex, $[Fe(bpp)_2]^{2+}$ [bpp = 2,6(bis(pyrazol-3-yl) pyridine)], into a ferromagnetic achiral 3D oxalate-based network, $[Fe(bpp)_2][MnCr(ox)_3]\cdot(bpp)\cdot(CH_3OH)$,[16] although spin crossover was not observed. In a further attempt, the coexistence of a spin crossover and magnetic ordering was successfully demonstrated in hybrid compounds obtained by insertion of a Fe^{III} complex, $[Fe^{III}(sal_2\text{-trien})]^+$ (H_2sal_2-trien = N,N'-disalicylidenetriethylene-tetramine) in homometallic[17] and bimetallic oxalate layers.[18] As a result, the compound $[Fe^{III}(sal_2\text{-trien})]_2[Mn^{II}_2(ox)_3]\cdot 4(H_2O)\cdot(C_3H_7NO)$ formed by homometallic Mn^{II} oxalate layers and inserted $[Fe(sal_2\text{-trien})]^+$ behaves as a weak ferromagnet below T_c = 8.1 K, exhibiting at the same time a gradual spin crossover from 300 to 80 K of half of the intercalated Fe^{III} complexes.[17] As far as the bimetallic oxalate layers are concerned, the magnetic properties of the compound $[Fe^{III}(sal_2\text{-trien})][Mn^{II}Cr^{III}(ox)_3]\cdot(CH_2Cl_2)$ formed by $[Fe^{III}(sal_2\text{-trien})]^+$ and $Mn^{II}Cr^{III}$ bimetallic layers, indicate the coexistence of a complete spin crossover transition from 300 to 160 K, and a ferromagnetic ordering below 5.4 K. It is interesting to notice that by changing the synthetic conditions the $[Fe^{III}(sal_2\text{-trien})]^+$ also stabilizes a 3D structure for the $Mn^{II}Cr^{III}$ bimetallic network. The resulting structure is similar to that of $[Fe(bpp)_2][MnCr(ox)_3]\cdot(bpp)\cdot(CH_3OH)$. This last compound shows a gradual and incomplete spin-crossover of 30 % of the Fe^{III} from 300 to 130 K, together with a ferromagnetic ordering of the 3D lattice below 5.2 K. The stabilization of two different oxalate networks with the same templating cation is a novel feature in this type of compounds. It can be explained by the structural flexibility of $[Fe^{III}(sal_2\text{-trien})]^+$ that presents a very different configuration in the two compounds.[18]

Although hybrid magnets with coexistence of magnetic ordering and spin crossover have been designed using this molecular approach, the preparation of

hybrid switchable magnets has not yet been reached. $[Fe^{III}(sal_2\text{-trien})][Mn^{II}Cr^{III}(ox)_3]\cdot(CH_2Cl_2)$ could be a good candidate for this purpose as it undergoes a complete spin-crossover. However, it is unexpected that the changes in structure of the intercalated compound due to spin crossover could modify the T_c of the 2D oxalate network, as 2D oxalate networks with different interlayer separations present similar T_c values. In this sense, compounds with a 3D network are expected to be better candidates because the T_c of 3D oxalate compounds is very sensistive to the size of the intercalated cation, *i.e.*, to the chemical pressure.[13f] Unfortunately, in the two 3D compounds obtained so far the occurrence of a spin-crossover and its influence on the ferromagnetic sublattice is very limited. In an attempt to improve these results, we have extended this strategy to derivatives of $[Fe^{III}(sal_2\text{-trien})]^+$ with different substituents on the position 5 of the salicylaldimine ring. From the structural point of view this could lead to new bimetallic oxalate networks more suitable for obtaining switching magnets. On the other hand, the presence of different substituent groups could tune the spin state of the inserted Fe^{III} complex. In general for this type of complexes electron-withdrawing groups, such as NO_2, favours the low-spin (LS) state whereas electron-donating groups, such as CH_3O, favours the high-spin (HS) state.[19]

In this work we report the preparation and structural and magnetic characterization of the hybrid compounds obtained by combining $[Fe^{III}(5\text{-}Xsal_2\text{-trien})]^+$ (X = NO_2 or CH_3O, see scheme 1) with the $Mn^{II}Cr^{III}$ bimetallic networks.

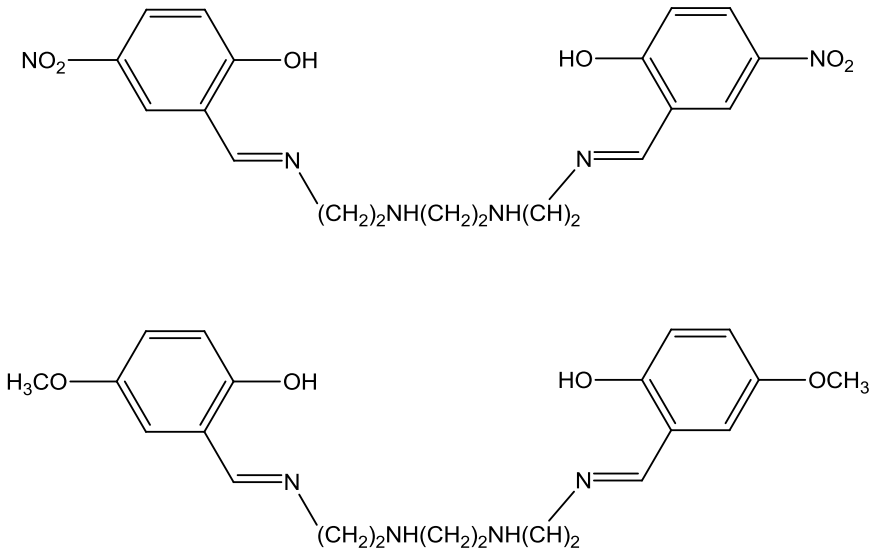

Scheme 1. H_2(5-NO_2sal$_2$-trien) (up) and H_2(5-CH_3Osal$_2$-trien) (down)

Experimental Section

Synthesis

The complexes [Fe^{III}(5-NO_2sal$_2$-trien)]PF_6 and [Fe^{III}(5-CH_3Osal$_2$-trien)]PF_6 were prepared according to literature methods.[19] $Ag_3[Cr(ox)_3]$ was prepared by metathesis from the corresponding potassium salt.[20] All other materials and solvents were commercially available and used without further purification.

[Fe^{III}(5-NO_2sal$_2$-trien)][$Mn^{II}Cr^{III}(ox)_3$]·(CH_3NO_2)·0.5(H_2O) (1). Crystals of this compound were obtained by slow diffusion of two solutions. The first solution was prepared by adding $MnCl_2·4H_2O$ (0.029 g, 0.148 mmol) to a suspension of $Ag_3Cr(Ox)_3$ (0.063 g, 0.098 mmol) in 6 mL of methanol. The AgCl precipitate was filtered off. The second solution was obtained by dissolving [Fe^{III}(5-NO_2sal$_2$trien)]PF_6 (0.064 g, 0.098 mmol) in 6 mL of nitromethane. After two weeks brown crystals were obtained.

[Fe^{III}(5-CH_3Osal$_2$-trien)][$Mn^{II}Cr^{III}(ox)_3$] (2). Crystals of this compound were obtained by slow diffusion of two solutions. The first solution was prepared by adding $MnCl_2 \cdot 4H_2O$ (0.032 g, 0.165 mmol) to a suspension of $Ag_3Cr(Ox)_3$ (0.069 g, 0.11 mmol) in 6 mL of methanol. The AgCl precipitate was filtered off. The second solution was obtained by dissolving [Fe^{III}(5-CH_3Osal$_2$trien)]PF_6 (0.067 g, 0.11 mmol) in 6 mL of 1,2-dichloroethane. After two weeks brown crystals were obtained.

Structural characterisation

Single crystal X-ray data of **1** and **2** were collected at 120 K on a Xcalibur, Sapphire3, Gemini diffractometer equipped with a graphite-monochromated Enhance (Mo) X-ray Source (λ = 0.71073 Å). The program CrysAlisPro, Oxford Diffraction Ltd., Version 1.171.33.52 was used for cell refinements and data reduction of the compounds. Empirical absorption correction was performed using spherical harmonics, implemented in SCALE3 ABSPACK scaling algorithm. Crystal structures were solved by direct methods with the SIR97 program,[21] and refined against all F^2 values with the SHELXL-97 program,[22] using the WinGX graphical user interface.[23] Non-hydrogen atoms were refined anisotropically (except as noted), and hydrogen atoms were placed in calculated positions refined using idealized geometries (riding model) and assigned fixed isotropic displacement parameters. The small size of the crystals of **1** and **2** gave rise to a very weak scattering. Due to this the number of reflections was not enough to carry out anisotropic refinement of all the atoms in **1**. Thus, only Mn, Cr and Fe atoms were refined anisotropically. In **1**, one of two crystallographically independent nitromethane solvent molecules was modeled in two orientations. In **2**, one of the two crystallographically independent [Fe^{III}(5-CH_3Osal$_2$-trien)]$^+$ complexes was modeled in two orientations. The other crystallographically independent [Fe^{III}(5-CH_3Osal$_2$-trien)]$^+$ complex could present some type of disorder that could not be solved. Due to this, short intermolecular distances (2.51 Å) and high U_{eq} are found in some atoms of these molecules. Carbon, nitrogen and oxygen atoms of the 5-CH_3Osal$_2$-trien ligand could only be

modeled isotropically due to the flexibility of the ligand. The use of restraints and/or constraints in the refinement of the structures is documented in the corresponding CIFs. Data collection and refinement statistics are collected in Table 1.

Table 1. Crystallographic data for compounds **1** and **2**.

Compound	**1**	**2**
Empirical formula	$C_{54}H_{52}Cr_2Fe_2Mn_2N_{14}O_{41}$	$C_{56}H_{56}Cr_2Fe_2Mn_2N_8O_{32}$
Formula weight	1878.66	1678.67
Crystal color	Brown	Brown
Temperature (K)	120(2)	120(2)
Wavelength, λ (*Å*)	0.71073	0.71073
Crystal system	Monoclinic	Orthorhombic
Space group	$P2_1$	$Pna2_1$
a (Å)	12.712(3)	20.8484(16)
b (Å)	15.933(3)	21.710(2)
c (Å)	18.379(4)	15.4856(13)
β (°)	106.59(3)	90
V (Å^3)	3567.5(12)	7009.0(11)
Z	2	4
D_c (Mg/m^3)	1.747	1.591
$\mu(Mo_{K\alpha})$ (mm^{-1})	1.146	1.145
θ range (°)	2.29 to 27.07	2.36 to 32.56
Reflns collected	20271	78783
Independent reflns, (R_{int})	10434 (0.0915)	22802 (0.1019)
L. S. parameters/ restraints	509/9	706/14
$R1(F)$,[a] [$I>2\sigma(I)$]	0.0730	0.0723
$wR2(F^2)$,[b] (all data)	0.1203	0.1778

[a] $R1(F) = \Sigma(||F_O| - |F_C||)/\Sigma|F_O|$; [b] $wR2(F^2) = [\Sigma w(F_O^2 - F_C^2)^2/\Sigma wF_O^4]^{1/2}$

Physical measurements

Magnetic susceptibility measurements were performed on polycrystalline samples using a magnetometer (Quantum Design MPMS-XL-5) equipped with a SQUID sensor. Variable-temperature measurements were carried out in the temperature range 2 - 400 K. The AC measurements were performed in the temperature range 2 - 10 K at different frequencies with an oscillating magnetic field of 0.395 mT. The magnetisation and hysteresis studies were performed between 5 and –5 T, cooling the samples at zero field. The Fe:Mn:Cr ratios were measured on a Philips ESEM X230 scanning electron microscope equipped with an EDAX DX-4 microsonde.

Results and Discussion

Synthesis

The method used to prepare $[Fe^{III}(5\text{-}NO_2sal_2\text{-}trien)][Mn^{II}Cr^{III}(ox)_3]\cdot(CH_3NO_2)\cdot 0.5(H_2O)$ (**1**) and $[Fe^{III}(5\text{-}CH_3Osal_2\text{-}trien)][Mn^{II}Cr^{III}(ox)_3]$ (**2**) is similar to what was used to prepare the compounds with $[Fe^{III}(sal_2\text{-}trien)]^+$.[18] It is based in the use of $Ag_3[Cr(ox)_3]$ to avoid the presence of alkali ions in the structure. It consists on the slow diffusion of a methanol solution containing the precursors of the oxalate network, Mn^{2+} and $[Cr(ox)_3]^{3-}$ ions, into a solution of $[Fe^{III}(5\text{-}Xsal_2\text{-}trien)]^+$ (X = NO_2 or CH_3O) in different solvents. In contrast to the compounds with $[Fe^{III}(sal_2\text{-}trien)]^+$ in which the use of different solvents to dissolve the Fe^{III} complex afforded compounds with different types of oxalate network (2D and 3D), only one type of oxalate network was obtained for each templating cation of $[Fe^{III}(5\text{-}Xsal_2\text{-}trien)]^+$ (X = NO_2 or CH_3O). In the case of $[Fe^{III}(5\text{-}NO_2sal_2\text{-}trien)]^+$ cation, the only solvent that led to crystals of adequate quality for X-ray single crystal diffraction was CH_3NO_2, whereas for $[Fe^{III}(5\text{-}CH_3Osal_2\text{-}trien)]^+$ cation, crystals of **2** were obtained with CH_2ClCH_2Cl whereas other solvents such as acetone or acetonitrile gave rise to crystals with a similar unit cell. It seems that the presence of CH_3NO_2 is necessary for the crystallisation of compound **1** as the solvent molecules enter in the structure (see below). The

composition of these crystals, checked by microanalysis, showed in all cases a Fe:Mn:Cr ratio of 1:1:1. The crystal structures of the two compounds have been solved by single-crystal X-ray diffraction. Attempts to obtain analogous compounds with other paramagnetic M^{2+} ions (M = Ni, Fe, Co and Cu) have been unsuccessful.

Structure of 1

The best solution to the structure of this compound is found in the chiral space group $P2_1$. Structural analysis applying any achiral space group does not converge to a normal solution. The crystal was solved as a racemic twin with a BASF parameter of 0.35785. In this case, the BASF coefficient is the Flack absolute structure parameter *x*.[24] Therefore, the structure resolution has been performed in a twinned crystal containing crystals of opposite chirality.

The structure is formed by anionic sheets in the *-101* plane of formula $[MnCr(ox)_3]^-$ with inter-lamellar $[Fe^{III}(5\text{-}NO_2sal_2\text{-}trien)]^+$ cations and nitromethane and water solvent molecules (Fig. 1). The anionic layer presents the well-known 2D honeycomb structure formed by an extended network with Mn^{II} and Cr^{III} ions linked through oxalate bridges. It is formed by oxalate ligands connecting Mn^{II} with Cr^{III} ions in such a way that each Mn^{II} is surrounded by three neighbouring Cr^{III} and vice versa (Fig. 2). These ions present octahedral coordination. The Mn^{II} and Cr^{III} are clearly distinguishable as they present different bond distances with oxalate ligands. Thus, there are two crystallographically independent Mn ions (Mn1 and Mn2) with Mn–O distances lying between 2.139(9) and 2.228(10) Å and two crystallographically independent Cr ions (Cr1 and Cr2) with Cr–O distances lying between 1.949(8) and 2.029(8) Å. These are typical Mn^{II}–O and Cr^{III}–O distances similar to those found in other oxalate networks. The neighbouring metal centres of these layers present alternated chirality as usual for this type of networks. In this structure all the Cr^{III} ions adopt a Δ configuration, whereas all the Mn^{II} adopt the Λ one. Therefore, the configuration of each metal ion is preserved in the neighbouring oxalate layers. Since we have started from a racemic mixture of $[Cr(ox)_3]^{3-}$ anion,

crystals of the two enantiomers have been obtained as expected. A similar behavior has been observed in other 2D oxalate structures.[11,25,26] The chirality of the $[Fe^{III}(5\text{-}NO_2sal_2\text{-}trien)]^+$ cations may be responsible of this first-order spontaneous resolution through chiral recognition between one of the enantiomers of $[Cr(ox)_3]^{3-}$ and $[Fe^{III}(5\text{-}NO_2sal_2\text{-}trien)]^+$. In agreement to this, one of the two crystallographically independent $[Fe^{III}(5\text{-}NO_2sal_2\text{-}trien)]^+$ complexes placed between the oxalate layers, [Fe1] (see below), which only adopts a Λ configuration, interacts through several short contacts with Cr1, which adopts a Δ configuration.

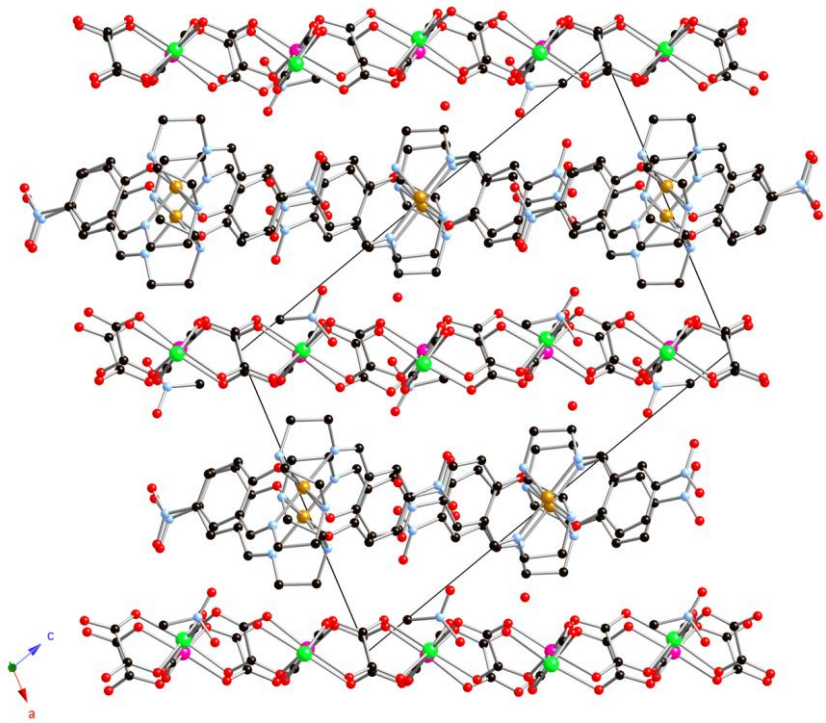

Fig. 1 Lateral view of the anionic and cationic layers of **1** (Fe (yellow), Cr (pink), Mn (green), C (black), N (blue), O (red)). Hydrogen atoms have been omitted for clarity. Only one of the two configurations of disordered nitromethane solvent molecule is shown for clarity.

Mean metal-metal distances between adjacent centres are in the range 5.416-5.456 Å. These distances are similar to those found in other 2D oxalate networks reported

in the literature.[2,3] The minimum distance between metals of different layers is 11.609 Å, which is higher than those found in other oxalate-based 2D compounds with decamethylferrocenium or alkylammonium cations (9.2-9.7 Å)[2,3] but similar to that of the 2D compound obtained by insertion of $[Fe^{III}(sal_2\text{-trien})]^+$ (11.6440(2) Å).[18] These anionic layers are stacked one over the other in an *AB*···fashion. In contrast to the structure of $[Fe^{III}(sal_2\text{- trien})][Mn^{II}Cr^{III}(ox)_3]\cdot CH_2Cl_2$ in which there is a certain undulation of the oxalate layer, the Mn^{II} and Cr^{III} ions and oxalate ligands form an almost perfect 2D layer in the structure of **1** (see Fig. 1). A possible explanation for this difference is the slightly larger interlayer distance in **1**. Finally, the minimum distance between the metallic ions from the oxalate network and the Fe atoms is 6.363 Å which is similar to that found in $[Fe^{III}(sal_2\text{-trien})][Mn^{II}Cr^{III}(ox)_3]\cdot CH_2Cl_2$.[18]

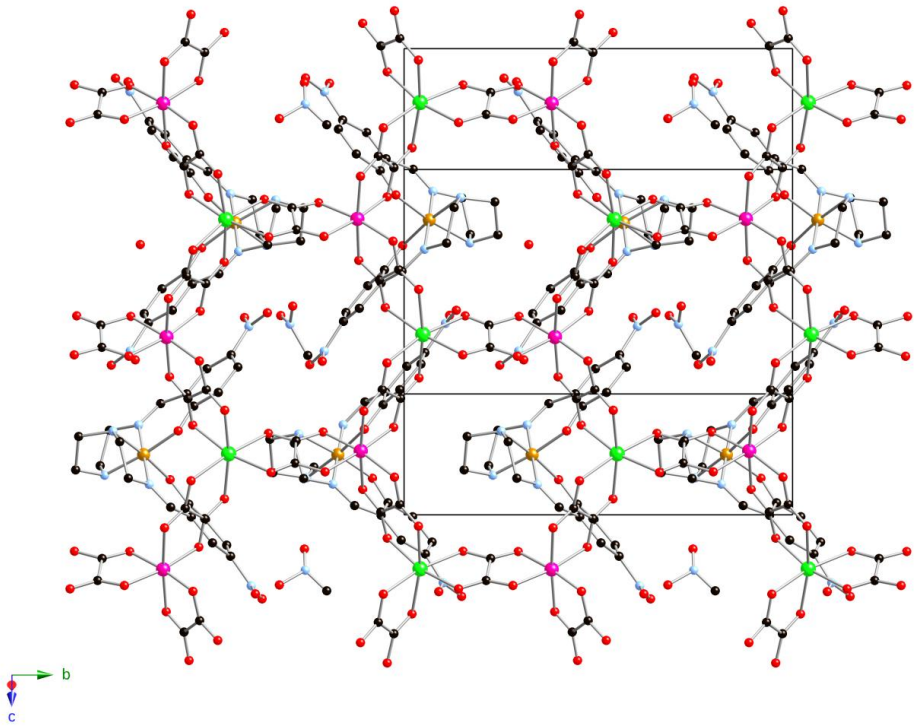

Fig. 2 Projection of **1** in the *-101* plane. (Fe (yellow), Cr (pink), Mn (green), C (black), N (blue), O (red)). Hydrogen atoms have been omitted for clarity. Only one of the two configurations of disordered nitromethane solvent molecule is shown for clarity.

The space between the oxalate layers is occupied by two crystallographically independent $[Fe^{III}(5\text{-}NO_2sal_2\text{-}trien)]^+$ complexes ([Fe1] and [Fe2]), two nitromethane and one water solvent molecules (Fig. 1 and 2). Fe^{III} ions present octahedral coordination. The average Fe–N and Fe–O bond distances are 1.955(10) and 1.898(8) Å in [Fe1] complexes and 1.972(12) and 1.882(9) Å in [Fe2] complexes. These values are in the range of those obtained for other LS $[Fe(sal_2\text{-}trien)]^+$ compounds, in full agreement with the magnetic measurements (see below), which indicate that all Fe are LS at 120 K (temperature at which the crystal structure has been determined). The dihedral angles, α, between the least squares planes of the two phenoxy rings are α = 89.002° ([Fe1] complex) and α = 94.248° ([Fe2] complex). The $[Fe^{III}(5\text{-}NO_2sal_2\text{-}trien)]^+$ cations lie with their longer axis parallel to the oxalate layers. The presence of the NO_2 group favours face-to-face interactions[27] between the aromatic rings of neighbouring $[Fe^{III}(5\text{-}NO_2sal_2\text{-}trien)]^+$ cations in contrast to the previous structures with $[Fe^{III}(sal_2\text{-}trien)]^+$ that presented mainly edge-to-face interactions.[18] Thus, each aromatic ring of [Fe1] complexes is connected through π···π stacking interactions with two neighbouring [Fe2] complexes forming a chain of alternating [Fe1] and [Fe2] complexes (see Fig. S1, ESI). In these chains, the two configurations of $[Fe^{III}(5\text{-}NO_2sal_2\text{-}trien)]^+$ complex are present as [Fe1] complexes are in the Λ configuration while [Fe2] complexes adopt the Δ configuration. [Fe1] and [Fe2] complexes belonging to the same chain present hydrogen bonds between the NO_2 group of each aromatic ring and the NH groups of the neighbouring complex. The complexes from different chains are connected through C–H···π interactions between the ethylene groups of one complex and the two aromatic rings of another complex. Furthermore, there are short contacts between N and O from NO_2 groups belonging to different chains. The two crystallographically independent nitromethane molecules occupy positions very close to the centre of the hexagonal rings of the oxalate network placed alternatively above and below the oxalate layer. One of the nitromethane molecules presents a disorder between two possible orientations. The water molecule occupies the holes between the

oxalate network and the layer of $[Fe^{III}(5\text{-}NO_2sal_2\text{-}trien)]^+$ cations.

Structure of 2

2 crystallises in the acentric orthorhombic space group *Pna2₁*, that contains metal centres of both chiralities. The structure of **2** is formed by an anionic 3D polymeric oxalate-bridged bimetallic network with $[Fe^{III}(5\text{-}CH_3Osal_2\text{-}trien)]^+$ cations occupying the cavities (Fig. 3). A very similar achiral 3D oxalate network has been found in the compound of formula $[In^{III}(sal_2\text{-}trien)][Mn^{II}Cr^{III}(ox)_3]\cdot(CH_3NO_2)\cdot 0.5(H_2O)$ that crystallizes in the same space group.[18] Other compounds with similar achiral 3D network reported in the literature are those of formula $[Fe(bpp)_2][MnCr(ox)_3]_2 \cdot bpp\cdot CH_3OH$ that crystallizes in the centrosymmetric *P2₁/n* space group,[16] $[Fe^{III}(sal_2\text{-}trien)][Mn^{II}Cr^{III}(ox)_3]\cdot(CH_3OH)$ and $[In^{III}(sal_2\text{-}trien)][Mn^{II}Cr^{III}(ox)_3]\cdot 0.25(H_2O) \cdot 0.25(CH_3OH)\cdot 0.25(CH_3CN)$ that crystallize in the acentric *Cc* space group.[18] This anionic polymeric structure is formed by bis-chelating oxalate ligands connecting Mn^{II} and Cr^{III} ions in such a way that each Mn^{II} is surrounded by three Cr^{III} and *vice versa*, building ten-membered rings in a (10,3) topology. The (10,3) decagon rings perpendicular to the *a* axis are formed by metal centers with the same chirality (see Fig. 3). Two of these neighbouring metal rings, that are linked trough two oxalate ligands, present opposite chirality (see Fig. 4).

Projection of the oxalate network on the *ab* plane is almost identical to that of the chiral 3D oxalate network in the *ab*, *bc* or *ac* planes (see Fig. 5). However, projection on the *ac* or *bc* planes (see Fig. 3 and 4) are different as a result of the different chirality of the neighbouring (10,3) decagon rings. Thus, in the *ac* projection an eclipsed disposition of the neighbouring oxalate rings is observed as a result of the heterochiral oxalate junctions among them (see Fig. 3). Mn and Cr present an octahedral coordination. Again, it is possible to distinguish between Mn^{II} and Cr^{III} ions of this oxalate network. Thus, there are two crystallographically independent Mn^{II} ions (Mn1 and Mn2) with Mn–O distances lying between 2.127(5) and 2.201(5) Å and two crystallographically independent Cr^{III} ions (Cr1 and Cr2) with

Cr–O distances lying between 1.951(6) and 1.990(5) Å. These are typical Cr^{III}–O and Mn^{II}–O distances similar to those found in other oxalate networks. Metal-metal distances between adjacent centers are in the range 5.362-5.426 Å. These metal-metal distances are shorter than those exhibited by **1**.

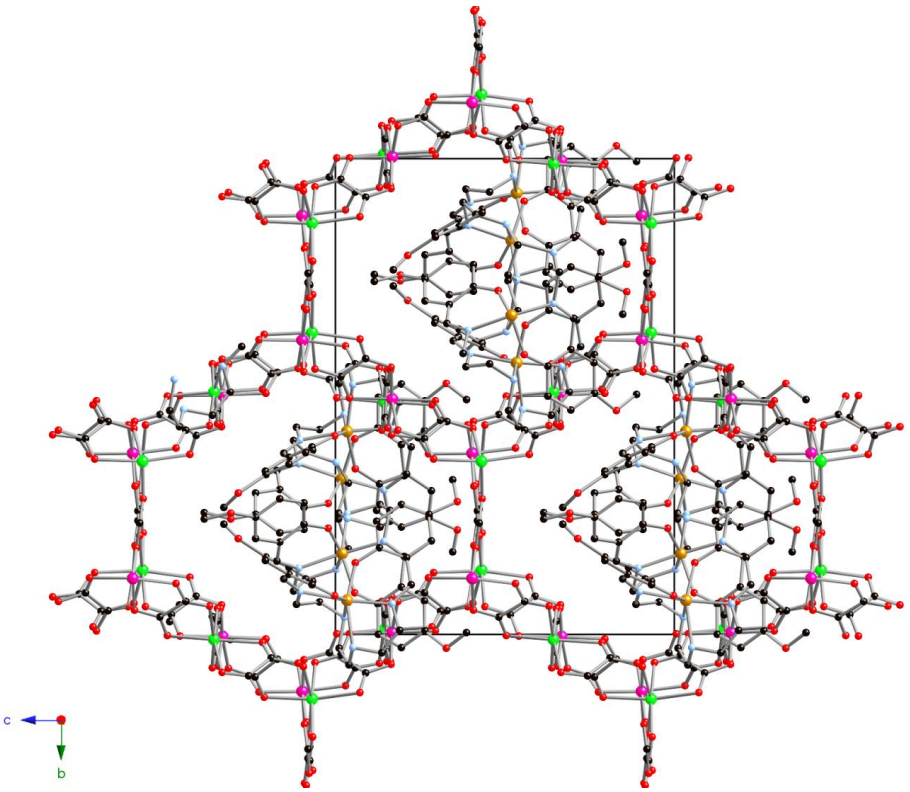

Fig. 3 Projection of **2** in the *bc* plane. (Fe (yellow), Cr (pink), Mn (green), C (black), N (blue), O (red)). Hydrogen atoms have been omitted for clarity. Only one of the two configurations of disordered $[Fe^{III}(5\text{-}CH_3O\ sal_2\text{-}trien)]^+$ molecule is shown for clarity.

This contrasts with the behavior exhibited by chiral 3D networks that normally present longer metal-metal distances than 2D structures. In addition, the minimum distance between the metallic ions from the oxalate network and the Fe atoms is much shorter than in compound **1**. Thus, a value of 5.518 Å is obtained between Cr1 and Fe1A.

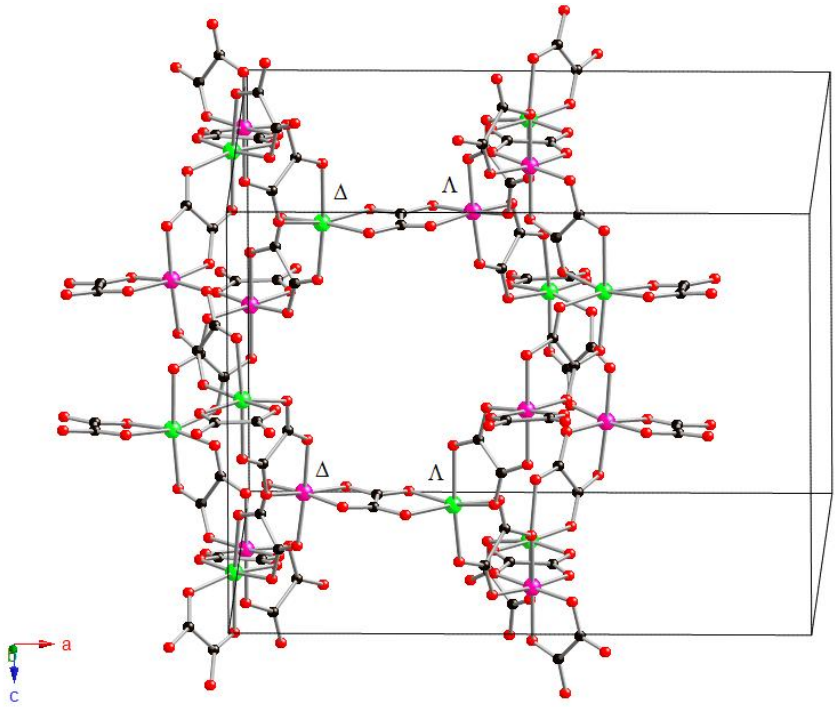

Fig 4. Two neighbouring ten-membered rings of the oxalate network of **2** of opposite chirality connected through two oxalate ligands along the *a* direction. (Fe (yellow), Cr (pink), Mn (green), C (black), N (blue), O (red)).

$[Fe(5\text{-}CH_3Osal_2\text{-}trien)]^+$ complexes are intercalated in the holes described by this 3D oxalate network. Fe^{III} present an octahedral coordination. There are two crystallographically independent $[Fe(5\text{-}CH_3Osal_2\text{-}trien)]^+$ complexes. One cation, ([Fe2] complex), presents Fe–N and Fe–O bond distances of 2.172(10) and 1.887(7) Å that are clearly similar to those of other HS complexes. Two complete orientations of the second cation site ([Fe1A] (~ 72 %) and [Fe1B] (~ 28 %) complexes) have been resolved in the refinement. Although the errors on their metric parameters are inevitably larger, the structure of one of these ([Fe1A] complex) is clearly consistent with it being HS (average Fe–N and Fe–O bond distances of 2.159(9) and 1.932(8) Å), while the other ([Fe1B complex) is apparently LS (average Fe–N and Fe–O bond distances of 1.96(2) and 1.86(2) Å). This indicates that at the temperature of the

structural study (120 K) 14 % of the Fe^{III} complexes are in the LS state in agreement with magnetic data (see below). A similar disorder of a $[Fe^{III}(sal_2\text{-trien})]^+$ site with two configuration being HS and LS has been found in the compound of formula $[Fe(sal_2\text{-trien})]ClO_4$.[28]

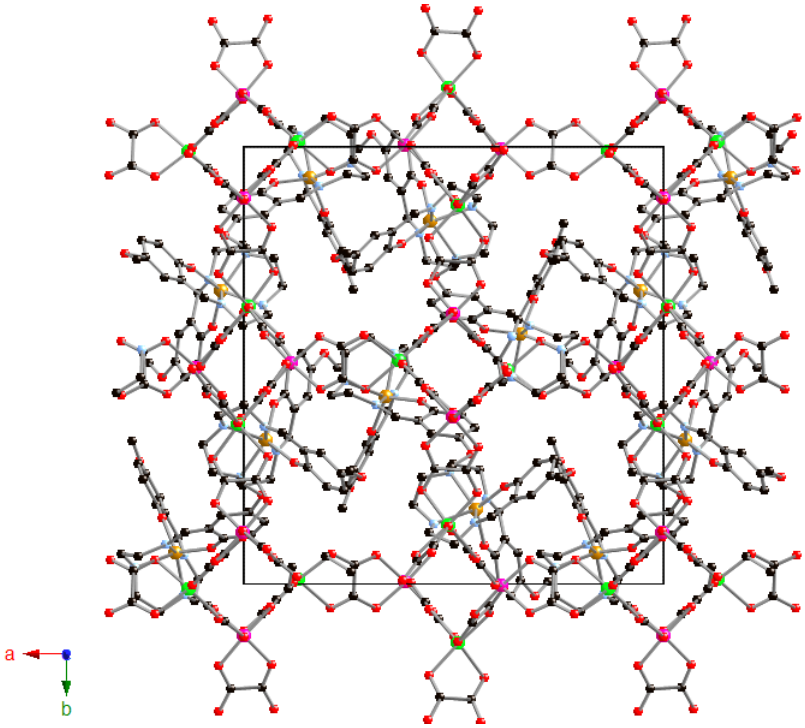

Fig. 5 Projection of **2** in the *ab* plane. (Fe (yellow), Cr (pink), Mn (green), C (black), N (blue), O (red)). Hydrogen atoms have been omitted for clarity. Only one of the two configurations of disordered $[Fe^{III}(5\text{-}CH_3O\text{-}sal_2\text{-trien})]^+$ molecule is shown for clarity.

In contrast to the structure of **1**, the intermolecular interactions between the complexes are not face-to-face (see Fig. S2, ESI). This can be explained by steric hindrance caused by the presence of the methoxy groups that difficult the face-to-face orientation of the neighbouring rings. Thus, the two aromatic rings from [Fe2] complex present short contacts with the ethylene groups of neighbouring [Fe1A] or [Fe1B] complexes. On the other hand, the ethylene groups of this [Fe2] present

short contacts with the phenoxy groups of another neighbouring [Fe1A] or [Fe1B] complex. Furthermore, [Fe2] and [Fe1B] are connected through hydrogen-bonds with the oxalate ligands. Dihedral angles, α, between the phenoxy rings of [Fe1A], [Fe1B] and [Fe2] are respectively 110.47°, 100.41° and 105.55°, respectively. The dihedral angles, α, between the least squares planes of the two phenoxy rings have very different values in the 2D or 3D structures presented in this paper. Thus, in the 2D compound **1** the two phenoxy rings are closer to 90°, the ideal value for an octahedral complex.

Magnetic properties of 1

The thermal dependence of the product of the molar magnetic susceptibility and temperature (χT) of **1** is shown in Fig. 6; χT shows a value of 8.0 emu·K·mol^{-1} at 400 K. Upon cooling down χT decreases gradually from 400 to 250 K from 8.0 to 6.8 emu·K·mol^{-1}. This last value is approximately equal to the sum of the expected contributions for the isolated paramagnetic ions with the Fe^{III} spin-crossover complex in a LS state. Therefore, in this range of temperatures there is a partial HS→LS spin conversion of the Fe^{III} complexes. This spin crossover is not complete since the χT at 400 K (8.0 emu·K·mol^{-1}) is still far for the expected value with all the Fe^{III} complexes in HS state (~ 10.6 emu·K·mol^{-1}), and corresponds approximately to a 66 % of the Fe^{III} in the LS state. Below 250 K there is an increase of χT, which is very sharp below 50 K. This indicates the presence of ferromagnetic interactions between neighbouring Mn^{II}–Cr^{III} magnetic ions of the oxalate network and suggests the onset of long-range ferromagnetic ordering, as observed for other M^{II}–Cr^{III} 2D oxalate networks.[2,3] To confirm the presence of long-range magnetic ordering and to determine precisely the critical temperatures, AC susceptibility measurements have been carried out. A maximum in the in-phase signal (χ') near T_c and an out-of-phase signal (χ'') that starts to appear at temperatures just below T_c is observed (Fig. 7). These signals are frequency independent as expected for a ferromagnet (Fig. 7). From this data the T_c of **1** is 5.6 K, similar to those reported for other 2D

Mn^{II}–Cr^{III} 2D oxalate compounds, but slightly higher than that of the 2D compound obtained with $[Fe^{III}(sal_2\text{-trien})]^+$ (T_c = 5.4 K).[18] In the ordered phase an additional peak in χ" at temperatures below 3 K is also detected. The presence of such a frequency-dependent peak has already been observed in other M^{II}–Cr^{III} 2D oxalate compounds. This can be related to the formation of magnetic domains and domain-wall movement.[29]

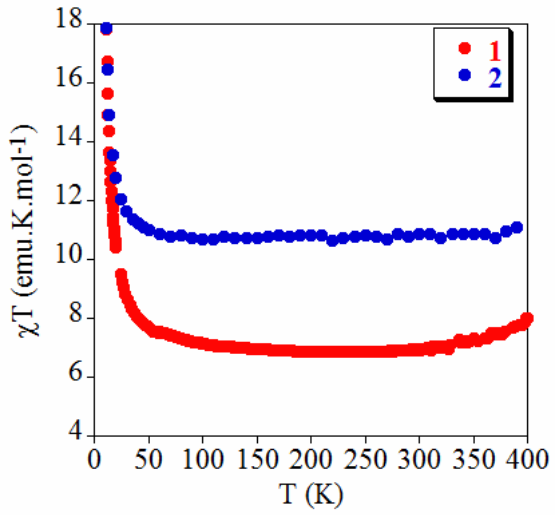

Fig. 6 Temperature dependence of the product of the molar magnetic susceptibility with temperature (χT) at 0.1 T for compounds **1** (red), **2** (blue).

To confirm the ferromagnetic ordering of the spins, isothermal magnetisation at 2 K has been performed (Fig. 8). This presents a sharp increase at low fields which is much faster than that expected for non-interacting Cr^{III} and Mn^{II} centers; this increase is more gradual at higher fields and no saturation is reached up to 5 T. The magnetisation (M) value at 5 T is 7.7 μ_B, which is slightly lower than the expected value for a parallel alignment of the spins in the bimetallic lattice with all the Fe^{III} in the LS state (9 μ_B). As for other M^{II}–Cr^{III} 2D oxalate compounds, this difference can be due to a spin canting of the ferromagnetic phase.[2] The hysteresis loops at 2 K shows that this compound is a soft ferromagnet with a coercive field of 0.5 mT.

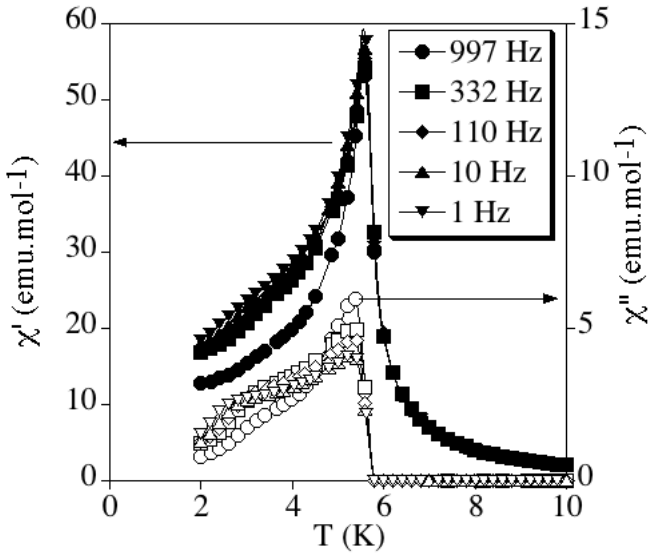

Fig 7. Temperature dependence of the in-phase AC susceptibility (χ') (filled symbols) and the out-of-phase AC susceptibility (χ'') (empty symbols) for **1.**

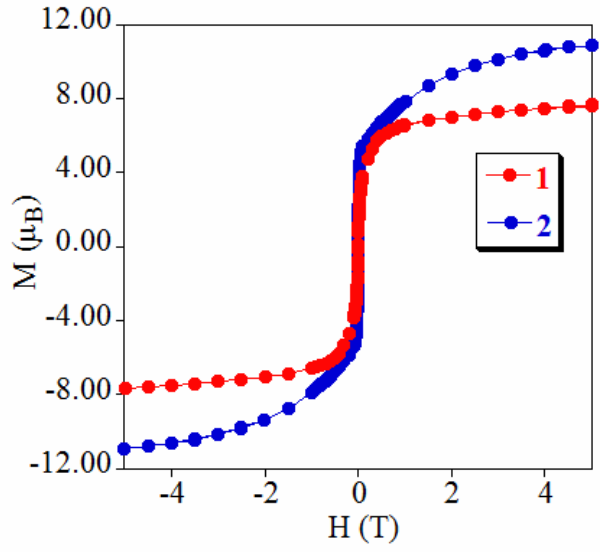

Fig. 8 Field dependence of the magnetization (M) for **1** (red) **2** (blue).

Magnetic properties of 2

The thermal dependence of χT for **2** is shown in Fig. 6. It shows a constant value of 10.7-10.8 emu·K·mol^{-1} from 400 to 100 K as temperature decreases which is much higher than that of compound **1**. This value is very close to the sum of the expected contributions for the isolated paramagnetic ions with 100 % of Fe^{III} in a HS state. This constant value in this range of temperature contrasts with the smooth increase of χT at decreasing temperature observed for the [Fe(sal_2-trien)]$^+$ compound with an analogous 3D achiral network.[18] It seems that the expected increase of χT due to the ferromagnetic coupling between the neighbouring Mn^{II}–Cr^{III} magnetic ions is compensated by the spin crossover transition of part of the inserted [Fe^{III}(5-CH_3Osal_2-trien)]$^+$ cation leading to an approximately constant value of χT. Indeed, the structure of this compound solved at 120 K shows that 14 % of the inserted [Fe^{III}(5-CH_3Osal_2-trien)]$^+$ complexes are in the LS state confirming this effect (see above). At temperatures below 100 K there is an increase of χT, which is very sharp below 50 K. This indicates the presence of ferromagnetic interactions between neighbouring Mn^{II}–Cr^{III} magnetic ions and the onset of long-range ferromagnetic ordering as usual for this type of compounds. The long-range ferromagnetic ordering is confirmed by AC susceptibility measurements (see Fig. 9) that show frequency-independent χ' and χ'' peaks. From this data the T_c of **2** is 5.1 K, which is very close to that found for the [Fe(sal_2-trien)]$^+$ compounds with an analogous 3D achiral network (5.2 K), and lower than that of compound **1** which presents a 2D network.[18]

Isothermal magnetisation at 2 K presents a sharp increase at low fields (below 0.1 T), and a hysteresis loop with a coercive field of *ca.* 0.6 mT, which is usual for this type of compounds (Fig. 8). In contrast to **1** in which there is only a slight linear increase of *M vs H* at fields above 0.1 T, the presence of a fraction of paramagnetic HS Fe^{III} produces a pronounced curvature in the *M vs H* curve with *M* increasing from 5.4 to 10.9 μ_B when *H* increases from 0.1 to 5 T. Although it is difficult to

evaluate the HS fraction from these measurements, we can say that the value of the *M* at *H* = 5 T (10.9 μ_B) is intermediate between the expected value for all the Fe^{III} in the HS state (13 μ_B) and the one for all the Fe^{III} in the LS state (9 μ_B). This indicates that from 300 to 2 K there is a partial spin crossover of the Fe^{III} ions. This spin crossover is far for being complete at 2 K as the *M* value at this temperature is closer to the expected one with all the Fe^{III} in the HS state. Mössbauer experiments are in progress to evaluate the LS/HS Fe^{III} ratio.

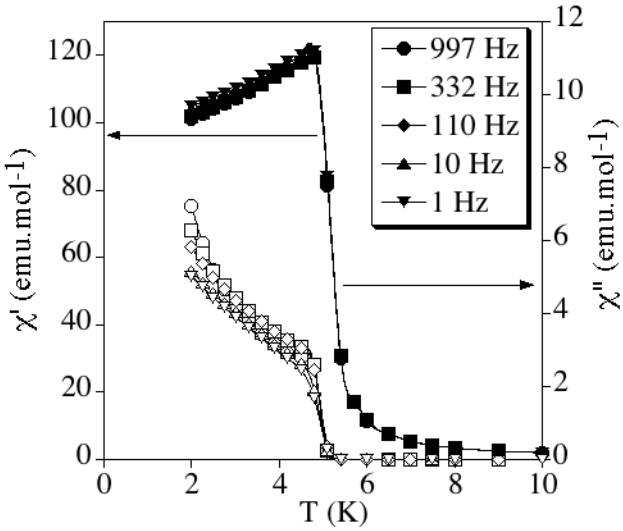

Fig. 9 Temperature dependence of the in-phase AC susceptibility (χ') (filled symbols) and the out-of-phase AC susceptibility (χ'') (empty symbols) for **2**.

Conclusion

We have reported in this paper the preparation of two novel hybrid compounds (**1** and **2**) formed by the insertion of two derivatives of the spin crossover $[Fe^{III}(sal_2\text{-trien})]^+$ cation into anionic coordination polymers based on bimetallic oxalate complexes. From the structural point of view, we have seen that the use of the $[Fe^{III}(5\text{-}NO_2sal_2\text{-trien})]^+$ complex, in which the presence of NO_2 groups favours π···π stacking interactions, gives rise to a 2D network in compound **1**, whereas the use of

$[Fe^{III}(5\text{-}CH_3Osal_2\text{-}trien)]^+$ complex, which prevent such interactions due to steric hindrance of the methoxy groups, leads to the formation of an achiral 3D network in compound **2**. This contrast with the flexibility of non-substituted $[Fe(sal_2\text{-}trien)]^+$ cation in which 2D and achiral 3D networks were obtained depending on the preparation conditions.[18] Furthermore, we have seen that the chirality of these templating cations may induce the formation of 2D chiral oxalate networks (compound **1**). This opens the way to the search for new magnetic effects derived from the chirality of the lattice, such as the magneto-chiral effect predicted by Rikken *et al*.[30] and observed recently in an enantiopure 2D oxalate compound.[9] From the point of view of the magnetic properties, we have shown that it is possible to tune the spin state of the inserted Fe^{III} compound depending on the electron-withdrawing or electron-donating character of the substituent of sal_2trien together with packing effects. Thus, the electron-withdrawing substituent NO_2, favours the LS state in compound **1**, whereas the electron-donating group CH_3O, favours the HS state in compound **2**. The magnetic properties indicate that there is a partial spin crossover of the inserted cation in these two compounds that coexists with a ferromagnetic ordering of the oxalate networks.

The possible use of these compounds as switchable magnets remains to be explored by applying light or pressure. For this purpose, the achiral 3D compound **2** seems a better candidate as it presents a 3D structure in which the chemical pressure effect is expected to be stronger than in the 2D structure. However, the preferred HS state of the inserted cation in this compound, might prevent any switching behavior, as seen for the 3D achiral compound obtained with $[Fe^{III}(sal_2\text{-}trien)]^+$.[18] To overcome this problem, other sal_2trien derivatives could be used. The results obtained in this paper may help to understand which candidates could be better suited to reach this goal. For instance, the use of a substituent with electron-withdrawing groups not favouring π···π stacking interactions such as CF_3 or disubstituted sal_2trien, is proposed to obtain 3D oxalate networks with a higher probability of spin-crossover of the inserted Fe^{III} complex.

Acknowledgements

Financial support from the European Union (MolSpinQIP and SPINMOL ERC Advanced Grant), the Spanish Ministerio de Ciencia e Innovación (Project Consolider-Ingenio in Molecular Nanoscience, CSD2007-00010, and projects CTQ2008-06720 and MAT2007-61584), and the Generalitat Valenciana (Prometeo Program) are gratefully acknowledged. The authors also thank J. M. Martínez-Agudo, University of Valencia, and Núria Clos, University of Barcelona, for magnetic characterization of the samples.

Notes and references

[1] (a) E. Coronado, P. Day, *Chem. Rev.,* 2004, **104**, 5419; (b) E. Coronado, J. R. Galán-Mascarós, *J. Mater. Chem.,* 2005, **15**, 66.

[2] (a) H. Tamaki, Z. J. Zhong, N. Matsumoto, S. Kida, M. Koikawa, N. Achiwa, Y. Hashimoto, H. Okawa, *J. Am. Chem. Soc.,* 1992, **114**, 6974; (b) H. Tamaki, M. Mitsumi, N. Nakamura, N. Matsumoto, S. Kida, H. Okawa, S. Ijima, *Chem. Lett.,* 1992, 1975; (c) C. Mathonière, S. G. Carling, D. Yuscheng, P. Day, *J. Chem. Soc., Chem. Commun.,* 1994, 1551; (d) C. Mathonière, J. Nutall, S. G. Carling, P. Day, *Inorg. Chem.,* 1996, **35**, 1201; (e) R. Pellaux, H. W. Schmalle, R. Huber, P. Fisher, T. Hauss, B. Ouladdiaf, S. Decurtins, *Inorg. Chem.,* 1997, **36**, 2301; (f) E. Coronado, J. R. Galán-Mascarós, C. J. Gómez-García, J. M. Martínez-Agudo, E. Martínez-Ferrero, J. C. Waerenborgh, M. Almeida, *J. Solid State Chem.,* 2001, **159**, 391; (g) K. S. Min, A. L. Rhinegold, J. S. Miller, *Inorg. Chem.,* 2005, **44**, 8433; (h) E. Coronado, J. R. Galán-Mascarós, C. Martí-Gastaldo, *J. Mater. Chem.,* 2006, **16,** 2685; (i) Z. Duan, Y. Zhang, B. Zhang. F. L. Pratt, *Inorg. Chem.,* 2009, **48**, 2140.

[3] (a) M. Clemente-León, J. R. Galán-Mascarós, C. J. Gómez-García, *Chem. Commun.,* 1997, 1727; (b) E. Coronado, J. R. Galán-Mascarós, C. J. Gómez-García, J. M. Martínez-Agudo, *Adv. Mater.,* 1999, **11**, 558; (c) E. Coronado, J. R. Galán-Mascarós, C. J. Gómez-García, J. Ensling, P. Gutlich, *Chem. Eur. J.,* 2000, **6**, 552.

[4] E. Coronado, C. Giménez-Saiz, C. J. Gómez-Garcia, F. M. Romero, A. Tarazón, *J. Mater. Chem.,* 2008, **18**, 929.

[5] (a) S. Bénard, P. Yu, J. P. Audière, E. Rivière, R. Clèment, J. Ghilhem, L. Tchertanov, K. Nakatami, *J. Am. Chem. Soc.,* 2000, **122**, 9444; (b) S. M. Aldoshin, N. A. Sanina, V. I. Minkin, N. A. Voloshin, V. N. Ikorskii, V. I. Ovcharenko, V. A. Smirnov, N. K. Nagaeva, *J. Mol. Struct.,* 2007, **826**, 6.

[6] S. Bénard, E. Rivière, P. Yu, K. Nakatami, J. F. Delouis, *Chem. Mater.,* 2001, **13,** 159.

[7] (a) E. Coronado, J. R. Galán-Mascarós, C. J. Gómez-García V. Laukhin, *Nature,* 2000, **408**, 447; (b) A. Alberola, E. Coronado, J. R. Galán-Mascarós, C. Giménez-Saiz, C. J. Gómez-García, *J. Am. Chem. Soc.,* 2003, **125**, 10774; (c) E. Coronado, J. R. Galán-Mascarós, C. J. Gómez-García, E. Martínez-Ferrero, S. Van Smaalen, *Inorg. Chem.,* 2004, **43,** 4808.

[8] M. Clemente-León, E. Coronado, J. C. Dias, A. Soriano-Portillo, R. D. Willett, *Inorg. Chem.,* 2008, **47**, 6458.

[9] C. Train, R. Gheorghe, V. Krstic, L. M. Chamoreau, N. S. Ovanesyan, G. L. J. A. Rikken, M. Gruselle, M. Verdaguer, *Nature Mater.,* 2008, **17**, 729.

[10] C. Train, T. Nuida, R. Gheorghe, M. Gruselle, S. Ohkoshi, *J. Am. Chem. Soc.,* 2009, **131**, 16838.

[11] H. Okawa, A. Shigematsu, M. Sadakiyo, T. Miyagawa, K. Yoneda, M. Ohba, H. Kitagawa, *J. Am. Chem. Soc.,* 2009, **131**, 13516.

[12] (a) F. D. Rochon, R. Melanson, M. Andruh, *Inorg. Chem.,* 1996, **35**, 6086; (b) M. Andruh, R. Melanson, C. V. Stager, F. D. Rochon, *Inorg. Chim. Acta,* 1996, 309; (c) N. Stanica, C. V. Stager, M. Cimpoesu, M. Andruh, *Polyhedron,* 1998, **17**, 1787; (d) G. Marinescu, M. Andruh, R. Lescouëzec, M. C. Muñoz, J. Cano, F. Lloret, M. Julve, *New J. Chem.,* 2000, **24**, 527; (e) S. Triki, F. Berezovsky, J. S. Pala, E. Coronado, C. J. Gómez-García, J. M. Clemente, A. Riou, P. Molinie, *Inorg. Chem.,* 2000, **39**, 3771; (f) G. Ballester, E. Coronado, C. Giménez-Saiz, F. M. Romero, *Angew. Chem. Int. Ed.,* 2001, **40**, 792; (g) E. Coronado, C. Giménez-Saiz, J. R. Galán-Mascarós, C. J. Gómez-García, C. Ruiz-Pérez, *Eur. J. Inorg. Chem.,* 2003, 2290; (h) E. Coronado, J. R. Galán-Mascarós, C. J. Gómez-García, C. Martí-Gastaldo, *Inorg. Chem.,* 2005, **44**, 6179; (i) E. Coronado, J. R. Galán-Mascarós, C. Martí-Gastaldo, *Inorg. Chem.,* 2006, **45**, 1882; (j) E. Coronado, J. R. Galán-Mascarós, C. Martí-Gastaldo, A. Murcia-Martínez, *Dalton Trans.,* 2006, 3294; (k) H. Z. Kou, O. Sato, *Inorg. Chem.,* 2007, **46**, 9513; (l) E. Cariati, R. Macchi, D. Roberto, R. Ugo, S. Galli, N. Casati, P. Macchi, A. Sironi, L. Bogani, A. Caneschi, D. Gatteschi, *J. Am. Chem. Soc.,* 2007, **129**, 9410; *(m)* H. Z. Kou, J. Tao, O. Sato, *Dalton Trans.,* 2008, 3652; (m) E. Coronado, J. R. Galán-Mascarós, C. Martí-Gastaldo, *Cryst. Eng. Comm.,* 2009, **11**, 2143; (n) Q.-X. Yao, L. Pan, X.-H. Jin, J. Li, Z.-F. Ju, J. Zhang, *Chem. Eur. J.,* 2009, **15**, 11890.

[13] (a) S. Decurtins, H. W. Schmalle, P. Schneuwly, H. R. Oswald, *Inorg. Chem.,* 1993, **32,** 1888; (b) S. Decurtins, H. W. Schmalle, P. Schneuwly, J. Ensling, P. Gütlich, *J. Am. Chem. Soc.,* 1994, **116**, 9521; (c) M. Hernández-Molina, F. Lloret, C. Ruiz-Pérez, M. Julve, M. *Inorg. Chem.,* 1998, **37**, 4141; (d) E. Coronado, J. R. Galán-Mascarós, C. J. Gómez-García, J. M. Martínez-Agudo, *Inorg. Chem.,* 2001, **40**, 113; (e) F. Pointillart, C. Train, M.

Gruselle, F. Villain, H. W. Schmalle, D. Talbot, P. Gredin, S. Decurtins, M. Verdaguer, *Chem. Mater.,* 2004, **16**, 832; (f) M. Clemente-León, E. Coronado, C. J. Gómez-García, A. Soriano-Portillo, *Inorg. Chem.,* 2006, **45**, 5653.

[14] (a) R. Andrés, M. Gruselle, B. Malézieux, M. Verdaguer, J. Vaissermann, *Inorg. Chem.,* 1999, **38**, 4637; (b) R. Andrés, M. Brissard, M. Gruselle, C. Train, J. Vaissermann, B. Malézieux, J. P. Jamet, M. Verdaguer, *Inorg. Chem.,* 2001, **40**, 4633.

[15] R. Sieber, S. Decurtins, H. Stoeckli-Evans, C. Wilson, D. Yufit, J. A. K. Howard, S. C. Capelli, A. Hauser, *Chem. Eur. J.*, 2000, **6**, 361.

[16] E. Coronado, J. R. Galán-Mascarós, M. C. Giménez-López, M. Almeida, J. C. Waerenborgh, *Polyhedron,* 2007, **26**, 1838.

[17] M. Clemente-León, E. Coronado, M. C. Giménez-López, A. Soriano-Portillo, J. C. Waerenborgh, F. S. Delgado, C. Ruiz-Pérez, *Inorg. Chem.,* 2008, **47**, 9111.

[18] M. Clemente-León, E. Coronado, M. López-Jordà, G. Mínguez Espallargas, A. Soriano-Portillo, J. C. Waerenborgh, *Chem. Eur. J.,* DOI: 10.1002/chem.200902668.

[19] M. F. Tweedle, L. J. Wilson, *J. Am. Chem. Soc.,* 1976*,* **98**, 4824.

[20] J. C. Baylar, E. M. Jones*,* (Ed. H. S. Booth), in *Inorganic Synthesis*, McGraw-Hill, New York, 1939, Vol 5, p. 35.

[21] A. Altomare, M. C. Burla, M. Camalli, G. L. Cascarano, C. Giacovazzo, A. Guagliardi, A. G. G. Moliterni, G. Polidori, R. Spagna, *J. Appl. Cryst*., 1999, **32**, 115-119.

[22] SHELXL-97: G. M. Sheldrick, University of Göttingen, Germany, **1997**.

[23] L. J. Farrugia, *J. Appl. Cryst.,* 1997, **32**, 837.

[24] (a) H.D. Flack, *Acta Cryst.*, **1983**, A39, 876; (b) G. Bernardinelli, H.D. Flack, *Acta Cryst.*, 1985, **A41**, 500.

[25] N. Ovanesyan, V. D. Makhaev, S. M. Aldoshin, P. Gredin, K. Boubekeur, C. Train, M. Gruselle, *Dalton Trans.,* 2005, 3101.

[26] M. Gruselle, C. Train, K. Boubekeur, P. Gredin, N. Ovanesyan, *Coord. Chem. Rev.,* 2006, **250**, 2491.

[27] C. Janiak, *J. Chem. Soc., Dalton Trans.,* 2000, 3885.

[28] R. Pritchard, S. A. Barrett, C. A. Kilner, M. A. Halcrow, *Dalton Trans.,* 2008, 3159.

[29] N. A. Chernova, Y. Song, P. Y. Zavalij, M. S. Wittingham, *Phys. Rev. B,* 2004, **70**, 144405.

[30] Rikken, G. L. J. A.; Raupach, E. *Nature,* 1997, **390**, 493.

Multifunctional magnetic materials obtained by insertion of spin-crossover Fe^{III} complexes into chiral 3D bimetallic oxalate-based ferromagnets

Inorganic Chemistry

Capítulo 6

Capítulo 6: Multifunctional magnetic materials obtained by insertion of spin-crossover Fe^{III} complexes into chiral 3D bimetallic oxalate-based ferromagnets

ABSTRACT. The syntheses, structures and magnetic properties of the compounds of formula $[Fe^{III}(5\text{-}Clsal_2\text{-}trien)][Mn^{II}Cr^{III}(ox)_3]\cdot 0.5(CH_3NO_2)$ **(1),** $[Fe^{III}(5\text{-}Brsal_2\text{-}trien)][Mn^{II}Cr^{III}(ox)_3]$ **(2)** and $[In^{III}(5\text{-}Clsal_2\text{-}trien)][Mn^{II}Cr^{III}(ox)_3]$ **(3)** are reported. The structure of the three compounds, that crystallize in the orthorhombic $P2_12_12_1$ chiral space group, presents a 3D chiral anionic network formed by Mn^{II} and Cr^{III} ions linked through oxalate ligands with inserted $[Fe^{III}(5\text{-}Clsal_2\text{-}trien)]^+$, $[Fe^{III}(5\text{-}Brsal_2\text{-}trien)]^+$ and $[In^{III}(5\text{-}Clsal_2\text{-}trien)]^+$ cations. The magnetic properties indicate that the three compounds undergo a long-range ferromagnetic ordering at ca. 5 K. On the other hand, the inserted Fe^{III} cations undergo a partial spin-crossover in the case of **1** and **2**.

Introduction

Molecular materials offer great possibilities in the search for novel combinations of properties in a single material. These materials may be prepared building up two-network hybrid solids formed by two molecular fragments with each network furnishing distinct physical properties. If the two networks are quasi-independent, a coexistence of the two physical properties is anticipated.[1] If the two molecular networks are coupled, the interplay between their properties may give rise to new properties.[1b] Finally, if one of these two networks changes its properties under application of an external stimulus, a switchable multifunctional material could be obtained in which the responsive network can influence the properties of the other network.[2]

Bimetallic oxalate-bridged complexes of formula $A[M^{II}M^{III}(ox)_3]$ (M^{III} = Cr, Fe, Ru, V, Mn; M^{II} = Mn, Fe, Co, Ni, Cu, Zn; A = Cation; ox = oxalate) have provided remarkable examples of this type of compounds.[3] They are composed by polymeric 2D[4] or 3D[5]

anionic networks, which furnish the cooperative magnetic properties (ferro- ferri- or canted antiferromagnetism), and a bulky charge-compensating molecular cation, which templates the network formation and adds a second physical property to the solid. Insertion of different cations into oxalate networks has led to compounds combining in the same compound the long-range magnetic ordering from the oxalate network with paramagnetism,[6] photochromism,[7] electric conductivity,[8] proton conduction,[9] chirality,[10] chirality and conductivity,[11] or ferroelectricity.[12]

The interplay between the properties of the two molecular networks has been observed in enantiopure oxalate-based magnets prepared by Train et al. that exhibit magneto-chiral dichroic effect and magnetization-induced second harmonic generation.[13] Although most of the chiral oxalate-based magnets reported so far present a 3D network and are formed with templating cations that are chiral metallic complexes such as $[Z^{II}(bpy)_3]^{2+}$ (Z = Ru, Fe, Co; bpy = bipyridine) and similar cations,[5,10a,10b] the interplay between chirality and magnetism has only been achieved in enantiopure 2D oxalate-based magnets. A possible explanation to this fact is that the optical properties of the 3D compounds are dominated by the absorption of the templating cation.[13a]

The design of switching magnets has been less explored. In this context, cationic spin crossover (SCO) complexes are particularly suitable for this purpose. This kind of molecular complexes change their spin state from low-spin (LS) to high-spin (HS) configurations under an external stimulus such as temperature, light-irradiation, or pressure. As this magnetic switching is accompanied by changes in the molecular size, the spin-crossover process should act as an internal pressure in the hybrid material and therefore might affect the long-range magnetic ordering in the extended magnetic network. In addition, the magnetic framework in which the spin-crossover molecule is inserted may affect the properties of this switchable molecule. Thus far, several examples have described the incorporation of SCO complexes into oxalate-based networks. While the first ones were solely restricted to Co(II) and Fe(II) complexes,[14] a

larger variety of compounds have been recently obtained with Fe(III) complexes of the hexadentate Schiff base ligand, sal_2-trien (H_2sal_2-trien = N,N' -disalicylidenetriethylene-tetramine) and derivatives that give rise to 2D and achiral 3D oxalate-based networks.[15,16] The only one showing coexistence of spin-crossover and ferromagnetism is the 2D compound, $[Fe^{III}(sal_2\text{-trien})][Mn^{II}Cr^{III}(ox)_3]\cdot(CH_2Cl_2)$, that presents a gradual spin crossover from 350 to 160 K, and a ferromagnetic ordering at 5.6 K.[16] Furthermore, it exhibits the conversion from the LS to HS state induced by light-irradiation, commonly known as the LIESST effect (light-induced excited spin-state trapping).[17] This is a very rare and unexpected property in a Fe^{III} spin-crossover complex as it has only been found in other two Fe^{III} complexes. Unfortunately, the photo-induced spin conversion of the inserted Fe^{III} complex has a negligible influence on the cooperative magnetic behavior of the oxalate network. This is not unexpected as 2D compounds with different interlayer separation have a very similar Curie temperature (T_c). In this sense, compounds with a 3D network are expected to be better candidates because the T_c of 3D oxalate compounds is very sensitive to the size of the intercalated cation.

In an attempt to insert spin-crossover molecules into a 3D oxalate lattice, we have extended this strategy to derivatives of $[Fe^{III}(sal_2\text{-trien})]^+$ with Cl and Br substituents on the position 5 of the salicylaldimine ring. This resulted in growth of a 3D chiral network in the compounds $[Fe^{III}(5\text{-Clsal}_2\text{-trien})][Mn^{II}Cr^{III}(ox)_3]\cdot 0.5(CH_3NO_2)$ (**1**), $[Fe^{III}(5\text{-Brsal}_2\text{-trien})][Mn^{II}Cr^{III}(ox)_3]$ (**2**) and the reference compound, $[In^{III}(5\text{-Clsal}_2\text{-trien})][Mn^{II}Cr^{III}(ox)_3]\cdot(CH_3NO_2)$ (**3**). The structure and magnetic properties of these compounds are reported in this paper.

Experimental Section

Complexes $[Fe^{III}(5\text{-Clsal}_2\text{-trien})]PF_6$, $[Fe^{III}(5\text{-Brsal}_2\text{-trien})]PF_6$ and $[In^{III}(5\text{-Clsal}_2\text{-trien})]PF_6$ were prepared according to literature methods.[18] $Ag_3[Cr(ox)_3]$ was prepared by metathesis from the corresponding potassium salt.[19] All other materials and solvents were commercially available and used without further purification.

$[Fe^{III}(5\text{-}Clsal_2\text{-}trien)][Mn^{II}Cr^{III}(ox)_3]\cdot 0.5(CH_3NO_2)$ (1), $[Fe^{III}(5\text{-}Brsal_2\text{-}trien)][Mn^{II}Cr^{III}(ox)_3]$ (2) and $[In^{III}(5\text{-}Clsal_2\text{-}trien)][Mn^{II}Cr^{III}(ox)_3]\cdot(CH_3NO_2)$ (3). Crystals of these compounds were obtained by slow diffusion of two solutions. The first solution was prepared by adding $MnCl_2\cdot 4H_2O$ (0.018 g, 0.09 mmol) to a suspension of $Ag_3Cr(Ox)_3$ (0.038 g, 0.06 mmol) in 3 mL of methanol. The AgCl precipitate was filtered. The second solution was obtained by dissolving $[Fe^{III}(5\text{-}Clsal_2trien)]PF_6$ (0.038 g, 0.06 mmol) in 3 mL of nitromethane (**1**), $[Fe^{III}(5\text{-}Brsal_2trien)]PF_6$ (0.043 g, 0.06 mmol) in 3 mL of acetonitrile (**2**), or $[In^{III}(5\text{-}Clsal_2trien)]PF_6$ (0.042 g, 0.06 mmol) in 3 mL of nitromethane (**3**). After two weeks brown (**1** and **2**) or violet (**3**) crystals were obtained. The composition of these crystals, checked by microanalysis, shows the following M: Mn: Cr: X (M = Fe, In, X = Cl and Br) ratios. Found: 1:1.2:1.1:2 (Fe:Mn:Cr:Cl) for **1**; 1:1.2:1.1:1.9 (Fe:Mn:Cr:Br) for **2** and 1:1.2:1.1:1.9 (In:Mn:Cr:Cl) for **3**. Calcd: 1:1:1:2 (M:Mn:Cr:X).

Structural Characterization. Single crystal X-ray data of **1**, **2** and **3** were collected at 120 K on a Xcalibur, Sapphire3, Gemini diffractometer equipped with a graphite-monochromated Enhance (Mo) X-ray Source (λ = 0.71073 Å). The program CrysAlisPro, Oxford Diffraction Ltd., Version 1.171.33.52 was used for cell refinements and data reduction of the compounds. Empirical absorption correction was performed using spherical harmonics, implemented in SCALE3 ABSPACK scaling algorithm. Crystal structures were solved by direct methods with the SIR97 program,[20] and refined against all F^2 values with the SHELXL-97 program[21] using the WinGX graphical user interface.[22] The three compounds exhibit a Flacks absolute parameter (*x*) close to 0.[23] This parameter lies within the range that indicates that the absolute structure is valid and that the three crystals are enantiopure. Non-hydrogen atoms were refined anisotropically, and hydrogen atoms were placed in calculated positions refined using idealized geometries (riding model) and assigned fixed isotropic displacement parameters. In **2**, the two terminal ethylene groups from $[Fe^{III}(5\text{-}Brsal_2\text{-}trien)]^+$ complexes were modeled in two orientations. Data collection and refinement statistics are collected in Table 1.

Table 1. Crystallographic data of **1** - **3**.

Compound	**1**	**2**	**3**
Empirical formula	$C_{26.5}H_{23.5}Cl_2CrFeMnN_{4.5}O_{15}$	$C_{26}H_{22}Br_2CrFe\ MnN_4O_{14}$	$C_{26}H_{22}Cl_2CrIn\ MnN_4O_{14}$
Formula weight	878.69	937.09	907.14
Crystal color	Brown	Brown	Violet
Temperature (K)	120	120	120
Wavelength (*Å*)	0.71073	0.71073	0.71073
Crystal system, Z	Orthorhombic, 4	Orthorhombic, 4	Orthorhombic, 4
Space group	$P2_12_12_1$	$P2_12_12_1$	$P2_12_12_1$
a (Å)	13.3082(3)	13.6797(11)	13.9216(11)
b (Å)	15.6219(4)	15.2785(9)	15.4812(14)
c (Å)	16.4727(5)	16.0478(13)	15.5450(13)
V (Å^3)	3424.66(16)	3354.1(4)	3350.31(5)
ρcalc (Mg/m^3)	1.704	1.856	1.798
$\mu(Mo_{K\alpha})$ (mm^{-1})	1.325	3.570	1.604
θ range (°)	3.02 - 32.60	2.87 - 26.45	12.36 -26.48
Reflns collected	55567	15601	21374
Independent reflns, (R_{int})	11701 (0.0616)	6553 (0.066)	6869 (0.153)
L. S. parameters/ restraints	478/1	440/0	436/0
$R1(F)$,[a] $I>2\sigma(I)$]	0.049	0.056	0.073
$wR2(F^2)$,[b] all data	0.111	0.108	0.144
$S(F^2)$,[c] all data	0.921	1.032	1.006

[a] $R1(F) = \Sigma(||F_O| - |F_C||)/\Sigma|F_O|$; [b] $wR2(F^2) = [\Sigma w(F_O^2 - F_C^2)^2/\Sigma wF_O^4]^{1/2}$; [c] $S(F^2) = [\Sigma w(F_O^2 - F_C^2)^2/(n - p)]^{1/2}$

Physical Measurements. Magnetic susceptibility measurements were performed on polycrystalline samples using a magnetometer (Quantum Design MPMS-XL-5) equipped with a SQUID sensor. Variable-temperature measurements were carried out in the

temperature range 2-300 K. The ac measurements were performed in the temperature range 2-10 K at different frequencies with an oscillating magnetic field of 0.395 mT. The magnetisation and hysteresis studies were performed between 5 and -5 T, cooling the samples at zero field. The M:Mn:Cr:X (M = Fe, In, X = Cl, Br) ratios were measured on a Philips ESEM X230 scanning electron microscope equipped with an EDAX DX-4 microsonde. Mössbauer spectra were collected in transmission mode using a conventional constant-acceleration spectrometer and a 25 mCi ^{57}Co source in a Rh matrix. The velocity scale was calibrated using α-Fe foil. The absorber was obtained by gently packing single crystals of **1** or **2** into a perspex holder. Low-temperature spectra were collected using a bath cryostat with the sample immersed in liquid He, for measurements at 4.1 and 2.2 K, or by using flowing He gas to cool the sample above 4.1 K (temperature stability of 0.2 K). The spectra were fitted to Lorentzian lines using a non-linear least-squares method.[24] Isomer shifts (Tables 2 and 3) are given relative to metallic α-Fe at room temperature.

Results and Discussion

Synthesis. The method used to prepare $[Fe^{III}(5\text{-}Clsal_2\text{-}trien)][Mn^{II}Cr^{III}(ox)_3]\cdot 0.5(CH_3NO_2)$ (**1**), $[Fe^{III}(5\text{-}Brsal_2\text{-}trien)][Mn^{II}Cr^{III}(ox)_3]$ (**2**) and $[In^{III}(5\text{-}Clsal_2\text{-}trien)][Mn^{II}Cr^{III}(ox)_3]$ (**3**) is similar to that used to prepare the compounds with $[Fe^{III}(sal_2\text{-}trien)]^+$ and the derivatives ($[Fe^{III}(5\text{-}Xsal_2\text{-}trien)]^+$ (X = NO_2 or CH_3O)).[15b,16] It is based in the use of $Ag_3[Cr(ox)_3]$ to avoid the presence of alkali ions in the structure. It consists on the slow diffusion of a methanol solution containing the precursors of the oxalate network, Mn^{2+} and $[Cr(ox)_3]^{3-}$ ions, into a solution of $[M^{III}(5\text{-}Xsal_2\text{-}trien)]^+$ (M = Fe or In, X = Cl or Br) in different solvents. In contrast to the compounds with $[Fe^{III}(sal_2\text{-}trien)]^+$ in which the use of different solvents to dissolve the Fe^{III} complex affords compounds with different types of oxalate network (2D for dichloromethane and 3D for acetonitrile), only one type of oxalate network, a chiral 3D network, is obtained for $[Fe^{III}(5\text{-}Xsal_2\text{-}trien)]^+$ (X = Cl or Br) in different solvents. The solvent that leads to best crystals for X-ray single crystal diffraction is CH_3NO_2, for $[Fe^{III}(5\text{-}Clsal_2\text{-}trien)]^+$, CH_3CN for $[Fe^{III}(5\text{-}Brsal_2\text{-}trien)]^+$ and

CH_3CN for $[In^{III}(5\text{-}Clsal_2\text{-}trien)]^+$ cations.[25] The composition of these crystals, checked by microanalysis, shows in all cases a M:Mn:Cr:X (M = Fe, In, X = Cl and Br) ratio of 1:1:1:2. The crystal structures of the three compounds have been solved by single-crystal X-ray diffraction. Attempts to obtain analogous compounds with other paramagnetic M^{2+} ions (M = Ni, Fe, Co and Cu) in the place of Mn^{2+} have been unsuccessful.

Structure. 1 - **3** crystallize in the chiral space group $P2_12_12_1$. As a racemic mixture of $[Cr(ox)_3]^{3-}$ and $[M^{III}(5\text{-}Xsal_2\text{-}trien)]^+$ ions has been used in the synthesis, crystals of both chiralities are obtained as expected.

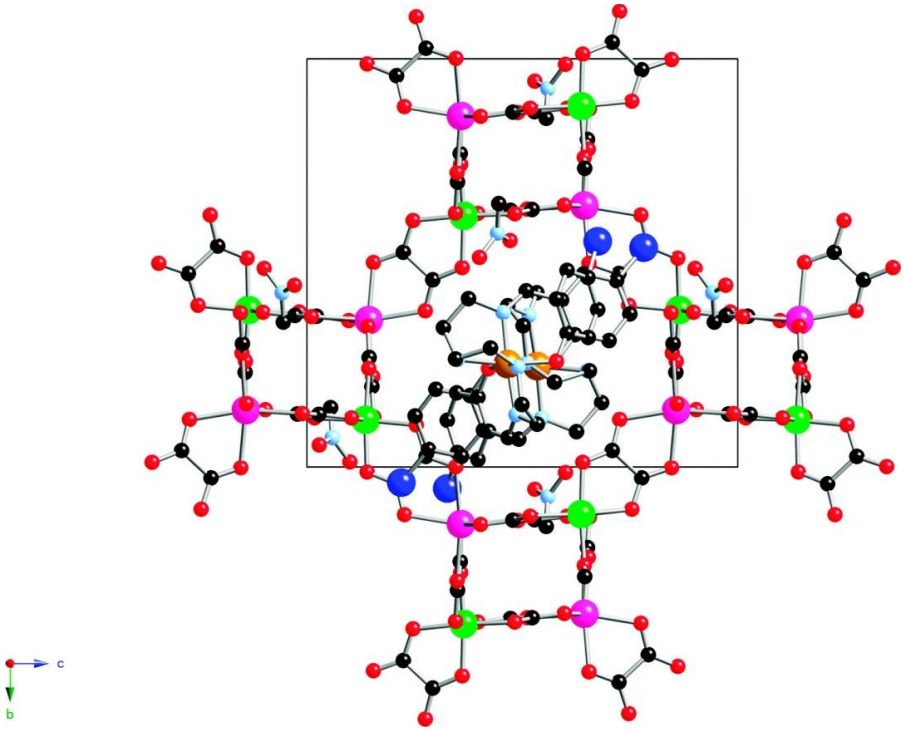

Figure1. Projection of **1** in the *bc* plane: Fe, yellow; Cr, green; Mn, pink; C, black; N, blue; O, red; Cl, dark blue. Hydrogen atoms have been omitted for clarity.

The structure of **1** is formed by an anionic 3D polymeric oxalate-bridged bimetallic network with $[Fe^{III}(5\text{-}Clsal_2\text{-}trien)]^+$ cations and nitromethane molecules occupying the

cavities. This anionic polymeric structure present the well-known 3D 3-connected decagonal oxalate-based anionic network (10,3) which is formed by oxalate ligands connecting Mn^{II} and Cr^{III} ions in such a way that each Mn^{II} is surrounded by three Cr^{III} and vice versa with all metal ions presenting the same chirality (Δ in the crystal used to solve the structure). The 3D oxalate chiral network of this compound presents some differences with those obtained with $[Z^{II}(bpy)_3]^{2+}$ templating cations. Whereas cations with D_3 symmetry lead to cubic networks, $[Fe^{III}(5\text{-}Clsal_2\text{-}trien)]^+$ cation gives rise to an orthorhombic network. The consequence of this lower symmetry is that it is possible to distinguish between Mn and Cr ions in the structure of **1** as they present different M-O bond length whereas they are disordered in the 3D compound obtained with $[Z^{II}(bpy)_3]^{2+}$. Thus, the two metals are crystallographically independent with mean Mn-O distances of 2.193(3) Å and Cr-O distances of 1.982(3) Å which are typical Mn^{II}-O and Cr^{III}-O distances. Metal-metal distances between adjacent centers are in the range 5.407(6)-5.462(6) Å. These metal-metal distances are longer than those exhibited by the 2D and 3D achiral structures obtained with $[Fe^{III}(sal_2\text{-}trien)]^+$ cations[15b,16] but shorter than those exhibited by other 3D oxalate-based chiral compounds. For instance, Mn–Cr distance in $[Ir(ppy)_2(bpy)][MnCr(ox)_3]\cdot 0.5H_2O$ is 5.503 Å.[5f] Another consequence of the lower symmetry of the oxalate network is that the projections in the *ab*, *bc* and *ac* planes are not completely equivalent. The bimetallic oxalate network of **1** defines channels that run along the *a*, *b* and *c* axis. In contrast with the 3D cubic lattice, in the orthorhombic one the channels running along the *a* axis (Figure 1) present a square shape while those running along the *b* (Figure 1SS, Suporting Information) and *c* axes (Figure 2SS, Suporting Information) are clearly elongated.

The $[Fe^{III}(5\text{-}Clsal_2\text{-}trien)]^+$ complexes and nitromethane molecules are enclosed in the holes described by this 3D oxalate network. There is one crystallographically independent $[Fe(5\text{-}Clsal_2\text{-}trien)]^+$ complex (Figure 2) and disordered nitromethane molecules. In the crystal used to solve the structure, Fe^{III} adopts a Λ configuration, which is the opposite to that shown by Mn^{II} and Cr^{III} ions in the chiral oxalate network. It

seems that in contrast to $[Z^{II}(bpy)_3]^{2+}$ cations, $[Fe(5\text{-}Clsal_2\text{-}trien)]^+$ cations induce the crystallisation of a 3D bimetallic oxalate-based network of opposite chirality.

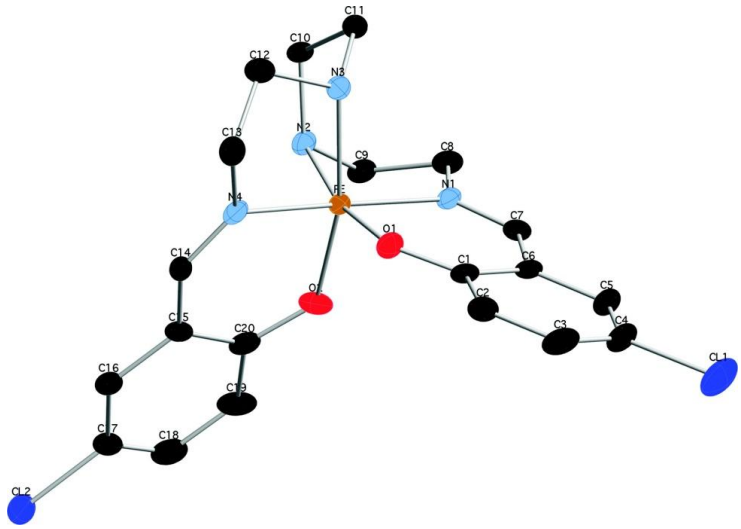

Figure2. Structural view of $[Fe^{III}(5\text{-}Clsal_2\text{-}trien)]^+$ cation in compound **1**: Fe, yellow; Cr, green; Mn, pink; C, black; N, blue; O, red; Cl, dark blue. Hydrogen atoms have been omitted for clarity.

A similar behavior has been observed for another $[Fe(sal_2\text{-}trien)]^+$ derivative ($[Fe(5\text{-}NO_2sal_2\text{-}trien)]^+$) which induce the crystallisation of a chiral 2D oxalate-based network in which all Cr^{III} centers and $[Fe(5\text{-}NO_2sal_2\text{-}trien)]^+$ presenting short intermolecular contacts are in the opposite configuration.[15b] It is also interesting to observe that $[Fe(5\text{-}Clsal_2\text{-}trien)]^+$ cations form chains that run along the *a* axis within the channels defined by the oxalate network (Figure 1). The CH groups from the two phenoxy rings of one $[Fe(5\text{-}Clsal_2\text{-}trien)]^+$ cation present numerous edge-to-face interactions with CH_2 and NH groups from one the two neighbouring $[Fe(5\text{-}Clsal_2\text{-}trien)]^+$ cation belonging to the same chain. At the same time the CH_2 and NH groups of this $[Fe(5\text{-}Clsal_2\text{-}trien)]^+$ cation are connected through edge-to-face interactions with the two phenoxy rings of the second $[Fe(5\text{-}Clsal_2\text{-}trien)]^+$ neighbour. Furthermore, they present hydrogen-bonds through the NH groups with oxalate ligands and numerous short contacts with oxygen

atoms from the oxalate network. Finally, the $[Fe(5\text{-}Clsal_2\text{-}trien)]^+$ cations from one chain are connected to the $[Fe(5\text{-}Clsal_2\text{-}trien)]^+$ cations of four neighbouring chains through short contacts between Cl atoms and CH_2 from ethylene groups. The nitromethane solvent molecules occupy the holes between the oxalate network and $[Fe(5\text{-}Clsal_2\text{-}trien)]^+$ cation. They have an ocuppancy of 0.5 CH_3 groups from nitromethane present short contacts with O atoms from the oxalate network, whereas NO_2 group have short contacts with CH and CH_2 groups from two $[Fe(5\text{-}Clsal_2\text{-}trien)]^+$ complexes belonging to the same chain. The average Fe–N and Fe–O bond distances of $[Fe^{III}(5\text{-}Clsal_2\text{-}trien)]^+$ complexes are 2.009(3) and 1.894(3) Å. These values are intermediate between those obtained for other HS and LS $[Fe(sal_2\text{-}trien)]^+$ compounds. We have to take into account that Mössbauer spectroscopy (see below) indicates that around 70 % of Fe is HS at 120 K (temperature at which the crystal structure has been determined).

The structures of **2** and **3** resemble that of **1** with $[Fe^{III}(5\text{-}Brsal_2\text{-}trien)]^+$ or $[In^{III}(5\text{-}Clsal_2\text{-}trien)]^+$ cations in the place of $[Fe^{III}(5\text{-}Clsal_2\text{-}trien)]^+$. The bimetallic oxalate 3D network is similar to that of **1**, but in contrast to **1**, solvent molecules are not found in these two structures. All metal ions from the oxalate network have the same chirality (Λ in the crystals used to solve the structures of **2** and **3**). The two metals are crystallographically independent with mean Mn-O distances of 2.192(5) Å for **2** and 2.186(8) for **3** and Cr-O distances of 1.973(5) Å for **2** and 1.973(7) for **3**. These distances are again the ones expected for Mn^{II}-O and Cr^{III}-O. Metal-metal distances between adjacent centers are in the range 5.393(5) - 5.432(5) Å for **2** and 5.385(7) - 5.409(7) Å for **3**.

$[Fe^{III}(5\text{-}Brsal_2\text{-}trien)]^+$ in **2** and $[In^{III}(5\text{-}Clsal_2\text{-}trien)]^+$ in **3** are intercalated in the holes described by the 3D oxalate network. There is one crystallographically independent $[M^{III}(5\text{-}Xsal_2\text{-}trien)]^+$ complex. In the crystals used to solve the structures of **2** and **3**, as for **1**, Fe^{III} and In^{III} adopt the opposite configuration (Δ) to that of Mn^{II} and Cr^{III} ions from the oxalate network (Λ). In **2**, the intermolecular interactions between $[Fe^{III}(5\text{-}Brsal_2\text{-}trien)]^+$ cations are similar to those of **1**. Thus, $[Fe^{III}(5\text{-}Brsal_2\text{-}trien)]^+$ cations ocuppy the

channels defined by the oxalate network forming chains that run along the *a* axis which are connected to the $[Fe^{III}(5\text{-}Brsal_2\text{-}trien)]^+$ cations of four neighbouring chains through short contacts between Br atoms and CH_2 from ethylene groups. In **3**, $[In^{III}(5\text{-}Clsal_2\text{-}trien)]^+$ also form chains but in this case they are only connected through short contacts between Cl atoms and CH_2 from ethylene groups with the $[In^{III}(5\text{-}Clsal_2\text{-}trien)]^+$ of two neighbouring chains.

The two ethylene groups closer to the phenoxy rings of $[Fe^{III}(5\text{-}Brsal_2\text{-}trien)]^+$ in **2** are disordered between two possible configurations. The average Fe–N and Fe–O bond distances of $[Fe^{III}(5\text{-}Brsal_2\text{-}trien)]^+$ complexes in **2** are 2.076(7) and 1.913(6) Å. These values are close to those obtained for other HS $[Fe(sal_2\text{-}trien)]^+$ compounds, in agreement with magnetic measurements and Mössbauer spectroscopy (see below), which indicate that around 60 % of Fe is HS at 120 K (temperature at which the crystal structure has been determined). The average In–N and In–O bond distances of $[In^{III}(5\text{-}Clsal_2\text{-}trien)]^+$ complexes in **3** are 2.253(8) and 2.114(7) Å.

Magnetic Properties. To get the magnetism of the MnCr oxalate lattice we will talk first of the magnetic properties of **3** as this compound contains a diamagnetic inserted cation. The thermal dependence of the product of the molar magnetic susceptibility times the temperature (χT) of **3** presents a value of 7.0 emu·K·mol^{-1} at 300 K, which is close to the sum of the expected contributions for the isolated paramagnetic ions (see Figure 3). Upon cooling down, χT increases gradually with a very abrupt increase below 50 K. This confirms the ferromagnetic interaction between Mn^{II} and Cr^{III} ions of the oxalate network and the onset of long-range ferromagnetic ordering, as observed for other Mn^{II}–Cr^{III} oxalate networks.[4-6] The χ^{-1} versus *T* curve of **3** is linear in the 50-300 K temperature range. This permits to fit it to a Curie-Weiss law ($\chi^{-1} = (T-\theta)/C$) leading to a Weiss constant, θ (K), of 5.5 K which is analogous to that obtained for a chiral 3D $Mn^{II}Cr^{III}$ oxalate network in the $[Ir(ppy)_2(bpy)][M^{II}Cr^{III}(ox)_3]\cdot 0.5H_2O$ compound (6.1 K).[5f] To confirm the presence of long-range magnetic ordering and to determine precisely the critical temperatures, *ac* susceptibility measurements were carried out. A maximum in

the in-phase signal (χ') near T_c and an out-of-phase signal (χ'') that starts to appear at temperatures just below T_c is observed (Figure 4). From these data the T_c of **3** is 5.0 K. As expected for a ferromagnet, these signals are frequency independent (Figure 4). In the ordered phase an additional peak in χ' and χ'' at temperatures below 3 K is also detected. The presence of such a frequency-dependent peak has already been observed in other 3D bimetallic oxalate compounds.[5f] It can be related with the formation of magnetic domains and domain-wall movement in the ordered phase.[26] The isothermal magnetisation (*M*) at 2 K shows a very sharp increase at low fields reaching a *M* value of 6.6 μ_B a 0.1 mT (Figure 5), confirming the ferromagnetic interactions between Mn^{II} and Cr^{III} ions. At fields above 0.1 T, only a slight linear increase of *M* versus *H* is observed as a consequence of spin canting in the ferromagnetic phase. A *M* value of 8.0 μ_B is obtained at 5 T, as expected for a $Mn^{II}Cr^{III}$ ferromagnet. A hysteresis loop of the magnetisation with a coercive field of 1 mT is observed at 2 K. All these features indicate a ferromagnetic behavior of this 3D oxalate network which is analogous to that obtained in the cubic 3D oxalate-based compounds.[5]

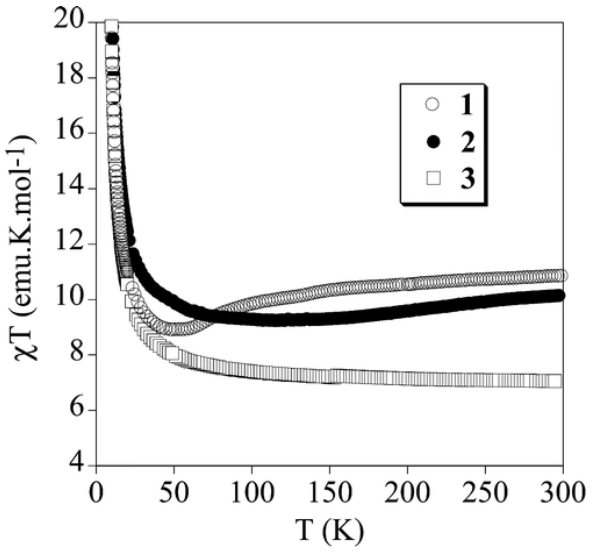

Figure 3. Temperature dependence of the product of the molar magnetic susceptibility with temperature (χT) at 0.1 for compounds **1** (empty circles), **2** (full circles), and **3** (empty squares).

To understand the magnetic properties of **1** and **2** we have to take into account the spin-crossover behavior of the inserted cation besides the ferromagnetic behavior of the MnCr oxalate lattice, mentioned above. χT of **1** and **2** shows higher values than that of **3** in all the range of temperature due to the paramagnetic contribution of the inserted Fe^{III} cation (see Figure 3). In the case of **1**, it presents a value of 10.9 emu·K·mol^{-1} at 300 K close to the sum of the expected contributions for the isolated paramagnetic ions with the Fe^{III} spin-crossover complex in a HS state. Upon cooling down, χT decreases gradually. This decrease is more abrupt below 100 K to reach a minimum of 8.9 emu·K·mol^{-1} around 60 K. This is consistent with a spin-crossover of around 50 % of Fe^{III} compounds from 300 to 60 K in agreement with the data obtained from Mössbauer spectroscopy (see below). χT of **2** is 10.0 emu·K·mol^{-1} at 300 K. This value is slightly lower to that obtained for **1** in agreement with the 13 % of Fe^{III} in the LS state at this temperature calculated from Mössbauer spectroscopy data. At lower temperatures, χT decreases very gradually to reach a minimum of 9.2 emu·K·mol^{-1} around 120 K, in agreement with Mössbauer data that suggest a progressive decrease of the HS fraction between 297 (87 % HS) and 100 K (61 % HS), which remains constant below this temperature. At temperatures below 80 K, χT of **2** is higher than that of **1** as a result of the smaller degree of HS→LS conversion of **2** (Figure 3). Below 50 K, **1** and **2** present a sharp increase of χT, as in the case of **3**, due to the onset of long-range ferromagnetic ordering.

Alternating Current susceptibility measurements of **1** and **2** are very similar to those of **3**. They show frequency independent peaks in χ' and χ'' and an additional peak in the ordered phase below 3 K (see Figure 4). From these data the T_c of **1** and **2** is 4.8 K. This indicates that the ferromagnetic behavior of the 3D oxalate network of **1** and **2** is analogous to that of **3** with a slight decrease of T_c that may be explained by the shorter Mn^{II}–Cr^{III} distances shown by **3** (5.407(6)-5.462(6) Å for **1,** 5.393(5)-5.432(5) Å for **2** and 5.385(7) and 5.409(7) Å for **3**) or by slight differences in the bonding angles.

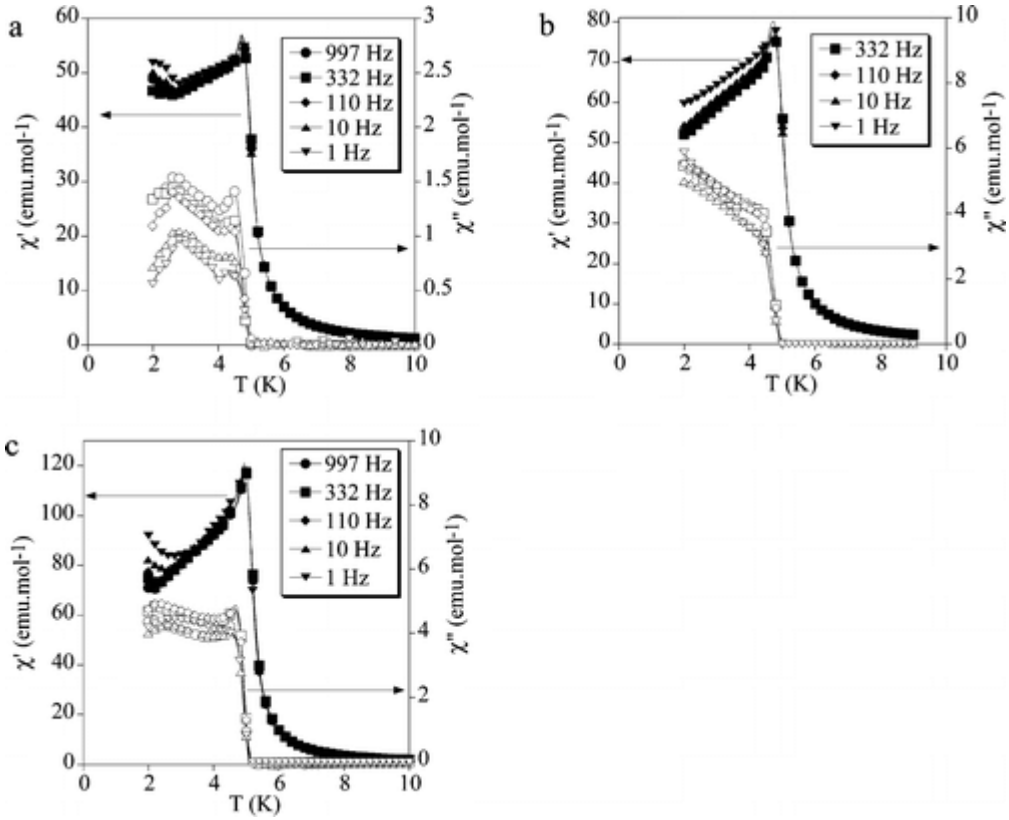

Figure 4. Temperature dependence of the in-phase *ac* susceptibility (χ') (filled symbols) and out-of-phase *ac* susceptibility (χ'') of **1** (a), **2** (b), and **3** (c)

The isothermal magnetisation of **1** and **2** at 2 K shows a very sharp increase at low fields, reaching a value of 6.1 μ_B in the two compounds at 0.1 mT, confirming the ferromagnetic interactions between Mn^{II} and Cr^{III} ions. At higher fields *M* has a continuous increase, which is more important than that of **3** due to the paramagnetic contribution of the inserted Fe^{III} cation. Furthermore, *M* of the two compounds does not saturate completely (see Figure 5). Due to this, *M* value obtained at 5 T (9.1 μ_B) for **1** is still lower than the expected value for a parallel alignement of the spins of Mn^{II} and Cr^{III} with 56 % of Fe^{III} in the HS state (11 μ_B) indicated by Mössbauer spectroscopy (see

below). This difference may be explained by the spin canting of the bimetallic oxalate network and nonsaturation of the *M* coming from the paramagnetic Fe^{III} complex. In **2**, the presence of a higher fraction of HS Fe^{III} than that of **1** produces a more pronounced curvature in the *M* vs *H* curve that reaches higher *M* values (Figure 5). Thus, *M* increases from 6.1 to 9.9 μ_B when *H* increases from 0.1 to 5 T. Again, this value is lower than the expected one for ~ 60 % of Fe^{III} in the HS state (~ 11.5 μ_B). A hysteresis loop of the magnetization with a coercive field of 3 mT is observed at 2 K for the two compounds.

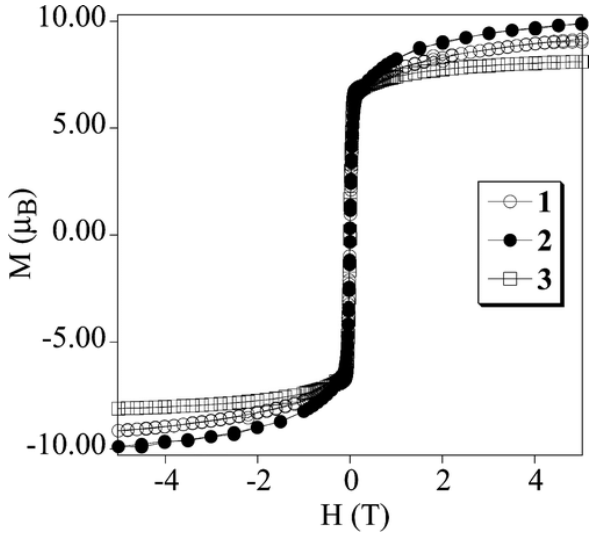

Figure5. Field dependence of the magnetisation (*M*) for **1** (empty circles), **2** (filled circles), and **3** (empty squares).

1 - **3** present slightly lower T_c than that of the cubic 3D chiral compound $[Ir(ppy)_2(bpy)][Mn^{II}Cr^{III}(ox)_3]\cdot 0.5H_2O$ (T_c = 5.1 K)[5f] in spite of the shorter Mn^{II}–Cr^{III} distances that they present. This could be attributed to other factors such as the differences in the relative orientation of the magnetic orbitals. If we compare with other 2D and 3D compounds obtained with $[Fe^{III}(sal_2\text{-trien})]^+$ and derivatives, the T_c value of **1** and **2** (4.8 K) is lower than that exhibited for Mn^{II}–Cr^{III} 2D oxalate (5.6 K) and achiral 3D compounds (5.2 K) with inserted $[Fe^{III}(sal_2\text{-trien})]^+$.[16] This could be explained by the longer Mn^{II}-Cr^{III} distances found in **1** and **2** with respect to these two compounds.

Furthermore, we have demonstrated that the decrease in T_c observed in the 3D series of bimetallic oxalates with respect to the 2D ones can be explained by the non-collinear alignment of the chiral axis in the 3D compounds, as they produce differences in the relative orientation of the magnetic orbitals.[27] On the other hand, in a chiral 3D lattice the T_c values should also be lower than those of achiral 3D lattices with inserted $[Fe^{III}(sal_2\text{-trien})]^+$ as observed for **1** and **2**. That is so because an achiral 3D lattice contains both homochiral (similar to those found in chiral 3D structures) and heterochiral (similar to those found in 2D structures) pairs of neighbouring magnetic ions.

Mössbauer spectroscopy. Mössbauer spectra of **1** and **2** shown in figures 6 and 7 are similar to those published for $[Fe^{III}(sal_2\text{-trien})][Mn^{II}Cr^{III}(ox)_3]\cdot(CH_3OH)$ between 2.2 and 295K and are therefore analysed with a similar model.[16]

For compound **1** only one contribution is observed at 295 K (Figure 6). It is an unresolved absorption centered at IS ~ 0.34 (295K) - 0.35 (4K) which gradually broadens as the temperature decreases and is assigned to HS Fe^{III}. A quadrupole doublet with estimated parameters typical of LS Fe^{III} appears in the 245 K spectrum. The relative area of the quadrupole doublet, and therefore the fraction of Fe^{III} in the LS state gradually increases with decreasing temperature down to 100 K. Below 100 K the increase of the LS fraction seems steeper until it reaches approximately 44 % at 70 K and stabilizes down to 4.2 K. At this temperature four peak maxima belonging to a sextet appear on the absorption band with an estimated magnetic hyperfine field of 52.8 T typical of HS Fe^{III} (S = 5/2) (table 2).

For compound **2** two contributions are clearly observed already at 295 K (Figure 7). One is a LS quadrupole doublet. The other one is an unresolved absorption centered at IS ~ 0.31 (295 K) to 0.50 (4 K) assigned to HS Fe^{III} which gradually broadens as the temperature decreases. At 4 K four peak maxima belonging to a sextet appear on the absorption band. This sextet becomes quite evident at 2.2 K with an estimated magnetic

hyperfine field of 53.2 T typical of HS Fe^{III} (S = 5/2). The fraction of Fe^{III} in the LS state increases with decreasing temperature down to 100 K, slowly between 295 and 230 K, fast between 230 and 190 K and again very slowly between 190 and 100 K, where it reaches a value of approximately 38 % (table 3).

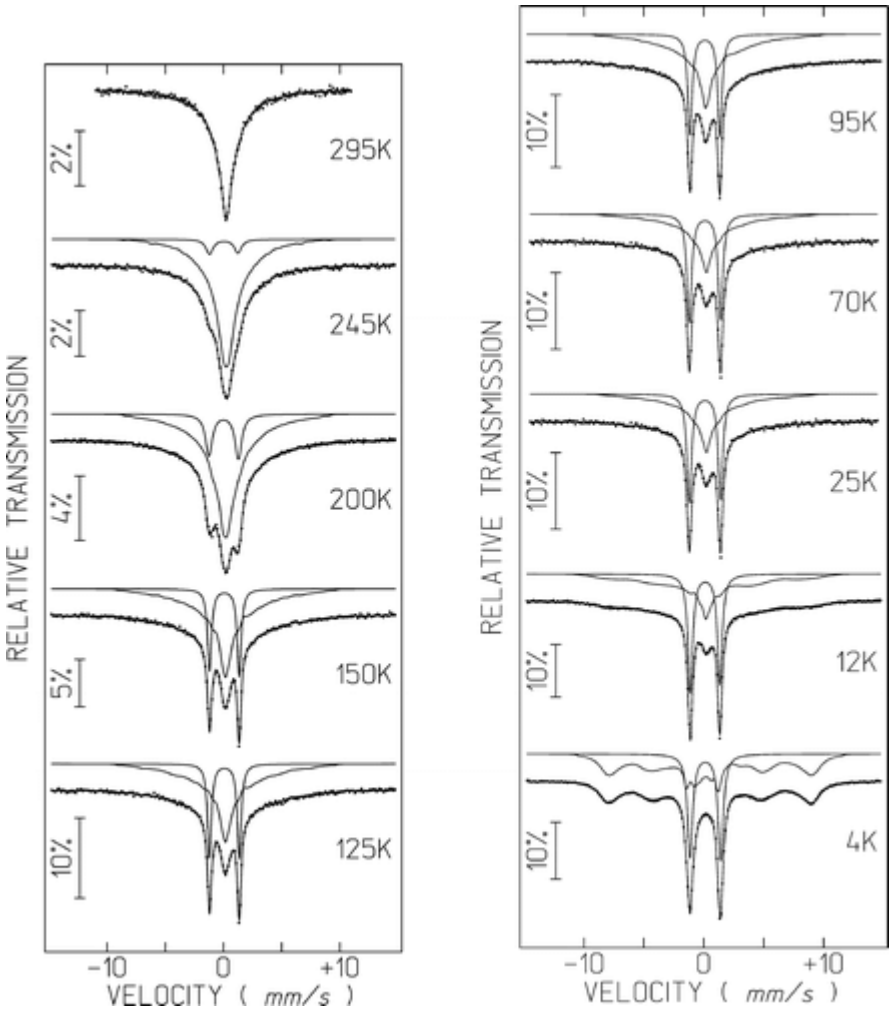

Figure 6. Mössbauer spectra of **1** taken at different temperatures. The lines over the experimental points are the sum of a doublet and a distribution of B_{hf} corresponding to LS and HS Fe^{III}. The estimated parameters for these doublets are collected in Table 2.

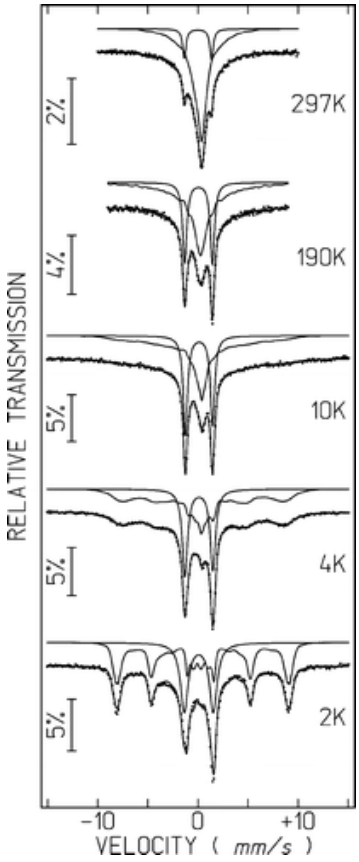

Figure 7. Mössbauer spectra of **2** taken at different temperatures. The lines over the experimental points are the sum of a doublet and a distribution of B_{hf} corresponding to LS and HS Fe^{III}. The estimated parameters for these doublets are collected in Table 2.

As discussed in detail in a previous paper, broadening of the HS Fe^{III} contribution may not be attributed to slow spin state interconversion since the LS Fe^{III} doublet peaks remain sharp with relatively thin line widths in the whole 300 - 2 K range.[16] Broadening of the HS Fe^{III} is rather due to slow relaxation of the HS Fe^{III} magnetic moments directions with a frequency (10^7 - 10^9 s^{-1}) whose reciprocal is on the same order of magnitude as the Mössbauer effect observation time. For both **1** and **2** compounds the relaxation frequency decreases with decreasing temperature as evidenced by the gradual broadening of the absorption until a sextet is observed at 4 K and below, in an identical way as observed for $[Fe^{III}(sal_2\text{-trien})][Mn^{II}Cr^{III}(ox)_3]\cdot(CH_3OH)$.[16] A similar effect

has been observed very recently at 3 K in a Fe^{III} complex with a hexadentate Schiff base ligand.[28]

Table 2. Estimated parameters from the Mössbauer spectra of **1** taken at different temperatures.[a]

T		IS	QS	B_{hf}	*I*
295 K	**LS Fe**				
	HS Fe	**0.34**	**0.00**		**100%**
245 K	**LS Fe**	**0.13**	**2.45**		**7%**
	HS Fe	**0.35**	**0.00**		**93%**
200 K	**LS Fe**	**0.16**	**2.51**		**17%**
	HS Fe	**0.35**	**0.10**		**83 %**
150 K	**LS Fe**	**0.19**	**2.55**		**25%**
	HS Fe	**0.33**	**0.10**		**75%**
125 K	**LS Fe**	**0.19**	**2.56**		**29%**
	HS Fe	**0.32**	**0.10**		**71%**
95 K	**LS Fe**	**0.21**	**2.50**		**34%**
	HS Fe	**0.33**	**0.11**		**66%**
70 K	**LS Fe**	**0.21**	**2.61**		**44%**
	HS Fe	**0.35**	**0.10**		**56%**
25 K	**LS Fe**	**0.22**	**2.51**		**44%**
	HS Fe	**0.35**	**0.10**		**56%**
12 K	**LS Fe**	**0.22**	**2.47**		**43%**
	HS Fe	**0.35**	**0.09**		**57%**
4 K	**LS Fe**	**0.23**	**2.51**		**44%**
	HS Fe	**0.35**	**0.28**	**52.8**	**56%**

Table 3. Estimated parameters from the Mössbauer spectra of **2** taken at different temperatures.[a]

T		IS	QS, ε	B_{hf}	*I*
295 K	**LS Fe**	**0.11**	**2.72**		**13%**
	HS Fe	**0.31**	**-0.29**		**87%**
230 K	**LS Fe**	**0.12**	**2.74**		**17%**
	HS Fe	**0.35**	**-0.13**		**83%**
190 K	**LS Fe**	**0.17**	**2.76**		**34%**
	HS Fe	**0.37**	**-0.05**		**66%**
100 K	**LS Fe**	**0.18**	**2.65**		**39%**
	HS Fe	**0.39**	**-0.11**		**61%**
10 K	**LS Fe**	**0.21**	**2.71**		**39%**
	HS Fe	**0.43**	**-0.15**		**61%**
4 K	**LS Fe**	**0.21**	**2.79**		**37%**
	HS Fe	**0.50**	**0.21**		**63%**
2 K	**LS Fe**	**0.19**	**2.89**		**38%**
	HS Fe	**0.49**	**0.21**	**53.2**	**62%**

[a] HS Fe and LS Fe: high-spin and low-spin Fe^{III}; IS (mm/s) isomer shift relative to metallic Fe at 295 K. QS (mm/s) quadrupole splitting of doublets; ε (mm/s), quadrupole shift for magnetic sextet; B_{hf} (T) magnetic hyperfine field. *I* relative area. Estimated standard deviations are <0.02 mm/s for IS, QS, and Γ, <0,5 T for Bhf, and <2% for *I*.

Conclusion

In this work we have reported the preparation of three novel compounds (**1** - **3**) formed by the insertion of the spin-crossover $[Fe^{III}(5\text{-}Clsal_2\text{-}trien)]^+$ and $[Fe^{III}(5\text{-}Brsal_2\text{-}trien)]^+$ cations and the reference compound with diamagnetic $[In^{III}(5\text{-}Clsal_2\text{-}trien)]^+$ cation into anionic coordination polymers based on bimetallic oxalate complexes. We confirm with this result that the use of different sal_2-trien derivatives is a suitable strategy to obtain a great variety of oxalate networks. Thus, we have seen previously that depending on the substituent, different type of networks can be obtained. Thus, $[Fe^{III}(5\text{-}NO_2sal_2\text{-}trien)]^+$ and $[Fe^{III}(5\text{-}CH_3Osal_2\text{-}trien)]^+$ complexes lead, respectively, to formation of a 2D and achiral 3D networks, in contrast with the flexibility of non-substituted $[Fe(sal_2\text{-}trien)]^+$ cation favouring 2D and achiral 3D networks by changing the preparation conditions. In this work, we extended this work to $[Fe^{III}(5\text{-}Xsal_2\text{-}trien)]^+$ (X = Cl, Br) complexes, and this has resulted in the growth of a different type of oxalate-based structure, a 3D chiral network. The different templating effect of these cations could be related to the intermolecular interactions. Thus, in $[Fe^{III}(5\text{-}NO_2sal_2\text{-}trien)]^+$ complex the presence of NO_2 groups favours π-π stacking interactions and this favours the growth of a 2D network, while $[Fe^{III}(5\text{-}CH_3Osal_2\text{-}trien)]^+$ complex, which make more difficult these interactions due to steric hindrance of the methoxy groups, leads to the formation of an achiral 3D network. In the three compounds reported in this paper the presence of smaller substituents (Cl or Br) favors a helical arrangement of the complexes and the growth of a 3D chiral network. Furthermore, this result shows that the formation of oxalate-based chiral 3D networks is not restricted to templating cations such as $[Z^{II}(bpy)_3]^{2+}$. We must take into account that, in contrast to 2D compounds, which admit a large variety of cations, in the 3D structures reported so far the templating cation might have the appropriate symmetry (D_3), size, and charge. This is the first time in which this type of chiral network is obtained with a cation of lower symmetry.

Beside the structural interest of these compounds, we have shown that the strategy reported in this paper gives rise to an unusual combination of three physical properties in the same compound, chirality, spin-crossover, and ferromagnetism in the case of **1**

and **2** and two properties, chirality and ferromagnetism, in the case of **3**. From the point of view of the onset of new properties, the combination of chirality and ferromagnetism could give rise to the observation of magneto-chiral dichroic effects. Notice that this effect has been observed in the weakly chiral 2D lattice.[13a] Still, in the strongly chiral 3D lattice this effect could not be studied as the charge transfer bands of the $[Z^{II}(bpy)_3]^{2+}$ counterions caused an intense absorption. For this purpose, compound **3** seems to be more promising since Fe^{III} cations of **1** and **2** have an intense absorption due to charge transfer bands and could dominate the optical properties as occurs in the 3D compounds containing $[Z(bpy)_3]^{2+}$ cations. In this context, **3** could be an ideal candidate to observe this effect due to the lack of absorption of the In^{III} complex.

On the other hand, a very promising possibility that remains to be explored is the tuning of the magnetic ordering of the $Mn^{II}Cr^{III}$ oxalate network by inducing the spin crossover of the cations applying light or pressure. Compounds **1** and **2** could be good candidates for this purpose as 3D oxalate networks are expected to be sensitive to the chemical pressure induced by the inserted cation. However, the possible switching effect induced by the presence of the spin-crossover cation could be limited by the gradual and not complete spin-crossover (less than 50 %) obtained for these compounds.

Associated Content

Supporting Information. Projections of the structure of **1** in the *ac* and *ab* planes and CIF files of the structures of **1** – **3**. This material is available free of charge via the Internet at http://pubs.acs.org.

Acknowledgment. Financial support from the EU (SPINMOL ERC Advanced Grant), the Spanish Ministerio de Ciencia e Innovación with FEDER cofinancing (Project Consolider-Ingenio in Molecular Nanoscience and projects MAT2007-61584 and CTQ-2008-06720), and the Generalitat Valenciana (Prometeo Program) are gratefully acknowledged.

References

[1] (a) E. Coronado, P. Day, *Chem. Rev.,* 2004, **104,** 5419; (b) E. Coronado, C. Martí-Gastaldo, E. Navarro-Moratalla, A. Ribera, S. J. Blundell, P. J. Baker, *Nat. Chem.,* 2010, **2**, 1031.

[2] (a) E. Coronado, M. C. Giménez-López, G. Levchenko, F. M. Romero, V. García-Baonza, A Milner, M. Paz-Pasternak, *J. Am. Chem. Soc.,* 2005, **127**, 4580; (b) E. Coronado, M. C. Giménez-López, T. Korzeniak, G. Levchenko, F. M. Romero, A. Segura, V. García-Baonza, J. C. Cezar, F. M. F. De Groot, A. Milner, M. Paz-Pasternak, *J. Am. Chem. Soc.,* 2008, **130**, 15519; (c) S. I.Ohkoshi, K. Imoto, Y. Tsunobuchi, S. Takano, H. Tokoro, *Nat. Chem.,* 2011, **3**, 564.

[3] M. Clemente-León, E. Coronado, C. Martí-Gastaldo, F. M. Romero, *Chem. Soc. Rev.,* 2011, **40**, 473.

[4] (a) H. Tamaki, Z. J. Zhong, N. Matsumoto, S. Kida, M. Koikawa, N. Achiwa, Y. Hashimoto, H. Okawa, *J. Am. Chem. Soc.,* 1992, **114,** 6974; (b) H. Tamaki, M. Mitsumi, N. Nakamura, N. Matsumoto, S. Kida, H. Okawa, S. Ijima, *Chem. Lett.,* 1992, 1975; (c) C. Mathonière, S. G. Carling, D. Yuscheng, P. Day, *J. Chem. Soc. Chem. Commun.,* 1994, 1551; (d) C. Mathonière, J. Nutall, S. G. Carling, P. Day, *Inorg. Chem.,* 1996, **35**, 1201; (e) R. Pellaux, H. W. Schmalle, R. Huber, P. Fisher, T. Hauss, B. Ouladdiaf, S. Decurtins, *Inorg. Chem.,* 1997, **36**, 2301; (f) E. Coronado, J. R. Galán-Mascarós, C. J. Gómez-García, J. M. Martínez-Agudo, E. Martínez-Ferrero, J. C. Waerenborgh, M. Almeida, *J. Solid State Chem.,* 2001, **159**, 391; (g) K. S. Min, A. L. Rhinegold, J. S. Miller, *Inorg. Chem.,* 2005, **44**, 8433; (h) E. Coronado, J. R. Galán-Mascarós, C. Martí-Gastaldo, *J. Mater. Chem.,* 2006, **16**, 2685.

[5] (a) S. Decurtins, H. W. Schmalle, P. Schneuwly, H. R. Oswald, *Inorg. Chem.,* 1993, **32**, 1888; (b) S. Decurtins, H. W. Schmalle, P. Schneuwly, J. Ensling, P. Gütlich, *J. Am. Chem. Soc.,* 1994, **116**, 9521; (c) M. Hernández-Molina, F. Lloret, C. Ruiz-Pérez, M. Julve, *Inorg. Chem.,* 1998, **37**, 4131; (d) E. Coronado, J. R. Galán-Mascarós, C. J. Gómez-García, J. M. Martínez-Agudo, *Inorg. Chem.,* 2001, **40**, 113; (e) F. Pointillart, C. Train, M. Gruselle, F. Villain, H. W. Schmalle, D. Talbot, P. Gredin, S. Decurtins, M. Verdaguer, *Chem. Mater.,* 2004, **16**, 832; (f) M. Clemente-León, E. Coronado, C. J. Gómez-García, A. Soriano-Portillo, *Inorg. Chem.,* 2006, **45**, 5653.

[6] (a) M. Clemente-León, J. R. Galán-Mascarós, C. J. Gómez-García, *Chem. Commun.,* 1997, 1727; (b) E. Coronado, J. R. Galán-Mascarós, C. J. Gómez-García, J. M. Martínez-Agudo, *Adv. Mater.,* 1999, **11**, 558; (c) E. Coronado, J. R. Galán-Mascarós, C. J. Gómez-García, J. Ensling, P. Gutlich, *Chem. Eur. J.,* 2000, **6**, 552.

[7] (a) S. Bénard, P. Yu, J. P. Audière, E. Rivière, R. Clèment, J. Ghilhem, L. Tchertanov, K. Nakatami, *J. Am. Chem. Soc.,* 2000, **122**, 9444; (b) S. M. Aldoshin, N. A. Sanina, V. I.

Minkin, N. A. Voloshin, V. N. Ikorskii, V. I. Ovcharenko, V. A.; Smirnov, N. K. Nagaeva, *J. Mol. Struct.,* 2007, **826**, 69.

[8] (a) E. Coronado, J. R. Galán-Mascarós, C. J. Gómez-García, V. Laukhin, *Nature,* 2000, **408**, 447; (b) A. Alberola, E. Coronado, J. R. Galán-Mascarós, C. Giménez-Saiz, C. J. Gómez-García, *J. Am. Chem. Soc.,* 2003, **125**, 10774; (c) E. Coronado, J. R. Galán-Mascarós, C. J. Gómez-García, E. Martínez-Ferrero, s. Van Smaalen, *Inorg. Chem.,* 2004, **43**, 4808.

[9] H. Okawa, A. Shigematsu, M. Sadakiyo, T. Miyagawa, K. Yoneda, M. Ohba H. Kitagawa, *J. Am. Chem. Soc.,* 2009, **131**, 13516.

[10] (a) R. Andrés, M. Gruselle, B. Malézieux, M. Verdaguer, J. Vaissermann, *Inorg. Chem.,* 1999, **38**, 4637; (b) R. Andrés, M. Brissard, M. Gruselle, C. Train, J. Vaissermann, B. Malézieux, J. P. Jamet, M. Verdaguer, *Inorg. Chem.,* 2001, **40**, 4633; (c) M. Clemente-León, E. Coronado, J. C. Dias, A. Soriano-Portillo, R. D. Willett, *Inorg. Chem.,* 2008, **47**, 6458.

[11] J. R. Galán-Mascarós, E. Coronado, P. A. Goddard, J. Singleton, A. I. Coldea, J. D. Wallis, A. J. Coles, A. Alberola, *J. Am. Chem. Soc.,* 2010, **132**, 9271.

[12] T. Endo, T. Akutagawa, S. I. Noro, T. Nakamura, *Dalton Trans.,* 2011, **40**, 1491.

[13] (a) C. Train, R. Gheorghe, V. Krstic, L. M. Chamoreau, N. S. Ovanesyan, G. L. J. A. Rikken, M. Gruselle, M. Verdaguer, *Nat. Mater.,* 2008, **17**, 729; (b) C. Train, T. Nuida, R. Gheorghe, M. Gruselle, S. Ohkoshi, *J. Am. Chem. Soc.,* 2009, **131**, 16838.

[14] (a) R. Sieber, S. Decurtins, H. Stoeckli-Evans, C. Wilson, D. Yufit, J. A. K. Howard, S. C. Capelli, A. Hauser, *Chem. Eur. J.,* 2000, **6**, 361; (b) E. Coronado, J. R. Galán-Mascarós, M. C. Giménez-López, M. Almeida, J. C. Waerenborgh, *Polyhedron,* 2007, **26**, 1838.

[15] (a) M. Clemente-León, E. Coronado, M. C. Giménez-López, A. Soriano-Portillo, J. C. Waerenborgh, F. S. Delgado, C. Ruiz-Pérez, *Inorg. Chem.,* 2008, **47**, 9111; (b) M. Clemente-León, E. Coronado, M. López-Jordà, M. *Dalton Trans.,* 2010, **39**, 4903.

[16] M. Clemente-León, E. Coronado, M. López-Jordà, G. Mínguez Espallargas, A. Soriano-Portillo, J. C. Waerenborgh, *Chem. Eur. J*., 2010, **16**, 2207.

[17] M. Clemente-León, E. Coronado, M. López-Jordà, C. Desplanches, S. Asthana, H. Wang, J.-F. Létard, *Chem. Sci.,* 2011, **2**, 1127.

[18] M. F. Tweedle, L. J. Wilson, *J. Am. Chem. Soc.,* 1976*,* **98**, 4824.

[19] J. C. Baylar, E. M. Jones, In *Inorganic Synthesis*; H. S. Booth, Ed. McGraw-Hill: New York, 1939; Vol. 1, p 35.

[20] A. Altomare, M. C. Burla, M. Camalli, G. L. Cascarano, C. Giacovazzo, A. Guagliardi, A. G. G. Moliterni, G. Polidori, R. Spagna, *J. Appl. Cryst*., 1999, **32**, 115.

[21] SHELXL-97: G. M. Sheldrick, University of Göttingen, Germany, 1997.

[22] L. J. Farrugia, *J. Appl. Cryst.,* 1997, **32**, 837.

[23] H. D. Flack, G. Bernardinelli, *J. Appl. Cryst.,* 2000, **33**, 1143.

[24] J. V. Rodrigues, I. C. Santos, V. Gama, R. T. Henriques, J. C. Waerenborgh, M. T. Duarte, M. Almeida, *J. Chem. Soc. Dalton Trans*., 1994, 2655.

[25] The use of CH_3NO_2, for $[Fe^{III}(5\text{-}Brsal_2\text{-}trien)]^+$ and CH_3CN for $[Fe^{III}(5\text{-}Clsal_2\text{-}trien)]^+$ gives rise to crystals with a similar unit cell but lower quality in the case of $[Fe^{III}(5\text{-}Brsal_2\text{-}trien)]^+$ and with a high content of impurities in the case of $[Fe^{III}(5\text{-}Clsal_2\text{-}trien)]^+$.

[26] N. A. Chernova, Y. Song, P. Y. Zavalij, M. S. Wittingham, *Phys. Rev. B,* 2004, **70**, 144405.

[27] R. S. Fishman, M. Clemente-León, E. Coronado, *Inorg. Chem.,* 2009, **48**, 3039.

[28] M. Griffin, S. Shakespeare, H. J. Shepherd, C. J. Harding, J.-F. Létard, C. Desplanches, A. E. Goeta, J. A. K. Howard, A. K. Powell, V. Mereacre, Y. Garcia, A. D. Naik, H. Müller-Bunz, G. G. Morgan, *Angew. Chem., Int. Ed.,* 2011, **50**, 896.

2D bimetallic oxalate-based ferromagnets with inserted $[Fe(4\text{-}Br\text{-}sal_2\text{-}trien)]^+$ & $[Fe(3\text{-}R\text{-}sal_2\text{-}trien)]^+$ (R = Br, Cl and CH_3O) Fe^{III} spin-crossover complexes

Capítulo 7

Capítulo 7: 2D bimetallic oxalate-based ferromagnets with inserted $[Fe(4\text{-}Br\text{-}sal_2\text{-}trien)]^+$ and $[Fe(3\text{-}R\text{-}sal_2\text{-}trien)]^+$ (R = Br, Cl and CH_3O) Fe^{III} spin-crossover complexes

The syntheses, structures and magnetic properties of the compounds of formula $[Fe^{III}(4\text{-}Br\text{-}sal_2\text{-}trien)][Mn^{II}Cr^{III}(ox)_3]_{0.67}Cl_{0.33}\cdot CH_3OH$_solvate (**1**), $[Fe^{III}(3\text{-}Br\text{-}sal_2\text{-}trien)][Mn^{II}Cr^{III}(ox)_3]\cdot(CH_3CN)_2$ (**2**), $[Fe^{III}(3\text{-}Cl\text{-}sal_2\text{-}trien)][Mn^{II}Cr^{III}(ox)_3]\cdot(CH_3OH)_2\cdot(CH_3CN)_2$ (**3**) and $[Fe^{III}(3\text{-}CH_3O\text{-}sal_2\text{-}trien)][Mn^{II}Cr^{III}(ox)_3]\cdot(CH_3OH)\cdot(H_2O)_{1.5}\cdot(CH_2Cl_2)_{0.5}$ (**4**) are reported. The four structures present a 2D honeycomb anionic layer formed by Mn^{II} and Cr^{III} ions linked through oxalate ligands and a cationic layer of the Fe^{III} complexes intercalated between the 2D oxalate networks. The main differences compared with previous 2D oxalate-based structures are the presence of double layers of cations in compounds **1**, **3** and **4** and porous channels in the structures of **1** and **4** filled with disordered solvent molecules. The magnetic properties indicate that the inserted Fe^{III} cations undergo an almost complete spin crossover above 300 K in **1** and a partial spin crossover in **3** and **4** that coexists with a ferromagnetic ordering of the oxalate network. In the case of **2**, the inserted cation remains in the HS from 2 to 300 K. Therefore, **1**, **3** and **4** are multifunctional compounds with coexistence of spin crossover and magnetic ordering. Conversely, photomagnetic characterization shows that **1** and **3** do not present LIESST effect in contrast to the 2D compound $[Fe^{III}(sal_2\text{-}trien)][Mn^{II}Cr^{III}(ox)_3]\cdot(CH_2Cl_2)$. These results could help to clarify this rare property for a Fe^{III} complex.

Introduction

Multifunctional materials that combine two (or more) physical properties of interest are one of the most promising topics in molecular magnetism because a wise choice of the constituent molecules allows the appearance in the same compound of an unusual combination of physical properties,[1] or even a mutual interplay -synergy- of the properties involved.[2] A suitable approach to obtain these materials is the hybrid

approach, in which two-network solids are constructed from two different molecular fragments (organic, inorganic or organometallic), with each network furnishing distinct properties to the solid.

Bimetallic oxalate-bridged complexes of formula $A[M^{II}M^{III}(ox)_3]$ (M^{III} = Cr, Fe, Ru, V, Mn; M^{II} = Mn, Fe, Co, Ni, Cu, Zn; A = cation; ox = oxalate) have provided many examples of multifunctional magnets.[3] These bimetallic salts are most often composed by polymeric 2D or 3D anionic networks,[4,5] which furnish the cooperative magnetic properties (ferro- ferri- or canted antiferromagnetism), and a bulky charge-compensating molecular cation, which templates the network formation. The insertion of different cations into oxalate networks has led to compounds combining in the same compound the long-range magnetic ordering from the oxalate network with paramagnetism,[6] photochromism,[7] electric conductivity,[8] proton conduction,[9] ferroelectricity,[10] chirality,[11] or chirality combined with conductivity[12] or proton conduction.[13] Finally, the chirality of the oxalate network combined with the magnetic ordering has led to new properties such as magneto-chiral dichroism[14] and magnetization-induced second-harmonic generation.[15]

Spin crossover cations are particularly suitable for the preparation of oxalate-based multifunctional magnetic materials since they represent one of the best examples of molecular bistability. These kinds of molecular complexes change their spin state from low-spin (LS) to high-spin (HS) configurations under an external stimulus such as temperature, light-irradiation or pressure. As this is accompanied by changes in the molecular size, the spin-crossover process should act as an internal pressure in the hybrid material and therefore, it might affect the long-range magnetic ordering in the extended magnetic network. This may lead to a way to design switching magnets in which the magnetic ordering of the oxalate network could be tuned by inducing the spin crossover phenomenon. So far, several examples have described the incorporation of Co^{II} and Fe^{II} spin crossover complexes into oxalate-based networks.[16] A larger variety of compounds has been obtained with Fe^{III} complexes of the hexadentate Schiff base

ligand, sal_2-trien (H_2sal_2-trien = N,N' -disalicylidenetriethylene-tetramine) and 5-X-sal_2-trien derivatives (X = Cl, Br, NO_2 CF_3O, and CH_3O) that give rise to 2D and 3D oxalate-based networks (see Scheme 1).[3,17] The most interesting results were obtained for the 2D compound, $[Fe^{III}(sal_2\text{-trien})][Mn^{II}Cr^{III}(ox)_3]\cdot(CH_2Cl_2)$. The magnetic properties of this compound indicate the coexistence of a complete spin crossover transition from 300 to 160 K, and a ferromagnetic ordering below 5.6 K.[17b] Furthermore, it exhibits the conversion from the LS to HS state induced by light-irradiation, commonly known as the LIESST effect (light-induced excited spin-state trapping).[18] This is a very rare and unexpected property in a Fe^{III} spin-crossover complex as it has only been found in other two Fe^{III} complexes.[19] As expected, the photo-induced spin conversion of the inserted Fe^{III} complex has a negligible influence on the cooperative magnetic behavior of the oxalate network. This is consistent with the 2D structure of the compound as for different interlayer separations, very similar critical temperatures have been observed.

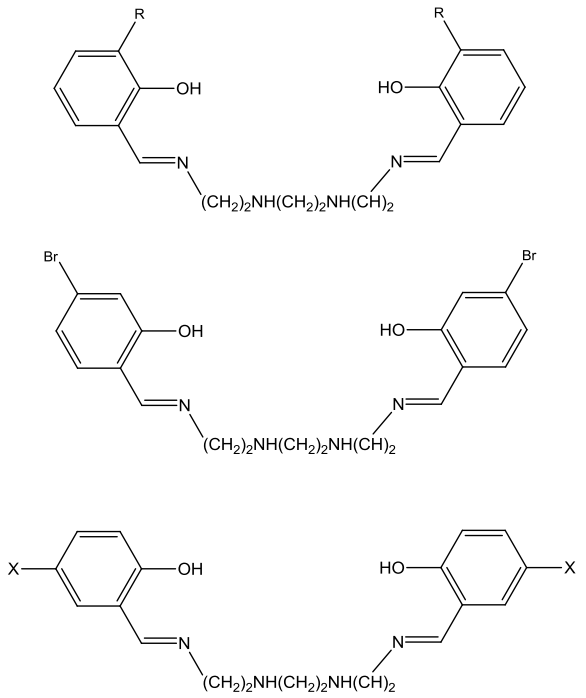

Scheme 1. H_2(3-R-sal_2-trien) (R = Br, Cl, CH_3O) (up), H_2(4-Br-sal_2-trien) (middle) and H_2(5-X-sal_2-trien) (X = Br, Cl, CH_3O, CF_3O and NO_2) (bottom)

In this work, $[Fe^{III}(4\text{-Br-sal}_2\text{-trien})]^+$ and $[Fe^{III}(3\text{-X-sal}_2\text{-trien})]^+$ (X = Br, Cl, CH_3O) complexes have been inserted into 2D oxalate-based networks in the search for new compounds with coexistence of spin crossover and magnetic ordering that could present LIESST effect. The structure and magnetic properties of the compounds of formula $[Fe^{III}(4\text{-Br-sal}_2\text{-trien})][Mn^{II}Cr^{III}(ox)_3]_{0.67}Cl_{0.33}\cdot CH_3OH$_solvate (**1**), $[Fe^{III}(3\text{-Br-sal}_2\text{-trien})][Mn^{II}Cr^{III}(ox)_3]\cdot(CH_3CN)_2$ (**2**), $[Fe^{III}(3\text{-Cl-sal}_2\text{-trien})][Mn^{II}Cr^{III}(ox)_3]\cdot(CH_3OH)_2\cdot(CH_3CN)_2$ (**3**) and $[Fe^{III}(3\text{-}CH_3O\text{-sal}_2\text{-trien})][Mn^{II}Cr^{III}(ox)_3]\cdot(CH_3OH)\cdot(H_2O)_{1.5}\cdot(CH_2Cl_2)_{0.5}$ (**4**) are reported in this paper. Photomagnetic characterisation of two of these compounds exhibiting spin crossover (**1** and **3**) have been performed.

Results and Discussion

Synthesis

The method to prepare **1**, **2**, **3** and **4** is similar to that used for the compounds with $[Fe^{III}(5\text{-X-sal}_2\text{-trien})]^+$ (X = H, Cl, Br, NO_2, CF_3O and CH_3O).[17] It is based on the use of $Ag_3[Cr(ox)_3]$ to avoid the presence of alkali ions in the structure. It consists of the slow diffucion of a methanol solution containing the precursors of the oxalate network, Mn^{2+} and $[Cr(ox)_3]^{3-}$ ions, into solutions of $[Fe^{III}(4\text{-Br-sal}_2\text{-trien})]^+$ or $[Fe^{III}(3\text{-X-sal}_2\text{-trien})]^+$ (X = Cl, Br, CH_3O) in different solvents. The best crystals for X-ray single-crystal diffraction are obtained in CH_3CN fro **1**, **2** and **3**, and CH_2Cl_2 for **4**. As observed for $[Fe^{III}(5\text{-X-sal}_2\text{-trien})]^+$ (X = Cl, Br, NO_2, CF_3O and CH_3O) derivatives, only one type of oxalate network -a 2D network- is obtained with different solvents. This is in contrast to what happens when $[Fe^{III}(sal_2\text{-trien})]^+$ is used as the cation. In that case, different solvents afford compounds with different types of oxalate network (2D for CH_2Cl_2 and 3D for CH_3CN). This may be related to the higher flexibility of $[Fe^{III}(sal_2\text{-trien})]^+$ complexes with respect to the substituents derivatives. The composition of crystals of these compounds, checked by microanalysis, shows a Fe/Mn/Cr/Cl ratio of 1:1:1:1 for **4**, a Fe/Mn/Cr/X (X = Cl or Br) ratio of 1:1:1:2 for **2** and **3** and Fe/Mn/Cr/Br/Cl ratio of 1:0.67:0.67:2:0.33 for **1**. In this last compound, Cl^- anions were found in the structure. Because of this, the stoichiometry of this compound (Fe/Mn/Cr/Br/Cl ratio of 1:0.67:0.67:2:0.33) is different

to the usual one (Fe/Mn/Cr ratio 1:1:1) for this type of compound. The presence of Cl^- in the solution is explained by the incomplete reaction between 1 equiv. of $Ag_3[Cr(ox)_3]$ and 1.5 equiv. of $MnCl_2$ due probably to the low solubility of $Ag_3[Cr(ox)_3]$. This leads to an excess of Cl^- that remains in the methanol solution containing the precursors of the oxalate network, $Mn2^+$ and $[Cr(ox)_3]^{3-}$, which is obtained after filtration of the AgCl precipitate. The crystal structures of the four compounds have been solved by single-crystal X-ray diffraction.

Structure

The structure of the four compounds consists of anionic layers with a 2D bimetallic oxalate network of formula $[MnCr(ox)_3]^-$ with inserted Fe^{III} cationic complexes and solvent molecules, and Cl^- anions in the case of **1**. The bimetallic oxalate layer presents in the four compounds the well-known honeycomb structure formed by an extended network with Mn^{II} and Cr^{III} ions linked through oxalate bridges with octahedral coordination. These oxalate ligands connect the Mn^{II} and Cr^{III} ions in such a way that each Mn^{II} is surrounded by three neighboring Cr^{III} and *vice-versa*.

*$[Fe^{III}(4\text{-}Br\text{-}sal_2\text{-}trien)][Mn^{II}Cr^{III}(ox)_3]_{0.67}Cl_{0.33}\cdot CH_3OH$_solvate (**1**)*

The structure of this compound was solved in the *P*-3 space group. The anionic bimetallic oxalate layer lies in the *ab* plane (Figure 1). It contains two crystallographically independent metals (Mn1/Cr1 and Mn2/Cr2) with M-O bond lengths lying between 2.058(3) and 2.086(3) Å. These bond lengths are intermediate between the ones expected for Cr^{III}-O and Mn^{II}-O. Therefore, it is not possible to distinguish between the two metals in this structure. The neighbouring metal centres of the bimetallic oxalate network present alternated chirality as usual for this type of network. These anionic layers are stacked one over the other in an *AA*···fashion. The minimum distance between metal ions belonging to different oxalate layers is 18.5675(7) Å (equal to the *c* parameter). This distance is much longer than those found in other oxalate-based 2D compounds with decamethylferrocenium or alkylammonium cations (9.2-9.7 Å)[4,6] or

with $[Fe^{III}(sal_2\text{-trien})]^+$ and derivatives (11.609-11.644 Å).[17b-c] This is due to the presence of a double layer of $[Fe^{III}(4\text{-Br-}sal_2\text{-trien})]^+$ complexes and Cl^- anions instead of the single layer found in other 2D structures. A similar interlayer distance was found in the compound $[Fe^{III}(sal_2\text{-trien})]_2[Mn^{II}_2(ox)_3]\cdot 4H_2O\cdot C_3H_7NO$ containing a double layer of $[Fe^{III}(sal_2\text{-trien})]^+$ between $[Mn^{II}_2(ox)_3]^{2-}$ layers.[17a]

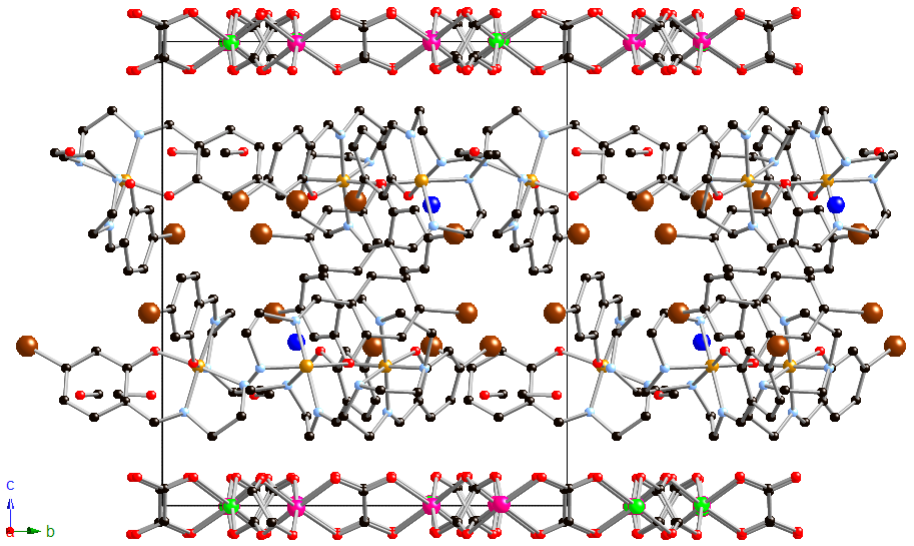

Figure 1. Projection of the structure of **1** in the *bc* plane. Fe (yellow), Br (brown), Cl (dark blue), C (black), N (blue), O (red), Mn (pink), Cr (green). Hydrogen atoms have been omitted for clarity.

The space between the oxalate layers is occupied by one crystallographically independent $[Fe^{III}(4\text{-Br-}sal_2\text{-trien})]^+$ complex, one chloride and one methanol molecule that form a double layer. Fe^{III} present the usual distorted octahedral symmetry of this type of complexes with average Fe-N and Fe-O bond distances of 1.967(3) and 1.888(4) Å respectively. These values are in the range of those obtained for other LS Schiff-Base complexes, in full agreement with the magnetic measurements (see below), which indicate that all Fe are LS at 120 K (temperature at which the crystal structure has been determined).

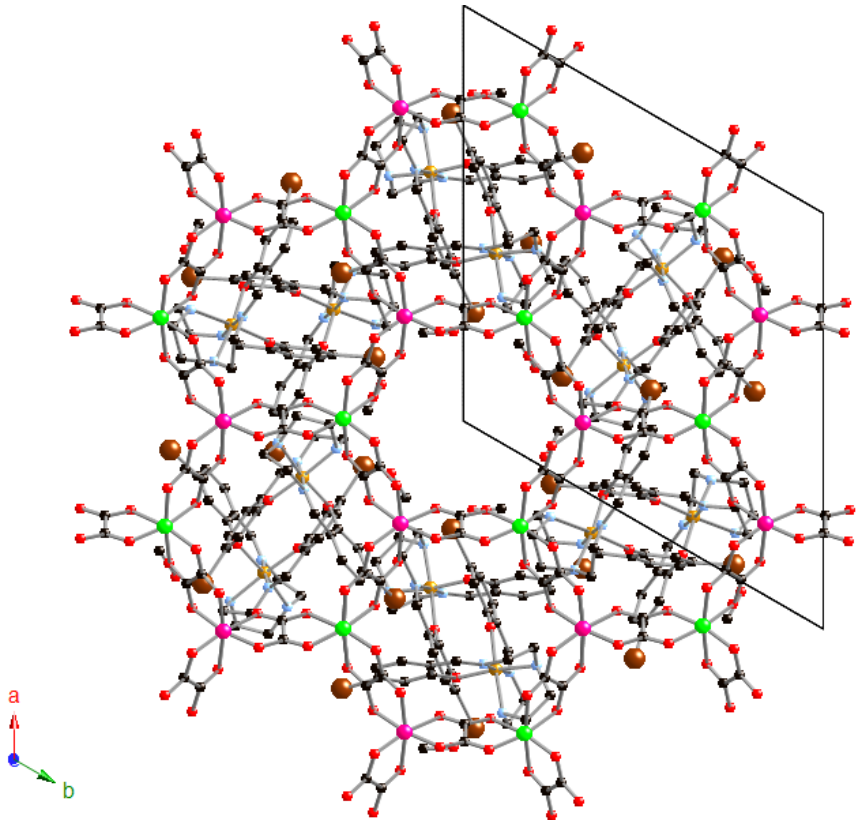

Figure 2. Projection of the structure of **1** in the *ab* plane. Fe (yellow), Br (brown), C (black), Cl (dark blue), N (blue), O (red), Mn (pink), Cr (green). Hydrogen atoms have been omitted for clarity.

The complexes lie with their longer axis almost parallel to the oxalate network. Thus, the phenoxy rings of these complexes are almost perpendicular to the bimetallic oxalate network (the dihedral angle between the least-squares planes of the phenoxy rings and that formed by the metals of the oxalate network are 71.5 and 81.0°). In each one of these layers, Cl^- is placed in a special position surrounded by three $[Fe^{III}(4\text{-Br-sal}_2\text{-trien})]^+$ complexes in the same layer related by a ternary axis. These three complexes form a hydrogen bond with a Cl^- anion through a NH group. Furthermore, there is a space between six $[Fe^{III}(4\text{-Br-sal}_2\text{-trien})]^+$ complexes belonging to the same layer that is

occupied by disordered solvent molecules. These hexagonal pores appear also in the other layer and are just behind and above the hexagonal channels described by the honeycomb bimetallic oxalate network. As a result, hexagonal channels occupied by disordered solvent molecules that run along the *c* axis are formed in this structure (see Figure 2). It is interesting to point out that not all the hexagonal channels are occupied by disordered solvent molecules. Thus, the *ab* projection of the structure show that one "empty" hexagonal channel is surrounded by six channels filled with $[Fe^{III}(4\text{-Br-sal}_2\text{-trien})]^+$ complexes. Cl^- anions are just behind and above along the *c* axis of Mn2/Cr2 ions. $[Fe^{III}(4\text{-Br-sal}_2\text{-trien})]^+$ complexes belonging to the different layers are linked through π-π stacking interactions and edge-to-face C-H···π interactions. Finally, there are numerous short contacts between the complexes and the oxalate network and methanol solvent molecules that form hydrogen bonds with a NH group of a neighbouring $[Fe^{III}(4\text{-Br-sal}_2\text{-trien})]^+$ complex.

*$[Fe^{III}(3\text{-Br-sal}_2\text{-trien})][Mn^{II}Cr^{III}(ox)_3]\cdot(CH_3CN)_2$ (**2**)*

This compound crystallizes in the triclinic space group *P-1*. The bimetallic oxalate layer lies in the *ac* plane and contains two crystallographically independent metals (Mn1/Cr1 and Mn2/Cr2) with M-O bond lengths lying between 2.065 (2) and 2.108 (2) Å (Figure 3). As in the case of **1**, it is not possible to distinguish between the two metals in the structure as they are intermediate between the ones expected for Cr^{III}-O and Mn^{II}-O. These anionic layers are stacked one over the other in an *AA*···fashion. The minimum distance between metal ions belonging to different oxalate layers is 12.8070(8) Å (equal to the *b* parameter). As this compound contains a single layer of $[Fe^{III}(3\text{-Br-sal}_2\text{-trien})]^+$ complexes, this distance is similar to those found in other oxalate-based 2D compounds with $[Fe^{III}(sal_2\text{-trien})]^+$ and derivatives (11.609-11.644 Å)[17b-c] and shorter than those found in **1**, **3** and **4** that contain a double layer. The space between the oxalate sheets is occupied by one crystallographically independent $[Fe^{III}(3\text{-Br-sal}_2\text{-trien})]^+$ complex and two crystallographically independent acetonitrile molecules.

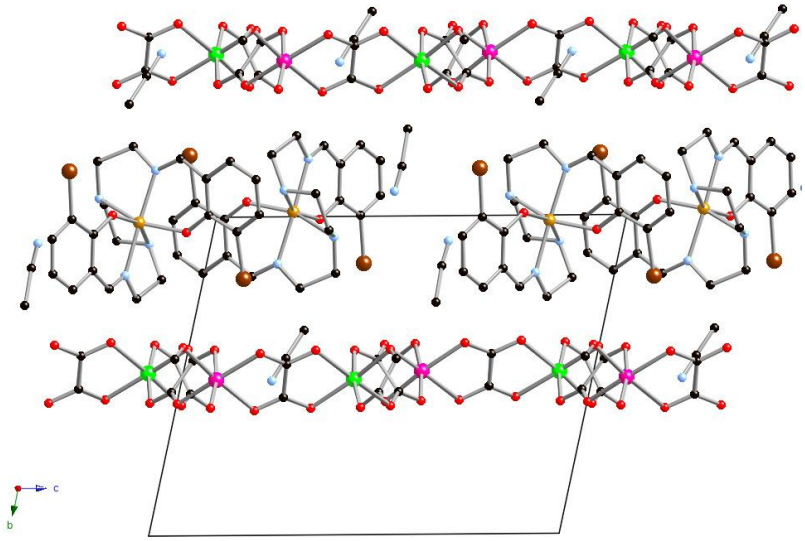

Figure 3. Projection of the structure of **2** in the *bc* plane. Fe (yellow), Br (brown), C (black), N (blue), O (red), Mn (pink), Cr (green). Hydrogen atoms have been omitted for clarity.

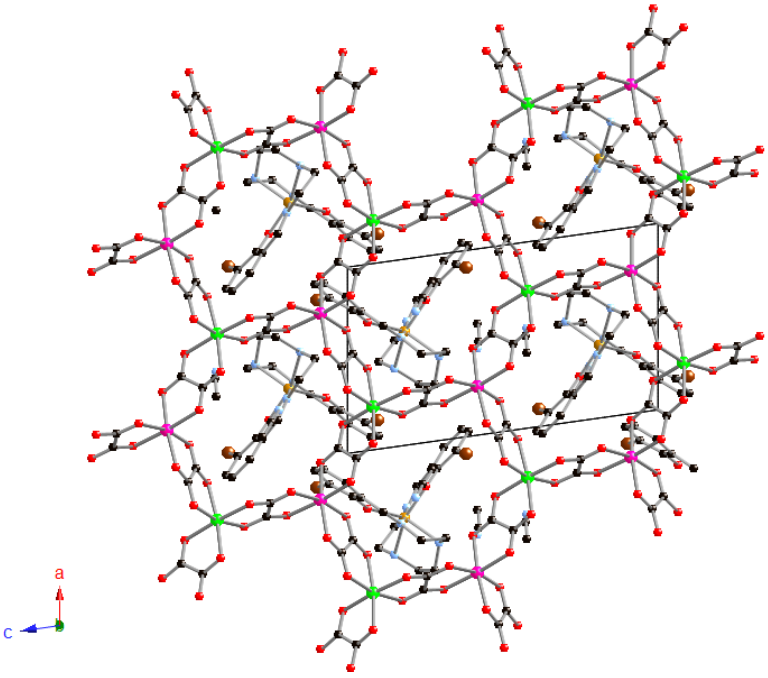

Figure 4. Projection of the structure of **2** in the *ac* plane. Fe (yellow), Br (brown), C (black), N (blue), O (red), Mn (pink), Cr (green). Hydrogen atoms have been omitted for clarity.

The average Fe-N and Fe-O bond lengths in $[Fe^{III}(3\text{-Br-sal}_2\text{-trien})]^+$ complexes are 2.152 (2) Å and 1.918 (2) Å, respectively. These values are typical values of HS Fe^{III} complexes in agreement with the magnetic properties. The cations lie with their longer axis parallel to the oxalate layers (Figure 3). This is confirmed by the dihedral angle between the least-squares planes of the phenoxy rings and that formed by the metals of the oxalate network (87.6 and 97.6°). $[Fe^{III}(3\text{-Br-sal}_2\text{-trien})]^+$ complexes form double chains running along the *a* axis (Figure 4 and Figure S1 of the Supporting information) separated by the acetonitrile solvent molecules. One of the two phenoxy rings of 3-Br-sal_2-trien, which is located in the internal part of the double chain, is involved in C–H···π and N–H···π interactions and π-π stacking interactions with two adjacent $[Fe^{III}(3\text{-Br-sal}_2\text{-trien})]^+$ complexes belonging to the other chain. The other phenoxy ring, which is located in the external part of the double chain, is connected through C–H···π interactions with an adjacent $[Fe^{III}(3\text{-Br-sal}_2\text{-trien})]^+$ complex belonging to the same chain. The two Br atoms of the complexes point alternatively above and below the cationic layer and present short interactions with the oxalate network. The $[Fe^{III}(3\text{-Br-sal}_2\text{-trien})]^+$ complexes of different double chains are connected through hydrogen bonds with the acetonitrile solvent molecules placed between the double layers. Finally, there are numerous short contacts between the cations and the bimetallic oxalate network.

*$[Fe^{III}(3\text{-Cl-sal}_2\text{trien})][Mn^{II}Cr^{III}(ox)_3]\cdot(CH_3OH)_2\cdot(CH_3CN)_2$ (**3**)*

The best solution to the structure of this compound was found in the chiral space group $P2_1$. The crystal was solved as a racemic twin with a BASF parameter of 0.66235. Therefore, the structure resolution has been performed in a twinned crystal containing crystals of opposite chirality. This compound presents a very different structure to that of compound **2**, in spite of the very similar templating cation. It seems that the small decrease in the size of the cation caused by the substitution of Br by Cl is enough to change the templating effect of the cation and to give rise to a very different structure.

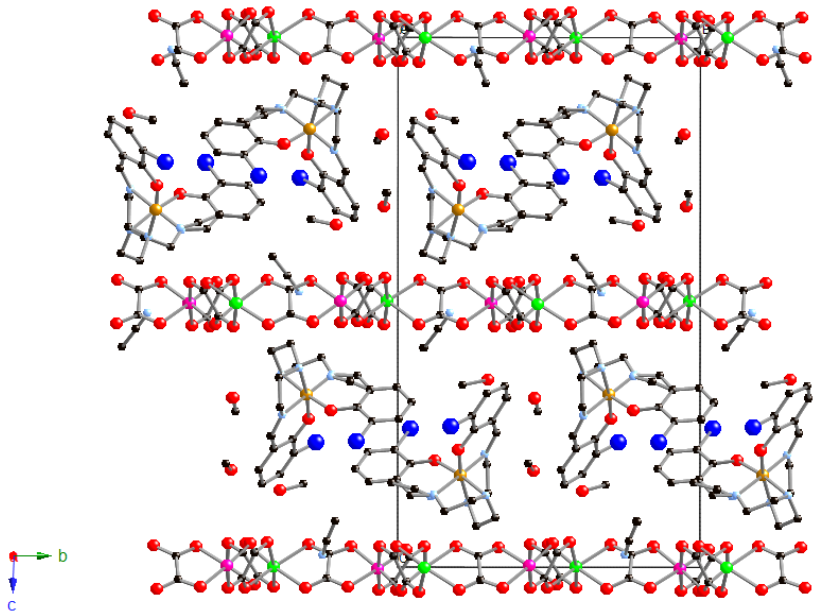

Figure 5. Projection of the structure of **3** in the *bc* plane. Fe (yellow), Cl (blue), C (black), N (blue), O (red), Mn (pink), Cr (green). Hydrogen atoms have been omitted for clarity.

In contrast to the two previous structures, the Mn^{II} and Cr^{III} of the bimetallic oxalate network are clearly distinguishable as they present different bond distances with oxalate ligands. Thus, there are two crystallographically independent Mn ions (Mn1 and Mn2) with Mn-O distances between 2.133(6) Å and 2.209(6) Å and two crystallographically independent Cr ions (Cr1 and Cr2) with Cr-O distances between 1.955(6) and 2.022(6) Å. These are typical Mn^{II}-O and Cr^{III}-O distances similar to those found in other oxalate networks. These anionic layers lies in the *ab* plane and are stacked one over the other in an *ABAB*···fashion (Figure 5). Metal centers Cr1 and Mn1 are located in the A layer whereas Mn2 and Cr2 are located in the B layer. The neighboring metal centers of these layers present alternated chirality as usual for this type of networks but in this structure all the Cr^{III} ions adopt Λ configuration, whereas all the Mn^{II} adopt the Δ configuration. Therefore, the configuration of each metal ion is preserved in the neighboring oxalate layers. Since we have started from a racemic mixture of $[Cr(ox)_3]^{3-}$ anion, crystals of the two enantiomers have been obtained.

The minimum distance between metal of different layers is 13.630 Å, which is longer than other 2D oxalate-based compounds with a single layer but not as long as that of other 2D oxalate-based compounds with a double layer of Fe^{III} complexes such as **1**. This intermediate interlayer distance is due to the presence of a double layer of $[Fe^{III}(3\text{-Cl-sal}_2\text{trien})]^+$ with a high degree of interpenetration between the two sublayers (see figure 5).

The space between oxalate layers is occupied by two crystallographically independent $[Fe^{III}(3\text{-Cl-sal}_2\text{-trien})]^+$ complexes (Fe1 and Fe2) and four crystallographically independent methanol and acetonitrile solvent molecules. The average Fe-N and Fe-O bond distances are 1.980(7) Å and 1.900(6) Å in Fe1 and 1.960(7) Å and 1.865(6) Å in Fe2. These values are typical of LS Fe^{III} complexes but the observation of higher Fe-N distances in Fe1 could indicate the presence of a fraction of Fe^{III} in the HS state, in agreement with magnetic properties (see below). Fe1 adopts a Δ configuration while Fe2 adopts a Λ configuration in the crystal used to solve the structure. In contrast to the structures of **1** and **2**, the cations do not lie with their longer axis parallel to the oxalate layers (Figure 5 and Figure S2 of the Supporting Information), but present an important tilting with respect to the oxalate layer. This is confirmed by the dihedral angle between the least-squares planes of the phenoxy rings and that formed by the metals of the oxalate network, which are far to be perpendicular in contrast to those of **1** and **2** (54.1 and 39.4° for Fe1 and 44.5 and 54.1° for Fe2). Note that one of the two phenoxy rings of Fe1 and Fe2 presents the same angle. This indicates that they are involved in π-π staking interactions as they present very short distances (six C-C distances between 3.421 and 3.553 Å). These dimers formed by the two crystallographically independent $[Fe^{III}(3\text{-Cl-sal}_2\text{-trien})]^+$ complexes are connected to other dimers by short Cl···Cl contacts (Cl-Cl distances of 3.304 and 3.307 Å) giving rise to double chains running along the *a* axis (see Figure S2 of the Supporting information). Finally, these two cations present numerous short contacts with methanol and acetonitrile solvent molecules (hydrogen bonds between NH groups and CH_3OH and CH_3CN molecules) and the oxalate network.

*Fe^{III}(3-CH_3O-sal$_2$-trien)][$Mn^{II}Cr^{III}(ox)_3$]·(CH_3OH)·(H_2O)$_{1.5}$·(CH_2Cl_2)$_{0.5}$ (**4**)*

This compound crystallizes in the monoclinic space group *$P2_1/n$*. The anionic layer lies in the *10-1* plane and contains two crystallographically independent metals with M-O bond lengths lying between 2.050(4) and 2.088(4) Å. Therefore, it is not possible to distinguish between Mn^{II} and Cr^{III} in the structure as in **1** and **2**. These anionic layers are stacked one over the other in an *AA*···fashion (see Figure 6). The minimum distance between metals ions of different layers is 14.865 Å, which is intermediate between those of **1** and **3** (the other two compounds with a double layer of Fe^{III} cations presented in this work) due a different degree of interpenetration of the two sublayers.

The space between oxalate layers is occupied by one crystallographically independent [Fe^{III}(3-MeO-sal$_2$-trien)]$^+$ complex and three water molecules, two methanol molecules and one dichloromethane crystallographically independent solvent molecules with an occupancy of 0.5. The average Fe-N and Fe-O bond distances are 2.131(4) and 1.913(4) Å respectively. These values are close to those found for other similar Fe^{III} HS complexes. However, they are shorter than those found for **2**. This indicates that a fraction of Fe^{III} complexes may be in the LS state in agreement with magnetic properties. As in the structure of **3**, the Fe^{III} complexes do not lie with their longer axis parallel to the oxalate layers (Figure 6). Indeed, the longer axis of these complexes is almost perpendicular to the oxalate layer. The dihedral angle between the least-squares planes of the phenoxy rings and that formed by the metals of the oxalate network are very different (52.0 and 84.9°), indicating a tilted disposition of the complexes. Two neighboring [Fe^{III}(3-MeO-sal$_2$-trien)]$^+$ complexes present short contacts through two CH···π edge-to-face interactions and two short contacts between O from the methoxy group and the same CH_2 involved in CH···π edge-to-face interactions. Furthermore, they are interconnected through numerous short contacts with the oxalate network and the disordered solvent molecules. They define some channels filled with disordered water and methanol solvent molecules that run along the [101] axis (see Figure 6).

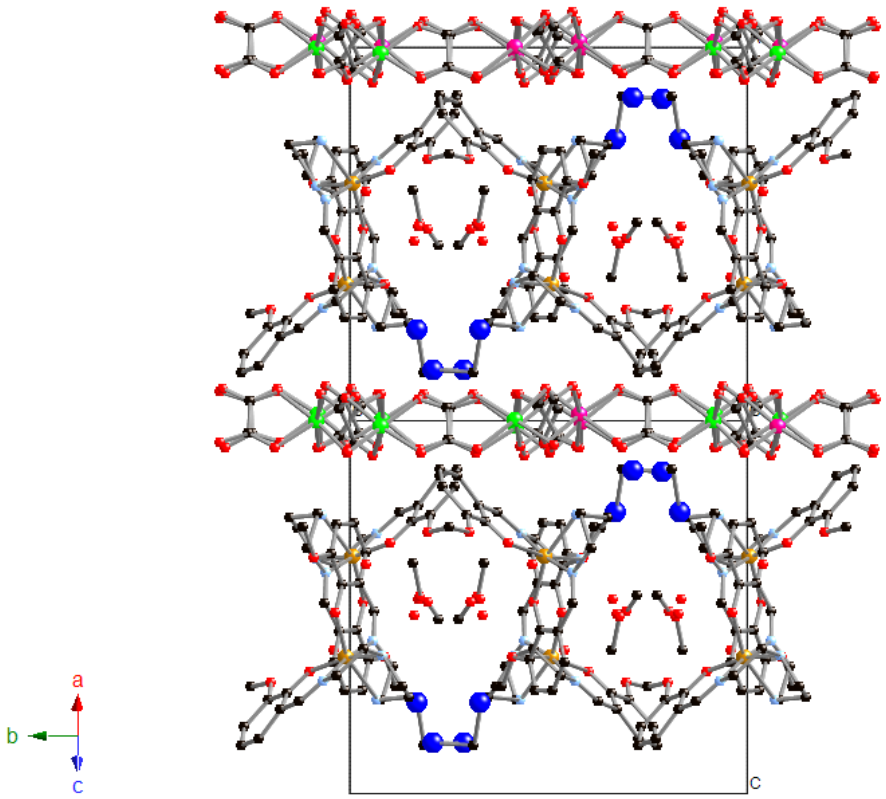

Figure 6. Lateral view of the bimetallic oxalate and cationic layers of **4**. Fe (yellow), C (black), N (blue), O (red), Mn (pink), Cr (green). Hydrogen atoms have been omitted for clarity.

Magnetic properties:

The thermal dependence of the product of the molar magnetic susceptibility times the temperature (χT) of **1** is shown in Figure 7. χT shows a value of 8.3 emu·K·mol^{-1} at 400 K. This value is approximately equal to the sum of the expected contributions for the isolated paramagnetic ions (1 Fe^{III}, 0.67 Mn^{II} and 0.67 Cr^{III}) with the 90 % of the Fe^{III} spin-crossover complex in a HS state. χT decreases abruptly from 400 to 270 K to reach a value of 5.4 emu·K·mol^{-1}. This value is close to the expected value for 100 % of Fe^{III} in the LS state (4.8 emu·K·mol^{-1}). From 270 to 140 K, χT shows a constant value consistent with almost all the Fe^{III} in the LS state. At lower temperatures, there is an increase of χT that is very sharp below 50 K. This indicates the presence of ferromagnetic interactions

between neighbouring Mn^{II}-Cr^{III} magnetic ions and suggests the onset of long-range ferromagnetic ordering, as observed for other 2D bimetallic oxalate networks. To confirm the presence of long-range magnetic ordering and to determine precisely the critical temperatures, alternating current (AC) susceptibility measurements were carried out. A maximum in the in-phase signal (χ') near T_c and an out-of-phase (χ'') that starts to appear at temperatures just below T_c is observed. From this data, the T_c of **1** is 5.2 K, similar to those reported for other Mn^{II}-Cr^{III} 2D oxalate compounds. As expected for a ferromagnet, these signals are frequency independent (Figure 8). The isothermal magnetization (M) at 2 K shows a very sharp increase at low fields which is much faster than that expected for non-interacting Mn^{II}-Cr^{III} centers; this increase is more gradual at higher fields and no saturation is reached even up to 5 T (Figure 9). The M value of 6.3 μ_B (μ_B = Bohr magneton) at 5 T, confirms a parallel alignment of the spins in this bimetallic lattice (spin only value of 6.4 μ_B). The hysteresis loop at 2 K shows that this compound is a soft ferromagnet with a coercive field of 7 mT.

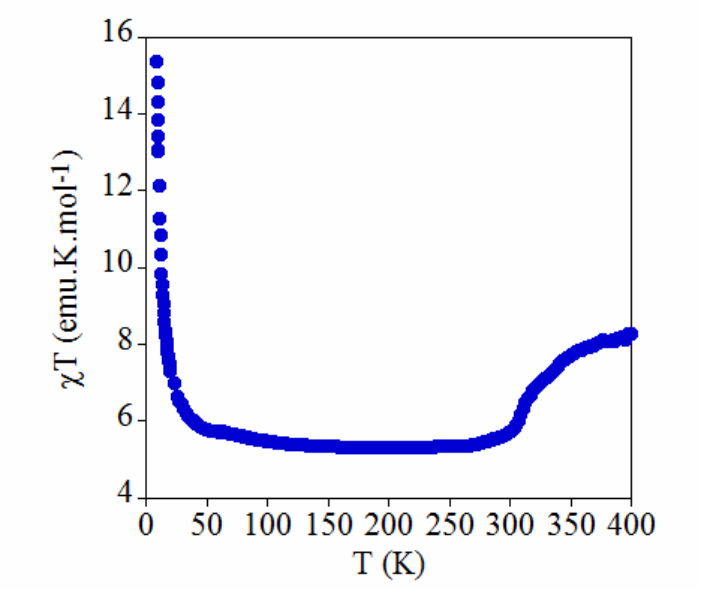

Figure 7. Temperature dependence of the product of the molar magnetic susceptibility with temperature (χT) at 0.1 T for compound **1** (empty circles).

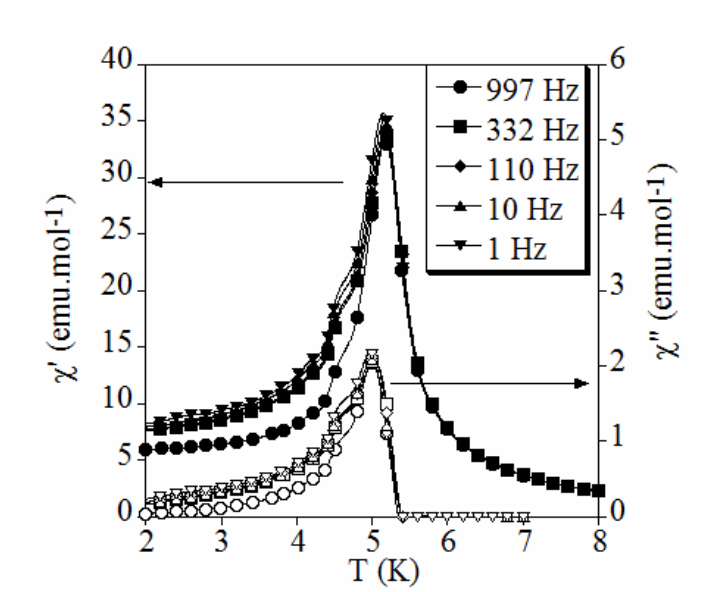

Figure 8. Temperature dependence of the in-phase AC susceptibility (χ') (filled symbols) and the out-of-phase AC susceptibility (χ") (empty symbols) for **1**.

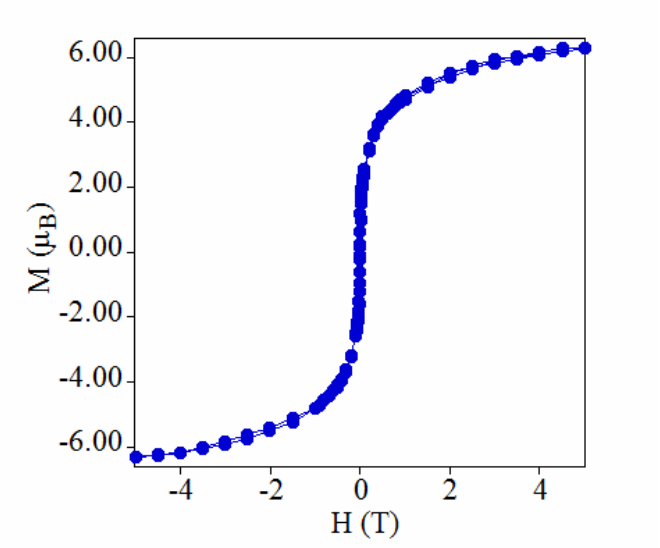

Figure 9. Field dependence of the magnetization (M) for **1** (empty circles).

The thermal dependence of χT of **2**, **3** and **4** is shown in figure 10. χT values of 11.3, 9.5 and 10.2 emu·K·mol^{-1} at 300 K are found for **2**, **3** and **4,** respectively. These values are consistent with Fe^{III} HS fractions of 100 % for **2**, 70 % for **3** and 90 % for **4**. At lower temperatures, χT of **2** increases whereas those of **3** and **4** decrease to reach minimum values of 9.0 and 9.8 emu·K·mol^{-1} respectively around 150 K. This indicates that **2** is in the HS state in the whole temperature range in agreement with structural data at 120 K and isothermal magnetisation at 2 K (see below) while **3** and **4** present a partial spin crossover which is quite gradual. At lower temperatures, χT increases gradually for the three compounds with a very abrupt increase below 50 K coming from the ferromagnetic MnCr oxalate layers. AC susceptibility measurements indicate that the T_c of **2**, **3** and **4** is respectively 5.4, 5.0 and 5.4 K, which are similar to that of **1** or those of other 2D $Mn^{II}Cr^{III}$ oxalate compounds, which are frequency independent (Figure S3 of the Supporting information).[17]

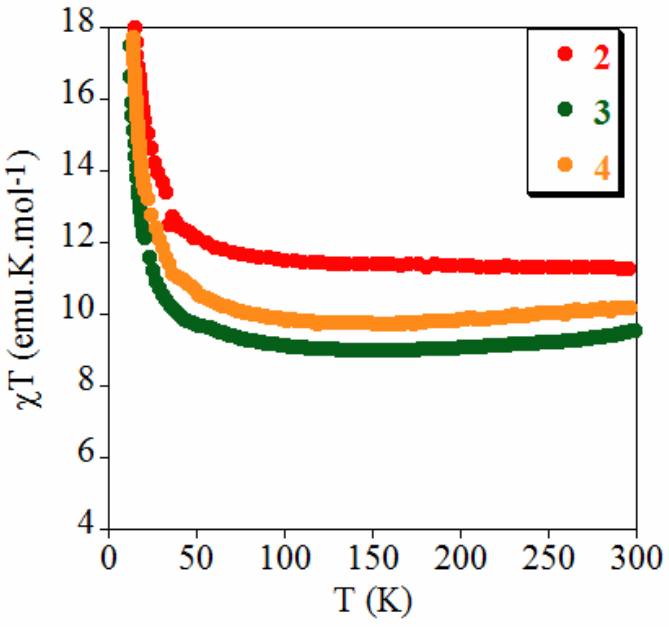

Figure 10. Temperature dependence of the product of the molar magnetic susceptibility with temperature (χT) at 0.1 T for compound **2** (empty circles), **3** (empty squares) and **4** (full circles).

The isothermal magnetization at 2 K of **2**, **3** and **4** is similar to that of **1** confirming the ferromagnetic nature of the MnCr layers (Figure S4 of the Supporting information). Furthermore, *M* values at 5 T are intermediate between the expected values for 100 % of Fe^{III} in the LS state (9 μ_B) and the expected ones for 100 % of Fe^{III} in the HS state (13 μ_B). This indicates that a significant fraction of Fe^{III} is in the HS state in the three compounds, which is higher in compound **2** in agreement with structural data. However, a quantitative estimation of the HS/LS fraction is difficult to extract from these data and Mössbauer measurements are needed to clarify this point.

Photomagnetic characterisation:

Photomagnetic characterisation of the two compounds of this family with the highest fraction of LS Fe^{III} at low temperatures (**1** and **3)** was performed. The two compounds were irradiated with red, green and IR light but the magnetization remained almost unchanged. Therefore, it seems that **1** and **3** do not present LIESST effect. The photomagnetic characterization of **2** and **4** is in progress taking into account that in the case of **4** only reverse LIESST could be expected as the cation is in the HS state in the whole temperature range.

The question remains why LIESST has been observed in other 2D oxalate-based compounds such as $[Fe^{III}(sal_2\text{-trien})][Mn^{II}Cr^{III}(ox)_3]\cdot(CH_2Cl_2)$[18] but not in **1** and **3**. Further work is necessary to answer to this question. At the moment, it remains unclear whether the absence of LIESST is linked to: (a) a too high thermal spin crossover temperature ($T_{1/2}$) and/or (b) structural differences between 2D networks and/or (c) the small amount of Fe^{III} that can undergo spin crossover. In the case of **1**, it could be related to the high $T_{1/2}$ as it has been shown that there is a linear correlation between the $T_{1/2}$ and *T*(LIESST) for iron (II) complexes.[20] Since the two temperatures are inversely proportional, a too high $T_{1/2}$ (a) may lead to a *T*(LIESST) too low to be detected. Conversely, the structural differences between the 2D structures of **1** and **3** and that of $[Fe^{III}(sal_2\text{-trien})][Mn^{II}Cr^{III}(ox)_3]\cdot(CH_2Cl_2)$ could explain the lack of LIESST behavior of these

compounds (b). Thus, the presence of a double layer of Fe^{III} complexes in **1** and **3** instead of the single one of $[Fe^{III}(sal_2\text{-trien})][Mn^{II}Cr^{III}(ox)_3]\cdot(CH_2Cl_2)$ gives rise to a decrease of the interactions with the oxalate network that could be necessary to observe LIESST effect.[18] Finally, the low amount of LS fraction at low temperature (c) of **3** make it difficult to observe the possible small increase of magnetization after light irradiation, as it would be difficult to distinguish this increase from the important magnetic signal of the oxalate network.

Conclusions

In this work we have reported the preparation of four novel compounds (**1**, **2**, **3** and **4**) formed by the insertion of the spin crossover cations $[Fe^{III}(4\text{-Br-sal}_2\text{-trien})]^+$, $[Fe^{III}(3\text{-Br-sal}_2\text{-trien})]^+$, $[Fe^{III}(3\text{-Cl-sal}_2\text{-trien})]^+$, and $[Fe^{III}(3\text{-CH}_3\text{O-sal}_2\text{-trien})]^+$ into anionic coordination polymers based on bimetallic oxalate complexes. We confirm with this result that the use of different sal_2-trien derivatives is a suitable strategy to obtain a great variety of oxalate networks. Thus, we have seen previously that depending on the substituent, different type of networks can be obtained. Thus, $[Fe(sal_2\text{-trien})]^+$, $[Fe^{III}(5\text{-NO}_2\text{-sal}_2\text{-trien})]^+$ and $[Fe^{III}(5\text{-CH}_3\text{O-sal}_2\text{-trien})]^+$ complexes, lead to the formation of 2D or achiral 3D networks. Conversely, $[Fe^{III}(5\text{-Xsal}_2\text{-trien})]^+$ (X = Cl, Br), gives rise to the growth of a 3D chiral network. The different templating effect of these cations could be related to the intermolecular interactions. For instance, in 5-substituted $[Fe^{III}(5\text{-Xsal}_2\text{-trien})]^+$ complexes, NO_2 groups favours π-π stacking interactions and the growth of a 2D network; with CH_3O groups, these interactions are more difficult due to steric hindrance and an achiral 3D network is formed. Finally, smaller substituents (Cl or Br) favour a helical arrangement of the complexes and the growth of a 3D chiral network. In contrast to this, the use of 3- or 4- substituted complexes gives rise in all cases to 2D networks. Furthermore, these 2D networks are very different to those obtained previously with $[Fe^{III}(sal_2\text{-trien})]^+$ and $[Fe^{III}(5\text{-NO}_2\text{-sal}_2\text{-trien})]^+$. The main difference is the different orientation of the Fe^{III} cations. In the previous compounds, these cations lie with their longer axis parallel to the oxalate network, while in the present case they show a certain

tilting angle. Such a disposition leads to double layers of cations in compounds **1**, **3** and **4** and to the presence of pores in the structures of **1** and **4** filled with disordered solvent molecules.

Apart from the structural interest of these compounds, the magnetic properties indicate that the inserted Fe^{III} cations undergo an almost complete spin crossover above 300 K in **1** and a partial spin crossover in **3** and **4** that coexists with a ferromagnetic ordering of the oxalate network. In the case of **2**, the inserted cation remains in the HS from 2 to 300 K. Therefore, **1**, **3** and **4** are multifunctional compounds with coexistence of spin crossover and magnetic ordering. Conversely, photomagnetic characterization shows that in contrast to the 2D compound $[Fe^{III}(sal_2\text{-trien})][Mn^{II}Cr^{III}(ox)_3]\cdot(CH_2Cl_2)$, **1** and **3** do not present LIESST effect. In attendance of the photomagnetic characterization of compounds **2** and **4**, this result may help to understand the factors affecting this very rare and unexpected property in a Fe^{III} spin-crossover complex. Thus, they could indicate that the intermolecular interactions between the cationic network and the oxalate network are of key importance. In fact, owing to the nature of the cationic network (double layer vs. single layer), these interactions are expected to be less pronounced in the present case (**1** and **3**) than in $[Fe^{III}(sal_2\text{-trien})][Mn^{II}Cr^{III}(ox)_3]\cdot(CH_2Cl_2)$. More examples of this type of compounds are needed to understand this point. Finally, the presence of pores with disordered solvent molecules in the structures of **1** and **4** could lead to new functionalities in addition to the magnetic ordering and the spin crossover such as solvent adsorption or proton conduction recently found in other 2D oxalate-based compounds.[9,13]

Experimental Section

Synthesis: Crystals of $[Fe^{III}(4\text{-Br-sal}_2\text{-trien})][Mn^{II}Cr^{III}(ox)_3]_{0.67}Cl_{0.33}\cdot CH_3OH$ (**1**), $[Fe^{III}(3\text{-Br-sal})_2\text{-trien}][Mn^{II}Cr^{III}(ox)_3]\cdot(CH_3CN)_2$ (**2**), $[Fe^{III}(3\text{-Cl-sal})_2\text{-trien}][Mn^{II}Cr^{III}(ox)_3]\cdot(CH_3OH)_2\cdot(CH_3CN)_2$ (**3**) and $[Fe^{III}(3\text{-}CH_3O\text{-sal}_2\text{-trien})][Mn^{II}Cr^{III}(ox)_3]\cdot(CH_3OH)\cdot(H_2O)_{1.5}\cdot(CH_2Cl_2)_{0.5}$ (**4**) were obtained by slow diffusion of two solutions. The first solution was prepared by

adding $MnCl_2 \cdot 4H_2O$ (14 mg, 0.067 mmol) to a suspension of $Ag_3Cr(ox)_3$ (38 mg, 0.06 mmol) in methanol (3 mL). The AgCl precipitate was filtered off. The second solution was obtained by dissolving compound **1** (43 mg, 0.06 mmol) in acetonitrile (3 mL), compound **2** (43 mg, 0.06 mmol) in acetonitrile (3 mL), compound **3** (38 mg, 0.06 mmol) in acetonitrile (3 mL) and compound **4** (37 mg, 0.06 mmol) in dichloromethane (3 mL). After 2 weeks brown-black crystals, in all cases, were obtained.

Structural Characterization: Single-crystal X-ray data of **1**-**4** were collected at 120 K on a Xcalibur, Sapphire3, Gemini diffractometer equipped with a graphite-monochromated Enhance (Mo) X-ray Source (λ = 0.71073 Å). The program CrysAlisPro, Oxford Diffracction Ltd., Version 1.171.33.52., was used for cell refinements and data reduction of the compounds. Empirical absorption correction was performed using spherical harmonics, implemented in SCALE3 ABSPACK scaling algorithm. Crystal structures were solved by direct methods with the SIR97 program[21] and refined against all F^2 values with the SHELXL-97 program[22] using the WinGX graphical user interface.[23] Non-hygrogen atoms were refined anisotropically, (except as noted) and hydrogen atoms were placed in calculated positions refined using idealized geometries (rinding model) and assigned fixed isotropic displacements parameters. The subroutine SQUEEZE[24] was used to remove the diffracting component of disordered solvents in **1** resulting in a void of ca. 1436.4 $Å^3$ and 387 electrons/cell omitted. This corresponds to ca. 12 CH_3CN + 12 H_2O molecules per cell. All non-hydrogen atoms were refined anisotropically. In **4**, the two aromatic rings from $[Fe^{III}(3\text{-MeO-sal})_2\text{-trien}]^+$ complexes were modeled in two orientations. In compound **3**, the small size of the crystal gave rise to a very weak scattering. Because of this the number of reflections was not enough to carry out anisotropic refinement of all the atoms, thus carbon atoms could only be modeled isotropically. Data collection and refinements statistics are collected in Table 1.

CCDC-900041 (for **1**), -900042 (for **2**), -900043 (for **3**), and -900044 (for **4**) contain the supplementary crystallographic data for this paper. These data can be obtained free of

charge from The Cambridge Crystallographic Data Centre via www.ccdc.cam.ac.uk/data_request/cif.

Table 1. Crystallographic data for compounds **1**, **2**, **3** and **4**.

Compound	**1**	**2**	**3**	**4**
Empirical formula	$Cl_{0.33}C_{29}Cr_{0.67}Br_2Fe Mn_{0.67}H_{36}O_{13}N_6$	$C_{30}CrBr_2FeMnH_{28} O_{14}N_6$	$Cl_2C_{32}CrFeMnH_{36} O_{16}N_6$	$ClC_{29.50}CrFeMnH_{36} O_{18.50}N_4$
Formula weight	975.41	1019.19	994.36	940.81
Crystal color	Black	Black	Black	Black
Temperature (K)	120(2)	120(2)	120(2)	120(2)
Wavelenght (Å)	0.71073	0.71073	0.71073	0.71073
Crystal system, Z	Trigonal, 6	Triclinic, 2	Monoclinic, 2	Monoclinic, 4
Space group	*P*-3	*P*-1	$P2_1$	$P2_1/n$
a (Å)	18.7107(5)	9.4310(6)	9.6700(4)	16.8977(13)
b (Å)	18.7107(5)	12.8070(8)	15.5850(7)	16.0300(8)
c (Å)	18.5675(7)	16.0680(10)	27.6340(14)	18.7421(12)
α(°)	90	101.392(5)	90	90
β (°)	90	96.264(5)	99.162(5)	116.454(9)
γ (°)	120	97.548(5)	90	90
V (Å^3)	5629.4(3)	1867.7(2)	4111.5(3)	4545.1(65)
ρcalc (Mg/m^3)	1.725	1.812	1.606	1.365
$\mu(Mo_{K\alpha})$(mm^{-1})	3.021	3.215	1.116	0.951
θ range (°)	2.43-29.83	2.30-32.26	2.36-32.27	2.42-32.30
Reflns collected	67242	42941	68834	68357
Independent reflns, *n*, (R_{int})	10053 (0.0929)	11416 (0.0666)	5321 (0.1371)	8477 (0.0957)
L. S. parameters/ restraints	394/1	498/0	716/1	541/2
$R1(F)$,[a] $I>2\sigma(I)$]	0.0398	0.0413	0.0472	0.0771
$wR2(F^2)$,[b] all data	0.0934	0.0851	0.0671	0.2486

[a] $R1(F) = S(|F_o| - |F_c|)/S|F_o|$ [b] $wR2(F^2) = [Sw(F_o^2 - F_c^2)^2/SwF_o^4]^{½}$

Physicals Measurements: Magnetic susceptibility measurements were performed on polycrystalline samples using a magnetometer (Quantum Design MPMS-XL-5) equipped with a SQUID sensor. Variable-temperature measurements were carried out in the temperature range 2-300 K. The AC measurements were performed in the temperature range 2-10 K at different frequencies with an oscillating magnetic field of 0.395 mT. The magnetization and hysteresis studies were performed between 5 and -5 T, cooling the samples at zero field. The photomagnetic measurements were performed using a Spectrum Physics Series 2025 Kr^+ laser coupled via an optical fibre to the cavity of a MPMS-55 Quantum Design SQUID magnetometer. The Fe:Mn:Cr:X (X = Cl, Br) ratios were measured on a Philips ESEM X230 scanning electron microscope equipped with an EDAX DX-4 microsonde.

Supporting Information (see footnote on the first page of this article): Structural views of the cationic layers of **2** and **3** and magnetic properties of **2**, **3** and **4**.

Acknowledgments

We thank the European Union (EU) (ERC Advanced grant SPINMOL, Project HINTS), the Spanish Ministerio de Economia y Competitividad (MINECO) (Project Consolider-Ingenio in Molecular Nanoscience, grant numbers CSD2007-00010, MAT2011-22785 and CTQ-2011-26507), and the Generalitat Valenciana (Prometeo Program) for finantial support. The authors also thank J. M. Martínez-Agudo and Dr. G. Agustí-López, University of Valencia, for assistance with the magnetic characterization and Prof. J. F. Létard, Dr. C. Desplanches and H. F. Wang, ICMCB, CNRS, Université Bordeaux 1, for the magnetic characterization under light irradiation.

[1] (a) E. Coronado, P. Day, *Chem. Rev.,* 2004, **104**, 5419; (b) E. Coronado, C. Martí-Gastaldo, E. Navarro-Moratalla, A. Ribera, S. J. Blundell, P. J. Baker, *Nat. Chem.*, 2010, **2**, 1031.

[2] (a) E. Coronado, M. C. Giménez-López, G. Levchenko, F. M. Romero, V. García-Baonza, A. Milner, M. Paz-Pasternak, *J. Am. Chem. Soc.*, 2005, **127**, 4580; (b) E. Coronado, M. C. Giménez-López, T. Korzeniak, G. Levchenko, F. M. Romero, A. Segura, V. García-Baonza, J. C. Cezar, F. M. F. De Groot, A. Milner, M. Paz-Pasternak, *J. Am. Chem. Soc.*, 2008, **130**, 15519; (c) S. I. Ohkoshi, K. Imoto, Y. Tsunobuchi, S. Takano, H. Tokoro, *Nat. Chem.*, 2011, **3**, 564.

[3] M. Clemente-León, E. Coronado, C. Martí-Gastaldo, F. M. Romero, *Chem. Soc. Rev.,* 2011, **40**, 473.

[4] (a) H. Tamaki, Z. J. Zhong, N. Matsumoto, S. Kida, M. Koikawa, N. Achiwa, Y. Hashimoto, H. Okawa, *J. Am. Chem. Soc.,* 1992, **114**, 6974; (b) H. Tamaki, M. Mitsumi, N. Nakamura, N. Matsumoto, S. Kida, H. Okawa, S. Ijima, *Chem. Lett.,* 1992, 1975; (c) C. Mathonière, J. Nutall, S. G. Carling, P. Day, *Inorg. Chem.,* 1996, **35**, 1201; (d) R. Pellaux, H. W. Schmalle, R. Huber, P. Fisher, T. Hauss, B. Ouladdiaf, S. Decurtins, *Inorg. Chem.,* 1997, **36**, 2301; (e) E. Coronado, J. R. Galán-Mascarós, C. J. Gómez-García, J. M. Martínez-Agudo, E. Martínez-Ferrero, J. C. Waerenborgh, M. Almeida, *J. Solid State Chem.,* 2001, **159**, 391; (f) K. S. Min, A. L. Rhinegold, J. S. Miller, *Inorg. Chem.,* 2005, **44**, 8433; (g) E. Coronado, J. R. Galán-Mascarós, C. Martí-Gastaldo*, J. Mater. Chem.,* 2006, **16**, 2685.

[5] (a) S. Decurtins, H. W. Schmalle, P. Schneuwly, H. R. Oswald, *Inorg. Chem.,* 1993, **32**, 1888; (b) S. Decurtins, H. W. Schmalle, P. Schneuwly, J. Ensling, P. Gütlich, *J. Am. Chem. Soc.,* 1994, **116**, 9521; (c) M. Hernández-Molina, F. Lloret, C. Ruiz-Pérez, M. Julve, *Inorg. Chem.,* 1998, **37**, 4131; (d) E. Coronado, J. R. Galán-Mascarós, C. J. Gómez-García and J. M. Martínez-Agudo, *Inorg. Chem.,* 2001, **40**, 113; (e) F. Pointillart, C. Train, M. Gruselle, F. Villain, H. W. Schmalle, D. Talbot, P. Gredin, S. Decurtins, M. Verdaguer, *Chem. Mater.,* 2004**, 16**, 832; (f) M. Clemente-León, E. Coronado, C. J. Gómez-García, A. Soriano-Portillo, *Inorg. Chem.,* 2006, **45**, 5653.

[6] (a) M. Clemente-León, E.Coronado, J. R. Galán-Mascarós, C. J. Gómez-García, *Chem. Commun.,* 1997, 1727; (b) E. Coronado, J. R. Galán-Mascarós, C. J. Gómez-García, J. M. Martínez-Agudo, *Adv. Mater.,* 1999, **11**, 558; (c) E. Coronado, J. R. Galán-Mascarós, C. J. Gómez-García, J. Ensling, P. Gutlich, *Chem. Eur. J.,* 2000, **6**, 552.

[7] (a) S. Bénard, P. Yu, J. P. Audière, E. Rivière, R. Clèment, J. Ghilhem, L. Tchertanov, K. Nakatami, *J. Am. Chem. Soc.,* 2000, **122**, 9444; (b) S. M. Aldoshin, N. A. Sanina, V. I. Minkin, N. A. Voloshin, V. N. Ikorskii, V. I. Ovcharenko, V. A. Smirnov, N. K. Nagaeva, *J. Mol. Struct.,* 2007, **826**, 69.

[8] (a) E. Coronado, J. R. Galán-Mascarós, C. J. Gómez-García, V. Laukhin, *Nature,* 2000, **408**, 447; (b) A. Alberola, E. Coronado, J. R. Galán-Mascarós, C. Giménez-Saiz, C. J. Gómez-García, *J. Am. Chem. Soc.,* 2003, **125**, 10774; (c) E. Coronado, J. R. Galán-Mascarós, C. J. Gómez-García, E. Martínez-Ferrero, S. Van Smaalen, *Inorg. Chem.,* 2004, **43**, 4808.

[9] (a) H. Okawa, A. Shigematsu, M. Sadakiyo, T. Miyagawa, K. Yoneda, M. Ohba, H. Kitagawa, *J. Am. Chem. Soc.,* 2009, **131**, 13516; (b) M. Sadayiko, H. Okawa, A. Shigematsu, M. Ohba, T. Yamada, H. Kitagawa, *J. Am. Chem. Soc.,* 2012, **134**, 5472.

[10] T. Endo, T. Akutagawa, S. I. Noro, T. Nakamura, *Dalton Trans.,* 2011, **40**, 1491.

[11] (a) R. Andrés, M. Gruselle, B. Malézieux, M. Verdaguer, J. Vaissermann, *Inorg. Chem.,* 1999, **38**, 4637; (b) R. Andrés, M. Brissard, M. Gruselle, C. Train, J. Vaissermann, B. Malézieux, J. P. Jamet, M. Verdaguer, *Inorg. Chem.,* 2001, **40**, 4633; (c) M. Clemente-León, E. Coronado, J. C. Dias, A. Soriano-Portillo, R. D. Willett, *Inorg. Chem.,* 2008, **47**, 6458.

[12] J. R. Galán-Mascarós, E. Coronado, P. A. Goddard, J. Singleton, A. I. Coldea, J. D. Wallis, S. J. Coles and A. Alberola, A. *J. Am. Chem. Soc.,* 2010, **132**, 9271.

[13] E. Pardo, C. Train, G. Contard, K. Boubekeur, O. Fabelo H. Liu, B. Dkhil, F. Lloret, K. Nakagawa, H. Tokoro, S. -I. Ohkoshi, M. Verdaguer, *J. Am. Chem. Soc.,* 2011, **133**, 15328.

[14] C. Train, R. Gheorghe, V. Krstic, L. M. Chamoreau, N. S. Ovanesyan, G. L. J. A. Rikken, M. Gruselle, M. Verdaguer, *Nature Mater.,* 2008, **17**, 729.

[15] C. Train, T. Nuida, R. Gheorghe, M. Gruselle, S. Ohkoshi, *J. Am. Chem. Soc.,* 2009, **131**, 16838.

[16] (a) R. Sieber, S. Decurtins, H. Stoeckli-Evans, C. Wilson, D. Yufit, J. A. K. Howard, S. C. Capelli, A. Hauser, *Chem. Eur. J.,* 2000, **6**, 361; (b) E. Coronado, J. R. Galán-Mascarós, M. C. Giménez-López, M. Almeida, J. C. Waerenborgh, *Polyhedron,* 2007, **26**, 1838.

[17] (a) M. Clemente-León, E. Coronado, M. C. Giménez-López, A. Soriano-Portillo, J. C. Waerenborgh, F. S. Delgado, C. Ruiz-Pérez, *Inorg. Chem.,* 2008, **47**, 9111; (b) M. Clemente-León, E. Coronado, M. López-Jordà, G. Mínguez Espallargas, A. Soriano-Portillo, J. C. Waerenborgh, *Chem. Eur. J.,* 2010, **16**, 2207; (c) M. Clemente-León, E. Coronado, M. López-Jordà, *Dalton Trans.,* 2010, **39**, 4903; (d) M. Clemente-León, E. Coronado, M. López-Jordà, J. C. Waerenborgh, *Inorg. Chem.,* 2011, **50**, 9122.

[18] M. Clemente-León, E. Coronado, M. López-Jordà, C. Desplanches, S. Asthana, H. Wang, J.-F. Létard, *Chem. Sci.,* 2011, **2**, 1121.

[19] (a) S. Hayami, Z. –Z. Gu, M. Shiro, Y. Einaga, A. Fujishima, O. Sato, *J. Am. Chem. Soc.,* 2000, **122**, 7126; (b) G. Juhász, S. Hayami, O. Sato, Y. Maeda, *Chem. Phys. Lett.,* 2002, **364**, 164; (c) S. Hayami, K. Hiki, T. Kawahara, Y. Maeda, D. Urakami, K. Inoue, M. Ohama, S. Kawata, O. Sato, *Chem. Eur. J.,* 2009, **15**, 3497.

[20] (a) T. Buchen, P. Gütlich, K. H. Sugiyarto, H. A. Goodwin, *Chem. Eur. J.,* 1996, **2**, 1134; (b) J.-F. Létard, P. Guionneau, L. Rabardel, J. A. K. Howard, A. E. Goeta, D. Chasseau, O. Kahn, *Inorg. Chem*., 1998, **37**, 4432; (c) J.-F. Létard, L. Capes, G. Chastanet, N. Moliner, S. Létard, J. A. Real, O. Kahn, *Chem. Phys. Lett*., 1999, **313**, 115; (d) S. Marcen, L. Lecren, L. Capes, H. A. Goodwin, J-F. Létard, *Chem. Phys. Lett*., 2002, **358**, 87; (e) J.-F. Létard, P. Guionneau, O. Nguyen, J. S. Costa, S. Marcen, G. Chastanet, M. Marchivie, L. Capes, *Chem. Eur. J.,* 2005, **11**, 4582; (f) J.-F. Létard, *J. Mater. Chem.,* 2006, **16**, 2550.

[21] A. Altomare, M. C. Burla, M. Camalli, G. L. Cascarano, C. Giacovazzo, A. Guagliardi, A. G. G. Moliterni, G. Polidori, R. Spagna, *J. Appl. Cryst*., 1999, **32**, 115.

[22] SHELXL-97: G. M. Sheldrick, University of Göttingen, Germany, 1997.

[23] L. J. Farrugia, *J. Appl. Cryst.,* 1997, **32**, 837.

[24] A. L. Spek, *J. Appl. Cryst.,* 2003, **36**, 7.

2D and 3D bimetallic oxalate-based ferromagnets prepared by insertion of Mn^{III}-salen type complexes

Dalton Transactions

Capítulo 8

Capítulo 8: 2D and 3D bimetallic oxalate-based ferromagnets prepared by insertion of Mn^{III}-salen type complexes

The syntheses, structures and magnetic properties of the compounds of formulae $[Mn((R)\text{-salmen})(CH_3OH)(CH_3CN)][MnCr(ox)_3](CH_3OH)_{0.5}(CH_3CN)_{1.25}$ (**(*R*)-1**), $[Mn((S)\text{-salmen})(CH_3OH)(CH_3CN)][MnCr(ox)_3](CH_3OH)_{0.5}(CH_3CN)_{1.25}$ (**(*S*)-1**), $[Mn((R)\text{-salmen})(CH_3OH)_2][MnCr(ox)_3](CH_2Cl_2)_{0.375}(CH_3OH)_{0.125}(H_2O)_{0.375}$ (**(*R*)-2**) and $[Mn((S)\text{-salmen})(CH_3OH)_2][MnCr(ox)_3](CH_2Cl_2)_{0.375}(CH_3OH)_{0.375}(H_2O)_{0.125}$ (**(*S*)-2**) (ox = oxalate, salmen^{2-} = N,N′-(1-methylethylene)bis(salicylideneiminato)), $[Mn(salpn)(CH_3OH)_{1.5}(CH_3CN)_{0.5}][MnCr(ox)_3](CH_3OH)_{0.82}(H_2O)_{0.93}$ (**3**) (salpn^{2-} = N,N′-(propane)bis(salicylideneiminate)) and $[Mn(saltmen)(CH_3OH)(CH_3CN)][MnCr(ox)_3](CH_3OH)$ (**4**) (saltmen^{2-} = N,N′-(1,1,2,2-tetramethylethylene)-bis(salicylidene-iminate)) are reported. These compounds are prepared by the insertion of Mn^{III}-Schiff base complexes into bimetallic oxalate networks. Different types of bimetallic oxalate networks are obtained for each templating cation. Thus, $[Mn((R)\text{-salmen})]^+$ and $[Mn((S)\text{-salmen})]^+$ chiral templating cations give rise to a 2D chiral bimetallic oxalate layer in acetonitrile in **(*R*)-1** and **(*S*)-1** compounds, whereas a new type of achiral 3D oxalate network is obtained with the same templating cation in dichloromethane in **(*S*)-2** and **(*R*)-2**. On the other hand, $[Mn(salpn)]^+$ and $[Mn(saltmen)]^+$ give rise respectively to a 3D chiral network and a 2D achiral network in **3** and **4** compounds. The magnetic properties of the four compounds indicate that they undergo a long-range ferromagnetic ordering at ca. 5 K.

Introduction

Bimetallic oxalate-based networks have provided many examples of multifunctional compounds.[1] These compounds are composed by polymeric anionic networks of bimetallic oxalate complexes,[2,3] which furnish the magnetic properties (ferro- ferri- or canted antiferromagnetism), and a bulky charge-compensating molecular cation,

which templates the network formation and adds a second physical property of interest. The insertion of different cations into oxalate networks has led to compounds combining the long-range magnetic ordering from the oxalate network with a second property such as paramagnetism,[4] photochromism,[5] electric conductivity,[6] proton conduction,[7] ferroelectricity,[8] chirality,[9] spin-crossover[10] or chirality combined with conductivity[11] or proton conduction.[12]

In these hybrid compounds, the dimensionality of the coordination network of their structures is controlled by the relative configuration of the adjacent metal ions linked by an oxalate bridge. Thus, a 2D honeycomb structure is obtained when the relative configurations are opposite, e.g. (Δ, Λ). On the contrary, if they are identical, (Λ, Λ) or (Δ, Δ), a chiral 3D network is formed.[13] The counter-ions associated with the formation of chiral 3D networks have been essentially chiral metallic complexes such as $[Z^{II}(bpy)_3]^{2+}$ (Z = Ru, Fe, Co; bpy = bipyridine), while 2D networks can be formed with a larger variety of templating cations with different shapes and sizes. Recent results have shown that the situation is more complicate. Thus, apart from these two types of structures, 3D networks with metals in the two configurations have been obtained with Fe^{II} and Fe^{III} complexes and triethylammonium cations very recently.[10b,c,14,15] For instance, Fe^{III} complexes of the hexadentate Schiff base ligand, sal_2-trien (H_2sal_2-trien = N,N'-disalicylidenetriethylene-tetramine) and 5-X-sal_2-trien derivatives (X = Cl, Br, NO_2 CF_3O, and CH_3O) as templating cations leads to a great variety of oxalate-based structures. Thus, 2D structures (with X = H in dichloromethane[10b] and X = NO_2[10c]), achiral 3D structures (X = H in acetonitrile,[10b] and X = CH_3O[10c]) or chiral 3D structures (with X = Cl or Br)[10d] have been obtained. All these examples outline the vital role of the cation in tailoring the assembling of the molecular building-blocks.

In this work, we have explored for the first time the use of a different type of templating cations, Mn^{III} salen-type complexes ($salen^{2-}$ = N,N'-ethylenebis-(salicylideneiminate), see scheme 1) in bimetallic oxalate-based networks. In

addition to the structural interest, these Mn^{III} complexes could confer novel properties to the hybrid materials, since these complexes have proven to be good building blocks for different magnetic materials such as single-chain magnets (SCM)[16] or single-molecule magnets (SMM)[17] thanks to their appropriate uniaxial anisotropy with a well-defined easy axis of the magnetization. In fact, dimers of this type of cations may present a SMM behavior. Therefore, coexistence of SMM of the inserted cation with the magnetic ordering from the oxalate network could be expected, if the dimer structure of the precursor is preserved.

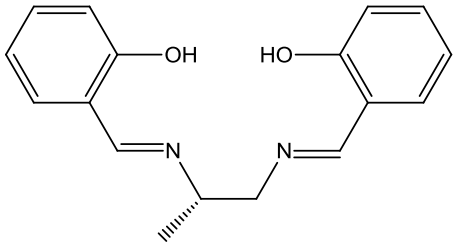

H_2((R)-salmen)

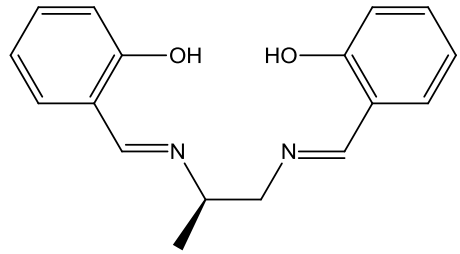

H_2((S)-salmen)

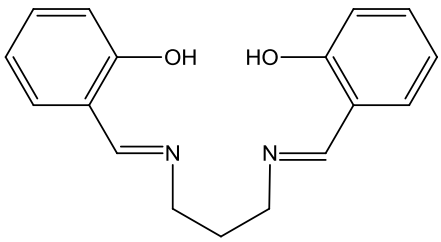

H_2-(salpn)

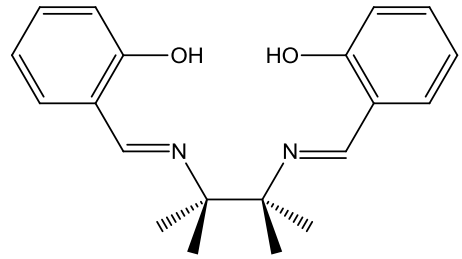

H_2(saltmen)

Scheme 1. H_2((*R*)-salmen), H_2((*S*)-salmen), H_2(salpn) and H_2(saltmen)

In the present case, we show that monomeric Mn^{III} species, instead of dimeric ones, are inserted into the bimetallic oxalate networks in all cases. Furthermore, the use of a chiral salen derivative ($salmen^{2-}$ = N,N'-(1-methylethylene)bis (salicylideneiminate)) having a chiral quaternary carbon leads to the introduction of

chirality in these hybrid magnets. A similar strategy has been sucessfully used to prepare enantiopure oxalate-based magnets, in which the combination of magnetic ordering and chirality leads to new properties such as the magneto-chiral dichroic effect and magnetisation-induced second harmonic generation.[18]

The compounds obtained with these Mn^{III} templating cations present different types of bimetallic oxalate networks: a 2D chiral structure in **(*S*)-1** and **(*R*)-1**, an achiral 3D oxalate network in **(*S*)-2** and **(*R*)-2**, a 3D chiral network in **3** and a 2D achiral network in **4**. The structures and magnetic properties of these compounds are presented in this paper.

Experimental Section

Synthesis

The complexes $[Mn(salpn)]ClO_4$,[19] $[Mn((R)\text{-salmen})]ClO_4$, $[Mn((S)\text{-salmen})]ClO_4$ and $[Mn(saltmen)]ClO_4$[20] have been prepared according to literature methods. $Ag_3[Cr(ox)_3]$ was prepared by metathesis from the corresponding potassium salt.[21] All other materials and solvents were commercially available and used without further purification.

$[Mn((R)\text{-salmen})(CH_3OH)(CH_3CN)][MnCr(ox)_3](CH_3OH)_{0.5}(CH_3CN)_{1.25}$ (**(*R*)-1**), $[Mn((S)\text{-salmen})(CH_3OH)(CH3CN)][MnCr(ox)_3](CH_3OH)_{0.5}(CH_3CN)_{1.25}$ (**(*S*)-1**), $[Mn((R)\text{-salmen})(CH_3OH)_2][MnCr(ox)_3](CH_2Cl_2)_{0.375}(CH_3OH)_{0.125}(H_2O)_{0.375}$ (**(*R*)-2**) and $[Mn((S)\text{-salmen})(CH_3OH)_2][MnCr(ox)_3](CH_2Cl_2)_{0.375}(CH_3OH)_{0.375}(H_2O)_{0.125}$ (**(*S*)-2**). Crystals of these compounds were obtained by slow difussion of two solutions. The first solution was prepared by adding $MnCl_2{\cdot}4H_2O$ (0.036 g, 0.182 mmol) to a suspension of $Ag_3Cr(ox)_3$ (0.077 g, 0.12 mmol) in 6 mL of methanol. The AgCl precipitate was filtered. The second solution was obtained by dissolving $[Mn((R)\text{-salmen})]ClO_4$ or $[Mn((S)\text{-salmen})]ClO_4$ (0.052 g, 0.12 mmol) in 6 mL of acetonitrile (**(*R*)-1** or **(*S*)-1**) or dichloromethane (**(*R*)-2** or **(*S*)-2**). After two weeks red crystals were obtained.

$[Mn(salpn)(CH_3OH)_{1.5}(CH_3CN)_{0.5}][MnCr(ox)_3]\cdot(CH_3OH)_{0.82}\cdot(H_2O)_{0.93}$ (3). Crystals of this compound were obtained by slow difussion of two solutions. The first solution was prepared by adding $MnCl_2\cdot 4H_2O$ (0.036 g, 0.182 mmol) to a suspension of $Ag_3Cr(ox)_3$ (0.077 g, 0.12 mmol) in 6 mL of methanol. The AgCl precipitate was filtered. The second solution was obtained by dissolving $[Mn(salpn)]ClO_4$ (0.052 g, 0.12 mmol) in 6 mL of acetonitrile. After two weeks red crystals were obtained.

$[Mn(saltmen)(CH_3OH)(CH_3CN)][MnCr(ox)_3]\cdot(CH_3OH)$ (4). Crystals of this compound were obtained by slow difussion of two solutions. The first solution was prepared by adding $MnCl_2\cdot 4H_2O$ (0.036 g, 0.182 mmol) to a suspension of $Ag_3Cr(ox)_3$ (0.077 g, 0.12 mmol) in 6 mL of methanol. The AgCl precipitate was filtered. The second solution was obtained by dissolving $[Mn(saltmen)]ClO_4$ (0.057 g, 0.12 mmol) in 6 mL of acetonitrile. After two weeks red crystals were obtained.

Structural characterisation

Single crystal X-ray data of **(*R*)-1**, **(*S*)-1**, **(*R*)-2**, **(*S*)-2**, **3** and **4** were collected at 120 K on a Xcalibur, Sapphire3, Gemini diffractometer equipped with a graphite-monochromated Enhance (Mo) X-ray Source (λ = 0.71073 Å). The program CrysAlisPro, Oxford Diffraction Ltd., Version 1.171.33.52 was used for cell refinements and data reduction of the compounds. Empirical absorption correction was performed using spherical harmonics, implemented in SCALE3 ABSPACK scaling algorithm. Crystal structures were solved by direct methods with the SIR97 program,[22] and refined against all F^2 values with the SHELXL-97 program,[23] using the WinGX graphical user interface.[24] **(*R*)-1**, **(*S*)-1**, **(*R*)-2**, **(*S*)-2** and **3** exhibit a Flack´s absolute parameter (*x*) close to 0.[25] This parameter lies within the range that indicates that the absolute structure is valid and that the five crystals are enantiopure. Non-hydrogen atoms were refined anisotropically, and hydrogen atoms were placed in calculated positions refined using idealized geometries (riding model) and assigned fixed isotropic displacement parameters. The use of restraints

and/or constraints in the refinement of the structures is documented in the corresponding CIFs. Data collection and refinement statistics are collected in Tables 1 and 2.

Physical measurements

Magnetic susceptibility measurements were performed on polycrystalline samples using a magnetometer (Quantum Design MPMS-XL-5) equipped with a SQUID sensor. Variable-temperature measurements were carried out in the temperature range 2 - 300 K. The AC measurements were performed in the temperature range 2 - 10 K at different frequencies with an oscillating magnetic field of 0.395 mT. The magnetisation and hysteresis studies were performed between 5 and -5 T, cooling the samples at zero field. The Mn:Cr ratios were measured on a Philips ESEM X230 scanning electron microscope equipped with an EDAX DX-4 microsonde.

Results

Synthesis

The following compounds [Mn((*R*)-salmen)(CH_3OH)(CH_3CN)][$MnCr(ox)_3$](CH_3OH)$_{0.5}$ (CH_3CN)$_{1.25}$ (**(*R*)-1**), [Mn((*S*)-salmen)(CH_3OH)(CH3CN)][$MnCr(ox)_3$](CH_3OH)$_{0.5}$ (CH_3CN)$_{1.25}$ (**(*S*)-1**), [Mn((*R*)-salmen)(CH_3OH)$_2$][$MnCr(ox)_3$](CH_2Cl_2)$_{0.375}$(CH_3OH)$_{0.125}$ (H_2O)$_{0.375}$ (**(*R*)-2**), [Mn((*S*)-salmen)(CH_3OH)$_2$][$MnCr(ox)_3$](CH_2Cl_2)$_{0.375}$(CH_3OH)$_{0.375}$ (H_2O)$_{0.125}$ (**(*S*)-2**) (salmen^{2-} = N,N′-(1-methylethylene) bis(salicylideneiminate)), [Mn(salpn)(CH_3OH)$_{1.5}$(CH_3CN)$_{0.5}$][$MnCr(ox)_3$]·(CH_3OH)$_{0.82}$·(H_2O)$_{0.93}$ (**3**) (salpn^{2-} = N,N′-(propane)bis(salicylideneiminate)) and [Mn(saltmen)(CH_3OH)(CH_3CN)][$MnCr(ox)_3$] (CH_3OH) (**4**) (saltmen^{2-} = N,N′-(1, 1,2,2-tetramethylethylene)bis(salicylideneiminate)) have been obtained.

Table 1. Crystallographic data for compounds (***R***)-**1**, (***S***)-**1**, (***R***)-**2** and (***S***)-**2**

Compound	(***R***)-**1**	(***S***)-**1**	(***R***)-**2**	(***S***)-**2**
Empirical formula	$C_{116}Cr_4Mn_8H_{109}O_{62}N_{17}$	$C_{116}Cr_4Mn_8H_{109}O_{62}N_{17}$	$Cl_3C_{103}Cr_4Mn_8H_{105}O_{66}N_8$	$Cl_3C_{103}Cr_4Mn_4H_{104}O_{66}N_8$
Formula weight	3380.72	3380.72	3226.52	3250.71
Crystal color	red	red	red	red
Temperature (K)	120(2)	120(2)	120(2)	120(2)
Wavelength (*Å*)	0.71073	0.71073	0.71073	0.71073
Crystal system, Z	Monoclinic, 1	Monoclinic, 1	Triclinic, 1	Triclinic, 1
Space group	$P2_1$	$P2_1$	$P1$	$P1$
a (Å)	9.2943(3)	9.2926(3)	15.2933(9)	15.2780(8)
b (Å)	32.5932(10)	32.5571(12)	15.5985(8)	15.5600(7)
c (Å)	11.8266(5)	11.8060(4)	18.1942(6)	18.1740(10)
α (°)	90	90	64.685(4)	64.665(5)
β (°)	90.608(3)	90.596(3)	77.986(4)	78.123(5)
γ (°)	90	90	61.077(6)	61.048(5)
V (Å^3)	3582.4(2)	3571.6(2)	3434.1(3)	3416.9(3)
ρcalc (Mg/m^3)	1.567	1.572	1.560	1.580
μ($Mo_{K\alpha}$) (mm^{-1})	1.067	1.070	1.166	1.172
θ range (°)	2.28 to 32.32	2.87 to 30.57	2.38 to 25.00	2.90 to 28.39
Reflns collected	23467	21833	16820	33799
Independent reflns, (R_{int})	9049 (0.0903)	15172 (0.0745)	11661 (0.0290)	21970 (0.0547)
L. S. parameters/ restraints	923/4	937/4	1679/84	1639/6
$R1(F)$,[a] $I>2\sigma(I)$]	0.0455	0.0591	0.0539	0.0777
$wR2(F^2)$,[b] all data	0.0881	0.1421	0.1415	0.2415

[a] $R1(F) = \Sigma(|F_O| - |F_C|)/\Sigma|F_O|$; [b] $wR2(F^2) = [\Sigma w(F_O^2 - F_C^2)^2/\Sigma wF_O^4]^{½}$;

The method used to prepare this family of compounds is analogous to that used to prepare other oxalate-based 2D and 3D $[M^{II}M^{III}(ox)_3]$ compounds. It is based on a slow diffusion in two phases. The first one containing $[Cr(ox)_3]^{3-}$ and Mn^{2+} ions is obtained after filtering a suspension of $Ag_3[Cr(ox)_3]$ and $MnCl_2$ in methanol. The second one is a solution of the Mn^{III} precursor in different solvents (CH_3CN for **(*S*)-1**, **(*R*)-1**, **3** and **4** and CH_2Cl_2 for **(*S*)-2** and **(*R*)-2**). In all cases, monomeric Mn^{III} species instead of dimers, have been formed. This result contrasts with what has been found for other salts of these cations.[16,17] The reason may be due to the presence of two coordinating solvent molecules (CH_3OH or CH_3CN) in the apical positions of Mn^{III}, which prevents the formation of dimeric cations. Notice that with unsubstituted $[Mn^{III}(salen)]^+$ templating cation, an achiral 3D bimetallic oxalate network with inserted $[Mn^{III}(salen)(H_2O)]_2^{2+}$ dimers is obtained.[26] It seems, therefore, that the small increse in the size of the precursors used in this work with respect to $[Mn^{III}(salen)]^+$ prevents the insertion of dimeric cations within the bimetallic oxalate network. Thus, although both monomer and dimer species may be in equilibrium in solution, only the monomer with two coordinated solvent molecules is inserted into bimetallic oxalate 2D or 3D structures for [Mn((*R*)-salmen)]$^+$, [Mn((*S*)-salmen)]$^+$, [Mn(salpn)]$^+$or [Mn(saltmen)]$^+$.

Two different types of structures have been obtained with [Mn((*R*)-salmen)]$^+$ or [Mn((*S*)-salmen)]$^+$ templating cations depending on the solvent used to dissolve this cation. Acetonitrile affords a chiral 2D bimetallic oxalate network whereas dichloromethane, nitromethane or acetone give rise to an achiral 3D network. Interestingly, the use of the same templating cation in different solvents affords different structures. This finding is very unusual for this type of oxalate compounds. The other example in which this occurs involves a flexible templating cation such as $[Fe(sal_2\text{-trien})]^+$.[10b] This complex gives rise to a 2D or achiral 3D structure depending on the solvent. As the relative orientation of the two phenoxy arms of this complex differ notably in the two compounds, we have proposed that these differences in configuration caused by the different solvent molecules explain the different

templating effect on the oxalate network. In the case of [Mn((*R)*-salmen)]$^{+}$ or [Mn((*S)*-salmen)]$^{+}$ cations, the different templating effect in the various solvents may be related to the presence of different solvent molecules coordinated to Mn^{III} in the two apical positions. Thus, the 3D structures of **(*R*)-2** and **(*S*)-2** contain only [Mn((*R/S)*-salmen)$(CH_3OH)_2]^{+}$ cations, whereas the 2D ones of **(*R*)-1** and **(*S*)-1** contain also [Mn((*R/S)*-salmen)$(CH_3CN)_2]^{+}$ cations together with [[Mn((*R/S)*-salmen)$(CH_3OH)_2]^{+}$ cations. It seems, therefore, that the acetonitrile solvent used in the syntheses of **(*R*)-1** and **(*S*)-1** enters in the coordination sphere of some Mn^{III} complexes and changes its templating effect.

Structure of (*R*)-1 and (*S*)-1

These compounds crystallize in the chiral space group $P2_1$. The structure is formed by bimetallic anionic sheets in the *ab* plane presenting a honeycomb pseudo-hexagonal structure alternating with layers containing [Mn((*R)*-salmen)$(CH_3OH)_2]^{+}$ and [Mn((*R)*-salmen)$(CH_3CN)_2]^{+}$ cations and solvent molecules. (Figure 1).

The anionic layer is formed by an extended network of Mn^{II} and Cr^{III} ions linked through oxalate bridges in such a way that each Mn^{II} is surrounded by three neighbouring Cr^{III} and *vice versa* (Figure 2). The Mn^{II} and Cr^{III} are clearly distinguishable as they present different bond distances with oxalate ligands. Thus, there are two crystallographically independent Mn ions (Mn1 and Mn2) with Mn–O distances lying between 2.148(3) and 2.219(3) Å for **(*R*)-1** and 2.143(3) and 2.203(3) Å for **(*S*)-1** and two crystallographically independent Cr ions (Cr1 and Cr2) with Cr–O distances lying between 1.963(3) and 1.990(3) Å for **(*R*)-1** and 1.966(3) and 1.992(3) for **(*S*)-1**. These are typical Mn^{II}–O and Cr^{III}–O distances similar to those found in other oxalate networks. The neighbouring metal centres of these layers present alternated chirality as usual for this type of networks. In the structure of **(*R*)-1** all the Cr^{III} ions adopt a Λ-configuration, whereas all the Mn^{II} adopt the Δ-one. On the contrary, in that of **(*S*)-1** all the Cr^{III} ions adopt a Δ-configuration, whereas all the Mn^{II} adopt the Λ-one. Therefore, the configuration of each metal ion is preserved in

the neighbouring oxalate layers and it is opposite in the two structures. Interestingly, although we have started from a racemic mixture of $[Cr(ox)_3]^{3-}$ anion, crystals of only one of the two enantiomers have been obtained. The minimum distance between metals of different layers is 11.8266(5) Å for **(*R*)-1** and 11.8060(4) for **(*S*)-1**, defined by the *c* parameter, which is higher than those found in other oxalate-based 2D compounds with decamethylferrocenium or alkylammonium cations (9.2-9.7 Å),[2,4] but similar to that of the 2D compounds obtained by insertion of bulkier $[Fe^{III}(sal_2\text{-trien})]^+$ (11.6440(2) Å) cations and derivatives.[10b] These oxalate-based layers are stacked one over the other in a *AA*···fashion defining hexagonal channels running along the *c* axis.

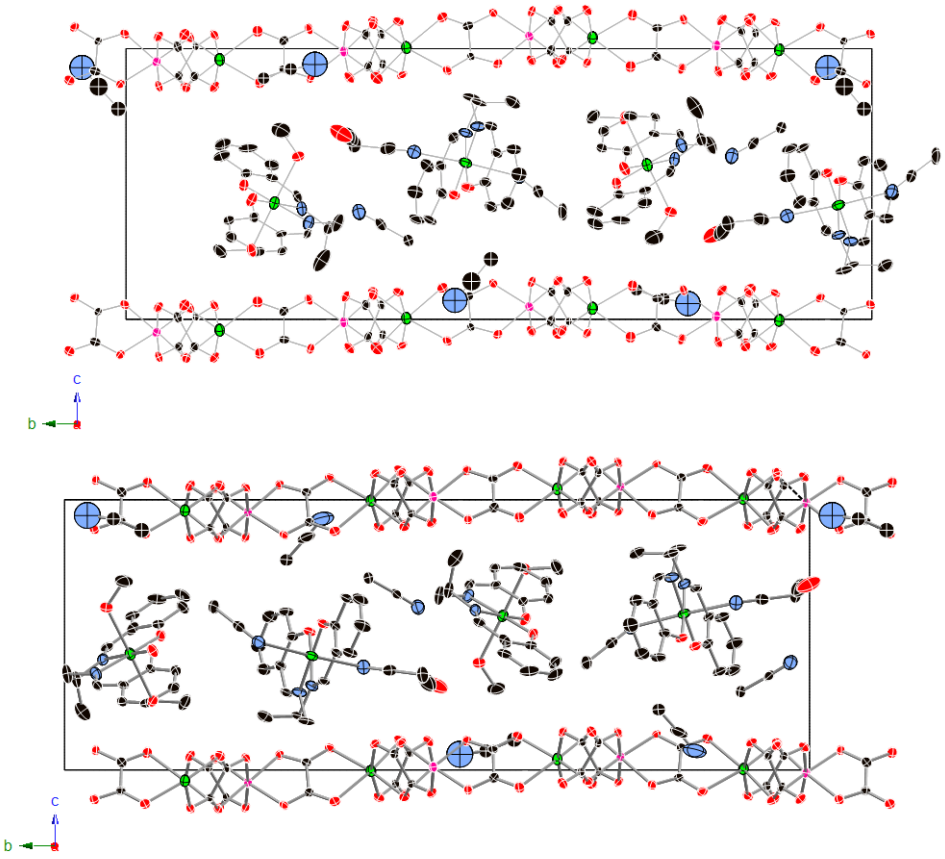

Fig. 1 Projection of **(*R*)-1** (up) and **(*S*)-1** (down) in the *bc* plane. (Cr (pink), Mn (green), C (black), N (blue), O (red)). Hydrogen atoms have been omitted for clarity.

The cationic layer intercalated between these oxalate layers is formed by two Mn^{III} complexes, $[Mn((R)\text{-salmen})(CH_3OH)_2]^+$ and $[Mn((R)\text{-salmen})(CH_3CN)_2]^+$ for **(*R*)-1** and $[Mn((S)\text{-salmen})(CH_3OH)_2]^+$ and $[Mn((S)\text{-salmen})(CH_3CN)_2]^+$ cations for **(*S*)-1** and acetonitrile and methanol solvent molecules. There are two crystallographically independent Mn ions (Mn3 and Mn4). Both Mn present a distorted octahedral geometry, in which the basal plane is formed by the coordination of the two imino nitrogens and the two phenolic oxygens from the salmen Schiff base. The two apical positions of Mn3 are occupied by the nitrogen atoms of two acetonitrile solvent molecules, whereas those of Mn4 are occupied by the oxygen atoms of two methanol solvent molecules. In these two Mn^{III} cations, the apical Mn-N (2.316(4) and 2.423(4) Å for **(*R*)-1** and 2.339(4) and 2.414(4) Å for **(*S*)-1**) or Mn-O distances (2.295(3) and 2.309(3) Å for **(*R*)-1** and 2.300(4) and 2.301(3) Å for **(*S*)-1**) are longer than the basal Mn-N (1.956(4)-1.982(4) Å for **(*R*)-1** and 1.966(4)-1.978(4) Å for **(*S*)-1**) and Mn-O (1.867(3)-1.886(3) Å for **(*R*)-1** and 1.873(3)-1.883(3) for **(*S*)-1**) ones as expected for Jahn-Teller distortion.

Neighbouring $[Mn((R)\text{-salmen})(CH_3OH)_2]^+$ or $[Mn((S)\text{-salmen})(CH_3OH)_2]^+$ complexes present π-π stacking interactions through the two phenoxy rings forming a chain that runs along the *a* axis. Coordinated CH_3OH molecules from these complexes form hydrogen bonds with the oxalate network and a non-coordinated CH_3OH molecule. $[Mn((R)\text{-salmen})(CH_3CN)_2]^+$ (or $[Mn((S)\text{-salmen})(CH_3CN)_2]^+$) cations present one short contact with a neighbouring $[Mn((R)\text{-salmen})(CH_3OH)_2]^+$ (or $[Mn((S)\text{-salmen})(CH_3OH)_2]^+$) complex through the coordinated acetonitrile molecule. $[Mn((R)\text{-salmen})(CH_3CN)_2]^+$ (or $[Mn((S)\text{-salmen})(CH_3CN)_2]^+$) cations present short contacts with the oxalate network and acetonitrile and solvent molecules. Acetonitrile and methanol solvent molecules occupy the holes between the cations and the bimetallic oxalate network.

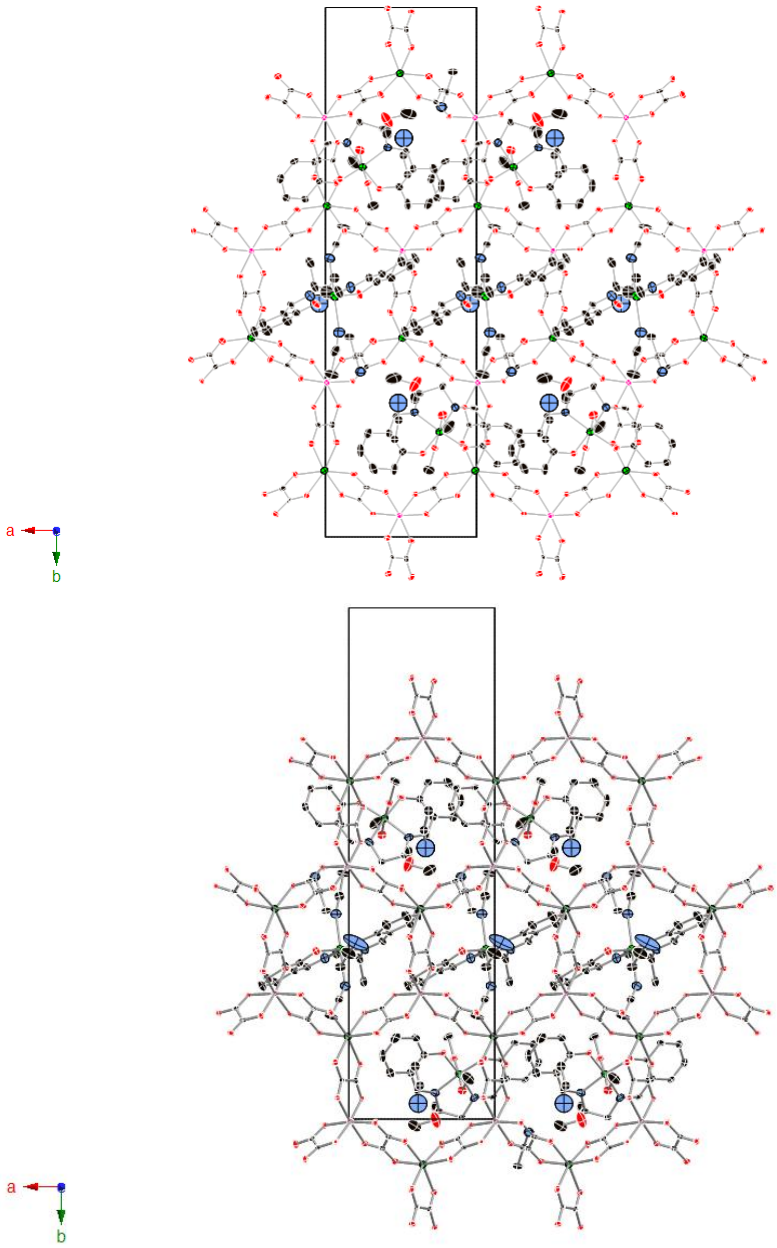

Fig. 2 Projection of **(*R*)-1** (up) and **(*S*)-1** (down) in the *ab* plane. (Cr (pink), Mn (green), C (black), N (blue), O (red)). Hydrogen atoms have been omitted for clarity.

Structure of (*R*)-2 and (*S*)-2

(*R*)-2 and **(*S*)-2** crystallise in the chiral triclinic space group *P1*. The structure is formed by an anionic 3D polymeric oxalate-bridged bimetallic network with $[Mn((R)\text{-salmen})(CH_3OH)_2]^+$ or $[Mn((S)\text{-salmen})(CH_3OH)_2]^+$ cations and solvent molecules occupying the cavities (Fig. 3). This anionic polymeric structure is formed by bis-chelating oxalate ligands connecting Mn^{II} and Cr^{III} ions in such a way that each Mn^{II} is surrounded by three Cr^{III} and *vice versa*. This oxalate network contains Mn and Cr ions of both chiralities. In the bimetallic oxalate network there are four crystallographically independent Mn^{II} ions (Mn1, Mn2, Mn3 and Mn4) with Mn–O distances lying between 2.132(5) and 2.212(6) Å for **(*R*)-2** and 2.127(6) and 2.197(6) Å for **(*S*)-2**, and four crystallographically independent Cr^{III} ions (Cr1, Cr2, Cr3 and Cr4) with Cr–O distances lying between 1.942(5) and 1.990(5) Å for **(*R*)-2** and 1.947(5) and 1.999(5) Å for **(*S*)-2**. These are typical Cr^{III}–O and Mn^{II}–O distances similar to those found in other oxalate networks. In the two compounds, there are half of Mn^{II} and Cr^{III} ions of both chiralities. Therefore, the two compounds present an achiral 3D oxalate-based network. This type of 3D achiral network is formed by helical strands that contain metals of one chirality running along the *b* axis. Thus, four of the eight crystallographically independent Mn and Cr ions (Cr1, Cr4, Mn2 and Mn4 in **(*R*)-2** and Cr3, Cr4 Mn2 and Mn3 in **(*S*)-2**) form a helical strand of Δ complexes, whereas the other four ones (Cr2, Cr3, Mn1 and Mn3 in **(*R*)-2** and Cr1, Cr2, Mn1 and Mn4 in **(*S*)-2**,) form a helical strand of Λ ones. Neighbouring helical strands, which are linked through oxalate ligands, present opposite chirality (see Fig. 4). In other achiral 3D oxalate networks of formulae $[Fe(bpp)_2][MnCr(ox)_3]_2\cdot bpp\cdot CH_3OH$,[14] $[Fe^{III}(sal_2\text{-trien})][Mn^{II}Cr^{III}(ox)_3]\cdot(CH_3OH)$, $[In^{III}(sal_2\text{-trien})][Mn^{II}Cr^{III}(ox)_3]\cdot 0.25(H_2O)\cdot 0.25(CH_3OH)\cdot 0.25(CH_3CN)$, $[In^{III}(sal_2\text{-trien})][Mn^{II}Cr^{III}(ox)_3]\cdot(CH_3NO_2)\cdot 0.5(H_2O)$[10b] and $[Fe^{III}(5\text{-}CH_3Osal_2\text{-trien})][Mn^{II}Cr^{III}(ox)_3]$,[10c] the neighbouring helical strands present the same chirality. This gives rise to 10,3 decagons with metals of the same chirality that are linked to another 10.3 decagon of opposite chirality. In contrast to this, in the structures of **(*R*)-2** and **(*S*)-2**, it is not

possible to find 10,3 decagons formed by metals of the same chirality.

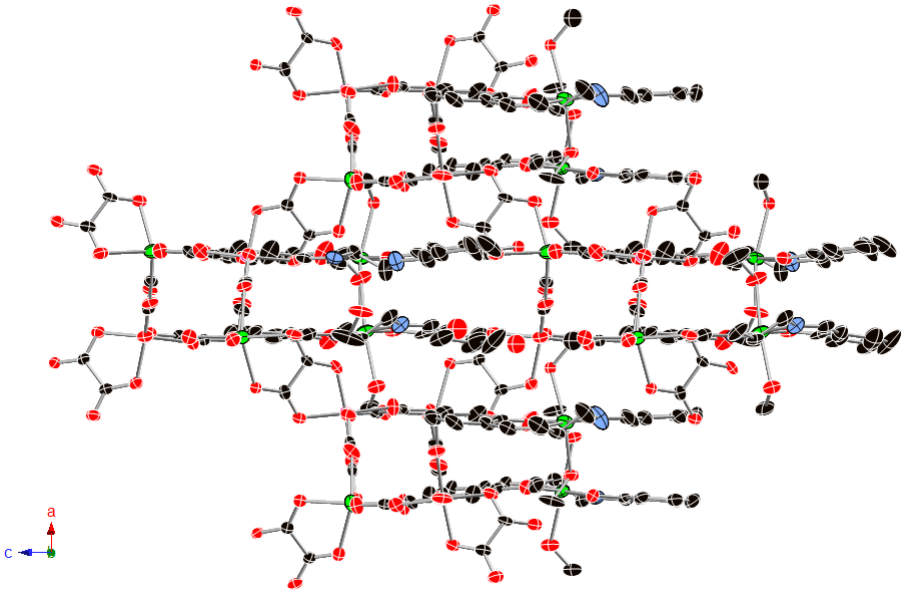

Fig 3. Projection of (**R**)-**2** in the *ac* plane. (Cr (pink), Mn (green), C (black), N (blue), O (red)). Hydrogen atoms and disordered solvent molecules have been omitted for clarity.

$[Mn((R)\text{-salmen})(CH_3OH)_2]^+$ and $[Mn((S)\text{-salmen})(CH_3OH)_2]^+$ cations and solvent molecules are intercalated in the holes described by this 3D oxalate network. There are four crystallographically independent $[Mn((R)\text{-salmen})(CH_3OH)_2]^+$ and $[Mn((S)\text{-salmen})(CH_3OH)_2]^+$ complexes (Mn5, Mn6, Mn7 and Mn8) and disordered dichloromethane, methanol and water molecules. The four Mn present a distorted octahedral geometry similar to that found in compounds **(*R*)-1** and **(*S*)-1**, in which the basal plane is formed by the coordination of the two imino nitrogens and the two phenolic oxygens from the salmen Schiff base. In contrast to **(*R*)-1** and **(*S*)-1,** there is only one type of complex, in which the two apical positions are occupied by the oxygen atoms of two methanol solvent molecules. In these four Mn^{III} cations, the apical Mn-O distances (between 2.230(5) and 2.384(11) Å for **(*R*)-2** and 2.233(6) and 2.338(13) Å for **(*S*)-2**) are longer than the basal Mn-N (between 1.971(7) and 2.005(7) Å for **(*R*)-2** and 1.962(8) and 2.007(6) Å for **(*S*)-2**) or Mn-O (between

1.846(6) and 1.915(5) Å for **(*R*)-2** and 1.838(6) and 1.914(5) Å for **(*S*)-2**) ones as expected for Jahn-Teller distortion. Two neighbouring $[Mn((R)\text{-salmen})(CH_3OH)_2]^+$ or $[Mn((S)\text{-salmen})(CH_3OH)_2]^+$ form a dimer linked trough short intermolecular contacts (Mn5 and Mn6 and Mn7 and Mn8). Thus, each pair of the four crystallographically independent $[Mn((R)\text{-salmen})(CH_3OH)_2]^+$ or $[Mn((S)\text{-salmen})(CH_3OH)_2]^+$ complexes presents two hydrogen bonds between oxygen atom of phenoxy ring and coordinated methanol of the neighbouring complex (See Fig. S1, ESI). Furthermore, Mn5 and Mn6 in **(*R*)-2** and Mn7 and Mn8 in **(*S*)-2** present π-π stacking interactions through the two phenoxy rings.

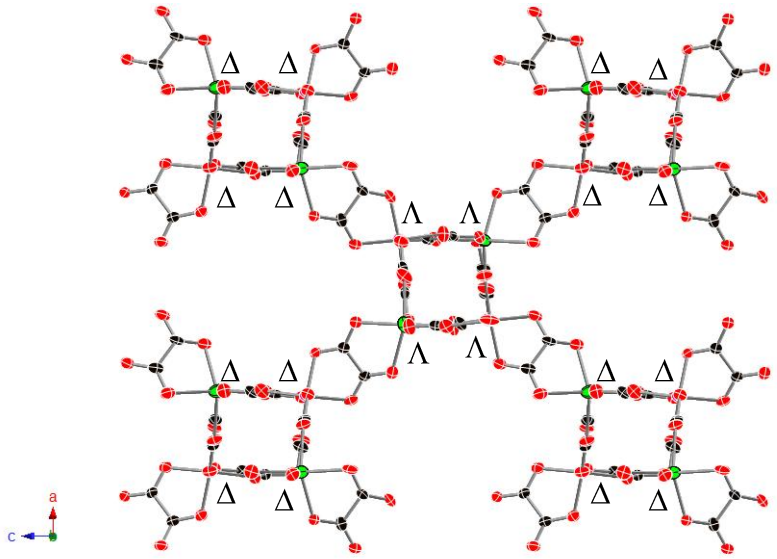

Fig. 4 Neighbouring helical strands of opposite chirality linked through oxalate ligands in (**(*R*)-2**).

On the other hand, there are numerous short contacts between the Mn^{III} complexes and the oxalate network. In most of them, the methyl group and hydrogen from the asymmetric carbon from the complexes are implied. Some of these interactions could be responsible of the formation of the chiral helical strands. Disordered dichloromethane, methanol and water solvent molecules

occupy the holes between the cations and the bimetallic oxalate network. The distribution of these disordered solvent molecules changes slightly in the two compounds.

Table 2. Crystallographic data for compounds **3** and **4**.

Compound	**3**	**4**
Empirical formula	$C_{105.28}Cr_4Mn_8H_{97.85}O_{69}N_{10}$	$C_{30}CrMn_2H_{32}O_{16}N_3$
Formula weight	3254.72	852.47
Crystal color	red	red
Temperature (K)	120(2)	120(2)
Wavelength (*Å*)	0.71073	0.71073
Crystal system, Z	Orthorhombic, 2	Triclinic, 2
Space group	$P2_12_12_1$	*P*-1
a (Å)	14.5286(4)	9.5551(5)
b (Å)	20.8778(7)	11.8076(5)
c (Å)	22.7570(6)	15.8509(8)
a (Å)	90	101.420(4)
β (°)	90	95.207(4)
γ(°)	90	93.581(4)
V (Å^3)	6902.8(4)	1739.77(15)
ρcalc (Mg/m^3)	1.567	1.627
μ(Mo$_{K\alpha}$) (mm^{-1})	1.107	1.099
θ range (°)	2.27 to 32.45	2.40 to 32.50
Reflns collected	22093	11477
Independent reflns, (R_{int})	7809 (0.0906)	3715 (0.1077)
L. S. parameters/ restraints	886/2	473/0
$R1(F)$,[a] $I>2\sigma(I)$]	0.0445	0.0576
$wR2(F^2)$,[b] all data	0.0944	0.1023

[a] $R1(F) = \Sigma(||F_O| - |F_C||)/\Sigma|F_O|$; [b] $wR2(F^2) = [\Sigma w(F_O^2 - F_C^2)^2/\Sigma wF_O^4]^{1/2}$;

Structure of 3

3 crystallizes in the chiral space group $P2_12_12_1$. As a racemic mixture of $[Cr(ox)_3]^{3-}$ ions has been used in the synthesis, crystals of both chiralities are obtained. The structure is formed by an anionic 3D polymeric oxalate-bridged bimetallic network with $[Mn^{III}(salpn)(CH_3CN)(CH_3OH)]^+$ and $[Mn^{III}(salpn)(CH_3OH)_2]^+$ cations and disordered methanol and acetonitrile solvent molecules occupying the cavities (Fig. 5). This anionic polymeric structure present the well-known 3D 3-connected 10-gon oxalate-based anionic network (10,3) which is formed by oxalate ligands connecting Mn^{II} and Cr^{III} ions in such a way that each Mn^{II} is surrounded by three Cr^{III} and *vice versa* with all metal ions presenting the same chirality (Λ in the crystal used to solve the structure).

Similar 3D chiral oxalate-based networks have been obtained in compounds $[Ni(phen)_3][NaCo(dto)_3]\cdot C_3H_6O$[27] (phen = phenantroline, dto = 1,2 dithiooxalate) and $[Fe^{III}(5\text{-X-sal}_2\text{-trien})][Mn^{II}Cr^{III}(ox)_3]$ (X = Cl, Br) that crystallize in the same space group as that of **3**.[10d] The orthorhombic 3D oxalate chiral networks of these compounds present the same connectivity as the cubic ones obtained with the smaller templating cation, $[Z^{II}(bpy)_3]^{2+}$,[3] with some differences as a consequence of the lowering in symmetry. In contrast with the other cubic heterometallic derivatives, in the structure of **3** there are two crystallographically independent Mn^{II} ions (Mn3 and Mn4) with Mn–O distances lying between 2.148(3) and 2.212(3) Å and two crystallographically independent Cr^{III} ions (Cr1 and Cr2) with Cr–O distances lying between 1.960(3) and 1.980(3) Å. Metal-metal distances between adjacent centers are in the 5.359-5.414 Å range. The bimetallic oxalate network of **3** defines channels that run along [100] (*a* axis) formed by helical strands of Λ complexes linked through oxalate ligands (see fig. 5). Furthermore, it forms channels perpendicular to the previous one running along [011] and [01-1] axes (See Fig. S2 and S3, ESI). This result is in contrast with the previously described orthorhombic chiral 3D oxalate networks in which the channels run along *a*, *b* and *c* axis. This is due to the larger unit cell of **3** compared with those of the previous compounds.

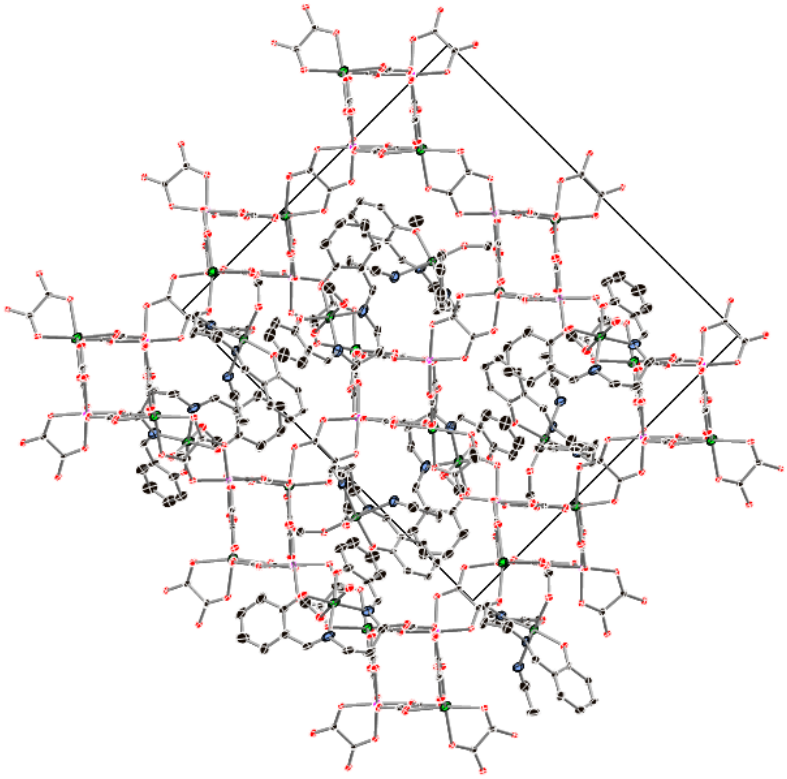

Fig. 5 Projection of **3** in the *bc* plane. (Cr (pink), Mn (green), C (black), N (blue), O (red)). Hydrogen atoms and disordered solvent molecules have been omitted for clarity.

The holes described by this 3D oxalate network are occupied by two Mn^{III} complexes, $[Mn(salpn)(CH_3OH)_2]^+$ and $[Mn(salpn)(CH_3CN)(CH_3OH)]^+$ and disordered methanol and water solvent molecules. There are two crystallographically independent Mn ions (Mn1 and Mn2). Both Mn present a distorted octahedral geometry similar to that exbited by Mn^{III} complexes in **1** and **2**. Thus, the two apical positions of Mn1 are occupied by one acetonitrile and methanol molecules, while those of Mn2 are occupied by two methanol solvent molecules. In this last case, one of the two coordinated methanol solvent molecules presents a disorder between two possible configurations. The apical Mn-N (2.405(4) Å) or Mn-O distances

(between 2.180(3) and 2.246(3) Å) are longer than the basal Mn-N (between 2.011(4) and 2.026(4) Å) and Mn-O (1.867(3)-1.903(3) Å) ones as expected for Jahn-Teller distortion.

Two neighbouring $[Mn(salpn)(CH_3OH)_2]^+$ and $[Mn(salpn)(CH_3CN)(CH_3OH)]^+$ molecules are linked through two hydrogen bonds between the oxygen atom of one of the phenoxy rings and coordinated methanol of the neighbouring complex (see Fig. S4, ESI). Furthermore, the other phenoxy ring is involved in a CH···π interaction with another $[Mn(salpn)(CH_3CN)(CH_3OH)]^+$ or $[Mn(salpn)(CH_3OH)_2]^+$ molecule. Finally, there are numerous short contacts with the oxalate network and solvent molecules.

Structure of 4

4 crystallizes in the triclinic space group *P-1*. The structure of this compound is formed by anionic sheets in the *ac* plane with inter-lamellar $[Mn(saltmen)(CH_3CN)(CH_3OH)]^+$ and methanol solvent molecules (Fig. 6). The anionic layer is formed by an extended network with Mn^{II} and Cr^{III} ions linked through oxalate bridges. It presents the 2D honeycomb structure already described for **1**. The neighbouring metal centers of these layers present alternated chirality as usual for this type of networks. There are two metals crystallographically independent with M–O distances lying between 2.055(3) and 2.094(3) Å. These distances are intermediate between the ones expected for Cr^{III}–O and Mn^{II}–O. Therefore, it is not possible to distinguish between the two metals in this structure. This indicates that Mn^{II} and Cr^{III} ions in these structures may have (Λ) or (Δ) configurations in the different layers and that the structure is not chiral in contrast to that of **(*R*)-1** and **(*S*)-1**. The minimum distance between metals of different layers is 11.8076(5) Å, defined by the *b* parameter, which is similar to that of **(*R*)-1** and **(*S*)-1**, as expected taking into account the similar size of the inserted cations in the two compounds. These oxalate-based layers are stacked one over the other in a *AA*··· fashion defining hexagonal channels running along the *b* axis (See Fig. S5, ESI).

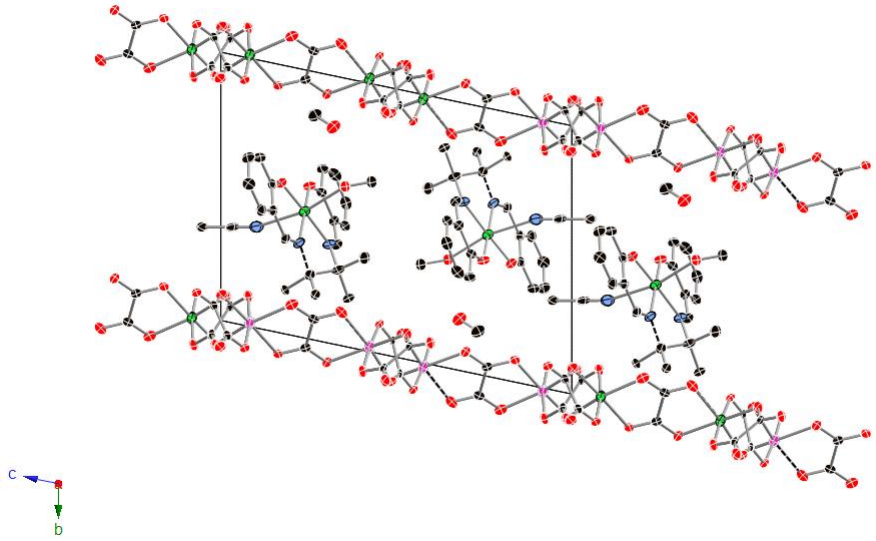

Fig. 6 Projection of **4** in the *bc* plane. (Cr (pink), Mn (green), C (black), N (blue), O (red)). Hydrogen atoms have been omitted for clarity.

The cationic layer intercalated between these oxalate layers is formed by $[Mn(saltmen)(CH_3CN)(CH_3OH)]^+$ cations and methanol solvent molecules. $[Mn(saltmen)(CH_3CN)(CH_3OH)]^+$ complexes are close to the center of the hexagonal channels of the bimetallic oxalate network mentioned above. There is one crystallographically independent Mn ion (Mn1). It presents a distorted octahedral geometry as in the previous compounds. One of the two apical positions of this ion is occupied by an acetonitrile solvent molecule, while the second one is occupied by a methanol solvent molecule. Again, the Mn-N (1.972(3) and 1.980(3) Å) and Mn-O (1.878(3) and 1.887(3) Å) basal distances are shorter than the apical ones (2.490(4) and 2.271(3) Å respectively) due to Jahn-Teller distortion. Two neighbouring $[Mn(saltmen)(CH_3CN)(CH_3OH)]^+$ complexes present two CH···π interactions between one methyl group from the 1,1,2,2-tetramethylethylene group and the phenoxy ring of the neighbouring complex forming a dimer. On the other hand, coordinated CH_3CN on the other side of the complex presents numerous short contacts with a coordinated CH_3CN of another neighbouring $[Mn(saltmen)(CH_3CN)(CH_3OH)]^+$

complex. The coordinated CH_3OH molecule forms a hydrogen bond with the non-coordinated CH_3OH molecule, which occupies the holes between the oxalate network and the Mn^{III} complexes. Finally, $[Mn(saltmen)(CH_3CN)(CH_3OH)]^+$ complex presents several short contacts with the oxalate network and the non-coordinated CH_3OH, that forms a hydrogen bond with the oxalate network.

Magnetic properties

The temperature dependence of the product of the magnetic susceptibility times the temperature (χT) under an applied field of 0.1 mT for the six compounds is shown in Fig. 7 and SI6, ESI. They present a similar behavior with χT values of 9.2-9.4 emu·K·mol^{-1} at 300 K in agreement with the expected value for non-interacting high-spin Mn^{III} (S = 2), high-spin Mn^{II} (S = 5/2) and Cr^{III} (S = 3/2) ions. A gradual increase of the χT product upon cooling is observed from 300 to 30 K. Below this temperature there is a sharp increase of the χT product. χ follows a Curie-Weiss law between 20 to 300 K with C and θ values shown in Table 3. This indicates the presence of ferromagnetic interactions between neighbouring M^{II}-Cr^{III} magnetic ions and the onset of long-range ferromagnetic ordering, as observed for other $Mn^{II}Cr^{III}$ 2D and 3D oxalate compounds. To confirm the presence of long-range magnetic ordering and to determine precisely the critical temperature (T_c), ac susceptibility measurements were carried out. As expected for samples presenting an ordered state, a maximum in the in-phase signal (χ') near T_c and an out-of-phase signal (χ'') that starts to appear at temperatures just below T_c is observed in the six compounds (Fig. 8, 9 and SI7-SI10, ESI). From these data the T_c of the compounds is around 5 K, which is similar to that of other 2D or 3D $Mn^{II}Cr^{III}$ bimetallic oxalate networks (see Table 3). These signals are almost frequency independent for **(*R*)-1** and **(*S*)-1**, whereas the other compounds present a small frequency dependence that could be explained by the presence of an additional peak in χ" at lower temperatures. These peaks have been observed in other 2D and 3D bimetallic oxalate compounds and can be related to the formation of magnetic domains and domain-wall movement.[10]

The ferromagnetic ordering is also confirmed by the field dependence of the magnetisation (*M*) at 2 K. In all the compounds, it shows a sharp increase at low fields tending to saturation above 2 T and reaching maximum values lower than the expected value for a parallel alignement of the spins (12 μ_B) (see Fig. SI11-SI13, ESI). The coercive fields at 2 K are close to 1 mT indicating that the compounds behave as soft ferromagnets (see Table 3).

In summary, the magnetic characterisation of the six compounds confirms the ferromagnetic ordering, which is very similar to that of other 2D and 3D bimetallic oxalate networks. On the other hand, the magnetic behavior of **(*R*)-1**, **(*S*)-1**, **(*R*)-2** and **(*S*)-2** indicates that, within the experimental error, neither T_c nor θ depend on the absolute configuration of the compounds, as observed in other enantiopure 2D bimetallic oxalate compounds.[18a]

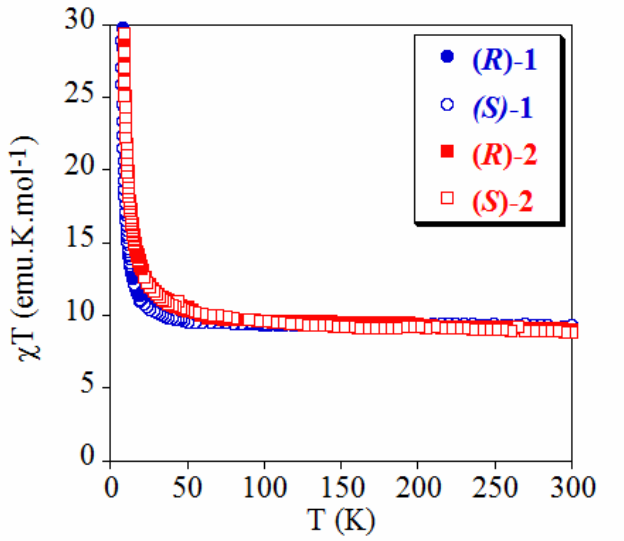

Fig. 7 Temperature dependence of the product of the molar magnetic susceptibility with temperature (χT) at 0.1 T for compounds **(*R*)-1** (full circles), **(*S*)-1** (empty circles), **(*R*)-2** (full squares) and **(*S*)-1** (empty squares).

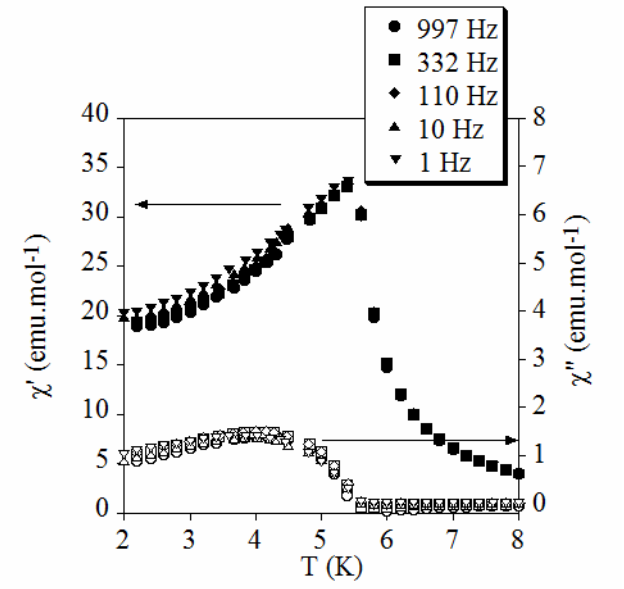

Fig. 8 Temperature dependence of the in-phase AC susceptibility (χ') (filled symbols) and the out-of-phase AC susceptibility (χ") (empty symbols) for ***(R)*-1**.

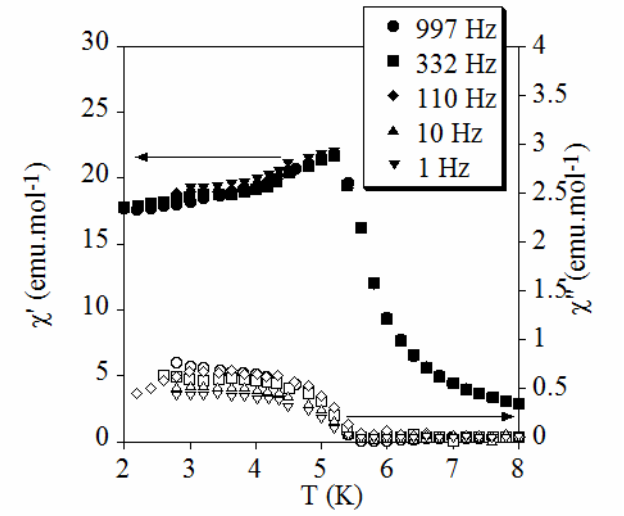

Fig. 9 Temperature dependence of the in-phase AC susceptibility (χ') (filled symbols) and the out-of-phase AC susceptibility (χ") (empty symbols) for ***(S)*-1**.

Table 3. Magnetic parameters for compounds (R)-**1**, (***S***)-**1**, (***R***)-**2**, (***S***)-**2, 3** and **4**.

Compound	T_c (K)	θ (K)	C (emu·K·mol^{-1})	M (μ_B) at 5 T and 2 K	H_{coer} (mT) at 2 K
(***R***)**-1**	5.5	5.5	9.0	10.2	0.8
(***S***)**-1**	5.5	3.5	9.3	10.2	0.2
(***R***)**-2**	5.2	7.0	9.1	10.8	1.9
(***S***)**-2**	5.2	7.7	8.8	11.2	1.8
3	5.4	2.8	8.8	9.5	1.4
4	5.6	6.0	9.4	10.4	1.3

Discussion

The use of derivatives of Mn^{III} salen-type complexes as templating cations has afforded different types of oxalate networks. Two different types of structures has been obtained with [Mn((*R)*-salmen)]$^+$ or [Mn((*S)*-salmen)]$^+$ that contain a chiral quaternary carbon atom depending on the solvent used to dissolve the cation. In acetonitrile, a chiral 2D bimetallic oxalate network has been obtained in compounds **(*R*)-1** and **(*S*)-1**, whereas in compounds **(*R*)-2** and **(*S*)-2**, a new type of achiral 3D network different to those reported before has been formed.

The enantioselective self-assembly of 2D oxalate-based compounds is a synthetic challenge due to the heterochiral arrangement of M^{II} and M^{III} ions in 2D structures.[13] In most of the reported 2D oxalato-bridged structures, M^{II} and M^{III} ions are disordered and it is not possible to distinguish among them. This contrasts with the structure of **(*R*)-1** and **(*S*)-1**, in which Cr^{III} and Mn^{II} of opposite configuration can be clearly differenciated as they present their characteristic M-O bond-lengh distances. Furthermore, Cr^{III} and Mn^{II} of the two compounds present the opposite configuration. Thus, in **(*R*)-1** all the Cr^{III} ions adopt a Λ-configuration, whereas all the Mn^{II} adopt the Δ-one. In contrast, in that of **(*S*)-1** all the Cr^{III} ions adopt a Δ-configuration, whereas all the Mn^{II} adopt the Λ-one. Therefore, the configuration of each metal ion is preserved in the neighbouring oxalate layers and it is opposite in

the two structures. This is a very unusual and interesting result. In most of the chiral 2D bimetallic oxalate networks found in the literature, it is not possible to separate the two enantiomers, as for the 2D structures obtained with a chiral tetraalkyl ammonium with four different alkyl chains[13,28] and those obtained with Fe^{III} complexes of the hexadentate Schiff base ligands, 5-NO_2-sal_2-trien[10c] and 3-Cl-sal_2-trien.[29] Until now, only a tetraalkylammonium with one chiral alkyl chain, appeared as a good chiral templating agent towards the formation of enantiopure 2D oxalate-based materials in compounds $[N((S)\text{-i-Bu})MePr_2][(\Lambda)Mn\text{-}(\Delta)\text{-}Cr(ox)_3]$ (i-Bu = $CH(CH_3)C_2H_5$; Me = CH_3; Pr = C_3H_7) and $[N((R)\text{-i-Bu})MePr_2][(\Delta)\text{-}Mn(\Lambda)\text{-}Cr(ox)_3]$.[13,18a] As in this previous result, the chirality of the $[Mn((R)\text{-salmen})(CH_3OH)_2]^+$ and $[Mn((R)\text{-salmen})(CH_3CN)_2]^+$ complexes, due to the presence of a quaternary C atom, may be responsible of this first-order spontaneous resolution through chiral recognition between one of the enantiomers of $[Cr(ox)_3]^{3-}$ and $[Mn((S)\text{-salmen})(CH_3OH)_2]^+$ and $[Mn((S)\text{-salmen})(CH_3CN)_2]^+$ cations. In agreement with this, the methyl groups of $[Mn((R)\text{-salmen})(CH_3OH)_2]^+$ and $[Mn((R)\text{-salmen})(CH_3CN)_2]^+$ cations, interact through several short contacts with the oxalate ligands.

On the other hand, the same templating chiral cations dissolved in a different solvent (dichloromethane, nitromethane or acetone) lead to a different network, a 3D structure with half of Mn^{II} and Cr^{III} ions of both chiralities, as that of compounds **(*R*)-2** and **(*S*)-2** obtained in dichloromethane. It seems then, that the presence of acetonitrile is necessary to form the 2D structure of **(*R*)-2** and **(*S*)-2**. The different templating effect of this cation in acetonitrile is related to the coordination of acetonitrile molecules to some of the Mn^{III} complexes in **(*R*)-1** and **(*S*)-1**, that changes their templating effect. This 3D achiral network is different to other achiral 3D oxalate networks found in the literature.[10b,c,14] In contrast to them, it does not contain 10,3 decagons with neighbouring Mn^{II} and Cr^{III} metals of the same chirality linked to another 10,3 decagon of opposite chirality, but helical strands with metals of the same chirality running along the c axis, which are linked to helical strands of the opposite chirality. Therefore, in this case the use of a chiral precursor has led to

a new type of 3D achiral structure.

Finally, the use of the achiral templating cations, $[Mn(salpn)]^+$ and $[Mn(salten)]^+$ gives rise to a chiral 3D network and an achiral 2D network respectively in compounds **3** and **4**. In the case of **3**, we have demonstrated that the formation of chiral oxalate-based networks is not limited to chiral templating cations. However, there is an important drawback of this strategy: crystals of both chiralities are obtained in the same synthesis in contrast to the obtention of enantiopure samples with the chiral precursors, $[Mn((R)\text{-salmen})]^+$ or $[Mn((S)\text{-salmen})]^+$, in **(*R*)-1** and **(*S*)-1**.

From the point of view of the physical properties, since all the derivatives of $[Mn^{III}(salen)]^+$ used in this work have led to the insertion of monomeric Mn^{III} species into oxalate-based bimetallic networks, they can be seen as hybrid magnets formed by a paramagnetic sublattice inserted into a 2D or 3D ferromagnetic network. The magnetic behavior of these networks is similar to that of other 2D or 3D oxalate-based compounds reported in the literature. Thus, the T_c values of the 2D compounds **(*R*)-1**, **(*S*)-1** and **4** (5.6 K) are identical to those of other $Mn^{II}Cr^{III}$ 2D oxalate compounds.[4,10e] The decrease of T_c of the 3D compounds, **(*R*)-2, (*S*)-2** (T_c = 5.2 K) and **3** (T_c = 5.4 K) is not unexpected, since usually 2D bimetallic oxalate compounds present higher T_c values than 3D ones. This has been explained by the non-collinear alignment of the chiral axis in the 3D compounds, which produces differences in the relative orientation of the magnetic orbitals.[30] The differences between the T_c of **(*R*)-2** and **(*S*)-2** and that of other bimetallic oxalate compounds with a 3D achiral structure such as $[Fe^{III}(5\text{-}CH_3Osal_2\text{-trien})][Mn^{II}Cr^{III}(ox)_3]$ (T_c = 5.1 K), $[Fe^{III}(sal_2\text{-trien})][Mn^{II}Cr^{III}(ox)_3]\cdot(CH_3OH)$ (T_c = 5.2 K) or $[Fe(bpp)_2][MnCr(ox)_3]\cdot bpp\cdot CH_3OH$, ($T_c$ = 3.0 K), may be explained by differences on the Mn^{II}–Cr^{III} distances and in the bonding angles. On the other hand, T_c of **3** (T_c = 5.4 K) is slightly higher than those found in $[Fe^{III}(5\text{-}Clsal_2\text{-trien})][Mn^{II}Cr^{III}(ox)_3]\cdot 0.5(CH_3NO_2)$, $[Fe^{III}(5\text{-}Brsal_2\text{-trien})][Mn^{II}Cr^{III}(ox)_3]$ and $[In^{III}(5\text{-}Clsal_2\text{-trien})][Mn^{II}Cr^{III}(ox)_3]\cdot(CH_3NO_2)$, the other compounds

with a similar 3D orthorhombic network (4.8-5 K)[10d] and compounds with a 3D cubic one (5.1 K).[3d,f,9b] This is not unusual as the T_c of this type of networks is very sensitive to the size of the inserted cation.[3f] Finally, the ferromagnetism of the 2D and 3D oxalate networks of these compounds may produce a Zeeman splitting of the S = 2 spins of the paramagnetic inserted Mn^{III} complexes. This effect has been studied by EPR (electronic paramagnetic resonance) spectroscopy in 2D compounds with inserted radical organic cations or decamethylferrocenium cations.[1,4] However, this is not possible in our systems as Mn^{III} complexes are EPR-silent.

The most promising result of these compounds is derived from the chirality of the oxalate network in compounds **(*S*)-1**, **(*R*)-1** and **3**, which opens the way to the search for new magnetic effects derived from the coexistence of chirality and ferromagnetism, such as the magneto-chiral effect predicted by Rikken et al.[31] and observed recently in an enantiopure 2D oxalate compound.[18a] Interestingly, in the case of **(*S*)-1** and **(*R*)-1**, it is possible to separate the two enantiomers by choosing the rigth chiral precursor. In the case of **3** obtained from an achiral precursor, a 50 % mixture of crystals of both enantiomers is obtained. Notice that magneto-chiral effect effect has been observed in the weakly chiral 2D lattice. Still, in the strongly chiral 3D lattice as that of **3**, this effect could be more important. Although it is not possible to perform enantiopure syntheses of this compound, this effect could be studied on single crystals.

Conclusion

In this article we have shown that the use of substituted Mn^{III}-salen complexes as templating cations is a suitable strategy to obtain different types of oxalate networks. The chiral templating cations $[Mn((R)\text{-salmen})]^+$ and $[Mn((S)\text{-salmen})]^+$ have led to a 2D chiral oxalate network in acetonitrile in **(*R*)-1** and **(*S*)-1** compounds, while a new type of achiral 3D oxalate network has been obtained in dichloromethane in compounds **(*S*)-2** and **(*R*)-2**. On the other hand, the achiral

templating cations, $[Mn(salpn)]^+$ and $[Mn(saltmen)]^+$, have given rise respectively to a 3D chiral network and a 2D achiral network in **3** and **4** compounds. All these complexes have led to the insertion of monomeric Mn^{III} species into oxalate-based bimetallic networks. Therefore, they are multifunctional compounds combining the ferromagnetic order of the 2D or 3D oxalate networks and the paramagnetism of the inserted Mn^{III} cation. The chirality of the oxalate network in compounds **(*S*)-1**, **(*R*)-1** and **3** may lead to new magnetic effects derived from the coexistence of chirality and ferromagnetism. Interestingly, in the case of **(*S*)-1** and **(*R*)-1**, this study could be performed in enantiopure samples, something very unusual for this type of compounds.

Acknowledgements

Financial support from the European Union (MolSpinQIP and SPINMOL ERC Advanced Grant), the Spanish Ministerio de Ciencia e Innovación (Projects Consolider-Ingenio in Molecular Nanoscience CSD2007-00010, MAT2011-22785 and CTQ2011-26507), and the Generalitat Valenciana (Prometeo Program) are gratefully acknowledged. The authors also thank José María Martínez-Agudo and Gloria Agustí-López, University of Valencia, for magnetic characterization of the samples.

Notes and references

[1] M. Clemente-León, E. Coronado, C. Martí-Gastaldo, F. M. Romero, *Chem. Soc. Rev.,* 2011, **40**, 473.

[2] (a) H. Tamaki, Z. J. Zhong, N. Matsumoto, S. Kida, M. Koikawa, N. Achiwa, Y. Hashimoto, H. Okawa, *J. Am. Chem. Soc.,* 1992, **114**, 6974; (b) H. Tamaki, M. Mitsumi, N. Nakamura, N. Matsumoto, S. Kida, H. Okawa, S. Ijima, *Chem. Lett.,* 1992, 1975; (c) C. Mathonière, S. G. Carling, D. Yuscheng, P. Day, *J. Chem. Soc., Chem. Commun.,* 1994, 1551; (d) C. Mathonière, J. Nutall, S. G. Carling, P. Day, *Inorg. Chem.,* 1996, **35**, 1201; (e) R. Pellaux, H. W. Schmalle, R. Huber, P. Fisher, T. Hauss, B. Ouladdiaf, S. Decurtins, *Inorg. Chem.,* 1997, **36**, 2301; (f) E. Coronado, J. R. Galán-Mascarós, C. J. Gómez-García, J. M. Martínez-Agudo, E. Martínez-Ferrero, J. C. Waerenborgh, M. Almeida, *J. Solid State Chem.,* 2001, **159**, 391; (g) K. S. Min, A. L. Rhinegold, J. S. Miller, *Inorg. Chem.,* 2005, **44**,

8433; (h) E. Coronado, J. R. Galán-Mascarós, C. Martí-Gastaldo, *J. Mater. Chem.,* 2006, **16,** 2685; (i) Z. Duan, Y. Zhang, B. Zhang. F. L. Pratt, *Inorg. Chem.,* 2009, **48**, 2140.

[3] (a) S. Decurtins, H. W. Schmalle, P. Schneuwly, H. R. Oswald, *Inorg. Chem.,* 1993, **32,** 1888; (b) S. Decurtins, H. W. Schmalle, P. Schneuwly, J. Ensling, P. Gütlich, *J. Am. Chem. Soc.,* 1994, **116**, 9521; (c) M. Hernández-Molina, F. Lloret, C. Ruiz-Pérez, M. Julve, M. *Inorg. Chem.,* 1998, **37**, 4141; (d) E. Coronado, J. R. Galán-Mascarós, C. J. Gómez-García, J. M. Martínez-Agudo, *Inorg. Chem.,* 2001, **40**, 113; (e) F. Pointillart, C. Train, M. Gruselle, F. Villain, H. W. Schmalle, D. Talbot, P. Gredin, S. Decurtins, M. Verdaguer, *Chem. Mater.,* 2004, **16**, 832; (f) M. Clemente-León, E. Coronado, C. J. Gómez-García, A. Soriano-Portillo, *Inorg. Chem.,* 2006, **45**, 5653.

[4] (a) M. Clemente-León, J. R. Galán-Mascarós, C. J. Gómez-García, *Chem. Commun.,* 1997, 1727; (b) E. Coronado, J. R. Galán-Mascarós, C. J. Gómez-García, J. M. Martínez-Agudo, *Adv. Mater.,* 1999, **11**, 558; (c) E. Coronado, J. R. Galán-Mascarós, C. J. Gómez-García, J. Ensling, P. Gutlich, *Chem. Eur. J.,* 2000, **6**, 552.

[5] (a) S. Bénard, P. Yu, J. P. Audière, E. Rivière, R. Clèment, J. Ghilhem, L. Tchertanov, K. Nakatami, *J. Am. Chem. Soc.,* 2000, **122**, 9444; (b) S. M. Aldoshin, N. A. Sanina, V. I. Minkin, N. A. Voloshin, V. N. Ikorskii, V. I. Ovcharenko, V. A. Smirnov, N. K. Nagaeva, *J. Mol. Struct.,* 2007, **826**, 6.

[6] (a) E. Coronado, J. R. Galán-Mascarós, C. J. Gómez-García V. Laukhin, *Nature,* 2000, **408**, 447; (b) A. Alberola, E. Coronado, J. R. Galán-Mascarós, C. Giménez-Saiz, C. J. Gómez-García, *J. Am. Chem. Soc.,* 2003, **125**, 10774; (c) E. Coronado, J. R. Galán-Mascarós, C. J. Gómez-García, E. Martínez-Ferrero, S. Van Smaalen, *Inorg. Chem.,* 2004, **43**, 4808; (d) B. Zhang, Y. Zhang, D. Zhu, *Chem. Commun.,* 2012, **48**, 197.

[7] (a) H. Okawa, A. Shigematsu, M. Sadakiyo, T. Miyagawa, K. Yoneda, M. Ohba, H. Kitagawa, *J. Am. Chem. Soc.,* 2009, **131**, 13516; (b) M. Sadayiko, H. Okawa, A. Shigematsu, ;.M. Ohba, T. Yamada, H. Kitagawa, *J. Am. Chem. Soc.,* 2012, **134**, 5472.

[8] T. Endo, T. Akutagawa, S. I. Noro, T. Nakamura, *Dalton Trans.,* 2011, **40**, 1491.

[9] (a) R. Andrés, M. Gruselle, B. Malézieux, M. Verdaguer, J. Vaissermann, *Inorg. Chem.,* 1999, **38**, 4637; (b) R. Andrés, M. Brissard, M. Gruselle, C. Train, J. Vaissermann, B. Malézieux, J. P. Jamet, M. Verdaguer, *Inorg. Chem.,* 2001, **40**, 4633; (c) M. Clemente-León, E. Coronado, J. C. Dias, A. Soriano-Portillo, R. D. Willett, *Inorg. Chem.,* 2008, **47**, 6458.

[10] (a) M. Clemente-León, E. Coronado, M. C. Giménez-López, A. Soriano-Portillo, J. C. Waerenborgh, F. S. Delgado, C. Ruiz-Pérez, *Inorg. Chem.,* 2008, **47**, 9111; (b) M. Clemente-León, E. Coronado, M. López-Jordà, G. Mínguez Espallargas, A. Soriano-

Portillo, J. C. Waerenborgh, *Chem. Eur. J.,* 2010, **16**, 2207; (c) M. Clemente-León, E. Coronado, M. López-Jordà, *Dalton Trans.,* 2010, **39**, 4903; (d) M. Clemente-León, E. Coronado, M. López-Jordà, J. C. Waerenborgh, *Inorg. Chem.,* 2011, **50**, 9122; (e) M. Clemente-León, E. Coronado, M. López-Jordà, C. Desplanches, S. Asthana, H. Wang, J.-F. Létard, *Chem. Sci.,* 2011, **2**, 1121.

[11] J. R. Galán-Mascarós, E. Coronado, P. A. Goddard, J. Singleton, A. I. Coldea, J. D. Wallis, S. J. Coles and A. Alberola, *J. Am. Chem. Soc.,* 2010, **132**, 9271.

[12] E. Pardo, C. Train, G. Contard, K. Boubekeur, O. Fabelo, H. Liu, B. Dkhil, F. Lloret, K. Nakagawa, H. Tokoro, S.-I. Ohkoshi, M. Verdaguer, *J. Am. Chem. Soc.,* 2011. **133**, 15328.

[13] C. Train, M. Gruselle, M. Verdaguer, *Chem. Soc. Rev.,* 2011, **40**, 3279.

[14] E. Coronado, J. R. Galán-Mascarós, M. C. Giménez-López, M. Almeida, J. C. Waerenborgh, *Polyhedron,* 2007, **26**, 1838.

[15] B. Zhang, Y. Zhang, D. Zhu, *Dalton Trans.,* 2012, **14**, 8509.

[16] (a) R. Clérac, H. Miyasaka, M. Yamashita, C. Coulon, *J. Am. Chem Soc.*, 2002, **124**, 12837; (b) M. Ferbinteanu, H. Miyasaka, W. Wernsdorfer, K. Nakata, K. Sugiura, M. Yamashita, C. Coulon, R. Clérac, *J. Am. Chem. Soc.,* 2005, **127**, 3090; (c) H. Miyasaka, R. Clérac, K. Mizushima, K. Sugiura, M. Yamashita, W. Wernsdorfer, C. Coulon, *Inorg. Chem.*, 2003, **42**, 8203; (d) A. Saitoh, H. Miyasaka; M. Yamashita, R. Clérac, *J. Mater. Chem.*, 2007, **17**, 2002; (e) H. Miyasaka, T. Madanbashi, A. Saitoh, N. Motokawa, R. Ishikawa, M. Yamashita, S. Bahr, W. Wernsdorfer, R. Clérac, *Chem. Eur. J.,* 2012, **18**, 3942.

[17] (a) H. Miyasaka, R. Clérac, W. Wernsdorfer, L. Lecren, C. Bonhomme, K. Sugiura, M. Yamashita, *Angew. Chem., Int. Ed.,* 2004, **43**, 2801; (b) H. J. Choi, J. J. Sokol, J. R. Long, *Inorg. Chem.*, 2004, **43**, 1606; (c) Z. Lu, M. Yuan, F. Pan, S. Gao, D. Zhang, D. Zhu, *Inorg. Chem.*, 2006, **45**, 3538; (d) C. Kachi-Terajima, H. Miyasaka, K. Sugiura, R. Clérac, H. Nojiri, *Inorg. Chem.*, 2006, **45**, 4381; (e) C. Kachi-Terajima, H. Miyasaka, A. Saitoh, N. Shirakawa, M. Yamashita, R. Clérac, *Inorg. Chem.*, 2007, **46**, 5861; (f) H. Miyasaka, A. Saitoh, S. Abe, *Coord. Chem. Rev.*, 2007, **251**, 2622; (g) Y. Sadawa, W. Kosaka, Y. Hayashi, H. Miyasaka, *Inorg. Chem.*, 2012, **51**, 4824.

[18] (a) C. Train, R. Gheorghe, V. Krstic, L. M. Chamoreau, N. S. Ovanesyan, G. L. J. A. Rikken, M. Gruselle, M. Verdaguer, *Nature Mater.,* 2008, **17**, 729; (b) C. Train, T. Nuida, R. Gheorghe, M. Gruselle, S. Ohkoshi, *J. Am. Chem. Soc.,* 2009, **131**, 16838.

[19] F. M. Ashmawy, C. A. McAuliffe, R. V. Parish, J. Tames, *J. Chem. Soc. Dalton Trans.,* 1985, 1391.

[20] L. Lecren, W. Wernsdorfer, Y. G. Li, A. Vindigni, H. Miyasaka, R. Clérac, *J. Am. Chem. Soc.,* 2007, **129**, 5045.

[21] J. C. Baylar, E. M. Jones, (Ed. H. S. Booth), in *Inorganic Synthesis*, McGraw-Hill, New York, 1939, Vol 5, p. 35.

[22] A. Altomare, M. C. Burla, M. Camalli, G. L. Cascarano, C. Giacovazzo, A. Guagliardi, A. G. G. Moliterni, G. Polidori, R. Spagna, *J. Appl. Cryst*., 1999, **32**, 115.

[23] G. M. Sheldrick, *Acta Crystallogr*., *Sect A: Fundam. Crystallogr.*, 2008, **64**, 112.

[24] L. J. Farrugia, *J. Appl. Cryst.,* 1997, **32**, 837.

[25] H, D. Flack, G. Bernardinelli, *J. Appl. Cryst.,* 2000, **33**, 1143.

[26] M. Clemente-León, E. Coronado, M. López-Jordà, F. Luis, manuscript in preparation.

[27] S. Decurtins, H. W. Schmalle, R. Pellaux, P. Schneuwly, A. Hauser, *Inorg. Chem.*, 1996, **35**, 1451.

[28] N. S. Ovanesyan, V. D. Makhaev, S. M. Aldoshin, P. Gredin, K. Boubekeur, C. Train, M. Gruselle, *J. Chem. Soc., Dalton Trans.*, 2005, 3101.

[29] M. Clemente-León, E. Coronado, M. López-Jordà, *Eur. J. Inorg.*, 2013, 753.

[30] R. S. Fishman, M. Clemente-León, E. Coronado, *Inorg. Chem.,* 2009, **48**, 3039.

[31] G. L. J. A. Rikken, E. Raupach, *Nature,* 1997, **390,** 493.

Insertion of a Single-Molecule-Magnet inside a ferromagnetic lattice based on a 3D bimetallic oxalate network: Towards molecular analogs of permanent magnets

Capítulo 9

Capítulo 9: Insertion of a Single-Molecule Magnet inside a ferromagnetic lattice based on a 3D bimetallic oxalate network: Towards molecular analogs of permanent magnets

ABSTRACT. The insertion of the single-molecule magnet (SMM) $[Mn^{III}(salen)(H_2O)]_2^{2+}$ ($salen^{2-}$ = N,N'-ethylenebis-(salicylideneiminate)) into a ferromagnetic bimetallic oxalate network affords the hybrid compound $[Mn^{III}(salen)(H_2O)]_2[Mn^{II}Cr^{III}(ox)_3]_2\cdot(MeOH)_3\cdot(H_2O)$ (**1**). This cationic Mn_2 cluster templates the growth of crystals formed by an unusual achiral 3D oxalate network. The magnetic properties of this hybrid magnet are compared with those of the analogous compounds $[Mn^{III}(salen)(H_2O)]_2[Zn^{II}Cr^{III}(ox)_3]_2\cdot(MeOH)_3\cdot(H_2O)$ (**2**) and $[In^{III}(sal_2\text{-trien})][Mn^{II}Cr^{III}(ox)_3]\cdot(H_2O)_{0.25}\cdot(CH_3OH)_{0.25}\cdot(CH_3CN)_{0.25}$ (**3**), which are used as reference compounds. In **2** it has been shown that the magnetic isolation between the Mn_2 clusters provided by their insertion into a paramagnetic oxalate network of Cr^{III} affords a SMM behavior with blocking temperatures well below 500 mK. In **3** the ferromagnetism coming from the bimetallic $Mn^{II}Cr^{III}$ network is observed at T_c = 5 K. Finally, in the hybrid compound **1** all the magnetic data are compatible with a coexistence of long-range ferromagnetic order and hysteresis and slow magnetic relaxation, typical of the SMM behavior. Interestigly, the interaction between the two networks induces important changes of the magnetic properties of **1** with respect to those of the reference compounds **2** and **3**.

Introduction

The development of permanent magnets for practical applications, chiefly as components of motors and generators, is oriented towards maximizing the product of the saturation magnetization times the coercive field, parameters that determine the maximum energy density that a magnet can store.[1] In metallic alloys, best performances have been achieved by a combination of 3d metals (Fe or Co), with high saturation magnetizations, and 4f ions such as Nd or Sm, which contribute to enhance the

magnetocrystalline anisotropy and thus also the magnetic coercivity.[2] In these materials, intrinsic relevant physical parameters are determined by composition and crystal structure and therefore the scope for design and improvement is somewhat limited.

Inspired by these materials, here we use a molecular approach, which combines these two ingredients - high saturation magnetizations and large magnetic anisotropy -, to design hybrid materials formed the insertion of a highly anisotropic single-molecule magnet (SMM) into an extended ferromagnetic lattice.

As ferromagnetic sublattice we have chosen the polymeric anionic networks $[M^{II}M^{III}(ox_3)]^{3-}$, which are formed by magnetic ions linked through oxalate ligands. When they contain as trivalent magnetic ions Cr^{III} or Ru^{III}, these bimetallic oxalate-based networks have shown to order as ferromagnets in a wide range of temperatures, ranging from 3 to 14 K, depending on the metal composition.[3] Furthermore, they are stabilized in presence of a bulky charge-compensating molecular cation, which templates the network formation and may add a second physical property of interest.[4,5] Thus, the insertion of different cations has provided many examples of multifunctional materials[6] combining the long-range magnetic ordering from the oxalate network with paramagnetism,[3c,7] photochromism,[8] electric conductivity,[9,10] proton conductivity,[11,12] ferroelectricity,[13] chirality, [14] or spin-crossover.[15] Notice that in these two-network compounds the electronic coupling between the two sublattices is very small and therefore a lack of interplay between the two properties has been observed in all the reported cases. The only exception to this rule has been found in materials combining chirality with magnetic ordering. In this case new properties such as the magneto-chiral dichroic effect and magnetization-induced second harmonic generation have been observed.[16] Still, this exception is only apparent as these two properties - chirality and magnetic ordering - are present in the same sublattice.

As source of magnetic anisotropy we have chosen the dimeric $[Mn^{III}(salen)(H_2O)]_2^{2+}$ ($salen^{2-}$ = N,N'-ethylenebis-(salicylideneiminate)). This type of complexes shows SMM

behavior[17] thanks to their uniaxial magnetic anisotropy with a well-defined easy magnetization axis. Although the $[Mn^{III}(salen)(H_2O)]_2(ClO_4)_2$ precursor itself does not behave as a SMM, because of the influence of interdimer interactions, SMM behavior of this cationic complex has been observed in salts of the bulky diamagnetic polyoxometalate $[XMo_6(OH)_6O_{18}]^{3-}$ (X = Al, Cr).[18] Therefore, the coexistence of the SMM behavior of the inserted $[Mn^{III}(salen)(H_2O)]_2^{2+}$ cation with the magnetic ordering of the oxalate network could be expected, provided that the dimer structure of the precursor is preserved and the dimers remain well isolated in the structure. In a previous work, we reported the insertion of other derivatives of $[Mn^{III}(salen)]^+$ complex into 2D and 3D oxalate-based structures.[19] Unfortunately, the Mn^{III} dimeric structure of the precursors was not preserved in these compounds, thus excluding any SMM behaviour. In contrast with this, the use of a $[Mn^{III}(salen)(H_2O)]_2(ClO_4)_2$ precursor results in the hybrid compound $[Mn^{III}(salen)(H_2O)]_2[Mn^{II}Cr^{III}(ox)_3]_2\cdot(MeOH)_3\cdot(H_2O)$ (**1**), which is formed by an achiral 3D oxalate-based bimetallic network with an inserted Mn_2^{III} dimer. In this work, we show that the interaction between these two constituents drastically modifies their respective magnetic properties with respect to those of the reference compounds $[Mn^{III}(salen)(H_2O)]_2[Zn^{II}Cr^{III}(ox)_3]_2\cdot(MeOH)_3\cdot(H_2O)$ (**2**) and $[In^{III}(sal_2\text{-trien})][Mn^{II}Cr^{III}(ox)_3]\cdot(H_2O)_{0.25}\cdot(CH_3OH)_{0.25}\cdot(CH_3CN)_{0.25}$ (**3**). The magnetic coupling between the two sublattices leads to an antiparallel arrangement between the magnetization of the oxalate lattice and that of the inserted SMM. The coupling effects also the magnetic relaxation of the SMM, which also transfer magnetic anisotropy to the oxalate lattice. As a result, the hybrid material behaves, below 1 K, as a permanent magnet with a relative high coercive field.

Experimental Section

$[Mn^{III}(salen)(H_2O)]_2(ClO_4)_2$ and $(NH_4)_3[Cr^{III}(ox)_3]$ were prepared according to literature methods.[20,21] $Ag_3[Cr^{III}(ox)_3]$ was prepared by metathesis from the corresponding potassium salt.[21] All other materials and solvents were commercially available and used without further purification.

$[Mn^{III}(salen)(H_2O)]_2[Mn^{II}Cr^{III}(ox)_3]_2\cdot(MeOH)_3\cdot(H_2O)$ (1). Crystals of **1** were obtained by slow difussion of two solutions. The first solution was prepared by adding $MnCl_2\cdot 4H_2O$ (0.080 g, 0.41 mmol) to a suspension of $Ag_3Cr(ox)_3$ (0.173 g, 0.27 mmol) in 9 mL of methanol. The AgCl precipitate was filtered. The second solution was obtained by dissolving $[Mn^{III}(salen)(H_2O)]_2(ClO4)_2$ (0.119 g, 0.135 mmol) in 9 mL of acetonitrile (**1**). After two weeks red crystals were obtained. Composition of these crystals, checked by microanalysis, shows a 2:1 Mn:Cr ratio.

$[Mn^{III}(salen)(H_2O)]_2[Zn^{II}Cr^{III}(ox)_3]_2\cdot(MeOH)_3\cdot(H_2O)$ (2). Crystals of **2** were obtained by slow difussion of two solutions. The first solution was prepared by adding $ZnCl_2$ (0.018 g, 0.14 mmol) to a suspension of $(NH_4)_3Cr(ox)_3$ (0.033 g, 0.09 mmol) in 4.5 mL of methanol and filtering. The second solution was obtained by dissolving $[Mn^{III}(salen)(H_2O)]_2(ClO4)_2$ (0.079 g, 0.09 mmol) in 4.5 mL of acetonitrile (**2**). After two weeks red crystals were obtained. Composition of these crystals, checked by microanalysis, shows a 1:1:1 Mn:Zn:Cr ratio.

Structural characterization

Single crystal X-ray data of **1** and **2** were collected at 120 K on a Xcalibur, Sapphire3, Gemini diffractometer equipped with a graphite-monochromated Enhance (Mo) X-ray Source (λ = 0.71073 Å). The program CrysAlisPro, Oxford Diffraction Ltd., was used for cell refinements and data reduction of the compounds. Empirical absorption correction was performed using spherical harmonics, implemented in SCALE3 ABSPACK scaling algorithm. Crystal structure of **1** was solved by direct methods with the SIR97 program,[22] and refined against all F^2 values with the SHELXL-97 program,[23] using the WinGX graphical user interface.[24] Non-hydrogen atoms of **1** were refined anisotropically and hydrogens atoms were placed in calculated positions refined using idealized geometries (riding model) and assigned fixed isotropic displacement parameters. Data collection and refinements statistics are collected in Table 1. **2** diffracted very weakly due to the small size of crystals. Due to this, it was not possible to solve the structure and only

single crystal unit cell measurements are presented in this paper. These measurements show that it is isostructural to **1**.[25]

Physical measurements

Magnetic susceptibility measurements were performed on polycrystalline samples using a magnetometer (Quantum Design MPMS-XL-5) equipped with a SQUID sensor and a physical properties measurement platform (Quantum Design PPMS) equipped with an inductive ac susceptometer. Variable-temperature measurements were carried out in the temperature range 2 - 300 K. AC susceptibility measurements were performed in the temperature range 2 - 10 K by applying a 0.395 mT in amplitude excitation magnetic field oscillating at frequencies $\omega/2\pi$ ranging from 10 to 10^4 Hz. Zero-field ac susceptibility studies were extended to the region of very low temperatures by using two different ac susceptometes, a conventional inductive susceptometer[26] and a micro-SQUID susceptometer installed in ^{3}He-^{4}He dilution refrigerators.[27] Magnetization and hysteresis studies were performed, between 9 and -9 T, using either the above mentioned commercial magnetometers (for T > 1.8 K) or a microHall magnetometer (for 0.4 K < T < 10 K).The Mn:Zn:Cr ratios were measured on a Philips ESEM X230 scanning electron microscope equipped with an EDAX DX-4 microsonde.

Results and discussion

Synthesis

The preparation method of this family of compounds is analogous to that used to synthesize other oxalate-based $[M^{II}M^{III}(ox)_3]$ compounds[5f,10b-g,19]. It is based in a slow diffusion of two phases: a) a methanol solution containing $[Cr(ox)_3]^{3-}$ and Mn^{2+} (Zn^{2+} in **2**), b) a solution of $[Mn^{III}(salen)(H_2O)]_2(ClO_4)_2$ ($[In^{III}(sal_2\text{-trien})]PF6$ in **3**)[15b] in CH_3CN. As a mentioned above, in **1** and **2** the structure of the dimer is preserved in the final compound. This result contrast to what has been observed for Mn^{III}-salen derivatives of higher size such as salmen, salpn or saltmen Mn^{III} complexes, which have been inserted

as monomerics species with two coordinated solvent molecules in the apical positions of the Mn^{III} complex.[19] It seems therefore that only $[Mn^{III}(salen)(H_2O)]_2^{2+}$ present the correct size and stability to template the formation of a 3D oxalate network.

Structure of $[Mn^{III}(salen)(H_2O)]_2[Mn^{II}Cr^{III}(ox)_3]_2\cdot(MeOH)_3\cdot(H_2O)$ (1)

1 crystallizes in the monoclinic centrosymmetric *C2/c* space group. The structure is formed by an anionic 3D polymeric oxalate-bridged bimetallic network. The cavities of this network are occupied by dinuclear $[Mn^{III}(salen)(H_2O)]_2^{2+}$ complexes and by disordered methanol and water solvent molecules. Mn^{II} and Cr^{III} ions from the oxalate network are connected through bis-chelating oxalate ligands in such a way that each Mn^{II} is surrounded by three Cr^{III} and *vice versa*, building ten-membered rings in a (10,3) topology that contains metal centers of both chiralities. A very similar 3D oxalate network has been found in the compounds of formula $[Fe^{III}(sal_2\text{-trien})][Mn^{II}Cr^{III}(ox)_3]\cdot CH_3OH$, $[In^{III}(sal_2\text{-trien})][Mn^{II}Cr^{III}(ox)_3]\cdot(H_2O)_{0.25}\cdot(CH_3OH)_{0.25}\cdot(CH_3CN)_{0.25}$ (**3**) that crystallize in the acentric *Cc* space group.[15b] Indeed, unit cell parameters of the three compounds are very close, indicating that the bimetallic oxalate networks are very similar.[28] The centrosymmetric symmetry of **1**, which is unusual for a 3D oxalate network,[19] may be a consequence of the higher symmetry of the inserted cation, which contains an inversion center, compared with $[Fe^{III}(sal_2\text{-trien})]^+$ or $[In^{III}(sal_2\text{-trien})]^+$. As a result, the achiral bimettalic oxalate network of **1** is formed by only two crystallographically independent metal atoms instead of the four as in $[Fe^{III}(sal_2\text{-trien})][Mn^{II}Cr^{III}(ox)_3]\cdot(CH_3OH)$ and **3**. Metal-oxygen distances in this network lie between 2.060(4) and 2.120(3) Å, which are intermediate between the ones expected for Cr^{III}-O and Mn^{II}-O. Therefore, it is not possible to distinguish between the two metals in the structure. The decagon rings (10,3) perpendicular to the *c* axis are formed by metal centers with the same chirality and are linked to other decagon rings of opposite chirality through oxalate bridges as usual for this type of structure. Therefore, it contains heterochiral and homochiral Mn-Cr junctions. Projections of the structure on the *110*, *ab*, *bc* and *ac* planes are shown in Figures 1 and SS1.

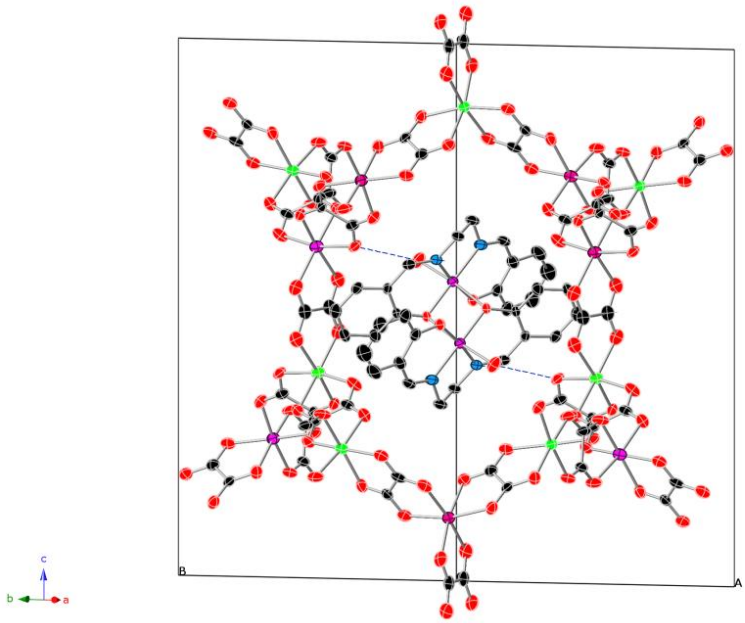

Figure 1. Projection on 110 plane of the structure of **1**; Mn (pink), Cr (green), C (black), N (blue), O (red); neighboring atoms corresponding to disordered Mn/Cr have been assigned as Mn and Cr separately for clarity; hydrogen atoms and disordered solvent molecules have been omitted for clarity. Hydrogen-Bonds are marked as blue dashed lines.

$[Mn^{III}(salen)(H_2O)]_2^{2+}$ dinuclear complexes and disordered water and methanol solvent molecules are intercalated in the holes described by this 3D oxalate network. There is only one crystallographically independent Mn atom (Mn3), which generates the dimer from an inversion center placed at the midpoint of the Mn···Mn vector. The dimer contains two μ-phenoxo bridges from one of the phenolate oxygen atoms of each salen ligand to the opposite metal center. The environment around each metal center in the complex can be described as a distorted octahedron in which the four equatorial positions are occupied by the N_2O_2 atoms of the quadridentate Schiff base ligand. One apical position is occupied by one water molecule (O1W), while the other one is occupied by a phenolate oxygen atom from the adjacent Mn^{III} complex of the dimer (O1). The equatorial Mn-O and Mn-N distances are 1.858(3)-1.905(3) Å and 1.972(4)-1.981(3) Å respectively, which are much shorter than the apical ones (Mn3-O1' distance

of 2.366(3) Å and Mn3-O1W of 2.198(3) Å) due to Jahn-Teller distortion as usual for this type of complexes. These distances are close to those found in $[Mn^{III}(salen)(H_2O)]_2^{2+}$ salts of $[XMo_6(OH)_6O_{18}]^{3-}$ (X = Al, Cr) polyoxometalate, which show SMM behavior, and significantly shorter than those of the ClO_4^- precursor salt[18] or other $[SiW_{12}O_{40}]^{4-}$ polyoxometalate salts not showing SMM behavior.[29]

Table 1 Crystallographic data of **1**.

Empirical formula	$C_{23.5}H_{14}CrMn_2N_2O_{17}$
Formula weight	758.25
Crystal color	Orange
Temperature (K)	120
Wavelength (*Å*)	0.71073
Crystal system, Z	Monoclinic, 8
Space group	*C*2/c
a (Å)	21.7488(6)
b (Å)	14.1837(5)
c (Å)	22.9477(7)
β (º)	92.190(3)
V (Å^3)	7073.7(4)
ρcalc (Mg/m^3)	1.424
μ($Mo_{K\alpha}$) (mm^{-1})	1.073
θ range (°)	2.44 to 32.54
Reflns collected	55567
Independent reflns, (R_{int})	12159 (0.1380)
L. S. parameters/ restraints	413/3
$R1(F)$,[a] $I>2\sigma(I)$]	0.0563
$wR2(F^2)$,[b] all data	0.1712
$S(F^2)$,[c] all data	0.769

[a] $R1(F) = S(||F_O| - |F_C||)/S|F_O|$; [b] $wR2(F^2) = [Sw(F_O^2 - F_C^2)^2/SwF_O^4]^{1/2}$; [c] $S(F^2) = [Sw(F_O^2 - F_C^2)^2/(n - p)]^{1/2}$

Water molecules from $[Mn^{III}(salen)(H_2O)]_2^{2+}$ form hydrogen-bonds with oxygen atoms from $[Mn^{II}Cr^{III}(ox)_3]^-$ network and methanol solvent molecules (see Figure 1). $[Mn^{III}(salen)(H_2O)]_2^{2+}$ dimers do not present hydrogen-bonds or π···π stacking interaction with other $[Mn^{III}(salen)(H_2O)]_2^{2+}$ dimers. There is only one short intermolecular contact between $[Mn^{III}(salen)(H_2O)]_2^{2+}$ dimers, which is due to C-H··· π interactions between two phenoxy rings.[30] In any case, the shorter interdimer Mn···Mn distance is 11.477 Å, which is longer than thant found for other salts of $[Mn^{III}(salen)(H_2O)]_2^{2+}$ presenting a SMM behavior (8.49 Å for $[Mn^{III}(salen)(H_2O)]_2$ $Na[AlMo_6(OH)_6O_{18}]\cdot(H_2O)$.[18] In conclusion, the insertion of these dinuclear complexes into the 3D bimetallic oxalate network provides a good magnetic isolation between these magnetic molecules. Unit cell measurements of crystal **2** show that it is isostructural to **1**.[25]

Magnetic properties

The spin of the two magnetic sublattices that form this compound are $S(Mn^{2+}) = 5/2$, $S(Cr^{3+}) = 3/2$, and $S([Mn^{III}(salen)(H_2O)]_2) = 4$, all with $g \approx 2$. In order to separately study the magnetic response of each sublattice, i.e. the inserted Mn^{III} dimeric cluster and the 3D bimetallic oxalate network, we have measured the magnetic properties of following samples; a) $[Mn^{III}(salen)(H_2O)]_2[Zn^{II}Cr^{III}(ox)_3]_2\cdot(MeOH)_3\cdot(H_2O)$ (**2**), formed by a Mn^{III} dimer inserted into a paramagnetic network, b) $[In^{III}(sal_2\text{-trien})][Mn^{II}Cr^{III}(ox)_3]\cdot(H_2O)_{0.25}\cdot(CH_3OH)_{0.25}\cdot(CH_3CN)_{0.25}$ (**3**), formed by a diamagnetic complex inserted into a ferromagnetic $Mn^{II}Cr^{III}$ network. Therefore, magnetic characterization of **2**, **3** and **1**, may enable to characterize separately the SMM behavior of the inserted cluster, the ferromagnetic behavior of the oxalate-based network and, finally, the interplay between these two magnetic lattices. We next give the results obtained for these three samples.

SMM behavior of 2: The zero-field ac magnetic susceptibility of this sample was measured, down to very low temperatures, via a combination of two set-ups: a commercial SQUID magnetometer and a microSQUID ac susceptometer installed inside the mixing chamber of a ^3He-^4He dilution refrigerator. The latter works between 20 mK and 2 K for frequencies in the range 10^{-2} Hz < $\omega/2\pi$ < 1MHz. The results are shown in

Figure 2. They show the typical SMM behavior, that is, a frequency-dependent superparamagnetic blocking of the in-phase susceptibility component χ' accompanied by maxima of the out-of-phase component χ''.

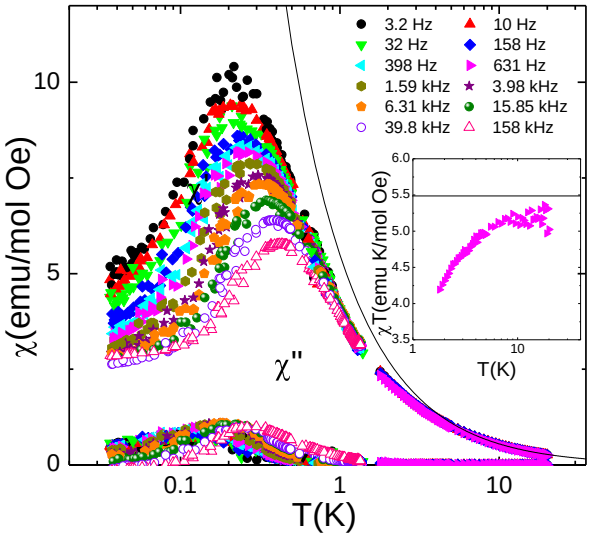

Figure 2. AC magnetic susceptibility of **2** measured at several frequencies. The inset shows $\chi'T$ measured at 631 Hz above 1 K. The solid lines give the theoretical paramagnetic contributions

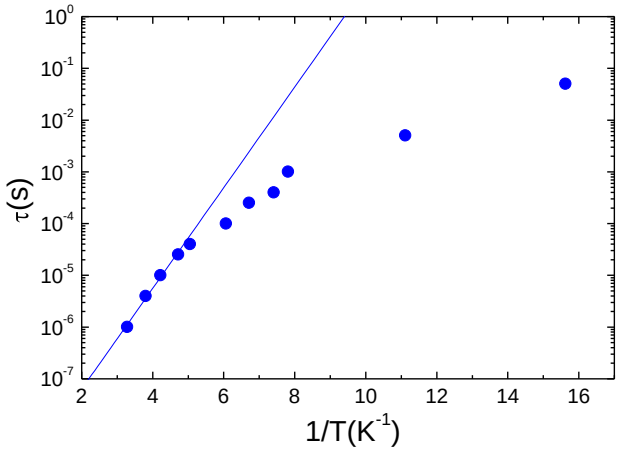

Figure 3. Arrhenius plot of the spin-lattice relaxation time of **2**. The solid line is a least-squares linear fit giving $U/k_B = 2.24$ K and $\tau_0 = 7\times10^{-10}$ s.

The Arrhenius plot obtained from these data is shown in Figure 3. Above T ≈ 0.2 K, it approximately follows Arrhenius law, with an activation energy U/k_B = 2.24 K and a pre-factor τ_0 = 7x10^{-10} s. Below 0.2 K, the effective energy barrier gradually decreases, probably marking the onset of a relaxation regime dominated by a temperature-independent process. The activation energy found by us is much smaller than the values reported previously for polyoxomethalate salts of $[Mn^{III}(salen)(H_2O)]_2^{2+}$, which range approximately from 10 to 23 K.[18,29] It is worth noticing, however, that these values were measured in the presence of magnetic fields, which block spin tunneling processes slowing down the magnetic relaxation. As we discuss next, a magnetic field also affects very strongly the spin dynamics of **2**.

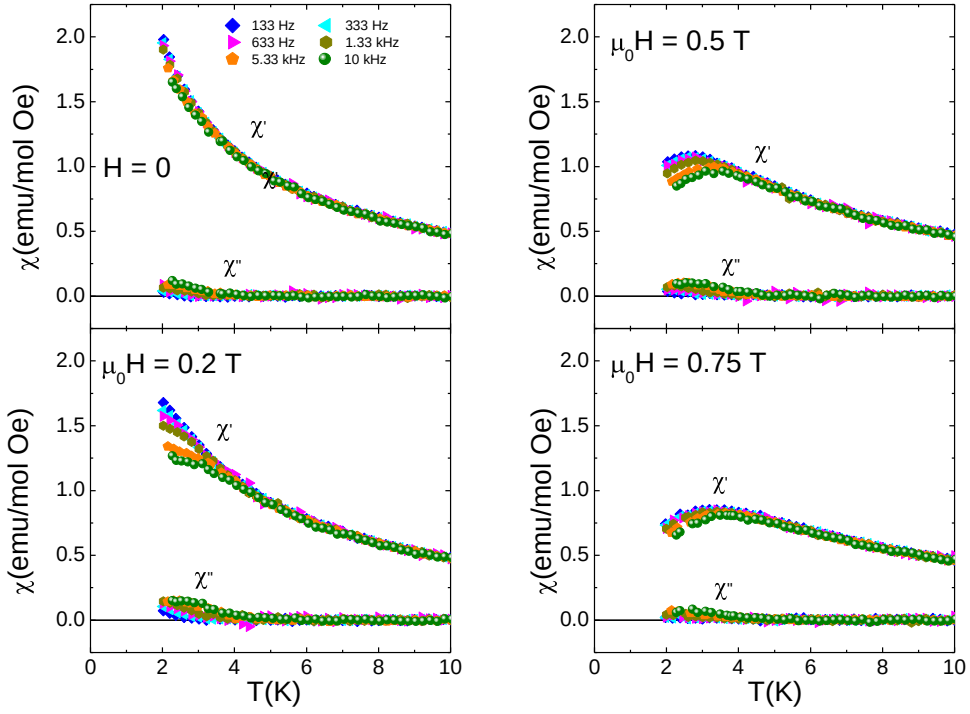

Figure 4. AC magnetic susceptibility of **2** measured at several frequencies and under different magnetic fields.

The temperature dependence of the ac susceptibility measured in the presence of dc magnetic fields *H* of varying intensity is shown in Figure 4. These data show the onset of the SMM behavior, although the maxima of χ'' become visible only for the highest frequencies ($\omega/2\pi$ > 1kHz). The blocking temperature, obtained from χ'' maxima measured at $\omega/2\pi$ = 10 kHz, is shown in Figure 5 as a function of *H*. These results reveal that *H* exerts a dramatic influence on the magnetic relaxation mechanisms. With increasing *H*, the susceptibility blocking shifts towards higher temperatures and then back again towards lower temperatures. This behavior, characteristic of many SMM, is compatible with a relaxation process involving quantum tunneling between magnetic states of opposite spin orientation. Tunneling dominates magnetic relaxation at sufficiently low fields, when such states are close to degenerate in energy. However, it becomes gradually blocked by the action of bias magnetic fields. Eventually, when tunneling is suppressed for all levels, relaxation must proceed via a (classical) thermally activated process above the magnetic anisotropy barrier, whose characteristic time decreases with increasing *H*.

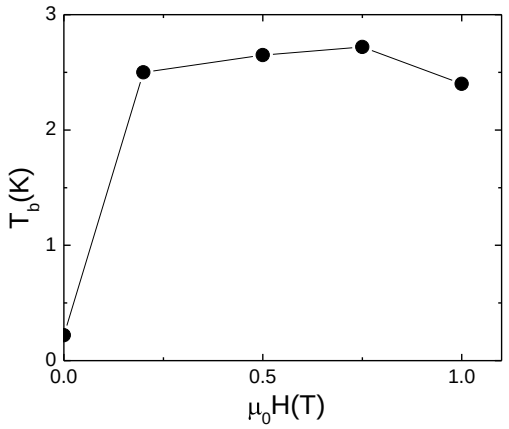

Figure 5. Superparamagnetic blocking temperature of **2** measured at a frequency $\omega/2\pi$ = 10 kHz.

Figure 6 shows the frequency-dependence of χ'' data measured at T = 2 K, normalized by the equilibrium susceptibility χ_T that has been obtained as the derivative

of the magnetization isotherm measured at the same temperature. Although the magnetic relaxation remains rather fast at any field (the χ'' maximum is always beyond the maximum attainable frequency of 10 kHz), it is clear that the magnetic relaxation time first increases with increasing H, for $0 < \mu_0 H < 0.5$ T, and then decreases, for higher fields intensities. Relaxation times determined from temperature and frequency dependent data measures at H = 0.5 T are also shown in Figure 6. They follow Arrhenius law with U/k_B = 30(3) K and $\tau_0 = 2\text{x}10^{-10}$ s. The activation energy is more than ten times larger than the value found at H = O, in full agreement with our interpretation, and even larger than the highest value of 23 K found for $[Mn^{III}(salen)(H_2O)]_2^{2+}$ and similar clusters in polyoxometalate lattices.[29] It is also possible to estimate roughly the second-order magnetic anisotropy parameter D from the relation $U = -DS^2$, which gives, D/k_B = -1.8 K for S = 4 or, equivalently, a magnetic anisotropy field $H_A = (2S\text{-}1)/g\cdot\mu_B$ = 9.3 T.

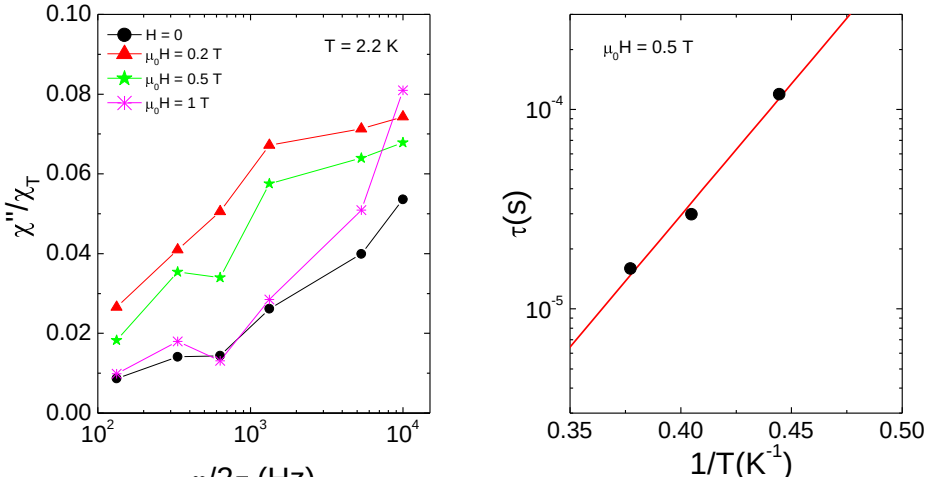

Figure 6. Left: Imaginary component of the ac susceptibility of **2** measured at T = 2.2 K for several intensities of the dc magnetic field H. Right: Arrhenius plot measured at $\mu_0 H$ = 0.5 T. The solid line is a least-squares linear fit that gives U/k_B = 30(3) K and $\tau_0 = 2\times10^{-10}$ s.

Although it is difficult to determinate the field-dependence of τ from ac susceptibility data because magnetic relaxation is too fast at almost any value of H (see

Figure 6), it is still possible to extract some qualitative information using the dependence of χ' and χ'' on *H*, which is shown in Figure 7 for T = 2 K. We observe, at any ω, that χ' first deviates from its equilibrium value χ_T and then it approaches it again. This dependence confirms that, upon increasing *H*, τ first increases (below approximately 0.2 T) and then it decreases. A rough estimate of τ can be obtained from the relaxation $\tau = \chi''/\omega\chi'$, which applies when the condition $\omega\tau << 1$ is fulfilled, as is approximately the case here, at least for $\omega/2\pi$ < 10kHz (remember Figure 6). Results obtained for $\omega/2\pi$ = 1.33 kHz confirm the expected dependence of τ on *H* and, thus, also our physical interpretation of the susceptibility data.

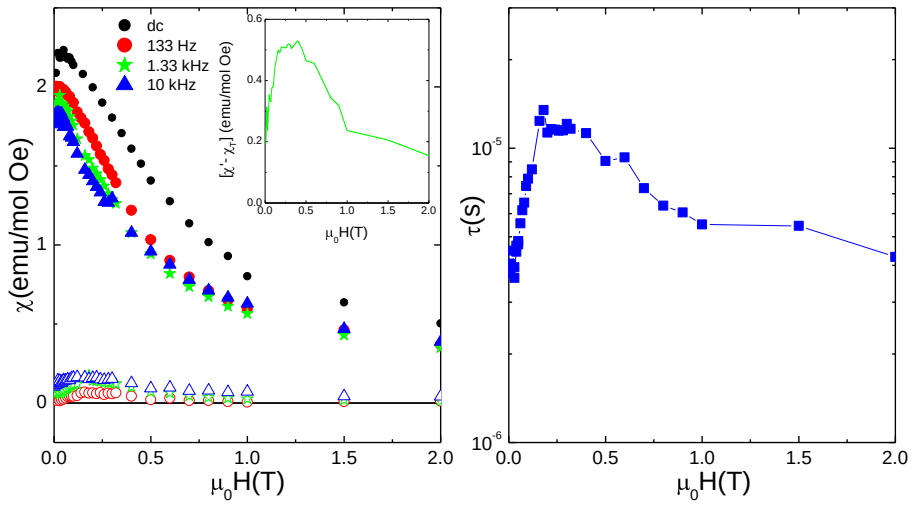

Figure 7. Left: AC susceptibility of **2** measured at T = 2 K as a function of *H*. Equilibrium (dc) data correspond to the numerical derivative of the isothermal magnetization curve measured at the same temperature (see below). The inset shows the difference between the equilibrium susceptibility and χ' measured at $\omega/2\pi$ = 1.33 kHz. Right: characteristic relaxation time determined from the relation $\tau = \chi''/\omega\chi'$ using data measured at $\omega/2\pi$ = 1.33 kHz.

Finally, Figure SS2 shows magnetization isotherms measured at several temperatures on a powdered sample of **2**. These curves are reasonably well reproduced by calculations done using a second-order anisotropy parameter D/k_B = -0.6 K, in a good

agreement with the value estimated from the fitting of the relaxation times. The differences between theory and experimental can be attributed to the presence of off-diagonal anisotropy terms, i.e. those involved in the tunneling phenomena observed at very low T.

Ferromagnetism of 3: The ac magnetic susceptibility of this sample has already been published.[15b] It shows a sharp peak near T = 5 K, which signals the onset of ferromagnetism with $\chi'' \neq 0$ in the ferromagnetic phase as usual for this family of compounds.[15] The ferromagnetic character of the ordered phase is confirmed by the magnetic field dependence of χ' and χ'', shown in Figure 8. Even relatively weak dc magnetic fields $H \sim 500$ Oe completely suppress the χ' divergence, as expected for a ferromagnetic phase transition. Notice that χ'' tends to vanish in the presence of a magnetic field, showing that magnetic relaxation processes become also considerably faster.

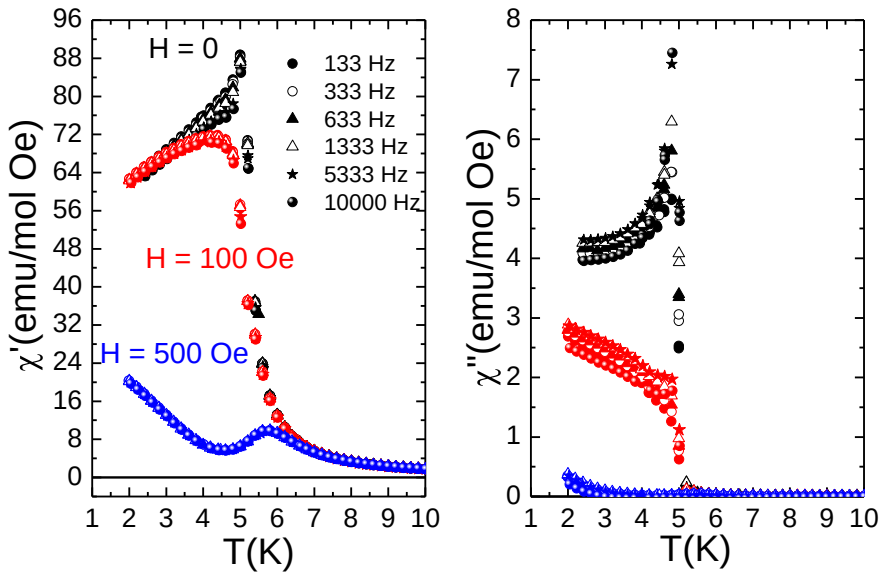

Figure 8. AC magnetic susceptibility (left, real component, right, imaginary component) of **3** measured at several frequencies and under the action of a dc magnetic field.

Interplay between SMM and ferromagnetism in 1: The ac susceptibility of this sample is shown in Figure 9. Data for 0.09 K < T < 2 K were measured using a home-made inductive ac susceptometer installed in a ^{3}He-^{4}He dilution refrigerator. As with the ferromagnetism **3** compound, the onset of ferromagnetism near 5 K is osbserved. It seems therefore that the insertion of the Mn_2 clusters has little effect on the Curie temperature (T_c) as observed for other 3D compounds with similar structure containing paramagnetic cations, which also present T_c close to that of **3**.[15b,c] Qualitatively, the magnetic susceptibilities of **1** and **3** are rather close to each other, as expected if one takes into account that the main contribution to χ' and χ'' arises from the strong response of the ferromagnetic fraction. The main difference is that χ' of the compound containing the Mn_2 SMM cluster (**1**) shows, between 2 and 5 K, a stronger variation with frequency than that of **3**. In addition, χ'' of **1** shows additional maxima between 2 and 4 K, which also show a strong dependence on frequency. This dependence can be fitted using an Arrhenius law with an effective activation energy U/k_B = 22(1) K and a prefactor $\tau_0 = 7\times10^{-9}$ s (see Figure 10).

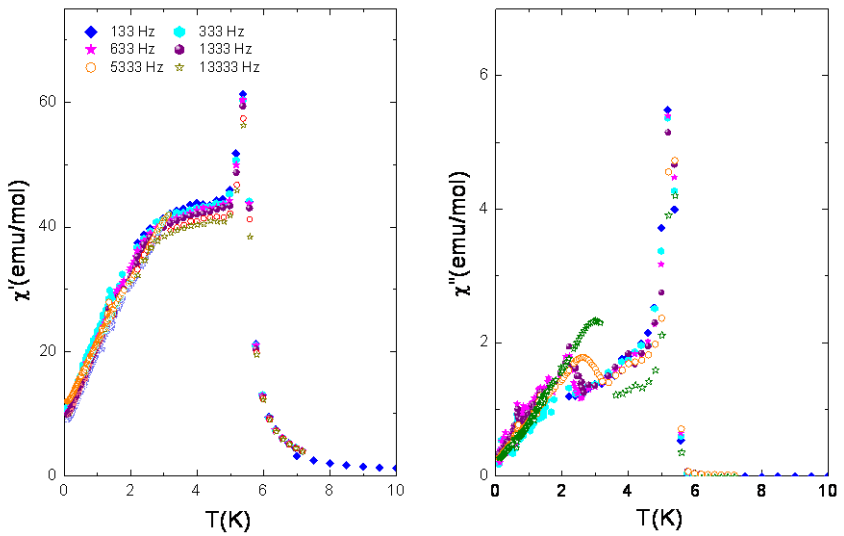

Figure 9. Real (left) and imaginary (right) components of the AC magnetic susceptibility of **1** measured at H = 0 and for several frequencies

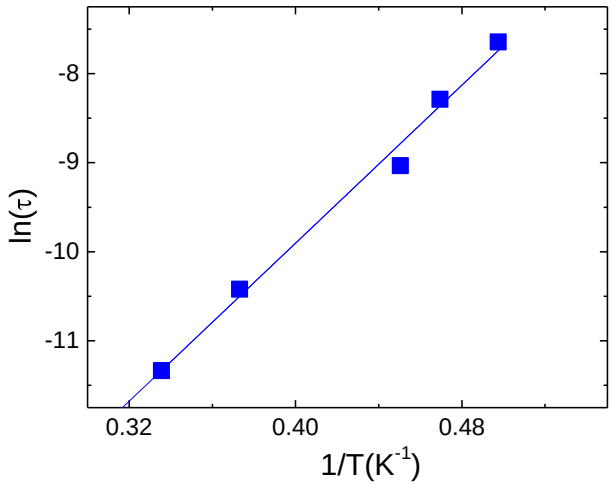

Figure 10. Arrhenius plot of **1** obtained from the frequency dependence of χ" maxima observed below 4 K. The solid line is a least-squares linear fit giving U/k_B = 22(1) K and $\tau_0 = 7\times10^{-9}$ s.

It is tempting to attribute the differences in the ac susceptibilities of **1** and **3** to a slow magnetic relaxation induced by the Mn_2 clusters. Yet, the magnetic response of **1** above 2 K constrasts sharply with the behavior of the isolated clusters (i.e. that measured on sample **2**, see Figure 2), which show blocking temperatures well below 500 mK, even for very high frequencies. Notice, however, that the ferromagnetic network generates, below T_c, a strong magnetic field on the sites occupied by the Mn_2 SMMs. This magnetic field likely slows down the spin reversal of the clusters. Indeed, magnetic measurements of **2** show that a magnetic field of about 0.2 T would be sufficient to shift the susceptibility blocking to temperatures close to 2-3 K (see Fig. 5 above).

Further evidence on the influence that the ferromagnetic oxalate network and the Mn_2 clusters exert on each other is provided by magnetization isotherms measured at T = 2.2 K, i. e. below T_c, which are shown in Fig. 11. Interestingly, these data clearly show that the magnetization of **1** is not a simple superposition of magnetization of each of the two components forming this hybrid material. At low fields ($\mu_0 H$ < 0.04 T), it increases linearly with a high slope, typical of a ferromagnetic material and associated with the displacement of domain walls.[15b,c] This initial ferromagnetic response is also observed in

compounds with inserted diamagnetic cations, such as **3**. There are, however, some important differences between these two. First, whereas after this linear regime, the magnetization of **3** is very close to saturation (8 μ_B as expected for one Mn(II) and one Cr(III) ions), the magnetization of **1** attains a much smaller value of about 3 μ_B. And second, the magnetization of **1** shows, above 0.05 T, a gradual and nonlinear increase, overcoming 10 μ_B at $\mu_0 H$ = 8 T. This increase cannot be fully ascribed to spin canting in the oxalate lattice. In **3**, for instance, spin canting gives rise to a magnetization change of less than 1 μ_B between $\mu_0 H$ = 0 and 5 T. These two properties can instead be associated with an antiferromagnetic coupling between the Mn_2-salen nanomagnets and the ferromagnetic oxalate network. At zero field, and below T_c, the hybrid would show a ferrimagnetic structure. Within this model, the saturation magnetization of the hybrid amounts to M_s = 5 μ_B + 3 μ_B - 4 μ_B = 4 μ_B, possibly reduced by spin canting effects in the oxalate network, which is not far from the magnetization attained by **1** at low magnetic fields.

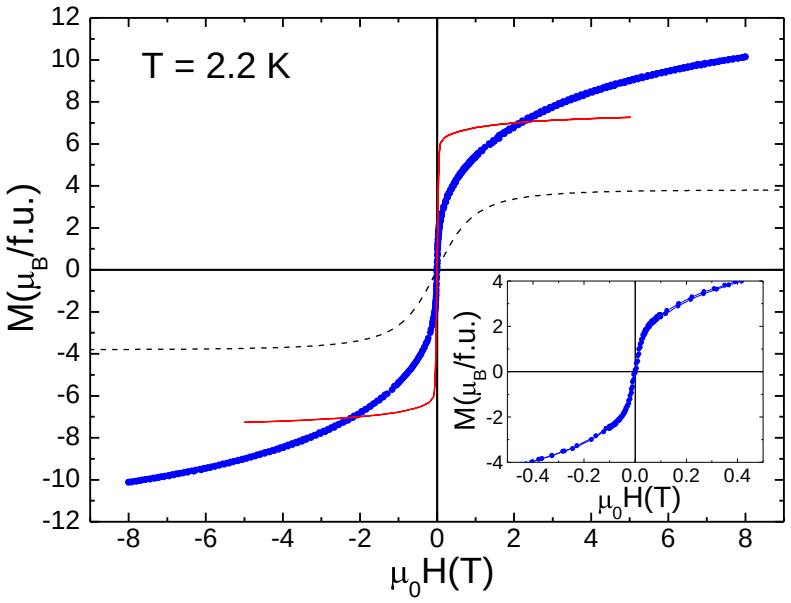

Figure 11. Magnetization isotherm of **1** (solid blue dots) and of **3** (solid red dots) measured at T = 2.2 K, that is, below T_c. The dashed black line shows the calculated paramagnetic response of Mn_2 salen clusters.

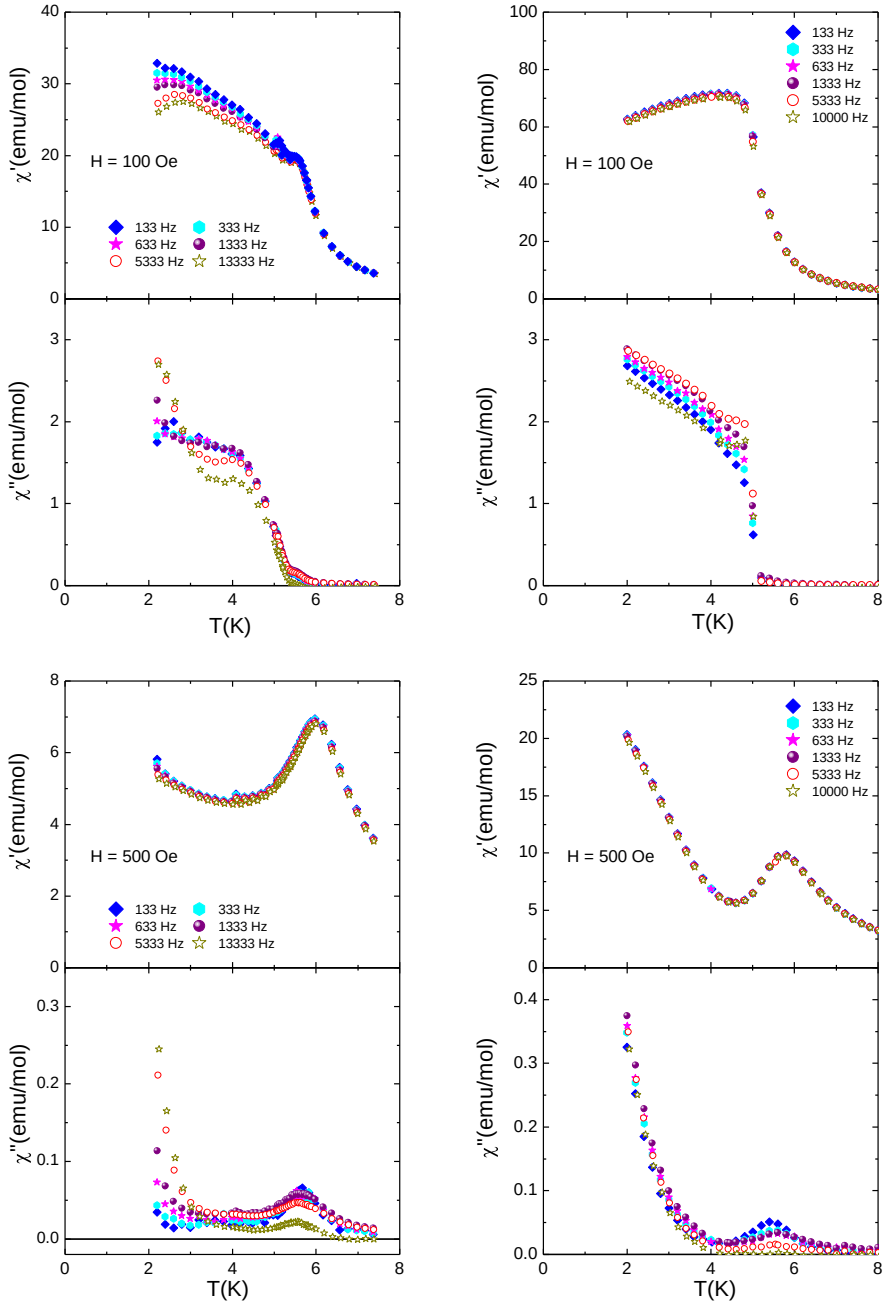

Figure 12. AC magnetic susceptibility of **1** measured at *H* = 100 Oe and 500 Oe and for several frequencies (left), compared with that measured on **3** (right).

The gradual nonlinear increase observed at high fields would result from the competition between the antiferromagnetic couplings and the Zeeman interaction with the external magnetic field, combined with the strong magnetic anisotropy of the clusters. This antiferromagnetic interaction could be mediated by the hydrogen bond between the water molecule coordinated to Mn(III) and one oxalate group described in the structural part (Fig. 1). Similar interactions between Mn_2 clursters, which involve a hydrogen bond with a water molecule coordinated to Mn(III), have been reported in the literature.[31]

The differences between the magnetic responses of the hybrid materials **1** and **3** manifest themselves also in the ac susceptibilities measured under a magnetic field (Fig. 12). As also happens at $H = 0$ (see Fig. 9), χ' of **1** depends more strongly on ω than that of the pure ferromagnetic compound **3**. It follows from these results that the magnetization dynamics is slowed down, with respect to those measured on the reference materials **2** and **3** by the mutual interaction between the Mn_2 clusters and the ferromagnetic oxalate network.

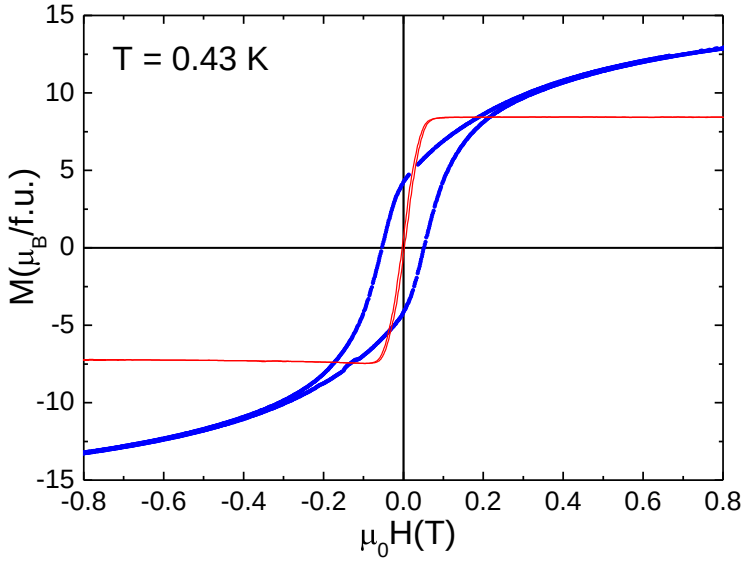

Figure 13. Magnetization hysteresis loops of **1** (solid blue dots) and of **3** (solid red line) measured at T = 0.43 K. the sweeping field rate was 6 mT/s.

A direct manifestation of this effect, shown in Figure 13, is the onset, below 1 K, of a large magnetization hysteresis in the hybrid material 1, which contrast sharply with the close to reversible behavior observed in the pure ferromagnetic compound 3.

As before, it is possible to estimate the characteristic magnetic relaxation time of the hybrid in the low-T region using the ratio $\chi''/\chi'\omega$. τ first increases with *H*, for *H* < 100 Oe, and then decreases again (Figure 14). This dependence agrees with the behavior of the Mn_2 clusters inserted into a paramagnetic oxalate network in the neighborhood of 0.2-0.3 T (Fig. 7). Again, this result is compatible with the fact that the interaction between Mn_2 and the ferromagnetic network efficiently suppresses quantum tunneling processes.

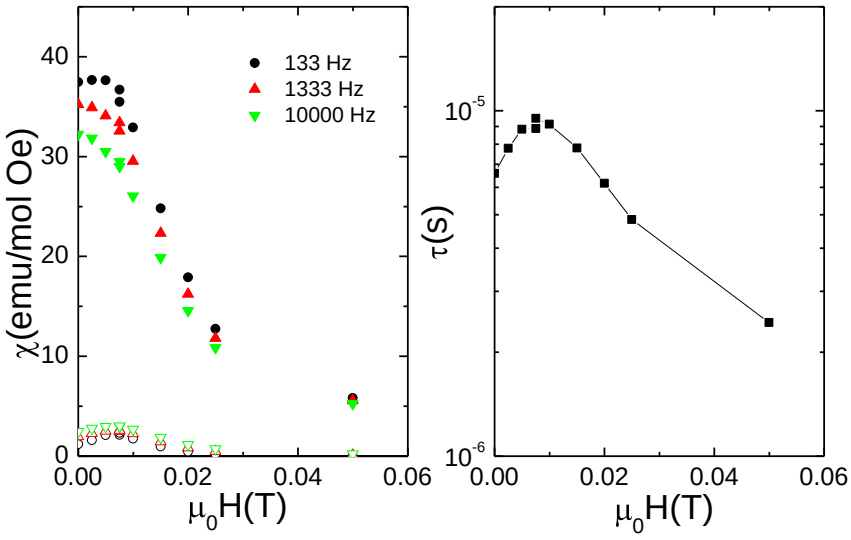

Figure 14. Left: AC magnetic susceptibility of **1** measured at T = 2 K vs *H* for several frequencies. Right: characteristic spin-lattice relaxation time obtained as $\tau \sim \chi''/\omega\chi'$ using data measured at $\omega/2\pi$ = 1333 Hz.

Conclusions

The insertion of $[Mn^{III}(salen)(H_2O)]_2^{2+}$ into bimetallic oxalate networks has given rise to an achiral 3D oxalate network in $[Mn^{III}(salen)(H_2O)]_2[Mn^{II}Cr^{III}(ox)_3]_2\cdot(MeOH)_3\cdot(H2O)$ (**1**) and $[Mn^{III}(salen)(H_2O)]_2[Zn^{II}Cr^{III}(ox)_3]_2\cdot(MeOH)_3\cdot(H2O)$ (**2**). The dimeric structure of the precursors is preserved in contrast to the use of larger Mn^{III}-salen derivatives, which lead to the insertion of Mn^{III} monomeric species into 2D or 3D oxalate networks. Therefore, the synthesis of these compounds represents the first successful attempt to insert a SMM molecule into a 3D oxalate network. In this context, we should point out that SMMs have already been inserted in other extended networks such as the TaS_2 layered superconductor.[32] Still, in these hybrid materials the SMM behavior does not seem to be influenced by the presence of the superconducting sublattice.

In the present case we have demonstrate the interplay between the SMM behavior and the ferromagnetism of the bimetallic oxalate network. Low-temperature magnetic characterization has shown that the magnetic isolation between the Mn_2 clusters provided by their insertion into a paramagnetic oxalate network affords a SMM behavior with blocking temperatures well below 500 mK in **2**. In the hybrid **1**, all magnetic data are compatible with a coexistence of long-range magnetic order, characteristic of the oxalate network, and a slow magnetic relaxation, typical of SMMs. Hoewever, the interaction between these two constituents drastically modifies their respective magnetic properties with respect to those of the reference compounds **2** and **3**, which present the separate properties of the SMM cluster and the ferromagnetic network resperctively. Thus, the coupling changes the spin dynamics of the Mn_2 clusters. In particular, in the ordered state the internal magnetic field generated by the MnCr oxalate network efficiently suppresses relaxation mechanisms mediated by quantum tunneling. In addition to this, the insertion of Mn_2 clusters into the MnCr oxalate network changes the ferromagnetism of the latter, which inherits the magnetic anisotropy and slow relaxation of the former. In particular, at low fields, the hybrid shows ferrimagnetic order resulting from the antiparallel arrangement of Mn_2 salen

nanomagnets and the magnetization of the oxalate lattice. In addition, the hybrid shows a large magnetization hysteresis below 1 K. This situation, which is totally new in the hybrid magnetic materials based on bimetallic oxalate lattices, resembles that found in alloys of 3d metals and lanthanide ions that, like $NdFe_{14}B$, are among the best permanent mangets known to date. The combination of extended molecular networks with long-range ferromagnetism, preferably above room temperature, and strongly anisotropic SMMs can therefore offer original possibilities for the design of molecule-based magnets with practical value.

Acknowledgment

Finantial support from the European Union (Project HINTS and ERC Advanced Grant SPINMOL), the Spanish MINECO (Project Consolider-Ingenio in Molecular Nanoscience CSD2007-00010, and projects MAT2011-22785 and CTQ-2011-26507), and the Generalitat Valenciana (Prometeo and ISIC-NANO Programs) are gratefully acknowledged. The authors also thank J. M. Martínez-Agudo, University of Valencia, for the magnetic measurements.

References

[1] R. Skomski, J. M. D. Coey, In *Permanent Magnetism*; Institute of Physics Publishing; Bristol, 1999.

[2] (a) R. K. Mishra, G. Thomas, T. Yoneyama, A. Fukuno, T. Ojima, *J. Appl. Phys.,* 1981, **52**, 2517; (b) M. Sagawa, S. Fujimura, M. Togawa, Y. Matsuura, *J. Appl. Phys.,* 1984, **55**, 2083.

[3] (a) H. Tamaki, Z. J. Zhong, N. Matsumoto, S. Kida, M. Koikawa, N. Achiwa, Y. Hashimoto, H. Okawa, *J. Am. Chem. Soc.,* 1992, **114**, 6974; (b) E. Coronado, J. R. Galán-Mascarós, C. J. Gómez-García, J. M. Martínez-Agudo, E. Martínez-Ferrero, J. C. Waerenborgh, M. Almeida, *J. Solid State Chem.*, 2001, **159**, 391; (c) E. Coronado, J. R. Galán-Mascarós, C. J. Gómez-García, J. Ensling, P. Gutlich, *Chem. Eur. J.,* 2000, **6**, 552.

[4] (a) H. Tamaki, M. Mitsumi, N. Nakamura, N. Matsumoto, S. Kida, H. Okawa, S. Ijima, *Chem. Lett.,* 1992, 1975; (b) C. Mathonière, S. G. Carling, D. Yuscheng, P. Day, *J. Chem. Soc. Chem. Commun.*, 1994, 1551; (c) C. Mathonière, J. Nutall, S. G. Carling, P. Day,

Inorg. Chem., 1996, **35**, 1201; (d) R. Pellaux, H. W. Schmalle, R. Huber, P. Fisher, T. Hauss, B. Ouladdiaf, S. Decurtins, *Inorg. Chem.*, 1997, **36**, 2301; (e) K. S.Min, A. L. Rhinegold, J. S. Miller, *Inorg. Chem.*, 2005, **44**, 8433; (f) E. Coronado, J. R. Galán-Mascarós, C. Martí-Gastaldo, *J. Mater. Chem.*, 2006, **16**, 2685 ; (g) Z. Duan, Y. Zhang, B. F. Zhang, L. Pratt, *Inorg. Chem.*, 2009, **48**, 2140.

[5] (a) S. Decurtins, H. W. Schmalle, P. Schneuwly, H. R. Oswald, *Inorg. Chem.*, 1993, **32**, 1888; (b) S. Decurtins, H. W. Schmalle, P. Schneuwly, J. Ensling, P. Gütlich, *J. Am. Chem. Soc.*, 1994, **116**, 9521; (c) M. Hernández-Molina, F. Lloret, C. Ruiz-Pérez, M. Julve, *Inorg. Chem.*, 1998, **37**, 4131; (d) E. Coronado, J. R. Galán-Mascarós, C. J. Gómez-García, J. M. Martínez-Agudo, *Inorg. Chem.*, 2001, **40**, 113; (e) F. Pointillart, C. Train, M. Gruselle, F. Villain, H. W. Schmalle, D. Talbot, P. Gredin, S. Decurtins, M. Verdaguer, M. *Chem. Mater.*, 2004, **16**, 832; (f) M. Clemente-León, E. Coronado, C. J. Gómez-García, A. Soriano-Portillo, *Inorg. Chem.*, 2006, **45**, 5653.

[6] M. Clemente-León, E. Coronado, C. Martí-Gastaldo, F. M. Romero, *Chem. Soc. Rev.*, **2011**, *40*, 473.

[7] (a) M. Clemente-León, J. R. Galán-Mascarós, C. J. Gómez-García, *Chem. Commun.*, 1997, 1727; (b) E. Coronado, J. R. Galán-Mascarós, C. J. Gómez-García, J. M. Martínez-Agudo, *Adv. Mater.*, 1999, **11**, 558.

[8] (a) S. Bénard, P. Yu, J. P. Audière, E. Rivière, R. Clèment, J. Ghilhem, L. Tchertanov, K. Nakatami, *J. Am. Chem. Soc.*, 2000, **122**, 9444; (b) S. M. Aldoshin, N. A. Sanina, V. I. Minkin, N. A. Voloshin, V. N. Ikorskii, V. I. Ovcharenko, V. A. Smirnov, N. K. Nagaeva, *J. Mol. Struct.*, 2007, **826**, 69.

[9] (a) E. Coronado, J. R. Galán-Mascarós, C. J. Gómez-García, V. Laukhin, *Nature*, 2000, **408**, 447; (b) A. Alberola, E. Coronado, J. R. Galán-Mascarós, C. Giménez-Saiz, C. J. Gómez-García, *J. Am. Chem. Soc.*, 2003, **125**, 10774; (c) E. Coronado, J. R. Galán-Mascarós, C. J. Gómez-García, E. Martínez-Ferrero, S. Van Smaalen, *Inorg. Chem.*, 2004, **43**, 4808 ; (d) *B.* Zhang, Y. Zhang, D. Zhu, *Chem. Commun.*, 2012, **48**, 197.

[10] J. R. Galán-Mascarós, E. Coronado, P. A. Goddard, J. Singleton, A. I. Coldea, J. D. Wallis, S. J. Coles, A. Alberola, *J. Am. Chem. Soc.*, 2010, **132**, 9271.

[11] (a) H. Okawa, A. Shigematsu, M. Sadakiyo, T. Miyagawa, K. Yoneda, M. Ohba, H. Kitagawa, *J. Am. Chem. Soc.*, 2009, **131**, 13516; (b) M. Sadayiko, H. Okawa, A. Shigematsu, M. Ohba, T. Yamada, H. Kitagawa, *J. Am. Chem. Soc.*, 2012, **134**, 5472 ; (c) H. Okawa, M. Sadakiyo, T. Yamada, M. Maesato, M. Ohba, H. Kitagawa, *J. Am. Chem. Soc.*, 2013, **135**, 2256.

[12] E. Pardo, C. Train, G. Contard, K. Boubekeur, O. Fabelo, H. Liu, B. Dkhil, F. Lloret, K. Nakagawa, H. Tokoro, S.-I. Ohkoshi, M. Verdaguer, *J. Am. Chem. Soc.*, 2011, **133**, 15328.

[13] (a) T. Endo, T. Akutagawa, S. I. Noro, T. Nakamura, *Dalton Trans.*, 2011, **40**, 1491; (b) E. Pardo, C. Train, H. Liu, L.-M. Chamoreau, B. Dkhil, K. Boubekeur, F. Lloret, K. Nakatani, H. Tokoro, S.-I. Ohkoshi, M. Verdaguer, *Angew. Chem., Int. Ed*., 2012, **51**, 8356.

[14] (a) R. Andrés, M. Gruselle, B. Malézieux, M. Verdaguer, J. Vaissermann, *Inorg. Chem.*, 1999, **38**, 4637 ; (b) R. Andrés, M. Brissard, M. Gruselle, C. Train, J. Vaissermann, B. Malézieux, J. P. Jamet, M. Verdaguer, *Inorg. Chem.*, 2001, **40**, 4633; (c) M. Clemente-León, E. Coronado, J. C. Dias, A. Soriano-Portillo, R. D. Willett, *Inorg. Chem.*, 2008, **47**, 6458.

[15] (a) M. Clemente-León, E. Coronado, M. C. Giménez-López, A. Soriano-Portillo, J. C. Waerenborgh, F. S. Delgado, C. Ruiz-Pérez, *Inorg. Chem.*, 2008, **47**, 9111; (b) M. Clemente-León, E. Coronado, M. López-Jordà, G. Mínguez Espallargas, A. Soriano-Portillo, J. C. Waerenborgh, *Chem. Eur. J*., 2010, **16**, 2207; (c) M. Clemente-León, E. Coronado, M. López-Jordà, *Dalton Trans.*, 2010, **39**, 4903; (d) M. Clemente-León, E. Coronado, M. López-Jordà, J. C. Waerenborgh, *Inorg. Chem.*, 2011, **50**, 9122; (e) M. Clemente-León, E. Coronado, M. López-Jordà, C. Desplanches, S. Asthana, H. Wang, J.-F. Létard, *Chem. Sci.*, 2011, **2**, 1121; (f) M. Clemente-León, E. Coronado, M. López-Jordà, *Eur. J. Inorg. Chem.*, 2013, 753; (g) A. Ben Djamâa, M. Clemente-León, E. Coronado, M. López-Jordà, *Polyhedron* 2013 doi: http://dx.doi.org/10.1016/j.poly.2013.03.015.

[16] (a) C. Train, R. Gheorghe, V. Krstic, L. M. Chamoreau, N. S. Ovanesyan, G. L. J. A. Rikken, M. Gruselle, M. Verdaguer, *Nat. Mater.*, 2008, **7**, 729; (b) C. Train, T. Nuida, R. Gheorghe, M. Gruselle, S. Ohkoshi, *J. Am. Chem. Soc.*, 2009, **131**, 16838.

[17] (a) H. Miyasaka, R. Clérac, W. Wernsdorfer, L. Lecren, C. Bonhomme, K. Sugiura, M. Yamashita, *Angew. Chem., Int. Ed.*, 2004, **43**, 2801; (b) H. J. Choi, J. J. Sokol, J. R. Long, *Inorg. Chem.*, 2004, **43**, 1606; (c) M. Ferbinteanu, H. Miyasaka, W. Wernsdorfer, K. Nakata, K. Sugiura, M. Yamashita, C. Coulon, R. Clérac, *J. Am. Chem. Soc.*, 2005, **127**, 3090; (d) *Z.* Lü, M. Yuan, F. Pan, S. Gao, S. Zhang, D. Zhu, *Inorg. Chem.*, 2006, **45**, 3538; (e) C. Kachi-Terajima, H. Miyasaka, K. Sugiura, R. Clérac, H. Nojiri, *Inorg. Chem.*, 2006, **45**, 4381; (f) C. Kachi-Terajima, H. Miyasaka, A. Saitoh, N. Shirakawa, M. Yamashita, R. Clérac, *Inorg. Chem.*, 2007, **46**, 5861; (g) H. Miyasaka, A. Saitoh, S. Abe, *Coord. Chem. Rev.*, 2007, **251**, 2622.

[18] Q. Wu, Y.-G. Li, Y.-H. Wang, R. Clérac, Y. Lu, E.-B. Wang, *Chem. Commun.*, **2009**, 5743.

[19] M. Clemente-León, E. Coronado, M. López-Jordà, *Dalton Trans.*, 2013, **42**, 5100.

[20] F. M. Ashmawy, C. A. McAuliffe, R. V. Parish, J. Tames, *J. Chem. Soc., Dalton Trans.*, 1985, 1391.

[21] J. C. Baylar, E. M. Jones, *Inorganic Synthesis*; H. S. Booth, Ed. McGraw-Hill: New York, 1939; Vol. 1, p 35.

[22] A. Altomare, M. C. Burla, M. Camalli, G. L. Cascarano, C. Giacovazzo, A. Guagliardi, A. G. G. Moliterni, G. Polidori, R. Spagna, *J. Appl. Cryst*., 1999, **32**, 115.

[23] SHELXL-97: G. M. Sheldrick, University of Göttingen, Germany, 1997.

[24] L. J. Farrugia, *J. Appl. Cryst.*, 1999, **32**, 837.

[25] Unit cell of **2** at 120 K: a = 21.54(2) Å, b = 13.99(2) Å, c = 22.73(3) Å; β = 91.71(3)°; V = 6903.0(7) Å^3.

[26] A. Morello, F. L. Mettes, O. N. Bakharev, H. B. Brom, L. J. de Jongh, F. Luis, J. F. Fernández, G. Aromí, *Phys. Rev. B*, 2006, **73**, 134406.

[27] (a) M. J. Martínez-Pérez, J. Sesé, F. Luis, D. Drung, T. Schurig, *J. Appl. Phys.*, 2010, **81**, 016108; (b) M. J. Martínez-Pérez, E. Bellido, R. de Miguel, J. Sesé, A. Lostao, C. Gómez-Moreno, D. Drung, T. Schurig, D. Ruiz-Molina, F. Luis, *Appl. Phys. Lett.*, 2011, **99**, 032504.

[28] Unit cell of [Fe(sal$_2$-trien)][MnCr(ox)$_3$]·(CH$_3$OH) at 120 K and **3** at 150 K taken from reference 15b are respectively: a = 21.9180(9) Å, b = 14.0330(9) Å, c = 22.4670 (15) Å; β = 92.639(4)°; V = 6903.0(7) Å^3; and a = 21.5690(7) Å, b = 14.1590(7) Å, c = 22.7360(9) Å; β = 91.116(2)°; V = 6942.5(5) Å^3.

[29] Y. Sadawa, W. Kosaka, Y. Hayashi, H. Miyasaka, *Inorg. Chem.*, 2012, **51**, 4824.

[30] C. Janiak, *J. Chem. Soc., Dalton Trans.*, 2000, 3885.

[31] L. Lecren, W. Wernsdorfer, Y.-G. Li, A. Vindigni, H. Miyasaka, R. Clérac, *J. Am. Chem. Soc.*, 2007, **129**, 5045.

[32] E. Coronado, C. Martí-Gastaldo, E. Navarro-Moratalla, E. Burzuri, E. Camon, F. Luis, *Adv. Mater.*, 2011, **23**, 5021.

Conclusiones finales y perspectivas

Capítulo 10

Capítulo 10: Conclusiones finales y perspectivas

En esta tesis se ha presentado la síntesis y caracterización de materiales multifuncionales basados en redes de oxalato que combinan el ordenamiento magnético de la red de oxalatos con una segunda propiedad. En concreto, se ha obtenido y caracterizado una familia de compuestos con complejos de transición de espín del tipo $[Fe^{III}(sal_2\text{-trien})]^+$ insertados en redes bimetálicas de oxalato. Además, se ha obtenido y caracterizado otra familia de compuestos formados por la inserción de complejos de bases de Schiff de Mn^{III} del tipo $[Mn(salen)]^+$ que pueden presentar un comportamiento de molécula imán. Los resultados más relevantes son los siguientes:

1- La utilización del complejo $[Fe^{III}(sal_2\text{-trien})]^+$ ha dado lugar, dependiendo de las condiciones de síntesis, a dos estructuras diferentes. En un caso se obtiene un compuesto de fórmula $[Fe^{III}(sal_2\text{-trien})][Mn^{II}Cr^{III}(ox)_3]\cdot CH_2Cl_2$ que presenta una estructura 2D. Las propiedades magnéticas de este compuesto nos indican la coexistencia de una transición de espín completa entre 150 y 350 K y un ordenamiento magnético a 5.6 K. El segundo compuesto $[Fe^{III}(sal_2\text{-trien})][Mn^{II}Cr^{III}(ox)_3]\cdot 0.75CH_3OH \cdot 0.5H_2O$, presenta una estructura 3D aquiral, con una transición de espín parcial y ordenamiento magnético a 5.2 K. La presencia de dos estructuras diferentes con el mismo complejo es un hecho inusual en la química de este tipo de compuestos que atribuimos a la flexibilidad que presenta el ligando orgánico del complejo $[Fe^{III}(sal_2\text{-trien})]^+$ al verse rodeado por las moléculas de disolvente. Estas pequeñas diferencias en la configuración del complejo parecen ser suficientes para dirigir el crecimiento de una red de oxalatos de forma distinta en los diferentes disolventes.

2- La estrategia utilizada nos ha permitido combinar en el compuesto $[Fe^{III}(sal_2\text{-trien})][Mn^{II}Cr^{III}(ox)_3]\cdot CH_2Cl_2$ dos propiedades que raramente aparecen juntas en un material, orden magnético y una transición de espín completa, aunque en intervalos de temperatura muy distintos. Para buscar una interacción entre estas dos propiedades, se ha intentado inducir la transición de espín mediante la luz (efecto

LIESST). La caracterización fotomagnética ha puesto de manifiesto que el compuesto presenta efecto LIESST por debajo de 42 K. Aunque la transición de espín fotoinducida no modifica de forma significativa la temperatura de ordenamiento magnético de la red bidimensional de oxalatos, el efecto LIESST de este compuesto es un resultado importante ya que este efecto es muy poco frecuente en complejos de Fe^{III}.

3- Para comprender, modular y extender este comportamiento se han sintetizado análogos del compuesto $[Fe^{III}(sal_2\text{-trien})][Mn^{II}Cr^{III}(ox)_3]\cdot CH_2Cl_2$ en otros disolventes halogenados ($CHCl_3$, CH_2Br_2 y $CHBr_3$). Los compuestos obtenidos de fórmula $[Fe^{III}(sal_2\text{-trien})][Mn^{II}Cr^{III}(ox)_3]\cdot CH_2Br_2$, $[Fe^{III}(sal_2\text{-trien})][Mn^{II}Cr^{III}(ox)_3]\cdot CHBr_3$, $[Fe^{III}(sal_2\text{-trien})][Mn^{II}Cr^{III}(ox)_3]\cdot CHCl_3$, mantienen la misma estructura 2D. El cambio de CH_2Cl_2 por disolventes más voluminosos aumenta la distancia interlaminar entre las capas de oxalato y disminuye la presión química sobre el compuesto de transición de espín insertado. Esto hace que la $T_{1/2}$ se desplace a temperaturas más bajas y por consiguiente la T_{LIESST} se desplaza a valores mayores. Por tanto, este sutil cambio estructural permite modular las temperaturas de transición de espín termo y fotoinducida lo que convierte a esta familia en un sistema modelo donde poder estudiar en detalle el efecto LIESST en complejos de Fe^{III}. De hecho, la versatilidad de estos compuestos ha permitido diluir el complejo de Fe^{III} con otros complejos similares de Ga^{III} que son diamagnéticos y que además no presentan bandas de absorción en el visible. Esto ha permitido estudiar la evolución de la transición de espín del complejo de Fe^{III} aislado por métodos espectroscópicos en el compuesto $[Ga_{0.99}Fe_{0.01}(sal_2\text{-trien})][Mn^{II}Cr^{III}(ox)_3]\cdot CH_2Cl_2$ que, al igual que el compuesto puro, presenta una transición de espín con la temperatura y efecto LIESST. La dilución del compuesto de Fe^{III} provoca que la transición de espín térmica sea más gradual. Además, al absorber menos luz en el visible, permite fotoexcitar un mayor número de complejos de Fe^{III}, a diferencia del compuesto puro en el que sólo es posible fotoexcitar el 40 %. Este resultado demuestra que para observar el efecto LIESST en un compuesto de Fe^{III} no es necesario tener cooperatividad en el sistema, lo que contrasta con los otros compuestos de Fe^{III} con efecto LIESST conocidos.

4- El análisis estructural de estos compuestos nos permite dilucidar los distintos factores que están implicados en la aparición del efecto LIESST en complejos de Fe^{III}. En los compuestos preparados con anterioridad, el $[Fe^{III}(pap)_2]ClO_4$ por ejemplo, el efecto LIESST se relacionó con la presencia de un ligando tridentado rígido que impone una geometría octaédrica muy distorsionada y con los efectos cooperativos originados por la presencia de fuertes interacciones intermoleculares del tipo π-π. Por el contrario, en los compuestos obtenidos en esta tesis que contienen un ligando más flexible, el origen del efecto LIESST estaría más relacionado, además de con la distorsión del octaedro en el estado de alto espín, con la presencia de la red 2D de oxalatos que es más rígida y establece numerosas interacciones intermoleculares con los complejos de Fe^{III} insertados.

5- En los compuestos derivados del complejo $[Fe^{III}(sal_2\text{-trien})^+$, se han obtenido distintos tipos de redes 2D o 3D en función del tipo y posición de los sustituyentes. Introduciendo un grupo nitro (NO_2) en la posición 5 del anillo aromático, se obtiene el compuesto $[Fe^{III}(5\text{-}NO_2\text{-}sal_2trien)][Mn^{II}Cr^{III}(ox)_3]\cdot MeNO_2\cdot 0.5H_2O$. Estos grupos favorecen interacciones de apilamiento π-π, lo que da lugar a una red 2D. Por otro lado, introduciendo grupos más voluminosos, como CF_3O/CH_3O en la misma posición se obtienen redes 3D aquirales en los compuestos $[Fe^{III}(5\text{-}CH_3O\text{-}sal_2trien)][Mn^{II}Cr^{III}(ox)_3]$ y $[Fe^{III}(5\text{-}CF_3O\text{-}sal_2trien)][Mn^{II}Cr^{III}(ox)_3]$, mientras que con grupos sustituyentes más pequeños, como Cl o Br, se produce un apilamiento helicoidal de los complejos de Fe^{III} que da lugar a una nueva estructura 3D quiral en los compuestos $[Fe^{III}(5\text{-}Cl\text{-}sal_2trien)][Mn^{II}Cr^{III}(ox)_3]\cdot 0.5MeNO_2$, $[Fe^{III}(5\text{-}Br\text{-}sal_2trien)][Mn^{II}Cr^{III}(ox)_3]$ y $[In^{III}(5\text{-}Cl\text{-}sal_2trien)][Mn^{II}Cr^{III}(ox)_3]$. Estos compuestos presentan un ordenamiento magnético alrededor de 5 K junto con la transición de espín térmica parcial. La única excepción se observa en los compuestos $[Fe^{III}(5\text{-}CH_3O\text{-}sal_2trien)][Mn^{II}Cr^{III}(ox)_3]$ y $[Fe^{III}(5\text{-}NO_2\text{-}sal_2trien)][Mn^{II}Cr^{III}(ox)_3]\cdot MeNO_2\cdot 0.5H_2O$, que permanecen en el estado de alto y bajo espín, respectivamente, entre 2 y 300 K. Por último, en los compuestos $[Fe^{III}(5\text{-}Cl\text{-}sal_2trien)][Mn^{II}Cr^{III}(ox)_3]\cdot 0.5MeNO_2$, $[Fe^{III}(5\text{-}Br\text{-}sal_2trien)][Mn^{II}Cr^{III}(ox)_3]$ y $[In^{III}(5\text{-}Cl\text{-}sal_2trien)][Mn^{II}Cr^{III}(ox)_3]$ se aporta una tercera propiedad al material

multifuncional, que es la quiralidad de la red. En estos sistemas la interacción de la quiralidad de la red con el ordenamiento magnético puede dar lugar a nuevas propiedades físicas como el dicroísmo magnetoquiral. Este aspecto se examinará en el futuro.

6- Con derivados de $[Fe^{III}(sal_2\text{-trien})]^+$ con sustituyentes en las posiciones 3 o 4, se ha obtenido los compuestos de fórmula $[Fe^{III}(4\text{-Br-sal}_2\text{trien})][Mn^{II}Cr^{III}(ox)_3]_{0.67}\cdot Cl_{0.33}\cdot MeOH$, $[Fe^{III}(3\text{-Cl-sal}_2\text{trien})][Mn^{II}Cr^{III}(ox)_3]\cdot(CH_3OH)_2\cdot(CH_3CN)_2$, $[Fe^{III}(3\text{-Br-sal}_2\text{trien})][Mn^{II}Cr^{III}(ox)_3]\cdot(CH_3CN)_2$, y $[Fe^{III}(3\text{-MeO-sal}_2\text{trien})][Mn^{II}Cr^{III}(ox)_3]\cdot(CH_3OH)\cdot(H_2O)_{1.5}\cdot(CH_2Cl_2)_{0.5}$, que presentan una estructura 2D. Todos ellos muestran un ordenamiento magnético alrededor de 5 K que coexiste con una transición de espín completa entre 300 y 400 K para $[Fe^{III}(4\text{-Br-sal}_2\text{trien})][Mn^{II}Cr^{III}(ox)_3]_{0.67}\cdot Cl_{0.33}\cdot MeOH$ y transiciones de espín parciales para $[Fe^{III}(3\text{-Cl-sal}_2\text{trien})][Mn^{II}Cr^{III}(ox)_3]\cdot(CH_3OH)_2\cdot(CH_3CN)_2$ y $[Fe^{III}(3\text{-Br-sal}_2\text{trien})][Mn^{II}Cr^{III}(ox)_3]\cdot(CH_3CN)_2$. El compuesto $Fe^{III}(3\text{-MeO-sal}_2\text{trien})][Mn^{II}Cr^{III}(ox)_3]\cdot(CH_3OH)\cdot(H_2O)_{1.5}\cdot(CH_2Cl_2)_{0.5}$ permanece en estado de alto espín entre 2 y 300 K. En dos de estos complejos se ha observado la presencia de poros en la estructura ocupados por moléculas de disolvente, lo que podría dar lugar a otros tipos de propiedades como absorción de disolventes o conducción de protones, recientemente observada en otras redes de oxalato.

7- En los compuestos 2D obtenidos con derivados de $[Fe^{III}(sal_2\text{-trien})]^+$, $[Fe^{III}(5\text{-NO}_2\text{-sal}_2\text{trien})][Mn^{II}Cr^{III}(ox)_3]\cdot MeNO_2\cdot 0.5H_2O$, $[Fe^{III}(4\text{-Br-sal}_2\text{trien})][Mn^{II}Cr^{III}(ox)_3]_{0.67}\cdot Cl_{0.33}\cdot MeOH$, $[Fe^{III}(3\text{-Cl-sal}_2\text{trien})][Mn^{II}Cr^{III}(ox)_3]\cdot(CH_3OH)_2\cdot(CH_3CN)_2$ no se observa el efecto LIESST. Las razones que pueden explicar la ausencia del efecto LIESST en estos compuestos son: (a) una $T_{1/2}$ demasiado alta; (b) la pequeña fracción de Fe^{III} que presenta transición de espín, y (c) la ausencia de interacciones fuertes con la red de oxalatos. Resultados preliminares de la caracterización espectroscópica del compuesto 3D quiral $[In^{III}(5\text{-Cl-sal}_2\text{trien})][Mn^{II}Cr^{III}(ox)_3]$ dopado con un 1 % de Fe muestran una relajación lenta del estado de alto espín fotoinducido, aunque mucho más rápida que la del compuesto $[Fe^{III}(sal_2\text{-trien})][Mn^{II}Cr^{III}(ox)_3]\cdot CH_2Cl_2$, lo que puede dificultar la

observación del efecto LIESST en este compuesto con un magnetómetro de tipo SQUID. Este resultado es prometedor porque el ordenamiento magnético de las redes 3D es mucho más sensible al tamaño del catión insertado, lo que abriría una posibilidad de modular el orden magnético de la red de oxalatos mediante irradiación del compuesto.

8- Por último, se han insertado complejos de Mn^{III} de $[Mn^{III}(salen)]^+$ y derivados en redes bimetálicas de oxalato, obteniendo una gran variedad de estructuras. El complejo $[Mn^{III}(salen)]^+$ da lugar al compuesto de fórmula $[Mn^{III}(salen)(H_2O)]_2[Mn^{II}Cr^{III}(ox)_3]_2\cdot(MeOH)_3\cdot(H_2O)$ y al análogo con una red paramagnética de fórmula $[Mn^{III}(salen)(H_2O)]_2[Zn^{II}Cr^{III}(ox)_3]_2\cdot(MeOH)_3\cdot(H_2O)$ formados por dímeros $[Mn^{III}(salen)(H_2O)]_2^{2+}$ insertados en una red 3D aquiral muy parecida a la obtenida con $[Fe^{III}(sal_2\text{-trien})]^+$. La conservación de la estructura del dímero de Mn^{III} del precursor permite observar un comportamiento de imán unimolecular en el compuesto paramagnético de Zn^{II}, aunque sólo a muy bajas temperaturas (por debajo de 0.5 K). La caracterización magnética del compuesto ferromagnético de Mn^{III} es consistente con la coexistencia de un ordenamiento magnético alrededor de 5 K y un comportamiento de imán unimolecular. Un resultado importante con este material es la observación de una interacción entre la red bimetálica de oxalatos y las moléculas imán que se manifiesta en el comportamiento magnético a bajas temperaturas. Esto abre una nueva estrategia molecular para la preparación de imanes permanentes y que consiste en introducir en un material ferromagnético una molécula imán que incorpora una alta anisotropía magnética. Por otro lado, cuando se utilizan derivados de $[Mn^{III}(salen)]^+$, en lugar de estabilizarse el dímero, se estabilizan los monómeros de Mn^{III} unidos a la base de Schiff tetradentada con dos moléculas de disolvente. Algunos de estos compuestos como $[Mn((R)\text{-salmen})(CH_3OH)_2][MnCr(ox)_3]\cdot(CH_2Cl_2)_{0.375}\cdot(CH_3OH)_{0.125}\cdot(H_2O)_{0.375}$ y $[Mn((S)\text{-salmen})(CH_3OH)_2][MnCr(ox)_3]\cdot(CH_2Cl_2)_{0.375}\cdot(CH_3OH)_{0.375}\cdot(H_2O)_{0.125}$ presentan estructuras 3D aquirales totalmente distintas a las obtenidas con anterioridad. El resultado más prometedor lo constituyen los compuestos $[Mn((R)\text{-salmen})(CH_3OH)(CH_3CN)][MnCr(ox)_3]\cdot(CH_3OH)_{0.5}\cdot(CH_3CN)_{1.25}$ y $[Mn((S)\text{-salmen})(CH_3OH)(CH_3CN)][MnCr(ox)_3]\cdot(CH_3OH)_{0.5}\cdot(CH_3CN)_{1.25}$, con una estructura 2D quiral, que

se pueden obtener de forma enantioméricamente pura eligiendo el precursor de quiralidad adecuada (*R* o *S*). Esto puede facilitar el estudio de nuevos fenómenos físicos derivados de la interacción entre orden magnético y quiralidad como el dicroísmo magnetoquiral antes mencionado.

Chapter 10: Concluding remarks and perspectives

In this thesis the synthesis and characterization of multifunctional oxalate-based networks that combine magnetic ordering from oxalate network with a second property has been presented. Specifically, a family of compounds with spin transition complexes $[Fe^{III}(sal_2\text{-trien})]^+$ inserted into bimetallic oxalate networks has been obtained and characterized. Furthermore, another family of compounds formed by the insertion of the Schiff base complexes of Mn^{III}, $[Mn^{III}(salen)]^+$ and derivatives, with single molecule magnet (SMM) behavior has also been obtained and characterized. The most important results are:

1- The use of the complex $[Fe^{III}(sal_2\text{-trien})]^+$ has led, depending on the synthesis conditions, to two different structures. In one case a compound of formula $[Fe^{III}(sal_2\text{-trien})][Mn^{II}Cr^{III}(ox)_3]\cdot CH_2Cl_2$ that shows a 2D honeycomb structure. The magnetic properties of this compound indicate the coexistence of a complete spin crossover between 150 and 350 K and a long-range ferromagnetic ordering of the oxalate networks at 5.6 K. The second compound $[Fe^{III}(sal_2\text{-trien})][Mn^{II}Cr^{III}(ox)_3]\cdot 0.75CH_3OH\cdot 0.5H_2O$ shows an achiral 3D structure, with a partial spin transition and magnetic order at 5.2 K. The presence of two different structures with the same complex is not common in the chemistry of this type of compounds. We think that this is related to the flexibility of the organic ligand of $[Fe^{III}(sal_2\text{-trien})]^+$ complex when it is surrounded by solvent molecules. These small differences in the complex configuration appear to be sufficient to direct the growth of different oxalate networks in different solvents.

2- This strategy has allowed us to combine, in the $[Fe^{III}(sal_2\text{-trien})][Mn^{II}Cr^{III}(ox)_3]\cdot CH_2Cl_2$ compound, two properties that rarely appear together in the same material, the magnetic ordering of the oxalate network and a complete spin transition, although in different ranges of temperature. To find an interaction between these two properties, we have tried to induce the spin transition through light (LIESST effect). The

photomagnetic characterization has shown that the compound present LIESST effect below 42 K. Although the photoinduced spin transition does not change significantly the magnetic ordering temperature of the bidimensional oxalate network, LIESST effect of this compound is an important result since this effect is rarely observed in Fe^{III} complexes.

3- Analogues of $[Fe^{III}(sal_2\text{-trien})][Mn^{II}Cr^{III}(ox)_3]\cdot CH_2Cl_2$ compound have been synthesized with another halogenated solvents ($CHCl_3$, CH_2Br_2 y $CHBr_3$) to understand, tune and extended this behavior. The compounds obtained of formula $Fe^{III}(sal_2\text{-trien})][Mn^{II}Cr^{III}(ox)_3]\cdot CH_2Br_2$, $[Fe^{III}(sal_2\text{-trien})][Mn^{II}Cr^{III}(ox)_3]\cdot CHBr_3$, $[Fe^{III}(sal_2\text{-trien})][Mn^{II}Cr^{III}(ox)_3]\cdot CHCl_3$, maintain the same 2D structure. The change of CH_2Cl_2 by a bulkier solvent, increases interlamellar distance between the layers of the oxalate network and reduces the chemical pressure on the inserted spin crossover compound. This induces a shift of $T_{1/2}$ to lower temperatures and therefore a shift of T_{LIESST} to larger values. Hence, this subtle change allows tuning the spin crossover temperature of the thermal and photoinduced spin-crossover providing a model system for studying in detail the LIESST effect in Fe^{III} complexes. In fact, the versatility of these compounds has allowed us to dilute Fe^{III} complex with similar but diamagnetic Ga^{III} complex, which does not present absorption bands in the visible. This has shown to be a suitable strategy to study the evolution of the spin transition of isolated Fe^{III} complex by spectroscopic methods in the compound $[Ga_{0.99}Fe_{0.01}(sal_2\text{-trien})][Mn^{II}Cr^{III}(ox)_3]\cdot CH_2Cl_2$ that, as the pure compound, presents a spin transition and LIESST effect. The dilution of the Fe^{III} complexes causes a more gradual spin transition. Furthermore, in contrast to the magnetic measurements on the pure Fe crystals, for which a light induced HS fraction of only 0.4 could be achieved, in the very dilute system it proved possible to achieve a quantitative population of the HS state. This is due to the comparatively weak optical density of the dilute crystals, which results in a good penetration and propagation of the light through the crystal, whereas the strong absorption of the pure Fe crystals only results in the photo-excitation of the complexes close to the surface and not in the bulk. These measurements on diluted samples confirm that, in contrast to other Fe^{III}

complexes presenting LIESST effect prepared previously, cooperativity is not necessary condition to observe the LIESST effect in Fe^{III} complexes, as cooperativity is excluded in these doped systems due to the long distances between the Fe^{III} centers.

4- Structural analysis of these compounds and other Fe^{III} complexes indicates that several factors may explain the LIESST effect in Fe^{III} complexes. In the case of $[Fe^{III}(pap)_2]^+$ complexes, the presence of a rigid tridentate ligand that induces a distorted octahedral geometry together with strong π-π interactions between the Fe^{III} complexes could be at the origin of this effect, while in the $[Fe^{III}(sal_2\text{-trien})]^+$ complexes reported in this thesis, which contain a more flexible ligand, it could be related to the interactions with a bimetallic oxalate extended network in addition to octahedral distortion in high spin state

5- The compounds obtained with derivatives of $[Fe^{III}(sal_2\text{-trien})]^+$, present different kinds of 2D and 3D oxalate networks depending on the type and position of substituents on the aromatic ring. A nitro group (NO_2) in the 5 position, favours π-π stacking interactions which give rise to a 2D network in $[Fe^{III}(5\text{-}NO_2\text{-}sal_2trien)][Mn^{II}Cr^{III}(ox)_3]\cdot MeNO_2\cdot 0.5H_2O$ compound. On the other hand, introducing bulky groups, as CF_3O or CH_3O in the same position, leads to achiral 3D networks in $[Fe^{III}(5\text{-}CH_3O\text{-}sal_2trien)][Mn^{II}Cr^{III}(ox)_3]$ and $[Fe^{III}(5\text{-}CF_3O\text{-}sal_2trien)][Mn^{II}Cr^{III}(ox)_3]$ compounds. Finally, smaller substituent groups, such as Cl or Br, favour an helical arrangements of Fe^{III} complexes, which result in a new chiral 3D structure in $[Fe^{III}(5\text{-}Cl\text{-}sal_2trien)][Mn^{II}Cr^{III}(ox)_3]\cdot 0.5MeNO_2$, $[Fe^{III}(5\text{-}Br\text{-}sal_2trien)][Mn^{II}Cr^{III}(ox)_3]$ and $[In^{III}(5\text{-}Cl\text{-}sal_2trien)][Mn^{II}Cr^{III}(ox)_3]$ compounds. These compounds show a magnetic ordering of the oxalate network about 5 K together with a partial thermal spin transition. The only exception is observed in $[Fe^{III}(5\text{-}CH_3O\text{-}sal_2trien)][Mn^{II}Cr^{III}(ox)_3]$ and $[Fe^{III}(5\text{-}NO_2\text{-}sal_2trien)][Mn^{II}Cr^{III}(ox)_3]\cdot MeNO_2\cdot 0.5H_2O$ compounds, which remain in the high spin and low spin state, respectively, between 2 and 300 K. Finally, in the compounds $[Fe^{III}(5\text{-}Cl\text{-}sal_2trien)][Mn^{II}Cr^{III}(ox)_3]\cdot 0.5MeNO_2$, $[Fe^{III}(5\text{-}Br\text{-}sal_2trien)][Mn^{II}Cr^{III}(ox)_3]$ and $[In^{III}(5\text{-}Cl\text{-}sal_2trien)][Mn^{II}Cr^{III}(ox)_3]$ a third property is provided to the multifunctional material, which is the

chirality of the oxalate network. In these systems, the interplay between the chirality and the magnetic ordering of the oxalate network could lead to new physical properties such as magnetochiral dichroism. This aspect will be studied in the future.

6- Derivatives of $[Fe^{III}(sal_2\text{-trien})]^+$ complex, with substituents in the 3 or 4 positions, give rise to 2D structures in compounds of formula $[Fe^{III}(4\text{-Br-sal}_2\text{trien})][Mn^{II}Cr^{III}(ox)_3]_{0.67}\cdot Cl_{0.33}\cdot MeOH$, $[Fe^{III}(3\text{-Cl-sal}_2\text{trien})][Mn^{II}Cr^{III}(ox)_3]\cdot(CH_3OH)_2\cdot(CH_3CN)_2$, $[Fe^{III}(3\text{-Br-sal}_2\text{trien})][Mn^{II}Cr^{III}(ox)_3]\cdot(CH_3CN)_2$, and $[Fe^{III}(3\text{-MeO-sal}_2\text{trien})][Mn^{II}Cr^{III}(ox)_3]\cdot(CH_3OH)\cdot(H_2O)_{1.5}\cdot(CH_2Cl_2)_{0.5}$. These compounds show a magnetic ordering about 5 K which coexists with a complete spin transition between 300 and 400 K for $[Fe^{III}(4\text{-Br-sal}_2\text{trien})][Mn^{II}Cr^{III}(ox)_3]_{0.67}\cdot Cl_{0.33}\cdot MeOH$ and partial spin transition for $[Fe^{III}(3\text{-Cl-sal}_2\text{trien})][Mn^{II}Cr^{III}(ox)_3]\cdot(CH_3OH)_2\cdot(CH_3CN)_2$ and $[Fe^{III}(3\text{-Br-sal}_2\text{trien})][Mn^{II}Cr^{III}(ox)_3]\cdot(CH_3CN)_2$ compounds. $Fe^{III}(3\text{-MeO-sal}_2\text{trien})][Mn^{II}Cr^{III}(ox)_3]\cdot(CH_3OH)\cdot(H_2O)_{1.5}\cdot(CH_2Cl_2)_{0.5}$ compound remains in high spin state between 2 and 300 K. In two of these complexes, the presence of pores with disordered solvent molecules could lead to new functionalities in addition to the magnetic ordering and the spin crossover such as solvent adsorption or proton conduction recently found in other 2D oxalate-based compounds.

7- In the 2D compounds, $[Fe^{III}(5\text{-NO}_2\text{-sal}_2\text{trien})][Mn^{II}Cr^{III}(ox)_3]\cdot MeNO_2\cdot 0.5H_2O$, $[Fe^{III}(4\text{-Br-sal}_2\text{trien})][Mn^{II}Cr^{III}(ox)_3]_{0.67}\cdot Cl_{0.33}\cdot MeOH$, $[Fe^{III}(3\text{-Cl-sal}_2\text{trien})][Mn^{II}Cr^{III}(ox)_3]\cdot(CH_3OH)_2\cdot(CH_3CN)_2$, LIESST effect is not observed. The reasons for the absence of LIESST effect may be: (a) a too high $T_{1/2}$ leading to a too fast HS-LS relaxation to be detected on the time scale of SQUID measurements; (b) the small amount of Fe^{III} that can undergo spin crossover, and (c) a different organization of the $[Fe(sal_2\text{-trien})]^+$ complexes in which only weak contacts with the oxalate network are established. Preliminary results of the spectroscopic characterization of the 3D chiral $[In^{III}(5\text{-Cl-sal}_2\text{trien})][Mn^{II}Cr^{III}(ox)_3]$ compound doped with 1 % of Fe^{III} shows a slow relaxation of the photoinduced high spin state, although much faster than that of $[Fe^{III}(sal_2\text{-trien})][Mn^{II}Cr^{III}(ox)_3]\cdot CH_2Cl_2$ compound, which may prevent the detection of LIESST effect with a SQUID

magnetometer. This result is promising because magnetic ordering in 3D networks is much more sensitive to changes of size of the inserted cation, opening the possibility to tune the magnetic ordering by irradiation.

8- Finally, $[Mn^{III}(salen)]^+$ complexes and derivatives have been inserted into bimetallic oxalate networks, leading to a great variety of structures. $[Mn^{III}(salen)]^+$ complex gives a compound of formula $[Mn^{III}(salen)(H_2O)]_2[Mn^{II}Cr^{III}(ox)_3]_2\cdot(MeOH)_3\cdot(H_2O)$ and an analogue of formula $[Mn^{III}(salen)(H_2O)]_2[Zn^{II}Cr^{III}(ox)_3]_2\cdot(MeOH)_3\cdot(H_2O)$ with a paramagnetic network. They are formed by $[Mn^{III}(salen)(H_2O)]_2^{2+}$ dimers inserted into a 3D achiral network very similar to that obtained with $[Fe^{III}(sal_2\text{-trien})]^+$ complex. The preservation of the dimeric structure of the Mn^{III} precursor allows a SMM behavior in the Zn^{II} paramagnetic compound, although at low temperatures (below 0.5 K). The magnetic characterization of the ferromagnetic compound $[Mn^{III}(salen)(H_2O)]_2[Mn^{II}Cr^{III}(ox)_3]_2\cdot(MeOH)_3\cdot(H_2O)$ is consistent with the coexistence of a magnetic ordering around 5 K and SMM behavior with important changes in the two properties which are attributed to the interplay between the bimetallic oxalate network and the SMM cluster. In particular, at low fields, the hybrid shows ferrimagnetic order resulting from the antiparallel arrangement of Mn_2 salen nanomagnets and the magnetization of the oxalate lattice. This situation, which is totally new in the hybrid magnetic materials based on bimetallic oxalato lattices, resembles that found in alloys of 3d metals and lanthanide ions that, like NdFe14B, are among the best permanent magnets known to date. The combination of extended molecular networks with long-range ferromagnetism, preferably above room temperature, and strongly anisotropic SMMs can therefore offer orifinal possibilities for the design of molecule-based magnets with practical value. On the other hand, the insertion of $[Mn^{III}(salen)]^+$ derivatives into bimetallic oxalates leads to the stabilization of Mn^{III} monomers coordinated to the tetradentate Shiff base ligand and two solvent molecules in contrast to the stabilization of the dimer observed for $[Mn^{III}(salen)]^+$. Some of these compounds such as $Mn((R)\text{-salmen})(CH_3OH)_2][MnCr(ox)_3]\cdot(CH_2Cl_2)_{0.375}\cdot(CH_3OH)_{0.125}\cdot(H_2O)_{0.375}$ and $[Mn((S)\text{-salmen})(CH_3OH)_2][MnCr(ox)_3]\cdot(CH_2Cl_2)_{0.375}\cdot(CH_3OH)_{0.375}\cdot(H_2O)_{0.125}$ show 3D achiral

structures completely different to those obtained previously. The most promising results are the compounds [Mn((*R*)-salmen)(CH_3OH)(CH_3CN)][$MnCr(ox)_3$]·$(CH_3OH)_{0.5}$ ·$(CH_3CN)_{1.25}$ and [Mn((*S*)-salmen)(CH_3OH)(CH_3CN)][$MnCr(ox)_3$]·$(CH_3OH)_{0.5}$·$(CH_3CN)_{1.25}$, with a 2D chiral structure which can be obtained enantiomerically pure by choosing the appropriate chiral precursor (*R* or *S*). This may facilitate the study of new physical phenomena arising from the interplay between magnetic ordering and chirality as the aforementioned magnetochiral dichroism.

Anexos

The surnames in all publications at ICMol are reported in alphabetical order

1. M. Clemente-León, E. Coronado, M. López-Jordà,

   ”2D and 3D bimetallic oxalate-based ferromagnets prepared by insertion of different Fe^{III} spin crossover complexes”
   Dalton Transactions, 2010, **39**, 4903-4910.

2. M. Clemente-León, E. Coronado, M. López-Jordà, G. Mínguez-Espallargas, A. Soriano-Portillo, J. C. Waerenborgh,

   “Multifunctional magnetic materials obtained by insertion of a spin-crossover Fe^{III} complex into bimetallic oxalate-based ferromagnets”
   Chemistry - A European Journal, 2010, **16**, 2207-2219.

3. M. Clemente-León, E. Coronado, M. López-Jordà, C. Desplanches, H. Wang, S. Asthana, J.-F. Létard,

   “A hybrid Magnet with coexistence of ferromagnetism and photoinduced Fe^{III} spin-crossover”
   Chemical Science, 2011, **2**, 1121-1127.

4. M. Clemente-León, E. Coronado, M. López-Jordà, J. C. Waerenborgh,

   “Multifunctional magnetic materials obtained by insertion of spin-crossover Fe^{III} complexes into chiral 3D oxalate-based network”
   Inorganic Chemistry, 2011, **50**, 9122-9130.

5. M. Clemente-León, E. Coronado, M. López-Jordà,

   “2D bimetallic oxalate-based ferromagnets with inserted $[Fe(4\text{-}Br\text{-}sal_2\text{-}trien)]^+$ and $[Fe(3\text{-}R\text{-}sal_2\text{-}trien)]^+$ (R = Br, Cl and CH_3O) Fe^{III} spin-crossover complexes”
   European Jornal of Inorganic Chemistry, 2013, 753-762.

6. M. Clemente-León, E. Coronado, M. López-Jordà,

   “2D and 3D bimetallic oxalate-based ferromagnets prepared by insertion of Mn^{III}-salen type complexes”
   Dalton Transactions, 2013, **42**, 5100-5110.

7. M. Clemente-León, E. Coronado, M. López-Jordà, J. C. Waerenborgh, C. Desplanches, H. Wang, J.-F. Létard, A. Hauser, A. Tissot,
"Stimuli responsive hybrid magnets: Tuning the photoinduced spin-crossover in Fe^{III} complexes inserted into layered magnets"
Accepted in JACS

8. M. Clemente-León, E. Coronado, C. J. Gómez-García, M. López-Jordà, A. Camón, F. Luis, A. Repollés,
"Insertion of a Single-Molecule Magnet inside a ferromagnetic lattice based on a 3D bimetallic oxalate network: Towards molecular analogs of permanent magnets"
Manuscript in preparation

2D and 3D bimetallic oxalate-based ferromagnets prepared by insertion of different Fe^{III} spin crossover complexes†

Miguel Clemente-León,*[a,b] Eugenio Coronado*[a] and Maurici López-Jordà[a]

Received 18th January 2010, Accepted 16th March 2010
First published as an Advance Article on the web 12th April 2010
DOI: 10.1039/c001067g

The syntheses, structures and magnetic properties of the compounds of formula $[Fe^{III}(5\text{-}NO_2sal_2\text{-}trien)][Mn^{II}Cr^{III}(ox)_3]\cdot CH_3NO_2\cdot 0.5H_2O$ (**1**) and $[Fe^{III}(5\text{-}CH_3Osal_2\text{-}trien)][Mn^{II}Cr^{III}(ox)_3]$ (**2**) are reported. The structure of **1**, that crystallizes in the $P2_1$ chiral space group, presents a 2D honeycomb anionic layer formed by Mn^{II} and Cr^{III} ions linked through oxalate ligands and a cationic layer of $[Fe^{III}(5\text{-}NO_2sal_2\text{-}trien)]^+$ complexes intercalated between the 2D oxalate network. The structure of **2**, that crystallizes in the $Pna2_1$ acentric space group, presents a 3D achiral anionic network formed by Mn^{II} and Cr^{III} ions linked through oxalate ligands with $[Fe(5\text{-}CH_3Osal_2\text{-}trien)]^+$ complexes intercalated within the 3D oxalate network. The magnetic properties of **1** and **2** indicate that both compounds undergo a long-range ferromagnetic ordering at *ca.* 5 K. On the other hand, the inserted Fe^{III} cations remain mainly in the low-spin (LS) state in the case of **1** and in the high-spin (HS) state in the case of **2**.

Introduction

For more than 30 years molecular magnetism has been a source of novel materials. The flexibility offered by the molecular approach has afforded the development of materials with novel and unprecedented properties. In this direction the multifunctional materials that combine two (or more) physical properties of interest are one of the most promising areas.[1] A wise choice of the constituent molecules could allow the appearance in the same compound of an unusual combination of physical properties, or even a mutual interplay or synergy of the properties involved. A suitable approach to obtain such materials is the so-called hybrid approach in which two network solids are constructed *via* self-assembling of two different molecular fragments (organic, inorganic or organometallic), with each network furnishing distinct properties to the solid.

Bimetallic oxalate-bridged complexes of formula $A[M^{II}M^{III}(ox)_3]$ (M^{III} = Cr, Fe, Ru, V, Mn; M^{II} = Mn, Fe, Co, Ni, Cu, Zn; A = cation; ox = oxalate) have provided many examples of hybrid magnets. These bimetallic salts are most often composed by polymeric 2D anionic networks, which furnish the cooperative magnetic properties (ferro-, ferri- or canted antiferromagnetism),[2] and a bulky charge-compensating molecular cation, which templates the network formation. In these compounds the cooperative magnetism of the oxalate network can co-exist with the electronic property provided by the cationic molecular lattice. Thus, paramagnetic decamethylferrocenium[3] or organic radical cations,[4] photochromic molecules,[5] NLO-active molecules,[6] organic π-electron donors,[7] and chiral molecules[8,9] have led to the formation of magnetic multilayers, photochromic magnets, ferromagnetic molecular metals or chiral magnets. New properties for this type of compounds such as the magnetisation-induced second harmonic generation,[10] observed in an enantiopure 2D oxalate-based magnet, and proton conduction, observed in a 2D oxalate-based magnet containing a hydrophilic ammonium cation,[11] have been reported very recently. Other magnetic networks, different from the 2D honeycomb-like networks can also be obtained depending on the nature of the templating cation (size, shape and charge) with dimensionalities ranging from 0D to 3D.[12] The most extensive one is represented by the family of 3D chiral structures in which the chirality of a templating cation of the type $[Z^{II}(bpy)_3]^{2+}$ (Z^{II} = Fe, Co, Ni, Ru; bpy = 2,2′-bipyridine) induces the building blocks to adopt an homochiral configuration,[13] which provides an opportunity to obtain chiral magnets.[13e,14] In addition, the hybrid character of these series also leads to examples in which the two sublattices are magnetic.[13d]

Spin crossover cations are particularly suitable to prepare multifunctional magnetic materials since they represent one of the best examples of molecular bistability. This may open a way to design switching magnets in which the magnetic ordering of the oxalate network could be tuned by inducing the spin crossover phenomenon applying external stimuli such as light or pressure.

The first example of the insertion of spin crossover cations into oxalate networks was reported by Decurtins *et al.* in a compound of formula $[Co(bpy)_3][LiCr(ox)_3]$.[15] This compound did not show coexistence of spin crossover and magnetic ordering since the oxalate network was paramagnetic. More recently, our group reported the insertion of the Fe^{II} spin-crossover complex, $[Fe(bpp)_2]^{2+}$ [bpp = 2,6-(bis(pyrazol-3-yl)pyridine)], into a ferromagnetic achiral 3D oxalate-based network, $[Fe(bpp)_2][MnCr(ox)_3]\cdot bpp\cdot CH_3OH$,[16] although spin crossover was not observed. In a further attempt, the coexistence of a spin crossover and magnetic ordering was successfully

[a]*Instituto de Ciencia Molecular, Universitat de València, Polígono de la Coma s/n, 46980, Valencia, Spain. E-mail: miguel.clemente@uv.es, eugenio.coronado@uv.es; Fax: 34 963543273; Tel: 34 963544405*
[b]*Fundació General de la Universitat de València, Universitat de València, Polígono de la Coma s/n, 46980, Valencia, Spain*

† Electronic supplementary information (ESI) available: Fig. S1: Plot of the layer of inorganic cations with intermolecular contacts of **1**; Fig. S2: Plot of the layer of inorganic cations of **2**. CCDC reference numbers 762043 and 762044. For ESI and crystallographic data in CIF or other electronic format see DOI: 10.1039/c001067g

demonstrated in hybrid compounds obtained by insertion of a Fe^{III} complex, $[Fe^{III}(sal_2\text{-trien})]^+$ (H_2sal_2-trien = *N*,*N*′-disalicylidenetriethylenetetramine) in homometallic[17] and bimetallic oxalate layers.[18] As a result, the compound $[Fe^{III}(sal_2\text{-trien})]_2[Mn^{II}_2(ox)_3]\cdot 4H_2O\cdot C_3H_7NO$ formed by homometallic Mn^{II} oxalate layers and inserted $[Fe(sal_2\text{-trien})]^+$ behaves as a weak ferromagnet below $T_c = 8.1$ K, exhibiting at the same time a gradual spin crossover from 300 to 80 K of half of the intercalated Fe^{III} complexes.[17] As far as the bimetallic oxalate layers are concerned, the magnetic properties of the compound $[Fe^{III}(sal_2\text{-trien})][Mn^{II}Cr^{III}(ox)_3]\cdot CH_2Cl_2$ formed by $[Fe^{III}(sal_2\text{-trien})]^+$ and $Mn^{II}Cr^{III}$ bimetallic layers, indicate the coexistence of a complete spin crossover transition from 300 to 160 K, and a ferromagnetic ordering below 5.4 K. It is interesting to note that by changing the synthetic conditions the $[Fe^{III}(sal_2\text{-trien})]^+$ also stabilizes a 3D structure for the $Mn^{II}Cr^{III}$ bimetallic network. The resulting structure is similar to that of $[Fe(bpp)_2][MnCr(ox)_3]\cdot bpp\cdot CH_3OH$. This last compound shows a gradual and incomplete spin-crossover of 30% of the Fe^{III} from 300 to 130 K, together with a ferromagnetic ordering of the 3D lattice below 5.2 K. The stabilization of two different oxalate networks with the same templating cation is a novel feature in this type of compounds. It can be explained by the structural flexibility of $[Fe^{III}(sal_2\text{-trien})]^+$ that presents a very different configuration in the two compounds.[18]

Although hybrid magnets with coexistence of magnetic ordering and spin crossover have been designed using this molecular approach, the preparation of hybrid switchable magnets has not yet been achieved. $[Fe^{III}(sal_2\text{-trien})][Mn^{II}Cr^{III}(ox)_3]\cdot CH_2Cl_2$ could be a good candidate for this purpose as it undergoes a complete spin-crossover. However, it is unexpected that the changes in structure of the intercalated compound due to spin crossover could modify the T_c of the 2D oxalate network, as 2D oxalate networks with different interlayer separations present similar T_c values. In this sense, compounds with a 3D network are expected to be better candidates because the T_c of 3D oxalate compounds is very sensitive to the size of the intercalated cation, *i.e.*, to the chemical pressure.[13f] Unfortunately, in the two 3D compounds obtained so far the occurrence of a spin-crossover and its influence on the ferromagnetic sublattice is very limited. In an attempt to improve these results, we have extended this strategy to derivatives of $[Fe^{III}(sal_2\text{-trien})]^+$ with different substituents on the position 5 of the salicylaldimine ring. From the structural point of view this could lead to new bimetallic oxalate networks more suitable for obtaining switching magnets. On the other hand, the presence of different substituent groups could tune the spin state of the inserted Fe^{III} complex. In solution for this type of complexes electron-withdrawing groups, such as NO_2, favours the low-spin (LS) state whereas electron-donating groups, such as CH_3O, favours the high-spin (HS) state.[19]

In this work we report the preparation and structural and magnetic characterization of the hybrid compounds obtained by combining $[Fe^{III}(5\text{-X}sal_2\text{-trien})]^+$ (X = NO_2 or CH_3O, see Scheme 1) with the $Mn^{II}Cr^{III}$ bimetallic networks.

Experimental

Synthesis

The complexes $[Fe^{III}(5\text{-}NO_2sal_2\text{-trien})]PF_6$ and $[Fe^{III}(5\text{-}CH_3Osal_2\text{-trien})]PF_6$ were prepared according to literature methods.[19]

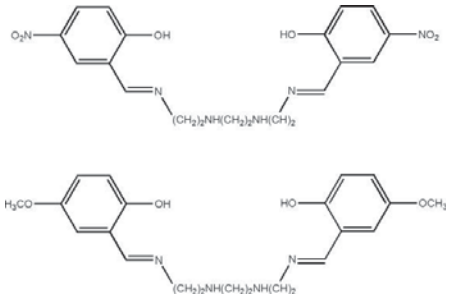

Scheme 1 $H_2(5\text{-}NO_2sal_2\text{-trien})$ (top) and $H_2(5\text{-}CH_3Osal_2\text{-trien})$ (bottom).

$Ag_3[Cr(ox)_3]$ was prepared by metathesis from the corresponding potassium salt.[20] All other materials and solvents were commercially available and used without further purification.

$[Fe^{III}(5\text{-}NO_2sal_2\text{-trien})][Mn^{II}Cr^{III}(ox)_3]\cdot CH_3NO_2\cdot 0.5H_2O$ (1). Crystals of this compound were obtained by slow diffusion of two solutions. The first solution was prepared by adding $MnCl_2\cdot 4H_2O$ (0.029 g, 0.148 mmol) to a suspension of $Ag_3Cr(ox)_3$ (0.063 g, 0.098 mmol) in 6 mL of methanol. The AgCl precipitate was filtered off. The second solution was obtained by dissolving $[Fe^{III}(5\text{-}NO_2sal_2trien)]PF_6$ (0.064 g, 0.098 mmol) in 6 mL of nitromethane. After two weeks brown crystals were obtained.

$[Fe^{III}(5\text{-}CH_3Osal_2\text{-trien})][Mn^{II}Cr^{III}(ox)_3]$ (2). Crystals of this compound were obtained by slow diffusion of two solutions. The first solution was prepared by adding $MnCl_2\cdot 4H_2O$ (0.032 g, 0.165 mmol) to a suspension of $Ag_3Cr(ox)_3$ (0.069 g, 0.11 mmol) in 6 mL of methanol. The AgCl precipitate was filtered off. The second solution was obtained by dissolving $[Fe^{III}(5\text{-}CH_3Osal_2trien)]PF_6$ (0.067 g, 0.11 mmol) in 6 mL of 1,2-dichloroethane. After two weeks brown crystals were obtained.

Structural characterisation

Single-crystal X-ray data of **1** and **2** were collected at 120 K on a Xcalibur, Sapphire3, Gemini diffractometer equipped with a graphite-monochromated Enhance (Mo) X-ray Source (λ = 0.71073 Å). The program CrysAlisPro, Oxford Diffraction Ltd., Version 1.171.33.52 was used for cell refinements and data reduction of the compounds. Empirical absorption correction was performed using spherical harmonics, implemented in SCALE3 ABSPACK scaling algorithm. Crystal structures were solved by direct methods with the SIR97 program,[21] and refined against all F^2 values with the SHELXL-97 program,[22] using the WinGX graphical user interface.[23] Non-hydrogen atoms were refined anisotropically (except as noted), and hydrogen atoms were placed in calculated positions refined using idealized geometries (riding model) and assigned fixed isotropic displacement parameters. The small size of the crystals of **1** and **2** gave rise to a very weak scattering. Due to this the number of reflections was not enough to carry out anisotropic refinement of all the atoms in **1**. Thus, only Mn, Cr and Fe atoms were refined anisotropically. In **1**, one of two crystallographically independent nitromethane solvent molecules was modeled in two orientations. In **2**, one of the two crystallographically independent $[Fe^{III}(5\text{-}CH_3Osal_2\text{-trien})]^+$ complexes was modeled in two orientations. The other

Table 1 Crystallographic data for compounds **1** and **2**

Compound	**1**	**2**
Empirical formula	$C_{54}H_{52}Cr_2Fe_2Mn_2N_{14}O_{41}$	$C_{56}H_{56}Cr_2Fe_2Mn_2N_8O_{32}$
Formula weight	1878.66	1678.67
Crystal color	Brown	Brown
T/K	120(2)	120(2)
Wavelength, λ/Å	0.71073	0.71073
Crystal system	Monoclinic	Orthorhombic
Space group	$P2_1$	$Pna2_1$
a/Å	12.712(3)	20.8484(16)
b/Å	15.933(3)	21.710(2)
c/Å	18.379(4)	15.4856(13)
β/°	106.59(3)	90
V/Å^3	3567.5(12)	7009.0(11)
Z	2	4
D_c/Mg m^{-3}	1.747	1.591
μ(Mo-Kα)/mm^{-1}	1.146	1.145
θ range/°	2.29–27.07	2.36–32.56
Reflns collected	20271	78783
Independent reflns (R_{int})	10434 (0.0915)	22802 (0.1019)
Least-squares parameters/restraints	509/9	706/14
$R1(F)^a(I > 2\sigma(I))$	0.0730	0.0723
$wR2(F^2)^b$ (all data)	0.1203	0.1778

^{a} $R1(F) = \sum(|F_o| - |F_c|)/\sum|F_o|$. ^{b} $wR2(F^2) = [\sum w(F_o^2 - F_c^2)^2/\sum wF_o^4]^{\frac{1}{2}}$.

crystallographically independent $[Fe^{III}(5\text{-}CH_3Osal_2\text{-}trien)]^+$ complex presents some type of disorder that could not be solved. Due to this, short intermolecular distances (2.51 Å) and high U_{eq} are found in some atoms of these molecules. Carbon, nitrogen and oxygen atoms of the 5-CH_3Osal_2-trien ligand could only be modeled isotropically due to the flexibility of the ligand. The use of restraints and/or constraints in the refinement of the structures is documented in the corresponding CIFs. Data collection and refinement statistics are collected in Table 1.

Physical measurements

Magnetic susceptibility measurements were performed on polycrystalline samples using a magnetometer (Quantum Design MPMS-XL-5) equipped with a SQUID sensor. Variable-temperature measurements were carried out in the temperature range 2-400 K. The AC measurements were performed in the temperature range 2–10 K at different frequencies with an oscillating magnetic field of 0.395 mT. The magnetisation and hysteresis studies were performed between 5 and −5 T, cooling the samples at zero field. The Fe : Mn : Cr ratios were measured on a Philips ESEM X230 scanning electron microscope equipped with an EDAX DX-4 Microsonde.

Results and discussion

Synthesis

The method used to prepare $[Fe^{III}(5\text{-}NO_2sal_2\text{-}trien)][Mn^{II}Cr^{III}(ox)_3]\cdot CH_3NO_2\cdot 0.5H_2O$ (**1**) and $[Fe^{III}(5\text{-}CH_3Osal_2\text{-}trien)][Mn^{II}Cr^{III}(ox)_3]$ (**2**) is similar to that used to prepare the compounds with $[Fe^{III}(sal_2\text{-}trien)]^+$.[18] This is based in the use of $Ag_3[Cr(ox)_3]$ to avoid the presence of alkali-metal ions in the structure. It consists of the slow diffusion of a methanol solution containing the precursors of the oxalate network, Mn^{2+} and $[Cr(ox)_3]^{3-}$ ions, into a solution of $[Fe^{III}(5\text{-}Xsal_2\text{-}trien)]^+$ (X = NO_2 or CH_3O) in different solvents. In contrast to the compounds with $[Fe^{III}(sal_2\text{-}trien)]^+$ in which the use of different solvents to dissolve the Fe^{III} complex afforded compounds with different types of oxalate networks (2D and 3D), only one type of oxalate network was obtained for each templating cation of $[Fe^{III}(5\text{-}Xsal_2\text{-}trien)]^+$ (X = NO_2 or CH_3O). In the case of $[Fe^{III}(5\text{-}NO_2sal_2\text{-}trien)]^+$ cation, the only solvent that led to crystals of adequate quality for X-ray single-crystal diffraction was CH_3NO_2, whereas for $[Fe^{III}(5\text{-}CH_3Osal_2\text{-}trien)]^+$ cation, crystals of **2** were obtained with CH_2ClCH_2Cl whereas other solvents such as acetone or acetonitrile gave rise to crystals with a similar unit cell. It seems that the presence of CH_3NO_2 is necessary for the crystallisation of compound **1** as the solvent molecules enter in the structure (see below). The composition of these crystals, checked by microanalysis, showed in all cases a Fe : Mn : Cr ratio of 1 : 1 : 1. The crystal structures of the two compounds have been solved by single-crystal X-ray diffraction. Attempts to obtain analogous compounds with other paramagnetic M^{2+} ions (M = Ni, Fe, Co and Cu) have been unsuccessful.

Structure of 1

The best solution to the structure of this compound is found in the chiral space group $P2_1$. Structural analysis applying any achiral space group does not converge to a normal solution. The crystal was solved as a racemic twin with a BASF parameter of 0.35785. In this case, the BASF coefficient is the Flack absolute structure parameter x.[24] Therefore, the structure resolution has been performed in a twinned crystal containing crystals of opposite chirality.

The structure is formed by anionic sheets in the $\bar{1}01$ plane of formula $[MnCr(ox)_3]^-$ with inter-lamellar $[Fe^{III}(5\text{-}NO_2sal_2\text{-}trien)]^+$ cations and nitromethane and water solvent molecules (Fig. 1). The anionic layer presents the well-known 2D honeycomb

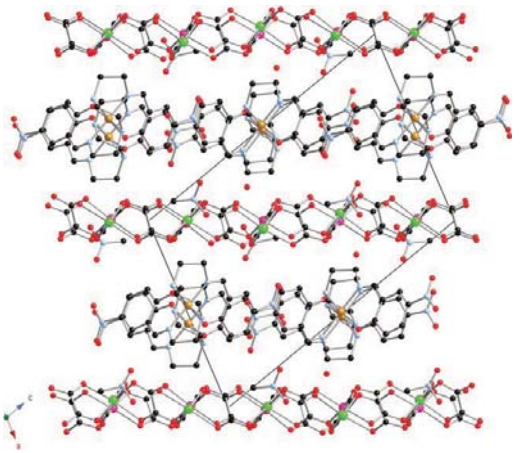

Fig. 1 Lateral view of the anionic and cationic layers of **1** (Fe (yellow), Cr (pink), Mn (green) C (black), N (blue), O (red)). Hydrogen atoms have been omitted for clarity. Only one of the two configurations of disordered nitromethane solvent molecule is shown for clarity.

structure formed by an extended network with Mn^{II} and Cr^{III} ions linked through oxalate bridges. It is formed by oxalate ligands connecting Mn^{II} with Cr^{III} ions in such a way that each Mn^{II} is surrounded by three neighbouring Cr^{III} and *vice versa* (Fig. 2). These ions present octahedral coordination. The Mn^{II} and Cr^{III} are clearly distinguishable as they present different bond distances with oxalate ligands. Thus, there are two crystallographically independent Mn ions (Mn1 and Mn2) with Mn–O distances lying between 2.139(9) and 2.228(10) Å and two crystallographically independent Cr ions (Cr1 and Cr2) with Cr–O distances lying between 1.949(8) and 2.029(8) Å. These are typical Mn^{II}–O and Cr^{III}–O distances similar to those found in other oxalate networks. The neighbouring metal centres of these layers present alternated chirality as usual for this type of networks. In this structure all the Cr^{III} ions adopt a Δ configuration, whereas all the Mn^{II} adopt the Λ configuration. Therefore, the configuration of each metal ion is preserved in the neighbouring oxalate layers. Since we have started from a racemic mixture of $[Cr(ox)_3]^{3-}$ anion, crystals of the two enantiomers have been obtained as expected. A similar behaviour has been observed in other 2D oxalate structures.[11,25,26] The chirality of the $[Fe^{III}(5\text{-}NO_2sal_2\text{-}trien)]^+$ cations may be responsible of this first-order spontaneous resolution through chiral recognition between one of the enantiomers of $[Cr(ox)_3]^{3-}$ and $[Fe^{III}(5\text{-}NO_2sal_2\text{-}trien)]^+$. In agreement to this, one of the two crystallographically independent $[Fe^{III}(5\text{-}NO_2sal_2\text{-}trien)]^+$ complexes placed between the oxalate layers, [Fe1] (see below), which only adopts a Λ configuration, interacts through several short contacts with Cr1, which adopts a Δ configuration.

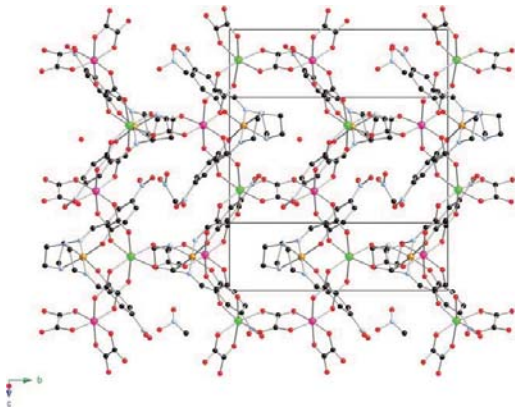

Fig. 2 Projection of **1** in the $\bar{1}01$ plane. (Fe (yellow), Cr (pink), Mn (green) C (black), N (blue), O (red)). Hydrogen atoms have been omitted for clarity. Only one of the two configurations of disordered nitromethane solvent molecule is shown for clarity.

Mean metal–metal distances between adjacent centres are in the range 5.416–5.456 Å. These distances are similar to those found in other 2D oxalate networks reported in the literature.[2,3] The minimum distance between metals of different layers is 11.609 Å, which is higher than those found in other oxalate-based 2D compounds with decamethylferrocenium or alkylammonium cations (9.2–9.7 Å)[2,3] but similar to that of the 2D compound obtained by insertion of $[Fe^{III}(sal_2\text{-}trien)]^+$ (11.6440(2) Å).[18] These anionic layers are stacked one over the other in an AB… fashion. In contrast to the structure of $[Fe^{III}(sal_2\text{-}trien)][Mn^{II}Cr^{III}(ox)_3]\cdot CH_2Cl_2$ in which there is a certain undulation of the oxalate layer, the Mn^{II} and Cr^{III} ions and oxalate ligands form an almost perfect 2D layer in the structure of **1** (see Fig. 1). A possible explanation for this difference is the slightly larger interlayer distance in **1**. Finally, the minimum distance between the metallic ions from the oxalate network and the Fe atoms is 6.363 Å which is similar to that found in $[Fe^{III}(sal_2\text{-}trien)][Mn^{II}Cr^{III}(ox)_3]\cdot CH_2Cl_2$.[18]

The space between the oxalate layers is occupied by two crystallographically independent $[Fe^{III}(5\text{-}NO_2sal_2\text{-}trien)]^+$ complexes ([Fe1] and [Fe2]), two nitromethane and one water solvent molecules (Fig. 1 and 2). Fe^{III} ions present octahedral coordination. The average Fe–N and Fe–O bond distances are 1.955(10) and 1.898(8) Å in [Fe1] complexes and 1.972(12) and 1.882(9) Å in [Fe2] complexes. These values are in the range of those obtained for other LS $[Fe(sal_2\text{-}trien)]^+$ compounds, in full agreement with the magnetic measurements (see below), which indicate that all Fe are LS at 120 K (temperature at which the crystal structure has been determined). The dihedral angles, α, between the least-squares planes of the two phenoxy rings are $\alpha = 89.002°$ ([Fe1] complex) and $\alpha = 94.248°$ ([Fe2] complex). The $[Fe^{III}(5\text{-}NO_2sal_2\text{-}trien)]^+$ cations lie with their longer axis parallel to the oxalate layers. The presence of the NO_2 group favours face-to-face interactions[27] between the aromatic rings of neighbouring $[Fe^{III}(5\text{-}NO_2sal_2\text{-}trien)]^+$ cations in contrast to the previous structures with $[Fe^{III}(sal_2\text{-}trien)]^+$ that presented mainly edge-to-face interactions.[18] Thus, each aromatic ring of [Fe1] complexes is connected through $\pi\cdots\pi$ stacking interactions with two neighbouring [Fe2] complexes forming a chain of alternating [Fe1] and [Fe2] complexes (see Fig. S1, ESI†). In these chains, the two configurations of the $[Fe^{III}(5\text{-}NO_2sal_2\text{-}trien)]^+$ complex are present with [Fe1] complexes in the Λ configuration while [Fe2] complexes adopt the Δ configuration. [Fe1] and [Fe2] complexes belonging to the same chain present hydrogen bonds between the NO_2 group of each aromatic ring and the NH groups of the neighbouring complex. The complexes from different chains are connected through C–H$\cdots\pi$ interactions between the ethylene groups of one complex and the two aromatic rings of another complex. Furthermore, there are short contacts between N and O from NO_2 groups belonging to different chains. The two crystallographically independent nitromethane molecules occupy positions very close to the centre of the hexagonal rings of the oxalate network placed alternatively above and below the oxalate layer. One of the nitromethane molecules presents a disorder between two possible orientations. The water molecule occupies the holes between the oxalate network and the layer of $[Fe^{III}(5\text{-}NO_2sal_2\text{-}trien)]^+$ cations.

Structure of 2

Complex **2** crystallises in the acentric orthorhombic space group $Pna2_1$, that contains metal centres of both chiralities. The structure of **2** is formed by an anionic 3D polymeric oxalate-bridged bimetallic network with $[Fe^{III}(5\text{-}CH_3Osal_2\text{-}trien)]^+$ cations occupying the cavities (Fig. 3). A very similar achiral 3D oxalate network has been found in the compound of formula $[In^{III}(sal_2\text{-}trien)][Mn^{II}Cr^{III}(ox)_3]\cdot CH_3NO_2\cdot 0.5H_2O$ that crystallizes in the same space group.[18] Other compounds

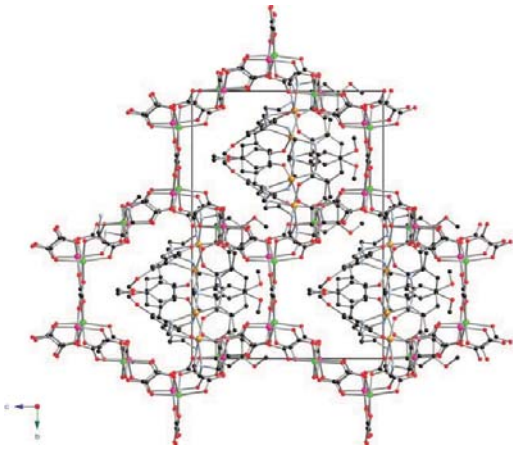

Fig. 3 Projection of **2** in the *bc* plane. (Fe (yellow), Cr (pink), Mn (green) C (black), N (blue), O (red)). Hydrogen atoms have been omitted for clarity. Only one of the two configurations of the disordered $[Fe^{III}(5\text{-}CH_3O\ sal_2\text{-}trien)]^+$ molecule is shown for clarity.

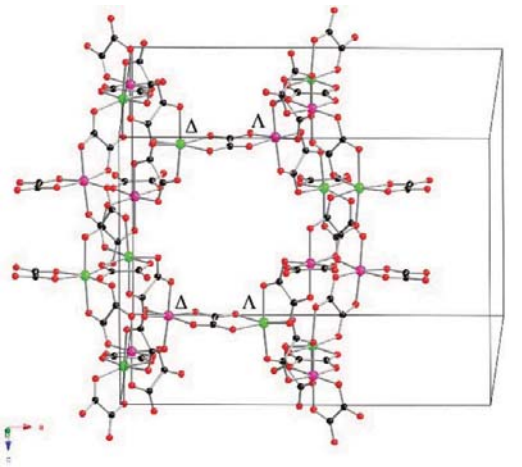

Fig. 4 Two neighbouring ten-membered rings of the oxalate network of **2** of opposite chirality connected through two oxalate ligands along the *a* direction. (Cr (pink), Mn (green) C (black), N (blue), O (red)).

with similar achiral 3D network reported in the literature are those of formula $[Fe(bpp)_2][MnCr(ox)_3]_2\cdot bpp\cdot CH_3OH$ that crystallizes in the centrosymmetric $P2_1/n$ space group,[16] $[Fe^{III}(sal_2\text{-}trien)][Mn^{II}Cr^{III}(ox)_3]\cdot CH_3OH$ and $[In^{III}(sal_2\text{-}trien)]$-$[Mn^{II}Cr^{III}(ox)_3]\cdot 0.25H_2O\cdot 0.25CH_3OH\cdot 0.25CH_3CN$ that crystallize in the acentric *Cc* space group.[18] This anionic polymeric structure is formed by bis-chelating oxalate ligands connecting Mn^{II} and Cr^{III} ions in such a way that each Mn^{II} is surrounded by three Cr^{III} and *vice versa*, building ten-membered rings in a (10,3) topology. The (10,3) decagon rings perpendicular to the *a* axis are formed by metal centers with the same chirality (see Fig. 3). Two of these neighbouring metal rings, that are linked trough two oxalate ligands, present opposite chirality (see Fig. 4). Projection of the oxalate network on the *ab* plane is almost identical to that of the chiral 3D oxalate network in the *ab*, *bc* or *ac* planes (see Fig. 5). However, projection on the *ac* or *bc* planes (see Fig. 3 and 4) are different as a result of the different chirality of the neighbouring (10,3) decagon rings. Thus, in the *bc* projection an eclipsed disposition of the neighbouring oxalate rings is observed as a result of the heterochiral oxalate junctions among them (see Fig. 3). Mn and Cr present an octahedral coordination. Again, it is possible to distinguish between Mn^{II} and Cr^{III} ions of this oxalate network. Thus, there are two crystallographically independent Mn^{II} ions (Mn1 and Mn2) with Mn–O distances lying between 2.127(5) and 2.201(5) Å and two crystallographically independent Cr^{III} ions (Cr1 and Cr2) with Cr–O distances lying between 1.951(6) and 1.990(5) Å. These are typical Cr^{III}–O and Mn^{II}–O distances similar to those found in other oxalate networks. Metal–metal distances between adjacent centers are in the range 5.362–5.426 Å. These metal–metal distances are shorter than those exhibited by **1**. This contrasts with the behaviour exhibited by chiral 3D networks that normally present longer metal–metal distances than 2D structures. In addition, the minimum distance between the metallic ions from the oxalate network and the Fe atoms is much shorter than in compound **1**. Thus, a value of 5.518 Å is obtained between Cr1 and Fe1A.

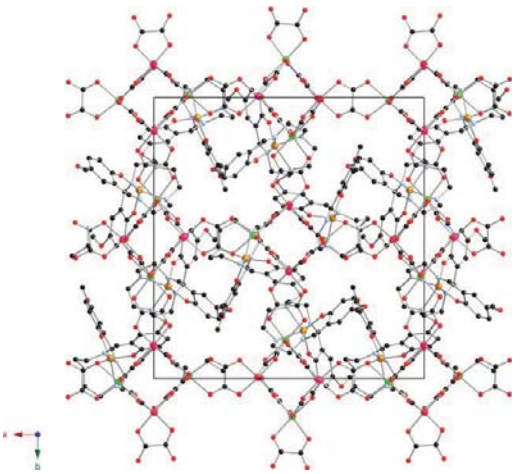

Fig. 5 Projection of **2** in the *ab* plane. (Fe (yellow), Cr (pink), Mn (green) C (black), N (blue), O (red)). Hydrogen atoms have been omitted for clarity. Only one of the two configurations of the disordered $[Fe^{III}(5\text{-}CH_3O\ sal_2\text{-}trien)]^+$ molecule is shown for clarity.

$[Fe(5\text{-}CH_3Osal_2\text{-}trien)]^+$ complexes are intercalated in the holes described by this 3D oxalate network. Fe^{III} presents an octahedral coordination. There are two crystallographically independent $[Fe(5\text{-}CH_3Osal_2\text{-}trien)]^+$ complexes. One cation, ([Fe2] complex), presents Fe–N and Fe–O bond distances of 2.172(10) and 1.887(7) Å that are clearly similar to those of other HS complexes. Two complete orientations of the second cation site ([Fe1A] (~72%) and [Fe1B] (~28%) complexes) have been resolved in the refinement. Although the errors on their metric parameters

are inevitably larger, the structure of one of these ([Fe1A] complex) is clearly consistent with it being HS (average Fe–N and Fe–O bond distances of 2.159(9) and 1.932(8) Å), while the other ([Fe1B complex) is apparently LS (average Fe–N and Fe–O bond distances of 1.96(2) and 1.86(2) Å). This indicates that at the temperature of the structural study (120 K) 14% of the Fe^{III} complexes are in the LS state in agreement with magnetic data (see below). A similar disorder of a $[Fe^{III}(sal_2\text{-trien})]^+$ site with two configurations being HS and LS has been found in the compound of formula $[Fe(sal_2\text{-trien})]ClO_4$.[28] In contrast to the structure of **1**, the intermolecular interactions between the complexes are not face-to face (see Fig. S2, ESI†). This can be explained by steric hindrance caused by the presence of the methoxy groups that hinders the face-to-face orientation of the neighbouring rings. Thus, the two aromatic rings from [Fe2] complex present short contacts with the ethylene groups of neighbouring [Fe1A] or [Fe1B] complexes. On the other hand, the ethylene groups of this [Fe2] present short contacts with the phenoxy groups of another neighbouring [Fe1A] or [Fe1B] complex. Furthermore, [Fe2] and [Fe1B] are connected through hydrogen bonds with the oxalate ligands. Dihedral angles α between the phenoxy rings of [Fe1A], [Fe1B] and [Fe2] are 110.47, 100.41 and 105.55°, respectively. The dihedral angles, α, between the least squares planes of the two phenoxy rings have very different values in the 2D or 3D structures presented in this paper. Thus, in the 2D compound **1** the two phenoxy rings are closer to 90°, the ideal value for an octahedral complex,

Magnetic properties of 1

The thermal dependence of the product of the molar magnetic susceptibility and temperature (χT) of **1** is shown in Fig. 6; χT shows a value of 8.0 emu K mol^{-1} at 400 K. Upon cooling down χT decreases gradually from 400 to 250 K from 8.0 to 6.8 emu K mol^{-1}. This last value is approximately equal to the sum of the expected contributions for the isolated paramagnetic ions with the Fe^{III} spin-crossover complex in a LS state. Therefore, in this range of temperatures there is a partial HS→LS spin conversion of the Fe^{III} complexes. This spin crossover is not complete since the χT at 400 K (8.0 emu K mol^{-1}) is still far for the expected value for all Fe^{III} complexes in HS state (~10.6 emu K mol^{-1}), and corresponds approximately to 66% of the Fe^{III} in the LS state. Below 250 K there is an increase of χT, which is very sharp below 50 K. This indicates the presence of ferromagnetic interactions between neighbouring Mn^{II}–Cr^{III} magnetic ions of the oxalate network and suggests the onset of long-range ferromagnetic ordering, as observed for other M^{II}–Cr^{III} 2D oxalate networks.[2,3] To confirm the presence of long-range magnetic ordering and to determine precisely the critical temperatures, AC susceptibility measurements have been carried out. A maximum in the in-phase signal (χ') near T_c and an out-of-phase signal (χ'') that starts to appear at temperatures just below T_c is observed (Fig. 7). These signals are frequency independent as expected for a ferromagnet (Fig. 7). From this data the T_c of **1** is 5.6 K, similar to those reported for other 2D Mn^{II}–Cr^{III} 2D oxalate compounds, but slightly higher than that of the 2D compound obtained with $[Fe^{III}(sal_2\text{-trien})]^+$ ($T_c = 5.4$ K).[18] In the ordered phase an additional peak in χ'' at temperatures below 3 K is also detected. The presence of such a frequency-dependent peak has already been observed in other M^{II}–Cr^{III} 2D oxalate compounds. This can be related to the formation of magnetic domains and domain-wall movement.[29]

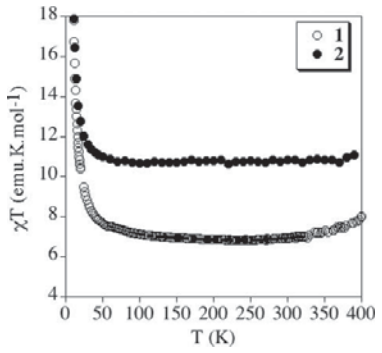

Fig. 6 Temperature dependence of the product of the molar magnetic susceptibility with temperature (χT) at 0.1 T for compounds **1** (empty circles) and **2** (full circles).

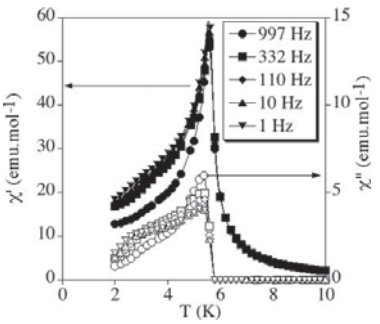

Fig. 7 Temperature dependence of the in-phase AC susceptibility (χ') (filled symbols) and the out-of-phase AC susceptibility (χ'') (empty symbols) for **1**.

To confirm the ferromagnetic ordering of the spins, isothermal magnetization at 2 K has been performed (Fig. 8). This presents a sharp increase at low fields which is much faster than that expected for non-interacting Cr^{III} and Mn^{II} centers; this increase is more

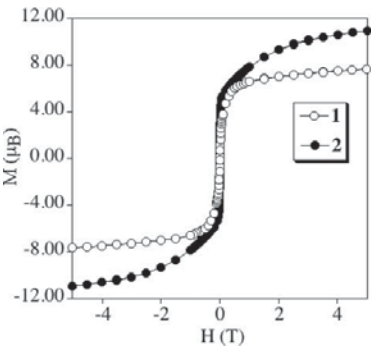

Fig. 8 Field dependence of the magnetization (M) for **1** (empty circles) and **2** (filled circles).

gradual at higher fields and no saturation is reached even up to 5 T. The magnetization (M) value at 5 T is 7.7 μ_B, which is slightly lower than the expected value for a parallel alignment of the spins in the bimetallic lattice with all the Fe^{III} in the LS state (9 μ_B). As for other M^{II}–Cr^{III} 2D oxalate compounds, this difference can be due to a spin canting of the ferromagnetic phase.[2] The hysteresis loops at 2 K shows that this compound is a soft ferromagnet with a coercive field of 0.5 mT.

Magnetic properties of 2

The thermal dependence of χT for **2** is shown in Fig. 6. It shows a constant value of 10.7–10.8 emu K mol^{-1} from 400 to 100 K as temperature decreases which is much higher than that of compound **1**. This value is very close to the sum of the expected contributions for the isolated paramagnetic ions with 100% of Fe^{III} in a HS state. This constant value in this range of temperature contrasts with the smooth increase of χT at decreasing temperature observed for the $[Fe(sal_2\text{-trien})]^+$ compound with an analogous 3D achiral network.[18] It seems that the expected increase of χT due to the ferromagnetic coupling between the neighbouring Mn^{II}–Cr^{III} magnetic ions is compensated by the spin crossover transition of part of the inserted $[Fe^{III}(5\text{-}CH_3Osal_2\text{-trien})]^+$ cation leading to an approximately constant value of χT. Indeed, the structure of this compound solved at 120 K shows that 14% of the inserted $[Fe^{III}(5\text{-}CH_3Osal_2\text{-trien})]^+$ complexes are in the LS state confirming this effect (see above). At temperatures below 100 K there is an increase of χT, which is very sharp below 50 K. This indicates the presence of ferromagnetic interactions between neighbouring Mn^{II}–Cr^{III} magnetic ions and the onset of long-range ferromagnetic ordering as usual for this type of compounds. The long-range ferromagnetic ordering is confirmed by AC susceptibility measurements (see Fig. 9) that show frequency-independent χ' and χ'' peaks. From this data the T_c of **2** is 5.1 K, which is very close to that found for the $[Fe(sal_2\text{-trien})]^+$ compounds with an analogous 3D achiral network (5.2 K), and lower than that of compound **1** which presents a 2D network.[18]

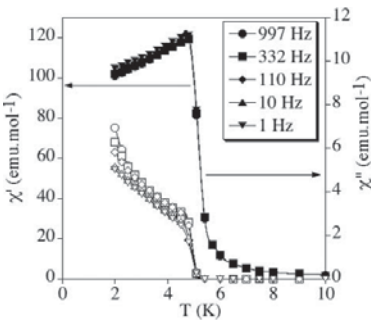

Fig. 9 Temperature dependence of the in-phase AC susceptibility (χ') (filled symbols) and the out-of-phase AC susceptibility (χ'') (empty symbols) for **2**.

Isothermal magnetization at 2 K presents a sharp increase at low fields (below 0.1 T), and a hysteresis loop with a coercive field of *ca.* 0.6 mT, which is usual for this type of compounds (Fig. 8). In contrast to **1** in which there is only a slight linear increase of M *vs.* H at fields above 0.1 T, the presence of a fraction of paramagnetic HS Fe^{III} produces a pronounced curvature in the M *vs.* H curve with M increasing from 5.4 to 10.9 μ_B when H increases from 0.1 to 5 T. Although it is difficult to evaluate the HS fraction from these measurements, we can say that the value of the M at H = 5 T (10.9 μ_B) is intermediate between the expected value for all the Fe^{III} in the HS state (13 μ_B) and the one for all the Fe^{III} in the LS state (9 μ_B). This indicates that from 300 to 2 K there is a partial spin crossover of the Fe^{III} ions. This spin crossover is far for being complete at 2 K as the M value at this temperature is closer to the expected one with all the Fe^{III} in the HS state. Mössbauer experiments are in progress to evaluate the LS/HS Fe^{III} ratio.

Conclusion

We have reported in this paper the preparation of two novel hybrid compounds (**1** and **2**) formed by the insertion of two derivatives of the spin crossover $[Fe^{III}(sal_2\text{-trien})]^+$ cation into anionic coordination polymers based on bimetallic oxalate complexes. From the structural point of view, we have seen that the use of the $[Fe^{III}(5\text{-}NO_2sal_2\text{-trien})]^+$ complex, in which the presence of NO_2 groups favours π–π stacking interactions, gives rise to a 2D network in compound **1**, whereas the use of $[Fe^{III}(5\text{-}CH_3Osal_2\text{-trien})]^+$ complex, which prevent such interactions due to steric hindrance of the methoxy groups, leads to the formation of an achiral 3D network in compound **2**. This contrasts with the flexibility of non-substituted $[Fe(sal_2\text{-trien})]^+$ cation in which 2D and achiral 3D networks were obtained depending on the preparation conditions.[18] Furthermore, we have seen that the chirality of these templating cations may induce the formation of 2D chiral oxalate networks (compound **1**). This opens the way to the search for new magnetic effects derived from the chirality of the lattice, such as the magneto-chiral effect predicted by Rikken *et al.*[30] and observed recently in an enantiopure 2D oxalate compound.[9] From the point of view of the magnetic properties, we have shown that it is possible to tune the spin state of the inserted Fe^{III} compound depending on the electron-withdrawing or electron-donating character of the substituent of sal_2trien together with packing effects. Thus, the electron-withdrawing substituent NO_2, favours the LS state in compound **1**, whereas the electron-donating group CH_3O, favours the HS state in compound **2**. The magnetic properties indicate that there is a partial spin crossover of the inserted cation in these two compounds that coexists with a ferromagnetic ordering of the oxalate networks.

The possible use of these compounds as switchable magnets remains to be explored by applying light or pressure. For this purpose, the achiral 3D compound **2** seems a better candidate as it presents a 3D structure in which the chemical pressure effect is expected to be stronger than in the 2D structure. However, the preferred HS state of the inserted cation in this compound, might prevent any switching behaviour, as seen for the 3D achiral compound obtained with $[Fe^{III}(sal_2\text{-trien})]^+$.[18] To overcome this problem, other sal_2trien derivatives could be used. The results obtained in this paper may help to understand which candidates could be better suited to reach this goal. For instance, the use of a substituent with electron-withdrawing groups not favouring π···π stacking interactions such as CF_3 or disubstituted sal_2trien, is proposed to obtain 3D oxalate networks with a higher probability of spin-crossover of the inserted Fe^{III} complex.

Acknowledgements

Financial support from the European Union (MolSpinQIP and SPINMOL ERC Advanced Grant), the Spanish Ministerio de Ciencia e Innovación (Project Consolider-Ingenio in Molecular Nanoscience, CSD2007-00010, and projects CTQ2008-06720 and MAT2007-61584), and the Generalitat Valenciana (Prometeo Program) are gratefully acknowledged. The authors also thank J. M. Martínez-Agudo, University of Valencia, and Núria Clos, University of Barcelona, for magnetic characterization of the samples.

References

1 (*a*) E. Coronado and P. Day, *Chem. Rev.*, 2004, **104**, 5419; (*b*) E. Coronado and J. R. Galán-Mascarós, *J. Mater. Chem.*, 2005, **15**, 66.
2 (*a*) H. Tamaki, Z. J. Zhong, N. Matsumoto, S. Kida, M. Koikawa, N. Achiwa, Y. Hashimoto and H. Okawa, *J. Am. Chem. Soc.*, 1992, **114**, 6974; (*b*) H. Tamaki, M. Mitsumi, N. Nakamura, N. Matsumoto, S. Kida, H. Okawa and S. Ijima, *Chem. Lett.*, 1992, 1975; (*c*) C. Mathonière, S. G. Carling, D. Yuscheng and P. Day, *J. Chem. Soc., Chem. Commun.*, 1994, 1551; (*d*) C. Mathonière, J. Nutall, S. G. Carling and P. Day, *Inorg. Chem.*, 1996, **35**, 1201; (*e*) R. Pellaux, H. W. Schmalle, R. Huber, P. Fisher, T. Hauss, B. Ouladdiaf and S. Decurtins, *Inorg. Chem.*, 1997, **36**, 2301; (*f*) E. Coronado, J. R. Galán-Mascarós, C. J. Gómez-García, J. M. Martínez-Agudo, E. Martínez-Ferrero, J. C. Waerenborgh and M. Almeida, *J. Solid State Chem.*, 2001, **159**, 391; (*g*) K. S. Min, A. L. Rhinegold and J. S. Miller, *Inorg. Chem.*, 2005, **44**, 8433; (*h*) E. Coronado, J. R. Galán-Mascarós and C. Martí-Gastaldo, *J. Mater. Chem.*, 2006, **16**, 2685; (*i*) Z. Duan, Y. Zhang, B. Zhang and F. L. Pratt, *Inorg. Chem.*, 2009, **48**, 2140.
3 (*a*) M. Clemente-León, J. R. Galán-Mascarós and C. J. Gómez-García, *Chem. Commun.*, 1997, 1727; (*b*) E. Coronado, J. R. Galán-Mascarós, C. J. Gómez-García and J. M. Martínez-Agudo, *Adv. Mater.*, 1999, **11**, 558; (*c*) E. Coronado, J. R. Galán-Mascarós, C. J. Gómez-García, J. Ensling and P. Gutlich, *Chem.–Eur. J.*, 2000, **6**, 552.
4 E. Coronado, C. Giménez-Saiz, C. J. Gómez-Garcia, F. M. Romero and A. Tarazón, *J. Mater. Chem.*, 2008, **18**, 929.
5 (*a*) S. Bénard, P. Yu, J. P. Audière, E. Rivière, R. Clèment, J. Ghilhem, L. Tchertanov and K. Nakatami, *J. Am. Chem. Soc.*, 2000, **122**, 9444; (*b*) S. M. Aldoshin, N. A. Sanina, V. I. Minkin, N. A. Voloshin, V. N. Ikorskii, V. I. Ovcharenko, V. A. Smirnov and N. K. Nagaeva, *J. Mol. Struct.*, 2007, **826**, 69.
6 S. Bénard, E. Rivière, P. Yu, K. Nakatami and J. F. Delouis, *Chem. Mater.*, 2001, **13**, 159.
7 (*a*) E. Coronado, J. R. Galán-Mascarós, C. J. Gómez-García and V. Laukhin, *Nature*, 2000, **408**, 447; (*b*) A. Alberola, E. Coronado, J. R. Galán-Mascarós, C. Giménez-Saiz and C. J. Gómez-García, *J. Am. Chem. Soc.*, 2003, **125**, 10774; (*c*) E. Coronado, J. R. Galán-Mascarós, C. J. Gómez-García, E. Martínez-Ferrero and S. Van Smaalen, *Inorg. Chem.*, 2004, **43**, 4808.
8 M. Clemente-León, E. Coronado, J. C. Dias, A. Soriano-Portillo and R. D. Willett, *Inorg. Chem.*, 2008, **47**, 6458.
9 C. Train, R. Gheorghe, V. Krstic, L. M. Chamoreau, N. S. Ovanesyan, G. L. J. A. Rikken, M. Gruselle and M. Verdaguer, *Nat. Mater.*, 2008, **7**, 729.
10 C. Train, T. Nuida, R. Gheorghe, M. Gruselle and S. Ohkoshi, *J. Am. Chem. Soc.*, 2009, **131**, 16838.
11 H. Okawa, A. Shigematsu, M. Sadakiyo, T. Miyagawa, K. Yoneda, M. Ohba and H. Kitagawa, *J. Am. Chem. Soc.*, 2009, **131**, 13516.
12 (*a*) F. D. Rochon, R. Melanson and M. Andruh, *Inorg. Chem.*, 1996, **35**, 6086; (*b*) M. Andruh, R. Melanson, C. V. Stager and F. D. Rochon, *Inorg. Chim. Acta*, 1996, **251**, 309; (*c*) N. Stanica, C. V. Stager, M. Cimpoesu and M. Andruh, *Polyhedron*, 1998, **17**, 1787; (*d*) G. Marinescu, M. Andruh, R. Lescouëzec, M. C. Muñoz, J. Cano, F. Lloret and M. Julve, *New J. Chem.*, 2000, **24**, 527; (*e*) S. Triki, F. Berezovsky, J. S. Pala, E. Coronado, C. J. Gómez-García, J. M. Clemente, A. Riou and P. Molinie, *Inorg. Chem.*, 2000, **39**, 3771; (*f*) G. Ballester, E. Coronado, C. Giménez-Saiz and F. M. Romero, *Angew. Chem., Int. Ed.*, 2001, **40**, 792; (*g*) E. Coronado, C. Giménez-Saiz, J. R. Galán-Mascarós, C. J. Gómez-García and C. Ruiz-Pérez, *Eur. J. Inorg. Chem.*, 2003, 2290; (*h*) E. Coronado, J. R. Galán-Mascarós, C. J. Gómez-García and C. Martí-Gastaldo, *Inorg. Chem.*, 2005, **44**, 6197; (*i*) E. Coronado, J. R. Galán-Mascarós and C. Martí-Gastaldo, *Inorg. Chem.*, 2006, **45**, 1882; (*j*) E. Coronado, J. R. Galán-Mascarós, C. Martí-Gastaldo and A. Murcia-Martínez, *Dalton Trans.*, 2006, 3294; (*k*) H. Z. Kou and O. Sato, *Inorg. Chem.*, 2007, **46**, 9513; (*l*) E. Cariati, R. Macchi, D. Roberto, R. Ugo, S. Galli, N. Casati, P. Macchi, A. Sironi, L. Bogani, A. Caneschi and D. Gatteschi, *J. Am. Chem. Soc.*, 2007, **129**, 9410; (*m*) H. Z. Kou, J. Tao and O. Sato, *Dalton Trans.*, 2008, 3652; (*n*) E. Coronado, J. R. Galán-Mascarós and C. Martí-Gastaldo, *CrystEngComm*, 2009, **11**, 2143; (*o*) Q.-X. Yao, L. Pan, X.-H. Jin, J. Li, Z.-F. Ju and J. Zhang, *Chem.–Eur. J.*, 2009, **15**, 11890.
13 (*a*) S. Decurtins, H. W. Schmalle, P. Schneuwly and H. R. Oswald, *Inorg. Chem.*, 1993, **32**, 1888; (*b*) S. Decurtins, H. W. Schmalle, P. Schneuwly, J. Ensling and P. Gütlich, *J. Am. Chem. Soc.*, 1994, **116**, 9521; (*c*) M. Hernández-Molina, F. Lloret, C. Ruiz-Pérez and M. Julve, M., *Inorg. Chem.*, 1998, **37**, 4131; (*d*) E. Coronado, J. R. Galán-Mascarós, C. J. Gómez-García and J. M. Martínez-Agudo, *Inorg. Chem.*, 2001, **40**, 113; (*e*) F. Pointillart, C. Train, M. Gruselle, F. Villain, H. W. Schmalle, D. Talbot, P. Gredin, S. Decurtins and M. Verdaguer, *Chem. Mater.*, 2004, **16**, 832; (*f*) M. Clemente-León, E. Coronado, C. J. Gómez-García and A. Soriano-Portillo, *Inorg. Chem.*, 2006, **45**, 5653.
14 (*a*) R. Andrés, M. Gruselle, B. Malézieux, M. Verdaguer and J. Vaissermann, *Inorg. Chem.*, 1999, **38**, 4637; (*b*) R. Andrés, M. Brissard, M. Gruselle, C. Train, J. Vaissermann, B. Malézieux, J. P. Jamet and M. Verdaguer, *Inorg. Chem.*, 2001, **40**, 4633.
15 R. Sieber, S. Decurtins, H. Stoeckli-Evans, C. Wilson, D. Yufit, J. A. K. Howard, S. C. Capelli and A. Hauser, *Chem.–Eur. J.*, 2000, **6**, 361.
16 E. Coronado, J. R. Galán-Mascarós, M. C. Giménez-López, M. Almeida and J. C. Waerenborgh, *Polyhedron*, 2007, **26**, 1838.
17 M. Clemente-León, E. Coronado, M. C. Giménez-López, A. Soriano-Portillo, J. C. Waerenborgh, F. S. Delgado and C. Ruiz-Pérez, *Inorg. Chem.*, 2008, **47**, 9111.
18 M. Clemente-León, E. Coronado, M. López-Jordà, G. Mínguez Espallargas, A. Soriano-Portillo and J. C. Waerenborgh, *Chem.–Eur. J.*, 2010, **16**, 2207, DOI: 10.1002/chem.200902668.
19 M. F. Tweedle and L. J. Wilson, *J. Am. Chem. Soc.*, 1976, **98**, 4824.
20 J. C. Baylar and E. M. Jones, in *Inorganic Synthesis*, ed. H. S. Booth, McGraw-Hill, New York, 1939, vol. 5, p. 35.
21 A. Altomare, M. C. Burla, M. Camalli, G. L. Cascarano, C. Giacovazzo, A. Guagliardi, A. G. G. Moliterni, G. Polidori and R. Spagna, *J. Appl. Crystallogr.*, 1999, **32**, 115–119.
22 *SHELXL-97*: G. M. Sheldrick, University of Göttingen, Germany, 1997.
23 L. J. Farrugia, *J. Appl. Crystallogr.*, 1999, **32**, 837.
24 (*a*) H. D. Flack, *Acta Crystallogr., Sect. A: Found. Crystallogr.*, 1983, **39**, 876; (*b*) G. Bernardinelli and H. D. Flack, *Acta Crystallogr., Sect. A: Found. Crystallogr.*, 1985, **41**, 500.
25 N. Ovanesyan, V. D. Makhaev, S. M. Aldoshin, P. Gredin, K. Boubekeur, C. Train and M. Gruselle, *Dalton Trans.*, 2005, 3101.
26 M. Gruselle, C. Train, K. Boubekeur, P. Gredin and N. Ovanesyan, *Coord. Chem. Rev.*, 2006, **250**, 2491.
27 C. Janiak, *J. Chem. Soc., Dalton Trans.*, 2000, 3885.
28 R. Pritchard, S. A. Barrett, C. A. Kilner and M. A. Halcrow, *Dalton Trans.*, 2008, 3159.
29 N. A. Chernova, Y. Song, P. Y. Zavalij and M. S. Wittingham, *Phys. Rev. B: Condens. Matter Mater. Phys.*, 2004, **70**, 144405.
30 G. L. J. A. Rikken and E. Raupach, *Nature*, 1997, **390**, 493.

DOI: 10.1002/chem.200902668

Multifunctional Magnetic Materials Obtained by Insertion of a Spin-Crossover Fe^{III} Complex into Bimetallic Oxalate-Based Ferromagnets

Miguel Clemente-León,*[a, b] Eugenio Coronado,*[a] Maurici López-Jordà,[a] Guillermo Mínguez Espallargas,[a] Alejandra Soriano-Portillo,[a] and João C. Waerenborgh[c]

Abstract: The syntheses, structures and magnetic properties of the compounds of formula $[Fe^{III}(sal_2\text{-trien})][Mn^{II}Cr^{III}(ox)_3]\cdot CH_2Cl_2$ (**1**; H_2sal_2-trien = *N*,*N*′-disalicylidenetriethylenetetramine, ox = oxalate), $[Fe^{III}(sal_2\text{-trien})][Mn^{II}Cr^{III}(ox)_3]\cdot CH_3OH$ (**2**), $[In^{III}(sal_2\text{-trien})][Mn^{II}Cr^{III}(ox)_3]\cdot 0.25\,H_2O\cdot 0.25\,CH_3OH\cdot 0.25\,CH_3CN$ (**3**), and $[In^{III}(sal_2\text{-trien})][Mn^{II}Cr^{III}(ox)_3]\cdot CH_3NO_2\cdot 0.5\,H_2O$ (**4**) are reported. The structure of **1** presents a 2D honeycomb anionic layer formed by Mn^{II} and Cr^{III} ions linked through oxalate ligands and a cationic layer of $[Fe(sal_2\text{-trien})]^+$ complexes intercalated between the 2D oxalate network. The structures of **2**, **3**, and **4** present a 3D achiral anionic network formed by Mn^{II} and Cr^{III} ions linked through oxalate ligands with $[Fe(sal_2\text{-trien})]^+$ or $[In(sal_2\text{-trien})]^+$ complexes and solvent molecules intercalated within the 3D oxalate network. The magnetic properties and Mössbauer spectroscopy of **1** and **2** indicate that these compounds undergo a long-range ferromagnetic ordering at around 5 K and a spin crossover of the intercalated $[Fe(sal_2\text{-trien})]^+$ complexes above 130 K, which is complete in the case of **1**. The magnetic properties of the compounds **3** and **4** confirm the ferromagnetic ordering of the bimetallic oxalate network.

Keywords: coordination chemistry · iron · magnetic properties · Moessbauer spectroscopy · spin crossover

Introduction

One of the most exciting developments in molecular magnetism is the preparation of multifunctional compounds. The versatility of molecular chemistry makes possible the design of new molecule-based materials that combine two (or more) physical properties of interest. Thus, a wise choice of the constituent molecules could allow the appearance in the same compound of an unusual combination of physical properties, or even a mutual interplay—synergy—of the properties involved. A suitable approach to obtaining such materials is the so-called hybrid approach in which two-network solids are constructed through the self-assembly of two different molecular fragments (organic, inorganic, or organometallic), with each network furnishing the solid with distinct properties.[1]

Bimetallic oxalate-bridged complexes of formula $A[M^{II}M^{III}(ox)_3]$ (M^{III} = Cr, Fe, Ru, V, Mn; M^{II} = Mn, Fe, Co, Ni, Cu, Zn; ox = oxalate; A = cation) have provided many examples of hybrid magnets. These bimetallic salts are most often composed of polymeric 2D anionic networks, which furnish the cooperative magnetic properties (ferro-, ferri-, or canted antiferromagnetism),[2] and a bulky charge-compensating molecular cation, which templates the network formation. In these compounds, the cooperative magnetism of the oxalate network can coexist with the electronic properties provided by the cationic molecular lattice. Some illustrative examples of this concept are provided by the use of paramagnetic decamethylferrocenium[3] or organic radical cations,[4] photochromic molecules,[5] nonlinear optical (NLO)-active molecules,[6] organic π-electron donors,[7] and chiral

[a] Dr. M. Clemente-León, Prof. E. Coronado, M. López-Jordà, Dr. G. Mínguez Espallargas, Dr. A. Soriano-Portillo
Instituto de Ciencia Molecular, Universidad de Valencia
Polígono de la Coma s/n, 46980 Paterna (Spain)
Fax: (+34) 963543273
E-mail: miguel.clemente@uv.es
eugenio.coronado@uv.es

[b] Dr. M. Clemente-León
Fundació General de la Universitat de València (FGUV)

[c] Dr. J. C. Waerenborgh
Dept. Quimica, Instituto Tecnológico e Nuclear/CFMC-UL
2686-953 Sacavém (Portugal)

Supporting information for this article is available on the WWW under http://dx.doi.org/10.1002/chem.200902668.

cations,[8] which lead to the formation of magnetic multilayers, photochromic magnets, ferromagnetic molecular metals, or chiral magnets. More recently, the magnetochiral dichroic effect has been observed for the first time on a chiral magnet in enantiopure 2D oxalate-based magnets prepared by Train et al.[9] Other magnetic networks, different from the 2D honeycomb-like network, can also be obtained depending on the nature of the templating cation (size, shape, and charge) with dimensionalities ranging from 0D to 3D.[10] The most extensive one is represented by the family of 3D chiral structures in which the chirality of a templating cation of the type $[Z^{II}(bpy)_3]^{2+}$ (Z^{II} = Fe, Co, Ni, Ru; bpy = 2,2′-bipyridine) induces the building blocks to adopt a homochiral configuration,[11] which provides an opportunity to obtain chiral magnets.[11e,12] In addition, the hybrid character of these series also leads to examples in which the two sublattices are magnetic.[11d]

In this context, spin-crossover cations are particularly suitable to prepare multifunctional magnetic materials since they represent one of the best examples of molecular bistability. This may open a way to design switching magnets in which the magnetic ordering of the oxalate network could be tuned, thus taking advantage of the possibility of inducing the spin-crossover phenomenon by applying an external stimuli such as light or pressure. However, this challenging goal requires first the preparation of hybrid materials formed by a magnetic network and a spin-crossover complex.

The first example of the insertion of spin-crossover cations into oxalate networks was reported by Decurtins et al. in a compound of formula $[Co(bpy)_3][LiCr(ox)_3]$.[13] In that case, the insertion of a Co^{II} complex into a 3D oxalate-based network resulted in the observation of spin crossover in the Co^{II} sublattice. However, the compound did not show coexistence of spin crossover and magnetic ordering since the oxalate network was paramagnetic. More recently, our group reported the insertion of the Fe^{II} spin-crossover complex $[Fe(bpp)_2]^{2+}$ (bpp = 2,6-bis(pyrazol-3-yl)pyridine) into a ferromagnetic achiral 3D oxalate-based network, $[Fe(bpp)_2][MnCr(ox)_3]\cdot bpp\cdot CH_3OH$,[14] although spin crossover was not observed as most Fe^{II} complexes remained in the low-spin (LS) state throughout the entire temperature range. The coexistence of a spin crossover and magnetic ordering has successfully been obtained very recently by insertion of Fe^{III} complexes in homometallic oxalate layers.[15] As a result, the compound $[\{Fe^{III}(sal_2\text{-trien})\}_2][Mn^{II}_2(ox)_3]\cdot 4H_2O\cdot C_3H_7NO$ (sal_2-trien = hexadentate ligand; see Scheme 1) formed by homometallic Mn^{II} oxalate layers and $[Fe(sal_2\text{-trien})]^+$ cations behaves as a weak ferromagnet below a critical temperature (T_c) of 8.1 K and exhibits at the same time a gradual spin crossover of half of the intercalated $[Fe(sal_2\text{-trien})]^+$ complexes from 300 to 80 K. In this compound, however, the two properties seem to be independent since the change in the spin state of the inserted $[Fe(sal_2\text{-trien})]^+$ cations after desolvation does not produce important changes in the magnetic ordering of the homometallic oxalate network.

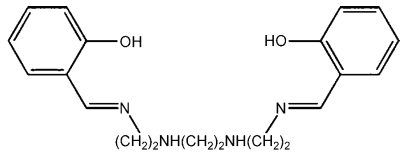

Scheme 1. H_2sal_2-trien.

In view of this first result, we have explored the insertion of the $[Fe(sal_2\text{-trien})]^+$ complex into bimetallic oxalate anionic networks. This approach has several advantages with respect to the previous one. On one hand, the use of bimetallic oxalate networks can give rise to ferro- or ferrimagnetism instead of weak ferromagnetism due to a spin canting in the antiferromagnetic state. On the other hand, the possibility of inserting the spin crossover complex into a 3D lattice could improve the effect of the spin crossover on the magnetic ordering of the oxalate network since the 3D oxalate networks are much more sensitive to small structural and size changes of the inserted cation than the 2D oxalate networks.[11f]

In this work we report the preparation and structural and magnetic characterization of the compounds $[Fe^{III}(sal_2\text{-trien})][Mn^{II}Cr^{III}(ox)_3]\cdot CH_2Cl_2$ (**1**), which presents a 2D oxalate-based anionic network, and $[Fe^{III}(sal_2\text{-trien})][Mn^{II}Cr^{III}(ox)_3]\cdot CH_3OH$ (**2**), $[In^{III}(sal_2\text{-trien})][Mn^{II}Cr^{III}(ox)_3]\cdot 0.25\,H_2O\cdot 0.25\,CH_3OH\cdot 0.25\,CH_3CN$ (**3**), and $[In^{III}(sal_2\text{-trien})][Mn^{II}Cr^{III}(ox)_3]\cdot CH_3NO_2\cdot 0.5\,H_2O$ (**4**), which present an achiral 3D oxalate-based anionic network. The compounds containing the diamagnetic $[In(sal_2\text{-trien})]^+$ complex have been studied as reference compounds.

Results and Discussion

Synthesis: The method used to prepare this family of compounds is analogous to that used to prepare the chiral oxalate 2D compound of formula $[(S)\text{-}\{PhCH(CH_3)N(CH_3)_3\}][Mn(CH_3CN)_{2/3}Cr(ox)_3]\cdot CH_3CN\cdot$(solvate).[8] It is based on the use of $Ag_3[Cr(ox)_3]$ to avoid the presence of alkali ions in the structure. It consists of the slow diffusion of a solution containing the precursors of the oxalate network, Mn^{2+} and $[Cr(ox)_3]^{3-}$ ions, in methanol, into a solution of $[M(sal_2\text{-trien})]^+$ (M^{III} = Fe or In) in different solvents. The use of different solvents to dissolve the $[M(sal_2\text{-trien})]^+$ complex gives rise to different structures. Thus, **1** is obtained by using CH_2Cl_2, **2** and **3** by using CH_3CN, and **4** by using CH_3NO_2. The composition of these crystals, checked by microanalysis, shows in all cases a M/Mn/Cr ratio of 1:1:1. Furthermore, crystals of **1** show the presence of Cl from CH_2Cl_2 in a ratio 2:1 with respect to Mn, Cr, and Fe. It has not been possible to obtain the crystal structure of the 2D oxalate network with the $[In(sal_2\text{-trien})]^+$ cation dissolved in dichloromethane. Due to this, we have tried with other solvents such as CH_3NO_2, but this has resulted in a new compound, **4**, that presents a 3D oxalate network slightly different to that of **2**

and **3**. The crystal structures of the four compounds have been solved by single-crystal X-ray diffraction. Unit cells of several crystals obtained in the same diffusion tube have been measured by single-crystal X-ray diffraction and give similar results in all cases. This excludes the possibility of crystallization of the different structures by using the same solvent mixture. Attempts to obtain analogous compounds with other paramagnetic M^{2+} ions (M = Ni, Fe, Co, and Cu), or with other M^{III} ions (M^{III} = Fe) in the place of Cr^{III} have been unsuccessful.

Structure of $[Fe^{III}(sal_2\text{-trien})][Mn^{II}Cr^{III}(ox)_3]\cdot CH_2Cl_2$ (1): The structure of this compound is formed by anionic sheets in the *bc* plane of formula $[MnCr(ox)_3]^-$ with interlamellar $[Fe(sal_2\text{-trien})]^+$ cations and dichloromethane solvent molecules (Figure 1). The anionic layer is formed by an extended

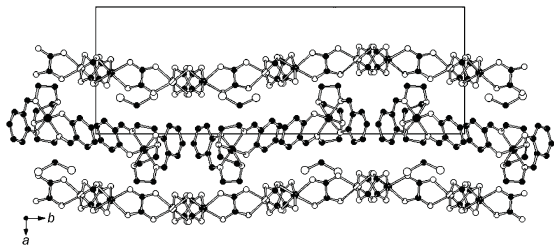

Figure 1. Projection on the *ab* plane of the structure of **1** (for clarity, neighboring atoms that correspond to disordered Mn/Cr have been assigned for Mn and Cr separately). Hydrogen atoms have been omitted for clarity.

network with Mn^{II} and Cr^{III} ions linked through oxalate bridges. It presents the well-known 2D honeycomb structure. It is formed by oxalate ligands connecting Mn^{II} with Cr^{III} ions in such a way that each Mn^{II} is surrounded by three neighboring Cr^{III} and vice versa (Figure 2). The neighboring metal centers of these layers present alternated chirality as is usual for this type of network. There are two metals that are crystallographically independent with M–O bond lengths lying between 2.061(3) and 2.107(3) Å. These bond lengths are intermediate between the ones expected for Cr^{III}–O and Mn^{II}–O. Therefore, it is not possible to distinguish between the two metals in this structure. Mean metal–metal distances between adjacent centers are in the range 5.3941(13)–5.4432(13) Å. These distances are similar to those found in other 2D oxalate networks reported in the literature[2,3] and shorter than those found in 3D systems.[11,13] The distance between metal ions of different layers is 11.6440(2) Å, which is higher than those found in other oxalate-based 2D compounds with decamethylferrocenium or alkylammonium cations (9.2–9.7 Å)[2,3] but lower than those of the $[\{Fe^{III}(sal_2\text{-trien})\}_2][Mn^{II}_2(ox)_3]\cdot 4H_2O\cdot C_3H_7NO$ compound (17.489(7) Å) in which a double layer of cations is necessary to compensate for the higher charge of the $[Mn^{II}_2(ox)_3]^{2-}$ anionic layer with respect to the $[M^{II}M^{III}(ox)_3]^-$ anionic layer.[15] These anionic layers are stacked one over the other in an *AA*… fashion. The Mn^{II} and Cr^{III} ions and oxalate ligands do not form a perfect 2D layer, as there is a certain amount of undulation of the inorganic layer (see Figure 1). The presence of ethylene groups from $[Fe(sal_2\text{-trien})]^+$ that extend alternatively above and below the layer of inserted $[Fe(sal_2\text{-trien})]^+$ complexes could be responsible for this effect. Finally, the minimum distance between the metallic ions from the oxalate network and the Fe atoms is 6.3795(9) Å.

The space between the oxalate layers is occupied by one crystallographically independent $[Fe(sal_2\text{-trien})]^+$ complex and one dichloromethane molecule (Figures 1 and 2). The

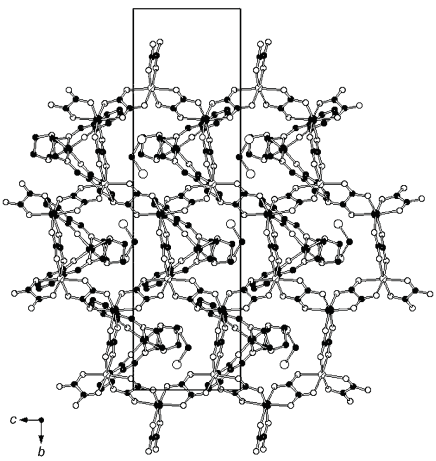

Figure 2. Projection on the *bc* plane of the structure of **1** (for clarity, neighboring atoms that correspond to disordered Mn/Cr have been assigned for Mn and Cr separately). Hydrogen atoms have been omitted for clarity.

$[Fe(sal_2\text{-trien})]^+$ cations lie with their longer axis parallel to the oxalate layers. They form double chains running along the *c* axis (Figure 1 and Figure 1SS in the Supporting Information) in which $[Fe(sal_2\text{-trien})]^+$ complexes are connected through C–H···π and N–H···π interactions.[16] Only one of the two phenoxy rings of sal_2-trien, which is placed in the internal part of the double chain, is involved in these C–H···π and N–H···π interactions with two adjacent $[Fe(sal_2\text{-trien})]^+$ complexes that belong to the same chain. These are edge-to-face interactions with a shortest distance of 3.592(7) Å between C4 and C1 of neighboring rings and 3.356(6) Å between C4 and N3 of neighboring rings (Figure 1SS in the Supporting Information). Furthermore, the phenoxy rings from $[Fe(sal_2\text{-trien})]^+$ complexes that belong to different double chains that are not involved in these interactions present short contacts with O atoms from the oxalate network ($d_{C16–O14}$ = 3.384(6) Å). Finally, there are short contacts between C atoms from ethylene groups of sal_2-trien and the oxalate ligands ($d_{C10–O13}$ = 3.152(6) Å). The average Fe–N and Fe–O bond lengths in $[Fe(sal_2\text{-trien})]^+$ complexes are

1.989(4) and 1.866(3) Å, respectively. These values are in the range of those obtained for other low-spin $[Fe(sal_2\text{-}trien)]^+$ compounds[17] and are in full agreement with the magnetic measurements and Mössbauer spectroscopy (see below), which indicate that all Fe are LS at 180 K (the temperature at which the crystal structure has been determined). On the other hand, the dichloromethane molecules occupy the holes situated in between the $[Fe(sal_2\text{-}trien)]^+$ cations and the oxalate network. They are placed alternatively above and below the layer formed by $[Fe(sal_2\text{-}trien)]^+$ cations. They present short contacts with oxalate ligands ($d_{Cl1\text{–}O10}=3.258(3)$ Å and $d_{Cl2\text{–}O12}=2.979(3)$ Å).

Structure of $[Fe^{III}(sal_2\text{-}trien)][Mn^{II}Cr^{III}(ox)_3]\cdot CH_3OH$ (2): The structure of **2** is formed by an anionic 3D polymeric oxalate-bridged bimetallic network with $[Fe(sal_2\text{-}trien)]^+$ cations and solvent molecules occupying the cavities (Figure 3).

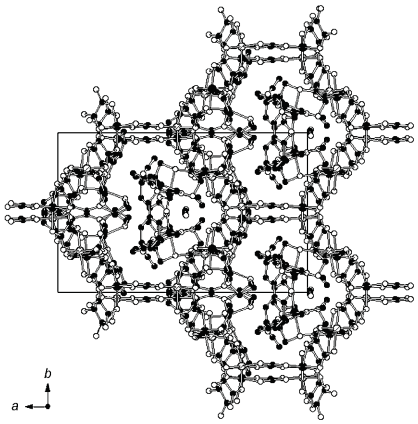

Figure 3. Projection on the *ab* plane of the structure of **2** (for clarity, neighboring atoms that correspond to disordered Mn/Cr have been assigned for Mn and Cr separately). Hydrogen atoms have been omitted for clarity.

This anionic polymeric structure is formed by bis-chelating oxalate ligands that connect Mn^{II} and Cr^{III} ions in such a way that each Mn^{II} is surrounded by three Cr^{III} and vice versa, thus building ten-membered rings in a (10,3) topology. In contrast to typical chiral structures exhibited by the oxalate-based 3D network, compound **2** possesses metal centers of both chiralities. In fact, **2** crystallizes in the acentric *Cc* space group. A similar achiral 3D oxalate network has been found in the compound of formula $[Fe(bpp)_2][\{MnCr(ox)_3\}_2]\cdot bpp\cdot CH_3OH$ that crystallizes in the centrosymmetric $P2_1/n$ space group.[14] The (10,3) decagon rings perpendicular to the *c* axis are formed by metal centers with the same chirality (see Figure 3). Two of these neighboring metal rings, which are linked through two oxalate ligands, present opposite chirality (see Figure 4). Projection of the oxalate network on the *ac* plane is almost identical to that of the chiral 3D oxalate network in the *ab*, *bc*, or *ac* planes

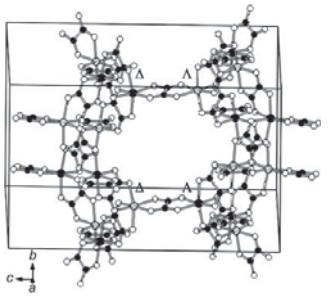

Figure 4. Two neighboring ten-membered rings of the oxalate network of **2** of opposite chirality connected through two oxalate ligands along the *c* direction (for clarity, neighboring atoms that correspond to disordered Mn/Cr have been assigned for Mn and Cr separately). Hydrogen atoms have been omitted for clarity.

(see Figure 5). However, projection on the *bc* or *ab* planes (see Figures 3 and 4) is different as a result of the different chirality of the neighboring (10,3) decagon rings. Thus, in

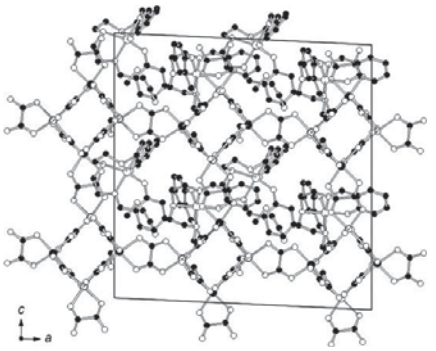

Figure 5. Projection on the *ac* plane of the structure of **2** (for clarity, neighboring atoms that correspond to disordered Mn/Cr have been assigned for Mn and Cr separately). Hydrogen atoms have been omitted for clarity.

the *ab* projection an eclipsed disposition of the neighboring oxalate rings is observed as a result of the heterochiral oxalate junctions among them (see Figure 3). This anionic network contains four metals that are crystallographically independent with M–O bond lengths lying between 2.004(14) and 2.141(13) Å. Again, these bond lengths are intermediate between the ones expected for Cr^{III}–O and Mn^{II}–O and hence it is not possible to distinguish between the two metals in this structure. Metal–metal distances between adjacent centers are in the range 5.396(3)–5.408(3) Å. These metal–metal distances are significantly shorter than those exhibited by the 3D chiral structures. For instance, the Mn–Cr distance in $[Ir(ppy)_2(bpy)][MnCr(ox)_3]\cdot 0.5\,H_2O$ is 5.503 Å.[11f] These metal–metal distances are shorter than those found for compound **1**, although it is important to

note that the crystal structure of compound **2** was determined at lower temperature (120 versus 180 K). In addition, the minimum distance between the metallic ions from the oxalate network and the Fe atoms is also shorter than in compound **1**. Thus, a value of 5.905(4) Å is obtained between Mn4/Cr4 and Fe1.

$[Fe(sal_2\text{-trien})]^+$ complexes and solvent molecules are intercalated in the holes described by this 3D oxalate network. There are two crystallographically independent $[Fe(sal_2\text{-trien})]^+$ complexes ([Fe1] and [Fe2]) and disordered methanol. The phenoxy rings from two neighboring crystallographically independent $[Fe(sal_2\text{-trien})]^+$ complexes present edge-to-face interactions with a shortest distance of 3.46(12) Å between C19 and C26 of neighboring rings. Furthermore, the [Fe1] complex presents hydrogen bonds through the NH groups with one disordered methanol molecule and one oxalate ligand ($d_{N3\cdots O3M}=3.11(2)$ and $d_{N2\cdots O24}=3.100(18)$ Å) and short contacts with oxalate ligands ($d_{C14\text{–}O19}=3.21(2)$ and $d_{C19\text{–}O22}=3.137(16)$ Å), whereas the [Fe2] complex forms hydrogen bonds with two disordered methanol molecules ($d_{N6\cdots O2M}=3.15(3)$ and $d_{O4\cdots O3M}=2.94(3)$ Å) and presents short contacts with oxalate ligands from the oxalate network ($d_{C29\text{–}O12}=3.05(3)$ Å). The average Fe–N and Fe–O bond lengths are 2.042(17) and 1.891(13) Å in [Fe1] complexes and 2.15(2) and 1.877(15) Å in [Fe2] complexes. These values are higher than those found in **1** and close to those obtained for other high-spin (HS) $[Fe(sal_2\text{-trien})]^+$ compounds. We have to take into account that magnetic measurements and Mössbauer spectroscopy (see below) indicates that around 28% of Fe is LS at 120 K (the temperature at which the crystal structure has been determined).

Interestingly, the use of the same templating cation in different solvents has afforded different structures. This finding is very unusual for this type of oxalate compound. The few examples in the literature in which that occurs involve either a change in the coordination mode of the oxalate ligand, or the presence of solvent molecules that complete the coordination of the metals from the oxalate network.[10k,l,18] In our case, the two different structures—a 2D and an achiral 3D oxalate network—present bis-chelating oxalate ligands that connect M^{II} and M^{III} ions. To our knowledge, this is a novel feature in this type of compound. A possible explanation may be related to the flexibility of $[Fe(sal_2\text{-trien})]^+$ cation. This complex presents two phenoxy arms projecting from the same face of the molecule.[17] The relative orientation of these arms differs notably in different compounds. Therefore, a different configuration of the phenoxy rings may have a different templating effect on the oxalate network, thus giving rise to different structures. Indeed, the configuration of $[Fe(sal_2\text{-trien})]^+$ cations in the structures of **1** and **2** confirms this point. The dihedral angles (α) between the least-squares planes of the two phenoxy rings have very different values in the 2D or 3D structures presented in this paper. Thus, $\alpha=71.65(13)°$ is present in **1**, whereas $\alpha=120.13(67)°$ ([Fe1] complex) and $\alpha=103.02(75)°$ ([Fe2] complex) are present in **2**. Whereas in the 2D compound the two phenoxy rings are clearly below 90°, the ideal value for an octahedral complex, the opposite behavior is observed in the 3D compound for the two crystallographically independent $[Fe(sal_2\text{-trien})]^+$ cations, which present α higher than 90°. Such a difference may be induced by the different solvent mixture used to dissolve the $[Fe(sal_2\text{-trien})]^+$ cations in the two compounds.

It is also possible to relate this configuration to the magnetic behavior of the $[Fe(sal_2\text{-trien})]^+$ complexes in the two compounds. Pritchard et al. have shown that there is a correlation between the disposition of the two phenoxy groups and the spin state of $[Fe(sal_2\text{-trien})]^+$ salts.[17] All $[Fe(sal_2\text{-trien})]^+$ compounds with LS state adopt a configuration with an α angle of 61.8–73.6°, whereas those presenting a HS state are much more structurally variable. They conclude that compounds presenting a low α angle, which is the preferred configuration for the LS state, can undergo a spin crossover. On the contrary, those presenting high α angles remain in the HS state, as the structural changes needed to adopt a LS state prevent the spin crossover from occurring. This is confirmed for the two compounds presented in this paper. Thus, in compound **1**, which shows a clear spin crossover (see below), $\alpha=71.65(13)°$, whereas in compound **2**, which remains mostly in the HS state throughout the entire temperature range, α values of 120.13(67) and 103.02(75)° are observed.

Structure of $[In^{III}(sal_2\text{-trien})][Mn^{II}Cr^{III}(ox)_3]\cdot 0.25\,H_2O\cdot 0.25\,CH_3OH\cdot 0.25\,CH_3CN$ (3): The structure of **3** resembles that of **2** with $[In(sal_2\text{-trien})]^+$ cations in the place of $[Fe(sal_2\text{-trien})]^+$ (see Figures 2SS, 3SS, and 4SS in the Supporting Information). The bimetallic oxalate 3D network is similar to that of **2**. It is formed by four metals that are crystallographically independent with M–O bond lengths that lie between 2.050(6) and 2.103(6) Å. Again, it is not possible to distinguish between Mn or Cr in this structure. Metal–metal distances between adjacent centers are in the range 5.3545(14)–5.4157(14) Å. The cavities of the oxalate network are occupied by two crystallographically independent $[In(sal_2\text{-trien})]^+$ complexes ([In1] and [In2]), and disordered water, methanol, and acetonitrile molecules. The disposition of the solvent molecules and $[In(sal_2\text{-trien})]^+$ differs with respect to that of **2**. In this case, the complex [In1] forms hydrogen bonds with one methanol molecule ($d_{N7\cdots O1M}=3.084(16)$ Å) and one water molecule ($d_{O50\cdots O1W}=3.038(13)$ Å), and has at the same time a short contact with an oxalate ligand ($d_{N7\text{–}O2}=3.269(13)$ Å) as well as C–H···π and N–H···π interactions with the neighboring [In2]. Apart from this short interaction between the two crystallographically independent complexes, [In2] presents one hydrogen bond with one water molecule ($d_{N2\cdots O1W}=3.033(10)$ Å) and two short interactions with an oxalate ligand ($d_{N3\text{–}O11}=3.199(7)$ and $d_{N3\text{–}O12}=3.122(7)$ Å). Dihedral angles between the phenoxy rings of [In1] and [In2] are, respectively, 120.22(52) and 102.96(60)°, similar to those found for $[Fe(sal_2\text{-trien})]^+$ complexes in compound **2**.

Structure of $[In^{III}(sal_2\text{-trien})][Mn^{II}Cr^{III}(ox)_3]\cdot CH_3NO_2\cdot 0.5H_2O$ (4): Compound **4** crystallizes in the acentric orthorhombic space group $Pna2_1$, which contains metal centers of both chiralities. It is formed by an anionic 3D polymeric oxalate-bridged bimetallic network similar to that of **2** and **3**. The cavities of this 3D network are occupied by the $[In(sal_2\text{-trien})]^+$ cations and nitromethane and water solvent molecules (Figure 6). In contrast to **2** and **3**, it is possible to

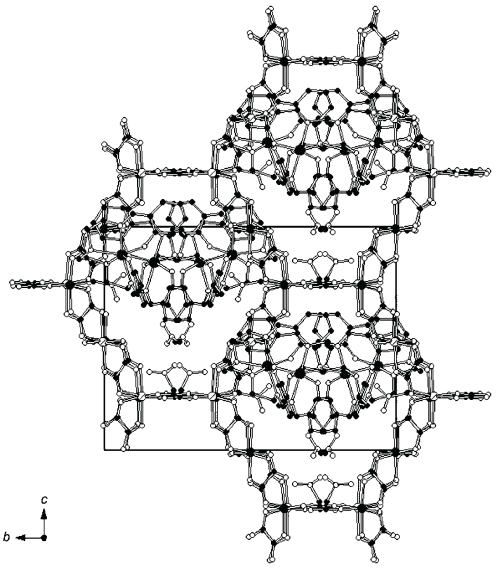

Figure 6. Projection on the *bc* plane of the structure of **4**. Hydrogen atoms have been omitted for clarity.

distinguish between Mn and Cr ions of this oxalate network. Thus, there are two crystallographically independent Mn ions (Mn1 and Mn2) with Mn–O bond lengths that lie between 2.151(6) and 2.196(6) Å and two crystallographically independent Cr ions (Cr1 and Cr2) with Cr–O bond lengths that lie between 1.957(6) and 1.988(6) Å. These are typical Cr^{III}–O and Mn^{II}–O distances similar to those found in other oxalate networks. Metal–metal distances between adjacent centers are in the range 5.3795(17)–5.4342(18) Å. These metal–metal distances are slightly shorter than those exhibited by **3** measured at the same temperature. This shortening may have some consequences on the magnetic properties (see below).

The (10,3) decagon rings formed by metal centers with the same chirality are in this case perpendicular to the *a* axis (Figure 6). Two of these neighboring metal rings, which are linked through two oxalate ligands, present opposite chirality as in the structure of **2** and **3** (see Figure 5SS in the Supporting Information). Projection of the oxalate network on the *ab* plane is almost identical to that of the chiral 3D oxalate network in the *ab*, *bc*, or *ac* planes (see Figure 6SS), whereas projections on the *bc* or *ac* planes (see Figure 6 and Figure 5SS in the Supporting Information) are different as a result of the different chirality of the neighboring (10,3) decagon rings, as observed for **2** and **3**. In this case, the eclipsed disposition of the neighboring rings is observed in the *bc* projection view (see Figure 6). In contrast to compounds **2** and **3**, which crystallize in a monoclinic space group, the eclipsed disposition of the rings is almost complete as a result of the higher symmetry of the space group of compound **4**.

The disposition of $[In(sal_2\text{-trien})]^+$ complexes and solvent molecules intercalated in the holes of this 3D oxalate network differs from that of **2** and **3**. There are two crystallographically independent $[In(sal_2\text{-trien})]^+$ complexes ([In1] and [In2]), one nitromethane molecule, and disordered nitromethane and water molecules. [In1] presents short contacts with the oxalate ligands through one of the two phenoxy rings ($d_{C14–O16}=2.924(11)$ and $d_{C15–O16}=3.168(11)$ Å). [In1] presents short contacts with two neighboring [In2] complexes. There are two types of short contacts. The first one is between the phenoxy ring of [In1] and one of the ethylene groups of [In2] ($d_{C19–C31}=3.280(18)$ and $d_{C19–N7}=3.237(15)$ Å). The second one is between one NH from [In1] and atoms from the phenoxy ring of [In2] ($d_{N3–C39}=3.218(11)$ and $d_{N3–C40}=3.294(11)$ Å). These are edge-to-face interactions. [In2] also presents short contacts with the oxalate ligands through one of the two phenoxy rings ($d_{C39–C55}=3.310(12)$ and $d_{C39–O28}=3.154(11)$ Å). Furthermore, the imine C linked to this phenoxy ring (C34) presents a short contact with another oxalate ligand ($d_{C34–O17}=2.901(12)$ Å). [In2] is also connected to two neighboring [In1] complexes through the short contacts mentioned above. The absence of methanol molecules in this structure could induce shorter contacts between neighboring $[M(sal_2\text{-trien})]^+$ complexes than those observed in compounds **2** or **3**. We have to take into account that methanol molecules of **2** and **3** are linked to sal_2-trien ligands through hydrogen bonds. Dihedral angles between the phenoxy rings of [In1] and [In2] are, respectively, 114.84(46) and 96.59(38)°.

Magnetic properties of 1: The thermal dependence of the product of the molar magnetic susceptibility with temperature (χT) of **1** is shown in Figure 7. χT shows a constant value of 10.0 emu K mol^{-1} from 400 to 350 K. This value is approximately equal to the sum of the expected contributions for the isolated paramagnetic ions with the Fe^{III} spin-crossover complex in a HS state. χT decreases gradually from 350 to 165 K as temperature decreases, with a more abrupt decrease below 300 K. The χT value at 165 K is 7.2 emu K mol^{-1}. This value of χT is consistent with the Mössbauer data that suggest that Fe^{III} is 94% LS at this temperature. Therefore, in this range of temperatures a full HS→LS spin conversion of the Fe^{III} complex takes place. At lower temperatures, there is an increase of χT that is very sharp below 50 K. This indicates the presence of ferromagnetic interactions between neighboring Mn^{II}–Cr^{III} magnetic ions and suggests the onset of long-range ferromagnetic ordering, as observed for other M^{II}–Cr^{III} 2D oxalate net-

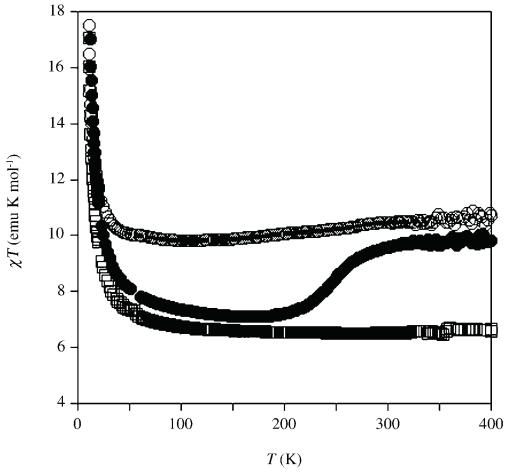

Figure 7. Temperature dependence of the product of the molar magnetic susceptibility with temperature (χT) at 0.1 T for compounds **1** (●), **2** (○), and **3** (□).

works.[2a,3] To confirm the presence of long-range magnetic ordering and to determine precisely the critical temperatures, alternating current (AC) susceptibility measurements were carried out. A maximum in the in-phase signal (χ') near T_c and an out-of-phase signal (χ'') that starts to appear at temperatures just below T_c is observed (Figure 8). From this data, the T_c of **1** is 5.4 K, similar to those reported for other Mn^{II}–Cr^{III} 2D oxalate compounds.[2a,3] These signals are frequency independent, as expected for a ferromagnet (Figure 8). In the ordered phase, an additional peak in χ'' at temperatures below 3 K is also detected. The presence of such a frequency-dependent peak has already been observed in other 2D M^{II}–Cr^{III} 2D oxalate compounds.[3] It can be related to the formation of magnetic domains and domain-wall movement.[19]

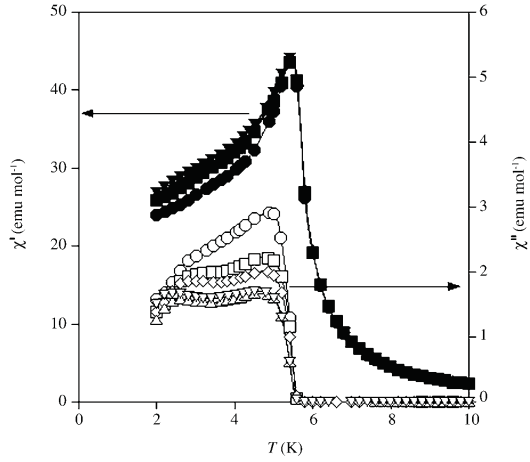

Figure 8. Temperature dependence of the in-phase AC susceptibility (χ') (filled symbols) and the out-of-phase AC susceptibility (χ'') (empty symbols) for **1**: ● 997 Hz, ■ 332 Hz, ◆ 110 Hz, ▲ 10 Hz, ▼ 1 Hz.

To confirm the ferromagnetic ordering of the spins, isothermal magnetization at 2 K was performed (Figure 9). It presented a sharp increase at low fields that is much faster than that expected for noninteracting Cr^{III} and Mn^{II} centers;

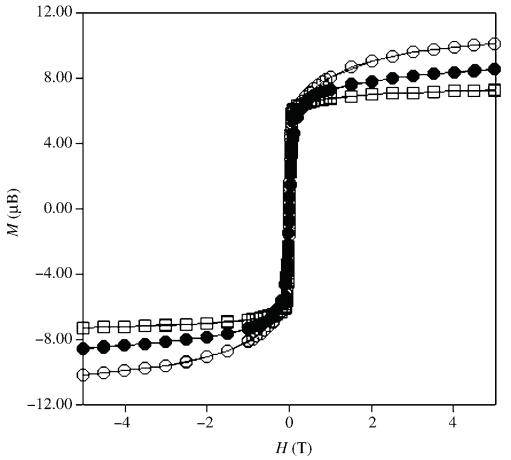

Figure 9. Field dependence of the magnetization (M) for **1** (●) **2** (○), and **3** (□).

this increase is more gradual at higher fields and no saturation is reached up to 5 T. The magnetization (M) value at 5 T is $8.5\mu_B$ (μ_B = Bohr magneton), which is slightly lower than the expected value for a parallel alignment of the spins in the bimetallic lattice ($9\mu_B$). It can be due to a spin canting of the ferromagnetic phase, as for other M^{II}–Cr^{III} 2D oxalate compounds.[3] The hysteresis loops at 2 K show that this compound is a soft ferromagnet with a coercive field of 2 mT.

The magnetic behavior of this compound after heating at 400 K under vacuum for 1 h has been studied because removal of solvent molecules may cause drastic changes in the spin-crossover behavior of this cation, as shown in other $[Fe(sal_2\text{-trien})]^+$ salts.[15,20] However, in contrast to similar compounds,[15] desolvation could not achieved, as microanalysis continued to show the presence of Cl in a 2:1 ratio with respect to Mn, Cr, and Fe.

Magnetic properties of 2 and 3: The thermal dependence of χT for **2** shows a value of 10.7 emu K mol^{-1} at 400 K (Figure 7). This value is close to the sum of the expected contributions for the isolated paramagnetic ions with 100% of Fe^{III} in a HS state. Furthermore, this value is 4.2 emu K mol^{-1} higher than that obtained for the reference

compound (**3**) with diamagnetic $[In(sal_2\text{-trien})]^+$ in the place of $[Fe(sal_2\text{-trien})]^+$. This confirms that $[Fe(sal_2\text{-trien})]^+$ is 100% HS at this temperature. χT presents a smooth decrease from 300 (10.5 emu K mol^{-1}) to 115 K (9.8 emu K mol^{-1}) as temperature decreases. The χT value of **2** at 300 K and the difference with that of **3** (4.0 emu K mol^{-1}) are consistent with the Mössbauer data that suggest that Fe^{III} is 93% HS at this temperature. On the other hand, the difference between χT values of **2** and **3** at 115 K is 3.1 emu K mol^{-1}, which is again consistent with the Mössbauer data that suggest that the fraction of LS Fe^{III} remains constant and close to 30% below 130 K. Therefore, the HS→LS spin conversion of 30% of the Fe^{III} complexes takes place between 300 and 130 K. This contrasts with the magnetic behavior of **1** that presents a complete spin conversion. At temperatures below 115 K there is an increase of χT, which is very sharp below 50 K. This indicates the presence of ferromagnetic interactions between neighboring Mn^{II}–Cr^{III} magnetic ions and the onset of long-range ferromagnetic ordering as usual for this type of compound. The χ^{-1} versus T curve of **3** is linear in the 50–300 K temperature range. This allows one to fit it to a Curie–Weiss law ($\chi^{-1} = (T-\theta)/C$, in which C is the Curie constant) and thus to a Weiss constant, θ, of 3.7 K, which is slightly lower than that obtained for a chiral 3D Mn^{II}–Cr^{III} oxalate network in the $[Ir(ppy)_2(bpy)][M^{II}Cr^{III}(ox)_3]\cdot 0.5\,H_2O$ compound (6.1 K).[11f] The long-range ferromagnetic ordering of the two compounds is confirmed by AC susceptibility measurements (see Figure 10) that show frequency-independent χ' and χ'' peaks. From this data, the T_c of compounds **2** and **3** is in both cases 5.2 K.

Isothermal magnetization at 2 K of the two compounds presents a sharp increase at low fields (below 0.1 T), and a hysteresis loop with a coercive field of approximately 3 mT, which is usual for this type of compound (Figure 9). In **3**, only the bimetallic oxalate sublattice is magnetic, so the magnetization tends to saturate and only a slight linear increase of M versus magnetic field (H) is observed at fields above 0.1 T as a consequence of spin canting in the ferromagnetic phase. In contrast, in **2**, the presence of a fraction of paramagnetic Fe^{III} produces a pronounced curvature in the M versus H curve with M increasing from 7.5 to 10 μ_B when H increases from 0.1 to 5 T. In these two compounds, the difference between the M values at 5 T (ca. 3 μ_B) is consistent with the presence of 70% of Fe^{III} in the HS state in **2**.

The magnetic behavior of **2** and **3** after desolvation has also been studied. In both cases, there are small differences with respect to the solvated sample. χT of the desolvated sample presents a more gradual decrease upon lowering the temperature, with values slightly higher than those of the initial sample from 300 to 100 K (see Figure 7SS in the Supporting Information). Thus, χT of the desolvated sample at 115 K is 0.3 emu K mol^{-1} higher than that of the solvated one. We could relate these differences to changes in the spin state of Fe^{III}. However, this is a very small effect that could be related also to structural changes in the oxalate network

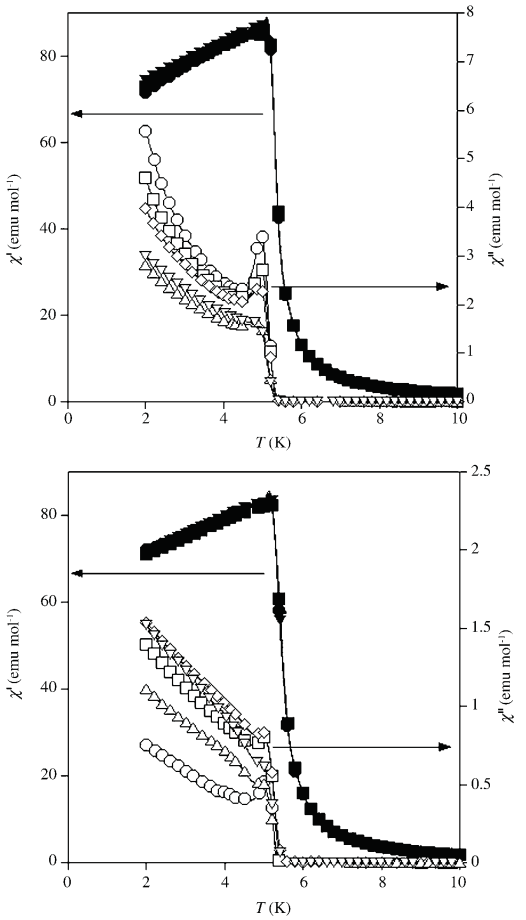

Figure 10. Temperature dependence of the in-phase AC susceptibility (χ') (filled symbols) and the out-of-phase AC susceptibility (χ'') (empty symbols) for **2** (top) and **3** (bottom): ● 997 Hz, ■ 332 Hz, ◆ 110 Hz, ▲ 10 Hz, ▼ 1 Hz.

(changes in distances and angles between the metallic centers). Thus, a slight increase of χT is also observed for the In^{III} analogoue, **3**, which does not contain a spin-crossover cation. Some differences appear also in AC susceptibility measurements of **2** and **3** with respect to the initial sample. Thus, both the χ' and χ'' peaks are shifted towards lower (T_c of 5.0 versus 5.2 K) temperatures and their intensity decreases with respect to the initial compound (see Figure 8SS in the Supporting Information). Again, these changes may be related to the oxalate network, as they occur in both compounds.

Magnetic properties of 4: χT of **4** presents a value of 6.5 emu K mol^{-1} at 300 K and an increase upon lowering the temperature, with a sharp increase below 50 K (Figure 9SS

in the Supporting Information). This confirms the ferromagnetic interaction between Mn^{II} and Cr^{III} ions of the oxalate network and the ferromagnetic behavior already observed in **2** and **3**. AC susceptibility measurements show a frequency-independent peak that starts to appear at 5.0 K and defines T_c (Figure 10SS in the Supporting Information). The isothermal magnetization at 2 K shows a very sharp increase at low fields and does not saturate completely at 5 T (see Figure 11SS in the Supporting Information). An M value of 7.8 μ_B is obtained at 5 T, as expected for a Mn^{II}–Cr^{III} ferromagnet. A hysteresis loop of the magnetization with a coercive field of 3 mT is observed at 2 K. All these features indicate that the ferromagnetic behavior of this 3D oxalate network is analogous to that of **3**. The slight decrease of T_c with respect to that of **2** and **3** may be explained by the slightly longer mean Mn^{II}–Cr^{III} distances shown by **4** (5.408 Å for **4** compared to 5.399 Å for **3**) and by slight differences in the bonding angles.

In any case, the T_c values obtained in the reported Mn^{II}–Cr^{III} 3D oxalate compound are all very close (5.2 K in **2** and **3**; 5.0 K in **4**) and similar to that shown by the chiral compound $[Ir(ppy)_2(bpy)][Mn^{II}Cr^{III}(ox)_3]\cdot 0.5H_2O$ (T_c = 5.1 K[11f]). Still, in the compound $[Fe(bpp)_2][MnCr(ox)_3]\cdot bpp\cdot CH_3OH$, which presents an achiral 3D oxalate network but longer Mn^{II}–Cr^{III} distances (5.503 Å), a significantly lower T_c value has been observed (T_c = 3.0 K).[14] It seems therefore that a correlation purely based on the Mn^{II}–Cr^{III} distances (longer for most of the chiral compounds) is not correct in this case, and other factors should also be involved. In this context we have demonstrated in a recent study that the decrease in T_c observed in the 3D series of bimetallic oxalates with respect to the 2D series can be explained by the noncollinear alignment of the chiral axis in the 3D compounds, as they produce differences in the relative orientation of the magnetic orbitals.[21] Hence, in an achiral 3D lattice, the T_c values should be intermediate between those shown by the 2D and the chiral 3D lattices if the distances between metals ions and other structural factors are kept similar. That is so because an achiral 3D lattice contains both homochiral (similar to those found in chiral 3D structures) and heterochiral (similar to those found in 2D structures) pairs of neighboring magnetic ions. Preliminary results in a chiral 3D analogue of **2** that exhibits a lower T_c value (4.8 K compared to 5.2 K in **2**) confirm this point.[22]

Mössbauer spectroscopy of 1: The Mössbauer spectrum of **1** obtained at 4 K shows only two well-defined peaks and may be fitted with a quadrupole doublet with isomer shift (IS) and quadrupole splitting (QS) typical of LS Fe^{III} (see Figure 11).[20a,23] Up to 160 K there is no change in the shape of the Mössbauer spectra. At 165 K, a very small absorption is observed between both peaks of the LS Fe^{III} doublet. This absorption increases as the temperature increases and may be fitted with two broad peaks with IS and QS typical for HS Fe^{III}.[20a,23] The coexistence of LS and HS Fe^{III} above 165 K, as well as the increase in the relative areas (I) of the HS Fe^{III} with increasing temperature, agree with magnetization data.

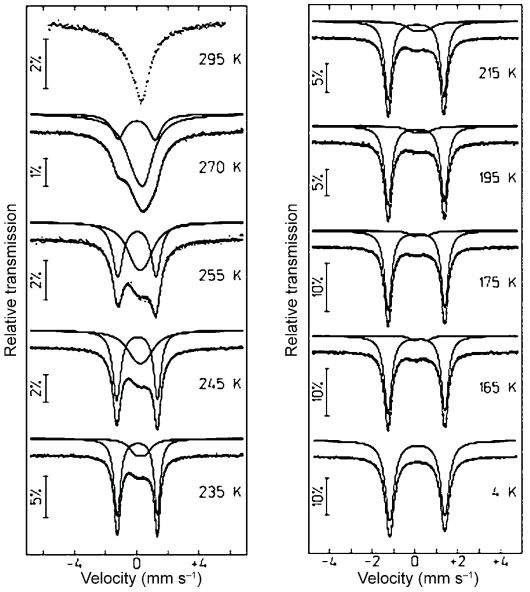

Figure 11. Mössbauer spectra of **1** taken at different temperatures. The lines over the experimental points are the sum of two doublets that correspond to HS and LS Fe^{III}. The estimated parameters for these doublets are collected in Table 1SS in the Supporting Information.

The HS Fe^{III} absorption peaks significantly broaden with increasing temperature and above 235 K the same is observed for LS Fe^{III} peaks. At 255 K, the LS Fe^{III} peaks, although quite broad, are still resolved, but at 270 K and above this is no longer the case. Such behavior of the spectra may be understood if a dynamic $^2T \leftrightarrow {}^6A$ spin interconversion occurs and the spin-state lifetimes are comparable to the Mössbauer timescale, 10^{-7} s.[23c] Up to 255 K, since the HS and LS signals are distinct, we may infer that the spin-state interconversion rate is still slow relative to the Mössbauer timescale. At 270 K, signals for the HS and LS species strongly overlap, and at 295 K it is not possible to distinguish them, although magnetic susceptibility data indicate that an appreciable LS population is still present at this temperature.

The estimated HS Fe^{III} fractions from Mössbauer and magnetization data are in good agreement up to 270 K. Between 165 and 255 K, the LS fraction deduced from magnetic susceptibility is slightly lower than the corresponding relative areas (I) estimated from the Mössbauer spectra (see Table 1SS in the Supporting Information). There are many effects that may contribute to differences between the values estimated from both techniques. In general, due to the shorter and stronger Fe–ligand chemical bonds in the LS Fe^{III} molecules, the recoilless fraction of these Fe^{III} species is higher than that of the HS Fe^{III}, particularly above 80 K.

Consequently, the estimated I for LS Fe^{III} may be higher than the actual fraction. Broad peaks in the spectra of compound **1** also lead to higher uncertainties in the estimated I. Moreover, the fraction of HS Fe^{III} deduced from magnetic susceptibility data may be overestimated, particularly at lower temperatures, due to the ferromagnetic coupling between Mn^{II} and Cr^{III} neighbors. It should also be noted that the ferromagnetic ordering that occurs in the oxalate layer, detected by magnetization data, has no effect in the Mössbauer spectra. The LS Fe^{III} remain paramagnetic below T_c.

Mössbauer spectroscopy of 2: In the Mössbauer spectra of **2**, two contributions are observed in the temperature range 2.2–297 K (see Figure 12). One is a quadrupole doublet with

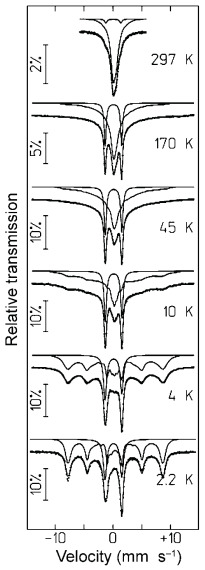

Figure 12. Mössbauer spectra of **2** taken at different temperatures. The lines over the experimental points are the sum of a doublet and a distribution of B_{hf} that corresponds to LS and HS Fe^{III}. The estimated parameters for these doublets are collected in Table 2SS in the Supporting Information.

estimated parameters typical of LS Fe^{III}. The other one consists of an unresolved absorption centered at IS≈0.34 (297 K)–0.45 mm s^{-1} (4 K). This contribution gradually broadens as the temperature decreases. At 10 K, the maxima of four peaks belonging to a sextet appears on the absorption band. This sextet is clearly observed at 4 K with an estimated magnetic hyperfine field B_{hf}≈51 T; the corresponding peaks sharpen down to 2.2 K (B_{hf}≈52 T). The estimated IS and B_{hf} for this contribution are typical of HS Fe^{III}.

Broadening of the HS Fe^{III} peaks was also observed in $[Fe(acac)_2trien]BPh_4$ and $[Fe(acac)_2trien]PF_6$[23a] (acac = acetylacetonate), and has been attributed to dynamic effects during the timescale 10^{-6}–10^{-8} s, the order of magnitude of the lifetime of the Mössbauer excited nuclear state.[23] These effects may be either related to the lifetimes of the electronic $S=1/2$ and $S=5/2$ states in the temperature range in which both states coexist, or to fluctuations of the directions of the Fe magnetic moments, μ_{Fe}, with a frequency along the order of 10^7 s^{-1}. When the spin-state interconversion between the HS and LS states is comparable or faster than the reciprocal of the Mössbauer time window, the corresponding doublets are expected to fuse into a single one with increasing temperature,[23c] as observed for compound **1**. Since both LS and HS Fe^{III} contributions are separately observed in the spectra of compound **2**, the fluctuations between spin states (frequencies $<10^7$ s^{-1}) are slow compared to the Mössbauer timescale at all measured temperatures. Therefore the HS Fe^{III} absorption broadening is only related to slow fluctuations of the magnetic hyperfine interaction caused by the slow relaxation of μ_{Fe} directions.

A sextet is observed when the frequency of fluctuation of the μ_{Fe} directions is lower than 10^7 s^{-1}.[24] This is the case when μ_{Fe} are magnetically ordered. However, such low frequencies may also be observed in the case of paramagnetic Fe atoms with slow μ_{Fe} relaxation. For compound **2**, one should be cautious since no sudden freezing of the μ_{Fe} in the $[Fe(sal_2\text{-trien})]^+$ occurs at the magnetic-ordering temperature of the $[MnCr(ox)_3]$ layers. Instead, a slow paramagnetic relaxation frequency of 10^7–10^9 s^{-1} is already observed at 170 K and it slows down gradually as the temperature decreases. Furthermore, no effect of the ferromagnetic ordering is observed in the LS Fe^{III} contribution, as in the case of compound **1**.

The LS Fe^{III} contributions to the spectra are well-defined quadrupole doublets within the 297–2.2 K temperature range. This means that, as usual, slow relaxation of μ_{Fe} is only observed for HS Fe^{III} and not for LS Fe^{III}. In fact, HS Fe^{III}, in the electronic ^6S state, is characterized by vanishing orbital momentum. The only relaxation mechanism available in this case is spin–spin (i.e., energy transfer may only occur between interacting spins). A sizeable orbital moment is, however, expected for LS Fe^{III}, and the corresponding spins may interact by means of spin–orbit and orbital–phonon coupling with the phonons, the so-called spin-lattice relaxation mechanism. This mechanism explains why μ_{Fe} relaxation is fast for LS Fe^{III}. By simulating the broad absorption of HS Fe^{III} with the distribution of B_{hf}, the estimated relative areas (Table 2SS in the Supporting Information) suggest that the fraction of HS Fe^{III} drops from around 93% at 297 K to around 72% at 130 K. Below this temperature, it remains approximately constant (≈70%) down to 2.2 K. At 4 and 2.2 K, the distribution of B_{hf} narrows significantly and, as mentioned above, is centered at B_{hf}≈51 and 52 T, respectively.

Conclusion

We have reported in this paper the first examples of molecular materials with coexistence of ferromagnetism and spin crossover. The materials are salts formed by the insertion of a spin-crossover Fe^{III} cation complex into anionic coordination polymers based on bimetallic oxalate complexes. From the chemical point of view, we have shown that the use of different mixed solvents and the same templating cation, which can adopt a variable configuration in the crystalline lattice, is a suitable strategy to obtain different oxalate networks. Thus, by changing the experimental conditions, two different oxalate networks, a 2D structure in compound **1** and an unusual achiral 3D structure in compounds **2**, **3**, and **4**, have been obtained with the same templating cation, $[Fe(sal_2\text{-trien})]^+$.

From the point of view of the physical properties, we have found that the magnetic properties and the Mössbauer spectroscopy of **1** indicate the coexistence of an almost complete spin crossover of 100% of Fe^{III} ions from 300 to 160 K, and a ferromagnetic ordering below 5.4 K in the layered magnet. In turn, **2** shows a gradual spin-crossover of 30% of the Fe^{III} from 300 to 130 K, together with a ferromagnetic ordering in the 3D lattice below 5.2 K. The preparation of the reference compounds **3** and **4** have allowed us to study the magnetic properties of the 3D lattice alone. They have shown that, in this case, the spin-crossover phenomenon does not influence the magnetic ordering. On the other hand, the magnetic properties of **2**, **3**, and **4** indicate that the ordering temperature of this achiral 3D network, T_c, is slightly higher than those observed in the chiral 3D analogues.

A very promising possibility provided by this hybrid strategy is to tune the magnetic ordering of the $Mn^{II}Cr^{III}$ oxalate network, thereby inducing the spin crossover of the intercalated spin-crossover cations by applying light or pressure. Compound **1** seems a better candidate for this purpose as it undergoes a complete spin-crossover; however, it is unexpected that the changes in the structure of the intercalated compound could modify the T_c of the 2D oxalate network, as 2D oxalate networks with different interlayer separations present similar T_c values. In fact, the spin-crossover transition can be seen as an internal anisotropic pressure that may induce small structural changes in the ferromagnetic sublattice. In this sense, compound **2**, which is formed by a 3D magnetic network, is expected to be much more sensitive to the influence of this internal pressure. Unfortunately, in this case the HS state is highly favored; therefore, the occurrence of a spin crossover and its influence on the ferromagnetic sublattice is very limited.

We can conclude that hybrid magnets with coexistence of magnetic ordering and spin crossover can be designed using this molecular approach. Although the preparation of hybrid switchable magnets has not yet been reached, the synthetic strategy presented in this paper opens the way to the preparation of these new type of magnets. Apart from this final goal, the versatility of this method to combine two molecular subnetworks in the same compound could give rise to new physical properties that stem from this unusual combination. This has been achieved in one of the compounds presented in this paper. Thus, in the ordered ferromagnetic state (below 5 K), the Mössbauer spectrum of **2** has shown the appearance of a sextet associated with HS Fe^{III}. However, this new phenomenon in $[Fe(sal_2\text{-trien})]^+$ compounds, the slow relaxation of the magnetic moment of HS Fe^{III}, is also observed at temperatures much higher than the magnetic ordering of the oxalate network. There is therefore no clear evidence of a relation between both phenomena.

Experimental Section

Synthesis: The complexes $[Fe(sal_2\text{-trien})]PF_6$ and $[In(sal_2\text{-trien})]PF_6$ were prepared according to literature methods.[23a] $Ag_3[Cr(ox)_3]$ was prepared by metathesis from the corresponding potassium salt.[25] All other materials and solvents were commercially available and used without further purification.

Compound 1: Crystals of this compound were obtained by slow diffusion of two solutions. The first solution was prepared by adding $MnCl_2{\cdot}4H_2O$ (0.053 g, 0.268 mmol) to a suspension of $Ag_3[Cr(ox)_3]$ (0.114 g, 0.179 mmol) in methanol (8 mL). The AgCl precipitate was filtered. The second solution was obtained by dissolving $[Fe(sal_2\text{-trien})]PF_6$ (0.100 g, 0.179 mmol) in dichloromethane (8 mL). After two weeks, brown crystals were obtained.

Compound 2: Crystals of this compound were obtained by slow diffusion of two solutions. The first solution was prepared by adding $MnCl_2{\cdot}4H_2O$ (0.053 g, 0.268 mmol) to a suspension of $Ag_3[Cr(ox)_3]$ (0.114 g, 0.179 mmol) in methanol (7 mL). The AgCl precipitate was filtered. The second solution was obtained by dissolving $[Fe(sal_2\text{-trien})]PF_6$ (0.100 g, 0.179 mmol) in acetonitrile (7 mL). After two weeks, brown crystals were obtained.

Compound 3: Crystals of this compound were obtained by slow diffusion of two solutions. The first solution was prepared by adding $MnCl_2{\cdot}4H_2O$ (0.053 g, 0.268 mmol) to a suspension of $Ag_3[Cr(ox)_3]$ (0.114 g, 0.179 mmol) in methanol (8 mL). The AgCl precipitate was filtered. The second solution was obtained by dissolving $[In(sal_2\text{-trien})]PF_6$ (0.110 g, 0.179 mmol) in acetonitrile (8 mL). After three weeks, violet crystals were obtained.

Compound 4: Crystals of this compound were obtained by slow diffusion of two solutions. The first solution was prepared by adding $MnCl_2{\cdot}4H_2O$ (0.072 g, 0.364 mmol) to a suspension of $Ag_3[Cr(ox)_3]$ (0.155 g, 0.242 mmol) in methanol (12 mL). The AgCl precipitate was filtered. The second solution was prepared by dissolving $[In(sal_2\text{-trien})]PF_6$ (0.150 g, 0.242 mmol) in nitromethane (12 mL). After three weeks, violet crystals were obtained.

Structural characterization: Single crystal X-ray data were collected at 180 K for compound **1**, 120 K for compound **2**, and 150 K for compounds **3** and **4** by using a Nonius KappaCCD diffractometer equipped with graphite-monochromated $Mo_{K\alpha}$ radiation ($\lambda = 0.71073$ Å). The Denzo and Scalepack programs were used for cell refinements and data reduction of the four compounds.[26] Crystal structures were solved by direct methods using the SIR97 program,[27] and refined against all F^2 values using the SHELXL-97 program.[28] Non-hydrogen atoms were refined anisotropically (except as noted); hydrogen atoms were placed in calculated positions that were refined using idealized geometries (riding model) and assigned fixed isotropic displacement parameters. In **3**, one of the two crystallographically independent sal_2-trien ligands was modeled in two orientations in a 59.7(10):40.3(10) ratio. Carbon, nitrogen, and oxygen atoms of some of the sal_2-trien ligands could only be modeled isotropically for compounds **2** and **3**, possibly due to the flexibility

Table 1. Crystallographic data for compounds **1**, **2**, **3**, and **4**.

Compound	**1**	**2**	**3**	**4**
formula	$C_{27}H_{26}Cl_2CrFeMnN_4O_{14}$	$C_{54}H_{56}Cr_2Fe_2Mn_2N_8O_{30}$	$C_{53.5}H_{52.5}Cr_2In_2Mn_2N_{8.5}O_{29}$	$C_{54}H_{48}Cr_2In_2Mn_2N_{10}O_{33}$
M_r	864.2065	1622.6329	1722.0495	1808.5270
crystal color	brown	brown	violet	violet
T [K]	180	120	150	150
crystal system	monoclinic	monoclinic	monoclinic	orthorhombic
Z	4	4	4	4
space group	$P2_1/c$	Cc	Cc	$Pna2_1$
a [Å]	11.6440(2)	21.9180(9)	21.5690(7)	20.4650(3)
b [Å]	31.7710(5)	14.0330(9)	14.1590(7)	21.2430(5)
c [Å]	9.5340(3)	22.4670(15)	22.7360(9)	16.2740(5)
β [°]	110.2370(11)	92.639(4)	91.116(2)	90
V [Å^3]	3309.30(13)	6903.0(7)	6942.2(5)	7074.9(3)
ρ_{calcd} [Mg m^{-3}]	1.735	1.561	1.659	1.698
$\mu(Mo_{K\alpha})$ [mm^{-1}]	1.367	1.157	1.405	1.378
θ range [°]	1.28 to 27.48	1.72 to 21.77	1.72 to 27.45	1.38 to 27.49
reflns collected	13485	8013	12959	15664
independent reflns (R_{int})	7451 (0.0471)	8006 (0.0273)	12955 (0.0617)	15664 (0.1364)
LS params/restraints	475/0	671/2	790/36	790/1
$R1(F)$[a] ($I>2\sigma(I)$)	0.0557	0.0798	0.0710	0.0621
$wR2(F^2)$[b] (all data)	0.1519	0.1435	0.1440	0.1120
$S(F^2)$[c] (all data)	1.116	1.017	0.970	1.033

[a] $R1(F)=S(|F_o|-|F_c|)/S|F_o|$. [b] $wR2(F^2)=[Sw(F_o^2-F_c^2)^2/SwF_o^4]^{1/2}$. [c] $S(F^2)=[Sw(F_o^2-F_c^2)^2/(n-p)]^{1/2}$.

of the ligand. The use of restraints and/or constraints in the refinement of the structures is documented in the corresponding CIFs. Data collection and refinement statistics are collected in Table 1. CCDC-749068 (**1**), -749069 (**2**), -749070 (**3**), and -749071 (**4**) contain the supplementary crystallographic data for this paper. These data can be obtained free of charge from The Cambridge Crystallographic Data Centre via www.ccdc.cam.ac.uk/data_request/cif.

Physical measurements: Magnetic susceptibility measurements were performed on polycrystalline samples by using a magnetometer (Quantum Design MPMS-XL-5) equipped with a SQUID sensor. Variable-temperature measurements were carried out in the temperature range 2–400 K. The AC measurements were performed in the temperature range 2–10 K at different frequencies with an oscillating magnetic field of 0.395 mT. The magnetization and hysteresis studies were performed between 5 and −5 T and by cooling the samples at zero field. The Fe/Mn/Cr/Cl and In/Mn/Cr ratios were measured using a Philips ESEM X230 scanning electron microscope equipped with an EDAX DX-4 microsonde. Mössbauer spectra were collected in transmission mode using a conventional constant-acceleration spectrometer and a 25 mCi ^{57}Co source in an Rh matrix. The velocity scale was calibrated using α-Fe foil. The absorber was obtained by pressing powdered single crystals of **1** or **2** into a Perspex holder. Low-temperature spectra were collected using a bath cryostat with the sample immersed in liquid He for measurements at 4.1 and 2.2 K, or by using flowing He gas to cool the sample above 4.1 K (temperature stability of 0.2 K). The spectra were fitted to Lorentzian lines using a nonlinear least-squares method.[29] Isomer shifts (Tables 1SS and 2SS in the Supporting Information) are given relative to metallic α-Fe at room temperature.

Acknowledgements

Financial support from the European Union (MolSpinQIP and SPINMOL ERC Advanced Grant), the Spanish Ministerio de Ciencia e Innovación (Project Consolider-Ingenio in Molecular Nanoscience, CSD2007-00010, and projects CTQ2005-09385-C03 and MAT2007-61584), and the Generalitat Valenciana (Prometeo Program) are gratefully acknowledged. The authors also thank J. M. Martínez-Agudo of the University of Valencia for assistance with the preparation and magnetic characterization of the samples.

[1] a) E. Coronado, P. Day, *Chem. Rev.* **2004**, *104*, 5419; b) E. Coronado, J. R. Galán-Mascarós, *J. Mater. Chem.* **2005**, *15*, 66.
[2] a) H. Tamaki, Z. J. Zhong, N. Matsumoto, S. Kida, M. Koikawa, N. Achiwa, Y. Hashimoto, H. Okawa, *J. Am. Chem. Soc.* **1992**, *114*, 6974; b) H. Tamaki, M. Mitsumi, N. Nakamura, N. Matsumoto, S. Kida, H. Okawa, S. Ijima, *Chem. Lett.* **1992**, 1975; c) C. Mathonière, S. G. Carling, D. Yuscheng, P. Day, *J. Chem. Soc. Chem. Commun.* **1994**, 1551; d) C. Mathonière, J. Nutall, S. G. Carling, P. Day, *Inorg. Chem.* **1996**, *35*, 1201; e) R. Pellaux, H. W. Schmalle, R. Huber, P. Fisher, T. Hauss, B. Ouladdiaf, S. Decurtins, *Inorg. Chem.* **1997**, *36*, 2301; f) E. Coronado, J. R. Galán-Mascarós, C. J. Gómez-García, J. M. Martínez-Agudo, E. Martínez-Ferrero, J. C. Waerenborgh, M. Almeida, *J. Solid State Chem.* **2001**, *159*, 391; g) K. S. Min, A. L. Rhinegold, J. S. Miller, *Inorg. Chem.* **2005**, *44*, 8433; h) E. Coronado, J. R. Galán-Mascarós, C. Martí-Gastaldo, *J. Mater. Chem.* **2006**, *16*, 2685.
[3] a) M. Clemente-León, J. R. Galán-Mascarós, C. J. Gómez-García, *Chem. Commun.* **1997**, 1727; b) E. Coronado, J. R. Galán-Mascarós, C. J. Gómez-García, J. M. Martínez-Agudo, *Adv. Mater.* **1999**, *11*, 558; c) E. Coronado, J. R. Galán-Mascarós, C. J. Gómez-García, J. Ensling, P. Gutlich, *Chem. Eur. J.* **2000**, *6*, 552.
[4] E. Coronado, C. Giménez-Saiz, C. J. Gómez-Garcia, F. M. Romero, A. Tarazón, *J. Mater. Chem.* **2008**, *18*, 929.
[5] a) S. Bénard, P. Yu, J. P. Audière, E. Rivière, R. Clèment, J. Ghilhem, L. Tchertanov, K. Nakatami, *J. Am. Chem. Soc.* **2000**, *122*, 9444; b) S. M. Aldoshin, N. A. Sanina, V. I. Minkin, N. A. Voloshin, V. N. Ikorskii, V. I. Ovcharenko, V. A. Smirnov, N. K. Nagaeva, *J. Mol. Struct.* **2007**, *826*, 69.
[6] S. Bénard, E. Rivière, P. Yu, K. Nakatami, J. F. Delouis, *Chem. Mater.* **2001**, *13*, 159.
[7] a) E. Coronado, J. R. Galán-Mascarós, C. J. Gómez-García V. Laukhin, *Nature* **2000**, *408*, 447; b) A. Alberola, E. Coronado, J. R. Galán-Mascarós, C. Giménez-Saiz, C. J. Gómez-García, *J. Am. Chem. Soc.* **2003**, *125*, 10774; c) E. Coronado, J. R. Galán-Mascarós, C. J. Gómez-García, E. Martínez-Ferrero, S. Van Smaalen, *Inorg. Chem.* **2004**, *43*, 4808.
[8] M. Clemente-León, E. Coronado, J. C. Dias, A. Soriano-Portillo, R. D. Willett, *Inorg. Chem.* **2008**, *47*, 6458.
[9] C. Train, R. Gheorghei, V. Krstic, L. M. Chamoreau, N. S. Ovanesyan, G. L. J. A. Rikken, M. Gruselle, M. Verdaguer, *Nat. Mater.* **2008**, *7*, 729.

[10] a) F. D. Rochon, R. Melanson, M. Andruh, *Inorg. Chem.* **1996**, *35*, 6086; b) M. Andruh, R. Melanson, C. V. Stager, F. D. Rochon, *Inorg. Chim. Acta* **1996**, *251*, 309; c) N. Stanica, C. V. Stager, M. Cimpoesu, M. Andruh, *Polyhedron* **1998**, *17*, 1787; d) G. Marinescu, M. Andruh, R. Lescouëzec, M. C. Muñoz, J. Cano, F. Lloret, M. Julve, *New J. Chem.* **2000**, *24*, 527; e) S. Triki, F. Berezovsky, J. S. Pala, E. Coronado, C. J. Gómez-García, J. M. Clemente, A. Riou, P. Molinie, *Inorg. Chem.* **2000**, *39*, 3771; f) G. Ballester, E. Coronado, C. Giménez-Saiz, F. M. Romero, *Angew. Chem.* **2001**, *113*, 814; *Angew. Chem. Int. Ed.* **2001**, *40*, 792; g) E. Coronado, C. Giménez-Saiz, J. R. Galán-Mascarós, C. J. Gómez-García, C. Ruiz-Pérez, *Eur. J. Inorg. Chem.* **2003**, 2290; h) E. Coronado, J. R. Galán-Mascarós, C. J. Gómez-García, C. Martí-Gastaldo, *Inorg. Chem.* **2005**, *44*, 6179; i) E. Coronado, J. R. Galán-Mascarós, C. Martí-Gastaldo, *Inorg. Chem.* **2006**, *45*, 1882; j) E. Coronado, J. R. Galán-Mascarós, C. Martí-Gastaldo, A. Murcia-Martínez, *Dalton Trans.* **2006**, 3294; k) H. Z. Kou, O. Sato, *Inorg. Chem.* **2007**, *46*, 9513; l) E. Cariati, R. Macchi, D. Roberto, R. Ugo, S. Galli, N. Casati, P. Macchi, A. Sironi, L. Bogani, A. Caneschi, D. Gatteschi, *J. Am. Chem. Soc.* **2007**, *129*, 9410; m) H. Z. Kou, J. Tao, O. Sato, *Dalton Trans.* **2008**, 3652.

[11] a) S. Decurtins, H. W. Schmalle, P. Schneuwly, H. R. Oswald, *Inorg. Chem.* **1993**, *32*, 1888; b) S. Decurtins, H. W. Schmalle, P. Schneuwly, J. Ensling, P. Gütlich, *J. Am. Chem. Soc.* **1994**, *116*, 9521; c) M. Hernández-Molina, F. Lloret, C. Ruiz-Pérez, M. Julve, *Inorg. Chem.* **1998**, *37*, 4141; d) E. Coronado, J. R. Galán-Mascarós, C. J. Gómez-García, J. M. Martínez-Agudo, *Inorg. Chem.* **2001**, *40*, 113; e) F. Pointillart, C. Train, M. Gruselle, F. Villain, H. W. Schmalle, D. Talbot, P. Gredin, S. Decurtins, M. Verdaguer, *Chem. Mater.* **2004**, *16*, 832; f) M. Clemente-León, E. Coronado, C. J. Gómez-García, A. Soriano-Portillo, *Inorg. Chem.* **2006**, *45*, 5653.

[12] a) R. Andrés, M. Gruselle, B. Malézieux, M. Verdaguer, J. Vaissermann, *Inorg. Chem.* **1999**, *38*, 4637; b) R. Andrés, M. Brissard, M. Gruselle, C. Train, J. Vaissermann, B. Malézieux, J. P. Jamet, M. Verdaguer, *Inorg. Chem.* **2001**, *40*, 4633.

[13] R. Sieber, S. Decurtins, H. Stoeckli-Evans, C. Wilson, D. Yufit, J. A. K. Howard, S. C. Capelli, A. Hauser, *Chem. Eur. J.* **2000**, *6*, 361.

[14] E. Coronado, J. R. Galán-Mascarós, M. C. Giménez-López, M. Almeida, J. C. Waerenborgh, *Polyhedron* **2007**, *26*, 1838.

[15] M. Clemente-León, E. Coronado, M. C. Giménez-López, A. Soriano-Portillo, J. C. Waerenborgh, F. S. Delgado, C. Ruiz-Pérez, *Inorg. Chem.* **2008**, *47*, 9111.

[16] C. Janiak, *J. Chem. Soc. Dalton Trans.* **2000**, 3885.

[17] R. Pritchard, S. A. Barrett, C. A. Kilner, M. A. Halcrow, *Dalton Trans.* **2008**, 3159.

[18] A. Alberola, E. Coronado, C. Giménez-Saiz, C. J. Gómez-García, F. M. Romero, A. Tarazón, *Eur. J. Inorg. Chem.* **2005**, 389.

[19] N. A. Chernova, Y. Song, P. Y. Zavalij, M. S. Wittingham, *Phys. Rev. B* **2004**, *70*, 144405.

[20] a) S. Floquet, S. Salunke, M. L. Boillot, R. Clément, F. Varret, K. Boukheddaden, E. Rivière, *Chem. Mater.* **2002**, *14*, 4164–4171; b) S. Floquet, M. C. Muñoz, E. Rivière, R. Clément, J. P. Audière, M. L. Boillot, *New J. Chem.* **2004**, *28*, 535.

[21] R. S. Fishman, M. Clemente-León, E. Coronado, *Inorg. Chem.* **2009**, *48*, 3039.

[22] Unpublished results.

[23] a) E. Sinn, G. Sim, E. V. Dose, M. F. Tweedle, L. J. Wilson, *J. Am. Chem. Soc.* **1978**, *100*, 3375; b) Y. Maeda, N. Tsutsumi Y. Takashima, *Inorg. Chem.* **1984**, *23*, 2440; c) M. Nihei, T. Shiga, Y. Maeda, H. Oshio, *Coord. Chem. Rev.* **2007**, *251*, 2606.

[24] N. N. Greenwood, T. C. Gibb, *Mossbauer Spectroscopy*, Chapman and Hall, London, **1971**, pp. 72–75.

[25] J. C. Baylar, E. M. Jones, *Inorganic Synthesis, Vol. 5* (Ed.: H. S. Booth), McGraw-Hill, New York, **1939**, p. 35.

[26] Z. Otwinowski, W. Minor, *Methods in Enzymology, Vol. 276* (Ed.: C. W. Carter, Jr., R. M. Sweet), Academic Press, New York, **1997**, p. 307.

[27] A. Altomare, M. C. Burla, M. Camalli, G. L. Cascarano, C. Giacovazzo, A. Guagliardi, A. G. G. Moliterni, G. Polidori, R. Spagna, *J. Appl. Crystallogr.* **1999**, *32*, 115–119.

[28] SHELXL-97: G. M. Sheldrick, University of Göttingen, Göttingen, **1997**.

[29] J. C. Waerenborgh, M. O. Figueiredo, J. M. P. Cabral, L. C. Pereira, *J. Solid State Chem.* **1994**, *111*, 300–309.

Received: September 28, 2009
Published online: December 28, 2009

View Article Online / Journal Homepage / Table of Contents for this issue
Dynamic Article Links

Chemical Science

Cite this: *Chem. Sci.*, 2011, **2**, 1121

www.rsc.org/chemicalscience

EDGE ARTICLE

A hybrid magnet with coexistence of ferromagnetism and photoinduced Fe(III) spin-crossover†

Miguel Clemente-León,*[a] Eugenio Coronado,*[a] Maurici López-Jordà,[a] Cédric Desplanches,[b] Saket Asthana,[b] Hongfeng Wang[b] and Jean-François Létard[b]

Received 11th January 2011, Accepted 4th March 2011
DOI: 10.1039/c1sc00015b

The insertion of a $[Fe(sal_2\text{-trien})]^+$ complex cation into a 2D oxalate network results in a hybrid magnet with coexistence of magnetic ordering and photoinduced spin-crossover (LIESST effect) in compound $[Fe^{III}(sal_2\text{-trien})][Mn^{II}Cr^{III}(ox)_3]\cdot(CH_2Cl_2)$ (**1**). A complete photomagnetic characterization together with a detailed structural analysis of the low-spin (LS) and high-spin (HS) structures of **1** is presented in order to understand such unusual behavior. This very rare and unexpected property in a Fe^{III} spin-crossover complex, has been attributed to the strong distortion exhibited by the metastable HS state. Furthermore, **1** has shown that, in contrast to what has been previously proposed, a cooperative spin-crossover is not a necessary condition to observe LIESST effect in Fe^{III} compounds. The photo-induced spin conversion of the inserted Fe^{III} complex has shown to have a negligible influence on the cooperative magnetic behaviour of the 2D oxalate network.

Introduction

Multifunctionality is one of the most appealing topics in chemical science. A rational approach to design multifunctional materials consists of building up two-network hybrid solids formed by two molecular fragments where each network furnishes distinct physical properties. If the two networks are quasi-independent, a coexistence of the two physical properties is anticipated.[1] If the two molecular networks are coupled, an interplay between their properties may be observed.[1b] Finally, if one of these two networks is physically (or chemically) responsive (*i.e.*, if it changes its properties under the application of an external stimulus, like for example light, pressure or temperature), a switchable multifunctional material can be obtained in which the responsive network can influence the properties of the other network.[2]

Bimetallic oxalate-bridged complexes of formula $A[M^{II}M^{III}(ox)_3]$ (M^{III} = Cr, Fe, Ru, V, Mn; M^{II} = Mn, Fe, Co, Ni, Cu, Zn; A = Cation; ox = oxalate) have provided remarkable examples of these types of materials.[3] They are composed by polymeric 2D[4] or 3D[5] anionic networks, which furnish the cooperative magnetic properties (ferro-, ferri- or canted antiferromagnetism), and a bulky charge-compensating molecular cation, which templates the network formation and adds a second physical property to the solid. The insertion of different cations into oxalate networks has led to compounds combining the long-range magnetic ordering from the oxalate network with paramagnetism,[6] photochromism,[7] electric conductivity,[8] proton conduction,[9] chirality[10] or very recently, chirality and conductivity in the same compound.[11]

The interplay between the properties of the two molecular networks has been observed, for example, in enantiopure 2D oxalate-based magnets prepared by Train *et al.* that exhibit magneto-chiral dichroic effect and magnetisation-induced second harmonic generation.[12]

The design of switchable magnets has been less explored. A promising approach to reach this goal consists of combining the bimetallic oxalate network with spin-crossover complexes. These kinds of molecular complexes change their spin state from low-spin (LS) to high-spin (HS) configurations when submitted to an external stimulus such as temperature, light-irradiation or pressure. As this magnetic switching is accompanied by changes in the molecular size, the spin-crossover process should act as an internal pressure in the hybrid material and therefore, it might affect the long-range magnetic ordering in the extended magnetic network.

Although several compounds combining spin-crossover cations and bimetallic oxalate anion networks have been reported,[13,14] the only one showing coexistence of spin-crossover and ferromagnetism is $[Fe^{III}(sal_2\text{-trien})][Mn^{II}Cr^{III}(ox)_3]\cdot(CH_2Cl_2)$ (**1**) reported very recently by our group.[14] This compound is formed by $[Fe(sal_2\text{-trien})]^+$ cations inserted between $Mn^{II}Cr^{III}$ bimetallic

[a]*Instituto de Ciencia Molecular, Universidad de Valencia, Catedrático José Beltrán 2, Paterna, 46980, Spain. E-mail: miguel.clemente@uv.es; Fax: +34 963543273; Tel: +34 963544405; eugenio.coronado@uv.es*
[b]*CNRS, Université de Bordeaux, ICMCB, 87 avenue du Dr A. Schweitzer, Pessac, F-33608, France*

† Electronic supplementary information (ESI) available: crystallographic data, intermolecular interactions, ZFC and FC magnetisation and AC measurements before and after irradiation, and details of the fitting of the magnetism of $[Mn^{II}Cr^{III}(ox)_3]$ layers. CCDC reference numbers 807172, 807173, 813345, 813714. For ESI and crystallographic data in CIF or other electronic format see DOI: 10.1039/c1sc00015b

oxalate layers. It presents a gradual spin-crossover transition from 350 to 160 K, and a ferromagnetic ordering at 5.6 K. Furthermore, by changing the synthetic conditions a second compound of formula $[Fe^{III}(sal_2\text{-trien})][Mn^{II}Cr^{III}(ox)_3]\cdot(CH_3OH)$ (**2**) has also been obtained. This compound shows an unusual non-chiral 3D network with inserted $[Fe(sal_2\text{-trien})]^+$ cations, exhibiting a gradual spin-crossover of 30% of the Fe(III) from 300 to 130 K, together with a ferromagnetic ordering at 5.2 K. Unfortunately, in these compounds no interplay between these two properties—spin-crossover and ferromagnetism—has been detected. This is probably due to the large difference in temperature at which the two phenomena occur. Thus, while the spin-crossover occurs at high temperatures (in the range 130–350 K), the ferromagnetic ordering occurs below 5.2–5.6 K.

A way to overcome this limitation is to take advantage of the photo-induced spin-crossover effect, also known as LIESST effect (light-induced excited spin-state trapping).[15] This phenomenon was originally established for Fe^{II} complexes at low-temperatures (typically below 50 K).[16] In principle, the relaxation *via* a tunneling process from the HS to the LS state is much faster in Fe^{III} compounds because the changes in the metal–ligand bond lengths between the two states are significantly smaller. However, there are two examples of Fe^{III} complexes showing the LIESST effect reported by Sato *et al.*[17,18] The explanation given by these authors for such unexpected behavior is related to the large structural distortion between the LS and HS states, with the intermolecular interactions playing an important role in the relaxation behavior.[18]

In this work, we will explore the possibility of using light irradiation to induce spin-crossover in these hybrid materials. We will show that the confinement of $[Fe(sal_2\text{-trien})]^+$ cations provided by the 2D bimetallic oxalate layers in **1** can also induce LIESST effect in Fe^{III} complexes. A complete photomagnetic characterization together with a detailed structural analysis of the LS and HS structures of **1** is presented in order to understand such unusual behavior. Finally, the possibility of using this family of compounds as switching magnets will be explored.

Results

Crystal structure of 1

The syntheses, crystal structures, Mössbauer spectroscopy and magnetic properties of **1** and **2** were reported previously.[14] In this work, four crystal structures of **1** at 92, 120, 250 and 300 K were solved to study the structural changes between the LS and HS structures.[19] Furthermore, we used for comparison the structural data at 180 K from the previous work[14] and measured the unit cell of one crystal between 92 and 290 K.

The structure of **1** is formed by anionic $[MnCr(ox)_3]^-$ sheets in the *bc* plane alternating with inter-lamellar $[Fe(sal_2\text{-trien})]^+$ cations and dichloromethane solvent molecules (see Fig. 1 and Fig. 2).

To evaluate the structural distortion between the LS and HS octahedral coordination geometries of $[Fe(sal_2\text{-trien})]^+$ in **1**, we have focused on the differences observed in the crystal structures measured at 120 and 300 K for the same crystal because they correspond roughly to the LS and HS structures.

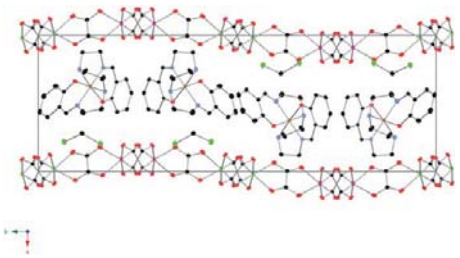

Fig. 1 Projection of the structure of **1** in the *ab* plane at 120 K. Fe (yellow), Cl (green) C (black), N (blue), O (red) Mn(pink), Cr(green). Hydrogen atoms have been omitted for clarity.

The first difference is a shortening of metal–ligand bond lengths as expected for a spin-crossover. Thus, the average Fe–N and Fe–O bond distances in the structure solved at 300 K are respectively, 2.124(4) and 1.890(4) Å, while those solved at 120 K are 1.975(2) and 1.866(2) Å. This results in average bond length differences $\Delta r_{HL,Fe-N} = 0.149$ Å and $\Delta r_{HL,Fe-O} = 0.024$ Å.

The second difference concerns the distortion of the octahedral coordination site, which is significantly larger for the HS state. Thus, at 300 K two of the three diagonals from the octahedron, defined by the bonds N(amine)–Fe–O(phenoxo) (N(amine) = N2,N3), differ strongly from 180° (158.08(19) and 161.23(15)°), while the remaining one, defined by the bond N(imine)–Fe–N(imine), is 176.78(15)° (N(imine) = N1,N4). On the contrary, the coordination octahedron is much more regular at 120 K. The three diagonals are much closer to 180° with N(amine)–Fe–O(phenoxo) angles of 173.18(10) and 173.82(9)° and N(imine)–Fe–N(imine) angle of 179.63(11)°. Different parameters have been used by several authors to quantify the distortions of $[Fe(sal_2\text{-trien})]^+$ salts, such as Σ and Θ (see Table 1).[20–22] As expected, angular and trigonal distortions, which are evaluated respectively by Σ and Θ, are much more important when the Fe^{III} complex is in the HS state (300 K). On the other hand, Σ and Θ parameters of the LS structures (92, 120 and 180 K) present very similar values while the structure with intermediate spin state (250 K) present intermediate values between the LS and HS structures as expected (see Table 1).

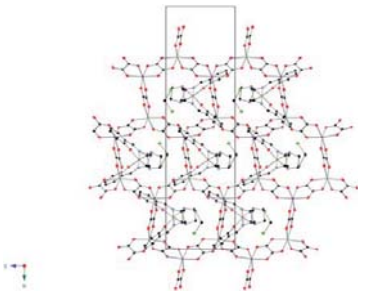

Fig. 2 Projection of the structure of **1** in the *bc* plane at 120 K. Fe (yellow), Cl (green) C (black), N (blue), O (red) Mn(pink), Cr(green). Hydrogen atoms have been omitted for clarity.

Table 1 Structural parameters of **1** and **2**

	Spin state	Mean Fe–N (Å)	Mean Fe–O (Å)	Σ (°)[a]	Θ (°)[b]
1 (300 K)	~ 80% HS	2.124(4)	1.890(4)	88	244
1 (250 K)	~ 50% HS	2.076(4)	1.871(3)	72	217
1 (180 K)	~ 90% LS	1.989(4)	1.866(3)	52	89
1 (120 K)	LS	1.975(2)	1.866(2)	49	87
1 (92 K)	LS	1.978(3)	1.864(2)	50	86
2 (120 K) [Fe1]	~ 72% HS	2.039(15)	1.886(12)	71	190
[Fe2]		2.14(2)	1.859(14)	89	235

[a] $\Sigma = \sum_{i=1}^{12} |90 - \alpha_i|$ where α_i are the 12 *cis*-N/O–Fe–N/O angles around the iron atom. [b] $\Theta = \sum_{j=1}^{24} |60 - \theta_j$ where θ_j are the 24 unique N/O–Fe–N/O angles measured on the projection of two triangular faces of the octahedron along their common pseudo-threefold axis.

The third difference concerns the structural disorder shown by one of the ethylene groups at 300 K, which can be solved by considering two possible configurations with occupancies of 58 and 42%. This disorder is not observed in the structures close to the LS state at 180, 120 and 92 K but it is maintained in the structure with ~50% of Fe^{III} in the HS state (250 K) with occupancies of 56 and 44%. Dichloromethane molecules that occupy the holes left by the $[Fe(sal_2\text{-trien})]^+$ cations and the oxalate network, present a similar disorder at 250 and 300 K, which disappears at 92, 120 and 180 K.

The crystal packing of $[Fe(sal_2\text{-trien})]^+$ complexes between the low and high temperature structures also presents some changes, which are reflected in the lattice parameters. Changes in the unit cell of **1** indicate a shortening of *a* and *b* axis from 300 to 92 K whereas the *c* axis remains almost constant with a small increase at decreasing temperature (see Fig. S1†). Furthermore, the β angle decreases gradually from 300 to 92 K. All these changes are more important in the spin-crossover region from 300 to 175 K indicating that they are associated with the change of spin state of $[Fe(sal_2\text{-trien})]^+$. To understand these changes, let us first describe the intermolecular contacts between the Fe^{III} complexes. In the present case, this packing is restricted in the *bc* plane as the Fe^{III} complexes are confined between two anionic bimetallic oxalate layers. They lie with their longer axis parallel to the oxalate layers, and they are connected through edge-to-face C–H···π and N–H···π interactions[23] (see Figs. S2 and S3†) forming double chains running along the *c* axis. From the two phenoxy rings of sal_2-trien, only the one placed in the internal part of the double chain is involved in these C–H···π and N–H···π interactions with four adjacent Fe^{III} complexes belonging to the same double chain. Furthermore, the phenoxy ring belonging to different double chains present π–π stacking interactions. Finally, there are numerous short contacts with the oxalate ligands of the two neighboring layers (see Figs S4 and S5†).

As the *a* parameter gives the separation between the oxalate layers (from 12.096(5) Å at 300 K to 11.5561(3) Å at 120 K), the shortening of *a* axis arises from the change in the spin state of the Fe^{III} complex. The most important consequence of this shortening is that at 120 K there are shorter contacts between O atoms from oxalate layers and CH groups from $[Fe(sal_2\text{-trien})]^+$ (see SI†). On the other hand, the most important effect of the shortening of *b* axis (from 32.135(5) Å at 300 K to 31.6369(7) Å at 120 K) is the presence of shorter contacts at 120 K between Fe^{III} complexes belonging to the same double chains through N–H···π edge-to-face interactions and between Fe^{III} complexes belonging to different double chains through π–π stacking interactions. On the contrary, offset π–π stacking interactions appear in the structure at 300 K between C atoms of phenoxy rings belonging to different double chains (in green in Figure S2†) with weaker contacts in the structure solved at 120 K (see SI†).

Change in the magnetic properties of 1 upon irradiation

In Fig. 3, we plot the magnetic behavior of **1** before and after light irradiation. Before irradiation χT shows a constant value of 10.0 emu·K mol^{-1} in the high temperature range (from 400 to 350 K), which is approximately equal to the sum of the expected contributions for the isolated paramagnetic ions with ~80% of Fe^{III} spin-crossover complex in a HS state. From 350 to 165 K, χT decreases gradually to reach a minimum χT value at 165 K of 7.2 emu·K mol^{-1}. This value is consistent with the Mössbauer data that indicates that Fe^{III} is 94% LS at this temperature.[14] Therefore, in this range of temperatures a HS → LS spin conversion of the Fe^{III} complex takes place. Below 165 K, χT increases due to the Mn^{II}–Cr^{III} ferromagnetic interactions within the bimetallic oxalate layers. This increase is very sharp at lower temperatures suggesting the onset of long-range ferromagnetic ordering at 5.6 K, as confirmed by AC susceptibility and field cooled (FC) and zero-field cooled (ZFC) magnetization measurements (Figs. S6 and S7†).[14]

During irradiation at 647 nm wavelength (power 8 mW cm^{-2}), at 10 K inside a SQUID cavity, an increase in χT was observed at low temperatures. Thus, after about 1.5 h the light irradiation was switched off. The temperature was then increased at 0.3 K min^{-1} and the magnetic susceptibility recorded. Below 50 K, the χT value after irradiation is clearly higher than the one before irradiation, while above 50 K, the two curves are superimposed (Fig. 3). This result suggests that a photomagnetic effect has occurred, which can be attributed to the spin photoconversion of

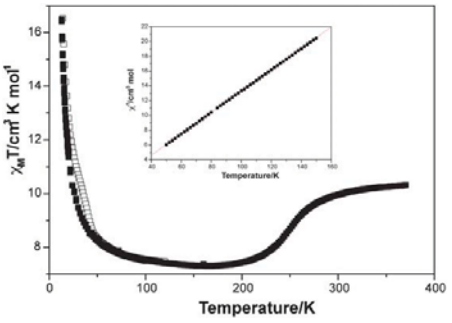

Fig. 3 Magnetic and Photo-Magnetic behaviour for compound **1**. ■ Magnetic behaviour measured in dark. □ Photo-magnetic behaviour measured after irradiation by 647 nm wavelength laser. Inserted graph: Curie–Weiss law between 50 K and 150 K.

the $[Fe(sal_2\text{-trien})]^+$ from its LS ground state at low temperature to its HS metastable state. In order to estimate the fraction of photoconverted Fe^{III}, the magnetism of the $Mn^{II}Cr^{III}$ bimetallic layers needs to be substrated as it presents a strong underlying magnetism. To estimate the magnetism of the bimetallic layers we have taken advantage of the fact that below the thermal spin transition (*i.e.* below 150 K) and well above the Curie temperature (*i.e.* above 50 K), the magnetic response can be satisfactorily simulated by a Curie–Weiss law (see inset in Fig. 3). Below 50 K, this simple Curie–Weiss law is unable to reproduce properly the χT values due to the vicinity of the ferromagnetic ordering. In this region, we have used the molecular field model proposed by Néel that explicitly takes into account the fact that there are two distinct sub-networks in the $Mn^{II}Cr^{III}$ layers.[24] Differences between experimental χT values and those obtained with this model are lower than 0.04 cm^3 K mol^{-1} in between 25 K and 175 K. Details of this fitting are given as supporting information.† In Fig. 4, we plot the temperature dependence of the fraction of HS Fe^{III} (γ_{HS}) before and after irradiation after subtracting the contribution from the $Mn^{II}Cr^{III}$ oxalate network.

γ_{HS} is almost zero below 170 K in the measurements performed in the dark. Increasing the temperature above 170 K leads to a gradual increase of γ_{HS} with a maximum value of 0.86 at 370 K in agreement with Mössbauer measurements.[14] γ_{HS} from the curve obtained after irradiation reaches a maximum value of 0.37 at 25 K. When the temperature increases, a decrease in γ_{HS} is observed, and γ_{HS} reaches 0 at about 75 K. At higher temperatures γ_{HS} curve is superimposed with that recorded in the dark. The T(LIESST), estimated from the minimum of the derivative of γ_{HS} by the temperature (inset in Fig. 4), is determined to be 41 K.[25] This represents somewhat the limit of the long-lived photo-induced lifetime of the HS state. In order to get some insight into the decay of the photoinduced HS state, some kinetics have been recorded at 10 K and every 2 K between 36 and 44 K (Fig. 5).

At 10 K, almost no decay of the photo-induced HS state was noticed. More precisely, the decrease of the HS fraction was less than 2% after 7 h. Fig. 5 shows the relaxation kinetics recorded between 36 and 44 K. The maximum of HS fraction at initial time, for a given kinetic is different: the higher the temperature, the lower the photoexcitation. This suggests that the kinetic process is thermally activated. Interestingly, these relaxation curves show strong deviation from a single exponential, with a marked stretched exponential behaviour, and with a fast component at earlier times and a long decay process at infinite time. For reproducing this type of curves, Hauser *et al.*[26] used a distribution of relaxation rates at a given temperature with a Gaussian distribution of the activation energy. Following this procedure, the relaxation curves of compound **1** can be satisfactorily fitted as illustrated by the solid lines in Fig. 5. The apparent activation energy, E_a (= 200 cm^{-1}), and the apparent preexponential factor, k_∞ (= 0.49 s^{-1}) of the activated region are calculated from the straight line of the $\ln k_{HL}(T)$ *vs.* $1/T$ plot. The standard deviation of the activation energy is 52 ± 6 cm^{-1}.

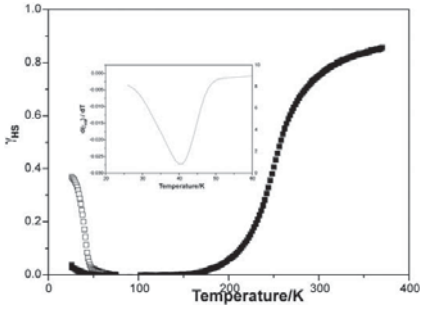

Fig. 4 Fraction of HS Fe^{III} (γ_{HS}) before (■) and after (□) irradiation). Inserted graph: χT derivative for photo-magnetism.

Effect of photoexcitation on the magnetic ordering

FC and ZFC magnetization (Fig. S6†) and AC susceptibility measurements (Fig. S7†) have been recorded between 2 and 10 K, before and after photoirradiation of 1.5 h at 10 K to test if the photoconversion of the Fe^{III} complex affects the Curie temperature (T_c) of the compound. We have to take into account that at 10 K the lifetime of the photoinduced HS state is very long, and consequently the HS fraction remains almost constant during the experiment. ZFC and FC magnetization measurements start to bifurcate at 5.6 K, both before and after irradiation. Similarly, AC susceptibility measurements show the appearance of an out-of-phase signal (χ'') below T_c = 5.6 K that remains almost constant upon irradiation, showing a shift to higher values by 0.1 K after photoirradiation.

Crystal structure and photomagnetism of 2

The structure of **2** was solved at 120 K.[14] It is formed by an anionic 3D polymeric oxalate-bridged bimetallic network with $[Fe(sal_2\text{-trien})]^+$ cations and methanol solvent molecules occupying the cavities. Magnetic measurements and Mössbauer spectroscopy[14] indicate that 100% of Fe^{III} complexes are in the HS at room temperature and the HS → LS spin conversion of 30% of the Fe^{III} complexes from 300 and 130 K. There are two crystallographically independent $[Fe(sal_2\text{-trien})]^+$ complexes ([Fe1] and [Fe2]). The average Fe–N and Fe–O bond distances

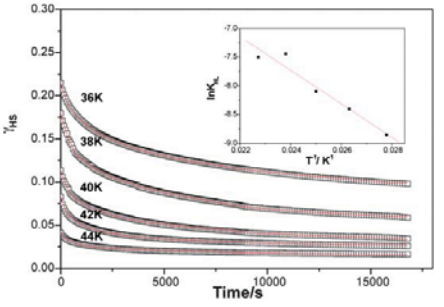

Fig. 5 Relaxation kinetics and simulation of the HS fraction *vs.* time at different temperatures. Inserted graph: $\ln k_{HL}(T)$ *vs.* $1/T$ dependence. k_{HL}corresponds to the rate constant for the HS → LS relaxation. The fitting procedure has been performed by adding a small residual HS at long time.

are close to those obtained for other high-spin (HS) $[Fe(sal_2\text{-}trien)]^+$ compounds (see Table 1). At lower temperatures, the HS fraction remains constant and there is a ferromagnetic ordering with a T_c of 5.2 K, as usual for this type of compounds. In contrast to **1**, this compound does not present LIESST effect.

Discussion

The lifetime of the HS photoexcited state has been rationalized by Hauser,[27] on the basis of a non-adiabatic multiphonon relaxation model. In the framework of this theory, the metal–ligand distance is taken as the reaction coordinate, related to only one vibrational mode, namely the completely symmetrical one. This is the so-called SCC (single configurational coordinate) approach. Based on this theory, it is possible to estimate theoretically the rate constant for the HS → LS relaxation (k_{HL}) at different temperatures for the different ions that could exhibit the LIESST effect such as Fe^{II}, Fe^{III} or Co^{II}.[28] The main difference between these three ions is the bond length difference between the LS and the HS states, being typically 0.2 Å for Fe^{II}, 0.13–0.16 Å for Fe^{III} and 0.09–0.12 Å for Co^{II}. This change in bond length difference is expected to directly affect the decay of the photo-induced state, being much faster for Co^{II} than for Fe^{II} and Fe^{III}. Particularly, according to SCC theory, the low-temperature (tunneling regime) lifetime of the HS state for Fe^{III} spin-crossover compounds is expected to be of the order of milliseconds, whereas it can go from seconds to months for Fe^{II} spin-crossover compounds. According to such a short lifetime, it should be impossible to observe the decay of the photoinduced state for Fe^{III} by using standard SQUID techniques. However, as mentioned above, the LIESST effect has been observed by Sato in two Fe^{III} complexes, $[Fe(pap)_2]^+$ and $[Fe(qsal)_2]^+$.[18] This author attributed such an extraordinary result to the strong distortion of the Fe^{III} site from its octahedral geometry, which can be enhanced by the presence of strong intermolecular interactions, such as π–π stacking. Thus, when passing from the ideal octahedral site $[Fe^{II}N_6]$ to a distorted $[Fe^{III}N_4O_2]$ geometry, in addition to the completely symmetrical vibrational mode, other vibrational modes such as the bending mode should also be taken into account.[18,29] This results in a displacement between the potential walls of the HS and LS states, which is larger than that expected considering only the changes in metal–ligand distances, and could explain the long lifetime of the photogenerated HS state.

To evaluate the distortion of $[Fe(sal_2\text{-}trien)]^+$ in **1**, we have focused our attention on the differences between the 120 and 300 K structures of the compound as they are close to the LS and HS structures. The structure at 120 K corresponds to the LS structure since magnetic and Mössbauer data indicate that 100% of the Fe^{III} are in the LS state at this temperature. On the other hand, the structure at 300 K is close to the HS structure as magnetic data indicate that around 80% of Fe^{III} are in the HS state at this temperature.[14]

The first difference between the two structures is a shortening in the Fe–N and Fe–O bond lengths as expected for a spin-crossover. Thus, the average bond length differences are $\Delta r_{HL,Fe-N} = 0.149$ Å and $\Delta r_{HL,Fe-O} = 0.024$ Å. If we take into account that at 300 K about 20% of Fe^{III} remains in the LS state, we could expect $\Delta r_{HL,Fe-N} = 0.186$ Å and $\Delta r_{HL,Fe-O} = 0.03$ Å values between the LS and HS states of this compound. These values are very close to those exhibited by the two Fe^{III} compounds known to date presenting LIESST effect (in $[Fe(pap)_2]X$, $\Delta r_{HL,Fe-N} = 0.19$ Å and $\Delta r_{HL,Fe-O} = 0.05$ Å, and in $[Fe(qsal)_2]Y$, $\Delta r_{HL,Fe-N} = 0.18$ Å and $\Delta r_{HL,Fe-O} = 0.02$ Å).[18] Notice that these values are also similar to those reported for $[Fe(sal_2\text{-}trien)][Ni(dmit)_2]$ ($\Delta r_{HL,Fe-N} = 0.188$ Å and $\Delta r_{HL,Fe-O} = 0.036$ Å)[30] which is the only other $[Fe(sal_2\text{-}trien)]^+$ salt reported so far for which both the LS and HS structural data are available.[31] This salt is the first example of $[Fe(sal_2\text{-}trien)]^+$ salt presenting a strong cooperative transition and wide hysteresis but no LIESST effect has been reported for this compound. Furthermore, the synthesis of this compound presents serious problems of reproducibility that could limit further studies.[32]

A second set of parameters accounting for angular and trigonal distortions from the ideal octahedron is provided by Σ and Θ parameters. However, Σ and Θ values of the 300 and 120 K structures lie in the range of those found for other HS and LS $[Fe(sal_2\text{-}trien)]^+$ compounds.[31] Therefore, it is difficult to get some conclusions from these parameters.

The third difference concerns the changes in selected bond angles (*cis* and *trans* N/O–Fe–N/O bond angles) between the LS and HS structures ($\Delta\measuredangle_{HL}$). In **1**, a value of $\Delta\measuredangle_{HL} = 93.64°$ is obtained. This value is intermediate between that of $[Fe(pap)_2]^+$ ($\Delta\measuredangle_{HL} = 136.06°$), for which LIESST effect is observed, and that of $[Fe(acpa)_2]^+$ ($\Delta\measuredangle_{HL} = 74.32°$), which does not present LIESST effect, but a larger value could be expected taking into account that there are still around 20% of Fe^{III} in the LS state in the structure solved at 300 K. Therefore, we can conclude that, in analogy with $[Fe(pap)_2]^+$, the strong distortion from the ideal octahedral geometry in **1** is at the origin of the LIESST effect.

In turn, a sharp structural difference between **1** and $[Fe(pap)_2]^+$ concerns the nature and dimensionality of the intermolecular interactions. Thus, while in $[Fe(pap)_2]^+$ the π–π 2D stacking between pyridine and phenyl rings seems to enhance the structural distortion of the LIESST complex, in **1**, π–π interactions between pairs of $[Fe(sal_2\text{-}trien)]^+$ complexes belonging to different chains coexist with edge-to-face CH–π and NH–π interactions. As a consequence, **1** shows a gradual spin-crossover with no hysteresis, while $[Fe(pap)_2]^+$ presents a cooperative spin-crossover with hysteresis. Furthermore, the decay of the photo-induced HS state of the two compounds follows a different relaxation kinetics. Whereas the time dependence of the HS fraction after photoexcitation of $[Fe(pap)_2]^+$ can be fitted to a sigmoidal-type curve as a result of self-acceleration of the HS → LS relaxation due to cooperative effects, the one from **1** can be fitted to a multiexponential curve with a fast component at earlier times and a long decay process at infinite times. The broad distribution of activation energies is the cause of this type of relaxation kinetics. These curves are typical of non-cooperative systems that rarely present a single-exponential behavior. It appears in poorly crystalline solids and in some cases it has been related to the presence of disorder in the structure in compounds presenting a cooperative spin-crossover.[33] Hence, it could have some relation with the disorder observed in the structure of **1** even it is only observed at high temperature. In any case, we can conclude that both the magnetic behavior and the decay of the photo-induced HS state in **1** indicate that in contrast to the

previous examples, cooperativity it is not a necessary condition to have LIESST effect in Fe^{III} compounds.

A second structural difference of **1** with respect to the other Fe^{III} compounds exhibiting LIESST effect is the presence of an anionic extended network (the bimetallic oxalate network) instead of a discrete small counterion. This rigid network could play a similar role in the stabilisation of the metastable HS state of **1** to that played by the strong π–π intermolecular interactions in $[Fe(pap)_2]^+$. In favour of this hypothesis are the numerous short contacts between the $[Fe(sal_2\text{-trien})]^+$ cations with the oxalate ligands, which are different in the low and high-temperature structures (see SI†). Maybe the interactions with the oxalate network enhance the distortion of the LIESST complex but, at the same time, they prevent a cooperative spin-crossover since they restrict the structural dimensionality to 2. Photomagnetic measurements on salts of $[Fe(sal_2\text{-trien})]^+$ and derivatives in different anionic environments are needed to clarify this point. This work is in progress in our group.[13d]

The question remains why no LIESST has been observed on the remaining 30% HS fraction at 10 K for compound **2**. Further work is necessary to answer to such question. For now, it remains unclear if the absence of LIESST is linked to: (a) a distortion effect and/or (b) the difference of rigidity between 2D and 3D networks and/or (c) the small amount of Fe^{III} that can be converted. As far as the distortion (a) is concerned, it would be helpful to compare the geometries of the $[Fe(sal_2\text{-trien})]^+$ complexes in the HS and the LS state. Unfortunately, this is not possible as the HS fraction remains at 70% at temperatures as low as 10 K. The influence of the rigidity of the network (b) can be seen in the fact that the contraction of the interlayer distance that follows the spin-crossover in **1** cannot be present in **2** that presents a more isotropic 3D network. Finally, the low amount of low spin fraction at low temperature (c) makes it difficult to observe the possible small increase of magnetic response under light, as it will be difficult to distinguish this increase from the important magnetic signal of the oxalate network. New compounds are to be synthesized, 2D and 3D, in order to have more data to draw conclusions.

Conclusions

In this work we have shown that the insertion of a $[Fe(sal_2\text{-trien})]^+$ complex cation into a 2D oxalate network results in a hybrid magnet with coexistence of magnetic ordering and photoinduced spin-crossover in compound **1**. The use of a molecular approach has led to the coexistence of two properties—ferromagnetism and photo-induced spin crossover—that normally do not appear together in the same compound. This could open the way to prepare switching magnets. Still, in the present case the photo-induced spin conversion of the inserted Fe^{III} complex has shown to have a negligible influence on the cooperative magnetic behaviour of the 2D oxalate network. This is not an unexpected result, as 2D oxalate networks with very different interlayer separations present similar T_c values. In this sense, hybrid compounds formed by insertion of these spin-crossover cations into a 3D oxalate network are expected to be more suitable, as this magnetic network has shown to be much more sensitive to the influence of an internal pressure. Unfortunately, the compound **2** obtained by insertion of a $[Fe(sal_2\text{-trien})]^+$ cation into a 3D oxalate network does not present LIESST effect.

Another remarkable result has been the observation of LIESST effect in **1**. This very rare and unexpected property in a Fe^{III} spin-crossover complex, has been attributed to the strong distortion exhibited by the metastable HS state. However, **1** has shown that, in contrast to what has been previously proposed, a cooperative spin-crossover is not a necessary condition to observe LIESST effect in Fe^{III} compounds. The presence of an extended anion network able to establish strong intermolecular interactions with the spin-crossover cation could also enhance this distortion. If this was true, the confinement of spin-crossover cations into extended networks could be a suitable strategy to induce LIESST effect on other Fe^{III} cations, or to improve LIESST properties in Fe^{II} complexes.

Finally, the discovery that $[Fe(sal_2\text{-trien})]^+$ complexes can present LIESST effect opens the way for the use of this compound in the preparation of new multifunctional switchable compounds with other properties different from the magnetic ones. An interesting possibility could be the switching of the conductivity in $[Fe(sal_2\text{-trien})]^+$ salts of $[Ni(dmit)_2]$ anions already reported in the literature.[34]

Acknowledgements

Financial support from the EU (SPINMOL ERC Advanced Grant to EC), the Spanish Ministerio de Ciencia e Innovación (Project Consolider-Ingenio in Molecular Nanoscience and projects MAT2007-61584 and CTQ-2008-06720) and the Generalitat Valenciana (Prometeo Program) are gratefully acknowledged.

Notes and references

1 (*a*) E. Coronado and P. Day, *Chem. Rev.*, 2004, **104**, 5419; (*b*) E. Coronado, C. Martí-Gastaldo, E. Navarro-Moratalla, A. Ribera, S. J. Blundell and P. J. Baker, *Nat. Chem.*, 2010, **2**, 1031.
2 (*a*) E. Coronado, M. C. Giménez-López, G. Levchenko, F. M. Romero, V. García-Baonza, A. Milner and M. Paz-Pasternak, *J. Am. Chem. Soc.*, 2005, **127**, 4580; (*b*) E. Coronado, M. C. Giménez-López, T. Korzeniak, G. Levchenko, F. M. Romero, A. Segura, V. García-Baonza, J. C. Cezar, F. M. F. De Groot, A. Milner and M. Paz-Pasternak, *J. Am. Chem. Soc.*, 2008, **130**, 15519.
3 M. Clemente-León, E. Coronado, C. Martí-Gastaldo and F. M. Romero, *Chem. Soc. Rev.*, 2011, **40**, 473.
4 (*a*) H. Tamaki, Z. J. Zhong, N. Matsumoto, S. Kida, M. Koikawa, N. Achiwa, Y. Hashimoto and H. Okawa, *J. Am. Chem. Soc.*, 1992, **114**, 6974; (*b*) H. Tamaki, M. Mitsumi, N. Nakamura, N. Matsumoto, S. Kida, H. Okawa and S. Ijima, *Chem. Lett.*, 1992, 1975; (*c*) C. Mathonière, S. G. Carling, D. Yuscheng and P. Day, *J. Chem. Soc., Chem. Commun.*, 1994, 1551; (*d*) C. Mathonière, J. Nutall, S. G. Carling and P. Day, *Inorg. Chem.*, 1996, **35**, 1201; (*e*) R. Pellaux, H. W. Schmalle, R. Huber, P. Fisher, T. Hauss, B. Ouladdiaf and S. Decurtins, *Inorg. Chem.*, 1997, **36**, 2301; (*f*) E. Coronado, J. R. Galán-Mascarós, C. J. Gómez-García, J. M. Martínez-Agudo, E. Martínez-Ferrero, J. C. Waerenborgh and M. Almeida, *J. Solid State Chem.*, 2001, **159**, 391; (*g*) K. S. Min, A. L. Rhinegold and J. S. Miller, *Inorg. Chem.*, 2005, **44**, 8433; (*h*) E. Coronado, J. R. Galán-Mascarós and C. Martí-Gastaldo, *J. Mater. Chem.*, 2006, **16**, 2685.
5 (*a*) S. Decurtins, H. W. Schmalle, P. Schneuwly and H. R. Oswald, *Inorg. Chem.*, 1993, **32**, 1888; (*b*) S. Decurtins, H. W. Schmalle, P. Schneuwly, J. Ensling and P. Gütlich, *J. Am. Chem. Soc.*, 1994, **116**, 9521; (*c*) M. Hernández-Molina, F. Lloret, C. Ruiz-Pérez and M. Julve, *Inorg. Chem.*, 1998, **37**, 4141; (*d*) E. Coronado, J. R. Galán-Mascarós, C. J. Gómez-García and J. M. Martínez-Agudo, *Inorg. Chem.*, 2001, **40**, 113; (*e*) F. Pointillart, C. Train, M. Gruselle, F. Villain, H. W. Schmalle, D. Talbot, P. Gredin, S. Decurtins and M. Verdaguer, *Chem. Mater.*, 2004, **16**, 832; (*f*)

M. Clemente-León, E. Coronado, C. J. Gómez-García and A. Soriano-Portillo, *Inorg. Chem.*, 2006, **45**, 5653.
6 (*a*) M. Clemente-León, J. R. Galán-Mascarós and C. J. Gómez-García, *Chem. Commun.*, 1997, 1727; (*b*) E. Coronado, J. R. Galán-Mascarós, C. J. Gómez-García and J. M. Martínez-Agudo, *Adv. Mater.*, 1999, **11**, 558; (*c*) E. Coronado, J. R. Galán-Mascarós, C. J. Gómez-García, J. Ensling and P. Gutlich, *Chem.–Eur. J.*, 2000, **6**, 552.
7 (*a*) S. Bénard, P. Yu, J. P. Audière, E. Rivière, R. Clèment, J. Ghilhem, L. Tchertanov and K. Nakatami, *J. Am. Chem. Soc.*, 2000, **122**, 9444; (*b*) S. M. Aldoshin, N. A. Sanina, V. I. Minkin, N. A. Voloshin, V. N. Ikorskii, V. I. Ovcharenko, V. A. Smirnov and N. K. Nagaeva, *J. Mol. Struct.*, 2007, **826**, 6.
8 (*a*) E. Coronado, J. R. Galán-Mascarós, C. J. Gómez-García and V. Laukhin, *Nature*, 2000, **408**, 447; (*b*) A. Alberola, E. Coronado, J. R. Galán-Mascarós, C. Giménez-Saiz and C. J. Gómez-García, *J. Am. Chem. Soc.*, 2003, **125**, 10774; (*c*) E. Coronado, J. R. Galán-Mascarós, C. J. Gómez-García, E. Martínez-Ferrero and S. Van Smaalen, *Inorg. Chem.*, 2004, **43**, 4808.
9 H. Okawa, A. Shigematsu, M. Sadakiyo, T. Miyagawa, K. Yoneda, M. Ohba and H. Kitagawa, *J. Am. Chem. Soc.*, 2009, **131**, 13516.
10 (*a*) R. Andrés, M. Gruselle, B. Malézieux, M. Verdaguer and J. Vaissermann, *Inorg. Chem.*, 1999, **38**, 4637; (*b*) R. Andrés, M. Brissard, M. Gruselle, C. Train, J. Vaissermann, B. Malézieux, J. P. Jamet and M. Verdaguer, *Inorg. Chem.*, 2001, **40**, 4633; (*c*) M. Clemente-León, E. Coronado, J. C. Dias, A. Soriano-Portillo and R. D. Willett, *Inorg. Chem.*, 2008, **47**, 6458.
11 J. R. Galán-Mascarós, E. Coronado, P. A. Goddard, J. Singleton, A. I. Coldea, J. D. Wallis, S. J. Coles and A. Alberola, *J. Am. Chem. Soc.*, 2010, **132**, 9271.
12 (*a*) C. Train, R. Gheorghe, V. Krstic, L. M. Chamoreau, N. S. Ovanesyan, G. L. J. A. Rikken, M. Gruselle and M. Verdaguer, *Nat. Mater.*, 2008, **17**, 729; (*b*) C. Train, T. Nuida, R. Gheorghe, M. Gruselle and S. Ohkoshi, *J. Am. Chem. Soc.*, 2009, **131**, 16838.
13 (*a*) R. Sieber, S. Decurtins, H. Stoeckli-Evans, C. Wilson, D. Yufit, J. A. K. Howard, S. C. Capelli and A. Hauser, *Chem.–Eur. J.*, 2000, **6**, 361; (*b*) E. Coronado, J. R. Galán-Mascarós, M. C. Giménez-López, M. Almeida and J. C. Waerenborgh, *Polyhedron*, 2007, **26**, 1838; (*c*) M. Clemente-León, E. Coronado, M. C. Giménez-López, A. Soriano-Portillo, J. C. Waerenborgh, F. S. Delgado and C. Ruiz-Pérez, *Inorg. Chem.*, 2008, **47**, 9111; (*d*) M. Clemente-León, E. Coronado and M. López-Jordà, *Dalton Trans.*, 2010, **39**, 4903.
14 M. Clemente-León, E. Coronado, M. López-Jordà, G. Mínguez Espallargas, A. Soriano-Portillo and J. C. Waerenborgh, *Chem.–Eur. J.*, 2010, **16**, 2207.
15 S. Decurtins, P. Gütlich, K. M. Hasselbach, A. Hauser and H. Spiering, *Inorg. Chem.*, 1985, **24**, 2174.
16 C. Enachescu, A. Hauser, J.-J. Girerd and M.-L. Boillot, *ChemPhysChem*, 2006, **7**, 1127.
17 (*a*) S. Hayami, Z.-Z. Gu, M. Shiro, Y. Einaga, A. Fujishima and O. Sato, *J. Am. Chem. Soc.*, 2000, **122**, 7126; (*b*) G. Juhász, S. Hayami, O. Sato and Y. Maeda, *Chem. Phys. Lett.*, 2002, **364**, 164.
18 S. Hayami, K. Hiki, T. Kawahara, Y. Maeda, D. Urakami, K. Inoue, M. Ohama, S. Kawata and O. Sato, *Chem.–Eur. J.*, 2009, **15**, 3497.
19 Crystal data for **1** at 300 K: $C_{27}H_{26}C_{l2}CrFeMnN_4O_{14}$, M = 864.21, monoclinic, space group $P2_1/c$ (no. 14), a = 12.096(5) Å;, b = 32.135(5) Å;, c = 9.467(5) Å;, β = 111.981(5)°, V = 3412(2) Å^3, Z = 4, μ = 1.325 mm^{-1}, F(000) = 1748, T = 300(2)K, 44282 reflections measured, 11352 unique (R_{int} = 0.0589), R_1 = 0.0635, wR_2 = 0.1689 for $I > 2\sigma(I)$. CCDC 807173. Crystal data for **1** at 250 K: $C_{27}H_{26}C_{l2}CrFeMnN_4O_{14}$, M = 864.21, monoclinic, space group $P2_1/c$ (no. 14), a = 11.9215(15) Å, b = 31.910(3) Å, c = 9.4841(11) Å, β = 111.535(13)°, V = 3356.1(6) Å^3, Z = 4, μ = 1.348 mm^{-1}, F(000) = 1748, T = 250(2)K, 43973 reflections measured, 11354 unique (R_{int} = 0.0590), R_1 = 0.0530, wR_2 = 0.1240 for $I > 2\sigma(I)$. CCDC 813345. Crystal data for **1** at 120 K: $C_{27}H_{26}C_{l2}CrFeMnN_4O_{14}$, M = 864.21, monoclinic, space group $P2_1/c$ (no. 14), a = 11.5561(3) Å, b = 31.6369(7) Å, c = 9.5457(3) Å, β = 109.984(3)°, V = 3279.77(15) Å^3, Z = 4, μ = 1.379 mm^{-1}, F(000) = 1748, T = 120(2)K, 26791 reflections measured, 10705 unique (R_{int} = 0.0302), R_1 = 0.0477, wR_2 = 0.0951 for $I > 2\sigma(I)$. CCDC 807172. Crystal data for **1** at 92 K: $C_{27}H_{26}C_{l2}CrFeMnN_4O_{14}$, M = 864.21, monoclinic, space group $P2_1/c$ (no. 14), a = 11.5602(4) Å;, b = 31.6268(12) Å;, c = 9.5237(4) Å;, β = 110.199(4)°, V = 3267.8(2) Å^3, Z = 4, μ = 1.379 mm^{-1}, F(000) = 1748, T = 92(2)K, 29715 reflections measured, 10846 unique (R_{int} = 0.0557), R_1 = 0.0546, wR_2 = 0.1230 for $I > 2\sigma(I)$. CCDC 813714. Crystal data of **1** at 180 K have been taken from ref. 14.
20 P. Guionneau, M. Marchivie, G. Bravic, J.-F. Létard and D. Chasseau, *Top. Curr. Chem.*, 2004, **234**, 97.
21 J. K. McCusker, A. L. Rheingold and D. N. Hendrickson, *Inorg. Chem.*, 1996, **35**, 2100.
22 M. Marchivie, P. Guionneau, J.-F. Létard and D. Chasseau, *Acta Crystallogr., Sect. B: Struct. Sci.*, 2005, **61**, 25.
23 C. Janiak, *J. Chem. Soc., Dalton Trans.*, 2000, 3885.
24 L. Néel, *Ann. Phys.*, 1948, **3**, 137.
25 J.-F. Létard, *J. Mater. Chem.*, 2006, **16**, 2550.
26 A. Hauser, J. Adler and P. Gütlich, *Chem. Phys. Lett.*, 1988, **152**, 468.
27 A. Hauser, *J. Chem. Phys.*, 1991, **94**, 2741.
28 A. Hauser, *Top. Curr. Chem.*, 2004, **234**, 155.
29 S. Schenker, A. Hauser and R. M. Dyson, *Inorg. Chem.*, 1996, **35**, 4676.
30 S. Dorbes, L. Valade, J. A. Real and C. Faulmann, *Chem. Commun.*, 2005, 69.
31 R. Pritchard, S. A. Barrett, C. A. Kilner and M. A. Halcrow, *Dalton Trans.*, 2008, 3159.
32 C. Faulmann, P. A. Szilágyi, K. Jacob, J. Chahine and L. Valade, *New J. Chem.*, 2009, **33**, 1268.
33 V. Mishra, R. Mukherjee, J. Linares, C. Balde, C. Desplanches, J.-F. Létard, E. Collet, L. Toupet, M. Castro and F. Varret, *Inorg. Chem.*, 2008, **47**, 7577.
34 C. Faulmann, S. Dorbes, J. A. Real and L. Valade, *J. Low Temp. Phys.*, 2006, **142**, 261.

Inorganic Chemistry

ARTICLE

pubs.acs.org/IC

Multifunctional Magnetic Materials Obtained by Insertion of Spin-Crossover Fe^{III} Complexes into Chiral 3D Bimetallic Oxalate-Based Ferromagnets

Miguel Clemente-León,*[,†] Eugenio Coronado,*[,†] Maurici López-Jordà,[†] and João C. Waerenborgh[‡]

[†]Instituto de Ciencia Molecular, Universidad de Valencia, Catedrático José Beltrán 2, 46980 Paterna, Spain

[‡]Department of Quimica, ITN/CFMC-UL, P-2686-953 Sacavém, Portugal

Supporting Information

ABSTRACT: The syntheses, structures, and magnetic properties of compounds of formula $[Fe^{III}(5\text{-Clsal}_2\text{-trien})][Mn^{II}Cr^{III}(ox)_3]\cdot 0.5(CH_3NO_2)$ (**1**), $[Fe^{III}(5\text{-Brsal}_2\text{-trien})][Mn^{II}Cr^{III}(ox)_3]$ (**2**), and $[In^{III}(5\text{-Clsal}_2\text{-trien})][Mn^{II}Cr^{III}(ox)_3]$ (**3**) are reported. The structure of the three compounds, which crystallize in the orthorhombic $P2_12_12_1$ chiral space group, presents a 3D chiral anionic network formed by Mn^{II} and Cr^{III} ions linked through oxalate ligands with inserted $[Fe^{III}(5\text{-Clsal}_2\text{-trien})]^+$, $[Fe^{III}(5\text{-Brsal}_2\text{-trien})]^+$, and $[In^{III}(5\text{-Clsal}_2\text{-trien})]^+$ cations. The magnetic properties indicate that the three compounds undergo long-range ferromagnetic ordering at ca. 5 K. On the other hand, the inserted Fe^{III} cations undergo a partial spin crossover in the case of **1** and **2**.

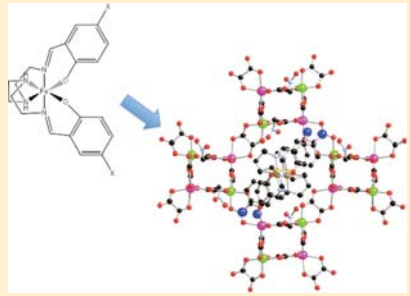

INTRODUCTION

Molecular materials offer great possibilities in the search for novel combinations of properties in a single material. These materials may be prepared building up two network hybrid solids formed by two molecular fragments with each network furnishing distinct physical properties. If the two networks are quasi-independent, a coexistence of the two physical properties is anticipated.[1] If the two molecular networks are coupled, the interplay between their properties may give rise to new properties.[1b] Finally, if one of these two networks changes its properties under application of an external stimulus, a switchable multifunctional material could be obtained in which the responsive network can influence the properties of the other network.[2]

Bimetallic oxalate-bridged complexes of formula $A[M^{II}M^{III}(ox)_3]$ (M^{III} = Cr, Fe, Ru, V, Mn; M^{II} = Mn, Fe, Co, Ni, Cu, Zn; A = cation; ox = oxalate) have provided remarkable examples of this type of compounds.[3] They are composed by polymeric 2D[4] or 3D[5] anionic networks, which furnish the cooperative magnetic properties (ferro-, ferri-, or canted antiferromagnetism), and a bulky charge-compensating molecular cation, which templates the network formation and adds a second physical property to the solid. Insertion of different cations into oxalate networks has led to compounds combining in the same compound the long-range magnetic ordering from the oxalate network with paramagnetism,[6] photochromism,[7] electric conductivity,[8] proton conduction,[9] chirality,[10] chirality and conductivity,[11] or ferroelectricity.[12]

The interplay between the properties of the two molecular networks has been observed in enantiopure oxalate-based magnets prepared by Train et al. that exhibit a magneto-chiral dichroic effect and magnetization-induced second-harmonic generation.[13] Although most of the chiral oxalate-based magnets reported so far present a 3D network and are formed with templating cations that are chiral metallic complexes such as $[Z^{II}(bpy)_3]^{2+}$ (Z = Ru, Fe, Co; bpy = bipyridine) and similar cations,[5,10a,10b] the interplay between chirality and magnetism has only been achieved in enantiopure 2D oxalate-based magnets. A possible explanation to this fact is that the optical properties of the 3D compounds are dominated by absorption of the templating cation.[13a]

The design of switching magnets has been less explored. In this context, cationic spin-crossover (SCO) complexes are particularly suitable for this purpose. This kind of molecular complex changes their spin state from low-spin (LS) to high-spin (HS) configurations under an external stimulus such as temperature, light irradiation, or pressure. As this magnetic switching is accompanied by changes in the molecular size, the spin-crossover process should act as an internal pressure in the hybrid material and therefore might affect the long-range magnetic ordering in the extended magnetic network. In addition, the magnetic framework in which the spin-crossover molecule is inserted may affect the properties of this switchable molecule. Thus far, several examples have described the incorporation of SCO

Received: June 16, 2011
Published: August 16, 2011

dx.doi.org/10.1021/ic201293f | *Inorg. Chem.* 2011, 50, 9122–9130

Table 1. Crystallographic Data of 1−3

	1	2	3
empirical formula	$C_{26.5}H_{23.5}Cl_2CrFeMnN_{4.5}O_{15}$	$C_{26}H_{22}Br_2CrFeMnN_4O_{14}$	$C_{26}H_{22}Cl_2CrInMnN_4O_{14}$
fw	878.69	937.09	907.14
cryst color	brown	brown	violet
temperature (K)	120	120	120
wavelength (Å)	0.71073	0.71073	0.71073
cryst syst, Z	orthorhombic, 4	orthorhombic, 4	orthorhombic, 4
space group	$P2_12_12_1$	$P2_12_12_1$	$P2_12_12_1$
a (Å)	13.3082(3)	13.6797(11)	13.9216(11)
b (Å)	15.6219(4)	15.2785(9)	15.4812(14)
c (Å)	16.4727(5)	16.0478(13)	15.5450(13)
V (Å^3)	3424.66(16)	3354.1(4)	3350.31(5)
ρ_{calcd} (Mg/m^3)	1.704	1.856	1.798
μ(Mo Kα) (mm^{-1})	1.325	3.570	1.604
θ range (deg)	3.02−32.60	2.87−26.45	2.36−26.48
reflns collected	55 567	15 601	21 374
independent reflns, n (R_{int})	11 701 (0.0616)	6553 (0.066)	6869 (0.152)
L. S. params/restraints	478/1	440/0	436/0
$R1(F)^a I > 2\sigma(I)$]	0.049	0.056	0.073
$wR2(F^2)^b$ all data	0.111	0.108	0.144
$S(F^2)^c$ all data	0.921	1.032	1.006

$^a R1(F) = \Sigma(||F_o| - |F_c||)/\Sigma|F_o|$. $^b wR2(F^2) = [\Sigma w(F_o^2 - F_c^2)^2/\Sigma wF_o^4]^{1/2}$. $^c \Sigma(F^2) = [\Sigma w(F_o^2 - F_c^2)^2/n - p]^{1/2}$.

complexes into oxalate-based networks. While the first ones were solely restricted to Co(II) and Fe(II) complexes,[14] a larger variety of compounds have been recently obtained with Fe(III) complexes of the hexadentate Schiff base ligand, sal$_2$-trien (H$_2$sal$_2$-trien = *N*,*N*′-disalicylidenetriethylene-tetramine) and derivatives that give rise to 2D and achiral 3D oxalate-based networks.[15,16] The only one showing coexistence of spin crossover and ferromagnetism is the 2D compound [Fe^{III}(sal$_2$-trien)][Mn^{II}Cr^{III}(ox)$_3$]·(CH$_2$Cl$_2$) that presents a gradual spin crossover from 350 to 160 K and a ferromagnetic ordering at 5.6 K.[16] Furthermore, it exhibits conversion from the LS to the HS state induced by light irradiation, commonly known as the LIESST effect (light-induced excited spin-state trapping).[17] This is a very rare and unexpected property in a Fe^{III} spin-crossover complex as it has only been found in two other Fe^{III} complexes. Unfortunately, the photoinduced spin conversion of the inserted Fe^{III} complex has a negligible influence on the cooperative magnetic behavior of the oxalate network. This is not unexpected as 2D compounds with different interlayer separation have a very similar Curie temperature (T_c). In this sense, compounds with a 3D network are expected to be better candidates because the T_c of 3D oxalate compounds is very sensitive to the size of the intercalated cation.

In an attempt to insert spin-crossover molecules into a 3D oxalate lattice, we extended this strategy to derivatives of [Fe^{III}(sal$_2$-trien)]$^+$ with Cl and Br substituents on position 5 of the salicylaldimine ring. This resulted in growth of a 3D chiral network in the compounds [Fe^{III}(5-Clsal$_2$-trien)][Mn^{II}Cr^{III}(ox)$_3$]·0.5(CH$_3$NO$_2$) (**1**), [Fe^{III}(5-Brsal$_2$-trien)][Mn^{II}Cr^{III}(ox)$_3$] (**2**), and the reference compound [In^{III}(5-Clsal$_2$-trien)][Mn^{II}Cr^{III}(ox)$_3$]·(CH$_3$NO$_2$) (**3**). The structure and magnetic properties of these compounds are reported in this paper.

EXPERIMENTAL SECTION

Complexes [Fe^{III}(5-Clsal$_2$-trien)]PF$_6$, [Fe^{III}(5-Brsal$_2$-trien)]PF$_6$, and [In^{III}(5-Clsal$_2$-trien)]PF$_6$ were prepared according to literature methods.[18] Ag$_3$[Cr(ox)$_3$] was prepared by metathesis from the corresponding potassium salt.[19] All other materials and solvents were commercially available and used without further purification.

[Fe^{III}(5-Clsal$_2$-trien)][Mn^{II}Cr^{III}(ox)$_3$]·0.5(CH$_3$NO$_2$) (1), [Fe^{III}(5-Brsal$_2$-trien)][Mn^{II}Cr^{III}(ox)$_3$] (2), and [In^{III}(5-Clsal$_2$-trien)][Mn^{II}Cr^{III}(ox)$_3$]·(CH$_3$NO$_2$) (3). Crystals of these compounds were obtained by slow difussion of two solutions. The first solution was prepared by adding MnCl$_2$·4H$_2$O (0.018 g, 0.09 mmol) to a suspension of Ag$_3$Cr(Ox)$_3$ (0.038 g, 0.06 mmol) in 3 mL of methanol. The AgCl precipitate was filtered. The second solution was obtained by dissolving [Fe^{III}(5-Clsal$_2$trien)]PF$_6$ (0.038 g, 0.06 mmol) in 3 mL of nitromethane (**1**), [Fe^{III}(5-Brsal$_2$trien)]PF$_6$ (0.043 g, 0.06 mmol) in 3 mL of acetonitrile (**2**), or [In^{III}(5-Clsal$_2$trien)]PF$_6$ (0.042 g, 0.06 mmol) in 3 mL of acetonitrile (**3**). After 2 weeks brown (**1** and **2**) or violet (**3**) crystals were obtained. The composition of these crystals, checked by microanalysis, shows the following M:Mn:Cr:X (M = Fe, In, X = Cl and Br) ratios. Found: 1:1.2:1.1:2 (Fe:Mn:Cr:Cl) for **1**; 1:1.2:1.1:1.9 (Fe:Mn:Cr:Br) for **2**, and 1:1.2:1.1:1.9 (In:Mn:Cr:Cl) for **3**. Calcd: 1:1:1:2 (M:Mn:Cr:X).

Structural Characterization. Single-crystal X-ray data of **1**−**3** were collected at 120 K on a Xcalibur, Sapphire3, Gemini diffractometer equipped with a graphite-monochromated Enhance (Mo) X-ray Source (λ = 0.71073 Å). The program CrysAlisPro, Oxford Diffraction Ltd., Version 1.171.33.52, was used for cell refinements and data reduction of the compounds. Empirical absorption correction was performed using spherical harmonics, implemented in SCALE3 ABSPACK scaling algorithm. Crystal structures were solved by direct methods with the SIR97 program[20] and refined against all F^2 values with the SHELXL-97 program[21] using the WinGX graphical user interface.[22] The three compounds exhibit a Flacks absolute parameter (x) close to 0.[23] This parameter lies within the range that indicates that the absolute structure is valid and that the three crystals are enantiopure. Non-hydrogen atoms were refined anisotropically, and hydrogen atoms were placed in calculated positions refined using idealized geometries (riding model) and assigned fixed isotropic displacement parameters. In **2**, the two terminal ethylene groups from [Fe^{III}(5-Brsal$_2$-trien)]$^+$ complexes were

dx.doi.org/10.1021/ic201293f |*Inorg. Chem.* 2011, 50, 9122–9130

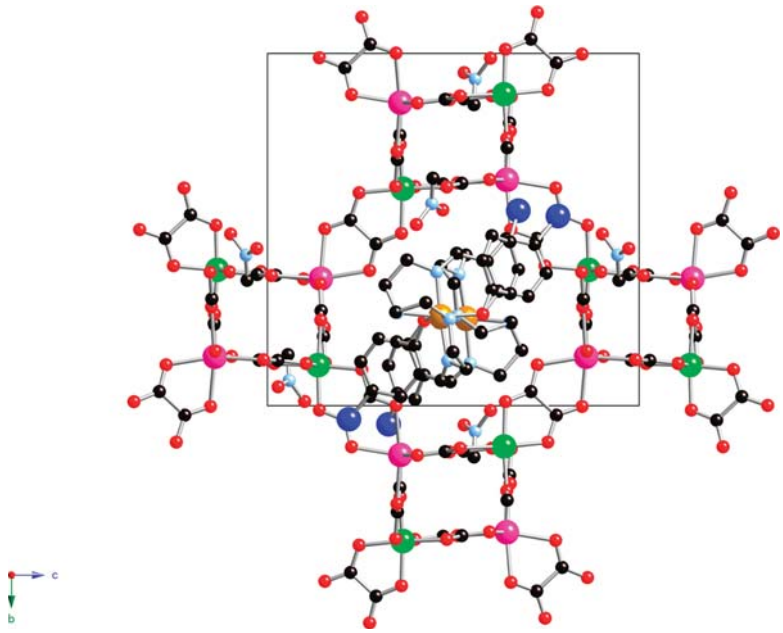

Figure 1. Projection of **1** in the *bc* plane: Fe, yellow; Cr, green; Mn, pink; C, black; N, blue; O, red; Cl, dark blue. Hydrogen atoms have been omitted for clarity.

modeled in two orientations. Data collection and refinement statistics are collected in Table 1.

Physical Measurements. Magnetic susceptibility measurements were performed on polycrystalline samples using a magnetometer (Quantum Design MPMS-XL-5) equipped with a SQUID sensor. Variable-temperature measurements were carried out in the temperature range 2−300 K. The ac measurements were performed in the temperature range 2−10 K at different frequencies with an oscillating magnetic field of 0.395 mT. The magnetization and hysteresis studies were performed between 5 and −5 T, cooling the samples at zero field. The M:Mn:Cr:X (M = Fe, In, X = Cl, Br) ratios were measured on a Philips ESEM X230 scanning electron microscope equipped with an EDAX DX-4 microsonde. Mössbauer spectra were collected in transmission mode using a conventional constant-acceleration spectrometer and a 25 mCi ^{57}Co source in a Rh matrix. The velocity scale was calibrated using α-Fe foil. The absorber was obtained by gently packing single crystals of **1** or **2** into a perspex holder. Low-temperature spectra were collected using a bath cryostat with the sample immersed in liquid He for measurements at 4.1 and 2.2 K or by using flowing He gas to cool the sample above 4.1 K (temperature stability of 0.2 K). The spectra were fitted to Lorentzian lines using a nonlinear least-squares method.[24] Isomer shifts (Tables 2 and 3) are given relative to metallic α-Fe at room temperature.

RESULTS AND DISCUSSION

Synthesis. The method used to prepare $[Fe^{III}(5\text{-}Clsal_2\text{-}trien)][Mn^{II}Cr^{III}(ox)_3]\cdot 0.5(CH_3NO_2)$ (**1**), $[Fe^{III}(5\text{-}Brsal_2\text{-}trien)][Mn^{II}Cr^{III}(ox)_3]$ (**2**), and $[In^{III}(5\text{-}Clsal_2\text{-}trien)][Mn^{II}Cr^{III}(ox)_3]$ (**3**) is similar to that used to prepare the compounds with $[Fe^{III}(sal_2\text{-}trien)]^+$ and the derivatives ($[Fe^{III}(5\text{-}Xsal_2\text{-}trien)]^+$ (X = NO_2 or CH_3O)).[15b,16] It is based on the use of $Ag_3[Cr(ox)_3]$ to avoid the presence of alkali ions in the structure. It consists of slow diffusion of a methanol solution containing the precursors of the oxalate network, Mn^{2+} and $[Cr(ox)_3]^{3-}$ ions, into a solution of $[M^{III}(5\text{-}Xsal_2\text{-}trien)]^+$ (M = Fe or In, X = Cl or Br) in different solvents. In contrast to the compounds with $[Fe^{III}(sal_2\text{-}trien)]^+$ in which the use of different solvents to dissolve the Fe^{III} complex affords compounds with different types of oxalate network (2D for dichloromethane and 3D for acetonitrile), only one type of oxalate network, a chiral 3D network, is obtained for $[Fe^{III}(5\text{-}Xsal_2\text{-}trien)]^+$ (X = Cl or Br) in different solvents. The solvent that leads to the best crystals for X-ray single-crystal diffraction is CH_3NO_2 for $[Fe^{III}(5\text{-}Clsal_2\text{-}trien)]^+$, CH_3CN for $[Fe^{III}(5\text{-}Brsal_2\text{-}trien)]^+$, and CH_3CN for $[In^{III}(5\text{-}Clsal_2\text{-}trien)]^+$ cations.[25] The composition of these crystals, checked by microanalysis, shows in all cases a M:Mn:Cr:X (M = Fe, In, X = Cl and Br) ratio of 1:1:1:2. The crystal structures of the three compounds have been solved by single-crystal X-ray diffraction. Attempts to obtain analogous compounds with other paramagnetic M^{2+} ions (M = Ni, Fe, Co, and Cu) in place of Mn^{2+} have been unsuccessful.

Structure. 1−**3** crystallize in the chiral space group $P2_12_12_1$. As a racemic mixture of $[Cr(ox)_3]^{3-}$ and $[M^{III}(5\text{-}Xsal_2\text{-}trien)]^+$ ions has been used in the synthesis, crystals of both chiralities are obtained as expected.

The structure of **1** is formed by an anionic 3D polymeric oxalate-bridged bimetallic network with $[Fe^{III}(5\text{-}Clsal_2\text{-}trien)]^+$ cations and nitromethane molecules occupying the cavities. This anionic polymeric structure has the well-known 3D 3-connected decagonal oxalate-based anionic network (10,3) which is formed by oxalate ligands connecting Mn^{II} and Cr^{III} ions in such a way that each Mn^{II} is surrounded by three Cr^{III} and vice versa with all metal ions presenting the same chirality (Δ in the crystal used to

dx.doi.org/10.1021/ic201293f |*Inorg. Chem.* 2011, 50, 9122–9130

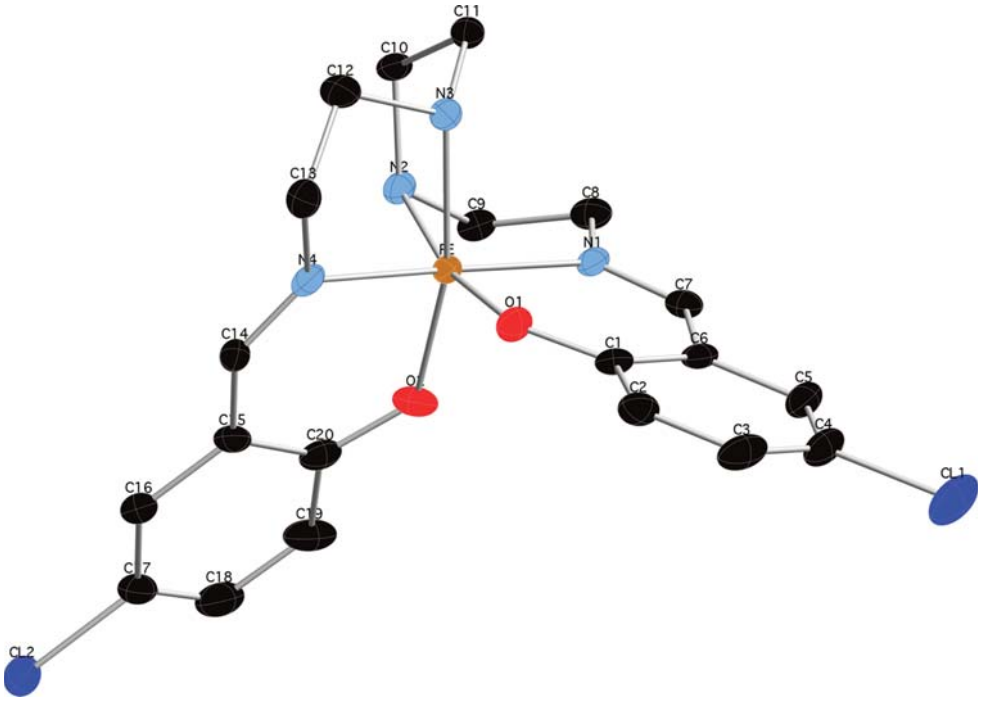

Figure 2. Structural view of $[Fe^{III}(5\text{-}Clsal_2\text{-}trien)]^+$ cation in compound **1**: Fe, yellow; C, black; N, blue; O, red; Cl, dark blue. Hydrogen atoms have been omitted for clarity.

solve the structure). The 3D oxalate chiral network of this compound has some differences with those obtained with $[Z^{II}(bpy)_3]^{2+}$ templating cations. Whereas cations with D_3 symmetry lead to cubic networks, the $[Fe^{III}(5\text{-}Clsal_2\text{-}trien)]^+$ cation gives rise to an orthorhombic network. The consequence of this lower symmetry is that it is possible to distinguish between Mn and Cr ions in the structure of **1** as they present different M−O bond lengths whereas they are disordered in the 3D compound obtained with $[Z^{II}(bpy)_3]^{2+}$. Thus, the two metals are crystallographically independent with mean Mn−O distances of 2.193(3) Å and Cr−O distances of 1.982(3) Å which are typical Mn^{II}−O and Cr^{III}−O distances. Metal−metal distances between adjacent centers are in the range 5.407(6)−5.462(6) Å. These metal−metal distances are longer than those exhibited by the 2D and 3D achiral structures obtained with $[Fe^{III}(sal_2\text{-}trien)]^+$ cations[15b,16] but shorter than those exhibited by other 3D oxalate-based chiral compounds. For instance, the Mn−Cr distance in $[Ir(ppy)_2(bpy)][MnCr(ox)_3]\cdot 0.5H_2O$ is 5.503 Å.[5f] Another consequence of the lower symmetry of the oxalate network is that the projections in the *ab*, *bc*, and *ac* planes are not completely equivalent. The bimetallic oxalate network of **1** defines channels that run along the *a*, *b*, and *c* axis. In contrast with the 3D cubic lattice, in the orthorhombic one the channels running along the *a* axis (Figure 1) present a square shape while those running along the *b* (Figure 1SS, Supporting Information) and *c* axes (Figure 2SS, Supporting Information) are clearly elongated.

The $[Fe^{III}(5\text{-}Clsal_2\text{-}trien)]^+$ complexes and nitromethane molecules are enclosed in the holes described by this 3D oxalate network. There is one crystallographically independent $[Fe(5\text{-}Clsal_2\text{-}trien)]^+$ complex (Figure 2) and disordered nitromethane molecules. In the crystal used to solve the structure, Fe^{III} adopts a Λ configuration, which is the opposite to that shown by Mn^{II} and Cr^{III} ions in the chiral oxalate network. It seems that in contrast to $[Z^{II}(bpy)_3]^{2+}$ cations, $[Fe(5\text{-}Clsal_2\text{-}trien)]^+$ cations induce crystallization of a 3D bimetallic oxalate-based network of opposite chirality. A similar behavior has been observed for another $[Fe(sal_2\text{-}trien)]^+$ derivative ($[Fe(5\text{-}NO_2sal_2\text{-}trien)]^+$), which induces crystallization of a chiral 2D oxalate-based network in which all Cr^{III} centers and $[Fe(5\text{-}NO_2sal_2\text{-}trien)]^+$ presenting short intermolecular contacts are in the opposite configuration.[15b] It is also interesting to observe that $[Fe(5\text{-}Clsal_2\text{-}trien)]^+$ cations form chains that run along the *a* axis within the channels defined by the oxalate network (Figure 1). The CH groups from the two phenoxy rings of one $[Fe(5\text{-}Clsal_2\text{-}trien)]^+$ cation present numerous edge-to-face interactions with CH_2 and NH groups from one of the two neighboring $[Fe(5\text{-}Clsal_2\text{-}trien)]^+$ cations belonging to the same chain. At the same time the CH_2 and NH groups of this $[Fe(5\text{-}Clsal_2\text{-}trien)]^+$ cation are connected through edge-to-face interactions with the two phenoxy rings of the second $[Fe(5\text{-}Clsal_2\text{-}trien)]^+$ neighbor. Furthermore, they present hydrogen bonds through the NH groups with oxalate ligands and numerous short contacts with oxygen atoms from the oxalate network. Finally, the $[Fe(5\text{-}Clsal_2\text{-}trien)]^+$ cations from one chain are connected to the $[Fe(5\text{-}Clsal_2\text{-}trien)]^+$ cations of four neighboring chains through short contacts between Cl atoms and CH_2 from ethylene groups.

dx.doi.org/10.1021/ic201293f |*Inorg. Chem.* 2011, 50, 9122–9130

The nitromethane solvent molecules occupy the holes between the oxalate network and the $[Fe(5\text{-}Clsal_2\text{-}trien)]^+$ cation. They have an ocuppancy of 0.5. CH_3 groups from nitromethane present short contacts with O atoms from the oxalate network, whereas NO_2 groups have short contacts with CH and CH_2 groups from two $[Fe(5\text{-}Clsal_2\text{-}trien)]^+$ complexes belonging to the same chain. The average Fe−N and Fe−O bond distances of $[Fe^{III}(5\text{-}Clsal_2\text{-}trien)]^+$ complexes are 2.009(3) and 1.894(3) Å. These values are intermediate between those obtained for other HS and LS $[Fe(sal_2\text{-}trien)]^+$ compounds. We have to take into account that Mössbauer spectroscopy (see below) indicates that around 70% of Fe is HS at 120 K (temperature at which the crystal structure has been determined).

The structures of **2** and **3** resemble that of **1** with $[Fe^{III}(5\text{-}Brsal_2\text{-}trien)]^+$ or $[In^{III}(5\text{-}Clsal_2\text{-}trien)]^+$ cations in the place of $[Fe^{III}(5\text{-}Clsal_2\text{-}trien)]^+$. The bimetallic oxalate 3D network is similar to that of **1**, but in contrast to **1**, solvent molecules are not found in these two structures. All metal ions from the oxalate network have the same chirality (Λ in the crystals used to solve the structures of **2** and **3**). The two metals are crystallographically independent with mean Mn−O distances of 2.192(5) Å for **2** and 2.186(8) Å for **3** and Cr−O distances of 1.973(5) Å for **2** and 1.973(7) Å for **3**. These distances are again the ones expected for Mn^{II}−O and Cr^{III}−O. Metal−metal distances between adjacent centers are in the range 5.393(5)−5.432(5) Å for **2** and 5.385-(7)−5.409(7) Å for **3**.

$[Fe^{III}(5\text{-}Brsal_2\text{-}trien)]^+$ in **2** and $[In^{III}(5\text{-}Clsal_2\text{-}trien)]^+$ in **3** are intercalated in the holes described by the 3D oxalate network. There is one crystallographically independent $[M^{III}(5\text{-}Xsal_2\text{-}trien)]^+$ complex. In the crystals used to solve the structures of **2** and **3**, as for **1**, Fe^{III} and In^{III} adopt the opposite configuration (Δ) to that of Mn^{II} and Cr^{III} ions from the oxalate network (Λ). In **2**, the intermolecular interactions between $[Fe^{III}(5\text{-}Brsal_2\text{-}trien)]^+$ cations are similar to those of **1**. Thus, $[Fe^{III}(5\text{-}Brsal_2\text{-}trien)]^+$ cations ocuppy the channels defined by the oxalate network, forming chains that run along the *a* axis which are connected to the $[Fe^{III}(5\text{-}Brsal_2\text{-}trien)]^+$ cations of four neighboring chains through short contacts between Br atoms and CH_2 from ethylene groups. In **3**, $[In^{III}(5\text{-}Clsal_2\text{-}trien)]^+$ also forms chains but in this case they are only connected through short contacts between Cl atoms and CH_2 from ethylene groups with the $[In^{III}(5\text{-}Clsal_2\text{-}trien)]^+$ of two neighboring chains.

The two ethylene groups closer to the phenoxy rings of $[Fe^{III}(5\text{-}Brsal_2\text{-}trien)]^+$ in **2** are disordered between two possible configurations. The average Fe−N and Fe−O bond distances of $[Fe^{III}(5\text{-}Brsal_2\text{-}trien)]^+$ complexes in **2** are 2.076(7) and 1.913(6) Å. These values are close to those obtained for other HS $[Fe(sal_2\text{-}trien)]^+$ compounds, in agreement with magnetic measurements and Mössbauer spectroscopy (see below), which indicate that around 60% of Fe is HS at 120 K (temperature at which the crystal structure has been determined). The average In−N and In−O bond distances of $[In^{III}(5\text{-}Clsal_2\text{-}trien)]^+$ complexes in **3** are 2.253(8) and 2.114(7) Å.

Magnetic Properties. To get the magnetism of the MnCr oxalate lattice we will talk first of the magnetic properties of **3** as this compound contains a diamagnetic inserted cation. The thermal dependence of the product of the molar magnetic susceptibility times the temperature (χT) of **3** presents a value of 7.0 emu·K·mol^{-1} at 300 K, which is close to the sum of the expected contributions for the isolated paramagnetic ions (see Figure 3). Upon cooling, χT increases gradually with a very abrupt increase below 50 K. This confirms the ferromagnetic

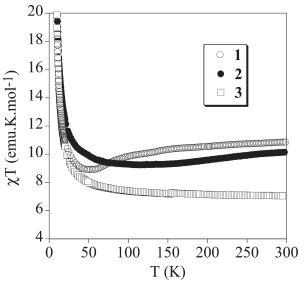

Figure 3. Temperature dependence of the product of the molar magnetic susceptibility with temperature (χT) at 0.1 T for compounds **1** (empty circles), **2** (full circles), and **3** (empty squares).

interaction between Mn^{II} and Cr^{III} ions of the oxalate network and the onset of long-range ferromagnetic ordering, as observed for other Mn^{II}−Cr^{III} oxalate networks.[4−6] The χ^{-1} versus T curve of **3** is linear in the 50−300 K temperature range. This permits one to fit it to a Curie−Weiss law ($\chi^{-1} = (T - \theta)/C$), leading to a Weiss constant, θ (K), of 5.5 K, which is analogous to that obtained for a chiral 3D $Mn^{II}Cr^{III}$ oxalate network in the $[Ir(ppy)_2(bpy)][M^{II}Cr^{III}(ox)_3]\cdot 0.5H_2O$ compound (6.1 K).[5f] To confirm the presence of long-range magnetic ordering and determine precisely the critical temperatures, ac susceptibility measurements were carried out. A maximum in the in-phase signal (χ') near T_c and an out-of-phase signal (χ'') that starts to appear at temperatures just below T_c is observed (Figure 4). From these data the T_c of **3** is 5.0 K. As expected for a ferromagnet, these signals are frequency independent (Figure 4). In the ordered phase an additional peak in χ' and χ'' at temperatures below 3 K is also detected. The presence of such a frequency-dependent peak has already been observed in other 3D bimetallic oxalate compounds.[5f] It can be related with formation of magnetic domains and domain−wall movement in the ordered phase.[26] The isothermal magnetization (M) at 2 K shows a very sharp increase at low fields, reaching a M value of 6.6 μ_B a 0.1 mT (Figure 5), confirming the ferromagnetic interactions between Mn^{II} and Cr^{III} ions. At fields above 0.1 T, only a slight linear increase of M versus H is observed as a consequence of spin canting in the ferromagnetic phase. A M value of 8.0 μ_B is obtained at 5 T, as expected for a $Mn^{II}Cr^{III}$ ferromagnet. A hysteresis loop of the magnetization with a coercive field of 1 mT is observed at 2 K. All these features indicate a ferromagnetic behavior of this 3D oxalate network which is analogous to that obtained in the cubic 3D oxalate-based compounds.[5]

To understand the magnetic properties of **1** and **2** we have to take into account the spin-crossover behavior of the inserted cation besides the ferromagnetic behavior of the MnCr oxalate lattice, mentioned above. χT of **1** and **2** shows higher values than that of **3** in all the range of temperatures due to the paramagnetic contribution of the inserted Fe^{III} cation (see Figure 3). In the case of **1**, it presents a value of 10.9 emu·K·mol^{-1} at 300 K close to the sum of the expected contributions for the isolated paramagnetic ions with the Fe^{III} spin-crossover complex in a HS state. Upon cooling, χT decreases gradually. This decrease is more abrupt below 100 K to reach a minimum of 8.9 emu·K·mol^{-1} around 60 K. This is consistent with a spin crossover of around 50% of Fe^{III} compounds from 300 to 60 K, in agreement with the

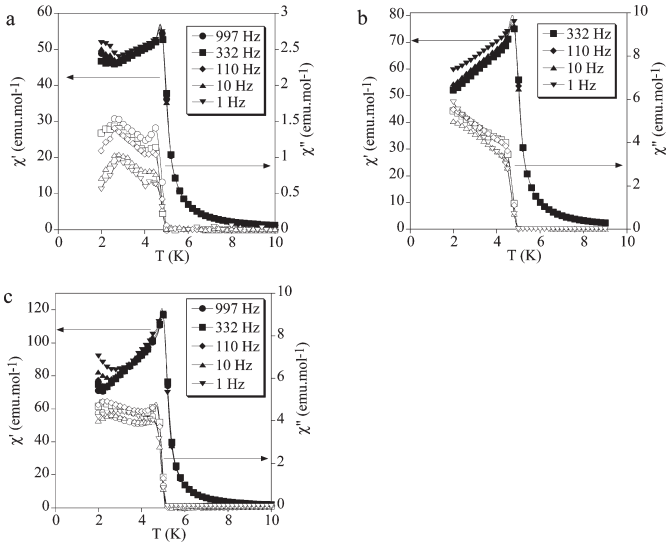

Figure 4. Temperature dependence of the in-phase ac susceptibility (χ') (filled symbols) and out-of-phase ac susceptibility (χ'') of **1** (a), **2** (b), and **3** (c).

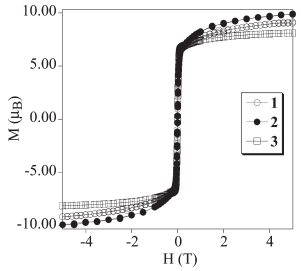

Figure 5. Field dependence of the magnetization (M) for **1** (empty circles), **2** (filled circles), and **3** (empty squares).

data obtained from Mössbauer spectroscopy (see below). χT of **2** is 10.0 emu·K·mol^{-1} at 300 K. This value is slightly lower than that obtained for **1**, in agreement with the 13% of Fe^{III} in the LS state at this temperature calculated from Mössbauer spectroscopy data. At lower temperatures, χT decreases very gradually to reach a minimum of 9.2 emu·K·mol^{-1} around 120 K, in agreement with Mössbauer data that suggest a progressive decrease of the HS fraction between 297 (87% HS) and 100 K (61% HS), which remains constant below this temperature. At temperatures below 80 K, χT of **2** is higher than that of **1** as a result of the smaller degree of HS → LS conversion of **2** (Figure 3). Below 50 K, **1** and **2** present a sharp increase of χT, as in the case of **3**, due to the onset of long-range ferromagnetic ordering.

Alternating current susceptibility measurements of **1** and **2** are very similar to those of **3**. They show frequency-independent peaks in χ' and χ'' and an additional peak in the ordered phase below 3 K (see Figure 4). From these data the T_c of **1** and **2** is 4.8 K. This indicates that the ferromagnetic behavior of the 3D oxalate network of **1** and **2** is analogous to that of **3** with a slight decrease of T_c that may be explained by the shorter Mn^{II}−Cr^{III} distances shown by **3** (5.407(6)−5.462(6) Å for **1**, 5.393(5)−5.432(5) Å for **2**, and 5.385(7) and 5.409(7) Å for **3**) or by slight differences in the bonding angles.

The isothermal magnetization of **1** and **2** at 2 K shows a very sharp increase at low fields, reaching a value of 6.1 μ_B in the two compounds at 0.1 mT, confirming the ferromagnetic interactions between Mn^{II} and Cr^{III} ions. At higher fields M has a continuous increase, which is more important than that of **3** due to the paramagnetic contribution of the inserted Fe^{III} cation. Furthermore, M of the two compounds does not saturate completely (see Figure 5). Due to this, the M value obtained at 5 T (9.1 μ_B) for **1** is still lower than the expected value for a parallel alignement of the spins of Mn^{II} and Cr^{III} with 56% of Fe^{III} in the HS state (11 μ_B) indicated by Mössbauer spectroscopy (see below). This difference may be explained by the spin canting of the bimetallic oxalate network and nonsaturation of the M coming from the paramagnetic Fe^{III} complex. In **2**, the presence of a higher fraction of HS Fe^{III} than that of **1** produces a more pronounced curvature in the M vs H curve that reaches higher M values (Figure 5). Thus, M increases from 6.1 to 9.9 μ_B when H increases from 0.1 to 5 T. Again, this value is lower than the expected one for ∼60% of Fe^{III} in the HS state (∼11.5 μ_B). A hysteresis loop of the magnetization with a coercive field of 3 mT is observed at 2 K for the two compounds.

1−**3** have a slightly lower T_c than that of the cubic 3D chiral compound $[Ir(ppy)_2(bpy)][Mn^{II}Cr^{III}(ox)_3]\cdot 0.5H_2O$ (T_c = 5.1 K)[5f] in spite of the shorter Mn^{II}−Cr^{III} distances that they present. This could be attributed to other factors such as the differences in the relative orientation of the magnetic orbitals. If we compare with other 2D and 3D compounds obtained with $[Fe^{III}(sal_2\text{-trien})]^+$ and derivatives, the T_c value of **1** and **2** (4.8 K) is lower than that exhibited for Mn^{II}−Cr^{III} 2D oxalate (5.6 K) and achiral

dx.doi.org/10.1021/ic201293f |*Inorg. Chem.* 2011, 50, 9122–9130

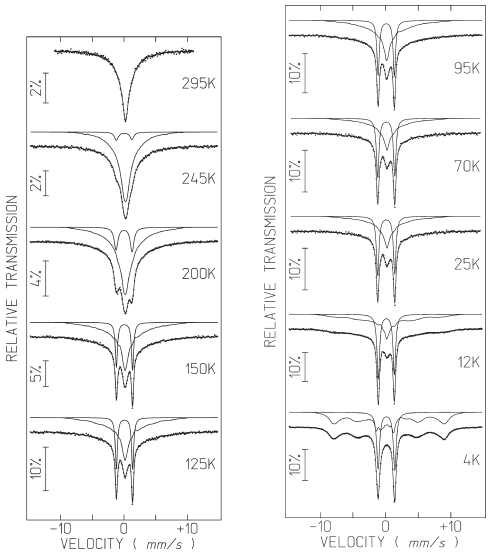

Figure 6. Mössbauer spectra of **1** taken at different temperatures. The lines over the experimental points are the sum of a doublet and a distribution of B_{hf} corresponding to LS and HS Fe^{III}. The estimated parameters for these doublets are collected in Table 2.

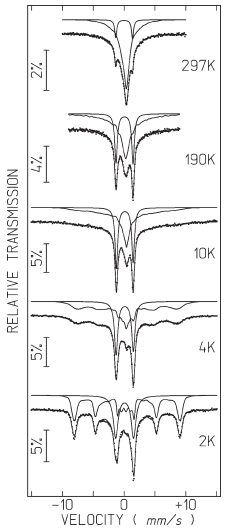

Figure 7. Mössbauer spectra of **2** taken at different temperatures. The lines over the experimental points are the sum of a doublet and a distribution of B_{hf} corresponding to LS and HS Fe^{III}. The estimated parameters for these doublets are collected in Table 3.

3D compounds (5.2 K) with inserted $[Fe^{III}(sal_2\text{-trien})]^+$.[16] This could be explained by the longer $Mn^{II}-Cr^{III}$ distances found in **1** and **2** with respect to these two compounds. Furthermore, we demonstrated that the decrease in T_c observed in the 3D series of

Table 2. Estimated Parameters from the Mössbauer Spectra of 1 Taken at Different Temperatures[a]

T		IS	QS	B_{hf}	I
295 K	LS Fe				
	HS Fe	0.34	0.0		100%
245 K	LS Fe	0.13	2.45		7%
	HS Fe	0.35	0.0		93%
200 K	LS Fe	0.16	2.51		17%
	HS Fe	0.35	0.1		83%
150 K	LS Fe	0.19	2.55		25%
	HS Fe	0.33	0.10		75%
125 K	LS Fe	0.19	2.56		29%
	HS Fe	0.32	0.10		71%
95 K	LS Fe	0.21	2.50		34%
	HS Fe	0.33	0.11		66%
70 K	LS Fe	0.21	2.61		44%
	HS Fe	0.35	0.10		56%
25 K	LS Fe	0.22	2.51		44%
	HS Fe	0.35	0.10		56%
12 K	LS Fe	0.22	2.47		43%
	HS Fe	0.35	0.09		57%
4 K	LS Fe	0.23	2.51		44%
	HS Fe	0.35	0.28	52.8	56%

[a] HS Fe and LS Fe: high-spin and low-spin Fe^{III}; IS (mm/s) isomer shift relative to metallic Fe at 295 K. QS (mm/s) quadrupole splitting of doublets; ε (mm/s), quadrupole shift for magnetic sextet; B_{hf} (T) magnetic hyperfine field. I relative area. Estimated standard deviations are <0.02 mm/s for IS, QS, and Γ, <0.5 T for B_{hf}, and <2% for I.

bimetallic oxalates with respect to the 2D ones can be explained by the noncollinear alignment of the chiral axis in the 3D compounds, as they produce differences in the relative orientation of the magnetic orbitals.[27] On the other hand, in a chiral 3D lattice the T_c values should also be lower than those of achiral 3D lattices with inserted $[Fe^{III}(sal_2\text{-trien})]^+$ as observed for **1** and **2**. That is so because an achiral 3D lattice contains both homochiral (similar to those found in chiral 3D structures) and heterochiral (similar to those found in 2D structures) pairs of neighboring magnetic ions.

Mössbauer Spectroscopy. Mössbauer spectra of **1** and **2** shown in Figures 6 and 7 are similar to those published for $[Fe^{III}(sal_2\text{-trien})][Mn^{II}Cr^{III}(ox)_3]\cdot CH_3OH$ between 2.2 and 295 K and are therefore analyzed with a similar model.[16]

For compound **1** only one contribution is observed at 295 K (Figure 6). It is an unresolved absorption centered at IS ≈ 0.34 (295 K) to 0.35 (4 K), which gradually broadens as the temperature decreases and is assigned to HS Fe^{III}. A quadrupole doublet with estimated parameters typical of LS Fe^{III} appears in the 245 K spectrum. The relative area of the quadrupole doublet and therefore the fraction of Fe^{III} in the LS state gradually increases with decreasing temperature down to 100 K. Below 100 K the increase of the LS fraction seems steeper until it reaches approximately 44% at 70 K and stabilizes down to 4.2 K. At this temperature four peak maxima belonging to a sextet appear on the absorption band with an estimated magnetic hyperfine field of 52.8 T typical of HS Fe^{III} ($S = 5/2$) (Table 2).

For compound **2** two contributions are clearly observed already at 295 K (Figure 7). One is a LS quadrupole doublet. The other one is an unresolved absorption centered at IS ≈ 0.31

dx.doi.org/10.1021/ic201293f |Inorg. Chem. 2011, 50, 9122–9130

Table 3. Estimated Parameters from the Mössbauer Spectra of 2 Taken at Different Temperatures[a]

T		IS	QS, ε	B_{hf}	I
295 K	LS Fe	0.11	2.72		13%
	HS Fe	0.31	−0.29		87%
230 K	LS Fe	0.12	2.74		17%
	HS Fe	0.35	−0.13		83%
190 K	LS Fe	0.17	2.76		34%
	HS Fe	0.37	−0.05		66%
100 K	LS Fe	0.18	2.65		39%
	HS Fe	0.39	−0.11		61%
10 K	LS Fe	0.21	2.71		39%
	HS Fe	0.43	−0.15		61%
4 K	LS Fe	0.21	2.79		37%
	HS Fe	0.50	0.21		63%
2 K	LS Fe	0.19	2.89		38%
	HS Fe	0.49	0.21	53.2	62%

[a] HS Fe and LS Fe: high-spin and low-spin Fe^{III}; IS (mm/s) isomer shift relative to metallic Fe at 295 K. QS (mm/s) quadrupole splitting of doublets; ε (mm/s), quadrupole shift for magnetic sextet; B_{hf} (T) magnetic hyperfine field. I relative area. Estimated standard deviations are <0.02 mm/s for IS, QS, and Γ, <0.5 T for B_{hf}, and <2% for I.

(295 K) to 0.50 (4 K) assigned to HS Fe^{III} which gradually broadens as the temperature decreases. At 4 K four peak maxima belonging to a sextet appear on the absorption band. This sextet becomes quite evident at 2.2 K with an estimated magnetic hyperfine field of 53.2 T typical of HS Fe^{III} (S = 5/2). The fraction of Fe^{III} in the LS state increases with decreasing temperature down to 100 K, slowly between 295 and 230 K, fast between 230 and 190 K and again very slowly between 190 and 100 K, where it reaches a value of approximately 38% (Table 3).

As discussed in detail in a previous paper, broadening of the HS Fe^{III} contribution may not be attributed to slow spin state interconversion since the LS Fe^{III} doublet peaks remain sharp with relatively thin line widths in the whole 300−2 K range.[16] Broadening of the HS Fe^{III} is rather due to slow relaxation of the HS Fe^{III} magnetic moments directions with a frequency (10^7−10^9 s^{-1}) whose reciprocal is on the same order of magnitude as the Mössbauer effect observation time. For both **1** and **2** the relaxation frequency decreases with decreasing temperature, as evidenced by the gradual broadening of the absorption until a sextet is observed at 4 K and below, in an identical way as observed for $[Fe^{III}(sal_2\text{-trien})][Mn^{II}Cr^{III}(ox)_3]\cdot(CH_3OH)$.[16] A similar effect has been observed very recently at 3 K in a Fe^{III} complex with a hexadentate Schiff base ligand.[28]

CONCLUSION

In this work we reported the preparation of three novel compounds (**1**−**3**) formed by insertion of the spin-crossover $[Fe^{III}(5\text{-Clsal}_2\text{-trien})]^+$ and $[Fe^{III}(5\text{-Brsal}_2\text{-trien})]^+$ cations and the reference compound with diamagnetic $[In^{III}(5\text{-Clsal}_2\text{-trien})]^+$ cation into anionic coordination polymers based on bimetallic oxalate complexes. We confirm with this result that the use of different sal_2-trien derivatives is a suitable strategy to obtain a great variety of oxalate networks. Thus, we have seen previously that depending on the substituent, different types of networks can be obtained. Thus, $[Fe^{III}(5\text{-NO}_2\text{sal}_2\text{-trien})]^+$ and $[Fe^{III}(5\text{-CH}_3\text{Osal}_2\text{-trien})]^+$ complexes lead, respectively, to formation of 2D and achiral 3D networks, in contrast with the flexibility of nonsubstituted $[Fe(sal_2\text{-trien})]^+$ cation favoring 2D and achiral 3D networks by changing the preparation conditions. In this work, we extended this work to $[Fe^{III}(5\text{-Xsal}_2\text{-trien})]^+$ (X = Cl, Br) complexes, and this has resulted in the growth of a different type of oxalate-based structure, a 3D chiral network. The different templating effect of these cations could be related to the intermolecular interactions. Thus, in $[Fe^{III}(5\text{-NO}_2\text{sal}_2\text{-trien})]^+$ complex the presence of NO_2 groups favors π−π stacking interactions, and this favors growth of a 2D network, while $[Fe^{III}(5\text{-CH}_3\text{Osal}_2\text{-trien})]^+$ complex, which makes more difficult these interactions due to steric hindrance of the methoxy groups, leads to formation of an achiral 3D network. In the three compounds reported in this paper the presence of smaller substituents (Cl or Br) favors a helical arrangement of the complexes and growth of a 3D chiral network. Furthermore, this result shows that formation of oxalate-based chiral 3D networks is not restricted to templating cations such as $[Z^{II}(bpy)_3]^{2+}$. We must take into account that, in contrast to 2D compounds, which admit a large variety of cations, in the 3D structures reported so far the templating cation might have the appropriate symmetry (D_3), size, and charge. This is the first time in which this type of chiral network is obtained with a cation of lower symmetry.

Besides the structural interest of these compounds, we have shown that the strategy reported in this paper gives rise to an unusual combination of three physical properties in the same compound, chirality, spin crossover, and ferromagnetism in the case of **1** and **2** and two properties, chirality and ferromagnetism, in the case of **3**. From the point of view of the onset of new properties, the combination of chirality and ferromagnetism could give rise to the observation of magneto-chiral dichroic effects. Notice that this effect has been observed in the weakly chiral 2D lattice.[13a] Still, in the strongly chiral 3D lattice this effect could not be studied as the charge transfer bands of the $[Z^{II}(bpy)_3]^{2+}$ counterions caused an intense absorption. For this purpose, compound **3** seems to be more promising since Fe^{III} cations of **1** and **2** have an intense absorption due to charge transfer bands and could dominate the optical properties as occurs in the 3D compounds containing $[Z(bpy)_3]^{2+}$ cations. In this context, **3** could be an ideal candidate to observe this effect due to the lack of absorption of the In^{III} complex.

On the other hand, a very promising possibility that remains to be explored is the tuning of the magnetic ordering of the $Mn^{II}Cr^{III}$ oxalate network by inducing the spin crossover of the cations applying light or pressure. Compounds **1** and **2** could be good candidates for this purpose as 3D oxalate networks are expected to be sensitive to the chemical pressure induced by the inserted cation. However, the possible switching effect induced by the presence of the spin-crossover cation could be limited by the gradual and not complete spin crossover (less than 50%) obtained for these compounds.

ASSOCIATED CONTENT

Supporting Information. Projections of the structure of **1** in the *ac* and *ab* planes and CIF files of the structures of **1**−**3**. This material is available free of charge via the Internet at http://pubs.acs.org.

AUTHOR INFORMATION

Corresponding Author

*Phone: (+34) 96 3544415. Fax: (+34) 96 354 3273. E-mail: miguel.clemente@uv.es (M.C.-L.); eugenio.Coronado@uv.es (E.C.).

ACKNOWLEDGMENT

Financial support from the EU (SPINMOL ERC Advanced Grant), the Spanish Ministerio de Ciencia e Innovación with FEDER cofinancing (Project Consolider-Ingenio in Molecular Nanoscience and projects MAT2007-61584 and CTQ-2008-06720), and the Generalitat Valenciana (Prometeo Program) are gratefully acknowledged.

REFERENCES

(1) (a) Coronado, E.; Day, P. *Chem. Rev.* **2004**, *104*, 5419. (b) Coronado, E.; Martí-Gastaldo, C.; Navarro-Moratalla, E.; Ribera, A.; Blundell, S. J.; Baker, P. J. *Nat. Chem.* **2010**, *2*, 1031.

(2) (a) Coronado, E.; Giménez-López, M. C.; Levchenko, G.; Romero, F. M.; García-Baonza, V.; Milner, A.; Paz-Pasternak, M. *J. Am. Chem. Soc.* **2005**, *127*, 4580. (b) Coronado, E.; Giménez-López, M. C.; Korzeniak, T.; Levchenko, G.; Romero, F. M.; Segura, A.; García-Baonza, V.; Cezar, J. C.; De Groot, F. M. F.; Milner, A.; Paz-Pasternak, M. *J. Am. Chem. Soc.* **2008**, *130*, 15519.(c) Ohkoshi, S. I.; Imoto, K.; Tsunobuchi, Y.; Takano, S.; Tokoro, H. *Nat. Chem.* **2011**, DOI: 10.1038/NCHEM.1067

(3) Clemente-León, M.; Coronado, E.; Martí-Gastaldo, C.; Romero, F. M. *Chem. Soc. Rev.* **2011**, *40*, 473.

(4) (a) Tamaki, H.; Zhong, Z. J.; Matsumoto, N.; Kida, S.; Koikawa, M.; Achiwa, N.; Hashimoto, Y.; Okawa, H. *J. Am. Chem. Soc.* **1992**, *114*, 6974. (b) Tamaki, H.; Mitsumi, M.; Nakamura, N.; Matsumoto, N.; Kida, S.; Okawa, H.; Ijima, S. *Chem. Lett.* **1992**, 1975. (c) Mathonière, C.; Carling, S. G.; Yuscheng, D.; Day, P. *J. Chem. Soc., Chem. Commun.* **1994**, 1551. (d) Mathonière, C.; Nutall, J.; Carling, S. G.; Day, P. *Inorg. Chem.* **1996**, *35*, 1201. (e) Pellaux, R.; Schmalle, H. W.; Huber, R.; Fisher, P.; Hauss, T.; Ouladdiaf, B.; Decurtins, S. *Inorg. Chem.* **1997**, *36*, 2301. (f) Coronado, E.; Galán-Mascarós, J. R.; Gómez-García, C. J.; Martínez-Agudo, J. M.; Martínez-Ferrero, E.; Waerenborgh, J. C.; Almeida, M. *J. Solid State Chem.* **2001**, *159*, 391. (g) Min, K. S; Rhinegold, A. L.; Miller, J. S. *Inorg. Chem.* **2005**, *44*, 8433. (h) Coronado, E.; Galán-Mascarós, J. R.; Martí-Gastaldo, C. *J. Mater. Chem.* **2006**, *16*, 2685.

(5) (a) Decurtins, S.; Schmalle, H. W.; Schneuwly, P.; Oswald, H. R. *Inorg. Chem.* **1993**, *32*, 1888. (b) Decurtins, S.; Schmalle, H. W.; Schneuwly, P.; Ensling, J.; Gütlich, P. *J. Am. Chem. Soc.* **1994**, *116*, 9521. (c) Hernández-Molina, M.; Lloret, F.; Ruiz-Pérez, C.; Julve, M. *Inorg. Chem.* **1998**, *37*, 4131. (d) Coronado, E.; Galán-Mascarós, J. R.; Gómez-García, C. J.; Martínez-Agudo, J. M. *Inorg. Chem.* **2001**, *40*, 113. (e) Pointillart, F.; Train, C.; Gruselle, M.; Villain, F.; Schmalle, H. W.; Talbot, D.; Gredin, P.; Decurtins, S.; Verdaguer, M. *Chem. Mater.* **2004**, *16*, 832. (f) Clemente-León, M.; Coronado, E.; Gómez-García, C. J.; Soriano-Portillo, A. *Inorg. Chem.* **2006**, *45*, 5653.

(6) (a) Clemente-León, M.; Galán-Mascarós, J. R.; Gómez-García, C. J. *Chem. Commun.* **1997**, 1727. (b) Coronado, E.; Galán-Mascarós, J. R.; Gómez-García, C. J.; Martínez-Agudo, J. M. *Adv. Mater.* **1999**, *11*, 558. (c) Coronado, E.; Galán-Mascarós, J. R.; Gómez-García, C. J.; Ensling, J.; Gutlich *Chem.—Eur. J.* **2000**, *6*, 552.

(7) (a) Bénard, S.; Yu, P.; Audière, J. P.; Rivière, E.; Clèment, R.; Ghilhem, J.; Tchertanov, L.; Nakatami, K. *J. Am. Chem. Soc.* **2000**, *122*, 9444. (b) Aldoshin, S. M.; Sanina, N. A.; Minkin, V. I.; Voloshin, N. A.; Ikorskii, V. N.; Ovcharenko, V. I.; Smirnov, V. A.; Nagaeva, N. K. *J. Mol. Struct.* **2007**, *826*, 69.

(8) (a) Coronado, E.; Galán-Mascarós, J. R.; Gómez-García, C. J.; Laukhin, V. *Nature* **2000**, *408*, 447. (b) Alberola, A.; Coronado, E.; Galán-Mascarós, J. R.; Giménez-Saiz, C.; Gómez-García, C. J. *J. Am. Chem. Soc.* **2003**, *125*, 10774. (c) Coronado, E.; Galán-Mascarós, J. R.; Gómez-García, C. J.; Martínez-Ferrero, E.; Van Smaalen, S. *Inorg. Chem.* **2004**, *43*, 4808.

(9) Okawa, H.; Shigematsu, A.; Sadakiyo, M.; Miyagawa, T.; Yoneda, K.; Ohba, M.; Kitagawa, H. *J. Am. Chem. Soc.* **2009**, *131*, 13516.

(10) (a) Andrés, R.; Gruselle, M.; Malézieux, B.; Verdaguer, M.; Vaissermann, J. *Inorg. Chem.* **1999**, *38*, 4637. (b) Andrés, R.; Brissard, M.; Gruselle, M.; Train, C.; Vaissermann, J.; Malézieux, B.; Jamet, J. P.; Verdaguer, M. *Inorg. Chem.* **2001**, *40*, 4633. (c) Clemente-León, M.; Coronado, E.; Dias, J. C.; Soriano-Portillo, A.; Willett, R. D. *Inorg. Chem.* **2008**, *47*, 6458.

(11) Galán-Mascarós, J. R.; Coronado, E.; Goddard, P. A.; Singleton, J.; Coldea, A. I.; Wallis, J. D.; Coles, S. J.; Alberola, A. *J. Am. Chem. Soc.* **2010**, *132*, 9271.

(12) Endo, T.; Akutagawa, T.; Noro, S. I.; Nakamura, T. *Dalton Trans.* **2011**, *40*, 1491.

(13) (a) Train, C.; Gheorghe, R.; Krstic, V.; Chamoreau, L. M.; Ovanesyan, N. S.; Rikken, G. L. J. A.; Gruselle, M.; Verdaguer, M. *Nat. Mater.* **2008**, *17*, 729. (b) Train, C.; Nuida, T.; Gheorghe, R.; Gruselle, M.; Ohkoshi, S. *J. Am. Chem. Soc.* **2009**, *131*, 16838.

(14) (a) Sieber, R.; Decurtins, S.; Stoeckli-Evans, H.; Wilson, C.; Yufit, D.; Howard, J. A. K.; Capelli, S. C.; Hauser, A. *Chem.—Eur. J.* **2000**, *6*, 361. (b) Coronado, E.; Galán-Mascarós, J. R.; Giménez-López, M. C.; Almeida, M.; Waerenborgh, J. C. *Polyhedron* **2007**, *26*, 1838.

(15) (a) Clemente-León, M.; Coronado, E.; Giménez-López, M. C.; Soriano-Portillo, A.; Waerenborgh, J. C.; Delgado, F. S.; Ruiz-Pérez, C. *Inorg. Chem.* **2008**, *47*, 9111. (b) Clemente-León, M.; Coronado, E.; López-Jordà, M. *Dalton Trans.* **2010**, *39*, 4903.

(16) Clemente-León, M.; Coronado, E.; López-Jordà, M.; Mínguez Espallargas, G.; Soriano-Portillo, A.; Waerenborgh, J. C. *Chem.—Eur. J.* **2010**, *16*, 2207.

(17) Clemente-León, M.; Coronado, E.; López-Jordà, M.; Desplanches, C.; Asthana, S.; Wang, H.; Létard, J.-F. *Chem. Sci.* **2011**, *2*, 1127.

(18) Tweedle, M. F.; Wilson, L. J. *J. Am. Chem. Soc.* **1976**, *98*, 4824.

(19) Baylar, J. C.; Jones, E. M. In *Inorganic Synthesis*; Booth, H. S., Ed.; McGraw-Hill: New York, 1939; Vol. 1, p 35.

(20) Altomare, A.; Burla, M. C.; Camalli, M.; Cascarano, G. L.; Giacovazzo, C.; Guagliardi, A.; Moliterni, A. G. G.; Polidori, G.; Spagna, R. *J. Appl. Crystallogr.* **1999**, *32*, 115.

(21) Sheldrick, G. M. *SHELXL-97*; University of Göttingen: Göttingen, Germany, 1997.

(22) Farrugia, L. J. *J. Appl. Crystallogr.* **1997**, *32*, 837.

(23) Flack, H. D.; Bernardinelli, G. *J. Appl. Crystallogr.* **2000**, *33*, 1143.

(24) Rodrigues, J. V.; Santos, I. C.; Gama, V.; Henriques, R. T.; Waerenborgh, J. C.; Duarte, M. T.; Almeida, M. *J. Chem. Soc., Dalton Trans.* **1994**, 2655.

(25) The use of CH_3NO_2 for $[Fe^{III}(5\text{-Brsal}_2\text{-trien})]^+$ and CH_3CN for $[Fe^{III}(5\text{-Clsal}_2\text{-trien})]^+$ gives rise to crystals with a similar unit cell but lower quality in the case of $[Fe^{III}(5\text{-Brsal}_2\text{-trien})]^+$ and with a high content of impurities in the case of $[Fe^{III}(5\text{-Clsal}_2\text{-trien})]^+$.

(26) Chernova, N. A; Song, Y.; Zavalij, P. Y.; Wittingham, M. S. *Phys. Rev. B* **2004**, *70*, 144405.

(27) Fishman, R. S.; Clemente-León, M.; Coronado, E. *Inorg. Chem.* **2009**, *48*, 3039.

(28) Griffin, M.; Shakespeare, S.; Shepherd, H. J.; Harding, C. J.; Létard, J. F.; Desplanches, C.; Goeta, A. E.; Howard, J. A. K.; Powell, A. K.; Mereacre, V.; Garcia, Y.; Naik, A. D.; Müller-Bunz, H.; Morgan, G. G. *Angew. Chem., Int. Ed.* **2011**, *50*, 896.

EurJIC European Journal of Inorganic Chemistry
ChemPubSoc Europe
FULL PAPER

DOI:10.1002/ejic.201201113

2D Bimetallic Oxalate-Based Ferromagnets with Inserted $[Fe(4\text{-}Br\text{-}sal_2\text{-}trien)]^+$ and $[Fe(3\text{-}R\text{-}sal_2\text{-}trien)]^+$ (R = Br, Cl and CH_3O) Fe^{III} Spin-Crossover Complexes

CLUSTER ISSUE

Miguel Clemente-León,*[a] Eugenio Coronado,*[a] and Maurici López-Jordà[a]

Keywords: Spin crossover / Magnetic properties / Oxalate complexes / Coordination chemistry / Schiff bases

The syntheses, structures and magnetic properties of the compounds of formula $[Fe^{III}(4\text{-}Br\text{-}sal_2\text{-}trien)][Mn^{II}Cr^{III}(ox)_3]_{0.67}Cl_{0.33}\cdot CH_3OH\_solvate$ (**1**), $[Fe^{III}(3\text{-}Br\text{-}sal_2\text{-}trien)][Mn^{II}Cr^{III}(ox)_3]\cdot(CH_3CN)_2$ (**2**), $[Fe^{III}(3\text{-}Cl\text{-}sal_2\text{-}trien)][Mn^{II}Cr^{III}(ox)_3]\cdot(CH_3OH)_2\cdot(CH_3CN)_2$ (**3**) and $[Fe^{III}(3\text{-}CH_3O\text{-}sal_2\text{-}trien)][Mn^{II}Cr^{III}(ox)_3]\cdot(CH_3OH)\cdot(H_2O)_{1.5}\cdot(CH_2Cl_2)_{0.5}$ (**4**) are reported. The four structures present a 2D honeycomb anionic layer formed by Mn^{II} and Cr^{III} ions linked through oxalate ligands and a cationic layer of the Fe^{III} complexes intercalated between the 2D oxalate network. The main differences compared with previous 2D oxalate-based structures are the presence of double layers of cations in compounds **1**, **3** and **4** and porous channels in the structures of **1** and **4** filled with disordered solvent molecules. The magnetic properties indicate that the inserted Fe^{III} cations undergo an almost complete spin crossover above 300 K in **1** and a partial spin crossover in **3** and **4** that coexists with a ferromagnetic ordering of the oxalate network. In the case of **2**, the inserted cation remains in the HS from 2 to 300 K. Therefore, **1**, **3** and **4** are multifunctional compounds with coexistence of spin crossover and magnetic ordering. Conversely, photomagnetic characterization shows that **1** and **3** do not present a LIESST effect in contrast to the 2D compound $[Fe^{III}(sal_2\text{-}trien)][Mn^{II}Cr^{III}(ox)_3]\cdot(CH_2Cl_2)$. These results could help to clarify this rare property for a Fe^{III} complex.

Introduction

Multifunctional materials that combine two (or more) physical properties of interest are one of the most promising topics in molecular magnetism because a wise choice of the constituent molecules allows the appearance in the same compound of an unusual combination of physical properties,[1] or even a mutual interplay – synergy – of the properties involved.[2] A suitable approach to obtain these materials is the hybrid approach, in which two-network solids are constructed from two different molecular fragments (organic, inorganic or organometallic), with each network furnishing distinct properties to the solid.

Bimetallic oxalate-bridged complexes of formula $A[M^{II}M^{III}(ox)_3]$ (M^{III} = Cr, Fe, Ru, V, Mn; M^{II} = Mn, Fe, Co, Ni, Cu, Zn; A = cation; ox = oxalate) have provided many examples of multifunctional magnets.[3] These bimetallic salts are most often composed of polymeric 2D or 3D anionic networks,[4–5] which furnish the cooperative magnetic properties (ferro-, ferri- or canted antiferromagnetism), and a bulky charge-compensating molecular cation, which templates the network formation. The insertion of different cations into oxalate networks has led to compounds combining in the same compound the long-range magnetic ordering from the oxalate network with paramagnetism,[6] photochromism,[7] electric conductivity,[8] proton conduction,[9] ferroelectricity,[10] chirality,[11] or chirality combined with conductivity[12] or proton conduction.[13] Finally, the chirality of the oxalate network combined with the magnetic ordering has led to new properties such as magneto-chiral dichroism[14] and magnetization-induced second-harmonic generation.[15]

Spin-crossover cations are particularly suitable for the preparation of oxalate-based multifunctional magnetic materials since they represent one of the best examples of molecular bistability. These kinds of molecular complexes change their spin state from low-spin (LS) to high-spin (HS) configurations under an external stimulus such as temperature, light irradiation or pressure. As this is accompanied by changes in the molecular size, the spin-crossover process should act as an internal pressure in the hybrid material and therefore, it might affect the long-range magnetic ordering in the extended magnetic network. This may lead to a way to design switching magnets in which the magnetic ordering of the oxalate network could be tuned by inducing the spin-crossover phenomenon. So far, several examples have described the incorporation of Co^{II} and Fe^{II} spin-crossover complexes into oxalate-based networks.[16] A

[a] Instituto de Ciencia Molecular, Universidad de Valencia, Catedrático José Beltrán 2, 46980 Paterna, Spain
Fax: +34-963543273
E-mail: miguel.clemente@uv.es
eugenio.coronado@uv.es

Supporting information for this article is available on the WWW under http://dx.doi.org/10.1002/ejic.201201113.

larger variety of compounds has been obtained with Fe^{III} complexes of the hexadentate Schiff base ligand, sal_2-trien (H_2sal_2-trien = *N*,*N*′-disalicylidenetriethylene-tetramine) and 5-X-sal_2-trien derivatives (X = Cl, Br, NO_2 CF_3O, and CH_3O) that give rise to 2D and 3D oxalate-based networks (see Scheme 1).[3,17] The most interesting results were obtained for the 2D compound, $[Fe^{III}(sal_2\text{-trien})][Mn^{II}Cr^{III}(ox)_3]\cdot(CH_2Cl_2)$. The magnetic properties of this compound indicate the coexistence of a complete spin-crossover transition from 300 to 160 K, and a ferromagnetic ordering below 5.6 K.[17b] Furthermore, it exhibits the conversion from the LS to HS state induced by light irradiation, commonly known as the LIESST effect (light-induced excited spin-state trapping).[18] This is a very rare and unexpected property in a Fe^{III} spin-crossover complex as it has only been found in two other Fe^{III} complexes.[19] As expected, the photo-induced spin conversion of the inserted Fe^{III} complex has a negligible influence on the cooperative magnetic behaviour of the oxalate network. This is consistent with the 2D structure of the compound as for different interlayer separations, very similar critical temperatures have been observed.

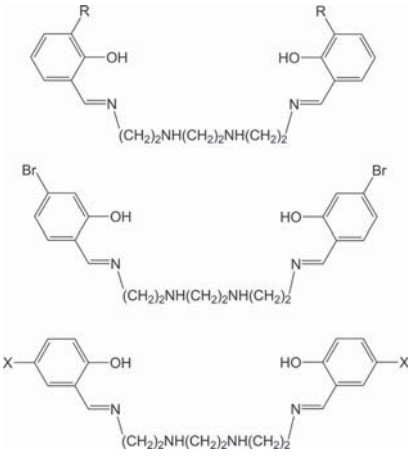

Scheme 1. H_2(3-R-sal_2-trien) (R = Br, Cl, CH_3O) (top), H_2(4-Br-sal_2-trien) (middle) and H_2(5-X-sal_2-trien) (X = Br, Cl, CH_3O, CF_3O and NO_2) (bottom).

In this work, $[Fe^{III}(4\text{-Br-}sal_2\text{-trien})]^+$ and $[Fe^{III}(3\text{-X-}sal_2\text{-trien})]^+$ (X = Br, Cl, CH_3O) complexes have been inserted into 2D oxalate-based networks in the search for new compounds with coexistence of spin crossover and magnetic ordering that could present the LIESST effect. The structure and magnetic properties of the compounds of formula $[Fe^{III}(4\text{-Br-}sal_2\text{-trien})][Mn^{II}Cr^{III}(ox)_3]_{0.67}Cl_{0.33}\cdot CH_3OH$_solvate (**1**), $[Fe^{III}(3\text{-Br-}sal_2\text{-trien})][Mn^{II}Cr^{III}(ox)_3]\cdot(CH_3CN)_2$ (**2**), $[Fe^{III}(3\text{-Cl-}sal_2\text{-trien})][Mn^{II}Cr^{III}(ox)_3]\cdot(CH_3OH)_2\cdot(CH_3CN)_2$ (**3**) and $[Fe^{III}(3\text{-}CH_3O\text{-}sal_2\text{-trien})][Mn^{II}Cr^{III}(ox)_3]\cdot(CH_3OH)\cdot(H_2O)_{1.5}\cdot(CH_2Cl_2)_{0.5}$ (**4**) are reported in this paper. Photomagnetic characterization of two of these compounds exhibiting spin crossover (**1** and **3**) has been performed.

Results and Discussion

Synthesis

The method to prepare **1**, **2**, **3** and **4** is similar to that used for the compounds with $[Fe^{III}(5\text{-X}sal_2\text{-trien})]^+$ (X = H, Cl, Br, NO_2 CF_3O, and CH_3O).[17] It is based on the use of $Ag_3[Cr(ox)_3]$ to avoid the presence of alkali ions in the structure. It consists of the slow diffusion of a methanol solution containing the precursors of the oxalate network, Mn^{2+} and $[Cr(ox)_3]^{3-}$ ions, into solutions of $[Fe^{III}(4\text{Br-}sal_2\text{-trien})]^+$ or $[Fe^{III}(3\text{X-}sal_2\text{-trien})]^+$ (X = Br, Cl, CH_3O) in different solvents. The best crystals for X-ray single-crystal diffraction are obtained in CH_3CN for **1**, **2** and **3**, and CH_2Cl_2 for **4**. As observed for $[Fe^{III}(5\text{-X}sal_2\text{-trien})]^+$ (X = Cl, Br, NO_2 CF_3O, and CH_3O) derivatives, only one type of oxalate network – a 2D network – is obtained with different solvents. This is in contrast to what happens when $[Fe^{III}(sal_2\text{-trien})]^+$ is used as the cation. In that case, different solvents afford compounds with different types of oxalate network (2D for CH_2Cl_2 and 3D for CH_3CN). This may be related to the higher flexibility of $[Fe^{III}(sal_2\text{-trien})]^+$ complexes with respect to the substituted derivatives. The composition of crystals of these compounds, checked by microanalysis, shows a Fe/Mn/Cr/Cl ratio of 1:1:1:1 for **4**, a Fe/Mn/Cr/X (X = Cl or Br) ratio of 1:1:1:2 for **2** and **3** and a Fe/Mn/Cr/Br/Cl ratio of 1:0.67:0.67:2:0.33 for **1**. In this last compound, Cl^- anions were found in the structure. Because of this, the stoichiometry of this compound (Fe/Mn/Cr/Cl ratio of 1:0.67:0.67:0.33) is different to the usual one (Fe/Mn/Cr ratio of 1:1:1) for this type of compound. The presence of Cl^- in the solution is explained by the incomplete reaction between 1 equiv. of $Ag_3[Cr(ox)_3]$ and 1.5 equiv. of $MnCl_2$ due probably to the low solubility of $Ag_3[Cr(ox)_3]$. This leads to an excess of Cl^- that remains in the methanol solution containing the precursors of the oxalate network, Mn^{2+} and $[Cr(ox)_3]^{3-}$, which is obtained after filtration of the AgCl precipitate. The crystal structures of the four compounds have been solved by single-crystal X-ray diffraction.

Structure

The structure of the four compounds consists of anionic layers with a 2D bimetallic oxalate network of formula $[MnCr(ox)_3]^-$ with inserted Fe^{III} cationic complexes and solvent molecules, and Cl^- anions in the case of **1**. The bimetallic oxalate layer presents in the four compounds the well-known honeycomb structure formed by an extended network with Mn^{II} and Cr^{III} ions linked through oxalate bridges with octahedral coordination. These oxalate ligands connect the Mn^{II} and Cr^{III} ions in such a way that each Mn^{II} is surrounded by three neighbouring Cr^{III} and vice versa.

$[Fe^{III}(4\text{-Br-}sal_2\text{-trien})][Mn^{II}Cr^{III}(ox)_3]_{0.67}Cl_{0.33}\cdot CH_3OH$_solvate (1)

The structure of this compound was solved in the $P\bar{3}$ space group. The anionic bimetallic oxalate layer lies in the

ab plane (Figure 1). It contains two crystallographically independent metals (Mn1/Cr1 and Mn2/Cr2) with M–O bond lengths lying between 2.058(3) and 2.086(3) Å. These bond lengths are intermediate between the ones expected for Cr^{III}–O and Mn^{II}–O. Therefore, it is not possible to distinguish between the two metals in this structure. The neighbouring metal centres of the bimetallic oxalate network present alternating chirality as usual for this type of network. These anionic layers are stacked one over the other in an *AA*···fashion. The minimum distance between metal ions belonging to different oxalate layers is 18.5675(7) Å (equal to the *c* parameter). This distance is much longer than those found in other oxalate-based 2D compounds with decamethylferrocenium or alkylammonium cations (9.2–9.7 Å)[4,6] or with $[Fe^{III}(sal_2\text{-trien})]^+$ and derivatives (11.609–11.644 Å).[17b–17c] This is due to the presence of a double layer of $[Fe^{III}(4\text{-Br-sal}_2\text{-trien})]^+$ complexes and Cl^- anions instead of the single layer found in other 2D structures. A similar interlayer distance was found in the compound $[Fe^{III}(sal_2\text{-trien})]_2[Mn^{II}_2(ox)_3]\cdot 4H_2O\cdot C_3H_7NO$ containing a double layer of $[Fe^{III}(sal_2\text{-trien})]^+$ between $[Mn^{II}_2(ox)_3]^{2-}$ layers.[17a]

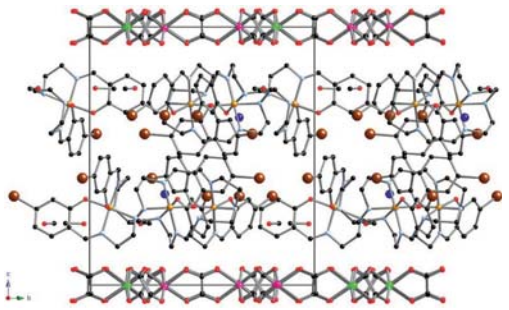

Figure 1. Projection of the structure of **1** in the *bc* plane. Fe (yellow), Br (brown), Cl (blue), C (black), N (blue), O (red) Mn (pink), and Cr (green). Hydrogen atoms have been omitted for clarity.

The space between the oxalate layers is occupied by one crystallographically independent $[Fe^{III}(4\text{-Br-sal}_2\text{-trien})]^+$ complex, one chloride and one methanol molecule that form a double layer. Fe^{III} present the usual distorted octahedral symmetry of this type of complex with average Fe–N and Fe–O bond lengths of 1.967(3) and 1.888(4) Å, respectively. These values are in the range of those obtained for other LS Schiff-base complexes, in full agreement with the magnetic measurements (see below), which indicate that all Fe are LS at 120 K (temperature at which the crystal structure has been determined). The complexes lie with their longer axis almost parallel to the oxalate network. Thus, the phenoxy rings of these complexes are almost perpendicular to the bimetallic oxalate network (the dihedral angle between the least-squares planes of the phenoxy rings and that formed by the metals of the oxalate network are 71.5 and 81.0°). In each one of these layers, Cl^- is placed in a special position surrounded by three $[Fe^{III}(4\text{-Br-sal}_2\text{-trien})]^+$ complexes in the same layer related by a ternary axis. These three complexes form a hydrogen bond with a Cl^- anion through a NH group. Furthermore, there is a space between six $[Fe^{III}(4\text{-Br-sal}_2\text{-trien})]^+$ complexes belonging to the same layer that is occupied by disordered solvent molecules. These hexagonal pores appear also in the other layer and are just behind and above the hexagonal channels described by the honeycomb bimetallic oxalate network. As a result, hexagonal channels occupied by disordered solvent molecules that run along the *c*-axis are formed in this structure (see Figure 2). It is interesting to point out that not all the hexagonal channels are occupied by disordered solvent molecules. Thus, the *ab* projection of the structure shows that one "empty" hexagonal channel is surrounded by six channels filled with $[Fe^{III}(4\text{-Br-sal}_2\text{-trien})]^+$ complexes. Cl^- anions are just behind and above along the *c*-axis of Mn2/Cr2 ions. $[Fe^{III}(4\text{-Br-sal}_2\text{-trien})]^+$ complexes belonging to the different layers are linked through π–π stacking interactions and edge-to-face C–H··π interactions. Finally, there are numerous short contacts between the complexes and the oxalate network and methanol solvent molecules that form hydrogen bonds with a NH group of a neighbouring $[Fe^{III}(4\text{-Br-sal}_2\text{-trien})]^+$ complex.

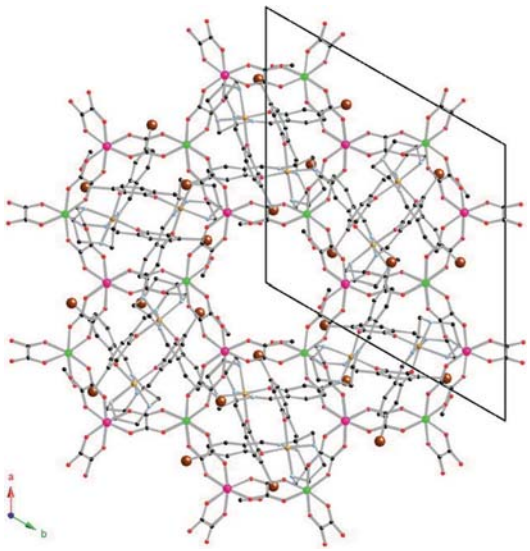

Figure 2. Projection of the structure of **1** in the *ab* plane. Fe (yellow), Br (brown), C (black), Cl (blue), N (blue), O (red), Mn (pink), and Cr (green). Hydrogen atoms have been omitted for clarity.

$[Fe^{III}(3\text{-Br-sal}_2\text{-trien})][Mn^{II}Cr^{III}(ox)_3]\cdot(CH_3CN)_2$ (2)

This compound crystallizes in the triclinic space group $P\bar{1}$. The bimetallic oxalate layer lies in the *ac* plane and contains two crystallographically independent metals (Mn1/Cr1 and Mn2/Cr2) with M–O bond lengths lying between 2.065(2) and 2.108(2) Å (Figure 3). As in the case of **1**, it is not possible to distinguish between the two metals in the structure as they are intermediate between the ones expected for Cr^{III}–O and Mn^{II}–O. These anionic layers are

stacked one over the other in an *AA*···fashion. The minimum distance between metal ions belonging to different oxalate layers is 12.8070(8) Å (equal to the *b* parameter). As this compound contains a single layer of $[Fe^{III}(3\text{-Br-sal}_2\text{-trien})]^+$ complexes, this distance is similar to those found in other oxalate-based 2D compounds with $[Fe^{III}(sal_2\text{-trien})]^+$ and derivatives (11.609–11.644 Å)[17b–17c] and shorter than those found in **1**, **3** and **4** that contain a double layer.

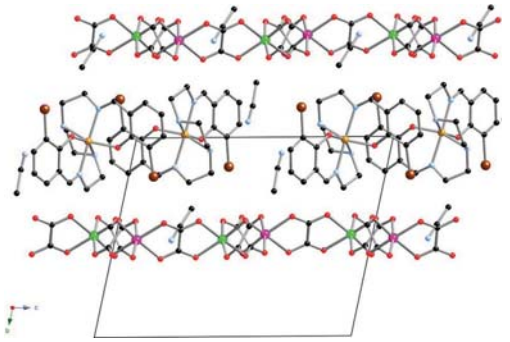

Figure 3. Projection of the structure of **2** in the *bc* plane. Fe (yellow), Br (brown), C (black), N (blue), O (red), Mn (pink), and Cr (green). Hydrogen atoms have been omitted for clarity.

The space between the oxalate sheets is occupied by one crystallographically independent $[Fe^{III}(3\text{-Br-sal}_2\text{-trien})]^+$ complex and two crystallographically independent acetonitrile molecules. The average Fe–N and Fe–O bond lengths in $[Fe^{III}(3\text{-Br-sal}_2\text{-trien})]^+$ complexes are 2.152(2) Å and 1.918(2) Å, respectively. These values are typical values for HS Fe^{III} complexes in agreement with the magnetic properties. The cations lie with their longer axis parallel to the oxalate layers (Figure 3). This is confirmed by the dihedral angle between the least-squares planes of the phenoxy rings and that formed by the metals of the oxalate network (87.6 and 97.6°). $[Fe^{III}(3\text{-Br-sal}_2\text{-trien})]^+$ complexes form double chains running along the *a*-axis (Figure 4 and Figure S1 of the Supporting Information) separated by the acetonitrile solvent molecules. One of the two phenoxy rings of 3-Br-sal_2-trien, which is located in the internal part of the double chain, is involved in C–H···π and N–H···π interactions and π–π stacking interactions with two adjacent $[Fe^{III}(3\text{-Br-sal}_2\text{-trien})]^+$ complexes belonging to the other chain. The other phenoxy ring, which is located in the external part of the double chain, is connected through C–H···π interactions with an adjacent $[Fe^{III}(3\text{-Br-sal}_2\text{-trien})]^+$ complex belonging to the same chain. The two Br atoms of the complexes point alternatively above and below the cationic layer and present short interactions with the oxalate network. The $[Fe^{III}(3\text{-Br-sal}_2\text{-trien})]^+$ complexes of different double chains are connected through hydrogen bonds with the acetonitrile solvent molecules placed between the double layers. Finally, there are numerous short contacts between the cations and the bimetallic oxalate network.

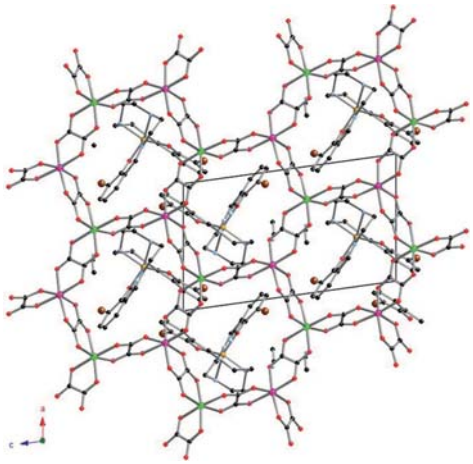

Figure 4. Projection of the structure of **2** in the *ac* plane. Fe (yellow), Br (brown), C (black), N (blue), O (red), Mn (pink), and Cr (green). Hydrogen atoms have been omitted for clarity.

$[Fe^{III}(3\text{-Cl-sal}_2\text{trien})][Mn^{II}Cr^{III}(ox)_3]\cdot(CH_3OH)_2\cdot(CH_3CN)_2$ (3)

The best solution to the structure of this compound was found in the chiral space group $P2_1$. The crystal was solved as a racemic twin with a BASF parameter of 0.66235. Therefore, the structure resolution has been performed in a twinned crystal containing crystals of opposite chirality. This compound presents a very different structure to that of compound **2**, in spite of the very similar templating cation. It seems that the small decrease in the size of the cation caused by the substitution of Br by Cl is enough to change the templating effect of the cation and to give rise to a very different structure.

In contrast to the two previous structures, the Mn^{II} and Cr^{III} of the bimetallic oxalate network are clearly distinguishable as they present different bond lengths with oxalate ligands. Thus, there are two crystallographically independent Mn ions (Mn1 and Mn2) with Mn–O distances between 2.133(6) and 2.209(6) Å and two crystallographically independent Cr ions (Cr1 and Cr2) with Cr–O distances between 1.955(6) and 2.022(6) Å. These are typical Mn^{II}–O and Cr^{III}–O distances similar to those found in other oxalate networks. These anionic layers lie in the *ab* plane and are stacked one over the other in an *ABAB*···fashion (Figure 5). Metal centres Cr1 and Mn1 are located in the A layer whereas Mn2 and Cr2 are located in the B layer. The neighbouring metal centres of these layers present alternating chirality as usual for this type of network but in this structure all the Cr^{III} ions adopt *Λ* configuration, whereas all the Mn^{II} ions adopt the *Δ* configuration. Therefore, the configuration of each metal ion is preserved in the neighbouring oxalate layers. Since we started from a racemic mixture of the $[Cr(ox)_3]^{3-}$ anion, crystals of the two enantiomers have been obtained. The minimum distance between metal of different layers is 13.630 Å, which is

longer than other 2D oxalate-based compounds with a single layer but not as long as that of other 2D oxalate-based compounds with a double layer of Fe^{III} complexes such as **1**. This intermediate interlayer distance is because of the presence of a double layer of $[Fe^{III}(3\text{-Cl-sal}_2\text{trien})]^+$ with a high degree of interpenetration between the two sublayers (see Figure 5).

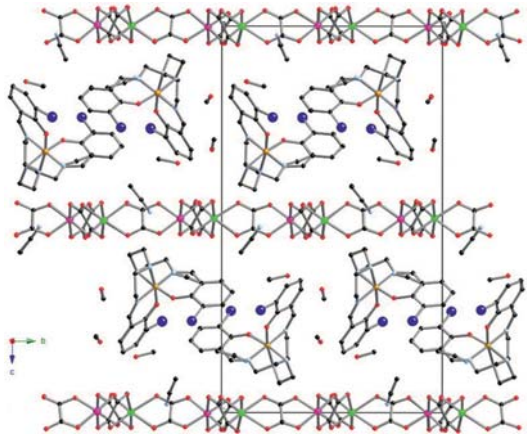

Figure 5. Projection of the structure of **3** in the *bc* plane. Fe (yellow), Cl (blue), C (black), N (blue), O (red), Mn (pink), and Cr (green). Hydrogen atoms have been omitted for clarity.

The space between oxalate layers is occupied by two crystallographically independent $[Fe^{III}(3\text{-Cl-sal}_2\text{-trien})]^+$ complexes (Fe1 and Fe2) and four crystallographically independent methanol and acetonitrile solvent molecules. The average Fe–N and Fe–O bond lengths are 1.980(7) and 1.900(6) Å in Fe1 and 1.960(7) and 1.865(6) Å in Fe2. These values are typical of LS Fe^{III} complexes but the observation of higher Fe–N distances in Fe1 could indicate the presence of a fraction of Fe^{III} in the HS state, in agreement with magnetic properties (see below). Fe1 adopts a *Δ* configuration while Fe2 adopts a *Λ* configuration in the crystal used to solve the structure. In contrast to the structures of **1** and **2**, the cations do not lie with their longer axis parallel to the oxalate layers (Figure 5 and Figure S2 of the Supporting Information), but present an important tilting with respect to the oxalate layer. This is confirmed by the dihedral angle between the least-squares planes of the phenoxy rings and that formed by the metals of the oxalate network, which are far from perpendicular in contrast to those of **1** and **2** (54.1 and 39.4° for Fe1 and 44.5 and 54.1° for Fe2). Note that one of the two phenoxy rings of Fe1 and Fe2 presents the same angle. This indicates that they are involved in π–π staking interactions as they present very short distances (six C–C distances between 3.421 and 3.553 Å). These dimers formed by the two crystallographically independent $[Fe^{III}(3\text{-Cl-sal}_2\text{-trien})]^+$ complexes are connected to other dimers by short Cl···Cl contacts (Cl–Cl distances of 3.304 and 3.307 Å) giving rise to double chains running along the *a*-axis (see Figure S2 of the Supporting Information). Finally, these two cations present numerous short contacts with methanol and acetonitrile solvent molecules (hydrogen bonds between NH groups and CH_3OH and CH_3CN molecules) and the oxalate network.

$[Fe^{III}(3\text{-}CH_3O\text{-}sal_2\text{-}trien)][Mn^{II}Cr^{III}(ox)_3]\cdot(CH_3OH)\cdot(H_2O)1.5\cdot(CH_2Cl_2)_{0.5}$ (4)

This compound crystallizes in the monoclinic space group $P2_1/n$. The anionic layer lies in the *10–1* plane and contains two crystallographically independent metals with M–O bond lengths lying between 2.050(4) and 2.088(4) Å. Therefore, it is not possible to distinguish between Mn^{II} and Cr^{III} in the structure as in **1** and **2**. These anionic layers are stacked one over the other in an *AA*···fashion (see Figure 6). The minimum distance between metal ions of different layers is 14.865 Å, which is intermediate between those of **1** and **3** (the other two compounds with a double layer of Fe^{III} cations presented in this work) due to a different degree of interpenetration of the two sublayers.

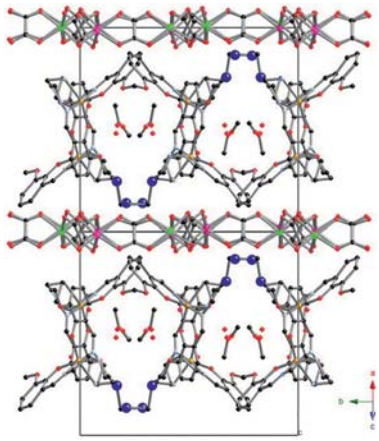

Figure 6. Lateral view of the bimetallic oxalate and cationic layers of **4**. Fe (yellow), C (black), N (blue), O (red), Mn (pink), and Cr (green). Hydrogen atoms have been omitted for clarity.

The space between oxalate layers is occupied by one crystallographically independent $[Fe^{III}(3\text{-MeO-sal}_2\text{-trien})]^+$ complex and three water, two methanol and one dichloromethane crystallographically independent solvent molecules with an occupancy of 0.5. The average Fe–N and Fe–O bond lengths are 2.131(4) and 1.913(4) Å, respectively. These values are close to those found for other similar Fe^{III} HS complexes. However, they are shorter than those found for **2**. This indicates that a fraction of Fe^{III} complexes may be in the LS state in agreement with magnetic properties. As in the structure of **3**, the Fe^{III} complexes do not lie with their longer axis parallel to the oxalate layers (Figure 6). Indeed, the longer axis of these complexes is almost perpendicular to the oxalate layer. The dihedral angle between the least-squares planes of the phenoxy rings and that formed by the metals of the oxalate network are very different (52.0 and 84.9°), indicating a tilted disposition of the complexes.

Two neighbouring $[Fe^{III}(3\text{-MeO-sal}_2\text{-trien})]^+$ complexes present short contacts through two CH···π edge-to-face interactions and two short contacts between O from the methoxy group and the same CH_2 involved in CH···π edge-to-face interactions. Furthermore, they are interconnected through numerous short contacts with the oxalate network and the disordered solvent molecules. They define some channels filled with disordered water and methanol solvent molecules that run along the [101] axis (see Figure 6).

Magnetic Properties

The thermal dependence of the product of the molar magnetic susceptibility times the temperature (χT) of **1** is shown in Figure 7. χT shows a value of 8.3 emu K mol^{-1} at 400 K. This value is approximately equal to the sum of the expected contributions for the isolated paramagnetic ions (1 Fe^{III}, 0.67 Mn^{II} and 0.67 Cr^{III}) with 90% of the Fe^{III} spin-crossover complex in a HS state. χT decreases abruptly from 400 to 270 K to reach a value of 5.4 emu K mol^{-1}. This value is close to the expected value for 100% of Fe^{III} in the LS state (4.8 emu K mol^{-1}). From 270 to 140 K, χT shows a constant value consistent with almost all the Fe^{III} in the LS state. At lower temperatures, there is an increase of χT that is very sharp below 50 K. This indicates the presence of ferromagnetic interactions between neighbouring Mn^{II}–Cr^{III} magnetic ions and suggests the onset of long-range ferromagnetic ordering, as observed for other 2D bimetallic oxalate networks. To confirm the presence of long-range magnetic ordering and to determine precisely the critical temperatures (T_c), alternating current (AC) susceptibility measurements were carried out. A maximum in the in-phase signal (χ') near T_c and an out-of-phase signal (χ'') that starts to appear at temperatures just below T_c is observed. From this data, the T_c of **1** is 5.2 K, similar to those reported for other Mn^{II}–Cr^{III} 2D oxalate compounds. As expected for a ferromagnet, these signals are frequency independent (Figure 8). The isothermal magnetization (M) at 2 K shows a very sharp increase at low fields which is much faster than that expected for noninteracting Mn^{II}–Cr^{III} centres; this increase is more gradual at higher fields and no saturation is reached even up to 5 T (Figure 9). The M value of 6.3 μ_B (μ_B is the Bohr magneton) at 5 T, confirms a parallel alignment of the spins in this bimetallic lattice (spin-only value of 6.4 μ_B). The hysteresis loop at 2 K shows that this compound is a soft ferromagnet with a coercive field of 7 mT.

The thermal dependence of χT of **2**, **3** and **4** is shown in Figure 10. χT values of 11.3, 9.5 and 10.2 emu K mol^{-1} at 300 K are found for **2**, **3** and **4**, respectively. These values are consistent with Fe^{III} HS fractions of 100% for **2**, 70% for **3** and 90% for **4**. At lower temperatures, χT of **2** increases whereas those of **3** and **4** decrease to reach minimum values of 9.0 and 9.8 emu K mol^{-1} respectively around 150 K. This indicates that **2** is in the HS state in the whole temperature range in agreement with structural data at 120 K and isothermal magnetization at 2 K (see below) while **3** and **4** present a partial spin crossover which is quite gradual. At lower temperatures, χT increases gradually for the three compounds with a very abrupt increase below

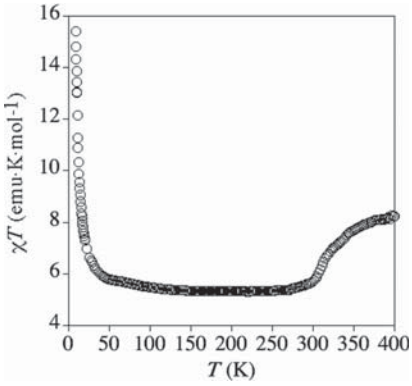

Figure 7. Temperature dependence of the product of the molar magnetic susceptibility with temperature (χT) at 0.1 T for compound **1** (empty circles).

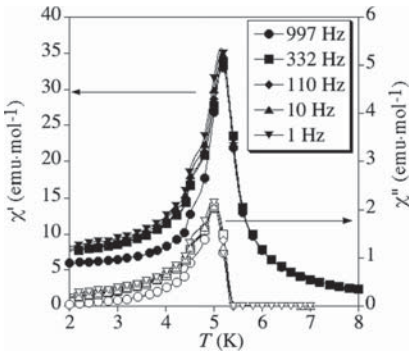

Figure 8. Temperature dependence of the in-phase AC susceptibility (χ') (filled symbols) and the out-of-phase AC susceptibility (χ'') (empty symbols) for **1**.

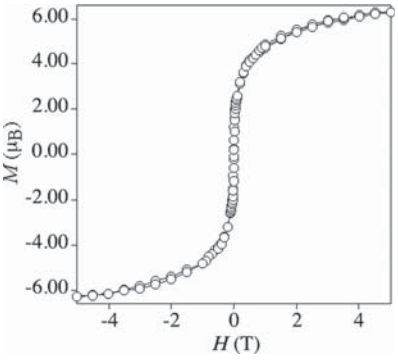

Figure 9. Field dependence of the magnetization (M) for **1** (empty circles).

50 K coming from the ferromagnetic MnCr oxalate layers. AC susceptibility measurements indicate that the T_c values of **2**, **3** and **4** are respectively 5.4, 5.0 and 5.4 K, which are similar to that of **1** or those of other 2D $Mn^{II}Cr^{III}$ oxalate compounds, which are frequency independent (Figure S3 of the Supporting Information).[17]

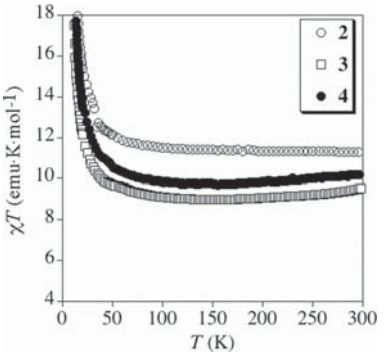

Figure 10. Temperature dependence of the product of the molar magnetic susceptibility with temperature (χT) at 0.1 T for compound **2** (empty circles), **3** (empty squares) and **4** (full circles).

The isothermal magnetization at 2 K of **2**, **3** and **4** is similar to that of **1** confirming the ferromagnetic nature of the MnCr layers (Figure S4 of the Supporting Information). Furthermore, M values at 5 T are intermediate between the expected values for 100% of Fe^{III} in the LS state (9 μ_B) and the expected ones for 100% of Fe^{III} in the HS state (13 μ_B). This indicates that a significant fraction of Fe^{III} is in the HS state in the three compounds, and is higher in compound **2** in agreement with structural data. However, a quantitative estimation of the HS/LS fraction is difficult to extract from these data and Mössbauer measurements are needed to clarify this point.

Photomagnetic Characterization

Photomagnetic characterization of the two compounds of this family with the highest fraction of LS Fe^{III} at low temperatures (**1** and **3**) was performed. The two compounds were irradiated with red, green and IR light but the magnetization remained almost unchanged. Therefore, it seems that **1** and **3** do not present a LIESST effect. The photomagnetic characterization of **2** and **4** is in progress taking into account that in the case of **4** only reverse LIESST could be expected as the cation is in the HS state in the whole temperature range.

The question remains why LIESST has been observed in other 2D oxalate-based compounds such as $[Fe^{III}(sal_2\text{-trien})][Mn^{II}Cr^{III}(ox)_3]\cdot(CH_2Cl_2)$[18] but not in **1** and **3**. Further work is necessary to answer to this question. At the moment, it remains unclear whether the absence of LIESST is linked to: (a) a too high thermal spin-crossover temperature ($T_{1/2}$) and/or (b) structural differences between 2D networks and/or (c) the small amount of Fe^{III} that can undergo spin crossover. In the case of **1**, it could be related to the high $T_{1/2}$ as it has been shown that there is a linear correlation between the $T_{1/2}$ and T(LIESST) for iron(II) complexes.[20] Since the two temperatures are inversely proportional, a too high $T_{1/2}$ (a) may lead to a T(LIESST) too low to be detected. Conversely, the structural differences between the 2D structures of **1** and **3** and that of $[Fe^{III}(sal_2\text{-trien})][Mn^{II}Cr^{III}(ox)_3]\cdot(CH_2Cl_2)$ could explain the lack of LIESST behaviour in these compounds (b). Thus, the presence of a double layer of Fe^{III} complexes in **1** and **3** instead of the single one of $[Fe^{III}(sal_2\text{-trien})][Mn^{II}Cr^{III}(ox)_3]\cdot(CH_2Cl_2)$ gives rise to a decrease of the interactions with the oxalate network that could be necessary to observe a LIESST effect.[18] Finally, the low amount of LS fraction at low temperature (c) of **3** make it difficult to observe the possible small increase of magnetization after light irradiation, as it would be difficult to distinguish this increase from the important magnetic signal of the oxalate network.

Conclusions

In this work we have reported the preparation of four novel compounds (**1**, **2**, **3** and **4**) formed by the insertion of the spin-crossover cations $[Fe^{III}(4\text{-Br-sal}_2\text{-trien})]^+$, $[Fe^{III}(3\text{-Br-sal}_2\text{-trien})]^+$, $[Fe^{III}(3\text{-Cl-sal}_2\text{-trien})]^+$, and $[Fe^{III}(3\text{-CH}_3\text{O-sal}_2\text{-trien})]^+$ into anionic coordination polymers based on bimetallic oxalate complexes. We confirm with this result that the use of different sal_2-trien derivatives is a suitable strategy to obtain a great variety of oxalate networks. Thus, we have seen previously that depending on the substituent, different types of network can be obtained. Thus, $[Fe(sal_2\text{-trien})]^+$, $[Fe^{III}(5\text{-NO}_2\text{-sal}_2\text{-trien})]^+$ and $[Fe^{III}(5\text{-CH}_3\text{O-sal}_2\text{-trien})]^+$ complexes, lead to the formation of 2D or achiral 3D networks. Conversely, $[Fe^{III}(5\text{-Xsal}_2\text{-trien})]^+$ (X = Cl, Br), gives rise to the growth of a 3D chiral network. The different templating effect of these cations could be related to the intermolecular interactions. For instance, in 5-substituted $[Fe^{III}(5\text{-Xsal}_2\text{-trien})]^+$ complexes, NO_2 groups favour π–π stacking interactions and the growth of a 2D network; with CH_3O groups, these interactions are more difficult due to steric hindrance and an achiral 3D network is formed. Finally, smaller substituents (Cl or Br) favour a helical arrangement of the complexes and the growth of a 3D chiral network. In contrast to this, the use of 3- or 4-substituted complexes gives rise in all cases to 2D networks. Furthermore, these 2D networks are very different to those obtained previously with $[Fe^{III}(sal_2\text{-trien})]^+$ and $[Fe^{III}(5\text{-NO}_2\text{-sal}_2\text{-trien})]^+$. The main difference is the different orientation of the Fe^{III} cations. In the previous compounds, these cations lie with their longer axis parallel to the oxalate network, while in the present case they show a certain tilting angle. Such a disposition leads to double layers of cations in compounds **1**, **3** and **4** and to the presence of pores in the structures of **1** and **4** filled with disordered solvent molecules.

Apart from the structural interest of these compounds, the magnetic properties indicate that the inserted Fe^{III} cat-

ions undergo an almost complete spin crossover above 300 K in **1** and a partial spin crossover in **3** and **4** that coexists with a ferromagnetic ordering of the oxalate network. In the case of **2**, the inserted cation remains in the HS state from 2 to 300 K. Therefore, **1**, **3** and **4** are multifunctional compounds with coexistence of spin crossover and magnetic ordering. Conversely, photomagnetic characterization shows that in contrast to the 2D compound $[Fe^{III}(sal_2\text{-trien})][Mn^{II}Cr^{III}(ox)_3]\cdot(CH_2Cl_2)$, **1** and **3** do not present a LIESST effect. In attendance of the photomagnetic characterization of compounds **2** and **4**, this result may help to understand the factors affecting this very rare and unexpected property in a Fe^{III} spin-crossover complex. Thus, they could indicate that the intermolecular interactions between the cationic network and the oxalate network are of key importance. In fact, owing to the nature of the cationic network (double layer vs. single layer), these interactions are expected to be less pronounced in the present case (**1** and **3**) than in $[Fe^{III}(sal_2\text{-trien})][Mn^{II}Cr^{III}(ox)_3]\cdot(CH_2Cl_2)$. More examples of this type of compound are needed to understand this point. Finally, the presence of pores with disordered solvent molecules in the structures of **1** and **4** could lead to new functionalities in addition to the magnetic ordering and spin crossover such as solvent adsorption or proton conduction recently found in other 2D oxalate-based compounds.[9,13]

Experimental Section

Syntheses: Crystals of $[Fe^{III}(4\text{-Br-sal}_2\text{-trien})][Mn^{II}Cr^{III}(ox)_3]_{0.67}Cl_{0.33}\cdot CH_3OH$ (**1**), $[Fe^{III}(3\text{-Br-sal})_2\text{-trien}][Mn^{II}Cr^{III}(ox)_3]\cdot(CH_3CN)_2$ (**2**), $[Fe^{III}(3\text{-Cl-sal})_2\text{-trien}][Mn^{II}Cr^{III}(ox)_3]\cdot(CH_3OH)_2\cdot(CH_3CN)_2$ (**3**) and $[Fe^{III}(3\text{-}CH_3O\text{-sal}_2\text{-trien})][Mn^{II}Cr^{III}(ox)_3]\cdot(CH_3OH)\cdot(H_2O)_{1.5}\cdot(CH_2Cl_2)_{0.5}$ (**4**) were obtained by slow diffusion of two solutions. The first solution was prepared by adding $MnCl_2\cdot 4H_2O$ (14 mg, 0.067 mmol) to a suspension of $Ag_3Cr(ox)_3$ (38 mg, 0.06 mmol) in methanol (3 mL). The AgCl precipitate was filtered off. The second solution was obtained by dissolving compound **1** (43 mg, 0.06 mmol) in acetonitrile (3 mL), compound **2** (43 mg, 0.06 mmol) in acetonitrile (3 mL), compound **3** (38 mg, 0.06 mmol) in acetonitrile (3 mL) and compound **4** (37 mg, 0.06 mmol) in dichloromethane (3 mL). After 2 weeks brown-black crystals, in all cases, were obtained.

Structural Characterization: Single-crystal X-ray data of **1**–**4** were collected at 120 K with a Xcalibur, Sapphire3, Gemini diffractometer equipped with a graphite-monochromated Enhance (Mo) X-ray source (λ = 0.71073 Å). The program CrysAlisPro, Oxford Diffraction Ltd., Version 1.171.33.52., was used for cell refinements and data reduction of the compounds. Empirical absorption correction was performed using spherical harmonics, implemented in the SCALE3 ABSPACK scaling algorithm. Crystal structures were solved by direct methods with the SIR97 program[21] and refined against all F^2 values with the SHELXL-97 program[22] using the WinGX graphical user interface.[23] Non-hydrogen atoms were refined anisotropically, (except as noted) and hydrogen atoms were placed in calculated positions refined using idealized geometries (riding model) and assigned fixed isotropic displacement parameters. The subroutine SQUEEZE[24] was used to remove the diffracting component of disordered solvents in **1** resulting in a void of ca. 1436.4 Å^3 and 387 electrons/cell omitted. This corresponds to ca. 12 CH_3CN + 12 H_2O molecules per cell. All non-hydrogen atoms were refined anisotropically. In **4**, the two aromatic rings from $[Fe^{III}(3\text{-MeO-sal})_2\text{-trien}]^+$ complexes were modelled in two orientations. In compound **3**, the small size of the crystal gave rise to a very weak scattering. Because of this the number of reflections was not enough to carry out anisotropic refinement of all the atoms, thus carbon atoms could only be modelled isotropically. Data collection and refinement statistics are collected in Table 1.

CCDC-900041 (for **1**), -900042 (for **2**), -900043 (for **3**), and -900044 (for **4**) contain the supplementary crystallographic data for this pa-

Table 1. Crystallographic data for compounds **1**, **2**, **3** and **4**.

	1	**2**	**3**	**4**
Empirical formula	$Cl_{0.33}C_{29}Cr_{0.67}Br_2FeMn_{0.67}H_{36}O_{13}N_6$	$C_{30}CrBr_2FeMnH_{28}O_{14}N_6$	$Cl_2C_{32}CrFeMnH_{36}O_{16}N_6$	$ClC_{29.50}CrFeMnH_{36}O_{18.50}N_4$
Formula weight	975.41	1019.19	994.36	940.81
Crystal colour	black	black	black	black
Temperature [K]	120(2)	120(2)	120(2)	120(2)
Wavelength [Å]	0.71073	0.71073	0.71073	0.71073
Crystal system, *Z*	trigonal, 6	triclinic, 2	monoclinic, 2	monoclinic, 4
Space group	$P\bar{3}$	$P\bar{1}$	$P2_1$	$P2_1/n$
a [Å]	18.7107(5)	9.4310(6)	9.6700(4)	16.8977(13)
b [Å]	18.7107(5)	12.8070(8)	15.5850(7)	16.0300(8)
c [Å]	18.5675(7)	16.0680(10)	27.6340(14)	18.7421(12)
α [°]	90	101.392(5)	90	90
β [°]	90	96.264(5)	99.162(5)	116.454(9)
γ [°]	120	97.548(5)	90	90
V [Å^3]	5629.4(3)	1867.7(2)	4111.5(3)	4545.1(65)
ρ(calcd.) [Mg m^{-3}]	1.725	1.812	1.606	1.365
μ(Mo-K_α) [mm^{-1}]	3.021	3.215	1.116	0.951
θ Range [°]	2.43–29.83	2.30–32.26	2.36–32.27	2.42–32.30
Reflections collected	67242	42941	68834	68357
Indep. refl., *n*, (R_{int})	10053 (0.0929)	11416 (0.0666)	5321 (0.1371)	8477 (0.0957)
L. S. parameters/ restraints	394/1	498/0	716/1	541/2
$R1(F)$,[a] [$I > 2\sigma(I)$]	0.0398	0.0413	0.0472	0.0771
$wR2(F^2)$,[b] all data	0.0934	0.0851	0.0671	0.2486

[a] $R1(F) = S(|F_o| - |F_c|)/S|F_o|$. [b] $wR2(F^2) = [Sw(F_o^2 - F_c^2)^2/SwF_o^4]^{1/2}$.

per. These data can be obtained free of charge from The Cambridge Crystallographic Data Centre via www.ccdc.cam.ac.uk/data_request/cif.

Physicals Measurements: Magnetic susceptibility measurements were performed on polycrystalline samples using a magnetometer (Quantum Design MPMS-XL-5) equipped with a SQUID sensor. Variable-temperature measurements were carried out in the temperature range 2–300 K. The AC measurements were performed in the temperature range 2–10 K at different frequencies with an oscillating magnetic field of 0.395 mT. The magnetization and hysteresis studies were performed between 5 and –5 T, cooling the samples at zero field. The photomagnetic measurements were performed with a Spectrum Physics Series 2025 Kr^+ laser coupled via an optical fibre to the cavity of a MPMS-55 Quantum Design SQUID magnetometer. The Fe/Mn/Cr/X (X = Cl, Br) ratios were measured with a Philips ESEM X230 scanning electron microscope equipped with an EDAX DX-4 microsonde.

Supporting Information (see footnote on the first page of this article): Structural views of the cationic layers of **2** and **3** and magnetic properties of **2**, **3** and **4**.

Acknowledgments

We thank the European Union (EU) (ERC Advanced grant SPINMOL, Project HINTS), the Spanish Ministerio de Economia y Competividad (MINECO) (Project Consolider-Ingenio in Molecular Nanoscience, grant numbers CSD2007-00010, MAT2011-22785 and CTQ-2011-26507), and the Generalitat Valenciana (Prometeo Program) for financial support. The authors also thank J. M. Martínez-Agudo and Dr. G. Agustí-López, University of Valencia, for assistance with the magnetic characterization and Prof. J. F. Létard, Dr. C. Desplanches and H. F. Wang, ICMCB, CNRS, Université Bordeaux 1, for the magnetic characterization under light irradiation.

[1] a) E. Coronado, P. Day, *Chem. Rev.* **2004**, *104*, 5419–5448; b) E. Coronado, C. Martí-Gastaldo, E. Navarro-Moratalla, A. Ribera, S. J. Blundell, P. J. Baker, *Nat. Chem.* **2010**, *2*, 1031–1036.

[2] a) E. Coronado, M. C. Giménez-López, G. Levchenko, F. M. Romero, V. García-Baonza, A. Milner, M. Paz-Pasternak, *J. Am. Chem. Soc.* **2005**, *127*, 4580–4581; b) E. Coronado, M. C. Giménez-López, T. Korzeniak, G. Levchenko, F. M. Romero, A. Segura, V. García-Baonza, J. C. Cezar, F. M. F. De Groot, A. Milner, M. Paz-Pasternak, *J. Am. Chem. Soc.* **2008**, *130*, 15519–15532; c) S. I. Ohkoshi, K. Imoto, Y. Tsunobuchi, S. Takano, H. Tokoro, *Nat. Chem.* **2011**, *3*, 564–569.

[3] M. Clemente-León, E. Coronado, C. Martí-Gastaldo, F. M. Romero, *Chem. Soc. Rev.* **2011**, *40*, 473–497.

[4] a) H. Tamaki, Z. J. Zhong, N. Matsumoto, S. Kida, M. Koikawa, N. Achiwa, Y. Hashimoto, H. Okawa, *J. Am. Chem. Soc.* **1992**, *114*, 6974–6979; b) H. Tamaki, M. Mitsumi, N. Nakamura, N. Matsumoto, S. Kida, H. Okawa, S. Ijima, *Chem. Lett.* **1992**, 1975–1978; c) C. Mathonière, J. Nutall, S. G. Carling, P. Day, *Inorg. Chem.* **1996**, *35*, 1201–1206; d) R. Pellaux, H. W. Schmalle, R. Huber, P. Fisher, T. Hauss, B. Ouladdiaf, S. Decurtins, *Inorg. Chem.* **1997**, *36*, 2301–2308; e) E. Coronado, J. R. Galán-Mascarós, C. J. Gómez-García, J. M. Martínez-Agudo, E. Martínez-Ferrero, J. C. Waerenborgh, M. Almeida, *J. Solid State Chem.* **2001**, *159*, 391–402; f) K. S. Min, A. L. Rhinegold, J. S. Miller, *Inorg. Chem.* **2005**, *44*, 8433–8441; g) E. Coronado, J. R. Galán-Mascarós, C. Martí-Gastaldo, *J. Mater. Chem.* **2006**, *16*, 2685–2689.

[5] a) S. Decurtins, H. W. Schmalle, P. Schneuwly, H. R. Oswald, *Inorg. Chem.* **1993**, *32*, 1888–1892; b) S. Decurtins, H. W. Schmalle, P. Schneuwly, J. Ensling, P. Gütlich, *J. Am. Chem. Soc.* **1994**, *116*, 9521–9528; c) M. Hernández-Molina, F. Lloret, C. Ruiz-Pérez, M. Julve, *Inorg. Chem.* **1998**, *37*, 4131–4135; d) E. Coronado, J. R. Galán-Mascarós, C. J. Gómez-García, J. M. Martínez-Agudo, *Inorg. Chem.* **2001**, *40*, 113–120; e) F. Pointillart, C. Train, M. Gruselle, F. Villain, H. W. Schmalle, D. Talbot, P. Gredin, S. Decurtins, M. Verdaguer, *Chem. Mater.* **2004**, *16*, 832–841; f) M. Clemente-León, E. Coronado, C. J. Gómez-García, A. Soriano-Portillo, *Inorg. Chem.* **2006**, *45*, 5653–5660.

[6] a) M. Clemente-León, E. Coronado, J. R. Galán-Mascarós, C. J. Gómez-García, *Chem. Commun.* **1997**, 1727–1728; b) E. Coronado, J. R. Galán-Mascarós, C. J. Gómez-García, J. M. Martínez-Agudo, *Adv. Mater.* **1999**, *11*, 558–561; c) E. Coronado, J. R. Galán-Mascarós, C. J. Gómez-García, J. Ensling, P. Gutlich, *Chem. Eur. J.* **2000**, *6*, 552–563.

[7] a) S. Bénard, P. Yu, J. P. Audière, E. Rivière, R. Clèment, J. Ghilhem, L. Tchertanov, K. Nakatami, *J. Am. Chem. Soc.* **2000**, *122*, 9444–9454; b) S. M. Aldoshin, N. A. Sanina, V. I. Minkin, N. A. Voloshin, V. N. Ikorskii, V. I. Ovcharenko, V. A. Smirnov, N. K. Nagaeva, *J. Mol. Struct.* **2007**, *826*, 69–74.

[8] a) E. Coronado, J. R. Galán-Mascarós, C. J. Gómez-García, V. Laukhin, *Nature* **2000**, *408*, 447–449; b) A. Alberola, E. Coronado, J. R. Galán-Mascarós, C. Giménez-Saiz, C. J. Gómez-García, *J. Am. Chem. Soc.* **2003**, *125*, 10774–10775; c) E. Coronado, J. R. Galán-Mascarós, C. J. Gómez-García, E. Martínez-Ferrero, S. Van Smaalen, *Inorg. Chem.* **2004**, *43*, 4808–4810.

[9] a) H. Okawa, A. Shigematsu, M. Sadakiyo, T. Miyagawa, K. Yoneda, M. Ohba, H. Kitagawa, *J. Am. Chem. Soc.* **2009**, *131*, 13516–13522; b) M. Sadayiko, H. Okawa, A. Shigematsu, M. Ohba, T. Yamada, H. Kitagawa, *J. Am. Chem. Soc.* **2012**, *134*, 5472–5475.

[10] T. Endo, T. Akutagawa, S. I. Noro, T. Nakamura, *Dalton Trans.* **2011**, *40*, 1491–1496.

[11] a) R. Andrés, M. Gruselle, B. Malézieux, M. Verdaguer, J. Vaissermann, *Inorg. Chem.* **1999**, *38*, 4637–4646; b) R. Andrés, M. Brissard, M. Gruselle, C. Train, J. Vaissermann, B. Malézieux, J. P. Jamet, M. Verdaguer, *Inorg. Chem.* **2001**, *40*, 4633–4640; c) M. Clemente-León, E. Coronado, J. C. Dias, A. Soriano-Portillo, R. D. Willett, *Inorg. Chem.* **2008**, *47*, 6458–6463.

[12] R. Galán-Mascarós, E. Coronado, P. A. Goddard, J. Singleton, A. I. Coldea, J. D. Wallis, S. J. Coles, A. Alberola, *J. Am. Chem. Soc.* **2010**, *132*, 9271–9273.

[13] E. Pardo, C. Train, G. Contard, K. Boubekeur, O. Fabelo, H. Liu, B. Dkhil, F. Lloret, K. Nakagawa, H. Tokoro, S.-I. Ohkoshi, M. Verdaguer, *J. Am. Chem. Soc.* **2011**, *133*, 15328–15331.

[14] C. Train, R. Gheorghe, V. Krstic, L. M. Chamoreau, N. S. Ovanesyan, G. L. J. A. Rikken, M. Gruselle, M. Verdaguer, *Nat. Mater.* **2008**, *7*, 729–734.

[15] C. Train, T. Nuida, R. Gheorghe, M. Gruselle, S. Ohkoshi, *J. Am. Chem. Soc.* **2009**, *131*, 16838–16843.

[16] a) R. Sieber, S. Decurtins, H. Stoeckli-Evans, C. Wilson, D. Yufit, J. A. K. Howard, S. C. Capelli, A. Hauser, *Chem. Eur. J.* **2000**, *6*, 361; b) E. Coronado, J. R. Galán-Mascarós, M. C. Giménez-López, M. Almeida, J. C. Waerenborgh, *Polyhedron* **2007**, *26*, 1838–1844.

[17] a) M. Clemente-León, E. Coronado, M. C. Giménez-López, A. Soriano-Portillo, J. C. Waerenborgh, F. S. Delgado, C. Ruiz-Pérez, *Inorg. Chem.* **2008**, *47*, 9111; b) M. Clemente-León, E. Coronado, M. López-Jordà, G. Mínguez Espallargas, A. Soriano-Portillo, J. C. Waerenborgh, *Chem. Eur. J.* **2010**, *16*, 2207–2219; c) M. Clemente-León, E. Coronado, M. López-Jordà, *Dalton Trans.* **2010**, *39*, 4903–4910; d) M. Clemente-León, E. Coronado, M. López-Jordà, J. C. Waerenborgh, *Inorg. Chem.* **2011**, *50*, 9122–9130.

[18] M. Clemente-León, E. Coronado, M. López-Jordà, C. Desplanches, S. Asthana, H. Wang, J.-F. Létard, *Chem. Sci.* **2011**, *2*, 1121–1127.

[19] a) S. Hayami, Z.-Z. Gu, M. Shiro, Y. Einaga, A. Fujishima, O. Sato, *J. Am. Chem. Soc.* **2000**, *122*, 7126–7127; b) G. Juhász, S. Hayami, O. Sato, Y. Maeda, *Chem. Phys. Lett.* **2002**, *364*,

164–170; c) S. Hayami, K. Hiki, T. Kawahara, Y. Maeda, D. Urakami, K. Inoue, M. Ohama, S. Kawata, O. Sato, *Chem. Eur. J.* **2009**, *15*, 3497–3508.
[20] a) T. Buchen, P. Gütlich, K. H. Sugiyarto, H. A. Goodwin, *Chem. Eur. J.* **1996**, *2*, 1134–1138; b) J.-F. Létard, P. Guionneau, L. Rabardel, J. A. K. Howard, A. E. Goeta, D. Chasseau, O. Kahn, *Inorg. Chem.* **1998**, *37*, 4432–4441; c) J.-F. Létard, L. Capes, G. Chastanet, N. Moliner, S. Létard, J. A. Real, O. Kahn, *Chem. Phys. Lett.* **1999**, *313*, 115–120; d) S. Marcen, L. Lecren, L. Capes, H. A. Goodwin, J.-F. Létard, *Chem. Phys. Lett.* **2002**, *358*, 87–95; e) J.-F. Létard, P. Guionneau, O. Nguyen, J. S. Costa, S. Marcen, G. Chastanet, M. Marchivie, L. Capes, *Chem. Eur. J.* **2005**, *11*, 4582–4589; f) J.-F. Létard, *J. Mater. Chem.* **2006**, *16*, 2550–2559.
[21] A. Altomare, M. C. Burla, M. Camalli, G. L. Cascarano, C. Giacovazzo, A. Guagliardi, A. G. G. Moliterni, G. Polidori, R. Spagna, *J. Appl. Crystallogr.* **1999**, *32*, 115–119.
[22] G. M. Sheldrick, *SHELXL-97*, Program for Crystal Structure Refinement, University of Göttingen, Germany, **1997**.
[23] L. J. Farrugia, *J. Appl. Crystallogr.* **1997**, *32*, 837–838.
[24] A. L. Spek, *J. Appl. Crystallogr.* **2003**, *36*, 7–13.
Received: September 20, 2012
Published Online: December 19, 2012

Dalton Transactions

RSC Publishing

PAPER

View Article Online
View Journal | View Issue

Cite this: *Dalton Trans.*, 2013, **42**, 5100

2D and 3D bimetallic oxalate-based ferromagnets prepared by insertion of Mn^{III}-salen type complexes†

Miguel Clemente-León,* Eugenio Coronado* and Maurici López-Jordà

The syntheses, structures and magnetic properties of the compounds of formulae [Mn((*R*)-salmen)-$(CH_3OH)(CH_3CN)$][$MnCr(ox)_3$]$(CH_3OH)_{0.5}(CH_3CN)_{1.25}$ (**(*R*)-1**), [Mn((*S*)-salmen)$(CH_3OH)(CH_3CN)$][$MnCr(ox)_3$]-$(CH_3OH)_{0.5}(CH_3CN)_{1.25}$ (**(*S*)-1**), [Mn((*R*)-salmen)$(CH_3OH)_2$][$MnCr(ox)_3$]$(CH_2Cl_2)_{0.375}(CH_3OH)_{0.125}(H_2O)_{0.375}$ (**(*R*)-2**) and [Mn((*S*)-salmen)$(CH_3OH)_2$][$MnCr(ox)_3$]$(CH_2Cl_2)_{0.375}(CH_3OH)_{0.375}(H_2O)_{0.125}$ (**(*S*)-2**) (ox = oxalate, salmen^{2-} = *N*,*N*′-(1-methylethylene)bis(salicylideneiminate)), [Mn(salpn)$(CH_3OH)_{1.5}(CH_3CN)_{0.5}$][$MnCr(ox)_3$]-$(CH_3OH)_{0.82}(H_2O)_{0.93}$ (**3**) (salpn^{2-} = *N*,*N*′-(propane)bis(salicylideneiminate)) and [Mn(saltmen)(CH_3OH)-(CH_3CN)][$MnCr(ox)_3$](CH_3OH) (**4**) (saltmen^{2-} = *N*,*N*′-(1,1,2,2-tetramethylethylene)bis(salicylideneiminate)) are reported. These compounds are prepared by the insertion of Mn^{III}–Schiff base complexes into bimetallic oxalate networks. Different types of bimetallic oxalate networks are obtained for each templating cation. Thus, [Mn((*R*)-salmen)]$^+$ and [Mn((*S*)-salmen)]$^+$ chiral templating cations give rise to a 2D chiral bimetallic oxalate layer in acetonitrile in **(*R*)-1** and **(*S*)-1** compounds, whereas a new type of achiral 3D oxalate network is obtained with the same templating cation in dichloromethane in **(*S*)-2** and **(*R*)-2**. On the other hand, [Mn(salpn)]$^+$ and [Mn(saltmen)]$^+$ give rise respectively to a 3D chiral network and a 2D achiral network in compounds **3** and **4**. The magnetic properties of the four compounds indicate that they undergo a long-range ferromagnetic ordering at *ca.* 5 K.

Received 13th December 2012,
Accepted 21st January 2013

DOI: 10.1039/c3dt32996h

www.rsc.org/dalton

Introduction

Bimetallic oxalate-based networks have provided many examples of multifunctional compounds.[1] These compounds are composed of polymeric anionic networks of bimetallic oxalate complexes,[2,3] which furnish the magnetic properties (ferro- ferri- or canted antiferromagnetism), and a bulky charge-compensating molecular cation, which templates the network formation and adds a second physical property of interest. The insertion of different cations into oxalate networks has led to compounds combining the long-range magnetic ordering from the oxalate network with a second property such as paramagnetism,[4] photochromism,[5] electric conductivity,[6] proton conduction,[7] ferroelectricity,[8] chirality,[9] spin-crossover[10] or chirality combined with conductivity[11] or proton conduction.[12]

In these hybrid compounds, the dimensionality of the coordination network of their structures is controlled by the relative configuration of the adjacent metal ions linked by an oxalate bridge. Thus, a 2D honeycomb structure is obtained when the relative configurations are opposite, *e.g.* (Δ, Λ). In contrast, if they are identical, (Λ, Λ) or (Δ, Δ), a chiral 3D network is formed.[13] The counter-ions associated with the formation of chiral 3D networks have been essentially chiral metallic complexes such as $[Z^{II}(bpy)_3]^{2+}$ (Z = Ru, Fe, Co; bpy = bipyridine), while 2D networks can be formed with a larger variety of templating cations with different shapes and sizes. Recent results have shown that the situation is more complicated. Thus, apart from these two types of structures, 3D networks with metals in the two configurations have been obtained with Fe^{II} and Fe^{III} complexes and triethylammonium cations very recently.[10b,c,14,15] For instance, Fe^{III} complexes of the hexadentate Schiff base ligand, sal_2-trien (H_2sal_2-trien = *N*,*N*′-disalicylidenetriethylene-tetramine) and 5-X-sal_2-trien derivatives (X = Cl, Br, NO_2 CF_3O, and CH_3O) as templating cations, lead to a great variety of oxalate-based structures. Thus, 2D structures (with X = H in dichloromethane[10b] and X = NO_2[10c]), achiral 3D structures (X = H in acetonitrile,[10b] and X = CH_3O)[10c] or chiral 3D structures (with X = Cl or Br)[10d] have been obtained. All these examples outline the vital role of the cation in tailoring the assembling of the molecular building-blocks.

Instituto de Ciencia Molecular, Universitat de València, Catedrático José Beltrán 2, 46980-Valencia, Spain. E-mail: miguel.clemente@uv.es, eugenio.coronado@uv.es; Fax: +34 963543273; Tel: +34 963544415

†Electronic supplementary information (ESI) available: Fig. S1 to SI5 are structural views of (***R*)-2**, **3** and **4**. Fig. SI6 to SI13 contain part of the magnetic characterisation of the six compounds. Crystallographic data in CIF format. CCDC 915417 for **3**, 915418 for **4**, 915419 for (***R*)-1**, 915420 for (***R*)-2**, 915421 for (***S*)-1**, and 915422 for (***S*)-2**. For ESI and crystallographic data in CIF or other electronic format see DOI: 10.1039/c3dt32996h

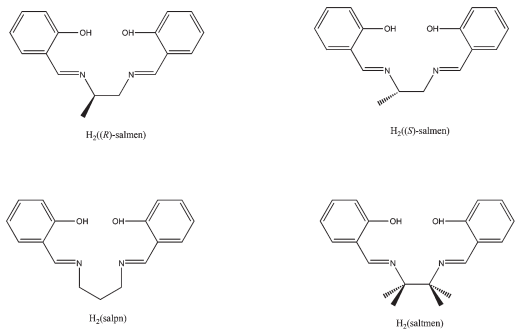

Scheme 1 H_2((*R*)-salmen), H_2((*S*)-salmen), H_2(salpn) and H_2(saltmen).

In this work, we have explored for the first time the use of a different type of templating cation, Mn^{III} salen-type complexes ($salen^{2-}$ = *N*,*N*′-ethylenebis-(salicylideneiminate), see Scheme 1) in bimetallic oxalate-based networks. In addition to the structural interest, these Mn^{III} complexes could confer novel properties to the hybrid materials, since these complexes have proven to be good building blocks for different magnetic materials such as single-chain magnets (SCM)[16] or single-molecule magnets (SMM)[17] thanks to their appropriate uniaxial anisotropy with a well-defined easy axis of the magnetization. In fact, dimers of this type of cation may present an SMM behavior. Therefore, coexistence of SMM of the inserted cation with the magnetic ordering from the oxalate network could be expected, if the dimer structure of the precursor is preserved.

In the present case, we show that monomeric Mn^{III} species, instead of dimeric ones, are inserted into the bimetallic oxalate networks in all cases. Furthermore, the use of a chiral salen derivative ($salmen^{2-}$ = *N*,*N*′-(1-methylethylene)bis(salicylideneiminate)) having a chiral quaternary carbon leads to the introduction of chirality into these hybrid magnets. A similar strategy has been successfully used to prepare enantiopure oxalate-based magnets, in which the combination of magnetic ordering and chirality leads to new properties such as the magneto-chiral dichroic effect and magnetisation-induced second harmonic generation.[18]

The compounds obtained with these Mn^{III} templating cations present different types of bimetallic oxalate networks: a 2D chiral structure in **(*S*)-1** and **(*R*)-1**, an achiral 3D oxalate network in **(*S*)-2** and **(*R*)-2**, a 3D chiral network in **3** and a 2D achiral network in **4**. The structures and magnetic properties of these compounds are presented in this paper.

Experimental section

Synthesis

The complexes $[Mn(salpn)]ClO_4$,[19] $[Mn((R)\text{-salmen})]ClO_4$, $[Mn((S)\text{-salmen})]ClO_4$ and $[Mn(saltmen)]ClO_4$[20] have been prepared according to literature methods. $Ag_3[Cr(ox)_3]$ was prepared by metathesis from the corresponding potassium salt.[21] All other materials and solvents were commercially available and used without further purification.

$[Mn((R)\text{-salmen})(CH_3OH)(CH_3CN)][MnCr(ox)_3](CH_3OH)_{0.5}(CH_3CN)_{1.25}$ (**(*R*)-1**), $[Mn((S)\text{-salmen})(CH_3OH)(CH_3CN)][MnCr(ox)_3](CH_3OH)_{0.5}(CH_3CN)_{1.25}$ (**(*S*)-1**), $[Mn((R)\text{-salmen})(CH_3OH)_2][MnCr(ox)_3](CH_2Cl_2)_{0.375}(CH_3OH)_{0.125}(H_2O)_{0.375}$ (**(*R*)-2**) and $[Mn((S)\text{-salmen})(CH_3OH)_2][MnCr(ox)_3](CH_2Cl_2)_{0.375}(CH_3OH)_{0.375}(H_2O)_{0.125}$ (**(*S*)-2**). Crystals of these compounds were obtained by slow diffusion of two solutions. The first solution was prepared by adding $MnCl_2{\cdot}4H_2O$ (0.036 g, 0.182 mmol) to a suspension of $Ag_3Cr(ox)_3$ (0.077 g, 0.12 mmol) in 6 mL of methanol. The AgCl precipitate was filtered. The second solution was obtained by dissolving $[Mn((R)\text{-salmen})]\text{-}ClO_4$ or $[Mn((S)\text{-salmen})]ClO_4$ (0.052 g, 0.12 mmol) in 6 mL of acetonitrile (**(*R*)-1** or **(*S*)-1**) or dichloromethane (**(*R*)-2** or **(*S*)-2**). After two weeks red crystals were obtained.

$[Mn(salpn)(CH_3OH)_{1.5}(CH_3CN)_{0.5}][MnCr(ox)_3](CH_3OH)_{0.82}(H_2O)_{0.93}$ (3). Crystals of this compound were obtained by slow diffusion of two solutions. The first solution was prepared by adding $MnCl_2{\cdot}4H_2O$ (0.036 g, 0.182 mmol) to a suspension of $Ag_3Cr(ox)_3$ (0.077 g, 0.12 mmol) in 6 mL of methanol. The AgCl precipitate was filtered. The second solution was obtained by dissolving $[Mn(salpn)]ClO_4$ (0.052 g, 0.12 mmol) in 6 mL of acetonitrile. After two weeks red crystals were obtained.

$[Mn(saltmen)(CH_3OH)(CH_3CN)][MnCr(ox)_3](CH_3OH)$ (4). Crystals of this compound were obtained by slow diffusion of two solutions. The first solution was prepared by adding $MnCl_2{\cdot}4H_2O$ (0.036 g, 0.182 mmol) to a suspension of $Ag_3Cr(ox)_3$ (0.077 g, 0.12 mmol) in 6 mL of methanol. The AgCl precipitate was filtered. The second solution was obtained by dissolving $[Mn(saltmen)]ClO_4$ (0.057 g, 0.12 mmol) in 6 mL of acetonitrile. After two weeks red crystals were obtained.

Structural characterisation

Single crystal X-ray data of **(*R*)-1**, **(*S*)-1**, **(*R*)-2**, **(*S*)-2**, **3** and **4** were collected at 120 K on a Xcalibur, Sapphire3, Gemini diffractometer equipped with a graphite-monochromated Enhance (Mo) X-ray Source (λ = 0.71073 Å). The program CrysAlisPro, Oxford Diffraction Ltd., Version 1.171.33.52 was used for cell refinements and data reduction of the compounds. Empirical absorption correction was performed using spherical harmonics, implemented in a SCALE3 ABSPACK scaling algorithm. Crystal structures were solved by direct methods with the SIR97 program,[22] and refined against all F^2 values with the SHELXL-97 program,[23] using the WinGX graphical user interface.[24] **(*R*)-1**, **(*S*)-1**, **(*R*)-2**, **(*S*)-2** and **3** exhibit a Flack's absolute parameter (x) close to 0.[25] This parameter lies within the range that indicates that the absolute structure is valid and that the five crystals are enantiopure. Non-hydrogen atoms were refined anisotropically, and hydrogen atoms were placed in calculated positions refined using idealized geometries (riding model) and assigned fixed isotropic displacement parameters. The use of restraints and/or constraints in the refinement of the structures is documented in the corresponding CIFs. Data

Table 1 Crystallographic data for compounds **(*R*)-1**, **(*S*)-1**, **(*R*)-2** and **(*S*)-2**

Compound	**(*R*)-1**	**(*S*)-1**	**(*R*)-2**	**(*S*)-2**
Empirical formula	$C_{116}Cr_4Mn_8H_{109}O_{62}N_{17}$	$C_{116}Cr_4Mn_8H_{109}O_{62}N_{17}$	$Cl_3C_{103}Cr_4Mn_8H_{105}O_{66}N_8$	$Cl_3C_{103}Cr_4Mn_8H_{104}O_{66}N_8$
Formula weight	3380.72	3380.72	3226.52	3250.71
Crystal color	Red	Red	Red	Red
Temperature (K)	120(2)	120(2)	120(2)	120(2)
Wavelength (Å)	0.71073	0.71073	0.71073	0.71073
Crystal system, *Z*	Monoclinic, 1	Monoclinic, 1	Triclinic, 1	Triclinic, 1
Space group	$P2_1$	$P2_1$	$P\bar{1}$	$P\bar{1}$
a (Å)	9.2943(3)	9.2926(3)	15.2933(9)	15.2780(8)
b (Å)	32.5932(10)	32.5571(12)	15.5985(8)	15.5600(7)
c (Å)	11.8266(5)	11.8060(4)	18.1942(6)	18.1740(10)
α (°)	90	90	64.685(4)	64.665(5)
β (°)	90.608(3)	90.596(3)	77.986(4)	78.123(5)
γ (°)	90	90	61.077(6)	61.048(5)
V (Å^3)	3582.4(2)	3571.6(2)	3434.1(3)	3416.9(3)
ρ_{calc} (Mg m^{-3})	1.567	1.572	1.560	1.580
μ ($Mo_{K\alpha}$) (mm^{-1})	1.067	1.070	1.166	1.172
θ range (°)	2.28 to 32.32	2.87 to 30.57	2.38 to 25.00	2.90 to 28.39
Reflns collected	23 467	21 833	16 820	33 799
Independent reflns, (R_{int})	9049 (0.0903)	15 172 (0.0745)	11 661 (0.0290)	21 970 (0.0547)
L. S. parameters/restraints	923/4	937/4	1679/84	1639/6
$R_1(F)$,[a] $I > 2\sigma(I)$]	0.0455	0.0591	0.0539	0.0777
w$R_2(F^2)$,[b] all data	0.0881	0.1421	0.1415	0.2415

[a] $R_1(F) = S(||F_o| - |F_c||)/S|F_o|$. [b] $wR_2(F^2) = [Sw(F_o^2 - F_c^2)^2/SwF_o^4]^{1/2}$.

Table 2 Crystallographic data for compounds **3** and **4**

Compound	**3**	**4**
Empirical formula	$C_{105.28}Cr_4Mn_8H_{97.85}O_{69}N_{10}$	$C_{30}CrMn_2H_{32}O_{16}N_3$
Formula weight	3254.72	852.4748
Crystal color	Red	Red
Temperature (K)	120(2)	120(2)
Wavelength (Å)	0.71073	0.71073
Crystal system, *Z*	Orthorhombic, 2	Triclinic, 2
Space group	$P2_12_12_1$	$P\bar{1}$
a (Å)	14.5286(4)	9.5551(5)
b (Å)	20.8778(7)	11.8076(5)
c (Å)	22.7570(6)	15.8509(8)
a (Å)	90	101.420(4)
β (°)	90	95.207(4)
γ (°)	90	93.581(4)
V (Å^3)	6902.8(4)	1739.77(15)
ρ_{calc} (Mg m^{-3})	1.567	1.627
μ ($Mo_{K\alpha}$) (mm^{-1})	1.107	1.099
θ range (°)	2.27 to 32.45	2.40 to 32.50
Reflns collected	22 093	11 477
Independent reflns (R_{int})	7809 (0.0906)	3715 (0.1077)
L. S. parameters/restraints	886/2	473/0
$R_1(F)$,[a] $I > 2\sigma(I)$]	0.0445	0.0576
w$R_2(F^2)$,[b] all data	0.0944	0.1023

[a] $R_1(F) = S(||F_o| - |F_c||)/S|F_o|$; [b] $wR_2(F^2) = [Sw(F_o^2 - F_c^2)^2/SwF_o^4]^{1/2}$;

collection and refinement statistics are collected in Tables 1 and 2.

Physical measurements

Magnetic susceptibility measurements were performed on polycrystalline samples using a magnetometer (Quantum Design MPMS-XL-5) equipped with a SQUID sensor. Variable-temperature measurements were carried out in the temperature range 2–300 K. The AC measurements were performed in the temperature range 2–10 K at different frequencies with an oscillating magnetic field of 0.395 mT. The magnetisation and hysteresis studies were performed between 5 and −5 T, cooling the samples at zero field. The Mn : Cr ratios were measured on a Philips ESEM X230 scanning electron microscope equipped with an EDAX DX-4 microsonde.

Results

Synthesis

The following compounds $[Mn((R)\text{-salmen})(CH_3OH)(CH_3CN)][MnCr(ox)_3](CH_3OH)_{0.5}(CH_3CN)_{1.25}$ (**(*R*)-1**), $[Mn((S)\text{-salmen})(CH_3OH)(CH_3CN)][MnCr(ox)_3](CH_3OH)_{0.5}(CH_3CN)_{1.25}$ (**(*S*)-1**), $[Mn((R)\text{-salmen})(CH_3OH)_2][MnCr(ox)_3](CH_2Cl_2)_{0.375}(CH_3OH)_{0.125}(H_2O)_{0.375}$ (**(*R*)-2**), $[Mn((S)\text{-salmen})(CH_3OH)_2][MnCr(ox)_3](CH_2Cl_2)_{0.375}(CH_3OH)_{0.375}(H_2O)_{0.125}$ (**(*S*)-2**) (salmen^{2-} = *N*,*N*′-(1-methylethylene)bis(salicylideneiminate)), $[Mn(salpn)(CH_3OH)_{1.5}(CH_3CN)_{0.5}][MnCr(ox)_3](CH_3OH)_{0.82}(H_2O)_{0.93}$ (**3**) (salpn^{2-} = *N*,*N*′-(propane)bis(salicylideneiminate)) and $[Mn(saltmen)(CH_3OH)(CH_3CN)][MnCr(ox)_3](CH_3OH)$ (**4**) (saltmen^{2-} = *N*,*N*′-(1,1,2,2-tetramethylethylene)bis(salicylideneiminate)) have been obtained.

The method used to prepare this family of compounds is analogous to that used to prepare other oxalate-based 2D and 3D $[M^{II}M^{III}(ox)_3]$ compounds. It is based on a slow diffusion in two phases. The first one containing $[Cr(ox)_3]^{3-}$ and Mn^{2+} ions is obtained after filtering a suspension of $Ag_3[Cr(ox)_3]$ and $MnCl_2$ in methanol. The second one is a solution of the Mn^{III} precursor in different solvents (CH_3CN for **(*S*)-1**, **(*R*)-1**, **3** and **4** and CH_2Cl_2 for **(*S*)-2** and **(*R*)-2**). In all cases, monomeric Mn^{III} species instead of dimers have been formed. This result

contrasts with what has been found for other salts of these cations.[16,17] The reason may be the presence of two coordinating solvent molecules (CH_3OH or CH_3CN) in the apical positions of Mn^{III}, which prevents the formation of dimeric cations. Notice that with an unsubstituted $[Mn^{III}(salen)]^+$ templating cation, an achiral 3D bimetallic oxalate network with inserted $[Mn^{III}(salen)(H_2O)]_2^{2+}$ dimers is obtained.[26] It seems, therefore, that the small increase in the size of the precursors used in this work with respect to $[Mn^{III}(salen)]^+$ prevents the insertion of dimeric cations within the bimetallic oxalate network. Thus, although both monomer and dimer species may be in equilibrium in solution, only the monomer with two coordinated solvent molecules is inserted into bimetallic oxalate 2D or 3D structures for $[Mn((R)\text{-salmen})]^+$, $[Mn((S)\text{-salmen})]^+$, $[Mn(salpn)]^+$ or $[Mn(saltmen)]^+$.

Two different types of structures have been obtained with $[Mn((R)\text{-salmen})]^+$ or $[Mn((S)\text{-salmen})]^+$ templating cations depending on the solvent used to dissolve this cation. Acetonitrile affords a chiral 2D bimetallic oxalate network whereas dichloromethane, nitromethane or acetone give rise to an achiral 3D network. Interestingly, the use of the same templating cation in different solvents affords different structures. This finding is very unusual for this type of oxalate compound. The other example in which this occurs involves a flexible templating cation such as $[Fe(sal_2\text{-trien})]^+$.[10b] This complex gives rise to a 2D or achiral 3D structure depending on the solvent. As the relative orientation of the two phenoxy arms of this complex differs notably in the two compounds, we have proposed that these differences in the configuration caused by the different solvent molecules explain the different templating effects on the oxalate network. In the case of $[Mn((R)\text{-salmen})]^+$ or $[Mn((S)\text{-salmen})]^+$ cations, the different templating effects in the various solvents may be related to the presence of different solvent molecules coordinated to Mn^{III} in the two apical positions. Thus, the 3D structures of **(*R*)-2** and **(*S*)-2** contain only $[Mn((R/S)\text{-salmen})(CH_3OH)_2]^+$ cations, whereas the 2D ones of **(*R*)-1** and **(*S*)-1** contain also $[Mn((R/S)\text{-salmen})(CH_3CN)_2]^+$ cations together with $[Mn((R/S)\text{-salmen})(CH_3OH)_2]^+$ cations. It seems, therefore, that the acetonitrile solvent used in the syntheses of **(*R*)-1** and **(*S*)-1** enters in the coordination sphere of some Mn^{III} complexes and changes its templating effect.

Structure of (*R*)-1 and (*S*)-1

These compounds crystallize in the chiral space group $P2_1$. The structure is formed by bimetallic anionic sheets in the *ab* plane presenting a honeycomb pseudo-hexagonal structure alternating with layers containing $[Mn((R)\text{-salmen})(CH_3OH)_2]^+$ and $[Mn((R)\text{-salmen})(CH_3CN)_2]^+$ cations and solvent molecules (Fig. 1).

The anionic layer is formed by an extended network of Mn^{II} and Cr^{III} ions linked through oxalate bridges in such a way that each Mn^{II} is surrounded by three neighbouring Cr^{III} and *vice versa* (Fig. 2). The Mn^{II} and Cr^{III} are clearly distinguishable as they present different bond distances with oxalate ligands. Thus, there are two crystallographically independent Mn ions (Mn1 and Mn2) with Mn–O distances lying between 2.148(3) and 2.219(3) Å for **(*R*)-1**, and 2.143(3) and 2.203(3) Å for **(*S*)-1**, and two crystallographically independent Cr ions (Cr1 and Cr2) with Cr–O distances lying between 1.963(3) and 1.990(3) Å for **(*R*)-1**, and 1.966(3) and 1.992(3) for **(*S*)-1**. These are typical Mn^{II}–O and Cr^{III}–O distances similar to those found in other oxalate networks. The neighbouring metal centres of these layers present alternated chirality as usual for this type of network. In the structure of **(*R*)-1** all the Cr^{III} ions adopt a *Λ*-configuration, whereas all the Mn^{II} adopt the *Δ*-one. In contrast, in that of **(*S*)-1** all the Cr^{III} ions adopt a *Δ*-configuration, whereas all the Mn^{II} adopt the *Λ*-one. Therefore, the configuration of each metal ion is preserved in the neighbouring oxalate layers and it is opposite in the two structures. Interestingly, although we have started from a racemic mixture of $[Cr(ox)_3]^{3-}$ anions, crystals of only one of the two enantiomers have been obtained. The minimum distance between metals of different layers is 11.8266(5) Å for **(*R*)-1** and 11.8060(4) for **(*S*)-1**, defined by the *c* parameter, which is higher than those found in other oxalate-based 2D compounds with decamethylferrocenium or alkylammonium cations (9.2–9.7 Å),[2,4] but similar to that of the 2D compounds obtained by insertion of bulkier $[Fe^{III}(sal_2\text{-trien})]^+$ (11.6440(2) Å) cations and derivatives.[10b] These oxalate-based layers are stacked one over the other in an *AA*... fashion defining hexagonal channels running along the *c* axis.

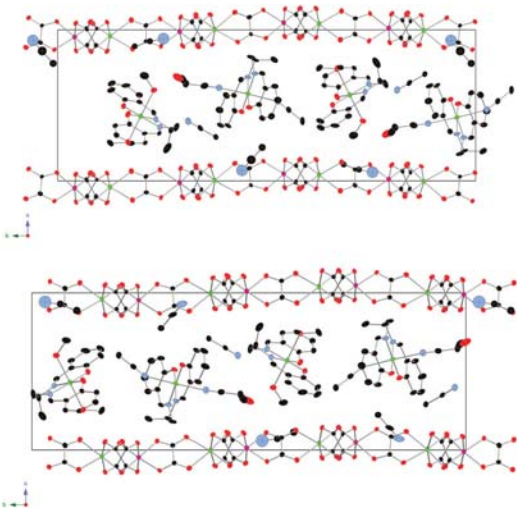

Fig. 1 Projection of **(*R*)-1** (up) and **(*S*)-1** (down) in the *bc* plane. (Cr (pink), Mn (green) C (black), N (blue), O (red)). Hydrogen atoms have been omitted for clarity.

The cationic layer intercalated between these oxalate layers is formed by two Mn^{III} complexes, $[Mn((R)\text{-salmen})(CH_3OH)_2]^+$ and $[Mn((R)\text{-salmen})(CH_3CN)_2]^+$ for **(*R*)-1**, and $[Mn((S)\text{-salmen})(CH_3OH)_2]^+$ and $[Mn((S)\text{-salmen})(CH_3CN)_2]^+$ cations for **(*S*)-1** and acetonitrile and methanol solvent molecules. There are two crystallographically independent Mn ions (Mn3 and Mn4). Both Mn present a distorted octahedral geometry, in which the

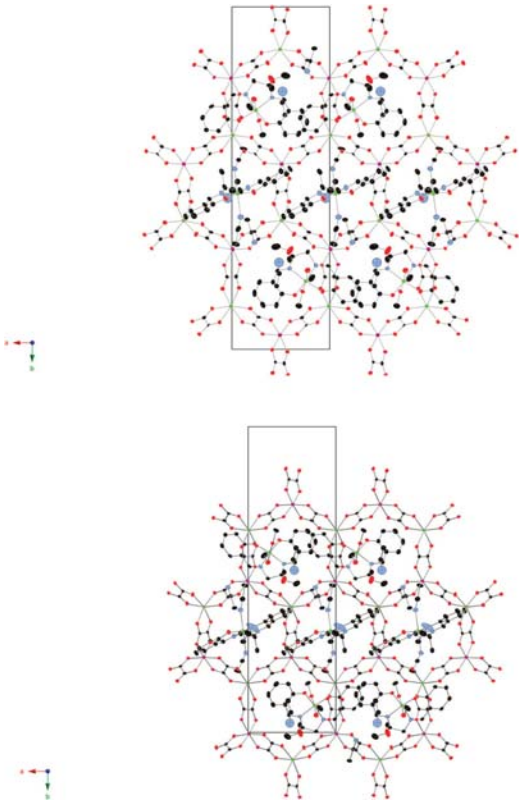

Fig. 2 Projection of **(*R*)-1** (up) and **(*S*)-1** (down) in the *ab* plane. (Cr (pink), Mn (green) C (black), N (blue), O (red)). Hydrogen atoms have been omitted for clarity.

basal plane is formed by the coordination of the two imino nitrogens and the two phenolic oxygens from the salmen Schiff base. The two apical positions of Mn3 are occupied by the nitrogen atoms of two acetonitrile solvent molecules, whereas those of Mn4 are occupied by the oxygen atoms of two methanol solvent molecules. In these two Mn^{III} cations, the apical Mn–N (2.316(4) and 2.423(4) Å for **(*R*)-1**, and 2.339(4) and 2.414(4) Å for **(*S*)-1**) or Mn–O distances (2.295(3) and 2.309(3) Å for **(*R*)-1**, and 2.300(4) and 2.301(3) Å for **(*S*)-1**) are longer than the basal Mn–N (1.956(4)–1.982(4) Å for **(*R*)-1**, and 1.966(4)–1.978(4) Å for **(*S*)-1**) and Mn–O (1.867(3)–1.886(3) Å for **(*R*)-1** and 1.873(3)–1.883(3) for **(*S*)-1**) ones as expected for Jahn–Teller distortion. Neighbouring $[Mn((R)\text{-salmen})(CH_3OH)_2]^+$ or $[Mn((S)\text{-salmen})(CH_3OH)_2]^+$ complexes present π–π stacking interactions through the two phenoxy rings forming a chain that runs along the *a* axis. Coordinated CH_3OH molecules from these complexes form hydrogen bonds with the oxalate network and a non-coordinated CH_3OH molecule. $[Mn((R)\text{-salmen})(CH_3CN)_2]^+$ (or $[Mn((S)\text{-salmen})(CH_3CN)_2]^+$) cations present one short contact with a neighbouring $[Mn((R)\text{-salmen})(CH_3OH)_2]^+$ (or $[Mn((S)\text{-salmen})(CH_3OH)_2]^+$) complex through the coordinated acetonitrile molecule. $[Mn((R)\text{-salmen})(CH_3CN)_2]^+$ (or $[Mn((S)\text{-salmen})(CH_3CN)_2]^+$) cations present short contacts with the oxalate network and acetonitrile and solvent molecules. Acetonitrile and methanol solvent molecules occupy the holes between the cations and the bimetallic oxalate network.

Structure of (*R*)-2 and (*S*)-2

(*R*)-2 and **(*S*)-2** crystallise in the chiral triclinic space group *P*1. The structure is formed by an anionic 3D polymeric oxalate-bridged bimetallic network with $[Mn((R)\text{-salmen})(CH_3OH)_2]^+$ or $[Mn((S)\text{-salmen})(CH_3OH)_2]^+$ cations and solvent molecules occupying the cavities (Fig. 3). This anionic polymeric structure is formed by bis-chelating oxalate ligands connecting Mn^{II} and Cr^{III} ions in such a way that each Mn^{II} is surrounded by three Cr^{III} and *vice versa*. This oxalate network contains Mn and Cr ions of both chiralities. In the bimetallic oxalate network there are four crystallographically independent Mn^{II} ions (Mn1, Mn2, Mn3 and Mn4) with Mn–O distances lying between 2.132(5) and 2.212(6) Å for **(*R*)-2** and 2.127(6) and 2.197(6) Å for **(*S*)-2**, and four crystallographically independent Cr^{III} ions (Cr1, Cr2, Cr3 and Cr4) with Cr–O distances lying between 1.942(5) and 1.990(5) Å for **(*R*)-2** and 1.947(5) and 1.999(5) Å for **(*S*)-2**. These are typical Cr^{III}–O and Mn^{II}–O distances similar to those found in other oxalate networks. In the two compounds, there are half of Mn^{II} and Cr^{III} ions of both chiralities. Therefore, the two compounds present an achiral 3D oxalate-based network. This type of 3D achiral network is formed by helical strands that contain metals of one chirality running along the *b* axis. Thus, four of the eight crystallographically independent Mn and Cr ions (Cr1, Cr4, Mn2 and Mn4 in **(*R*)-2** and Cr3, Cr4 Mn2 and Mn3 in **(*S*)-2**) form a helical strand of Δ complexes, whereas the other four ones (Cr2, Cr3, Mn1 and Mn3 in **(*R*)-2** and Cr1, Cr2, Mn1 and Mn4 in **(*S*)-2**) form a helical strand of Λ ones. Neighbouring helical strands, which are linked through oxalate ligands, present opposite chirality (see Fig. 4). In other achiral 3D oxalate networks of formulae $[Fe(bpp)_2][MnCr(ox)_3]_2\cdot bpp\cdot CH_3OH$,[14] $[Fe^{III}(sal_2\text{-trien})][Mn^{II}Cr^{III}(ox)_3]\cdot(CH_3OH)$, $[In^{III}(sal_2\text{-trien})][Mn^{II}Cr^{III}(ox)_3]\cdot$

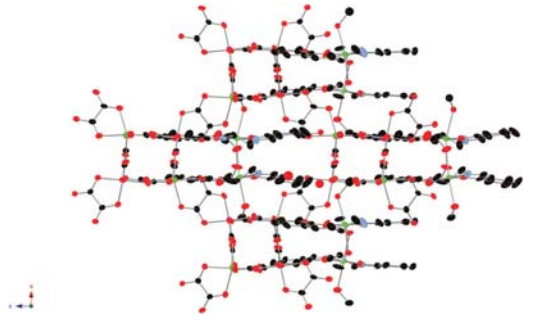

Fig. 3 Projection of **(*R*)-2** in the *ac* plane. (Cr (pink), Mn (green) C (black), N (blue), O (red)). Hydrogen atoms and disordered solvent molecules have been omitted for clarity.

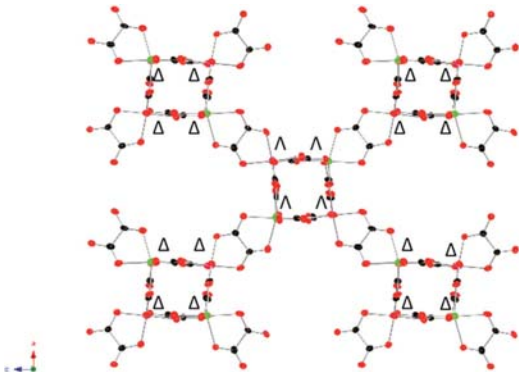

Fig. 4 Neighbouring helical strands of opposite chirality linked through oxalate ligands in (**(*R*)-2**).

$0.25(H_2O)\cdot0.25(CH_3OH)\cdot0.25(CH_3CN)$, $[In^{III}(sal_2\text{-trien})][Mn^{II}Cr^{III}(ox)_3]\cdot(CH_3NO_2)\cdot0.5(H_2O)$[10b] and $[Fe^{III}(5\text{-}CH_3Osal_2\text{-trien})][Mn^{II}Cr^{III}(ox)_3]$,[10c] the neighbouring helical strands present the same chirality. This gives rise to 10,3 decagons with metals of the same chirality that are linked to another 10,3 decagon of opposite chirality. In contrast to this, in the structures of **(*R*)-2** and **(*S*)-2**, it is not possible to find 10,3 decagons formed by metals of the same chirality.

$[Mn((R)\text{-salmen})(CH_3OH)_2]^+$ and $[Mn((S)\text{-salmen})(CH_3OH)_2]^+$ cations and solvent molecules are intercalated in the holes described by this 3D oxalate network. There are four crystallographically independent $[Mn((R)\text{-salmen})(CH_3OH)_2]^+$ and $[Mn((S)\text{-salmen})(CH_3OH)_2]^+$ complexes (Mn5, Mn6, Mn7 and Mn8) and disordered dichloromethane, methanol and water molecules. The four Mn present a distorted octahedral geometry similar to that found in compounds **(*R*)-1** and **(*S*)-1**, in which the basal plane is formed by the coordination of the two imino nitrogens and the two phenolic oxygens from the salmen Schiff base. In contrast to **(*R*)-1** and **(*S*)-1**, there is only one type of complex, in which the two apical positions are occupied by the oxygen atoms of two methanol solvent molecules. In these four Mn^{III} cations, the apical Mn–O distances (between 2.230(5) and 2.384(11) Å for **(*R*)-2**, and 2.233(6) and 2.338(13) Å for **(*S*)-2**) are longer than the basal Mn–N (between 1.971(7) and 2.005(7) Å for **(*R*)-2** and 1.962(8) and 2.007(6) Å for **(*S*)-2**) or Mn–O (between 1.846(6) and 1.915(5) Å for **(*R*)-2** and 1.838(6) and 1.914(5) Å for **(*S*)-2**) ones as expected for Jahn–Teller distortion. Two neighbouring $[Mn((R)\text{-salmen})(CH_3OH)_2]^+$ or $[Mn((S)\text{-salmen})(CH_3OH)_2]^+$ form a dimer linked through short intermolecular contacts (Mn5 and Mn6 and Mn7 and Mn8). Thus, each pair of the four crystallographically independent $[Mn((R)\text{-salmen})(CH_3OH)_2]^+$ or $[Mn((S)\text{-salmen})(CH_3OH)_2]^+$ complexes presents two hydrogen bonds between an oxygen atom of the phenoxy ring and coordinated methanol of the neighbouring complex (see Fig. S1, ESI†). Furthermore, Mn5 and Mn6 in **(*R*)-2** and Mn7 and Mn8 in **(*S*)-2** present π–π stacking interactions through the two phenoxy rings. On the other hand, there are numerous short contacts between the Mn^{III} complexes and the oxalate network. In most of them, the methyl group and hydrogen from the asymmetric carbon from the complexes are implied. Some of these interactions could be responsible for the formation of the chiral helical strands. Disordered dichloromethane, methanol and water solvent molecules occupy the holes between the cations and the bimetallic oxalate network. The distribution of these disordered solvent molecules changes slightly in the two compounds.

Structure of 3

3 crystallizes in the chiral space group $P2_12_12_1$. As a racemic mixture of $[Cr(ox)_3]^{3-}$ ions has been used in the synthesis, crystals of both chiralities are obtained. The structure is formed by an anionic 3D polymeric oxalate-bridged bimetallic network with $[Mn^{III}(salpn)(CH_3CN)(CH_3OH)]^+$ and $[Mn^{III}(salpn)(CH_3OH)_2]^+$ cations and disordered methanol and acetonitrile solvent molecules occupying the cavities (Fig. 5). This anionic polymeric structure presents the well-known 3D 3-connected 10-gon oxalate-based anionic network (10,3) which is formed by oxalate ligands connecting Mn^{II} and Cr^{III} ions in such a way that each Mn^{II} is surrounded by three Cr^{III} and *vice versa* with all metal ions presenting the same chirality (*Λ* in the crystal used to solve the structure).

Similar 3D chiral oxalate-based networks have been obtained in compounds $[Ni(phen)_3][NaCo(dto)_3]\cdot C_3H_6O$[27] (phen = phenanthroline, dto = 1,2 dithiooxalate) and $[Fe^{III}(5\text{-X-}sal_2\text{-trien})][Mn^{II}Cr^{III}(ox)_3]$ (X = Cl, Br) that crystallize in the same space group as that of **3**.[10d] The orthorhombic 3D oxalate chiral networks of these compounds present the same connectivity as the cubic ones obtained with the smaller templating cation, $[Z^{II}(bpy)_3]^{2+}$,[3] with some differences as a consequence of the lowering in symmetry. In contrast with the other cubic heterometallic derivatives, in the structure of **3** there are two crystallographically independent Mn^{II} ions (Mn3 and Mn4) with Mn–O distances lying between 2.148(3) and 2.212(3) Å

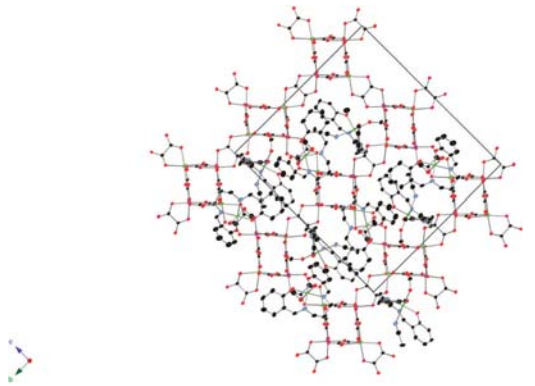

Fig. 5 Projection of **3** in the *bc* plane. (Cr (pink), Mn (green) C (black), N (blue), O (red)). Hydrogen atoms and disordered solvent molecules have been omitted for clarity.

and two crystallographically independent Cr^{III} ions (Cr1 and Cr2) with Cr–O distances lying between 1.960(3) and 1.980(3) Å. Metal–metal distances between adjacent centers are in the 5.359–5.414 Å range. The bimetallic oxalate network of **3** defines channels that run along [100] (*a* axis) formed by helical strands of *Λ* complexes linked through oxalate ligands (see Fig. 5). Furthermore, it forms channels perpendicular to the previous one running along [011] and [01$\bar{1}$] axes (see Fig. S2 and S3, ESI†). This result is in contrast with the previously described orthorhombic chiral 3D oxalate networks in which the channels run along *a*, *b* and *c* axes. This is due to the larger unit cell of **3** compared with those of the previous compounds.

The holes described by this 3D oxalate network are occupied by two Mn^{III} complexes, $[Mn(salpn)(CH_3OH)_2]^+$ and $[Mn(salpn)(CH_3CN)(CH_3OH)]^+$ and disordered methanol and water solvent molecules. There are two crystallographically independent Mn ions (Mn1 and Mn2). Both Mn present a distorted octahedral geometry similar to that exhibited by Mn^{III} complexes in **1** and **2**. Thus, the two apical positions of Mn1 are occupied by one acetonitrile and methanol molecule, while those of Mn2 are occupied by two methanol solvent molecules. In this last case, one of the two coordinated methanol solvent molecules presents a disorder between two possible configurations. The apical Mn–N (2.405(4) Å) or Mn–O distances (between 2.180(3) and 2.246(3) Å) are longer than the basal Mn–N (between 2.011(4) and 2.026(4) Å) and Mn–O (1.867(3)–1.903(3) Å) ones as expected for Jahn–Teller distortion. Two neighbouring $[Mn(salpn)(CH_3OH)_2]^+$ and $[Mn(salpn)(CH_3CN)(CH_3OH)]^+$ molecules are linked through two hydrogen bonds between the oxygen atom of one of the phenoxy rings and coordinated methanol of the neighbouring complex (see Fig. S4, ESI†). Furthermore, the other phenoxy ring is involved in a CH–π interaction with another $[Mn(salpn)(CH_3CN)(CH_3OH)]^+$ or $[Mn(salpn)(CH_3OH)_2]^+$ molecule. Finally, there are numerous short contacts with the oxalate network and solvent molecules.

Structure of 4

4 crystallizes in the triclinic space group $P\bar{1}$. The structure of this compound is formed by anionic sheets in the *ac* plane with inter-lamellar $[Mn(saltmen)(CH_3CN)(CH_3OH)]^+$ and methanol solvent molecules (Fig. 6). The anionic layer is formed by an extended network with Mn^{II} and Cr^{III} ions linked through oxalate bridges. It presents the 2D honeycomb structure already described for **1**. The neighbouring metal centers of these layers present alternated chirality as usual for this type of networks. There are two metals crystallographically independent with M–O distances lying between 2.055(3) and 2.094(3) Å. These distances are intermediate between the ones expected for Cr^{III}–O and Mn^{II}–O. Therefore, it is not possible to distinguish between the two metals in this structure. This indicates that Mn^{II} and Cr^{III} ions in these structures may have (*Λ*) or (*Δ*) configurations in the different layers and that the structure is not chiral in contrast to that of **(*R*)-1** and **(*S*)-1**. The minimum distance between metals of different layers is 11.8076(5) Å, defined by the *b* parameter, which is similar to that of **(*R*)-1** and **(*S*)-1**, as expected taking into account the similar size of the inserted cations in the two compounds. These oxalate-based layers are stacked one over the other in an *AA*... fashion defining hexagonal channels running along the *b* axis (see Fig. S5, ESI†).

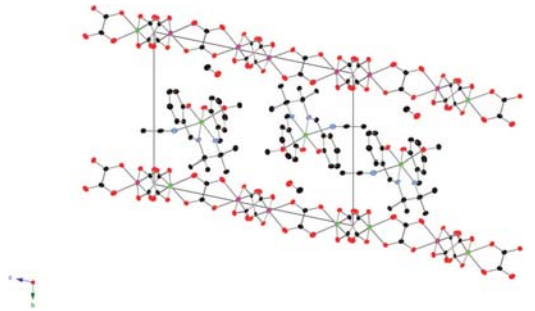

Fig. 6 Projection of **4** in the *bc* plane. (Cr (pink), Mn (green) C (black), N (blue), O (red)). Hydrogen atoms have been omitted for clarity.

The cationic layer intercalated between these oxalate layers is formed by $[Mn(saltmen)(CH_3CN)(CH_3OH)]^+$ cations and methanol solvent molecules. $[Mn(saltmen)(CH_3CN)(CH_3OH)]^+$ complexes are close to the center of the hexagonal channels of the bimetallic oxalate network mentioned above. There is one crystallographically independent Mn ion (Mn1). It presents a distorted octahedral geometry as in the previous compounds. One of the two apical positions of this ion is occupied by an acetonitrile solvent molecule, while the second one is occupied by a methanol solvent molecule. Again, the Mn–N (1.972(3) and 1.980(3) Å) and Mn–O (1.878(3) and 1.887(3) Å) basal distances are shorter than the apical ones (2.490(4) and 2.271(3) Å respectively) due to Jahn–Teller distortion. Two neighbouring $[Mn(saltmen)(CH_3CN)(CH_3OH)]^+$ complexes present two CH–π interactions between one methyl group from the 1,1,2,2-tetramethylethylene group and the phenoxy ring of the neighbouring complex forming a dimer. On the other hand, coordinated CH_3CN on the other side of the complex presents numerous short contacts with a coordinated CH_3CN of another neighbouring $[Mn(saltmen)(CH_3CN)(CH_3OH)]^+$ complex. The coordinated CH_3OH molecule forms a hydrogen bond with the non-coordinated CH_3OH molecule, which occupies the holes between the oxalate network and the Mn^{III} complexes. Finally, the $[Mn(saltmen)(CH_3CN)(CH_3OH)]^+$ complex presents several short contacts with the oxalate network and the non-coordinated CH_3OH, which forms a hydrogen bond with the oxalate network.

Magnetic properties

The temperature dependence of the product of the magnetic susceptibility times the temperature (χT) under an applied field of 0.1 mT for the six compounds is shown in Fig. 7 and SI6, ESI.† They present a similar behavior with χT values of 9.2–9.4 emu K mol^{-1} at 300 K in agreement with the expected

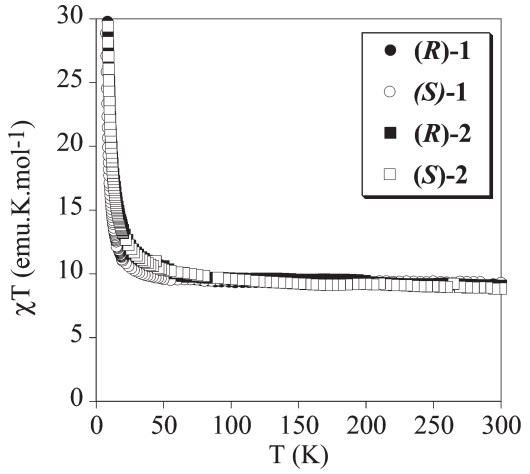

Fig. 7 Temperature dependence of the product of the molar magnetic susceptibility with temperature (χT) at 0.1 T for compounds **(*R*)-1** (full circles), **(*S*)-1** (empty circles), **(*R*)-2** (full squares) and **(*S*)-1** (empty squares).

Table 3 Magnetic parameters for compounds **(*R*)-1**, **(*S*)-1**, **(*R*)-2**, **(*S*)-2**, **3** and **4**

Compound	T_c (K)	θ (K)	C (emu K mol^{-1})	M (μ_B) at 5 T and 2 K	H_{coer} (mT) at 2 K
(*R*)-1	5.5	5.5	9.0	10.2	0.8
(*S*)-1	5.5	3.5	9.3	10.2	0.2
(*R*)-2	5.2	7.0	9.1	10.8	1.9
(*S*)-2	5.2	7.7	8.8	11.2	1.8
3	5.4	2.8	8.8	9.5	1.4
4	5.6	6.0	9.4	10.4	1.3

value for non-interacting high-spin Mn^{III} (S = 2), high-spin Mn^{II} (S = 5/2) and Cr^{III} (S = 3/2) ions. A gradual increase of the χT product upon cooling is observed from 300 to 30 K. Below this temperature there is a sharp increase of the χT product. χ follows a Curie–Weiss law between 20 and 300 K with C and θ values shown in Table 3. This indicates the presence of ferromagnetic interactions between neighbouring M^{II}–Cr^{III} magnetic ions and the onset of long-range ferromagnetic ordering, as observed for other $Mn^{II}Cr^{III}$ 2D and 3D oxalate compounds. To confirm the presence of long-range magnetic ordering and to determine precisely the critical temperature (T_c), ac susceptibility measurements were carried out. As expected for samples presenting an ordered state, a maximum in the in-phase signal (χ') near T_c and an out-of-phase signal (χ'') that starts to appear at temperatures just below T_c is observed in the six compounds (Fig. 8, 9 and SI7–SI10, ESI†). From these data the T_c of the compounds is around 5 K, which is similar to that of other 2D or 3D $Mn^{II}Cr^{III}$ bimetallic oxalate networks (see Table 3). These signals are almost frequency independent for **(*R*)-1** and **(*S*)-1**, whereas the other compounds present a small frequency dependence that could be explained by the presence of an additional peak in χ'' at lower temperatures. These peaks have been observed in other 2D and 3D bimetallic

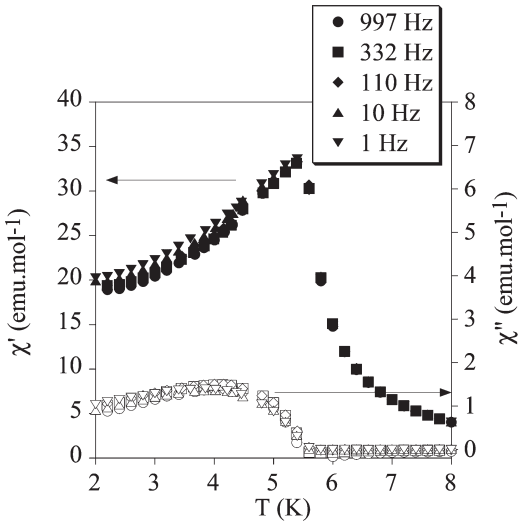

Fig. 8 Temperature dependence of the in-phase AC susceptibility (χ') (filled symbols) and the out-of-phase AC susceptibility (χ'') (empty symbols) for **(*R*)-1**.

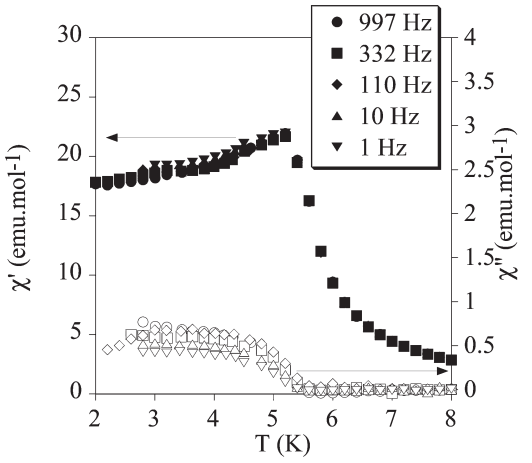

Fig. 9 Temperature dependence of the in-phase AC susceptibility (χ') (filled symbols) and the out-of-phase AC susceptibility (χ'') (empty symbols) for **(*S*)-1**.

oxalate compounds and can be related to the formation of magnetic domains and domain-wall movement.[10] The ferromagnetic ordering is also confirmed by the field dependence of the magnetisation (M) at 2 K. In all the compounds, it shows a sharp increase at low fields tending to saturation above 2 T and reaching maximum values lower than the expected value for a parallel alignment of the spins (12 μ_B) (see Fig. SI11–SI13, ESI†). The coercive fields at 2 K are close to 1 mT indicating that the compounds behave as soft ferromagnets (see Table 3).

In summary, the magnetic characterisation of the six compounds confirms the ferromagnetic ordering, which is very similar to that of other 2D and 3D bimetallic oxalate networks. On the other hand, the magnetic behavior of **(*R*)-1**, **(*S*)-1**, **(*R*)-2** and **(*S*)-2** indicates that, within the experimental error, neither T_c nor θ depend on the absolute configuration of the compounds, as observed in other enantiopure 2D bimetallic oxalate compounds.[18a]

Discussion

The use of derivatives of Mn^{III} salen-type complexes as templating cations has afforded different types of oxalate networks. Two different types of structures have been obtained with $[Mn((R)\text{-salmen})]^+$ or $[Mn((S)\text{-salmen})]^+$ that contain a chiral quaternary carbon atom depending on the solvent used to dissolve the cation. In acetonitrile, a chiral 2D bimetallic oxalate network has been obtained in compounds **(*R*)-1** and **(*S*)-1**, whereas in compounds **(*R*)-2** and **(*S*)-2**, a new type of achiral 3D network different from those reported before has been formed.

The enantioselective self-assembly of 2D oxalate-based compounds is a synthetic challenge due to the heterochiral arrangement of M^{II} and M^{III} ions in 2D structures.[13] In most of the reported 2D oxalato-bridged structures, M^{II} and M^{III} ions are disordered and it is not possible to distinguish among them. This contrasts with the structure of **(*R*)-1** and **(*S*)-1**, in which Cr^{III} and Mn^{II} of opposite configuration can be clearly differentiated as they present their characteristic M–O bond-length distances. Furthermore, Cr^{III} and Mn^{II} of the two compounds present the opposite configuration. Thus, in **(*R*)-1** all the Cr^{III} ions adopt a Λ-configuration, whereas all the Mn^{II} adopt the Δ-one. In contrast, in that of **(*S*)-1** all the Cr^{III} ions adopt a Δ-configuration, whereas all the Mn^{II} adopt the Λ-one. Therefore, the configuration of each metal ion is preserved in the neighbouring oxalate layers and it is opposite in the two structures. This is a very unusual and interesting result. In most of the chiral 2D bimetallic oxalate networks found in the literature, it is not possible to separate the two enantiomers, as for the 2D structures obtained with a chiral tetraalkyl ammonium with four different alkyl chains[13,28] and those obtained with Fe^{III} complexes of the hexadentate Schiff base ligands, 5-NO_2-sal$_2$-trien[10c] and 3-Cl-sal$_2$-trien.[29] Until now, only a tetraalkylammonium with one chiral alkyl chain appeared as a good chiral templating agent towards the formation of enantiopure 2D oxalate-based materials in compounds $[N((S)\text{-i-Bu})MePr_2][(\Lambda)Mn\text{-}(\Delta)Cr(ox)_3]$ (i-Bu = $CH(CH_3)\text{-}C_2H_5$; Me = CH_3; Pr = C_3H_7) and $[N((R)\text{-i-Bu})MePr_2][(\Delta)Mn\text{-}(\Lambda)Cr(ox)_3]$.[13,18a] As in this previous result, the chirality of the $[Mn((R)\text{-salmen})(CH_3OH)_2]^+$ and $[Mn((R)\text{-salmen})(CH_3CN)_2]^+$ complexes, due to the presence of a quaternary C atom, may be responsible for this first-order spontaneous resolution through chiral recognition between one of the enantiomers of $[Cr(ox)_3]^{3-}$ and $[Mn((S)\text{-salmen})(CH_3OH)_2]^+$ and $[Mn((S)\text{-salmen})(CH_3CN)_2]^+$ cations. In agreement with this, the methyl groups of $[Mn((R)\text{-salmen})(CH_3OH)_2]^+$ and $[Mn((R)\text{-salmen})(CH_3CN)_2]^+$ cations interact through several short contacts with the oxalate ligands.

On the other hand, the same templating chiral cations dissolved in a different solvent (dichloromethane, nitromethane or acetone) lead to a different network, a 3D structure with half of Mn^{II} and Cr^{III} ions of both chiralities, as that of compounds **(*R*)-2** and **(*S*)-2** obtained in dichloromethane. It seems then that the presence of acetonitrile is necessary to form the 2D structure of **(*R*)-2** and **(*S*)-2**. The different templating effects of this cation in acetonitrile are related to the coordination of acetonitrile molecules to some of the Mn^{III} complexes in **(*R*)-1** and **(*S*)-1**, which changes their templating effect. This 3D achiral network is different from other achiral 3D oxalate networks found in the literature.[10b,c,14] In contrast to them, it does not contain 10,3 decagons with neighbouring Mn^{II} and Cr^{III} metals of the same chirality linked to another 10,3 decagon of opposite chirality, but helical strands with metals of the same chirality running along the *c* axis, which are linked to helical strands of the opposite chirality. Therefore, in this case the use of a chiral precursor has led to a new type of 3D achiral structure.

Finally, the use of the achiral templating cations, $[Mn(salpn)]^+$ and $[Mn(salten)]^+$, gives rise to a chiral 3D network and an achiral 2D network respectively in compounds **3** and **4**. In the case of **3**, we have demonstrated that the formation of chiral oxalate-based networks is not limited to chiral templating cations. However, there is an important drawback of this strategy: crystals of both chiralities are obtained in the same synthesis in contrast to the obtention of enantiopure samples with the chiral precursors, $[Mn((R)\text{-salmen})]^+$ or $[Mn((S)\text{-salmen})]^+$, in **(*R*)-1** and **(*S*)-1**.

From the point of view of the physical properties, since all the derivatives of $[Mn^{III}(salen)]^+$ used in this work have led to the insertion of monomeric Mn^{III} species into oxalate-based bimetallic networks, they can be seen as hybrid magnets formed by a paramagnetic sublattice inserted into a 2D or 3D ferromagnetic network. The magnetic behavior of these networks is similar to that of other 2D or 3D oxalate-based compounds reported in the literature. Thus, the T_c values of the 2D compounds **(*R*)-1**, **(*S*)-1** and **4** (5.6 K) are identical to those of other $Mn^{II}Cr^{III}$ 2D oxalate compounds.[4,10e] The decrease of T_c of the 3D compounds, **(*R*)-2**, **(*S*)-2** (T_c = 5.2 K) and **3** (T_c = 5.4 K), is not unexpected, since usually 2D bimetallic oxalate compounds present higher T_c values than 3D ones. This has been explained by the non-collinear alignment of the chiral axis in the 3D compounds, which produces differences in the relative orientation of the magnetic orbitals.[30] The differences between the T_c of **(*R*)-2** and **(*S*)-2** and that of other bimetallic oxalate compounds with a 3D achiral structure, such as $[Fe^{III}(5\text{-}CH_3Osal_2\text{-trien})][Mn^{II}Cr^{III}(ox)_3]$ (T_c = 5.1 K), $[Fe^{III}(sal_2\text{-trien})][Mn^{II}Cr^{III}(ox)_3]\cdot(CH_3OH)$ (T_c = 5.2 K) or $[Fe(bpp)_2][MnCr(ox)_3]\cdot bpp\cdot CH_3OH$, ($T_c$ = 3.0 K), may be explained by differences in the Mn^{II}–Cr^{III} distances and in the bonding angles. On the other hand, T_c of **3** (T_c = 5.4 K) is slightly higher than those found in $[Fe^{III}(5\text{-}Clsal_2\text{-trien})][Mn^{II}Cr^{III}(ox)_3]\cdot 0.5(CH_3NO_2)$,

$[Fe^{III}(5\text{-}Brsal_2\text{-}trien)][Mn^{II}Cr^{III}(ox)_3]$ and $[In^{III}(5\text{-}Clsal_2\text{-}trien)]$-$[Mn^{II}Cr^{III}(ox)_3]\cdot(CH_3NO_2)$, the other compounds with a similar 3D orthorhombic network (4.8–5 K)[10d] and compounds with a 3D cubic one (5.1 K).[3d,f,9b] This is not unusual as the T_c of this type of network is very sensitive to the size of the inserted cation.[3f] Finally, the ferromagnetism of the 2D and 3D oxalate networks of these compounds may produce a Zeeman splitting of the $S = 2$ spins of the paramagnetic inserted Mn^{III} complexes. This effect has been studied by EPR (electronic paramagnetic resonance) spectroscopy in 2D compounds with inserted radical organic cations or decamethylferrocenium cations.[1,4] However, this is not possible in our systems as Mn^{III} complexes are EPR-silent.

The most promising result of these compounds is derived from the chirality of the oxalate network in compounds **(*S*)-1**, **(*R*)-1** and **3**, which opens the way to the search for new magnetic effects derived from the coexistence of chirality and ferromagnetism, such as the magneto-chiral effect predicted by Rikken *et al.*[31] and observed recently in an enantiopure 2D oxalate compound.[18a] Interestingly, in the case of **(*S*)-1** and **(*R*)-1**, it is possible to separate the two enantiomers by choosing the right chiral precursor. In the case of **3** obtained from an achiral precursor, a 50% mixture of crystals of both enantiomers is obtained. Notice that the magneto-chiral effect has been observed in the weakly chiral 2D lattice. Still, in the strongly chiral 3D lattice as that of **3**, this effect could be more important. Although it is not possible to perform enantiopure syntheses of this compound, this effect could be studied on single crystals.

Conclusion

In this article we have shown that the use of substituted Mn^{III}-salen complexes as templating cations is a suitable strategy to obtain different types of oxalate networks. The chiral templating cations $[Mn((R)\text{-salmen})]^+$ and $[Mn((S)\text{-salmen})]^+$ have led to a 2D chiral oxalate network in acetonitrile in **(*R*)-1** and **(*S*)-1** compounds, while a new type of achiral 3D oxalate network has been obtained in dichloromethane in compounds **(*S*)-2** and **(*R*)-2**. On the other hand, the achiral templating cations, $[Mn(salpn)]^+$ and $[Mn(saltmen)]^+$, have given rise respectively to a 3D chiral network and a 2D achiral network in **3** and **4** compounds. All these complexes have led to the insertion of monomeric Mn^{III} species into oxalate-based bimetallic networks. Therefore, they are multifunctional compounds combining the ferromagnetic order of the 2D or 3D oxalate networks and the paramagnetism of the inserted Mn^{III} cation. The chirality of the oxalate network in compounds **(*S*)-1**, **(*R*)-1** and **3** may lead to new magnetic effects derived from the coexistence of chirality and ferromagnetism. Interestingly, in the case of **(*S*)-1** and **(*R*)-1**, this study could be performed in enantiopure samples, something very unusual for this type of compound.

Acknowledgements

Financial support from the European Union (MolSpinQIP and SPINMOL ERC Advanced Grant), the Spanish Ministerio de Ciencia e Innovación (Projects Consolider-Ingenio in Molecular Nanoscience CSD2007-00010, MAT2011-22785 and CTQ-2011-26507), and the Generalitat Valenciana (Prometeo Program) is gratefully acknowledged. The authors also thank José María Martínez-Agudo and Gloria Agustí-López, University of Valencia, for magnetic characterization of the samples.

Notes and references

1 M. Clemente-León, E. Coronado, C. Martí-Gastaldo and F. M. Romero, *Chem. Soc. Rev.*, 2011, **40**, 473–497.
2 (*a*) H. Tamaki, Z. J. Zhong, N. Matsumoto, S. Kida, M. Koikawa, N. Achiwa, Y. Hashimoto and H. Okawa, *J. Am. Chem. Soc.*, 1992, **114**, 6974; (*b*) H. Tamaki, M. Mitsumi, N. Nakamura, N. Matsumoto, S. Kida, H. Okawa and S. Ijima, *Chem. Lett.*, 1992, 1975; (*c*) C. Mathonière, S. G. Carling, D. Yuscheng and P. Day, *J. Chem. Soc., Chem. Commun.*, 1994, 1551; (*d*) C. Mathonière, J. Nutall, S. G. Carling and P. Day, *Inorg. Chem.*, 1996, **35**, 1201; (*e*) R. Pellaux, H. W. Schmalle, R. Huber, P. Fisher, T. Hauss, B. Ouladdiaf and S. Decurtins, *Inorg. Chem.*, 1997, **36**, 2301; (*f*) E. Coronado, J. R. Galán-Mascarós, C. J. Gómez-García, J. M. Martínez-Agudo, E. Martínez-Ferrero, J. C. Waerenborgh and M. Almeida, *J. Solid State Chem.*, 2001, **159**, 391; (*g*) K. S. Min, A. L. Rhinegold and J. S. Miller, *Inorg. Chem.*, 2005, **44**, 8433; (*h*) E. Coronado, J. R. Galán-Mascarós and C. Martí-Gastaldo, *J. Mater. Chem.*, 2006, **16**, 2685; (*i*) Z. Duan, Y. Zhang, B. Zhang and F. L. Pratt, *Inorg. Chem.*, 2009, **48**, 2140.
3 (*a*) S. Decurtins, H. W. Schmalle, P. Schneuwly and H. R. Oswald, *Inorg. Chem.*, 1993, **32**, 1888; (*b*) S. Decurtins, H. W. Schmalle, P. Schneuwly, J. Ensling and P. Gütlich, *J. Am. Chem. Soc.*, 1994, **116**, 9521; (*c*) M. Hernández-Molina, F. Lloret, C. Ruiz-Pérez and M. Julve, *Inorg. Chem.*, 1998, **37**, 4141; (*d*) E. Coronado, J. R. Galán-Mascarós, C. J. Gómez-García and J. M. Martínez-Agudo, *Inorg. Chem.*, 2001, **40**, 113; (*e*) F. Pointillart, C. Train, M. Gruselle, F. Villain, H. W. Schmalle, D. Talbot, P. Gredin, S. Decurtins and M. Verdaguer, *Chem. Mater.*, 2004, **16**, 832; (*f*) M. Clemente-León, E. Coronado, C. J. Gómez-García and A. Soriano-Portillo, *Inorg. Chem.*, 2006, **45**, 5653.
4 (*a*) M. Clemente-León, J. R. Galán-Mascarós and C. J. Gómez-García, *Chem. Commun.*, 1997, 1727; (*b*) E. Coronado, J. R. Galán-Mascarós, C. J. Gómez-García and J. M. Martínez-Agudo, *Adv. Mater.*, 1999, **11**, 558; (*c*) E. Coronado, J. R. Galán-Mascarós, C. J. Gómez-García, J. Ensling and P. Gutlich, *Chem.–Eur. J.*, 2000, **6**, 552.
5 (*a*) S. Bénard, P. Yu, J. P. Audière, E. Rivière, R. Clèment, J. Ghilhem, L. Tchertanov and K. Nakatami, *J. Am. Chem. Soc.*, 2000, **122**, 9444; (*b*) S. M. Aldoshin, N. A. Sanina, V. I. Minkin, N. A. Voloshin, V. N. Ikorskii,

V. I. Ovcharenko, V. A. Smirnov and N. K. Nagaeva, *J. Mol. Struct.*, 2007, **826**, 6.

6 (*a*) E. Coronado, J. R. Galán-Mascarós, C. J. Gómez-García and V. Laukhin, *Nature*, 2000, **408**, 447; (*b*) A. Alberola, E. Coronado, J. R. Galán-Mascarós, C. Giménez-Saiz and C. J. Gómez-García, *J. Am. Chem. Soc.*, 2003, **125**, 10774; (*c*) E. Coronado, J. R. Galán-Mascarós, C. J. Gómez-García, E. Martínez-Ferrero and S. Van Smaalen, *Inorg. Chem.*, 2004, **43**, 4808; (*d*) B. Zhang, Y. Zhang and D. Zhu, *Chem. Commun.*, 2012, **48**, 197–199.

7 (*a*) H. Okawa, A. Shigematsu, M. Sadakiyo, T. Miyagawa, K. Yoneda, M. Ohba and H. Kitagawa, *J. Am. Chem. Soc.*, 2009, **131**, 13516–13522; (*b*) M. Sadayiko, H. Okawa, A. Shigematsu, M. Ohba, T. Yamada and H. Kitagawa, *J. Am. Chem. Soc.*, 2012, **134**, 5472–5475.

8 T. Endo, T. Akutagawa, S. I. Noro and T. Nakamura, *Dalton Trans.*, 2011, **40**, 1491–1496.

9 (*a*) R. Andrés, M. Gruselle, B. Malézieux, M. Verdaguer and J. Vaissermann, *Inorg. Chem.*, 1999, **38**, 4637–4646; (*b*) R. Andrés, M. Brissard, M. Gruselle, C. Train, J. Vaissermann, B. Malézieux, J. P. Jamet and M. Verdaguer, *Inorg. Chem.*, 2001, **40**, 4633–4640; (*c*) M. Clemente-León, E. Coronado, J. C. Dias, A. Soriano-Portillo and R. D. Willett, *Inorg. Chem.*, 2008, **47**, 6458–6463.

10 (*a*) M. Clemente-León, E. Coronado, M. C. Giménez-López, A. Soriano-Portillo, J. C. Waerenborgh, F. S. Delgado and C. Ruiz-Pérez, *Inorg. Chem.*, 2008, **47**, 9111; (*b*) M. Clemente-León, E. Coronado, M. López-Jordà, G. Mínguez Espallargas, A. Soriano-Portillo and J. C. Waerenborgh, *Chem.–Eur., J.*, 2010, **16**, 2207–2219; (*c*) M. Clemente-León, E. Coronado and M. López-Jordà, *Dalton Trans.*, 2010, **39**, 4903–4910; (*d*) M. Clemente-León, E. Coronado, M. López-Jordà and J. C. Waerenborgh, *Inorg. Chem.*, 2011, **50**, 9122–9130; (*e*) M. Clemente-León, E. Coronado, M. López-Jordà, C. Desplanches, S. Asthana, H. Wang and J.-F. Létard, *Chem. Sci.*, 2011, **2**, 1121–1127.

11 J. R. Galán-Mascarós, E. Coronado, P. A. Goddard, J. Singleton, A. I. Coldea, J. D. Wallis, S. J. Coles and A. Alberola, *J. Am. Chem. Soc.*, 2010, **132**, 9271–9273.

12 E. Pardo, C. Train, G. Contard, K. Boubekeur, O. Fabelo, H. Liu, B. Dkhil, F. Lloret, K. Nakagawa, H. Tokoro, S.-I. Ohkoshi and M. Verdaguer, *J. Am. Chem. Soc.*, 2011, **133**, 15328–15331.

13 C. Train, M. Gruselle and M. Verdaguer, *Chem. Soc. Rev.*, 2011, **40**, 3279–3312.

14 E. Coronado, J. R. Galán-Mascarós, M. C. Giménez-López, M. Almeida and J. C. Waerenborgh, *Polyhedron*, 2007, **26**, 1838–1844.

15 B. Zhang, Y. Zhang and D. Zhu, *Dalton Trans.*, 2012, **14**, 8509–8511.

16 (*a*) R. Clérac, H. Miyasaka, M. Yamashita and C. Coulon, *J. Am. Chem. Soc.*, 2002, **124**, 12837; (*b*) M. Ferbinteanu, H. Miyasaka, W. Wernsdorfer, K. Nakata, K. Sugiura, M. Yamashita, C. Coulon and R. Clérac, *J. Am. Chem. Soc.*, 2005, **127**, 3090; (*c*) H. Miyasaka, R. Clérac, K. Mizushima, K. Sugiura, M. Yamashita, W. Wernsdorfer and C. Coulon, *Inorg. Chem.*, 2003, **42**, 8203; (*d*) A. Saitoh, H. Miyasaka, M. Yamashita and R. Clérac, *J. Mater. Chem.*, 2007, **17**, 2002; (*e*) H. Miyasaka, T. Madanbashi, A. Saitoh, N. Motokawa, R. Ishikawa, M. Yamashita, S. Bahr, W. Wernsdorfer and R. Clérac, *Chem.–Eur. J.*, 2012, **18**, 3942–3954.

17 (*a*) H. Miyasaka, R. Clérac, W. Wernsdorfer, L. Lecren, C. Bonhomme, K. Sugiura and M. Yamashita, *Angew. Chem., Int. Ed.*, 2004, **43**, 2801–2805; (*b*) H. J. Choi, J. J. Sokol and J. R. Long, *Inorg. Chem.*, 2004, **43**, 1606; (*c*) M. Ferbinteanu, H. Miyasaka, W. Wernsdorfer, K. Nakata, K. Sugiura, M. Yamashita, C. Coulon and R. Clérac, *J. Am. Chem. Soc.*, 2005, **127**, 3090; (*d*) Z. Lu, M. Yuan, F. Pan, S. Gao, D. Zhang and D. Zhu, *Inorg. Chem.*, 2006, **45**, 3538–3548; (*e*) C. Kachi-Terajima, H. Miyasaka, K. Sugiura, R. Clérac and H. Nojiri, *Inorg. Chem.*, 2006, **45**, 4381; (*f*) C. Kachi-Terajima, H. Miyasaka, A. Saitoh, N. Shirakawa, M. Yamashita and R. Clérac, *Inorg. Chem.*, 2007, **46**, 5861; (*g*) H. Miyasaka, A. Saitoh and S. Abe, *Coord. Chem. Rev.*, 2007, **251**, 2622; (*h*) Y. Sadawa, W. Kosaka, Y. Hayashi and H. Miyasaka, *Inorg. Chem.*, 2012, **51**, 4824–4832.

18 (*a*) C. Train, R. Gheorghe, V. Krstic, L. M. Chamoreau, N. S. Ovanesyan, G. L. J. A. Rikken, M. Gruselle and M. Verdaguer, *Nat. Mater.*, 2008, **17**, 729; (*b*) C. Train, T. Nuida, R. Gheorghe, M. Gruselle and S. Ohkoshi, *J. Am. Chem. Soc.*, 2009, **131**, 16838.

19 F. M. Ashmawy, C. A. McAuliffe, R. V. Parish and J. Tames, *J. Chem. Soc., Dalton Trans.*, 1985, 1391–1397.

20 L. Lecren, W. Wernsdorfer, Y. G. Li, A. Vindigni, H. Miyasaka and R. Clérac, *J. Am. Chem. Soc.*, 2007, **129**, 5045–5051.

21 J. C. Baylar and E. M. Jones, in *Inorganic Synthesis*, ed. H. S. Booth, McGraw-Hill, New York, 1939, vol. 5, p. 35.

22 A. Altomare, M. C. Burla, M. Camalli, G. L. Cascarano, C. Giacovazzo, A. Guagliardi, A. G. G. Moliterni, G. Polidori and R. Spagna, *J. Appl. Crystallogr.*, 1999, **32**, 115.

23 G. M. Sheldrick, *Acta Crystallogr., Sect. A: Fundam. Crystallogr.*, 2008, **64**, 112.

24 L. J. Farrugia, *J. Appl. Crystallogr.*, 1999, **32**, 837.

25 H. D. Flack and G. Bernardinelli, *J. Appl. Crystallogr.*, 2000, **33**, 1143.

26 M. Clemente-León, E. Coronado, M. López-Jordà and F. Luis, manuscript in preparation.

27 S. Decurtins, H. W. Schmalle, R. Pellaux, P. Schneuwly and A. Hauser, *Inorg. Chem.*, 1996, **35**, 1451–1460.

28 N. S. Ovanesyan, V. D. Makhaev, S. M. Aldoshin, P. Gredin, K. Boubekeur, C. Train and M. Gruselle, *Dalton Trans.*, 2005, 3101.

29 M. Clemente-León, E. Coronado and M. López-Jordà, *Eur. J. Inorg. Chem.*, DOI: 10.1002/ejic.201201113, in press.

30 R. S. Fishman, M. Clemente-León and E. Coronado, *Inorg. Chem.*, 2009, **48**, 3039.

31 G. L. J. A. Rikken and E. Raupach, *Nature*, 1997, **390**, 493.

Stimuli responsive hybrid magnets: Tuning the photoinduced spin-crossover in Fe(III) complexes inserted into layered magnets.

Miguel Clemente-León,*[a] Eugenio Coronado,*[a] Maurici López-Jordà,[a] João C. Waerenborgh,[b] Cédric Desplanches,[c] Hongfeng Wang,[c] Jean-François Létard,[c] Andreas Hauser,[d] Antoine Tissot[d]

[a]Instituto de Ciencia Molecular (ICMol), Universidad de Valencia, Catedrático José Beltrán 2, 46980 Paterna, Spain

[b]IST/ITN, Instituto Superior Técnico, Universidade Técnica de Lisboa, CFMC-UL, 2686-953 Sacavém, Portugal

[c]Université de Bordeaux, ICMCB, 87 avenue du Dr. A. Schweitzer, Pessac, F-33608, France

[d]Département de Chimie Physique, Université de Genève, 30 Quai Ernest-Ansermet, CH-1211 Genève 4, Switzerland

ABSTRACT: The insertion of a $[Fe(sal_2\text{-trien})]^+$ complex cation into a 2D oxalate network in the presence of different solvents results in a family of hybrid magnets with coexistence of magnetic ordering and photoinduced spin-crossover (LIESST effect) in compounds $[Fe^{III}(sal_2\text{-trien})][Mn^{II}Cr^{III}(ox)_3]\cdot CHCl_3$ (**1·CHCl₃**), $[Fe^{III}(sal_2\text{-trien})][Mn^{II}Cr^{III}(ox)_3]\cdot CHBr_3$ (**1·CHBr₃**) and $[Fe^{III}(sal_2\text{-trien})][Mn^{II}Cr^{III}(ox)_3]\cdot CH_2Br_2$ (**1·CH₂Br₂**). The three compounds crystallize in a 2D honeycomb anionic layer formed by Mn^{II} and Cr^{III} ions linked through oxalate ligands and a layer of $[Fe(sal_2\text{-trien})]^+$ complexes and solvent molecules ($CHCl_3$, $CHBr_3$, or $CHCl_3$) intercalated between the 2D oxalate network. The magnetic properties and Mössbauer spectroscopy indicate that they undergo long-range ferromagnetic ordering at 5.6 K and a spin crossover of the intercalated $[Fe(sal_2\text{-trien})]^+$ complexes at different temperatures $T_{1/2}$. The three compounds present a LIESST effect with a relaxation temperature T_{LIESST} inversely proportional to $T_{1/2}$. The isostructural paramagnetic compound, $[Fe^{III}(sal_2\text{-trien})][Zn^{II}Cr^{III}(ox)_3]\cdot CH_2Cl_2$ (**2·CH₂Cl₂**) was also prepared. This compound presents a partial spin crossover of the inserted Fe^{III} complex as well as a LIESST effect. Finally, spectroscopic characterization of the Fe^{III} doped compound $[Ga_{0.99}Fe_{0.01}(sal_2trien)][Mn^{II}Cr^{III}(ox)_3]\cdot CH_2Cl_2$ (**3·CH₂Cl₂**) shows a gradual and complete thermal spin crossover and a LIESST effect on the isolated Fe^{III} complexes. This result confirms that cooperativity is not a necessary condition to observe the LIESST effect in an Fe^{III} compound.

INTRODUCTION

Multifunctionality is one of the most appealing topics in chemical science. A rational approach to design multifunctional materials consists of creating hybrid solids constituted of two networks formed by two molecular fragments, where each network furnishes distinct physical properties.[1] A coexistence of the two physical properties is anticipated if the two networks are quasi-independent. Materials for which physical properties can be tuned by applying an external stimulus are attracting considerable interest in view of their potential applications as chemical switches, memories or molecular sensors.[2] Most of the responsive magnetic materials obtained so far are one-network materials in which the magnetic order is tuned by light or pressure.[3] Two-network materials formed by a magnetic lattice and a switchable molecular component, are promising candidates for the preparation of multifunctional responsive materials.

A potential source for this type of materials is the bimetallic oxalate-bridged complexes that have provided remarkable examples of multifunctional magnetic materials.[4] An interesting example prepared by our group is the compound $[Fe^{III}(sal_2\text{-trien})][Mn^{II}Cr^{III}(ox)_3]\cdot CH_2Cl_2$ (**1·CH₂Cl₂**, H_2sal_2-trien = N,N'-disalicylidenetriethylenetetramine, ox = oxalate).[5] This compound shows an unusual combination of properties in the same compound; a spin crossover (SCO) transition of the inserted complex cation and a ferromagnetic ordering of the oxalate network. Unfortunately, no interplay between these two properties has been detected due to the large difference in temperature at which the two phenomena occur. Thus, while the spin crossover occurs at comparatively high temperatures, that is, in the range of 130 - 350 K, the ferromagnetic ordering occurs below 5.2 - 5.6 K. A way to overcome this limitation is to take advantage of the photoinduced spin-crossover effect, also known as LIESST effect (Light-Induced Excited Spin-State Trapping) originally established for Fe^{II} complexes at temperatures typically below 50 K.[6] Light irradiation at low temperatures, induces a LIESST effect for **1·CH₂Cl₂** with a T(LIESST) = 41 K, which defines the limiting temperature above which the photoinscribed information is erased.[7] The photo-induced spin conversion of the inserted Fe^{III} complex, however, has a negligible influence on the magnetic behavior of the 2D oxalate network. This is not unexpected, as 2D oxalate

networks with very different interlayer separations present a similar behavior.

Although the preparation of a switchable magnet has not been achieved, the LIESST effect of this compound constitutes a remarkable finding, as this phenomenon is rarely observed in Fe^{III} complexes. SCO Fe^{II} compounds present an average bond length change of about 0.20 Å between the LS and HS state, whereas that of Fe^{III} SCO complexes is about 0.13 Å. Obviously, the structural reorganization influences the kinetics of the spin-state interconversion. It is presumed that the lifetime of the photoinduced excited HS state for Fe^{III} complexes is shorter than that for Fe^{II} complexes, as the smaller energy barrier between the HS and LS states in Fe^{III} complexes cannot prevent the relaxation of the metastable HS state back to the LS ground state effectively. Only a few examples of Fe^{III} complexes showing the LIESST effect have been reported by Sato, Hayami et al., namely $[Fe^{III}(pap)_2]^+$, $[Fe^{III}(qsal)_2]^+$ and $[Fe^{III}(qnal)_2]^+$ (Hpap = 2-(2-pyridilmethylamino)phenol, Hqsal = 2-[(8-quinolinylimino)mehyl]phenol and Hqnal = 1-((8-quinolinylimino)methyl)-2-naphthalenol).[8-10] The LIESST effect of these compounds is attributed to the strong distortion of the Fe^{III} sites from their octahedral geometry, which is enhanced by the presence of strong intermolecular interactions, such as π-π stacking.[9] In contrast to the above Fe^{III} complexes in the form of salts of small anions such as BF_4^- or ClO_4^-, **1·CH$_2$Cl$_2$** presents an extended 2D anionic network formed by Mn^{II} and Cr^{III} ions linked through oxalate ligands. $[Fe^{III}(sal_2\text{-trien})]^+$ cations and CH_2Cl_2 solvent molecules are intercalated between these oxalate layers.[5] Besides **1·CH$_2$Cl$_2$**, other compounds formed by the insertion of $[Fe^{III}(sal_2\text{-trien})]^+$ or $[Fe^{III}(X\text{-}sal_2\text{-trien})]^+$ (X = 5-Cl, 5-Br, 5-NO_2, 5-CH_3O, 4-Br, 3-Br, 3-Cl and 3-CH_3O) into 2D or 3D bimetallic oxalate networks have been prepared by us,[5,11] but the LIESST effect has so far only been observed in **1·CH$_2$Cl$_2$**.[7]

In this work, a family of compounds with a similar structure to that of **1·CH$_2$Cl$_2$** has been prepared by replacing CH_2Cl_2 with other halogenated solvents. Furthermore, a fraction of the Fe^{III} spin crossover complexes of **1·CH$_2$Cl$_2$** have been replaced with the diamagnetic dopant, $[Ga^{III}(sal_2\text{-trien})]^+$ complex, to prepare compounds of formula $[Ga^{III}_{1-x}Fe^{III}_x(sal_2\text{-trien})][Mn^{II}Cr^{III}(ox)_3]\cdot CH_2Cl_2$. The aim of this work is to obtain new Fe^{III} compounds presenting a LIESST effect that could provide more data to understand this rare property. On the other hand, substitution of the solvent molecule may allow tuning the temperatures of the thermal and photo-induced spin-crossover of the inserted Fe^{III} cations. We have to take into account that replacement of the solvent molecules induces changes in the internal chemical pressure of the inserted Fe^{III} SCO complex and in the intermolecular interactions with the oxalate network, that are key factors for the SCO properties. Finally, dilution of the $[Fe^{III}(sal_2\text{-trien})]^+$ complex with an inert $[Ga^{III}(sal_2\text{-trien})]^+$ complex reduces cooperativity and may help to clarify the role of intermolecular interactions between SCO complexes in this type of compound. An additional advantage of dilution is that it permits to perform spectroscopic characterization on single crystals, which is not possible for pure Fe^{III} compounds due to the strong absorption of $[Fe^{III}(sal_2\text{-trien})]^+$ complexes.

EXPERIMENTAL SECTION

Synthesis: $[Fe(sal_2\text{-trien})]PF_6$ and $[Ga(sal_2\text{-trien})]PF_6$ were prepared according to literature methods.[12] $Ag_3[Cr(ox)_3]$ was prepared by metathesis from the corresponding potassium salt.[13] All other materials and solvents were commercially available and used without further purification. Single crystals of the five compounds $[Fe^{III}(sal_2\text{-trien})][Mn^{II}Cr^{III}(ox)_3]\cdot CHCl_3$ (**1·CHCl$_3$**), $[Fe^{III}(sal_2\text{-trien})][Mn^{II}Cr^{III}(ox)_3]\cdot CHBr_3$ (**1·CHBr$_3$**), $[Fe^{III}(sal_2\text{-trien})][Mn^{II}Cr^{III}(ox)_3]\cdot CH_2Br_2$ (**1·CH$_2$Br$_2$**), $[Fe^{III}(sal_2\text{-trien})][Zn^{II}Cr^{III}(ox)_3]\cdot CH_2Cl_2$ (**2·CH$_2$Cl$_2$**) and $[Ga^{III}_{1-x}Fe^{III}_x(sal_2\text{-trien})][Mn^{II}Cr^{III}(ox)_3]\cdot CH_2Cl_2$ (**3·CH$_2$Cl$_2$**, x = 0.01) were obtained by slow diffusion of two solutions. The first solution was prepared by adding $MnCl_2\cdot 4H_2O$ (0.040 g, 0.202 mmol for **1·CHBr$_3$**, **1·CHCl$_3$** and **1·CH$_2$Br$_2$**) or $ZnCl_2$ (0.075 g, 0.536 mmol for **2·CH$_2$Cl$_2$**) to a suspension of $Ag_3Cr(ox)_3$ (0.086 g, 0.134 mmol) in 9 mL of methanol. The AgCl precipitate was filtered. The second solution was obtained by dissolving $[Fe(sal_2\text{-trien})]PF_6$ (0.075 g, 0.134 mmol) in 9 mL of chloroform (**1·CHCl$_3$**), bromoform (**1·CHBr$_3$**), dibromomethane (**1·CH$_2$Br$_2$**) and dichloromethane (**2·CH$_2$Cl$_2$**), or a mixture of 0.1 and 9.9 mL of 15 mM solutions of $[Fe(sal_2\text{-trien})]PF_6$ and $[Ga(sal_2\text{-trien})]PF_6$, respectively, in dichloromethane (**3·CH$_2$Cl$_2$**). After two weeks brown or violet (**3·CH$_2$Cl$_2$**) crystals were obtained.

Structural characterization: Single crystals of all five compounds were mounted on glass fibres using a viscous hydrocarbon oil to coat the crystal and then transferred directly to the cold nitrogen stream for data collection. X-ray data were collected at 100 and 300 K for **1·CHCl$_3$**, **1·CHBr$_3$** and **1·CH$_2$Br$_2$**, at 120 K for **2·CH$_2$Cl$_2$** and at 300 K for **3·CH$_2$Cl$_2$** on a diffractometer equipped with a graphite-monochromated Enhance (Mo) X-ray Source (λ = 0.71073 Å). The program CrysAlisPro, Oxford Diffraction Ltd., was used for unit cell determinations and data reduction. Empirical absorption correction was performed using spherical harmonics, implemented in the SCALE3 ABSPACK scaling algorithm. Crystal structures were solved by direct methods with the SIR97 program,[14] and refined against all F^2 values with the SHELXL-97 program,[15] using the WinGX graphical user interface.[16] Non-hydrogen atoms were refined anisotropically (except as noted), and hydrogen atoms were placed in calculated positions refined using idealized geometries (riding model) and assigned fixed isotropic displacement parameters. In compound **1.CHCl$_3$**, the small size of the crystals gave rise to a very weak scattering. Due to this, the number of reflections was not enough to carry out anisotropic refinement of all the atoms. Thus, carbon atoms at 100 K and carbon, nitrogen and oxygen atoms at 300 K could only be modeled isotropically. Furthermore, this caused a too low observed / unique reflections ratio in the structure solved at 300 K. This problem disappeared in the structure of the same crystal solved at 100 K. Data collection and refinement statistics are collected in Table 1. CCDC-929201 to 929208 contain the supplementary crystallographic data for this paper. These data can be obtained free of charge from The Cambridge Crystallographic Data Centre via www.ccdc.cam.ac.uk/data_request/cif.

Physical measurements: Magnetic susceptibility measurements were performed on polycrystalline samples using a magnetometer (Quantum Design MPMS-XL-5) equipped with a SQUID sensor. Variable-temperature measurements were carried out in the temperature range 2 - 400 K. The AC measurements were performed in the temperature range 2 - 10 K at different frequencies with an oscillating magnetic field of 0.395 mT. The magnetization and hysteresis studies were performed between 5 and −5 T, cooling the samples at zero field. The Ga:Fe:M:Cr:X (M = Mn or Zn, and X = Br or Cl) ratios were measured on a Philips ESEM X230 scanning electron microscope equipped with an EDAX DX-4 microprobe.

Mössbauer spectra were collected in transmission mode using a conventional constant-acceleration spectrometer and a 25 mCi ^{57}Co source in a Rh matrix. The velocity scale was calibrated using an α-Fe foil. The absorber was obtained by gently packing single crystals of **1·CHCl$_3$**, **1·CHBr$_3$** and **1·CH$_2$Br$_2$** into a perspex holder. Low-temperature spectra were collected using a bath cryostat with the sample immersed in liquid He for measurements at 4.2 K, or by using flowing He gas to cool the sample above 4.2 K (temperature stability of 0.5 K). The spectra were fitted to Lorentzian lines using a non-linear least-squares method.[17] Isomer shifts are given relative to metallic α-Fe at room temperature.

Variable temperature optical single crystal absorption spectra of **3·CH$_2$Cl$_2$** were recorded with a commercial double beam spectrometer (Varian, Cary 5000). To this end a small crystal was mounted with silver paste so as to cover an aperture on a copper sample holder, which in turn was mounted on the cold finger of an optical close cycle cryostat (Janis, Sumitomo SHI-4.5) capable of achieving a base temperature of 4 K.

RESULTS

Synthesis. The method used to prepare the family of five compounds of the present work was described in the experimental section and is analogous to that used to prepare **1·CH$_2$Cl$_2$**.[5] In previous work, two different types of structures were obtained depending on the solvent used to dissolve[Fe^{III}(sal$_2$-trien)]PF$_6$.[5] A 2D bimetallic oxalate network is obtained with CH_2Cl_2 in **1·CH$_2$Cl$_2$**, while a 3D bimetallic oxalate network is obtained with CH_3CN and CH_3NO_2. In this work, we have discovered that the halogenated solvents, $CHCl_3$, $CHBr_3$ and CH_2Br_2, give rise to 2D structures similar to that of **1·CH$_2$Cl$_2$**. This confirms that the formation of 2D or 3D networks is controlled by the size and configuration of the templating cation, which change in the different solvents. An interesting example of how subtle changes lead to 2D or 3D structures is the use of other [M^{III}(sal$_2$-trien)]$^+$ complexes in the same solvent (CH_2Cl_2). Thus, the largest cation, [In^{III}(sal$_2$-trien)]$^+$, gives rise to a 3D structure[18] while the smallest one, [Ga^{III}(sal$_2$-trien)]$^+$,[19] leads to a 2D one. Therefore, the halogenated solvents, CH_2Cl_2, CH_2Br_2, $CHCl_3$ and $CHBr_3$ lead to 2D structures with [Fe^{III}(sal$_2$-trien)]$^+$ because they induce a configuration of the cation suitable for the growth of the 2D network, which is also stabilized by the insertion of the solvent molecules. When a similar cation of larger size such as [In^{III}(sal$_2$-trien)]$^+$ is used, the 3D network is favored and the solvent molecules do not enter the structure. This allows preparing 2D compounds containing two different cations of similar size and to dilute the SCO Fe^{III} complexes with diamagnetic Ga^{III} complexes. In the compounds of formula [Ga$^{III}_{1-x}$Fe$^{III}_x$(sal$_2$-trien)][Mn^{II}Cr^{III}(ox)$_3$]·CH_2Cl_2, most of the [Fe^{III}(sal$_2$-trien)]$^+$ complexes of **1·CH$_2$Cl$_2$** are replaced by the diamagnetic [Ga^{III}(sal$_2$-trien)]$^+$ complexes. They are prepared by mixing the [Ga^{III}(sal$_2$-trien)]PF$_6$ and [Fe^{III}(sal$_2$-trien)]PF$_6$ precursors in the desired ratio.

The composition of the compounds was checked by microanalysis, which shows the presence of the solvent molecules in the structures. Thus, a 1:1:1:3 Fe:M (Mn or Zn):Cr:X (X = Cl or Br) ratio was found for **1·CHCl$_3$** and **1·CHBr$_3$**, while a 1:1:1:2 ratio is found for **1·CH$_2$Br$_2$** and **2·CH$_2$Cl$_2$**. The Ga:Fe ratio for [Ga$^{III}_{1-x}$Fe$^{III}_x$(sal$_2$-trien)][Mn^{II}Cr^{III}(ox)$_3$]·CH_2Cl_2 was found to be close to the ratio of the solutions used in the synthesis. For the lightly doped compound [Ga$^{III}_{1-x}$Fe$^{III}_x$(sal$_2$-trien)][Mn^{II}Cr^{III}(ox)$_3$]·CH_2Cl_2, (x=0.01, **3·CH$_2$Cl$_2$**) used for optical spectroscopic characterization, the iron content was found to be less than 1 % and could not determined accurately. Still, the presence of Fe in the single crystals of **3·CH$_2$Cl$_2$** is verified by the presence of the characteristic LMCT bands in the absorption spectrum (see below).

Structure. The single crystal X-ray diffraction study of **1·CHCl$_3$**, **1·CHBr$_3$**, **1·CH$_2$Br$_2$**, **2·CH$_2$Cl$_2$** and **3·CH$_2$Cl$_2$** shows that they present very similar structures to that of **1·CH$_2$Cl$_2$**. Indeed, their unit cell parameters are very close to the one of **1·CH$_2$Cl$_2$** (see Table 1). The structures of **1·CHCl$_3$**, **1·CHBr$_3$** and **1·CH$_2$Br$_2$** were solved at 100 and 300 K as at these temperatures the Fe^{III} complexes are close to 100 % in the LS or the HS state, respectively. On the other hand, the structure of **2·CH$_2$Cl$_2$** could only be solved at 120 K due to the lower quality of the crystals and the only partial spin crossover exhibited by this compound (see below).

As in the case of **1·CH$_2$Cl$_2$**, the four compounds are formed by anionic [M^{II}Cr^{III}(ox)$_3$]$^-$ (M = Mn or Zn) sheets in the *bc* plane alternating with inter-lamellar [Fe^{III}(sal$_2$-trien)]$^+$ cationic complexes and solvent molecules (see Figure 1). The anionic layers present a 2D honeycomb structure with two crystallographically independent metals linked through oxalate ligands. The intermediate metal-oxygen distances with respect to the ones expected for Cr^{III}–O and Mn^{II}–O (Zn^{II}–O for **2·CH$_2$Cl$_2$**), do not allow distinguishing between the two metals in these structures. The cationic layer contains one crystallographically independent [Fe^{III}(sal$_2$-trien)]$^+$ (or [Ga^{III}(sal$_2$-trien)]$^+$ in **3·CH$_2$Cl$_2$**) complex and one solvent molecule (CH_2Cl_2, $CHCl_3$, $CHBr_3$ or CH_2Br_2).

We will now focus on the differences between the crystal structures measured at 100 and 300 K as they may help to understand the structural changes associated with the spin crossover. Furthermore, they will be compared with those observed in **1·CH$_2$Cl$_2$**. We will look first at the usual changes in the coordination geometry of the Fe^{III} complex between the LS and HS states (Fe-N or Fe-O bond lengths and distortions from the octahedral geometry) and then at the differences in crystal packing.

The first effect of lowering the temperature is a shortening on metal-ligand bond lengths (see Table 2), which is similar to that found for **1·CH$_2$Cl$_2$** (average bond length differences of Δr_{HL}(Fe-N) = 0.149 Å and Δr_{HL}(Fe-O) = 0.024 Å.[7] The small variation in these values between the different compounds may be attributed to a different fraction of Fe^{III} complexes undergoing spin crossover from 300 to 100 K.

The second difference concerns the distortion of the octahedral coordination site, which is larger for the HS state as observed in **1·CH$_2$Cl$_2$**.[7] Thus, at 300 K the angles of two of the three diagonals from the octahedron, defined by the bonds N(amine)-Fe-O(Phenoxo), N(amine) = N2, N3, differ strongly from 180º, while the remaining one, defined by the bond N(imine)-Fe-N(imine), N(imine) = N1, N4, is closer to 180º. The coordination octahedron is much more regular at 100 K with angles of all three diagonals closer to 180º (see Table 2).

The third difference between the LS and HS structures is related to the disorder of the ethylene groups of [Fe(sal$_2$-trien)]$^+$ and solvent molecules. At 300 K, two of the three ethylene groups of [Fe(sal$_2$-trien)]$^+$ in **1·CHBr$_3$** and **1·CHCl$_3$** and the three of them in **1·CH$_2$Br$_2$** present a disorder, which has been solved by considering two possible configurations with occupancies of 62 and 38 % for **1·CHBr$_3$**, 69 and 31 % for **1·CHCl$_3$** and 63 and 37 % for **1·CH$_2$Br$_2$**. This disorder is not observed in the structures of these compounds solved at 100 K. This disorder could be related to the presence of HS Fe^{III} complexes as it disappears at low temperatures where Fe is in the LS state. On the other hand, in **1·CH$_2$Br$_2$** one over the two Br atoms of the CH_2Br_2 solvent presents a disorder at 300 K that could be solved assuming two possible configurations with occupancies of 85 and 15 %. This disorder disappears at 100 K. **1·CH$_2$Cl$_2$** presents a similar disorder in the ethylene groups and in the Cl atoms of CH_2Cl_2 molecules at 250 and 300 K, which disappears below 180 K.[7] This disorder is not present for $CHBr_3$ or $CHCl_3$ solvent molecules in **1·CHCl$_3$** and **1·CHBr$_3$**.

Finally, the crystal packing of [Fe^{III}(sal$_2$-trien)]$^+$ complexes in the four neat compounds also presents important differences between low and high temperature structures. As in the case of **1·CH$_2$Cl$_2$**, the *a* parameter, which gives the interlayer separation, decreases with the temperature (see Table 1). Therefore, the spin crossover from HS to LS states leads to a decrease of the interlayer separation. This shortening results in contacts between O atoms from oxalate layers and CH or CH_2 groups from [Fe^{III}(sal$_2$-trien)]$^+$, which are shorter at 100 K than at 300 K. Therefore, stronger interactions with the oxalate network are expected when the Fe^{III} complexes are in the LS state (see Tables S1 - S6 of the supporting information). On the other hand, interlayer distances of **1·CH$_2$Cl$_2$** are shorter than those of **1·CHCl$_3$**, **1·CHBr$_3$** and **1·CH$_2$Br$_2$** (11.5602(4) Å at 92 K and 12.096(5) Å at 300 K for 1·CH_2Cl_2)[7] at the same temperatures. Two factors could explain these differences: the change of CH_2Cl_2 by the more voluminous $CHCl_3$, $CHBr_3$ or CH_2Br_2 solvents, and a different fraction of [Fe^{III}(sal$_2$-trien)]$^+$ in the HS state. Thus, at low temperatures, when almost 100 % of Fe^{III} are in the LS state, a comparison of the *a* parameter for **1·CHCl$_3$** and **1·CH$_2$Br$_2$** at 100 K with that of **1·CH$_2$Cl$_2$** at 92 K demonstrates that the interlayer distance increases with the volume of the solvent. In the case of **1·CHBr$_3$**, ~25% of Fe^{III} are in the HS state at this temperature (see Mössbauer data below). This may be an additional factor contributing to the increase in interlayer separation. This indicates that the internal pressure on the inserted [Fe^{III}(sal$_2$-trien)]$^+$ complexes decreases as the size of the solvent increases. This could explain the stabilization of the HS state in the presence of the bulkier solvents. Magnetic measurements and Mössbauer spectra are consistent with this feature (see below).

Magnetic properties. The thermal dependence of the product of the molar magnetic susceptibility times the temperature (χ_MT) of the three compounds is shown in Figure 2. The values for χ_MT are 10.9, 10.1 and 9.9 cm^3·K·mol^{-1} at 300 K for **1·CHCl$_3$**, **1·CHBr$_3$** and **1·CH$_2$Br$_2$**, respectively. These values are close to the sum of the expected contributions for the isolated paramagnetic ions with most of the Fe^{III} spin-crossover complexes in the HS state. The lower χ_MT values of **1·CHBr$_3$** and **1·CH$_2$Br$_2$** with respect of that of **1·CHCl$_3$** indicate that in these two compounds there is still a small Fe^{III} LS fraction at 300 K. This is consistent with Mössbauer data at 250 K (see below and Table 3). χ_MT decreases gradually in the three compounds from 300 K to reach minimum values at 140 K for **1·CH$_2$Br$_2$**, 95 K for **1·CHCl$_3$** and 80 K for **1·CHBr$_3$**. Mössbauer data (see below) indicate that almost 100 % of Fe^{III} are in the LS state below 80 K for **1·CH$_2$Br$_2$** and **1·CHCl$_3$**. In the case of **1·CHBr$_3$** at 77 K, there is still a significant fraction of Fe^{III} in the HS state (~18 %), that disappears at 4 K. Therefore, the three compounds undergo an almost complete spin crossover with different $T_{1/2}$ values ($T_{1/2}$ = temperature of 50% HS→LS spin conversion). These values, calculated from Mössbauer data, are 230 K for **1·CH$_2$Br$_2$**, 180 K for **1·CHCl$_3$** and 140 K for **1·CHBr$_3$**. This confirms that the presence of bulkier solvent molecules shifts $T_{1/2}$ towards lower values due to the lowering of the chemical pressure on the inserted [Fe^{III}(sal$_2$-trien)]$^+$ complexes. At lower temperatures χ_MT increases due to the ferromagnetic interactions between neighboring Mn^{II}–Cr^{III} magnetic ions as observed for **1·CH$_2$Cl$_2$** and other M^{II}–Cr^{III} 2D oxalate networks. AC susceptibility measurements confirm the presence of long-range magnetic ordering and permit to determine precisely the critical temperatures (T_c). A maximum in the in-phase signal (χ_M') near T_c and an out-of-phase signal (χ_M'') that starts to appear at temperatures just below T_c is observed in the three compounds (Figure 3). From this data the T_c of the three compounds is 5.6 K, which is similar to that of **1·CH$_2$Cl$_2$** and other 2D Mn^{II}–Cr^{III} 2D oxalate compounds.[5,11a,c] These signals are frequency independent as expected for a ferromagnet.

Isothermal magnetization at 2 K of the three compounds shows the expected behavior for a ferromagnet (Figure S1 in SI). The magnetization (M) value at 5 T of the three compounds is 8.7 μ_B, which is close to the expected value of 9 μ_B for a parallel alignment of the spins in the bimetallic lattice with Fe^{III} in the LS state, thus confirming the complete HS→LS spin conversion at this temperature for the three compounds. The hysteresis loops at 2 K show that these compounds are soft ferromagnets with coercive

fields of 3 mT for **1·CHBr$_3$** and 1 mT for **1·CH$_2$Br$_2$** and **1·CHCl$_3$**.

The temperature dependence of χ_MT for **2·CH$_2$Cl$_2$** is shown in Figure S2 in SI. χ_MT shows a value of 4.5 cm^3·K·mol^{-1} at 300 K. This value is approximately equal to the sum of the expected contributions for the isolated paramagnetic ions (Cr^{III} and Fe^{III}) with ca. 50 % of the Fe^{III} spin-crossover complexes in a HS state. χ_MT decreases gradually from 300 to 150 K. Below this temperature, the decrease is less abrupt and reaches a plateau below 100 K with χ_MT values of 2.3 cm^3·K·mol^{-1} close to the expected value for isolated Cr^{III} ions and 100 % of the Fe^{III} complexes in a LS state. Finally, below 10 K, there is a decrease of a χ_MT that can be due to spin-orbit coupling and zero-field splitting effects. These results demonstrates that inside the bimetallic oxalate framework the two metals are ordered in such a way that each Cr^{III} center is surrounded by three non-magnetic Zn centers and that a 50 % HS→LS spin conversion takes place from 300 to 100 K.

Photomagnetic properties. 1·CHCl$_3$, 1·CH$_2$Br$_2$, 1·CHBr$_3$ and **2·CH$_2$Cl$_2$** were introduced into SQUID at 10 K and irradiated with red light (λ = 647 nm). An increase of the magnetic signal was observed. After about 1 hour, the irradiation was switched off. The temperature was then increased at a rate of 0.3 K min^{-1} and the magnetic susceptibility recorded. For the four compounds, χ_MT recorded at low temperature after irradiation is higher than the value recorded in the dark. Upon increasing the temperature, the difference vanishes and becomes zero above a temperature between 60 and 80 K, depending on the compound. In order to see clearly the magnetic differences after and before irradiation, χ_MT after irradiation was subtracted to the one recorded before irradiation using an interpolation procedure. Interpolated differences are presented in Figure 4. At 20 K, the differences in χ_MT values are 1.5, 0.8, 1.0 and 0.45 cm^3·K·mol^{-1} respectively for **1·CHCl$_3$, 1·CH$_2$Br$_2$, 1·CHBr$_3$** and **2·CH$_2$Cl$_2$**. Taking the mean values of 4.375 cm^3·K·mol^{-1} for Fe^{III} HS and 0.6 cm^3·K·mol^{-1} for Fe^{III} LS, the fraction of Fe^{III} photoconverted after irradiation is calculated to be 40, 21, 26 and 13% for **1·CHCl$_3$, 1·CH$_2$Br$_2$, 1·CHBr$_3$** and **2·CH$_2$Cl$_2$**, respectively. As already described, the difference in χ_MT decreases when the temperature increases, being zero when the temperature is higher than 80 K. For the four compounds, T(LIESST) temperatures, defined as the minimum of the derivate of this χ_MT difference with regard to temperature, are respectively 58, 45, 62 and 45 K.

In order to get some insight into the decay of the photo-induced HS state, HS→LS relaxation curves were recorded for **1·CHCl$_3$, 1·CH$_2$Br$_2$** and **1·CHBr$_3$**. These are presented in Figure S3 in SI. For the three compounds, the relaxation curves show strong deviations from single exponential in the shape of stretched exponentials. The best fit (solid lines in Figure S3 in SI) was obtained with a distribution of relaxation rate constants at a given temperature from a Gaussian distribution of activation energies as already observed in **1·CH$_2$Cl$_2$**.[7] The apparent activation energy, E_a, apparent pre-exponential factor, k_∞, and standard deviation of the mean activation energy, σ, are reported in Table S7 in SI for the three compounds. These curves are typical of non-cooperative systems, which rarely show a single-exponential behavior, because of inhomogeneous distributions due to poorly crystalline solids and the presence of disorder.[20] Hence, in the present case the deviations could be related to the disorder observed in the ethylene groups of $[Fe^{III}(sal_2\text{-trien})]^+$ in **1·CHCl$_3$, 1·CH$_2$Br$_2$** and **1·CHBr$_3$**, indicating different possible configurations of the cations in the HS state.

Mössbauer spectroscopy. Mössbauer spectra of **1·CHCl$_3$, 1·CH$_2$Br$_2$** and **1·CHBr$_3$** shown in Figures 5, 6 and 7 are similar to those published for **1·CH$_2$Cl$_2$**, the achiral 3D compound $[Fe^{III}(sal_2trien)][Mn^{II}Cr^{III}(ox)_3]\cdot CH_3OH$, or other compounds formed by the insertion of $[Fe^{III}(5X\text{-}sal_2\text{-}trien)]^+$ (X = Cl, Br) into chiral 3D oxalate networks.[5,11b] In the present compounds, only a quadrupole doublet with estimated parameters typical of LS Fe^{III} is observed at 4K (Table 3). Above 77 K for **1·CHCl$_3$** and **1·CHBr$_3$** and 160 K for **1·CH$_2$Br$_2$**, an unresolved absorption, centered at IS ~ 0.30-0.36 mm/s at 295 K, is observed. This broad absorption is assigned to HS Fe^{III}. As discussed in detail in previous papers[5,11b] broadening of the HS Fe^{III} contribution below 180 K may hardly be attributed to a slow spin state interconversion, since the LS Fe^{III} doublet peaks remain sharp with relatively thin line widths. In the 4-180 K temperature range broadening of the HS Fe^{III} seems to be rather due to slow relaxation of the HS Fe^{III} magnetic moments directions with a frequency (10^7 - 10^9 s^{-1}) whose reciprocal is of the same order of magnitude of the Mössbauer effect observation time. Below the temperatures referred to above, all the Fe centers are present as LS Fe^{III} and therefore no sextets are observed at 4 K in contrast to $[Fe(5\text{-}Cl\text{-}sal_2trien)][MnCr(ox)_3]\cdot 0.5CH_3NO_2$, $[Fe(5\text{-}Br\text{-}sal_2trien)][MnCr(ox)_3]$ and $[Fe(sal_2trien)][MnCr(ox)_3]\cdot CH_3OH$ where a significant fraction of Fe^{III} was still in the HS state at temperatures ≤ 4 K.[5,11b]

The temperature dependence of the estimated relative areas of the HS and LS Fe^{III} subspectra of the three compounds are plotted in Figure S4 of the supporting information. They follow the same trend as the temperature dependence of χ_MT and permit to calculate the transition temperature $T_{1/2}$.

Spectroscopic measurements on the diluted system. The spin-crossover behavior of this family of Fe^{III} complexes has been studied by optical spectroscopy on single crystals. It is not possible to perform this type of measurements with the pure Fe compounds because the ligand-metal charge transfer (LMCT) absorption bands of the Fe complexes are very intense in the visible region and saturate the signal. Therefore, doped $[Ga^{III}_{1-x}Fe^{III}_x(sal_2\text{-}trien)][Mn^{II}Cr^{III}(ox)_3]\cdot CH_2Cl_2$ crystals were prepared. They show much less intense absorption bands, as Ga^{III} complexes do not absorb in the visible region of the spectrum. For good quality spectra, it was necessary to reduce the Fe content to 1 mole% (**3·CH$_2$Cl$_2$**).

Absorption spectra at different temperatures on a single crystal of **3·CH$_2$Cl$_2$** were recorded in order to follow the thermal spin crossover of the compound (Figure 8a). At room temperature, the characteristic LMCT band of the HS Fe^{III} complex is observed as a shoulder at around 500 nm of an intense band centered at 570 nm assigned to the spin

allowed $^4A_2 \rightarrow {}^4T_2$ *d-d* transition of $[Cr(ox)_3]^{3-}$ of the bimetallic oxalate network. The latter practically does not change with temperature. Upon cooling, a band around 650 nm, due to an LMCT absorption of the LS complex, gradually appears and increases in intensity. At the same time, the intensity of the above-mentioned HS band decreases. The temperature dependence of the HS fraction was monitored by analyzing the evolution of the absorbance of the LMCT absorption bands. For a quantitative evaluation of the resultant thermal spin transition, the evolution of the optical density at 665 nm as a function of temperature has been normalized with the data from the magnetic measurements performed on **1·CH$_2$Cl$_2$**.[5] Comparison of this result with magnetic data of the pure Fe compound **1·CH$_2$Cl$_2$** is shown in Figure 8b. For both compounds a gradual variation of the HS fraction is observed, with an estimated HS fraction at room temperature of 80%. For the doped system **3·CH$_2$Cl$_2$**, $T_{1/2}$ is shifted to lower temperatures ($T_{1/2}$ = 225 K) compared to **1·CH$_2$Cl$_2$** ($T_{1/2}$ = 245 K).[7] Furthermore, the transition is more gradual in **3·CH$_2$Cl$_2$** than in the pure Fe compound **1·CH$_2$Cl$_2$**. This observation can be explained by the lack of cooperative interactions in lightly doped crystals.

For LIESST experiments the sample was irradiated at 5 K with a continuous diode pumped solid-state laser at 690 nm. Irradiation at this wavelength, which is within the LMCT absorption of the LS species, resulted in a light-induced population of the metastable HS state at the expense of the LS state. Irradiation for only 2 minutes at 1 mW/mm^2 in fact resulted in an almost quantitative transformation from the LS state to the photo-excited HS state (Figure 9a), since the absorption spectrum of **3·CH$_2$Cl$_2$** in the photo-excited state at low temperature is almost identical to the one obtained at room temperature. Absorption spectra after photo-excitation were subsequently recorded between 5 and 70 K with a heating rate of 0.3 K/min. The HS fraction at every temperature was calculated from the evolution of the absorbance at 665 nm, taking the spectrum at 5 K as the LS reference and the one obtained just after irradiation at this temperature as the HS reference. The HS fraction remains close to 100 % from 5 to 30 K. At higher temperatures it decreases to reach a value close to zero at around 60 K (Figure 9b). This gives a T(LIESST) of 43 K, which is similar to the result obtained from the magnetic measurements for the pure Fe compound **1·CH$_2$Cl$_2$**.[7] In contrast to the magnetic measurements on the pure Fe crystals, for which a light induced HS fraction of only 0.4 could be achieved,[7] in the very dilute system it proved possible to achieve a quantitative population of the HS state. This is due to the comparatively weak optical density of the dilute crystals, which results in a good penetration and propagation of the light through the crystal, whereas the strong absorption of the pure Fe crystals only results in the photo-excitation of the complexes close to the surface and not in the bulk.

DISCUSSION

T(LIESST). In the quest for high T(LIESST) values, chemists have searched for parameters allowing to rationalize and predict the T(LIESST) value, in order to reach the highest T(LIESST) possible. Létard et al. have proposed a relationship between T(LIESST) and $T_{1/2}$ for Fe(II) complexes.[21] They proposed that these two experimental parameters are related by a linear relationship, T(LIESST) = $T_0 - 0.3\ T_{1/2}$. T_0 has been proposed to be equal to 100, 120, 150, 180 and 200 K for monodentate, bidentate, tridentate, macrocyclic ligands and Prussian Blue analogs, respectively. Sato et al. have looked for an analogous relationship for the Fe^{III} complexes presenting a LIESST effect. Thus, they reported a linear relationship T(LIESST) = $T_0 - 0.4T_{1/2}$, with T_0 = 185 K for the six compounds derived from the $[Fe(pap)]^+$ complex.[8c] In a second article, two more examples of Fe^{III} complexes presenting a LIESST effect containing the complex $[Fe(qsal)_2]^+$, were added.[9] These two compounds were shown to have substantially lower T(LIESST) values than expected from the above relation.

The T(LIESST) / $T_{1/2}$ values for the SCO compounds based on $[Fe^{III}(sal_2\text{-trien})]^+$ inserted into bimetallic oxalate networks as well as the other compounds reported by Sato et al.[8,9] are given in Table 4 and Figure 10.

All the $[Fe(pap)_2]^+$ complexes (points 1 to 6) lie quite close to the line with T_0 = 150 K, the one obtained for tridentate ligands in Fe^{II} complexes using the relation of Létard et al.[20] Since the pap$^-$ ligand is tridentate in nature, it can be supposed that the Fe^{III} complexes exhibiting a LIESST effect follow the same law as Fe^{II} complexes. The two $[Fe(qsal)_2]^+$ compounds (points 7 and 8) lie sensibly below this line, although the qsal$^-$ ligand is also tridentate. Sato et al. indicated that this could be due to the incomplete LIESST effect of this complex.[9] The four $[Fe^{III}(sal_2\text{-trien})][Mn^{II}Cr^{III}(ox)_3]\cdot S$ (S = CH_2Cl_2, $CHCl_3$, CH_2Br_2, $CHBr_3$) compounds (points 9 - 12) lie notably lower than the previous Fe^{III} compounds. This behavior is significantly different to that of the pap$^-$ ligand. Indeed, the sal$_2$-trien^{2-} ligand is a hexadentate ligand. Thus, a priori, we would have expected the T(LIESST) / $T_{1/2}$ points to be situated on an upper line (T_0 = 180 K for example). A possible explanation may be related to the flexibility of the ligand. Tridentate pap$^-$ and qsal$^-$ ligands are both entirely conjugated in contrast to the sal$_2$-trien^{2-} ligand, which possesses three flexible ethylene bridges $-CH_2CH_2-$. A high flexibility has been recognized as a factor decreasing T(LIESST).[21]

Sato et al. have related the low T(LIESST) of $[Fe(qsal)_2]NCS$ and $[Fe(qsal)_2]NCSe$ to the low photoconversion. Approximately 17 % and 8 % of LS species were transformed into photo-induced HS species at 5 K for $[Fe(qsal)_2]NCS$ and $[Fe(qsal)_2]NCSe$ respectively. It seems however, that in $[Fe^{III}(sal_2\text{-trien})][Mn^{II}Cr^{III}(ox)_3]\cdot S$ compounds, the situation is more complex. For example, **1·CHCl$_3$** presents a T(LIESST) of 58 K with a photoconversion of about 40 % whereas **1·CHBr$_3$** presents a slightly higher T(LIESST) of 62 K with a photoconversion of about 26 %. In the dilute system **3·CH$_2$Cl$_2$**, the photoconversion is 100% and T(LIESST) is 43 K.

Origin of the LIESST effect in Fe^{III} complexes. The lifetime of the HS photoexcited state has been rationalized on the basis of a non-adiabatic mutiphonon relaxation model.[22] Within the framework of this theory, the Single Configurational Coordinate (SCC) approach considers the Metal-Ligand distance as the reaction coordinate, related to only one vibrational mode, the completely symmetrical one. According to SCC theory, the low-temperature (tunneling regime) lifetime of the HS state for Fe^{III} spin-

crossover compounds is expected to be of the order of milliseconds, whereas it can go from seconds to months for Fe^{II} spin-crossover compounds. With this short lifetime, it should be impossible to observe the decay of the photoinduced state for Fe^{III} by using standard SQUID techniques. However, as mentioned above, the LIESST effect has been observed by Sato et al. in several Fe^{III} complexes.[8-10] These authors attributed their observations to the strong distortion of the Fe^{III} site from octahedral geometry, enhanced by the presence of strong intermolecular interactions such as π-π stacking. Thus, when passing from the ideal octahedral $[Fe^{II}N_6]$ site to a distorted $[Fe^{III}N_4O_2]$ geometry, in addition to the completely symmetrical vibrational mode, other vibrational modes such as bending modes should also be taken into account.[9,23] This results in a displacement between the potential walls of the HS and LS states, which is larger than that expected considering only the changes in metal-ligand distances, and could explain the long lifetime of the photogenerated HS state.

To evaluate the structural changes of $[Fe(sal_2\text{-trien})]^+$ in **1·CH_2Cl_2**, **1·CH_2Br_2**, **1·$CHCl_3$** and **1·$CHBr_3$**, we have focused our attention on the differences between the 100 and 300 K structures as they are close to the LS and HS structures. A limitation of this comparison is that we assume the photoinduced and high temperature HS states to present similar structures. X-ray structure determination of crystals of **1·CH_2Cl_2** after light irradiation at 10 K is in progress to verify this.

As the shortening in the Fe-N and Fe-O bond lengths between the HS and LS structures in these compounds are similar to those of other Fe^{III} complexes, other structural factor such as the distortion of the octahedral geometry may be at the origin of the LIESST effect in these compounds. To evaluate and compare this distortion with that of other Fe^{III} complexes, we have used the program SHAPE that can be obtained from its authors upon request.[24] This program calculates continuous shape measures of a set of points (e.g. atomic positions) relative to the vertices of ideal polyhedra and has already been used to find structure-property correlations in SCO complexes.[25] It also calculates the path deviation function for the minimal distortion interconversion path between the two ideal polyhedra (octahedron and a trigonal prism in our case). In the present case, SHAPE calculations show that at all temperatures, the coordination geometry around Fe falls along the minimal distortion path between a perfect octahedron and a perfect trigonal prism with a deviation of less than 10%. We have then calculated the generalized coordinate between the two ideal polyhedra that gives the trigonal prismacity of a given coordination sphere with respect to a pure octahedron. Thus, complexes with a perfect octahedral geometry or a perfect trigonal prismatic one would have generalized coordinate values of 0% and 100%, respectively. Figure 11 shows that the changes of the generalized coordinate of the Fe^{III} complexes of **1·CH_2Cl_2** with the temperature follow the same trend as the increase of HS fraction extracted from magnetic and Mössbauer measurements.[5] The distortion of the octahedral geometry of these complexes from the LS to the HS state follows then a Bailar twist with a higher distortion for the HS state. The trigonal prismacity of the Fe^{III} complexes of **1·$CHCl_3$**, **1·$CHBr_3$** and **1·CH_2Br_2** in the LS and HS state are similar to those of **1·CH_2Cl_2** at the same temperatures with small differences that can be related to small differences in the LS/HS ratio (see Figure 11). Therefore, the HS Fe^{III} complexes in **1·CH_2Cl_2**, **1·$CHCl_3$**, **1·$CHBr_3$** and **1·CH_2Br_2** present a Bailar distortion with respect to the LS complexes.

To see whether the LIESST effect could be related to this distortion, the trigonal distortion of other $[Fe(sal_2\text{-trien})]^+$ salts in which LIESST is not detected, such as the reference compound, $[Fe(sal_2\text{-trien})]ClO_4$ and the compound $[Fe^{III}(sal_2\text{-trien})][Mn^{II}Cr^{III}(ox)_3]\cdot CH_3OH$, were calculated.[5,7,26] The results show that they present a similar trigonal distortion as those of $[Fe(sal_2\text{-trien})]^+$ salts presenting a LIESST effect.[27] Then, the same method was used to evaluate the distortion of other Fe^{III} complexes not presenting a LIESST effect such as $[Fe(acpa)_2]^+$. This complex presents a Bailar twist in $[Fe(acpa)_2]BPh_4$ that follows the same trend as the magnetic measurements (see Figure 11), but the relative changes are much smaller than those found for the $[Fe^{III}(sal_2\text{-trien})]^+$ salts. Finally, the distortion of the octahedral geometry of $[Fe^{III}(pap)_2]^+$, the Fe^{III} complex exhibiting the clearest LIESST effect, has been evaluated. In this case the coordination geometry is far from the pure octahedral one even for the LS state. In contrast to $[Fe(sal_2\text{-trien})]^+$ complexes, the changes of the coordination sphere from LS to HS do not follow a Bailar distortion. This may be related to the tridentate character of the pap ligands that favors a different type of distortion path (D_{2d}) rather than the trigonal twist.[25a]

We conclude that the Fe^{III} complexes exhibiting a LIESST effect present a large distortion of the octahedral geometry in their HS state. However, in $[Fe^{III}(sal_2\text{-trien})]^+$ salts, other factors may contribute to this rare property as several salts of this cation with a similar distortion of the octahedral geometry do not present a LIESST effect such as the ClO_4^- and 3D $[Mn^{II}Cr^{III}(ox)_3]^-$ salts. In the case of $[Fe^{III}(pap)_2]^+$ salts, which present a different distortion of the octahedral geometry between the LS and HS states, it has been proposed that cooperative interactions due to strong π-π stacking intermolecular interactions may be at the origin of the LIESST effect. This factor cannot be used to explain the LIESST effect of $[Fe^{III}(sal_2\text{-trien})]^+$ compounds as they do not present abrupt spin-crossover transitions characteristic of cooperative systems. Furthermore, spectroscopic measurements on single crystals of the doped compound **3·CH_2Cl_2**, which is isostructural to **1·CH_2Cl_2**, confirm that the LIESST effect in this type of compound is not related to cooperativity. An important structural difference between the compounds reported in this paper and the other Fe^{III} compounds exhibiting a LIESST effect is the presence of the bimetallic, anionic extended oxalate network, instead of discrete small counterions. This rigid network could play an important role in the stabilization of the metastable HS state. In favor of this hypothesis are the numerous short contacts between the $[Fe(sal_2\text{-trien})]^+$ cations and the oxalate ligands, which are different in the low and high-temperature structures. These interactions may stabilize the photo-generated LIESST complex and prevent fast relaxation to the LS ground state. In other words, the increase of volume of the $[Fe^{III}(sal_2\text{-trien})]^+$ complexes after the photoinduced spin-

crossover may result in new interactions with the bimetallic oxalate layers, which prevent fast relaxation to the LS ground state. A structure determination of the metastable LIESST state is in progress to confirm this hypothesis, but this is not a trivial task.

Possible explanations for the absence of LIESST in other $[Fe(sal_2\text{-trien})]^+$ complexes inserted in 2D or 3D extended oxalate-based networks are:[7,11c] (a) a too high $T_{1/2}$ leading to a too fast HS-LS relaxation to be detected on the time scale of SQUID measurements; (b) the small amount of Fe^{III} that can undergo spin crossover, and (c) a different organization of the $[Fe(sal_2\text{-trien})]^+$ complexes in which only weak contacts with the oxalate network are established. Synthesis of more Fe^{III} complexes showing LIESST together with further characterization are needed to understand this unusual property.

CONCLUSION

We have demonstrated that the substitution of CH_2Cl_2 for other halogenated solvents in the synthesis of the 2D oxalate-based ferromagnet of formula $[Fe^{III}(sal_2\text{-trien})][Mn^{II}Cr^{III}(ox)_3]\cdot CH_2Cl_2$ permits the preparation of a family of compounds with an analogous structure that maintain the interesting physical properties of this compound, i. e., a coexistence of magnetic ordering and the LIESST effect. The subtle structural changes provide a model system for studying in detail the LIESST effect in Fe^{III} complexes. In fact, the change of solvent modifies the chemical pressure exerted on the inserted cation leading to different temperatures of the thermal and photoinduced spin crossover for each compound. Thus, the bulkiest $CHBr_3$ solvent increases the interlayer separation between layers in the structure of **1·CHBr$_3$** and favors the HS state, while the opposite is observed for the solvent of smallest volume, that is, CH_2Cl_2. As a consequence, **1·CHBr$_3$** and **1·CH$_2$Cl$_2$** present respectively the lowest and highest $T_{1/2}$ and the highest and lowest T_{LIESST} of this family of compounds. Therefore, substitution of CH_2Cl_2 in **1·CH$_2$Cl$_2$** by the bulkier $CHBr_3$, CH_2Br_2 and $CHCl_3$ solvent molecules has proven to be a successful strategy to obtain Fe^{III} complexes exhibiting a LIESST effect at higher temperatures.

The versatility of this system has also allowed us to show that the replacement of Fe^{III} complexes by the diamagnetic Ga^{III} is a successful strategy to perform a spectroscopic characterization on single crystals. Thus, we have demonstrated that $[Ga_{1-x}Fe_x(sal_2trien)][Mn^{II}Cr^{III}(ox)_3]\cdot CH_2Cl_2$, x = 0.01 (**3·CH$_2Cl_2$**) also presents a complete thermal spin crossover and a quantitative LIESST effect. These measurements on diluted samples confirm that, in contrast to the results obtained by Sato et al.,[8,9] cooperativity is not a necessary condition to observe the LIESST effect in Fe^{III} complexes, as cooperativity is excluded in these doped systems due to the long distance between the Fe^{III} centers.

Structural analysis of these compounds and other Fe^{III} complexes indicates that several factors may explain the LIESST effect in Fe^{III} complexes. In the case of $[Fe^{III}(pap)_2]^+$ complexes, the presence of a rigid tridentate ligand that induces a distorted octahedral geometry together with strong π-π interactions between the Fe^{III} complexes could be at the origin of this effect, while in the $[Fe^{III}(sal_2\text{-trien})]^+$ complexes reported here, which contain a more flexible ligand, it could be related to the interactions with a bimetallic oxalate extended network. Further experiments are needed to confirm this point.

ASSOCIATED CONTENT

Supporting Information. Magnetization curves of **1·CH$_2$Br$_2$**, **1·CHCl$_3$** and **1·CHBr$_3$**, the temperature dependence of $\chi_M T$ for **2·CH$_2$Cl$_2$**, relaxation kinetics and simulation of the $\chi_M T$ product vs. time at different temperatures of **1·CH$_2$Br$_2$**, **1·CHCl$_3$** and **1·CHBr$_3$**, temperature dependence of the estimated relative areas of HS Fe^{III} from the Mössbauer spectra for compounds **1·CH$_2$Br$_2$**, **1·CHCl$_3$** and **1·CHBr$_3$** and tables with the intermolecular contacts and the parameters from the relaxation kinetics curves of **1·CH$_2$Br$_2$**, **1·CHCl$_3$** and **1·CHBr$_3$**. This material is available free of charge via the Internet at http://pubs.acs.org.

AUTHOR INFORMATION

Corresponding Author

* E-mail: miguel.clemente@uv.es, eugenio.coronado@uv.es.

ACKNOWLEDGMENT

Financial support from the European Union (MolSpinQIP and SPINMOL ERC Advanced Grant), the Spanish Ministerio de Economía y Competitividad (Projects Consolider-Ingenio in Molecular Nanoscience CSD2007-00010, MAT2011-22785 and CTQ-2011-26507), and the Generalitat Valenciana (Prometeo Program) are gratefully acknowledged. The authors also thank J. M. Martínez-Agudo and Dr. Gloria Agustí-López, University of Valencia, for magnetic characterization of the samples, Prof. S. Hayami and Prof. O. Sato by kindly providing the structural data of $[Fe^{III}(pap)_2]PF_6.CH_3OH$ compound and Prof. S. Alvárez by kindly providing the SHAPE program and for helpful discussions. AT acknowledges a Marie-Curie Fellowship of the European Union. C. Besnard is acknowledged for the structure determination of the compound **3·CH$_2$Cl$_2$**.

REFERENCES

(1) (a) Coronado E.; Day, P. *Chem. Rev.* **2004**, *104*, 5419. (b) Coronado, E.; Martí-Gastaldo, C.; Navarro-Moratalla, E.; Ribera, A.; Blundell S. J.; Baker, P. J. *Nat. Chem.* **2010**, *2*, 1031. (c) Coronado, E.; Martí-Gastaldo, C.; Navarro-Moratalla, E.; Burzuri, E.; Camon, E.; Luis, F. *Adv. Mater.* **2011**, *23*, 5021.

(2) Coronado, E.; Mínguez Espallargas, G. *Chem. Soc. Rev.* **2013**, *42*, 1525.

(3) (a) Sato, O.; Iyoda, T.; Fujishima, A.; Hashimoto, K. *Science*, **1996**, *272*, 704. (b) Coronado, E.; Giménez-López, M. C.; Levchenko, G.; Romero, F. M.; García-Baonza, V.; Milner A.; Paz-Pasternak, M. *J. Am. Chem. Soc.* **2005**, *127*, 4580. (b) Coronado, E.; Giménez-López, M. C.; Korzeniak, T.; Levchenko, G.; Romero, F. M.; Segura, A.; García-Baonza, V.; Cezar, J. C.; De Groot, F. M. F.; Milner A.; Paz-Pasternak, M. *J. Am. Chem. Soc.* **2008**, *130*, 15519. (c) Ohkoshi, S.–I.; Imoto, K.; Takano, S.; Tokoro, H. *Natur. Chem.* **2011**, *3*, 564.

(4) (a) Bénard, S.; Yu, P.; Audière, J. P.; Rivière, E.; Clèment, R.; Ghilhem, J.; Tchertanov, L.; Nakatami, K. *J. Am. Chem. Soc.* **2000**, *122*, 9444. (b) Coronado, E.; Galán-Mascarós, J. R.; Gómez-García C. J.; Laukhin, V. *Nature* **2000**, *408*, 447. (c) Train, C.; Gheorghe, R.; Krstic, V.; Chamoreau, L. M.; Ovanesyan, N. S.; Rikken, G. L. J. A.; Gruselle M.; Verdaguer, M. *Nat. Mater.* **2008**, *7*, 729. (d) Okawa, H.; Shigematsu, A.; Sadakiyo, M.; Miyagawa, T.; Yoneda, K.; Ohba M.; Kitagawa, H. *J. Am. Chem. Soc.* **2009**, *131*, 13516. (e) Train, C.; Nuida, T.; Gheorghe, R.; Gruselle, M.; Ohkoshi, S. *J. Am. Chem. Soc.* **2009**, *131*, 16838. (f) Clemente-León, M.; Coronado, E.; Martí-

Gastaldo C.; Romero, F. M. *Chem. Soc. Rev.* **2011**, *40*, 473. (g) Pardo, E.; Train, C.; Liu, H.; Chamoreau, L.-M.; Dkhil, B.; Boubekeur, K.; Lloret, F.; Nakatani, K.; Tokoro, H.; Ohkoshi, S.-I.; Verdaguer, M. *Angew. Chem. Int. Ed.* **2012**, *51*, 8356. (h) Sadayiko, M.; Okawa, H.; Shigematsu, A.; Ohba, M.; Yamada, T.; Kitagawa, H. *J. Am. Chem. Soc.* **2012**, *134*, 5472. (i) Okawa, H.; Sadakiyo, M.; Yamada, T.; Maesato, M.; Ohba, M.; Kitagawa, H. *J. Am. Chem. Soc.* **2013**, *135*, 2256.

(5) Clemente-León, M.; Coronado, E.; López-Jordà, M.; Mínguez Espallargas, G.; Soriano-Portillo, A.; Waerenborgh, J. C. *Chem. Eur. J.* **2010**, *16*, 2207.

(6) (a) Decurtins, S.; Gütlich, P.; Köhler, C. P.; Spiering, H.; Hauser, A. *Chem. Phys. Lett.* **1984,** *105*, 1. (b) Hauser, A. *Top. Curr. Chem.* **2004**, *234,* 155.

(7) Clemente-León, M.; Coronado, E.; López-Jordà, M.; Desplanches, C.; Asthana, S.; Wang, H.; Létard, J.-F. *Chem. Sci.* **2011**, *2*, 1121.

(8) (a) Hayami, S.; Gu, Z. –Z.; Shiro, M.; Einaga, Y.; Fujishima, A.; Sato, O. *J. Am. Chem. Soc.* **2000**, *122*, 7126. (b) Juhász, G.; Hayami, S.; Sato, O.; Maeda, Y. *Chem. Phys. Lett.* **2002**, *364*, 164. (c) Hayami, S.; Kawahara, T.; Maeda, Y.; Inoue, K.; Sato, O. *J. Radioanal. Nucl. Chem.* **2005**, *266*, 521.

(9) Hayami, S.; Hiki, K.; Kawahara, T.; Maeda, Y.; Urakami, D.; Inoue, K.; Ohama, M.; Kawata, S.; Sato, O. *Chem. Eur. J.* **2009**, *15*, 3497.

(10) Shimizu, T.; Komatsu, Y.; Kamihata, H.; Lee, Y. H.; Fuyuhiro, A.; Iijima, S.; Hayami, S. *J. Incl. Phenom. Macrocycl. Chem.* **2011**, *71*, 363.

(11) (a) Clemente-León, M.; Coronado, E.; López-Jordà, M. *Dalton Trans.* **2010**, *39*, 4903. (b) Clemente-León, M.; Coronado, E.; López-Jordà, M.; Waerenborgh, J. C. *Inorg. Chem.* **2011**, *50*, 9122. (c) Clemente-León, M.; Coronado, E.; López-Jordà, M. *Eur. J. Inorg. Chem.* **2013**, 753.

(12) Tweedle, M. F.; Wilson L. J. *J. Am. Chem. Soc*. **1976**, *98*, 4824.

(13) Baylar, J. C.; Jones, E. M. *Inorganic Synthesis*; Booth, H. S.; Ed.; McGraw-Hill: New York, 1939; Vol. 1, p 35.

(14) Altomare, A.; Burla, M. C.; Camalli, M.; Cascarano, G. L.; Giacovazzo, C.; Guagliardi, A.; Moliterni, A. G. G.; Polidori, G.; Spagna, R. *J. Appl. Cryst*. **1999**, *32*, 115.

(15) SHELXL-97: G. M. Sheldrick, University of Göttingen, Germany, **1997**.

(16) Farrugia, L. J. *J. Appl. Cryst.***1997**, *32*, 837.

(17) Rodrigues, J. V.; Santos, I. C.; Gama, V.; Henriques, R. T.; Waerenborgh, J. C.; Duarte, M. T.; Almeida, M. *J. Chem. Soc. Dalton Trans*. **1994**, 2655.

(18) Unit cell of compound $[In^{III}(sal_2\text{-trien})][Mn^{II}Cr^{III}(ox)_3]$ obtained in CH_2Cl_2 measured with single crystal X-ray diffraction (a = 15.841(12) Å, b = 20.639(16) Å and c = 21.285(18)Å, β = 90°, V = 6947(10)Å^3) is similar to that of other 3D compounds obtained in CH_3CN or CH_3NO_2 such as compound **4** from reference 5.

(19) Unit cell of compound $[Ga^{III}(sal_2\text{-trien})][Mn^{II}Cr^{III}(ox)_3]\cdot CH_2Cl_2$ measured with single crystal X-ray diffraction (a = 11.851(8) Å, b = 31.972(18) Å and c = 9.486(7)Å, β = 111.62(6)°, V = 3342(4)Å^3) is similar to that of the 2D compound obtained in CH_2Cl_2 with $[Fe^{III}(sal_2\text{-trien})]$ (**1·CH$_2$Cl$_2$**).

(20) Mishra, V.; Mukherjee, R.; Linares, J.; Baldé, C.; Desplanches, C.; Létard, J.-F.; Collet, E.; Toupet, L.; Castro, M.; Varret, F. *Inorg. Chem.* **2008**, *47*, 7577.

(21) (a) Létard, J.-F. ; Guionneau, P.; Nguyen, O.; Sanchez Costa, J.; Marcen, S.; Chastanet, G.; Marchivie, M.; Goux-Capes, L. *Chem. Eur. J.* **2005**, *11*, 4582. (b) Létard, J.-F. *J. Mater. Chem.* **2006**, *16*, 2550.

(22) Hauser, A. *J. Chem. Phys.* **1991**, *94*, 2741.

(23) Schenker, S.; Hauser A.; Dyson, R. M. *Inorg. Chem.* **1996**, *35*, 4676.

(24) Llunell, M.; Casanova, D.; Cirera, J.; Bofill, J. M.; Alemany, P.; Alvarez, S.; Pinski, M.; Avnir. D. SHAPE (2.0); Barcelona 2010)

(25) (a) Alvárez, S. *J. Am. Chem. Soc.* **2003**, *125*, 6795. (b) Matouzenko, G. S.; Borshch, S. A.; Jeanneau. E.; Bushuev, M. B. *Chem. Eur. J.* **2009**, *15*, 1252.

(26) Pritchard, R.; Barrett, S. A.; Kilner, C. A.; Halcrow M. A. *Dalton Trans.* **2008**, 3159.

(27) Trigonal prismacity of the two crystallographically independent iron atoms of $[Fe^{III}(sal_2\text{-trien})][Mn^{II}Cr^{III}(ox)_3]\cdot CH_3OH$ is 29.1 and 34.9 % at 120 K, temperature at which 70 % of Fe^{III} is in the HS state. Trigonal prismacity of the four crystallographically independent iron atoms of $[Fe^{III}(sal_2\text{-trien})]ClO_4$ is 37.4 and 41.8 % for the HS Fe^{III} and 14.1 and 19.2 % for the LS Fe^{III} at 105 K. At this temperature half of the Fe^{III} is in the HS state (see reference 26).